

Chemical characterization and source attribution of aviation-related ultrafine particles

Dissertation
zur Erlangung des Doktorgrades
der Naturwissenschaften

vorgelegt beim Fachbereich 14 Biochemie, Chemie und Pharmazie
der Johann Wolfgang Goethe - Universität
in Frankfurt am Main

von
Florian Ungeheuer
aus Bad Vilbel

Frankfurt 2023
(D 30)

vom Fachbereich 14 Biochemie, Chemie und Pharmazie der

Johann Wolfgang Goethe - Universität als Dissertation angenommen.

Dekan: Prof. Dr. Clemens Glaubitz

Gutachter : Prof. Dr. Alexander L. Vogel
Prof. Dr. Martin U. Schmidt

Datum der Disputation : 20.07.2023

Abstract

Large international airports were identified as sources of ultrafine particles (UFPs) (Hu et al., 2009; Yu et al., 2012; Hsu et al., 2013; Keuken et al., 2015; Hudda and Fruin, 2016). Since September 2017 UFP emissions originating from the Frankfurt International Airport, Germany are monitored by the Hessian Agency for Nature Conservation, Environment and Geology (HLNUG) showing elevated UFP concentrations during airport operating hours (05:00–23:00 CET) (Ditas et al., 2022). Referring to that, the organic chemical composition of aviation-related UFPs emerging from the Frankfurt Airport was analysed by performing a comprehensive non-target screening of UFP filter samples.

Aluminium-filter samples were collected at an air quality monitoring station 4 km north of the Frankfurt Airport, using a 13-stage impactor system (Nano-MOUDI). The chemical characterization of UFPs in the size range of 10-18 nm, 18-32 nm and 32-56 nm was accomplished by ultra-high-performance liquid chromatography, heated electrospray ionisation and mass analysis using an Orbitrap high-resolution mass spectrometer. Non-target screening revealed that the majority of detected compounds belong to homologous series of two different types of organic esters, which are base stocks of aircraft lubrication oils.

In reference to five different jet engine lubrication oils of various manufacturers, the corresponding lubricant base stocks and their additives, two amines and one organophosphate, were identified in the UFPs by the use of matching retention time, exact mass and MS/MS fragmentation pattern of single organic molecules. The quantitative analysis of the jet engine oil constituents in the aviation-related UFPs with diameters < 56 nm was accomplished by standard addition. By characterizing the Nano-MOUDI, loss factors for each size stage were determined and used for correction accordingly. Particle-number size distribution measurements, conducted parallel to the filter sampling, enabled the determination of the jet engine oil contribution to the UFP mass.

Furthermore, the nucleation and particle formation potential of a commonly used synthetic jet engine lubrication oil was investigated in the laboratory. Thermodenuder experiments at 20 °C and 300 °C were carried out to monitor the gas-to-particle partitioning behaviour of jet engine oils. At 300 °C a significantly higher number of particles with a mean diameter of ~10 nm are formed, leading to a more than fivefold increase in total particle numbers compared to 20 °C. Particle diameters of the newly formed oil particles in the laboratory experiment appeared in the same size region as UFPs emerging from Frankfurt Airport. Particles originating from the Frankfurt city centre direction showed larger diameters.

Results indicate that aircraft emissions strongly influence the total mass of 10-18 nm particles. The jet oil fraction decreases for bigger particles (e.g., 18-56 nm), implying that these oils form new particles in the cooling exhaust gases of aircraft engines. In addition, non-target screening and *in vitro* bioassays on aviation-related PM_{2.5} filter samples were combined to provide indications for potential toxicologically relevant compounds in dependence of different wind directions and airport operations. Most recently, the applied non-target screening method was also used to identify seasonal variations in the organic aerosol composition in Beijing.

Acknowledgements

Table of Content

1.	Introduction to aerosol research.....	1
1.1	Motivation	1
1.2	Ultrafine particles – Occurrence and health effects	3
1.3	Focus of this thesis	8
2.	Aviation-related ultrafine particles	9
3.	Methods.....	13
3.1	Mass spectrometry (MS) – An overview	13
3.2	Ion trap mass analyser – Orbitrap	14
3.3	Tandem mass spectrometry (MS/MS).....	18
3.4	Electrospray ionisation (ESI)	20
3.5	Ultra-high performance liquid chromatography (UHPLC).....	21
3.6	Non-target analysis.....	23
3.7	Quantitative analysis	24
3.8	Particle-number size distribution	25
3.9	Sampling of atmospheric particulate matter.....	27
4.	The Projects.....	30
4.1	Identification and source attribution of organic compounds in ultrafine particles near Frankfurt International Airport.....	30
4.2	Nucleation of jet engine oil vapours is a large source of aviation-related ultrafine particles	51
4.3	Occurrence and in vitro toxicity of organic compounds in urban background PM _{2.5}	68
4.4	Nontarget Screening Exhibits a Seasonal Cycle of PM _{2.5} Organic Aerosol Composition in Beijing	73
5.	Publications	77
5.1	Identification and source attribution of organic compounds in ultrafine particles near Frankfurt International Airport.....	77
5.2	Nucleation of jet engine oil vapours is a large source of aviation-related ultrafine particles	110
5.3	Occurrence and in vitro toxicity of organic compounds in urban background PM _{2.5}	141
5.4	Nontarget Screening Exhibits a Seasonal Cycle of PM _{2.5} Organic Aerosol Composition in Beijing	183
6.	Summary and Outlook	221

7.	Zusammenfassung.....	226
8.	Personal Contribution to the Publications	232
9.	References	235
10.	Curriculum Vitae	257

Except where stated otherwise by reference or acknowledgment, the work presented was generated by myself under the supervision of my advisors during my doctoral studies.

Whenever a figure, table or text is identical to a previous publication, it is stated explicitly in the thesis that copyright permission and/or co-author agreement has been obtained.

The following parts of the thesis have been previously published:

- Figure(s) “1-3; 6; 7; 9; 11-24”

- Table(s) “1-2”

1. Introduction to aerosol research

1.1 Motivation

Atmospheric aerosol has a diverse and strong influence on our planet Earth. Aerosols defined as liquid or solid particles suspended in a gas, play a major role in the global energy budget affecting Earth's climate and impairing human health (Seinfeld and Pandis, 2016). Different sources and processes can cause the emission of particulate matter to the atmosphere divisible into natural- and anthropogenic sources. Land use change and combustion of fossil- and biofuels are mainly attributable to human activities whereas for example dust and biological material like pollen are of natural origin (Heald and Spracklen, 2015; Shrivastava et al., 2017). Furthermore particulate matter like sea salt, biological materials and mineral dust, which is directly emitted to the atmosphere, is referred as primary particles. The formation of secondary particles like sulphate aerosol, from dimethyl sulphide emission from phytoplankton, occurs in the atmosphere by conversion of gaseous precursors through processes like nucleation, condensation and different chemical reactions (Haywood and Boucher, 2000; Hallquist et al., 2009; Moise et al., 2015). Furthermore, airborne particulate matter is differentiated based on aerodynamic diameter with particles smaller than 10 μm , referred as coarse mode particles (PM_{10}). Particles smaller than 2.5 μm in diameter are designated as fine particulate matter ($\text{PM}_{2.5}$; accumulation mode) and with a diameter below 0.1 μm as ultrafine particles (UFPs). These particles can be further subdivided into the nuclei mode ($< 10 \text{ nm}$) and Aitken mode (10-100 nm) (Seinfeld and Pandis, 2016). Atmospheric aerosol influences Earth's energy budget in different ways, which can be divided into direct and indirect effects. Direct effects include the scattering and absorption of solar- and terrestrial radiation, changing the global radiative budget, whereas the indirect effects are based on the influence of aerosols towards clouds (Haywood and Boucher, 2000). Atmospheric aerosol affects the lifetime and cloud albedo as higher particle concentrations lead to smaller sized cloud droplets. In this regard aerosol particles need to be activated as cloud condensation nuclei (CCN) (Twomey, 1977; Albrecht, 1989; Mei et al., 2013). The Intergovernmental Panel on Climate Change (IPCC) states that the overall effective radiative forcing of atmospheric aerosol is negative, implying a net cooling effect (IPCC, 2021). The development of mankind and the associated industrialisation lead to an increasing alteration of Earth's surface condition and the gaseous and aerosol phase emission regime, both in quantity and quality. For example, different food production and further land

use changes lead to stronger applications of nitrogen fertilizers and an increase in animal husbandry activities, which cause a consequent rising in gaseous precursors emission that can lead to formation of aerosol particles as well. In this regard the emission of ammonia and nitrogen oxides results in the formation of inorganic ammonium nitrate aerosol (Heald and Spracklen, 2015; Bauer et al., 2016). Nevertheless not only anthropogenic emissions are significant to air quality, human health and climate, as biogenic emissions like airborne bacteria and pollen can trigger human diseases and also act as CCN (Fröhlich-Nowoisky et al., 2016).

Air pollution is linked to respiratory diseases like asthma and lung cancer (Newby et al., 2015). Accordingly NO₂ pollution is seen as a contributor to paediatric asthma globally (Anenberg et al., 2022). These negative health effects as well as cardiovascular diseases, which are triggered by inhalation of airborne particulate matter, are a consequence of various adverse processes in the human body like oxidative stress at the cellular level and inflammatory reactions (Mills et al., 2009). Current research results implicate an annual excess mortality rate in the European Union (EU-28) of 659,000 and a reduction of the mean life expectancy by ~2.2 years caused by air pollution (Lelieveld et al., 2019), whereas the European Environment Agency (EEA) designates 307,000 premature death to PM_{2.5} exposure in the EU-27 for 2019. In order to address this problem, the World Health Organisation (WHO) guidelines reduced the annual average concentration exposition level from airborne PM_{2.5} from 10 µg m⁻³ in 2005 to 5 µg m⁻³ in 2021 (WHO, 2006, 2021). From the years 2000 to 2019, ~86% of urban inhabitants were facing PM_{2.5} concentrations exceeding the WHO 2005 limits (Southerland et al., 2022). Application of the new WHO guidelines of 2021 would have reduced the number of premature death in the EU-27 in 2019 by at least 72% compared to 2005 levels (EEA, 2021). Despite no limit is set so far, in the WHO report (2021) the monitoring of ultrafine particles (UFPs) was recommended as well.

The adverse effects on human health and Earth's energy budget are strictly affected not only by PM concentrations but also by their chemical composition as well. For these reasons, we need to apply measuring techniques, which get constantly further optimized in order to chemically characterize aerosol particles, being indispensable for the understanding of the aerosol driven processes. In this regards, the complexity of the topic is made even more challenging due to the fact that Earth's atmosphere acts as a huge oxidative reactor that promotes continuous changes in airborne chemical species due to successive reactions (Jimenez et al., 2009; Shrivastava et al., 2017).

1.2 Ultrafine particles – Occurrence and health effects

Ultrafine particles (UFPs) are specified as particles smaller than 100 nm in diameter and are of very low mass compared to larger sized particles. These type of particles can be found in high numbers in the urban environment with a vast variety of emission sources whereby their emission is strongly connected to primary aerosols (Allan et al., 2010). The nature of the source affects the particles size range as well as the number concentration with the highest numbers originating from the traffic sector and coal use in the 30-50 nm range. Bigger sized particles are released for example through industrial combustion processes and agricultural waste burning. Nucleation of vapours can as well lead to the formation of UFPs mostly under influence of sulphuric acid, ammonia and organic molecules in the gas phase. This oxidation-driven process initially causes the formation of particles smaller than 2 nm in diameter. Formation of new particles can also be observed in engine exhaust plumes when hot fumes get rapidly cooled by contact with ambient air (Paasonen et al., 2016). As particle growth progresses, the increase in diameter starts to get more and more dominated by organics. The particles increase their size by taking up condensable vapours, this process is in competition with coagulation with bigger sized particles (Riipinen et al., 2012). Reaching diameters of ~50 nm and above, particles can act as cloud condensation nuclei (Seinfeld and Pandis, 2016). In order to escape the nucleation valley of death, it is necessary to reach particle sizes larger than 10 nm. This required rapid growth is mainly driven by gas phase supersaturation (Wang et al., 2020). Consequently, secondary organic aerosol formation can also contribute to the overall ultrafine-particle mass burden.

Based on airborne measurements Junkermann and Hacker (2018) concluded that the majority of anthropogenic UFP emissions results from fossil fuel combustion. Nevertheless, industrial processes like arc welding (Cena et al., 2014) and also restaurant cooking (Vert et al., 2016) can lead to particle emissions in the ultrafine size range. Furthermore, a study from Japan concluded that automobile traffic exhaust and coal- and fuel combustion contributed most to the ultrafine particle mass burden in an urban industrial area (Fujitani et al., 2021). It is worth to be mentioned that biogenic secondary organic aerosol is also a possible source for ultrafine particles, contributing to the overall ultrafine particle mass in urban areas (Zhu et al., 2002a; Zhu et al., 2002b; Morawska et al., 2008; Paasonen et al., 2016, Rönkkö et al., 2017).

The here presented study focuses on airports as a major source of UFPs which has already been the subject of various publications, mainly focusing on physical measurements and not

providing detailed chemical information (Hu et al., 2009; Yu et al., 2012; Keuken et al., 2015; Stafoggia et al., 2016; Yu et al., 2017; Habre et al., 2018; Fushimi et al., 2019; Rivas et al., 2020). Due to the large number of sources and resulting chemical complexity of the particles composition, especially in the urban environment, it is indispensable to investigate possible exposure health effects. Research should focus on the burden in the direct surrounding of local sources as indoor infiltration of UFPs seems to be more relevant than PM_{2.5} and PM₁₀ (Chen et al., 2020; Hudda et al., 2020). Possible workplace exposure should also be considered.

UFPs are of very small size enabling deep penetration of human tissue leading to oxidative stress, inflammatory reactions and cell membrane damages (Nel et al., 2006; Jonsdottir et al., 2019; Ohlwein et al., 2019) (Figure 1). These health effects depend on the particle size, mass and number concentration (Yu et al., 2017). Although health effects of UFPs are still not adequately investigated, an increasing number of studies in the field of Nanotoxicology give insight into possible health-damaging consequences of exposure. Furthermore, it should be considered that compounds with no toxicological relevance can become deleterious by forming nano-sized structures (Oberdörster et al., 2005).

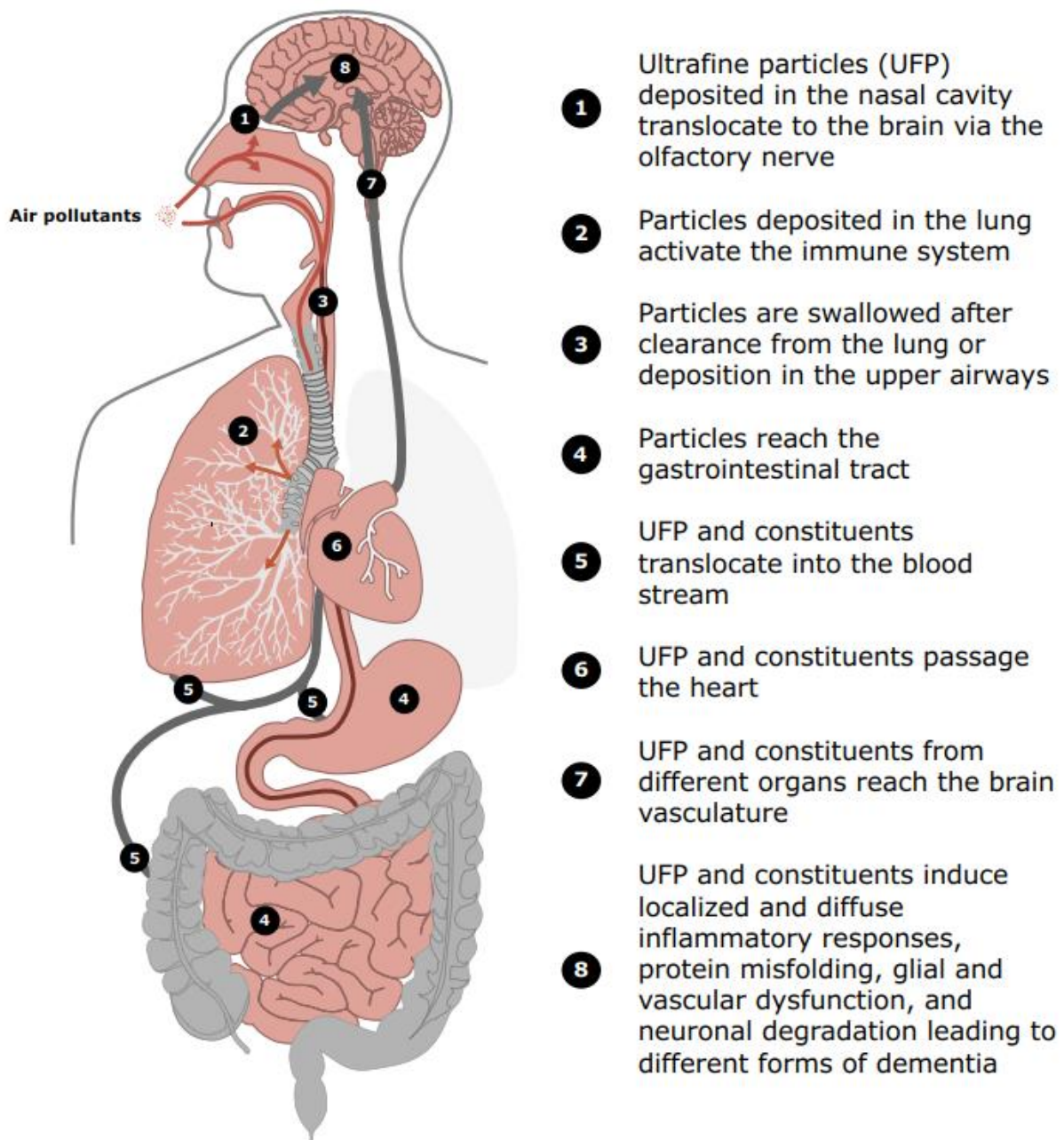


Figure 1. Overview about the circulation and impact of fine and ultrafine particles within the human body. Taken from Peters (2023).

The very small size of UFPs (≤ 100 nm) is responsible for a more diffusional driven behaviour in the respiratory tract in contrast to fine (< 2.5 μm) and coarse (2.5 – 10 μm) particles affected by gravitational sedimentation and inertial impaction (Kim and Jaques, 2000; Oberdörster et al., 2005). It is likely that they can enter the blood circulation by reaching the alveoli and penetrating the pulmonary epithelium (Oberdörster et al., 2002; Oberdörster et al., 2005; Lu et al., 2020). Stronger retention in the lungs due to hindered phagocytosis by alveolar macrophages is additionally increased in people with respiratory diseases like asthma and

chronic obstructive pulmonary disease (COPD), possibly exacerbating the symptomatology (Chalupa et al., 2004; Terzano et al., 2010; Kim et al., 2020; Chatkin et al., 2021).

Miller et al. (2017) was able to demonstrate in human-based studies that inhaled nanoparticles distribute organism-wide within minutes to hours and are still detectable after months of exposure. Translocation and accumulation of smaller sized particles was increased towards sites of vascular inflammation with the liver as the main burdened organ (Oberdörster et al., 2002; Miller et al., 2017). Miller et al. (2017) also stated that there are remaining open questions on how nanoparticles translocate and accumulate in the human body.

Studies indicate that UFPs have an influence on humans via different mechanisms compared to PM_{2.5}, and being able to create synergetic effects with transition metals (Costa and Dreher, 1997; Campen et al., 2001; WHO, 2013). The ability to damage mitochondria (Li et al., 2003; Oberdörster et al., 2005) and the central nervous system as a possible translocation site (Oberdörster et al., 2004) were also identified.

The harmful effects are based on their special characteristics like large surface areas, ability to oppose macrophage phagocytosis, high oxidant capacity and tendency to induce pulmonary inflammation (Chalupa et al., 2004). UFPs are supposed to initiate stronger proinflammatory effects compared to fine- and coarse-mode particles with increased oxidative stress (Donaldson et al., 2000; Donaldson et al., 2002; Li et al., 2003). The extent of inflammation is positively correlated with surface area (Donaldson et al., 2002; MacNee and Donaldson, 2003). UFPs with large surface areas can function as carriers for large amounts of airborne pollutants (Oberdörster, 2001) with more reactive groups at the surface able to catalyse chemical reactions as formation of reactive oxygen species (ROS) (Li et al., 2003; Delfino et al., 2005; Oberdörster et al., 2005; Nel et al., 2006; Leikauf et al., 2020).

As lung deposition rates are dependant of particle size and human activity, smaller particle sizes with greater diffusivity and higher minute ventilation during exercise lead to higher particle number deposition (Jaques and Kim, 2000; Kim and Jaques, 2000; Daigle et al., 2003). This could be especially relevant for the airport ground staff with physically demanding occupations and exposure to the highest concentrations of UFPs as acute systemic inflammation caused by airport-related UFPs was already declared (Habre et al., 2018). This could lead to the necessity of testing studies with personal nanoparticle samplers. Habre et al. (2018) states that health effects of airport-related UFP exposure are distinct to road traffic-related emissions while He et al. (2020) indicates no differences. Lammers et al. (2020) found an association between short-term exposure to high UFP concentrations and the health status of young healthy adults, however the effects were relatively small. In a large cohort study of workers at Copenhagen

airport no association between cardiovascular diseases and UFP exposure was found (Møller et al., 2020). Nevertheless Merzenich et al. (2021) concluded after performing a scoping review that scientific knowledge on health hazards regarding airport apron workers is still sparse which highlights the need for further toxicological studies with realistic test conditions. A cohort study in the Los Angeles airport area, investigating the development of malignant brain tumours, reported a 12% increased risk for each increase of UFP exposure by 6,700 particles cm^{-3} (Wu et al., 2021). In this context, a hazard ratio of 1.112 in developing a malignant brain tumour per UFP increase of 10,000 particles cm^{-3} , adjusted for other air pollutants and socio-demographic factors, was reported by a study from Toronto (Weichenthal et al., 2020).

Most of the health studies use inert surrogate particles made of materials like Teflon, titanium dioxide (TiO_2), gold, latex and carbon black to investigate possible health effects of an UFP exposure (Oberdörster, 2001; MacNee and Donaldson, 2003; Miller et al., 2017). Although the particle size properties used are similar to ambient UFPs, the chemical composition is still different. As jet engine oils have been identified in aviation-related UFPs (Yu et al., 2010; Timko et al., 2010; Yu et al., 2012; Fushimi et al., 2019; Yu et al., 2019), a more detailed assessment of their contribution to the UFPs chemical composition may be valuable to enable a better impact assessment of their health effects.

In vitro toxicity testing can be performed as a first approach to gain insight into possible toxicological effects of aviation-related particulate matter. As these tests require a certain amount of sampled particle mass, which is difficult to attain for UFPs, $\text{PM}_{2.5}$ samples can be used as surrogate. Due to the high filtration efficiency of glass fibre filters, the sampled fraction also includes the ultrafine fraction although their toxicological effects are likely masked by larger particles. Toxicity testing using various types of bioassays is a widespread technique for the risk assessment of a variety of contaminants in the environment (Völker et al., 2017; Schreiber et al., 2018). Assays based on bacterial bioluminescence are suitable for the assessment of pollutants as the luminescence is correlated with the bacterium's metabolic activity (Völker et al., 2017). The Microtox assay based on the bioluminescence of the bacterium *A. fischeri* gives insight about the baseline toxicity as it is non-specific regarding toxicological effects (Escher et al., 2014). This test was already utilised for the evaluation of atmospheric particulate matter (Turóczy et al., 2012; Roig et al., 2013; Aammi et al., 2017). Furthermore assays targeting a specific endpoint, like the inhibition of the acetylcholinesterase enzyme (AChE) can be carried out. For example organophosphorus compounds, as used in jet engine oils, can act as AChE inhibitors causing neurotoxic effects (Carletti et al., 2013; Chang et al., 2020).

1.3 Focus of this thesis

Large international airports were identified as sources of UFPs (Hu et al., 2009; Yu et al., 2012; Hsu et al., 2013; Keuken et al., 2015; Hudda and Fruin, 2016). The Hessian Agency for Nature Conservation, Environment and Geology started in September 2017 to monitor UFP emissions from Frankfurt International Airport. Wind coming from the airport direction during airport operating hours (05:00–23:00 CET) resulted in the measurement of higher UFP concentrations (Ditas et al., 2022). Most of the studies that are dealing with this topic undertake physical measurements providing information for example about the particles mass, size and number distribution. Accordingly, information on the chemical composition of these particles is rather scarce. Increasing knowledge of chemical composition can also improve the assessment of potential health hazards from exposure to aviation-related ultrafine particles.

Hence, UFPs emerging from the Frankfurt Airport were chemically characterized by using ultra-high performance liquid chromatography with high-resolution mass spectrometry and performing a comprehensive non-target screening. In total four studies are described in this thesis. The first conducted study (Ungeheuer et al., 2021) revealed that in aviation-related UFPs (smaller than 56 nm) detected organic compounds are dominated by jet engine lubrication oils. In the second study (Ungeheuer et al., 2022), the contribution of engine oils to the aviation-related UFPs was analysed. Therefore, the oils gas-to-particle partitioning behaviour was investigated to determine the nucleation ability of jet engine oil vapours to improve the understanding of the oils behaviour being released into the environment. Additionally, the fraction of jet engine oil was determined in UFPs collected near Frankfurt Airport. For this quantitative analysis the determination of sampling artefacts is necessary.

Insight into the chemical composition of aviation-related ultrafine particles was achieved in the first two studies by non-target screening and quantitative analysis. As air pollution is generally seen as a risk factor to human health (Yang et al., 2020; Samet et al., 2000), the aim of the third study (Wallraff et al., 2022) was to get a first impression of the toxicity of aviation-related aerosol. In this regard, the organic fraction of PM_{2.5} was analysed, as the mass of the collected UFP samples was not sufficient for toxicity testing. The toxicological outcome combined with a non-target screening allowed a first indication of certain compound classes being of toxicological relevance.

In the fourth study (Ma et al., 2022) non-target screening and hierarchical cluster analysis (HCA) was applied on ambient PM_{2.5} filters from Beijing. Haze episodes in Beijing and anthropogenic emissions as influencing factor were investigated by several studies (Bryant et

al., 2020; Wang et al., 2018). To reduce emissions, the identification of organic aerosol sources is essential and therefore the aerosols chemical composition and related transformation processes must be elucidated.

2. Aviation-related ultrafine particles

Airports have been identified as a major source of UFPs (Hu et al., 2009; Yu et al., 2012; Keuken et al., 2015; Stafoggia et al., 2016; Yu et al., 2017; Habre et al., 2018; Fushimi et al., 2019; Rivas et al., 2020). Emissions due to airport activities lead to a higher ambient particle number concentration in the surrounding of airports, with only limited information about the chemical composition of the particles available (Hudda et al., 2014; Hudda et al., 2018; Hudda et al., 2020). They can be transported further distances from the source (up to 18 km) reaching densely populated residential areas, as large airports are usually located in the close vicinity of metropolitan cities (Keuken et al., 2015; Hudda and Fruin, 2016; Zhang et al., 2020). Furthermore, transport and indoor infiltration of aviation-related UFPs seems to be more relevant than PM_{2.5} and PM₁₀ (Chen et al., 2020; Hudda et al., 2020). Different aircraft engine operation conditions are associated with varying amounts of particulate matter emissions, take-off is often designated as the status with the highest UFP emissions (Zhu et al., 2011; Hsu et al., 2012; Hsu et al., 2013; Keuken et al., 2015; Pirhadi et al., 2020). As these particles are typically formed during combustion and via gas-to-particle conversion (Pekkanen and Kulmala, 2004), road traffic is also a contributor to be taken into account. Due to a certain size dependency on the respective source, it is partially possible to differentiate between emission sources. The number of particles emitted by jet engines are dominated by particles with a diameter smaller than ~30 nm, which is significantly smaller compared to particles from road traffic emissions (Riley et al., 2016; Masiol et al., 2017; Shirmohammadi et al., 2017; Stacey, 2019; Pirhadi et al., 2020). This is in accordance with a study near Schiphol Airport (Netherlands), which concluded that the road traffic contribution to UFPs is less significant compared to aviation as a source based on the results from a site in 7 km distance to the airport (Keuken et al., 2015).

Due to the COVID-19 pandemic, the European flight traffic in 2020 declined by 55% and by 44% in 2021 compared to 2019 with actual forecasts predicting a full recovery of flight movements between mid-2023 and after 2027 depending on the pandemic course (Eurocontrol,

2021b, 2021a, 2022). The predicted emissions of the flight sector will still partially or fully influence local and global air pollution and global warming (Lee et al., 2009; Masiol and Harrison, 2014; Yu et al., 2017; Kärcher, 2018). Pre-pandemic forecasts indicated an increase of flights in Europe in the range of 1.9% per year with 16.2 million movements in 2040 (Eurocontrol, 2018).

Various studies examined the exhaust of aircrafts and found dependencies between particle emissions, their chemical composition, engine design and the engine operating state (Timko et al., 2010; Yu et al., 2010; Timko et al., 2013; Beyersdorf et al., 2014). It is often distinguished between the idle and the take-off status of aircrafts concerning particulate emissions. The idle state is mainly characterized by higher nucleation-mode particle number concentrations due to a stronger nucleation of organic and sulphate precursors and a lower soot surface area as condensation sink (Herndon et al., 2008; Timko et al., 2013). It is stated that at low thrust levels a dominant fraction of the emitted particulate matter components are volatile and tend to condense under formation of nucleation mode particles via mixing with ambient air (Wey et al., 2007; Yu et al., 2017; Stacey, 2019). The volatile organic fraction of the emitted particles increases through photochemical aging (Kılıç et al., 2018). In this regard transmission electron microscopy analysis of nucleation mode particles from aircraft exhaust showed their relatively volatile character (Mazaheri et al., 2013). The non-volatile fraction is dominated by black carbon, which absorbs visible light and is a component of soot resulting from incomplete combustion (Penner and Novakov, 1996; Petzold et al., 2013). The ratio of volatile organics/non-volatile organics varies mainly depending on the operating state and the used jet fuel (Timko et al., 2010; Timko et al., 2013; Beyersdorf et al., 2014; Keuken et al., 2015). It appears that black carbon is a minor fraction of airport-related particulate emissions (Keuken et al., 2015), whereby technological advances led to reduced emissions over time (Lee et al., 2010).

Jet engine oil constituents have been identified in aviation-related UFPs (Yu et al., 2010; Timko et al., 2010; Yu et al., 2012; Fushimi et al., 2019; Yu et al., 2019). This is a consequence of the jet engine design, where rotating parts of the turbines need to be lubricated and other parts like bearings to be cooled. Due to obstructed seals of the oil circulating system and a technically required venting system, nanometre-sized oil droplets are released into the atmosphere. Recovery of the oil used for lubrication is achieved through an oil-air separator, typically made of a casing including a rotating porous metal foam in a housing. The metal foam together with

the housing are often called 'breather'. This breather can be either located inside a bearing chamber (internal design) or externally receiving the flows from the bearing chambers (external design). Oil gets separated from air by centrifugation, whereby the oil droplets are thrown against the inner walls of the casing and are thereby recovered. Smaller oil droplets enter the porous foam where they either coalesce and are again transported to the casing walls or are released to the atmosphere (Eastwick et al., 2006). Oil droplets smaller than $\sim 0.5 \mu\text{m}$ can pass the breather and are vented to the atmosphere. The pressure drop within the breather setup is a limiting factor for the breather design. This can be especially critical at engine idling conditions with low sealing air pressure. The oil seals within the bearing chambers partially lose their tightness if a high pressure drop occurs leading to increased oil emissions. Whereby lower pressure drops lead to a reduced separation efficiency. The breather design considers certain aspects as temperature stability, physical dimensions, separation efficiency and in this regard the level of pressure drop. Reduction of oil emissions and an improved separation efficiency can be achieved by the use of better sealings. An enhanced air-oil separation efficiency is beneficial as it leads to less oil emissions and therefore to technical, maintenance and environmental benefits. In general, oil droplets below the breather cut-off size should be prevented from reaching the breather as they cannot be retained (Willenborg et al., 2008). In this context it should be kept in mind that with increasing thrust, the diameter of jet engine oil droplets increases (Yu et al., 2010).

The exposure of turbine and hydraulic oils to aircraft crews and ground-staff has been linked to health effects such as disorientation, headache, respiratory problems and weakness (van Netten and Leung, 2000; Winder and Balouet, 2001; Winder and Balouet, 2002). Besides AChE inhibition, one possible etiological factor is the inhibition of the neurotoxic esterase (NTE) by organophosphorus compounds, which are present as additives in aircraft lubrication oil (Freudenthal et al., 1993; Ehrich et al., 1993; Eyer, 1995; O'Callaghan, 2003). The symptoms mentioned are likely induced through an exposure with organophosphorus compounds, summarised under the expression organophosphorus-induced delayed neuropathy (OPIDN). The formation of potentially harmful chemicals during aircraft operations requires further elucidation, as Boer et al. (2015) states that bleed air in aircraft cabins contains tricresyl phosphate concentrations below effect thresholds and therefore cannot explain observed symptoms.

In order to assess further possible detrimental effects on human health, it is important to determine the chemical composition of UFPs near airports in order to identify their sources

during airport operations, and finally, to mitigate their emission. Due to the low mass of UFPs, the typical sampling and extraction methods need to be refined in order to characterize particles with aerodynamic diameters < 56 nm, requiring detection limits of low picogram levels of single organic molecules. Nevertheless, it is necessary to shed a light on the formation process of aviation-related UFPs. In this regard, the chemical characterization can provide an indication for further research. Performing a non-target screening gives an overview about the organic chemical composition and enables the possibility to identify distinct contributors to the UFPs chemical composition.

In the context of the study presented here, jet engine lubrication oils have been identified accounting for most of the detected signals. This led to lab-based thermodenuder experiments to see whether the high particle number concentrations emerging from airports can be attributed to the nucleation of hot jet engine oil vapours in aircraft exhaust plumes, rapidly cooling down by contact with ambient air.

3. Methods

3.1 Mass spectrometry (MS) – An overview

The invention of mass spectrometry goes back to 1898 when Willy Wien recognized that a beam of positively charged ions called canal rays, discovered by Eugen Goldstein in 1886, can be deflected in a magnetic field. The first mass spectrometer was built by Thomson in 1907, which enabled a first mass detection using electric and magnetic fields. Francis William Aston further improved the technique and was successful in discovering different isotopes with his setup accounted in 1919 (Squires, 1998). Until now more great improvements were achieved in mass spectrometry enabling significantly enhanced resolving power and sensitivity. Mass spectrometry is nowadays a widely used technique in the field of analytical chemistry with the principle aim to get as much information about a molecular compound based on its mass information. It is for example used in the field of protein identification (proteomics) to improve the understanding of the functioning and role of proteins, applied among other things for new drug discovery. More applications are the identification of pollutants in the ecosystem, to develop mitigation strategies and also to enlighten chemical transformations in water, soil and the atmosphere. Mass spectrometry in the field of atmospheric sciences is widely used to identify compounds present both in the gas phase and in the particle phase (Hoffmann et al., 2011; Laskin et al., 2018). In order to be able to analyse organic as well as inorganic analytes regarding their individual mass, they need to be ionised in the first step. Therefore, to be more precise, not the mass of a compound is detected rather the mass-to-charge ratio (m/z). Isotopic ratios are also taken into account. After the ionisation, the charged compounds or fragments (depending on the ionisation technique, as explained below) are first separated regarding their m/z and then qualitatively and quantitatively detected using an appropriate detector system. The separation of ions is achieved by varying electrical or magnetic fields or by the time needed to travel a defined trajectory in so called time-of-flight mass spectrometers (ToF-MS).

The basic build of a mass spectrometer always consists of an ion source, a mass analyser and detector. The recorded mass spectrum is a representation of the ions abundance shown as signal intensity against their individual m/z .

As mentioned, the ionisation of compounds allows them to be characterized in function of the mass-to-charge ratio (m/z). Apart from the fact that there are several ionization techniques, they

can basically be divided into two families: hard and soft. The main difference between them is the ability to fragment the compounds of interest or gently charge them, keeping the molecules intact or almost intact.

Electron-impact ionisation (EI) is one of the most commonly used ionisation techniques in connection to a prior gas chromatographic separation: within this technique, analytes get fragmented by impact of electrons with a certain energy, commonly 70 eV, which destroy the molecules by collision. As a result, EI ionisation produces a fragmentation pattern, which is unique for each analyte and can be useful to gain information about its molecular structure.

Soft ionisation techniques are typically represented by chemical ionisation in which the ionisation occurs non-destructive by charging the analytes using a reactant gas (Gross and Roepstorff, 2011). Electrospray ionisation, which is also referred as a soft ionisation technique, will be discussed more detailed separately, as it was the technique of choice used in this work. Besides the already mentioned time-of-flight (ToF) mass analyser the presumably most frequently used type of analyser is the quadrupole. The underlying principle is that mass separation is achieved by a changing electrical field, which directly influences the motion of the ionised analytes according to their m/z . Linear quadrupole systems are built of four cylindrical rods (Glish and Vachet, 2003). Another type of detector is the ion trap which is discussed later on as it is the basis of the Orbitrap system used in this work for the chemical characterization of atmospheric aerosol.

Decisive for the performance of a mass spectrometer is the mass resolution and accuracy. High resolutions are necessary to detect neighbouring ion signals with similar m/z . Resolution is defined as the smallest m/z value ($\Delta m/z$) which can still be resolved for a certain peak m/z ($R = \frac{m/z}{\Delta m/z}$). $\Delta m/z$ is specified as the full width at half of the peak maximum (FWHM). Mass accuracy is crucial for deriving the elemental composition of compounds based on mass information and therefore essential for non-target analysis. It is defined as the difference between the measured mass and the theoretical mass, normally specified in parts per million (ppm) (Bristow, 2006; Sparkman, 2011).

3.2 Ion trap mass analyser – Orbitrap

Quadrupole ion trap mass analysers use a three-dimensional electrical field set up between two hyperbolic- and one ring electrodes to trap ions on stable trajectories. The ions of interest can

thereby be formed inside or outside the ion trap. To measure the mass of the trapped ions, their trajectories need to be made unstable by adjusting the radio frequency voltage of the ring electrode, which results in a mass selective distraction (Glish and Vachet, 2003). Although the working principle is different to the basic principle mentioned before, the Orbitrap analyser is also considered as an ion trap. This type of mass analyser is based on the general approach of trapping ions in an orbital trajectory first introduced in 1923 by K. H. Kingdon (Kingdon, 1923). He was able to show that ions with sufficient tangential velocity circle around a charged wire in an electrostatic field. Later on R. D. Knight conducted an experiment in which laser produced ions were, orbitally trapped, excited and ejected (Knight, 1981). The driving force for the development of the Orbitrap analyser was to be able to reach a resolving power and mass accuracy similar to Fourier transform ion cyclotron resonance analysers (FT-ICR) without the high costs and space needed to operate a strong magnetic field (Gross and Roepstorff, 2011). The first commercially available linear trap quadrupole (LTQ) Orbitrap system was released in 2005 by Thermo Fisher Scientific including a linear ion trap mass spectrometer combined with an Orbitrap mass analyser (Makarov et al., 2006).

The Orbitrap analyser consists of three electrodes, a spindle-shaped central electrode and a surrounding two-piece outer electrode. Applying a voltage between the inner electrode and the outer electrode results in an electric field with strong axial and radial field forces. As a consequence, injected ions oscillate axial along the inner electrode, with the radial forces directing them on orbital trajectories towards the central electrode with balancing centrifugal forces. The axial oscillations induce an image current in the outer electrode, which can be converted into a mass spectrum by Fourier transformation, as the m/z can be determined using the frequency of the axial oscillation (Scigelova and Makarov, 2006; Zubarev and Makarov, 2013; Nolting et al., 2019) (Figure 2).

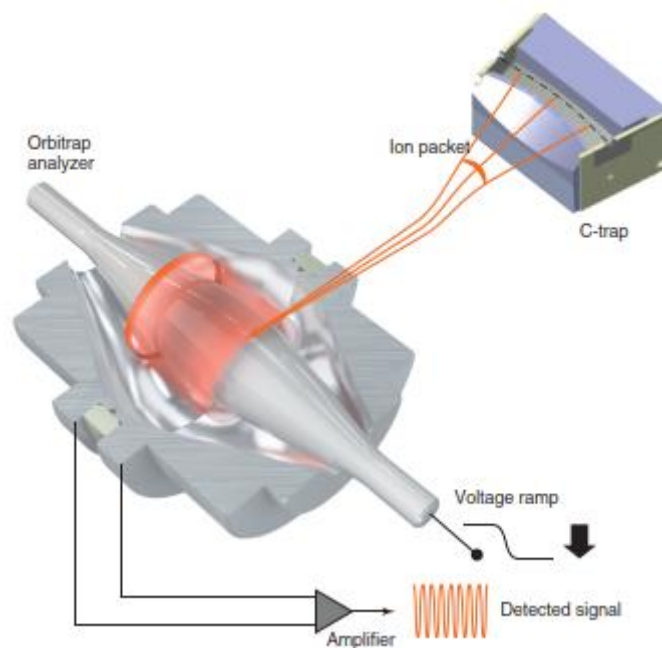


Figure 2. Schematic of the Orbitrap analyser and C-trap. Taken from Hecht et al. (2019).

To analyse complex mixtures it was necessary to connect the discontinuous Orbitrap analyser with continuously working ion sources like electrospray ionisation (Hardman and Makarov, 2003). Therefore, an ion storage device, which is used to accumulate ion packages with subsequent tangential injection into the electrical field offset to the centre, was implemented the so called C-trap.

Meanwhile Orbitrap systems were further improved regarding sensitivity and scan speed to fulfil the requirements for more complex applications. Enhanced ion source optics, ion trap mass analyser and a separate fragmentation cell were implemented. As the first available Orbitrap system contained only the option to carry out fragmentation experiments, using low energy ion trap-based collision induced dissociation (CID) with limitations towards structure elucidation, a new cell for higher energy collision-induced dissociation (HCD) was implemented (Figure 3). The HCD-cell contains a multipole arrangement, is filled with an inert gas and located next to the C-trap. Compounds of interest become accelerated towards the collision gas molecules by adjusting the electrode voltages, resulting in fragmentation through impaction (Olsen et al., 2007). This type of fragmentation provides a lower mass cut-off regarding the formed fragments compared to CID fragmentation. Also higher fragment numbers are usually obtained, which improves the structure identification of small molecules. The C-trap functions in that respect as a distributor of ions between the HCD-cell and the Orbitrap mass analyser (Eliuk and Makarov, 2015). In 2008 – with the release of the Exactive MS system – the ion trap setup of the LTQ Orbitrap was replaced by a multipole and in 2011

the Q Exactive series was launched employing a quadrupole mass filter incorporating faster cycle times and introducing multiplexed scan modes (Figure 3). The improved duty cycle is a consequence of the option of filling the C-trap or HCD cell during an ongoing Orbitrap scan (Michalski et al., 2011). Additional improvements to an Orbitrap Q Exactive Plus mass spectrometer enabled the detection of analytes up to 70,000 m/z (Fort et al., 2017). Further on, the Tribrid line of Orbitrap mass spectrometer integrated three types of mass analysers expanding the number of possible experiments. Current generation Orbitrap systems – like the used Q Exactive Focus Hybrid Quadrupole-Orbitrap (Figure 4) – reach mass accuracies with external- and internal calibration between 2-3 ppm and < 1 ppm (Hecht et al., 2019). Moreover, by reaching resolutions of above 1,000,000 at m/z 200 Orbitrap systems became an effective alternative to FT-ICR MS systems in the field of petroleomics (Schmidt et al., 2018).

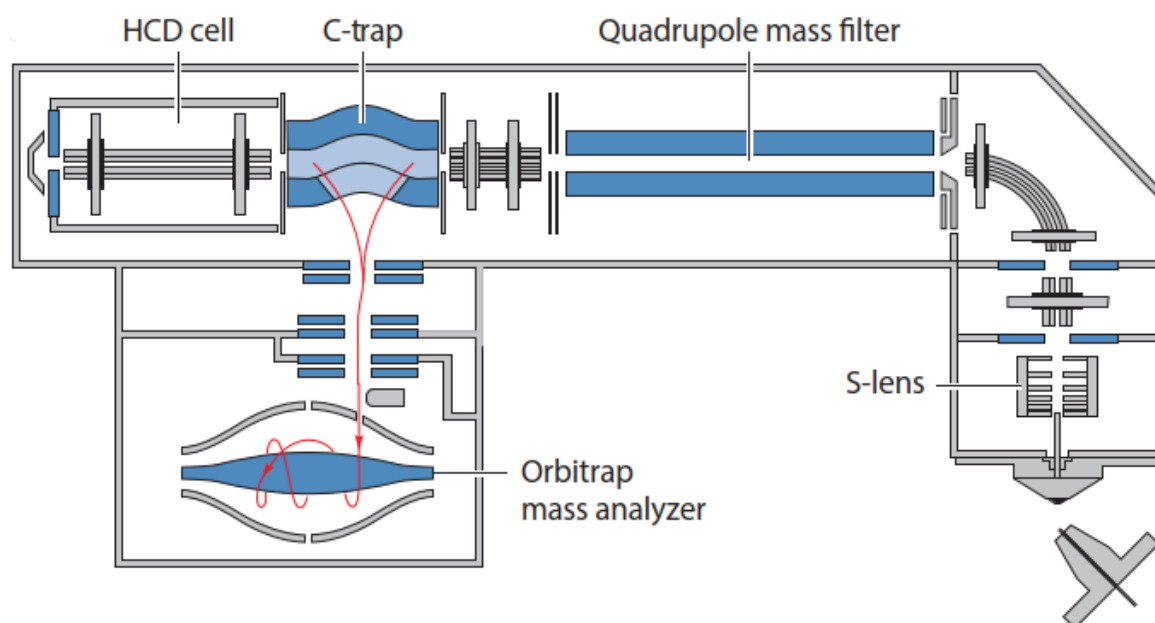


Figure 3. Schematic showing the setup of the Q Exactive mass spectrometer. Taken from Eliuk and Makarov (2015).

In order to perform non-target screening of complex environmental samples, the implementation of high-resolution accurate mass analysis (HR/AM) is essential to identify the elemental composition of unknown compounds using exact mass, isotopic and fragmentation pattern. Orbitrap mass spectrometer are utilised in atmospheric sciences to chemically characterize airborne particulate matter and shed a light on atmospheric transformation processes. The application is versatile, among other things they are used to analyse PM_{2.5} filter samples, atmospheric organic aerosol in real time and to reconstruct past organic aerosol

composition based on glacier ice cores (Wang et al., 2017; Zuth et al., 2018; Vogel et al., 2019; Wang et al., 2021).



Figure 4. The Vanquish Flex - Q Exactive Focus Hybrid Quadrupole Orbitrap System used.

3.3 Tandem mass spectrometry (MS/MS)

The term tandem mass spectrometry describes experiments with more than one stage of mass spectrometric analysis with a change of the compounds molecular structure taking place in between. In the first step, an analyte called precursor ion gets isolated and fragmented by increasing the compounds internal energy through collision with an inert gas, referred as collision-induced dissociation (CID) (McLuckey, 1992). Next, the produced product ions are analysed in another mass spectrometric scan describing a mass spectrometric experiment of second order (MS^2). Repetition of this sequence leads to experiments of higher MS orders (MS^n). Advantageous of these types of experiments is that by selecting precursor ions for analysis, the chemical noise due to high numbers of ions reaching the mass analyser is reduced noticeable in form of improved detection limits. Fragmentation experiments make it possible

to elucidate the molecular structure of compounds in complex samples by analysing the formed product ions (Nozière et al., 2015).

Two possible modes of operation are the precursor-ion- and the product-ion scan. The first experiment focuses on the detection of a specific product ion and therefore identifies all analytes which dissociate to form this type of fragment. The product-ion mode is aimed to identify selected analytes by detecting all the formed product ions. Furthermore, a neutral loss experiment offers the possibility to identify selected compounds by addressing a specific mass loss after fragmentation. Reaction monitoring is often used for quantification, as in this type of experiment both the analytes and product ions are specified, which enhances accuracy as the ratio of the formed product ions can be monitored. As trapping-based mass spectrometers normally use the same analyser for each MS-stage, they are referred as tandem-in-time instruments with the option to higher order MS/MS experiments, using one analyser (Glish, 1994). If different analysers are used for the different MS-stages, the instruments operate tandem-in-space. Using one analyser for several MS-stages increases the MS/MS efficiency as no ion transfer losses between the analysers occur and longer dissociation times are applicable. On the other hand precursor ion- and neutral loss scans are not possible (Glish and Vachet, 2003). The product-ion scan combined with a chromatographic separation and authentic standards provides the most clear identification of all techniques, making an unambiguous compound identification possible. In this context HR/AM measurements are also useful to elucidate the product ion identity (Kahnt et al., 2014). The other variants of tandem mass spectrometry are also used in some particular use cases in atmospheric aerosol characterization (Nozière et al., 2015).

Tandem mass spectrometry is a common technique to chemically characterize atmospheric particulate matter in order to gain structural information or to confirm the identity of detected compounds (Kitanovski et al., 2012; Zuth et al., 2018; Vogel et al., 2019; Brüggemann et al., 2019). In this work we used MS/MS experiments in the form of product-ion scanning in order to identify as many as possible analytes by database matching (database: <https://www.mzcloud.org/>).

3.4 Electrospray ionisation (ESI)

Yamashita and Fenn (1984) reported about the formation of ions if a solution passes a small capillary with a voltage applied. They established a new ionisation technique based on their findings. Single ions in the gas phase are generated in the ESI source by a potential difference between the mass spectrometer inlet and the small capillary at atmospheric pressure. The required voltage depends on the used solvent and size of the capillary tip (Glish and Vachet, 2003). Depending on the charging state of the inlet and the capillary, positively or negatively charged droplets containing both analyte and solvent molecules are formed exiting the capillary. Due to the potential difference a separation of the differently charged ions occurs. Ions which get attracted by the capillary are discharged (Ikonomou et al., 1991). In contrast ions directing towards the inlet enrich at the surface of the droplets, forming a cone named after Taylor (1964) with the surface tension as countering force. At some point the charge repulsion (Coulomb forces) within the droplets reaches a critical level (Raleigh limit) so that the surface tension is exceeded and smaller droplets are emitted (Coulomb explosion). This process is supported by the evaporation of the solvent either through a heated gas flow or a heated transfer capillary into the mass spectrometer or both (Gross and Roepstorff, 2011; Kromidas, 2017).

The final formation of the individual ionised species is still under debate. The charge residue model (CRM) assumes that the process of droplet size reduction repeats itself until only single charged molecules are left in the droplets. Ongoing solvent evaporation leads then to charged analytes in the gas phase (Felitsyn et al., 2002). Contrasting this, the ion evaporation model (IEM) says that the droplets size is reduced until single ions are sent out (Iribarne, 1976; Thomson and Iribarne, 1979). It is assumed that the formation of small ions follow the IEM model and that for bigger ions the CRM model is applicable (Kearle, 2000). The resulting analyte ions are then transferred into the high vacuum of the mass spectrometer.

With the development of ESI it became feasible to analyse thermally unstable, large and non-volatile compounds and to use solvent-based separation techniques like ultra-high performance liquid chromatography prior to mass spectrometric analysis. The development of ESI was especially beneficial for the analysis of large biological molecules, as they can be ionised unscathed ('soft ionisation') without any mass restrictions. Often high molecular weight compounds like proteins and oligonucleotides are charged multiple times leading to a reduction of their m/z to a level suitable for a wider range of mass spectrometers. Multiple charging is

only rarely seen for small molecules (Glish and Vachet, 2003; Gross and Roepstorff, 2011). Ionisation by ESI occurs through adduct formation by protonation, deprotonation or attaching for example sodium $[\text{Na}^+]$ or potassium $[\text{K}^+]$ ions. Molecular ions holding a negative charge ($[\text{M} - \text{H}]^-$) are formed by deprotonation in the negative-mode. Positively charged molecular ions ($[\text{M} + \text{H}]^+$, $[\text{M} + \text{Na}]^+$) are generated by adduct formation within the positive-mode. Suppression of the ionisation of certain analytes can occur as higher concentrated analytes can focus a large part of the charges on themselves.

In this work, we used ESI to ionise organic compounds as soft as possible to be able to determine the molecular composition based on their exact mass. Since the ionisation efficiency of compounds depends on their functionality, authentic standards are essential for a subsequent precise quantification.

3.5 Ultra-high performance liquid chromatography

(UHPLC)

Chromatography is an analytical method used to separate compounds in mixtures. It was first introduced by the botanist Michail Tswett in 1906 who achieved the separation of leaf dyes using an adsorbent packed column (Ettre and Sakodynskii, 1993). The basic principle of chromatography is that the various compounds in a mixture interact differently with the mobile- and stationary phase whereby they get separated. At first the sample solution is injected into a mobile liquid- or gas phase which moves along a stationary phase. Due to the different strength of interactions of the analytes with the surface of the stationary phase they elute at different times from the column. Consequently, the retention time is substance specific and can therefore be used for compound identification using authentic standards.

Furthermore, a method for the detection of the separated components needs to be applied. Often UV/Vis detectors are coupled with UHPLC systems. In this work a high-resolution Orbitrap mass spectrometer for the subsequent analysis was used. Recording of the detector signal over the elution time returns a chromatogram. The interaction of an analyte solved in the mobile phase with the stationary phase can be described through constantly re-establishing distribution equilibria. If the overall equilibrium, described by a partition coefficient, is more on the side of the mobile phase a substance is less retarded. Compounds that do not interact with the stationary

phase and get detected shortly after injection allow to identify the dead time, which is column specific. The separation efficiency can be described through the number of theoretical plates which depends on the column length and the theoretical plate height first introduced by Martin and Synge (1941). Lower heights of the theoretical plates are beneficial for the column efficiency. The peak width, respectively the time period a certain compound is eluting from the column, is defined by the Eddy- and longitudinal diffusion and the mass transfer between the two phases. As a consequence, columns smaller in diameter and packed with smaller particles as stationary phase became more and more utilised. The longitudinal diffusion can be reduced through increasing the flow rate which has in return a negative impact on the separation efficiency due to a reduced mass transfer. The extent of diffusion is also analyte specific with lower molecular masses advantageous for the separation.

UHPLC is widely utilised in the pharmaceutical, forensic and industrial field as well as for the analysis of foods regarding possible contaminants. The used setups generally utilise reservoirs for solvents of different polarity, an injector and pump system and a UHPLC column for the actual separation of the analytes. Two methods of operation are distinguished, isocratic elution just uses one constant ratio of the solvent volumes for compound separation whereas a better efficiency often can be reached by varying the ratio during the chromatography, named gradient elution. By changing the polarity of the solvent mixture over time a better separation within shorter time periods is achieved. The pump systems are subject to special requirements as they need to resist chemical decay, generate high pressures and to guarantee constant flows with high reproducibility.

In this work, a Vanquish Flex system of Thermo Fisher Scientific was used utilising a binary pump setup. This system can generate pressures up to 1000 bar mixing two solvents for a high-pressure gradient (Thermo Fisher Scientific, 2021).

In liquid chromatography two different mode of operation are used. Normal phase chromatography is a working method utilising a polar stationary phase and a non-polar solvent as mobile phase; one application of this method is the separation of steroids and sugars. If the stationary phase consists of an immobilised polar liquid bound to a solid phase like silica gel, gradient elution cannot be used. More often reversed-phase chromatography is used for compound separation utilising a non-polar stationary phase and a polar mobile phase. Within this type of column the effective separation phase is covalently bound to a solid phase, normally particulate silica gel. This general type of stationary phase is used for normal phase as well as for reversed phase chromatography. In this work the Accucore C₁₈ (Thermo Fisher Scientific)

reversed-phase column was used. The C₁₈-groups protrude vertically from the bound particle surfaces interacting with the analytes through adsorption. The retention efficiency and applicable analyte concentration generally increases with the length of the bounded alkyl chains (Otto, 2006). The chromatographic separation of polar compounds can be achieved using normal-phase columns, whereby in combination with ESI reduced ionisation efficiencies are obtained due to the use of non-polar pure organic solvents. Furthermore, the solubility of polar organic analytes in the mobile phase can be limited. To encounter these problems a new type of chromatography was introduced based on hydrophilic interactions. Hydrophilic interaction chromatography (HILIC) utilises a polar stationary phase in combination with a water- polar organic solvent mixture as mobile phase (Nguyen and Schug, 2008). These type of columns are also used in atmospheric sciences for the characterization of polar organic compounds like organosulphates (Spolnik et al., 2018).

3.6 Non-target analysis

The screening for target compounds in environmental samples presuppose that compounds have already been identified with regard to environmental relevance or human health. This type of analysis requires the availability of reference standards, measured with the same analysis settings in parallel (Schymanski et al., 2015). In contrast, in a non-target analysis, the three-dimensional space of retention time, m/z , and intensity is searched for peak signals without preselecting target compounds (Figure 5). Target- and non-target analysis can be combined to get a more comprehensive overview about the chemical composition. The extraction and ionization method used influences the chemical composition of the sample extracts and thus also the substances that can be identified. Non-target analysis, a software-based approach, required the further development of high-resolution mass spectrometry and the coupling with gas or liquid chromatography to precisely measure the exact mass of structural intact compounds after ionization. Following the mass spectrometric detection of compounds, an algorithm is applied to the measurement data in order to identify formed adducts and, in this context, identify compounds based on their exact mass. This approach enables the detection of unexpected compounds and also the retrospective search for compounds of concern in already measured samples.

The identification of substances within the targeted screening approach is based on the analysis of single peaks using extracted ion chromatograms. In contrast, the non-target screening

approach holistically identifies chromatographic peaks based on exact mass, isotopic pattern and MS² fragmentation pattern. The identification process can be further improved by including database matching of recorded fragmentation spectra. Finally, the software uses these characteristics to determine molecular formulae of the detected compounds. If an exact mass deviation can be assigned to adducts, clusters, fragments or isotopic differences, simultaneously eluting peak signals are combined to one compound. At the end of a non-target analysis, the identification of the substances is often supported by measuring the respective standards, if available. In this regard, the software identification of low intensity signals can be improved by analysing reference standards and the samples data within one non-target project. With this approach compounds can be discovered that will then be the subject of targeted measurements in future analyses (Schymanski et al., 2015).

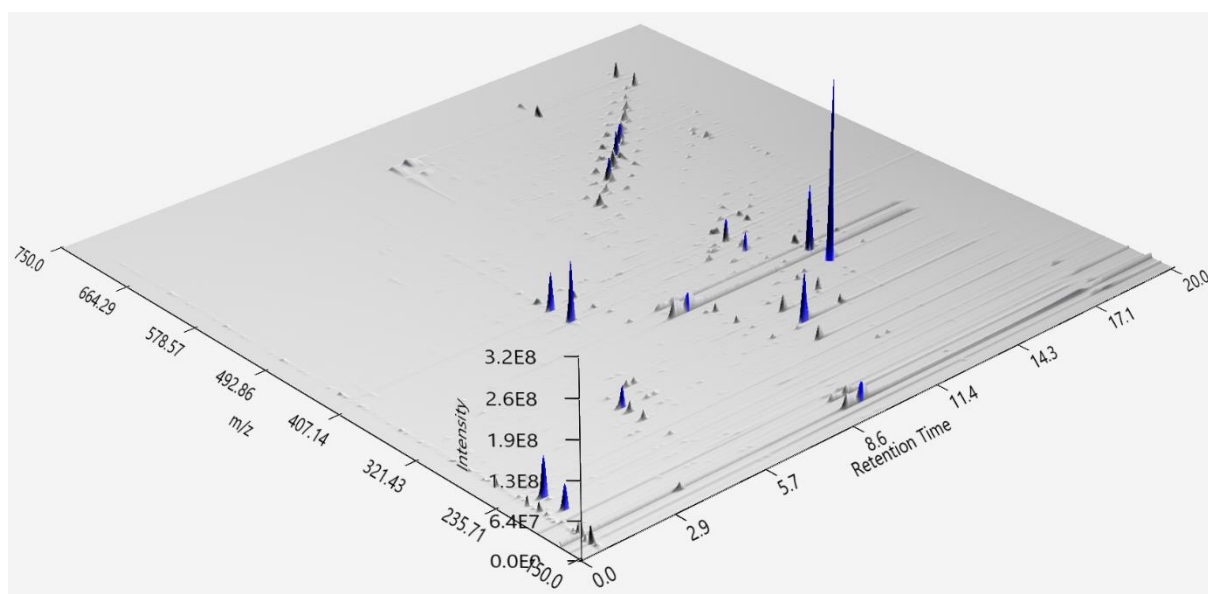


Figure 5. Three-dimensional space of retention time, m/z and intensity of a Frankfurt Airport UFP sample (32-56 nm; by MZmine2).

3.7 Quantitative analysis

The concentration of compounds in solvent extracts of ambient filters can be determined by external calibration using authentic or surrogate standards. Based on a series of different compound dilutions, the known concentrations are fitted with the corresponding signal intensity responses. The resulting correlation makes it possible to quantify compounds based on their measured peak signal intensity. Generally test measurements of the samples and dilutions of the reference standards are conducted to assess the calibration range covering the concentrations

present in the samples. Several different standard concentrations are then analysed, with each calibration point being measured multiple times. The resulting calibration curve needs to be assessed regarding their linear response range between concentration and signal intensity. In case the calibration does not show full linearity, the concentration range needs to be adjusted. Matrix effects, for example due to adsorption on suspended particulate material or on glass surfaces, are not taken into account with this quantification method. To overcome this limitation, the standard addition method can be used for quantification. In this case, the substances to be quantified are added directly to the sample extracts. Therefore, different dilutions of the authentic standards have to be prepared and added gradually. This spiking process leads to an increase in the concentration of the compounds and thus the signal intensity. The measurement of the extracts with differently increased concentrations results in the representation of a calibration curve. It should be noted that linearity exists over the entire concentration range. Based on this, the concentration of the target compounds in the native sample can be determined by extrapolating the compounds response to zero (Ellison and Thompson, 2008).

For the assessment of an analysis method, the limit of detection (LOD) and the limit of quantification (LOQ) can be determined. The first metric describes the lowest concentration of a compound that can be detected qualitatively with a certain degree of confidence. The LOQ is defined as the lowest analyte concentration which can be quantified with a certain degree of confidence. These metrics are described by the standard DIN 32645 of the German Institute for Standardization (DIN).

3.8 Particle-number size distribution

Particle number size distributions are widely used for the characterization of airborne aerosol like aviation-related UFPs (Hudda and Fruin, 2016; Pirhadi et al., 2020). By representing the total particle number in a specific volume and the associated particle sizes, this type of distributions can help to identify the source of particle emissions and their spread. Biomass- and wood burning and other combustion processes, as in automobiles or for power generation, generally lead to the formation of particles in the size range of a few nanometres up to one micrometre. Secondary formed aerosol by photochemistry in the atmosphere is predominantly smaller than one micrometre in diameter, whereas primary aerosol like dust, sea salt, plant material and pollens are normally larger than one micrometre. The particles lifetime in the

atmosphere is influenced by their size (Seinfeld and Pandis, 2016). Larger sized particles in the coarse mode range ($< 10 \mu\text{m}$) are emitted, for example, from road traffic due to abrasion of brake pads and tires (Fujitani et al., 2021).

Ultrafine particles ($< 0.1 \mu\text{m}$) are of very low mass compared to larger sized particles, and can be found in high numbers in the urban environment (Kumar et al., 2014) (Figure 6).

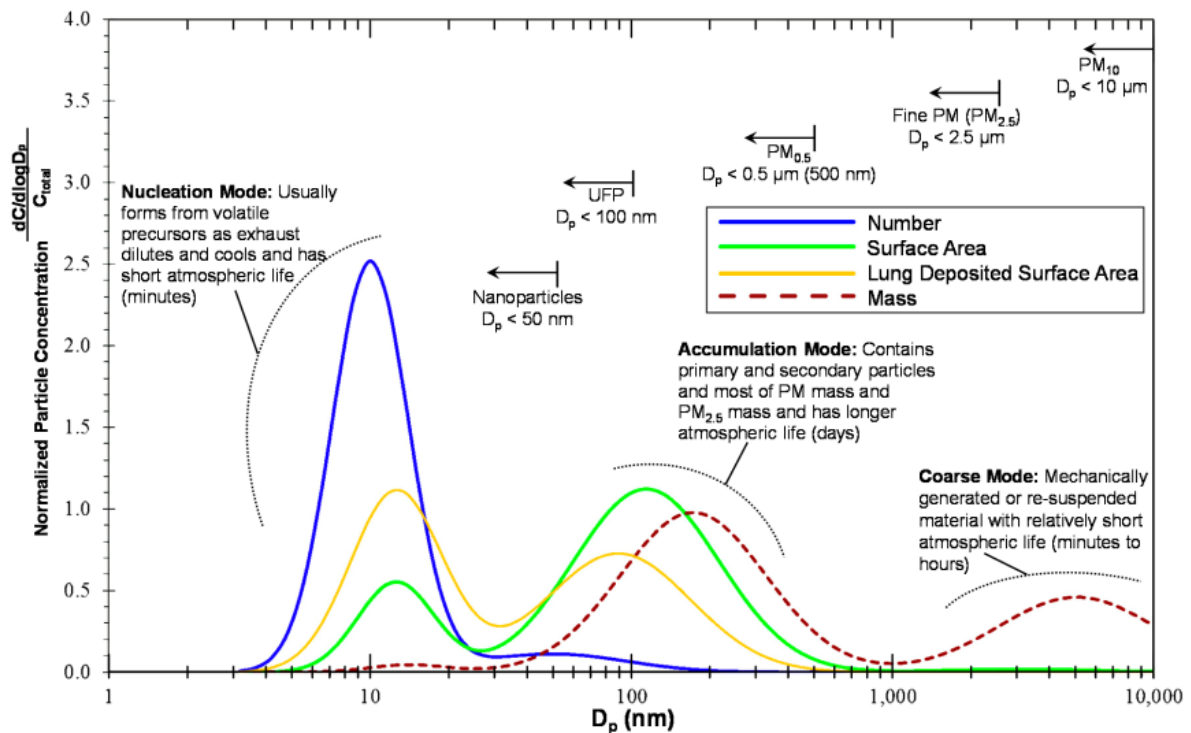


Figure 6. Particle size distribution including the ultrafine-, fine and coarse mode particles size range. The particles number, surface area, lung deposited surface area, and mass are shown. Taken from Baldauf et al. (2016).

Accordingly, UFP emissions emerging from the Frankfurt Airport were characterized regarding their specific number size distribution (Ditas et al., 2022). Commercially available condensation particle counters (CPC) can reach a lower limit of detection of $\sim 3 \text{ nm}$ (Hermann et al., 2007; Mordas et al., 2008). Therefore, particles need to be enlarged by condensing a solvent like butanol or water onto their surface. After growing to nearly the same size (magnitude of a few micrometres) they can be detected optically. The lowest instruments cut-off diameter, which describes the diameter at which 50% of the particles are counted, is $\sim 1 \text{ nm}$ reached by another type of instrument (Particle size magnifier; PSM) (Vanhanen et al., 2011; Kulkarni, 2011). As CPCs can only measure particle numbers, an instrument for size selection must be used beforehand to determine particle-number size distributions. Scanning mobility particle sizers (SMPS) as employed in this work combine CPC particle counting with a size selection based on the principle of differential mobility analysers (DMA). DMAs classify

aerosol particles depending on their electrical mobility, which describes the particles migration velocity in a defined electrical field. This parameter depends on the particle size, morphology and number of elementary charges. After applying a defined charge distribution onto the particles of the aerosol sample they are injected and directed along the cylindrical construct by a gas flow. The applied electrical field between the outer and inner electrodes drags the particles perpendicular to the flow direction towards the inner electrode. Only particles with a specific electrical mobility can reach the outlet port. The remaining particles either impact earlier on the inner electrode or more downstream not reaching the exit port. SMPS instruments can measure particle-number size distributions by continuously changing the voltage and therefore the electrical field. Thereby varying particle sizes are detected successively (Wang and Flagan, 1990; Kulkarni, 2011).

3.9 Sampling of atmospheric particulate matter

Besides the direct chemical analysis of atmospheric particulate matter using online instrumentation, offline sampling with subsequent analysis is widely used. In this field inertial classifiers and especially impactor systems are most common. One example for an impaction based sampler is the Micro Orifice Uniform Deposition Impactor (Nano-MOUDI) (Marple et al., 1991), used in this work. Size-dependant (aerodynamic diameter) separation of particles is achieved by taking advantage of the different particles inertia. Only particles with a sufficiently low inertia can follow the air stream and bigger sized particles impact on a substrate for subsequent analysis. Whether a particle is collected or follows the air stream depends on the air velocity, the size of the impaction plate and the particle size. This dependency is explained by the Stokes number setting the dimension of the impaction plate in relation to the distance a particle would need to stop. Impactors, a type of inertial classifiers, are used for particle separation at which defined cut-sizes determine whether a larger particle impacts on a plate or a smaller particle follows the air stream. For the subsequent analysis of the deposited particles, impaction plates are covered with a removable substrate like aluminium foils. The efficiency of this size-dependant separation process can be described through collection efficiency curves taking into account the fraction of particles impacted. Often a cascade of impactors is used in series to separate various particle size fractions gaining information about the size distribution. Cascade impactors make use of a stagewise increasing air velocity to collect smaller particles

in succession. This size collection range can be extended to very small sizes by applying lower pressures within the stages or by utilising nozzles with lower diameters.

The used Nano-MOUDI sampler makes use of these modifications being therefore classified as a micro-orifice impactor. This type of cascade impactor works under the principle of inertial impaction (Marple et al., 1991) and consists of 13 stages with the last three stages used for sampling. Stagewise the diameter of the nozzles decreases with simultaneous increasing number of nozzles to reach sufficient flow rates. In comparison low pressure cascade impactors use much lower pressures however the utilised nozzles are similar as in standard impactors.

Difficulties in collecting particles using impactors are filter overloading, interstage losses and bounce off. Particle bounce from higher to lower stages can be prevented by coating the impaction substrate, applying a sticky substance selected based on the chemical composition, mass stability and particle analysis technique. Particle overload of the sampling substrate can be attenuated through rotation of the impaction plates. Diffusional losses are relevant for very small particles like the analysed UFPs, due to a low sampling pressure. Sampling losses depend on the characteristics of the collected particles. Solid particles undergo stronger bounce off, lower interstage losses and tend to stronger filter overloading than more adhesive particles. For particles < 100 nm wall losses are most relevant (Weiden et al., 2009).

Another way of attaining a representative sample of atmospheric particulate matter is using a filtration technique enabling the sampling of higher air volumes instead of an impaction based deposition method (Turpin et al., 2000). Within this approach a filter is used to remove particles suspended in air and deposit them on a surface to gain a transportable and storable sample for subsequent analysis. Often an impactor is used upstream to a filter to separate a certain particle size fraction before collection. This approach is also utilised in high-volume samplers as used in this work for PM_{2.5} collection. The efficiency of transport of particles from the inlet to the filter can be affected by electrostatic wall-loss effects, temperature differences and inertial-, gravitational- and diffusional wall deposition. Fibrous filters like glass fibre filters used by default for high-volume air sampling are characterized by their particle filtration efficiency larger than 99% due to their high specific surface area making also gas phase adsorption possible (Turpin et al., 2000). Due to the high filtration efficiency the sampling of PM_{2.5} also leads to the collection of UFPs. Particles get retained after impaction or diffusion onto the fibres. Furthermore, this type of filter is relatively inert, temperature stable and pressure drops are less relevant (Kulkarni, 2011).

Shortcomings of particle sampling are compound volatilisation (blow off) and adsorption of gas phase constituents (blow on) (Jacobson et al., 2000). In this regard, a pressure drop can lead to volatilisation of particle-bound compounds (Turpin et al., 2000). Rebound from the collection surface called thermal rebound (Givehchi and Tan, 2014) of nanoparticles down to 3 nm is not of relevance (Kim et al., 2006). Sampling artefacts due to chemical transformation of deposited compounds can occur regardless of the sampling method.

4. The Projects

4.1 Identification and source attribution of organic compounds in ultrafine particles near Frankfurt International Airport

This chapter describes the content of the first paper of this study (Ungeheuer et al., 2021), which focuses on the chemical characterization of aviation-related ultrafine particles using non-target screening. To further improve the subsequent identification of compounds, fragmentation and thermal decomposition experiments as well as a source attribution analysis were performed.

In September 2017 the Hessian Agency for Nature Conservation, Environment and Geology started to monitor UFP emissions originating from the Frankfurt International Airport as various studies identified large international airports as sources of UFPs (Hu et al., 2009; Yu et al., 2012; Hsu et al., 2013; Keuken et al., 2015; Hudda and Fruin, 2016). Based on particle size distribution measurements it could be shown that during the operating hours of the Frankfurt Airport (05:00–23:00 CET) higher UFP concentrations are measured when the wind was coming from the airport direction (Ditas et al., 2022). Based on that, the chemical characterization of UFPs emerging from the Frankfurt Airport was intended by performing a comprehensive non-target screening of UFP filter samples.

Frankfurt Airport, one of the largest airports in Europe, is located in the Rhine-Main metropolitan area in around 12 km distance to the city centre of Frankfurt. In 2019 the year of the sampling campaign 2.1 million tons of cargo and more than 70.5 million passengers have been transported by more than 500,000 flight operations shared over four runways (Fraport AG, 2020). In 2020 the European flight traffic declined by 55% and by 44% in 2021 compared to 2019, due to the COVID-19 pandemic. Full recovery of flight movements is expected between mid-2023 and after 2027, depending on the course of the Covid-19 pandemic (Eurocontrol, 2021b, 2021a, 2022). The correlation between flight movements and UFP emissions at Frankfurt Airport, which certainly applies for large international airports in general, implies that the recovery of the aviation sector will also lead to higher UFP emissions (Rose et al., 2020; Ditas et al., 2022).

Ambient filter sampling

UFP filter sampling took place from August to October 2019 at the time of the highest traffic volume at Frankfurt Airport to date. The air quality monitoring station, operated by the Hessian Agency for Nature Conservation, Environment and Geology, used as sampling site is located 4 km north of Frankfurt Airport in the city forest (Frankfurt Schwanheim; F-Schwanheim) (Figure 7). Highly frequented streets are not located within a distance of 1 km. Due to the size of the airport and the proximity to the airport, samples taken at this station are considered to generally represent emissions of large international airports. In order to characterize the airport outflow, sampling only took place during the operating hours (5:00 – 23:00 CET) and southerly wind direction. Due to the low mass of UFPs the sampling times varied between 18 to 54 hours. Particle size distribution measurements in F-Schwanheim show a strong deviation between airport-influenced- and background measurements regarding number concentration and distribution shape. Furthermore, these measurements point out the exceptional high number concentrations detected at the monitoring site in October 2019 (Ditas et al., 2022).

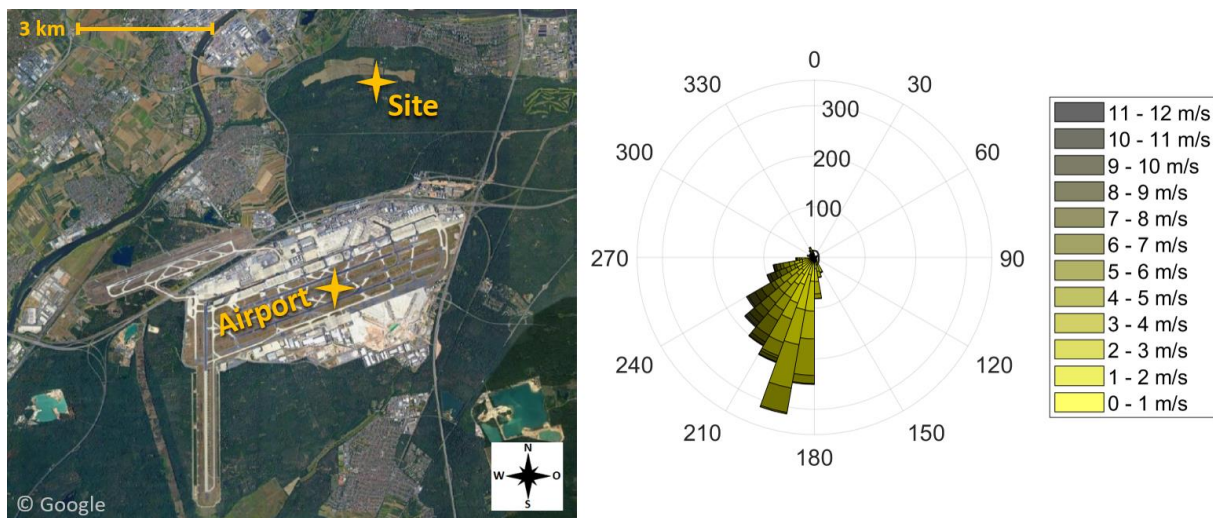


Figure 7: Map showing the sampling site 4 km north of Frankfurt Airport. The southerly wind direction during the eight sampling periods is depicted by the wind rose. Taken from Ungeheuer et al. (2021).

For the sampling of UFPs a Micro Orifice Uniform Deposition Impactor was used (Nano-MOUDI, Model 115, MSP, Minneapolis, MN, USA) utilising 13 impactor stages for size segregation and being able to collect particles < 100 nm on the last four stages. Particle size distribution measurements in F-Schwanheim show that aviation-related particulate emissions mainly contribute to the < 30 nm size fraction (Ditas et al., 2022). Hence, we only sampled on the last three stages covering aerodynamic diameters between 0.010 - 0.018 μm , 0.018 - 0.032 μm and 0.032 - 0.056 μm . The 13 impaction plates of the Nano-MOUDI were covered with

aluminium foils to sample particles by impaction. The foils of the upper ten stages were coated with grease to prevent larger particles reaching the lower stages by bounce-off (Figure 8). The filters were stored in metal boxes at $-20\text{ }^{\circ}\text{C}$ to avoid transformation and evaporation of compounds altering the outcome of the non-target screening. Field blanks in the same size range $< 56\text{ nm}$ were collected for 115 hours without actively sampling.

The collected UFP samples cover the average UFP emissions emerging from Frankfurt Airport with contributions of different types of aircraft engines, fuels, jet engine oils and operating conditions. Besides the meteorological conditions and the sampling time the actual thrust of aircraft engines affects their particle emissions (Timko et al., 2014; Lobo et al., 2015; Yu et al., 2017).

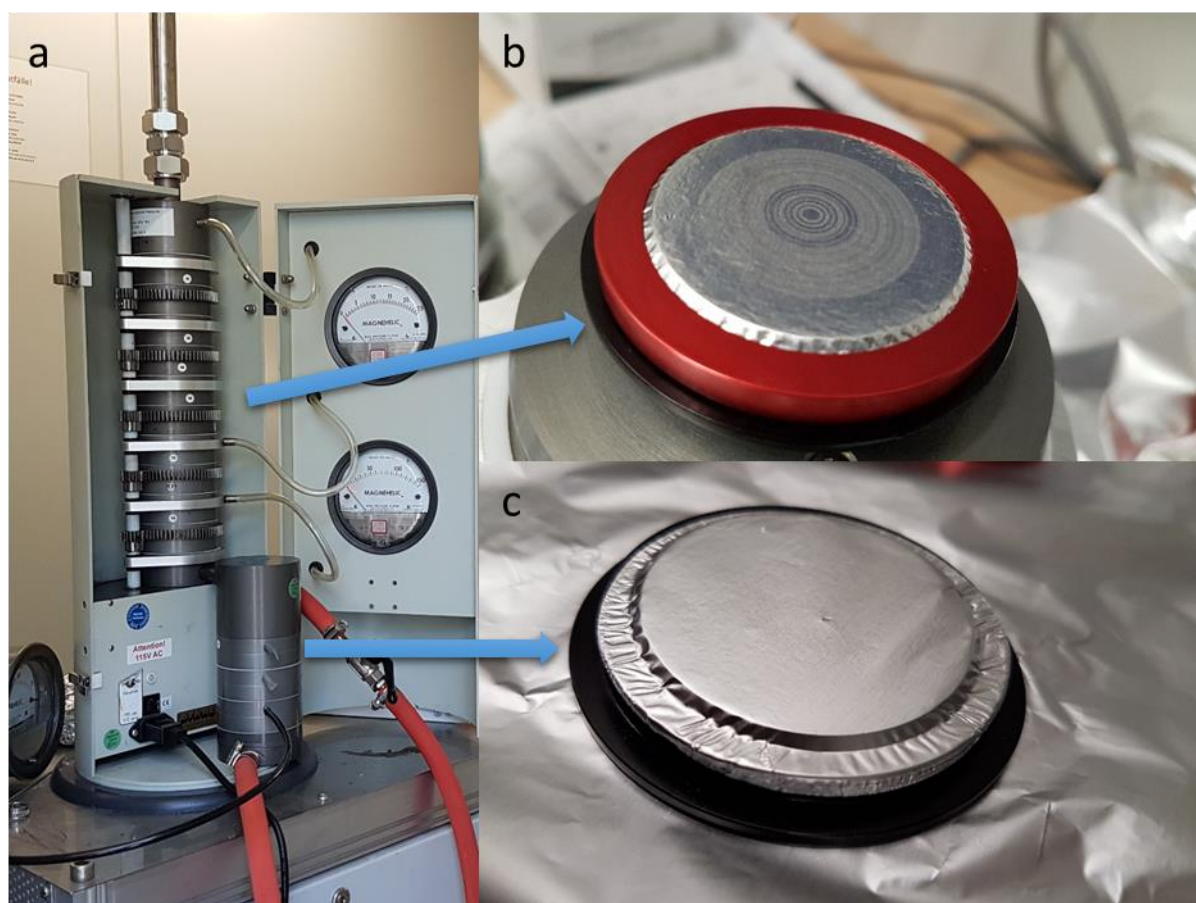


Figure 8. The Nano-MOUDI sampler used for the collection of ambient aviation-related ultrafine particles (a). Aluminium foils after Nano-MOUDI sampling on the ten upper stages (b) and on the three lower stages (c; 32-56 nm).

Jet engine lubrication oils

In order to identify jet engine oil constituents in UFPs five different jet oils of different brands, selected according to the recommendations for various engine types, were analysed. These oils are mainly used for cooling and the reduction of friction within turbines. They are mainly composed of a synthetic ester base stock like pentaerythritol esters or trimethylolpropane esters and different additives. Amine additives are used as stabilizers (Wu et al., 2013) whereas organophosphate constituents serve as anti-wear agents and metal deactivators (Wyman et al., 1987; Du Han and Masuko, 1998) (Figure 9).

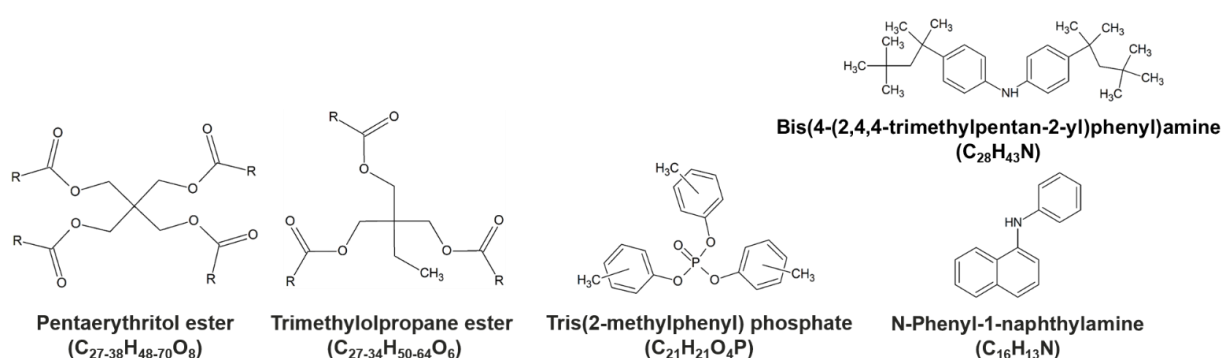


Figure 9. Most prominent jet engine lubrication oil constituents. Taken from Ungeheuer et al. (2022).

The analysed oils were: Mobil Jet Oil II (ExxonMobil, Irving, TX, USA), Mobil Jet Oil 254 (Exxon-Mobil, Irving, TX, USA), Aeroshell 500 (Royal Dutch Shell, The Hague, Netherlands), Turbo Oil 2197 and 2380 (Eastman, TN, USA) (Figure 10). The Mobil Jet Oil II has the highest market share (Winder and Balouet, 2002), the market share of the other oils is unknown.



Figure 10. The analysed jet engine oils (Mobil Jet Oil II, Mobil Jet Oil 254, AeroShell 500, Eastman Turbo Oil 2197 and Eastman Turbo Oil 2380).

Filter extraction procedure

Although UFPs are characterized by high particle number concentrations, their low mass makes it necessary to develop a filter extraction method reaching highest possible extract concentrations. Particle size distribution measurements indicated that the sampled particle mass is at most in the low microgram range. Because concentrating extracts through solvent evaporation can lead to volatilization of compounds, high extract concentrations have been sought by reducing the amount of solvent used for extraction. Furthermore, no extract filtration was conducted accounting for the adsorptive behaviour of the jet engine oil constituents. Pure methanol was used for the filter extraction as testing different mixtures of solvents (50% acetonitrile, 50% methanol; 60% methanol, 40% water; 60% acetonitrile, 40% water) showed lower extraction efficiencies based on detected signal intensities and number of non-target screening identifications.

After sampling no deposited particulate matter was visible onto the filter surface, hence the area below the nozzle array of each impactor stage was chosen for extraction. The cut out filter material with a diameter of 2.5 cm was cut in small pieces (~ 2.5 mm x 2.5 mm) using ceramic scissors. Extraction was carried out within 2 x 20 min on an orbital shaker (300 rpm) after adding 100 μ L and 50 μ L pure methanol (OptimaTM LC/MS grade, Fisher scientific),

respectively. Ultrasonic extraction was discarded due to a possible chemical transformation of the sample composition owing to the formation of free radicals (Riesz et al., 1985). Two UFP samples were extracted a third time solely using 50 μL of methanol to identify a possible extraction loss caused by the adsorptive behaviour of the jet engine oil constituents. To ensure that the entire filter surface gets in contact with the solvent, glass vials equipped with flat-bottom micro inserts with a maximal volume of 200 μL (LLG Labware; \O x H: 6 x 31 mm) were used for extraction. Both solvent extracts were combined and then aliquoted into three glass vials including 100 μL micro inserts with conical bottoms (VWR, \O xH: 6x31 mm) ensuring a sufficient solvent level for the UHPLC injection of 5 μL . One vial was used for the analysis of the native sample. Using the standard addition method authentic standards were added to the other two vials for quantification of the jet oil constituents. The sample extracts were measured directly after extraction. In total 48 filter samples were collected including 9 field blanks. In the end 22 filter samples and 3 field blanks were analysed. The other filters were used for method development and testing further analytical methods to analyse metals and organic-, inorganic carbon.

Chromatographic separation and mass spectrometric analysis

The mass spectrometric analysis of the ambient UFP filter samples was realised using an Orbitrap high-resolution mass spectrometer (Q Exactive Focus Hybrid Quadrupole-Orbitrap, Thermo Fisher Scientific). Chromatographic separation of the chemical composition was achieved by ultra-high-performance liquid chromatography (UHPLC) (Vanquish Flex, Thermo Fisher Scientific). Heated electrospray ionisation (HESI) was utilized for compound ionisation, forming negatively and positively charged molecular ions. To separate the organic composition based on polarity a reversed-phase column (Accucore C18, 150 x 2.1 mm, 2.6 μm particle size, Thermo Fisher Scientific), thermostated at 40 $^{\circ}\text{C}$ (still air) was used. An improved chromatographic separation was achieved by applying a solvent gradient using ultrapure water (18.2 M Ωcm ; Millipak[®] Express 40: 0.22 μm , Millipore; Milli-Q[®] Reference AC, Merck) (solvent A) and methanol (Optima[®] LC/MS grade, Thermo Fisher Scientific) (solvent B) as the UHPLC solvents. The flow rate of the mobile phase was 400 $\mu\text{L min}^{-1}$. Both solvents were acidified using formic acid (0.1% by volume; LiChropur[®], Merck; purity: 98 – 100%) to enhance the chromatographic separation and ionisation efficiency in the positive mode. Based on test measurements revealing the non-polar character of most of the detected compounds, the chromatographic separation started with 60% solvent B (0–0.5 min). This high organic fraction

of the mobile phase allowed to inject large volumes of pure organic solvent based sample extracts without impairment of the chromatographic separation. The gradient was then raised to 90% solvent B (0.5–11 min), followed by a final increase to 99% (11–16 min). The slowed rise of the gradient between 90 – 99% solvent B was implemented to better separate the single synthetic esters of the jet oil base stocks. After reducing solvent B to 60% (16–17 min), the system equilibrated the starting conditions within 3 min. The total runtime of the method was 20 min, the sample injection volume 5 μL .

Different settings regarding the ESI source were adjusted to optimise the ionisation process like the spray voltage, transfer capillary temperature, auxiliary gas flow and temperature. After testing, both the positive and negative mode run the same settings (3.5 kV spray voltage, 40 psi sheath gas (nitrogen), 8 psi auxiliary gas (nitrogen), 350 °C gas temperature) but due to a lower number of compounds in the negative mode the spray voltage was reduced from 3.5 kV to 2.5 kV. The MS-system was calibrated reaching a mass accuracy < 2 ppm using Pierce™ (Negative Ion Calibration Solution, LTQ Velos ESI Positive Ion Calibration Solution, Thermo Fisher Scientific) calibration solutions. Within the mass spectrometric analysis, a resolution of ~70 k at mass-to-charge ratio (m/z) 200 was reached, scanning in the positive mode between 150 – 750 m/z and in the negative mode between 50 – 700 m/z . Data was recorded in profile mode, and to further improve compound identification a tandem mass spectrometry based method was implemented (data-dependent MS² (dd-MS²)).

Due to the low mass of UFPs and therefore low filter loadings determining the LOD and LOQ of tri-*o*-cresyl phosphate (TCP) and pentaerythritol tetrahexanoate (C₂₉H₅₂O₈) make it possible to evaluate the suitability of the MS-system for the analysis. These thresholds were determined based on external calibration. Different compound concentrations in a dilution series are fitted with the corresponding signal intensity responses. Based on this correlation it is possible to determine compound concentrations in ambient samples. This type of quantification method does not consider matrix effects. Five points were calibrated between 0.001–1 ng μL^{-1} using authentic standards (tri-*o*-cresyl phosphate: \geq 97.0%, Sigma-Aldrich; pentaerythritol tetrahexanoate: 95%, Carbosynth Ltd) with each concentration measured three times. The LOD and LOQ for tri-*o*-cresyl phosphate was: 0.021 ng μL^{-1} and 0.060 ng μL^{-1} and for pentaerythritol tetrahexanoate: 0.007 ng μL^{-1} and 0.018 ng μL^{-1} . The procedure follows the standard DIN 32645. Both calibration curves only showed a small linear response range between concentration and signal intensity, hence only three calibration points ranging between 0.001–0.1 ng μL^{-1} were used. This is presumably a consequence of the compounds adsorptive behaviour which probably applies to all the ester base stock compounds as well. Consequently,

the standard addition method was chosen for quantification within the next study to take matrix effects into account.

Non-target screening

Besides focusing on several target compounds an overview about the chemical composition of environmental samples can be achieved by applying a non-target screening. This software-based approach enables the detection of unsuspected compounds and also to retrospectively search for compounds of concern. The Compound Discoverer (CD) software (version 3.2.0.261, Thermo Fisher Scientific) used in this study as well as the MZmine2 software utilize the two-dimensional space of m/z and retention time for compound identification. They identify chromatographic peaks based on exact mass, isotopic pattern and MS^2 fragmentation pattern. Furthermore, these fragmentation spectra can be matched with databases to further improve the identification process (database: [mzCloud – Advanced Mass Spectral Database](#), last access: 23 February 2022). Based on these characteristics the software identifies compounds and calculates molecular formulae. Co-eluting peak signals are assigned as one compound if an exact mass deviation can be attributed to adducts, clusters, fragments or isotopic differences. Analysing identification standards and ambient samples within one non-target project improves the software identification, enabling also the identification of low intensity signals. Hence the spectra of the described jet oils ($1 \mu\text{g mL}^{-1}$ in methanol (Optima[®] LC/MS grade, Thermo Fisher Scientific)), the field blanks and the UFP samples were processed in one experiment. The non-target settings were iteratively optimised leading to the following criteria: a sample-to-blank ratio of 5, a minimum peak area of 1.0×10^5 after field blank correction and a 5 ppm mass tolerance for compound detection. The minimum retention time was set to 0.7 min, accounting for the column dead time of 0.6 min. Molecular formulae were calculated allowing elemental combinations of C_{1-90} , H_{1-190} , O_{0-20} , N_{0-4} , S_{0-3} , P_{0-1} , Cl_{0-4} , and Br_{0-3} with a mass tolerance of 2 ppm. All assigned molecular formulae are classified regarding their elemental composition (CHO, CHN, CHNO, CHOS, CHNOS, CHOP, other). Tris(2-butoxyethyl) phosphate ($C_{18}H_{39}O_7P$, m/z 399.2506 ± 4 ppm, $[M+H]^+$), presumably a lab contamination, was filtered out due to its wide spectrum of applications: plasticizer, flame retardant and floor finish (Lewis Sr. et al., 2016).

Fragmentation based structural elucidation

Structural information of the compounds detected by the non-target screening were obtained by HCD fragmentation applying a normalized collision energy (NCE) of 30. Two modes of operation were used in combination, full-scan- and dd-MS² measurements. At first the exact mass of signals is determined, additionally the discovery mode possibly records fragmentation spectra of highly abundant signals if an estimated peak apex is reached. Processing the data with CD, a list of compounds different from the blanks can be obtained which can be used within the confirmation mode. This inclusion list is then used in a second measurement to record high-quality MS² spectra. This approach improves the database identification process and enables to obtain fragmentation spectra of low-intensity compounds.

For these measurements the described jet engine lubrication oils were used as qualitative identification standards to unambiguously identify the jet oil constituents in the UFP samples based on exact mass, retention time and MS² fragmentation pattern. Structural isomers cannot be differentiated based on fragmentation experiments. Confirmation of the absence of the tri-*o*-isomer of tricresyl phosphate in the ambient UFP samples and jet engine oils can be achieved based on retention times.

According to Schymanski et al. (2014) the confidence in compound identification can be divided into five levels. Level 1 represents the highest level of identification certainty by using reference standards. Whereas level 5 describes the lowest level of identification confidence if only the compounds measured exact mass is available. Database matching (database: <https://www.mzcloud.org/>) results in a level 2 (Probable structure) identification confidence. Targeting the identification of the jet engine oil constituents authentic standards were used to match their exact mass, retention times and fragmentation pattern and therefore reaching a level 1 (Confirmed structure) confidence.

Chemical characterization of UFPs by non-target screening

The positive-ionisation mode revealed almost 1000 compounds, whereas a large fraction was also detected in the field blanks and therefore filtered out. Applying the sample-to-blank ratio > 5 to the average of six samples of the 0.032-0.056 μm size fraction resulted in ~200 organic compounds. In this size fraction sample-to-blank ratios > 100 were reached by approximately 30 compounds. More than 100 organic compounds in the two smaller size fractions (0.010-0.018 μm , 0.018-0.032 μm) showed a sample-to-blank ratio > 5 averaged over 8 samples

respectively (Figure 11). The most abundant compounds in the 0.032-0.056 μm particle size range showed higher signal intensities by a factor of 5 to 10 compared to 0.010-0.032 μm particles due to higher mass concentrations. Hence, the number of detected compounds is also increased compared to the two smaller size bins. Applying the same data filtering onto the measurements in the negative-ionisation mode resulted in only 16 compounds. Presumably this low number of detected compounds is a consequence of a low influence of oxidation products from biogenic emissions.

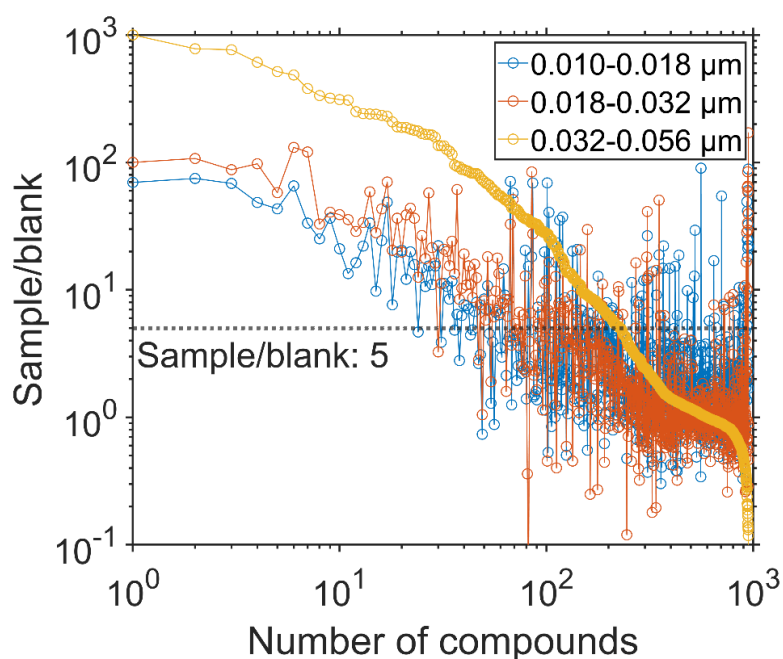


Figure 11. The average of all samples within each size fraction (0.010-0.018, 0.018-0.032, 0.032-0.056 μm) is used to plot the compounds sample-to-blank ratios against the number of detected compounds in the positive-ionisation mode. The sample-to-blank ratio of 5 is marked showing the compounds to be analysed after data filtering. Taken from Ungeheuer et al. (2021).

The chemical composition of the UFP samples can be depicted using molecular fingerprints, focusing on different chemical characteristics. The various plots retention time vs. molecular weight (MW), Van Krevelen diagram, Kroll diagram and Kendrick mass defect vs. MW are shown in Figure 12 for 0.032-0.056 μm particles. MW was used for plotting, converting the measured mass-to-charge ratios. The detected compounds are represented as coloured circles. The colouring describes the belonging to different molecular groups, while the measured signal intensity is represented by their area. Compounds with no molecular formula attributable are marked as "other".

Figure 12a mainly shows CHO containing compounds, including a homologous series of pentaerythritol esters ($\text{C}_{27-38}\text{H}_{48-70}\text{O}_8$) in group 1. CD identification artefacts were manually

removed based on adduct specific exact mass differences and retention time. Measured $[M+Na]^+$, $[M+K]^+$ and $[M+NH_4]^+$ signals of the pentaerythritol esters were misinterpreted by CD as $[M+H]^+$ adducts. The detected homologous series of pentaerythritol esters can be attributed to emissions of jet engine oils as these esters are commonly utilised as base stock material (Winder and Balouet, 2002). Automotive oil base stocks consist mostly of crude-oil based petroleum hydrocarbons (Vazquez-Duhalt, 1989), hence being distinguishable from aviation-related jet oils. Trimethylolpropane esters ($C_{27-34}H_{50-64}O_6$) also used as jet engine oil base stock material appear in group 2. Fragments of pentaerythritol esters can be observed in group 3. These fragments show a mass difference to the pentaerythritol esters at the same retention times, explainable by the neutral loss of fatty-acid fragments (e.g. $C_5H_{10}O_2$, $C_7H_{14}O_2$, $C_8H_{16}O_2$, and $C_{10}H_{20}O_2$). Although electrospray is known as very soft ionisation technique, fragmentation of the pentaerythritol esters presumably occurs in the HESI source during ionization. Ion formation was optimized in order to prevent fragmentation by adjusting the auxiliary gas heater temperature from 350 to 200 °C in 50 °C steps, and the spray voltage from 3.5 to 2.0 kV in 0.5 kV steps. Both parameters were identified as most relevant for the ionization process, nevertheless suppression of fragmentation was not achieved.

The non-target screening implies that most of the organic fraction of the sampled UFPs is attributable to jet engine lubrication oils with only a minor fraction of compounds remaining unidentified (other). The large signal at 5.2 min is likely attributable to decanedioic acid-1,10-diethyl ester ($C_{14}H_{26}O_4$) and its fragments. The homologous series of pentaerythritol- and trimethylolpropane esters used in the Mobil Jet Oil II (Figure 13) and Eastman Turbo Oil 2380 (Figure 14) as base stock have been clearly detected in the UFP samples (Figure 12 group 1-2). It is important to note that the used HESI technique is only capable of ionizing organic compounds carrying functional groups.

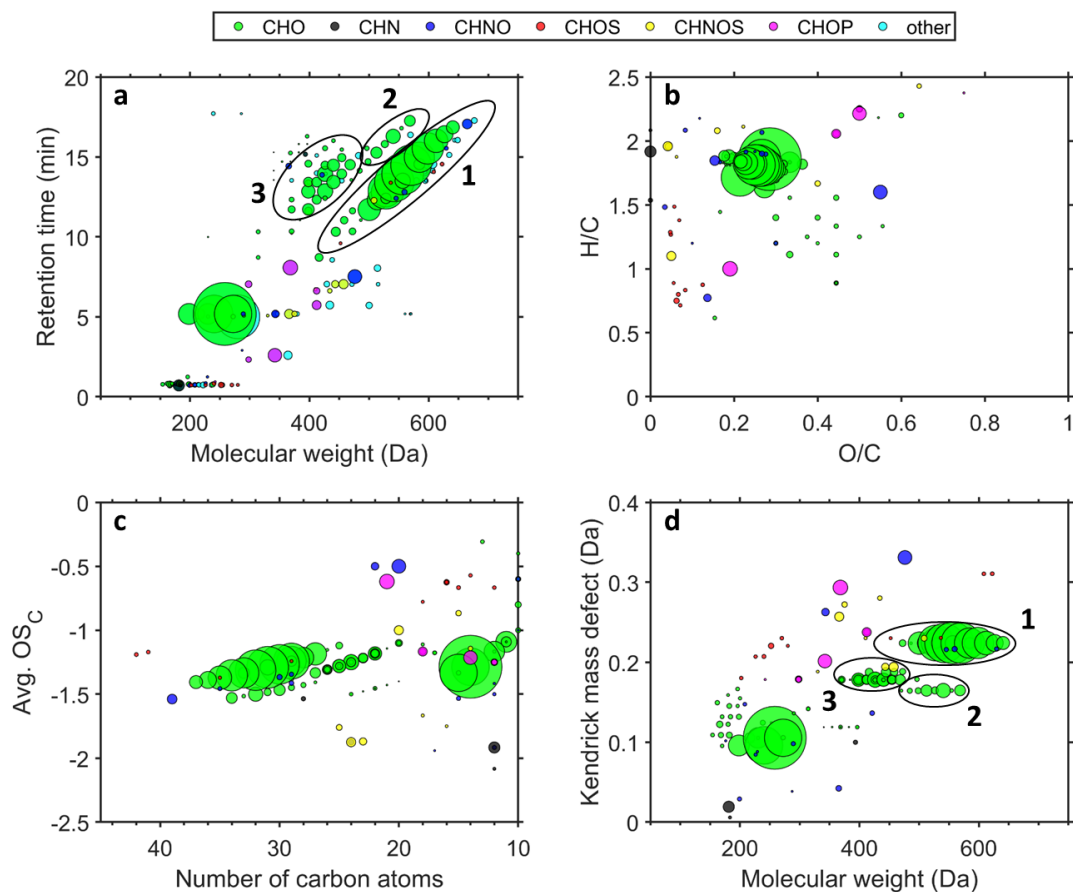


Figure 12. The chemical composition of UFPs in the size range 0.032-0.056 μm is averaged over six samples and depicted using molecular fingerprints (retention time vs. MW (a)), Van Krevelen diagram (b), Kroll diagram (c), Kendrick mass defect vs. MW (d). Taken from Ungeheuer et al. (2021).

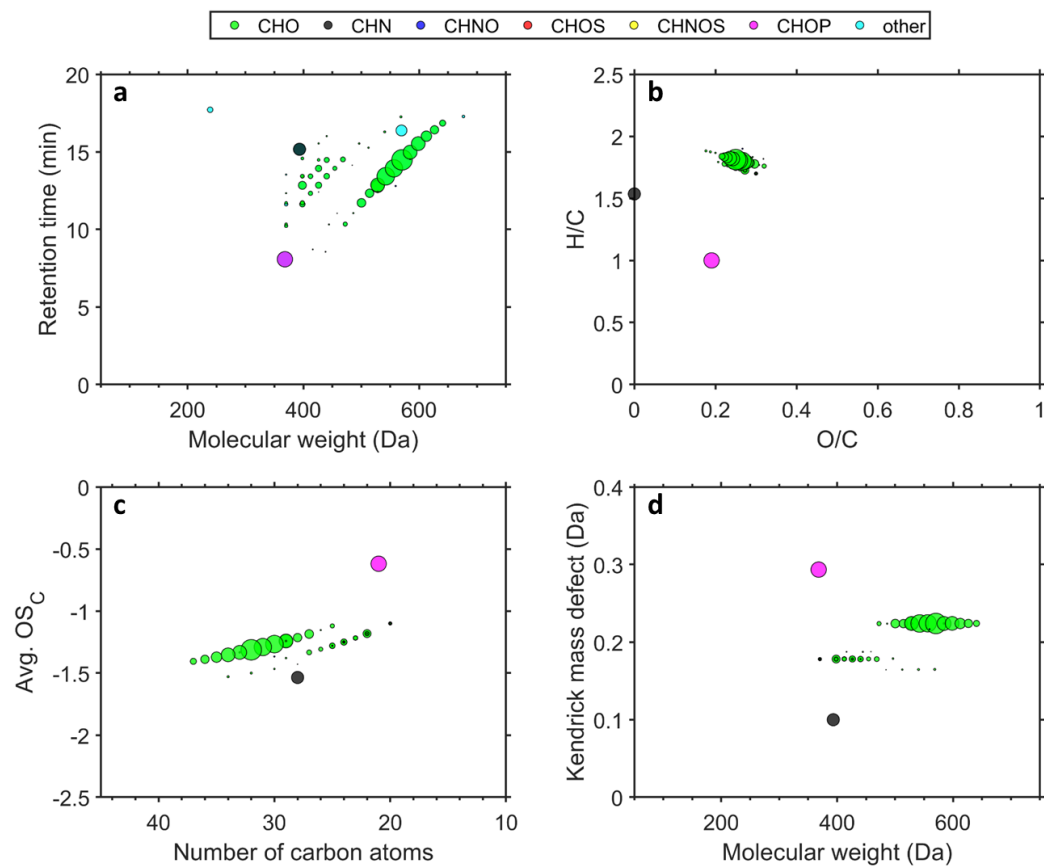


Figure 13. Mobil Jet Oil II (ExxonMobil) molecular fingerprints (Retention time vs. MW (a), Van Krevelen diagram (b), Kroll-diagram (c), Kendrick mass defect vs. MW (d)). Taken from Ungeheuer et al. (2021).

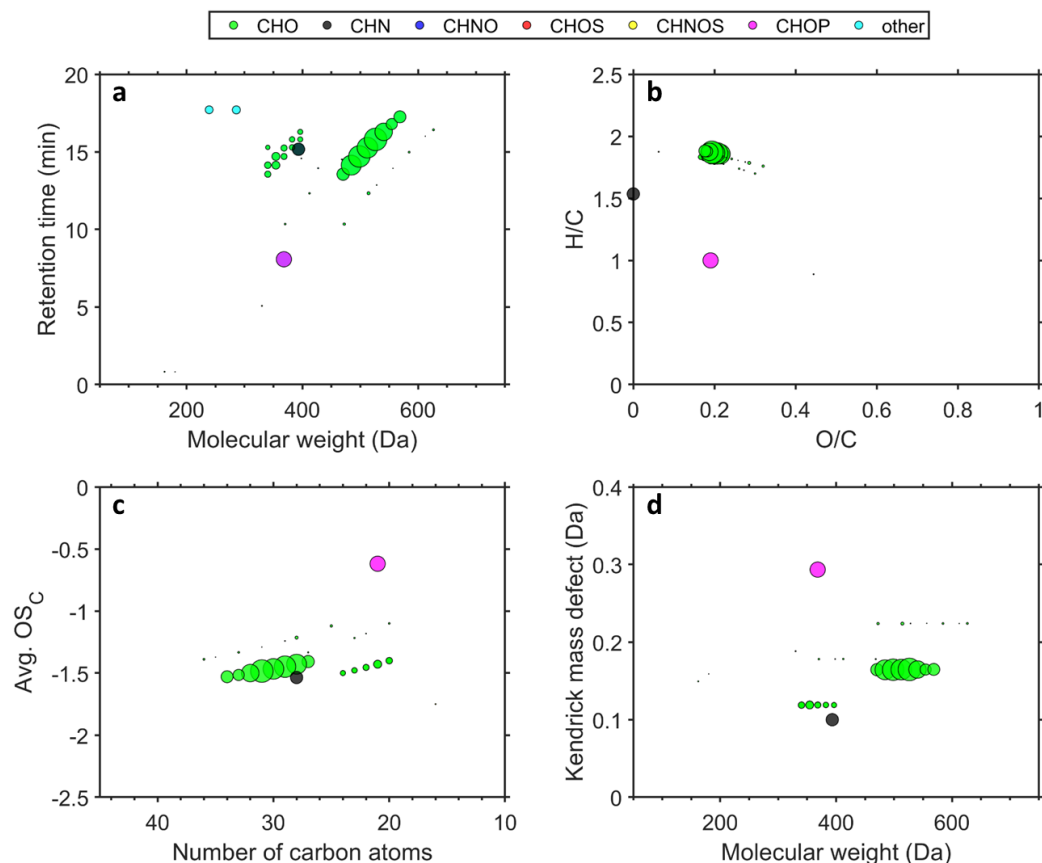


Figure 14. Turbo Oil 2380 (Eastman) molecular fingerprints (Retention time vs. MW (a), Van Krevelen diagram (b), Kroll-diagram (c), Kendrick mass defect vs. MW (d)). Taken from Ungeheuer et al. (2021).

The hydrogen-to-carbon (H/C) and oxygen-to-carbon (O/C) ratio can give insight about the aromaticity and whether compound oxidation occurred. The Van Krevelen diagram (Figure 12b) describes the chemical composition based on these two ratios, simplifying the identification of compounds mainly consisting of single-ring aromatic moieties having an H/C ratio around 1. The results imply that only a minor fraction of the detected compounds show aromaticity ($H/C \leq 1$). The jet oil anti-wear additive tricresyl phosphate appears at $H/C = 1$ and $O/C = 0.2$ as a magenta circle, containing a cresol moiety (three single aromatic rings). Based on the O/C ratios < 0.6 it can be stated that jet engine oils do not become oxidized reaching the monitoring station in 4 km distance. The O/C ratios of the analysed jet oils range between 0.2-0.4 (exemplary see Figures 13-14).

Oxidative transformation of a complex chemical composition can be analysed by calculating the average carbon oxidation state (avg. OS_C) plotted against the number of carbon atoms (n_C). Functionalization, fragmentation and oligomerization are transformations occurring in the atmosphere leading to a shift of the OS_C and n_C values (Kroll et al., 2011). The avg. OS_C was calculated not correcting for oxygen atoms attached to non-carbon atoms (Equation 1):

$$avg. OS_C \approx 2 * O/C - H/C \quad (1)$$

This simplified equation is appropriate for compounds only containing carbon, hydrogen and oxygen atoms. Consequently functional groups containing oxygen atoms, like phosphate groups, lead to OS_C values higher than the average oxidation state of the oxygen atoms implies. Atmospheric particulate matter mainly influenced by biogenic emissions exhibits a larger variability in their avg. OS_C values (Kroll et al., 2011; Vogel et al., 2019) compared with the analysed aviation-related UFPs (Figure 12c). The lubrication oil emissions only span a small range of OS_C values indicating no significant oxidative chemical transformation, confirming the characteristic of jet engine oils to be stable against oxidation. In this regard N-phenyl-1 naphthylamine ($C_{16}H_{13}N$) and alkylated diphenyl amine ($C_{28}H_{43}N$) additives serve as radical scavengers (Wu et al., 2013). Furthermore, Duangkaewmanee and Petsom (2011) reported that tricresyl phosphate can improve the oxidation inhibition ability of antioxidant mixtures in lubrication oils. The synthetic esters (CHO) contain 27-37 carbon atoms which shows that they are large molecules having low vapour pressures making it likely that these constituents stay in the particle phase.

Homologous series of hydrocarbons can be identified in complex chemical compositions by plotting the Kendrick mass defect vs. MW (Figure 12d). Compounds only differing in their number of CH_2 groups appear on a horizontal line since they all exhibit the same mass defect. Therefore, the molecular composition of compounds forming a homologous series can be deduced based on only one identified compound. Standardizing the IUPAC mass on $^{12}CH_2$ with an exact mass of 14 Da yields the Kendrick mass (Kendrick, 1963). The Kendrick mass defect (KMD) results from the difference between the Kendrick mass and the nominal mass (Equation 2):

$$KMD = nominal\ mass - (IUPAC\ mass * \frac{14.00000}{14.01565}) \quad (2)$$

The homologous series of pentaerythritol- and trimethylolpropane esters (group 1-2) and related fragments (group 3) form horizontal lines in Figure 12d.

Source attribution based on the synthetic esters pattern

The fraction of each single base stock ester with regard to the sum of all esters was analysed. Figure 15 shows the comparison of the synthetic esters pattern between the five different jet engine oils and the ambient-UFP samples. The pentaerythritol- and trimethylolpropane esters were analysed in all 22 filter samples, the spread of the single ester fractions is depicted by

boxes. The jet engine oil fractions of the individual synthetic esters are illustrated by coloured symbols. Four of the five jet engine lubrication oils utilize a pentaerythritol ester ($C_{27-38}H_{48-70}O_8$) base stock, the ester composition of these oils matches well the UFP samples composition. The pattern of the Mobil Jet Oil II most closely matches the median values of the ambient ester pattern. This is in line with this oil having the highest market share. Accordingly, jet engine oil emissions can be named as the source of the pentaerythritol esters detected in the aviation-related UFP samples. In addition, trimethylolpropane esters ($C_{27-34}H_{50-64}O_6$) have been detected in the UFP samples. This type of base stock is only used in the Eastman Turbo Oil 2380, and not in the other four oils. These esters contribute much less to the chemical composition of the UFPs compared to the pentaerythritol esters, presumably because of a minor use of this base stock type in jet engine lubrication oils. The different base stocks used in the five analysed jet oils can be distinguished by the individual molecular fingerprints and chromatograms of the oils (exemplary see Figures 13-14 & Figure 16).

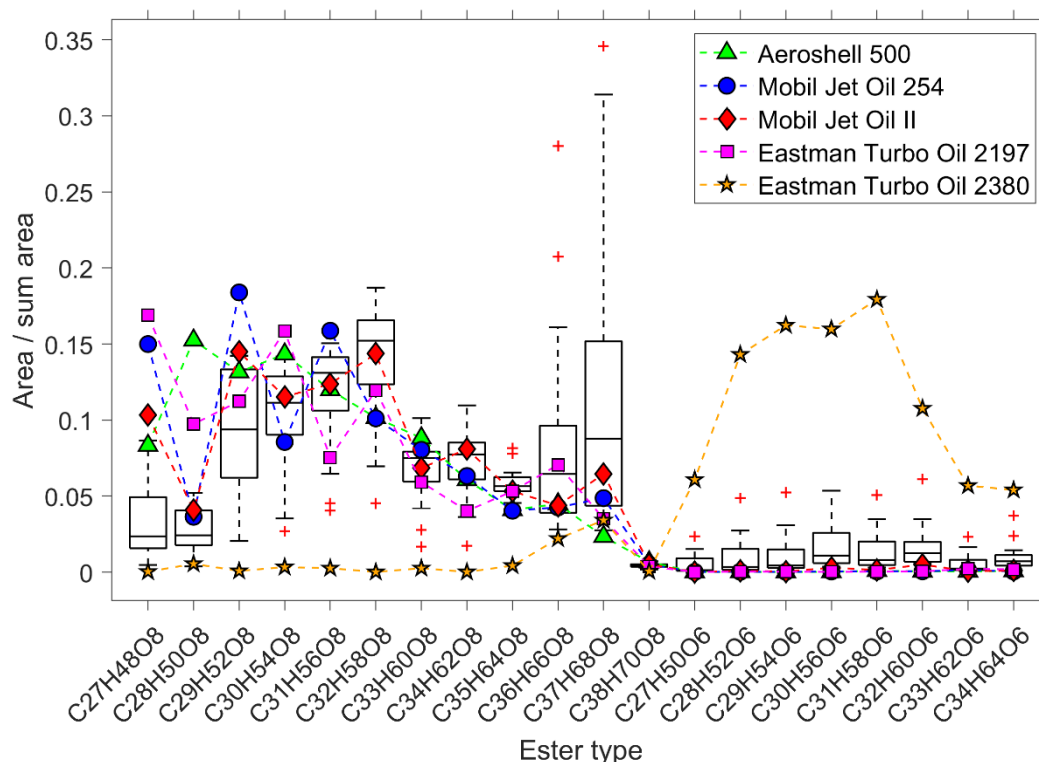


Figure 15. Boxplot which compares the spread of the pentaerythritol- and trimethylolpropane ester ratios in the 22 ambient-UFP samples (boxes) with the corresponding ratios of the five different jet engine lubrication oils (coloured symbols). The x axis represents the different ester types and the y axis the ratio of the peak area of each ester compound to the overall area of all esters. The interquartile range is indicated by the bottom and top edges of the boxes, and the median inside the boxes is depicted by an horizontal line. The spread to the most extreme values is indicated by whiskers, and outliers (outside $\pm 2.7\sigma$) as red "+" symbols. Taken from Ungeheuer et al. (2021).

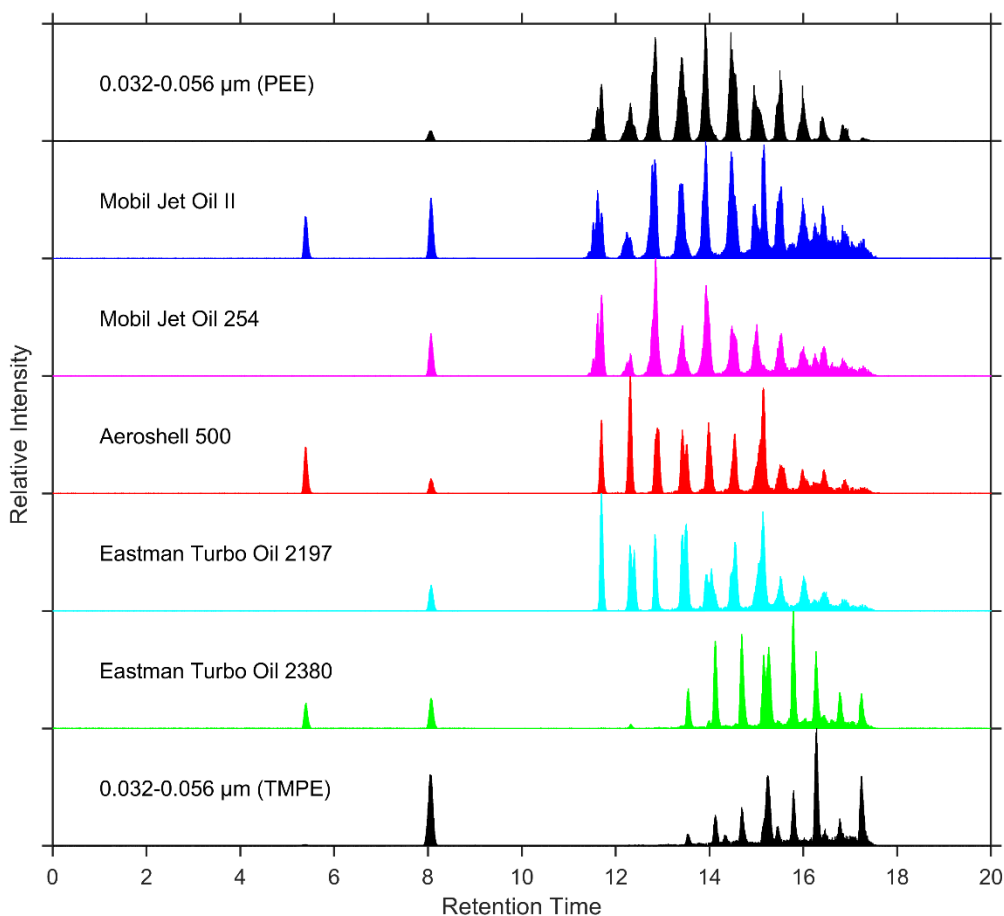


Figure 16. Extracted ion chromatograms (XIC) of an airport-sample (UFP size: 0.032-0.056 μm). A matching pattern with the major compounds of five different jet oils can be observed: $m/z \pm 4$ ppm 220.1120 (RT: 5.40 min, $[\text{M}+\text{H}]^+$, N-phenyl-1-naphthylamine, $\text{C}_{16}\text{H}_{13}\text{N}$), $m/z \pm 4$ ppm 394.3468 (RT: 15.16 min, $[\text{M}+\text{H}]^+$, alkylated diphenyl amine, $\text{C}_{28}\text{H}_{43}\text{N}$), $m/z \pm 4$ ppm 391.1069 (RT: 8.05 min, $[\text{M}+\text{Na}]^+$, tricresyl phosphate, $\text{C}_{21}\text{H}_{21}\text{O}_4\text{P}$) and homologous series of $m/z \pm 4$ ppm 523.3241 - 677.4962 (RT: 11.70 – 17.27 min, $[\text{M}+\text{Na}]^+$, pentaerythritol esters, $\text{C}_{27-38}\text{H}_{48-70}\text{O}_8$, PEE) and $m/z \pm 4$ ppm 493.3499 - 591.4595 (RT: 13.53 – 17.24 min, $[\text{M}+\text{Na}]^+$, trimethylolpropane esters, $\text{C}_{27-34}\text{H}_{50-64}\text{O}_6$, TMPE). The same sample (0.032-0.056 μm) was depicted once with the focus on the pentaerythritol esters (PEE) and once with the focus on the trimethylolpropane esters (TMPE). Taken from Ungeheuer et al. (2021).

Compound verification based on fragmentation experiments

The molecular structure of compounds can be elucidated by performing MS^2 fragmentation experiments. The created fragments have lower masses reducing the number of possible structural combinations of the measured molecular composition. Chemical bonds within molecules differ in their energy mostly leading to the formation of distinct fragments. These fragments can be used to deduce the structure of compounds and to unambiguously verify the identity of compounds in ambient samples using authentic standards.

Verification of the jet engine oil constituents detected in the ambient-UFP samples was conducted by performing fragmentation experiments of the homologous series of

pentaerythritol- ($C_{27-38}H_{48-70}O_8$) and trimethylolpropane esters ($C_{27-34}H_{50-64}O_6$), tricresyl phosphate ($C_{21}H_{21}O_4P$), N-phenyl-1-naphthylamine ($C_{16}H_{13}N$) and alkylated diphenyl amine (bis(4-(1,1,3,3 tetramethylbutyl)phenyl)amine; $C_{28}H_{43}N$). Fushimi et al. (2019) reported these compounds as molecular markers for jet engine oil emissions, not used in automotive lubrication oils. Mobil Jet Oil II by ExxonMobil was used as authentic standard to compare the fragmentation pattern of tricresyl phosphate (Figure 17a), alkylated diphenyl amine (Figure 17b) and the pentaerythritol ester $C_{29}H_{52}O_8$ (Figure 17c) detected in the ambient-UFP samples. The structure of tricresyl phosphate features three aromatic moieties bridged by an phosphate group. Fragmentation leads to the abstraction of one aromatic moiety including the bridging oxygen atom of the phosphate group, yielding the fragment ion at m/z 261.0674 ($C_{14}H_{14}O_3P$) consisting of only two aromatic moieties. The fragment at m/z 91.0543 (C_7H_7) corresponds to the abstracted aromatic ring structure without the oxygen atom of the phosphate group. Alkylated diphenylamine seems to be more stable regarding the used fragmentation settings compared to the other jet engine oil constituents, not showing a pronounced fragmentation pattern. The fragment ion at m/z 134.0964 ($C_9H_{12}N$) can be related to one of the two aromatic rings linked to the nitrogen atom and parts of one alkyl side chain. Fragmentation of the pentaerythritol esters, utilized as base stock material in jet oils, was analysed based on pentaerythritol tetrahexanoate ($C_{29}H_{52}O_8$), one constituent of the homologous series. The characteristic fragmentation pattern shows a fragment ion at m/z 399.2737 ($C_{22}H_{39}O_6$), corresponding to one ester molecule after abstraction of one side chain ($C_7H_{13}O_2$). Ester bond cleavage releases an aliphatic side chain fragment ion at m/z 113.0960 ($C_7H_{13}O$). The signal intensity of N-phenyl-1-naphthylamine in the ambient-UFP samples was insufficient to record a clear fragmentation spectrum. This is possibly explainable by a minor utilization of this additive in jet engine oils, functioning as a radical scavenger (Wu et al., 2013), potentially undergoing a faster atmospheric degradation. Additionally, the obtained MS² fragmentation pattern of tricresyl phosphate and N-phenyl-1-naphthylamine by analysing the jet engine oils agreed with the corresponding fragmentation spectra of the mzcloud database.

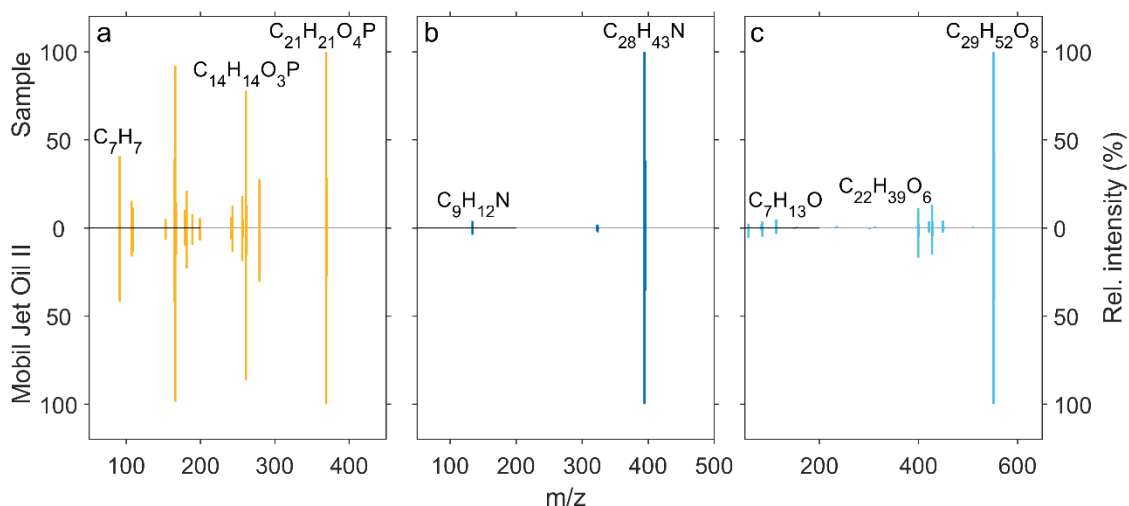


Figure 17. The MS² fragmentation patterns of tricresyl phosphate (a; C₂₁H₂₁O₄P), alkylated diphenyl amine (b; C₂₈H₄₃N) and one pentaerythritol ester (c; C₂₉H₅₂O₈) measured in an ambient-UFP sample (0.032-0.056 μm) (upward spectra) and the Mobil Jet Oil II by ExxonMobil (downward spectra) confirm their matching identity. Taken from Ungeheuer et al. (2021).

Analysis of TCP isomers in the UFP samples

Detrimental health effects have been associated with a tricresyl phosphate exposure holding a neurotoxic potential by acting as an acetylcholinesterase (AChE) inhibitor and endocrine disruptor (Chang et al., 2020; Ji et al., 2020). Targeted screening by selected-ion monitoring (SIM) was performed to gain insight about the TCP isomer composition in aviation-related UFPs, as the potential health effects of the isomers vary. The identified TCP peak signal in the UFP samples elutes after 8.06 min, while the purchased tri-*ortho* isomer standard elutes earlier at 7.82 min. Therefore it can be stated that the tri-*ortho* isomer of tricresyl phosphate was not present in the collected UFPs, the measured peak signal is presumably attributable to overlapping peak signals of different *meta*- and *para*-isomers. This is beneficial concerning possible detrimental health effects of a tri-*o*-cresyl phosphate exposure which possibly occur due to formation of cyclic phosphate metabolites (Eto et al., 1962). The absence of tri-*o*-cresyl phosphate in the airport samples is consistent with the reduction of this isomer in jet engine lubrication oils (Winder and Balouet, 2002; Nola et al., 2008). Accordingly, the tri-*ortho* isomer of TCP was also not detected by other studies analysing various sample types (Solbu et al., 2010; Solbu et al., 2011). Nevertheless, it should be considered that the toxicity of isomers featuring only one methyl group in ortho-position is possibly higher compared to isomers with the methyl groups only in meta- and para-position (Hanhela et al., 2005).

Further organophosphate compounds like triphenyl phosphate (TPP), a high-production-volume chemical, were detected in the airport-related UFP samples. TPP used as flame retardant and plasticizer (Wei et al., 2015) is described as AChE inhibitor and endocrine

disruptor bearing a neurotoxic potential (Chen et al., 2015; Shi et al., 2018). Aircraft ground maintenance can also potentially lead to the release of organophosphates into the environment (Solbu et al., 2010). Accordingly, the detected TPP is probably originating from hydraulic oils, with presumably further sources beyond airport operations being relevant.

Identification of the thermal decomposition product TMP-P

Trimethylolpropane phosphate (TMP-P), a neurotoxin can be formed when trimethylolpropane esters (TMPEs), which are used as base stock material in jet engine lubrication oils, are combined with a phosphate additive with a final share of only 2% (Callahan et al., 1989; Centers, 1992). In contrast combining phosphate additives with the more commonly used pentaerythritol ester base stock does not lead to the formation of TMP-P (Wyman et al., 1987). The formation of TMP-P takes place between 250-750 °C, possibly with all phosphates regardless of the structure. As the activation energy of the reaction is low, the formation of TMP-P is probably not highly temperature-dependant (Wright, 1996). TMP-P starts to decompose reaching the upper reaction-temperature limit, thereby the actual yield of TMP-P is determined by the balance between formation and degradation reactions (Callahan et al., 1989). The ability of TMP-P to bind to γ -aminobutyric acid (GABA) receptors, particularly at the picrotoxinin site, affects neurotransmission processes, implying its convulsive potency to affect the nervous system (Bowery et al., 1976; Bowery et al., 1977; Mattsson, 1980; Simmonds, 1982; Ticku and Ramanjaneyulu, 1984). TMP-P was not detected in different studies (van Netten and Leung, 2000; Solbu et al., 2011), while it could be identified in the UFP samples by fragmentation resulting in a characteristic phosphate fragment. The continued use of jet engine lubrication oils based on TMPEs could be the reason that TMP-P is detectable in aviation-related UFPs. The analysed Eastman Turbo Oil 2380 is based on a trimethylolpropane ester base stock, showing a different pattern regarding the jet oil marker compounds compared with the other analysed jet oils based on pentaerythritol ester formulations (Figure 16). The Eastman Turbo Oil 2380 is probably the successor to the Exxon 2380 oil, which was mentioned as a TMP-P source (Callahan et al., 1989). The TMP-P detected in the UFP samples was verified by simulating the thermal decomposition process in a laboratory experiment using the Eastman Turbo Oil 2380 heated to temperatures of 250-450 °C in 50 °C steps for 4 h each. Subsequently the jet oil was analysed and a signal at m/z 179.0467 ($[M+H]^+$, TMP-P, $C_6H_{11}O_4P$) could be detected from 400 °C on. The unambiguous identification of TMP-P in the UFP samples was confirmed by comparing the retention time with the signal from the oil experiment. Starting at

400 °C the fraction of TMP-P rises with increasing temperature. The relative fraction of tricresyl phosphate rises, due to its temperature-stability in contrast to the trimethylolpropane esters. They show a decreasing trend at temperatures above 400 °C. Between 250-350 °C the fraction of both amine additives ($C_{16}H_{13}N$, $C_{28}H_{43}N$) decreases, being no longer detectable from 400 °C on (Figure 18).

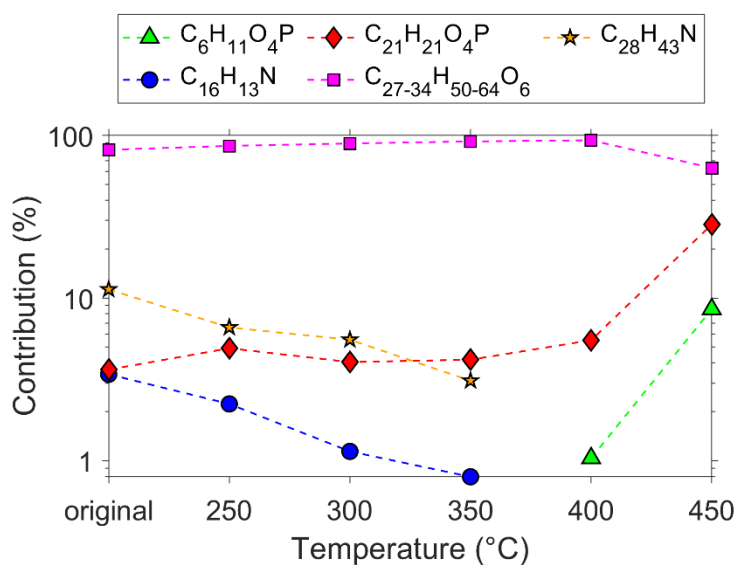


Figure 18. Outcome of the temperature experiment using the Eastman Turbo Oil 2380. The contribution (%) of the different oil constituents is defined as the ratio of the area of each single compound relative to the total area of all constituents. Taken from Ungeheuer et al. (2021).

4.2 Nucleation of jet engine oil vapours is a large source of aviation-related ultrafine particles

This chapter describes the content of the second paper of this study (Ungeheuer et al., 2022), which focuses on the ability of jet engine oil vapours to form new particles and on the oil fraction in aviation-related ultrafine particles. Thermodenuder experiments and a volatility analysis were performed to investigate the nucleation ability. To reliably quantify the oil fraction, the particle sampler used was characterized in terms of sampling losses.

The non-target screening of airport-related UFPs in the previous study (Ungeheuer et al., 2021) showed that the spectrum of detected organic compounds in aviation-related UFPs < 56 nm is dominated by jet engine lubrication oils. Following this non-target study, the nucleation ability of jet engine oil vapours was investigated by studying their gas-to-particle partitioning behaviour. Furthermore this was supported by a quantitative analysis of the whole spectrum of jet engine oil constituents in particles with aerodynamic diameters < 56 nm collected near Frankfurt Airport. This quantitative characterization requires the detection of organic molecules down to a few picograms. In this regard the determination of possible sampling losses is required. The results show that jet oil vapours during engine exhaust plume cooldown reach gas-phase supersaturation leading to new-particle formation (Figure 19).

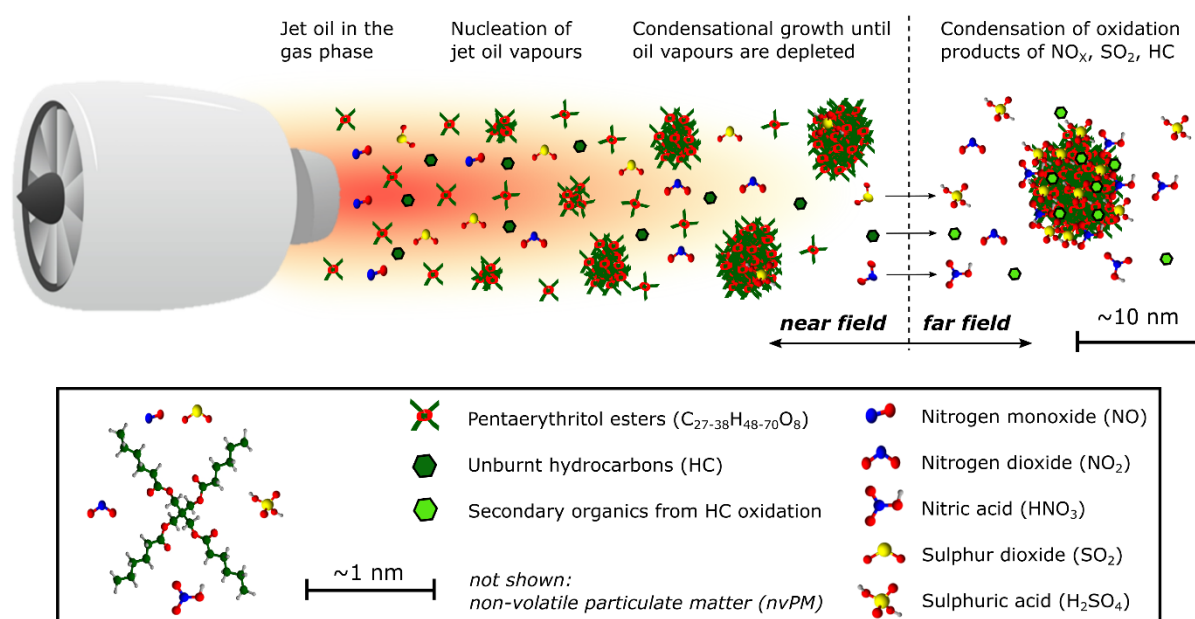


Figure 19. Illustration of the UFP formation from the emissions of aircraft turbofans, via fast nucleation and growth of jet oil vapours in the near field. Taken from Ungeheuer et al. (2022).

Quantification of the jet engine oil constituents in UFPs

The UFP filter sampling, sample preparation and extraction procedure is described comprehensively in the previous study (Ungeheuer et al., 2021). Targeted measurements of the jet engine oil constituents were carried out by using ultra-high performance liquid chromatography (UHPLC)/heated electrospray ionization (HESI) combined with an Orbitrap high-resolution mass spectrometer (HRMS). Chromatographic separation of the jet engine oil constituents was accomplished using a C₁₈ reversed phase column (Accucore C₁₈, Thermo Fisher Scientific). More details regarding the used instrument settings can be found in the previous study.

Quantification was realised by selected ion monitoring (SIM) with a resolution of ~35k. At maximum only four compounds were detected simultaneously in a SIM time window using an inclusion list to attain highest possible detection sensitivity. The inclusion list was created based on prior measurements of ambient samples and the purchased jet engine oils. The target compounds were N-phenyl-1-naphthylamine (C₁₆H₁₃N, CAS: 90-30-2), 1,4-Dihydroxyanthraquinone (C₁₄H₈O₄, CAS: 81-64-1), tri-*o*-cresyl phosphate (C₂₁H₂₁O₄P, CAS: 78-30-8), pentaerythritol esters (C₂₇₋₃₈H₄₈₋₇₀O₈), trimethylolpropane esters (C₂₇₋₃₄H₅₀₋₆₄O₆) and Bis(4-(2,4,4-trimethylpentan-2-yl)phenyl)amine (C₂₈H₄₃N, CAS: 15721-78-5). Quantification of the trimethylolpropane ester base stock was conducted based on the measured full scan MS-spectra as these esters were detected in the course of the data analysis. Concentrations were obtained by applying a correction factor of 1.95 to switch from full-MS to SIM mode. This factor was determined based on the surrogate standard pentaerythritol tetrahexanoate (C₂₉H₅₂O₈) measured in both modes. Quantification of each compound was achieved by the use of a standard addition method with authentic standards. This method was chosen to account for the tendency of the target compounds to adsorb on surfaces leading to possible matrix effects. For quantification of the oil additives N-phenyl-1-naphthylamine (≥ 98.0%, Sigma-Aldrich), tri-*o*-cresyl phosphate (≥ 97.0%, Sigma-Aldrich), Bis(4-(2,4,4-trimethylpentan-2-yl)phenyl)amine (90%, Fluorochem) and 1,4-Dihydroxyanthraquinone (≥ 98.0%, Sigma-Aldrich) were used. Pentaerythritol tetrahexanoate (95%, Carbosynth Ltd) was utilized for both types of oil base stocks.

The measured signal intensity is directly linked to the ionization efficiency of the compounds in the HESI source mainly dependent on their functional groups. Hence, pentaerythritol tetrahexanoate was used to quantify all pentaerythritol esters with total carbon chain length between C₂₇ – C₃₈ attached to the ester groups. Dilutions of the jet engine oil constituents were

prepared in methanol. Pentaerythritol tetrahexanoate was concentrated to $1.5 \text{ ng } \mu\text{L}^{-1}$ and the four additives to $0.08 \text{ ng } \mu\text{L}^{-1}$ in the first dilution. The second dilution contained the different constituents in a four times higher concentration. Measurements of single UFP filter samples and quantification by external calibrations were used to evaluate the concentration ranges of the ambient filter samples. The solvent extracts were divided onto three vials $20 \mu\text{L}$ each and $3 \mu\text{L}$ of both dilutions were added. The native sample concentration was adjusted accordingly by adding $3 \mu\text{L}$ of pure methanol. After the first spiking series the final concentrations were $0.196 \text{ ng } \mu\text{L}^{-1}$ for pentaerythritol tetrahexanoate and $0.010 \text{ ng } \mu\text{L}^{-1}$ for each additive. The vials of the second spiking series contained the constituents in a four times higher concentration. Hence, each UFP filter sample was measured three times leading to a total of 75 measurements. The software Xcalibur (version 4.2.47, Thermo Fisher Scientific) was used to determine the signal areas through automatic integration. The results were checked manually. For pentaerythritol tetrahexanoate the calibration range was $0.2\text{-}0.8 \text{ ng } \mu\text{L}^{-1}$ and for N-phenyl-1-naphthylamine, 1,4-Dihydroxyanthraquinone, Bis(4-(2,4,4-trimethylpentan-2-yl)phenyl)amine and tri-*o*-cresyl phosphate $0.01\text{-}0.04 \text{ ng } \mu\text{L}^{-1}$. The jet engine oil constituents were quantified in the native samples applying a linear regression for each compound in every UFP sample based on the spiked samples. The final results were corrected with the individual purity of the calibration standards. Finally 25 ambient filter samples including 3 blank samples were analysed with 23 compounds being quantified. In the final results pentaerythritol- and trimethylolpropane esters have been grouped together considering only their summed total mass. Mixtures of those ester compounds with a wide range of different carbon chain lengths are used in jet engine oils as base stock. The jet engine oil mass of the deposited UFPs was determined after subtraction of the field blank values.

Characterization of the Nano-MOUDI sampler

The very low mass of UFPs (total particle mass collected after 30-50 hours of sampling in the sub-microgram range) makes the quantitative analysis challenging. Furthermore accounting for sampling artefacts is just as difficult as necessary for quantifying the jet engine oil mass fraction. Despite several shortcomings MOUDI and Nano-MOUDI samplers are commonly utilized for the collection and subsequent analysis of UFPs (Díaz-Robles et al., 2014; Andrade-Oliva et al., 2020; Focsa et al., 2020; Takegawa et al., 2021). Characterization of the Nano-MOUDI sampler was carried out in a lab experiment making use of different surrogate compounds with different chemical functional groups. To account for sampling losses pentaerythritol tetrahexanoate was used as representative for jet engine oil base stocks. These

synthetic ester base stocks make up the largest fraction of jet engine oils. Volatilisation of semi-volatile compounds is expected to be relevant as the three nano-stages (10-18 nm, 18-32 nm, 32-56 nm) exhibit a reduced pressure down to approximately 1/6 of the ambient pressure (~17.2 kPa; 18-32 nm stage). Generally, wall losses are most important for particles < 100 nm (Weiden et al., 2009). Within the lab experiment nanoparticles of pentaerythritol tetrahexanoate ($C_{29}H_{52}O_8$) were generated and sampled by the Nano-MOUDI. Quantifying the collected particle mass and comparing with the mass based on the measured particle-number size distributions revealed a correction factor for each nano-stage < 56 nm. Particles with an aerodynamic diameter between 32-56 nm showed a loss of 28% and a loss of 40% was determined for 18-32 nm particles. The sampled mass of 10-18 nm particles was insufficient to experimentally obtain a loss factor for the smallest size stage. Therefore calculation of the loss factor was undertaken assuming that sampling losses of particles < 100 nm is mainly driven by their diffusivity. The sampling condition of the 18-32 nm stage with a pressure of 17.2 kPa and 20°C were used to determine the dependency between diffusion coefficient and corresponding particle diameter. Calculations resulted in a loss of ~58% for the 10-18 nm particles by using the experimentally determined losses of the two larger stages, the particles mean geometric diameters and a damping term on the diffusion coefficient equation. As the 18-32 nm stage pressure was used, the estimated loss factor for the smallest size stage can be evaluated as conservative since the 10-18 nm stage features a lower pressure leading to a higher diffusivity and in this regard to higher losses. The quantified ambient jet oil filter mass was corrected applying these loss factors. Subsequently, the mass fraction of jet oils regarding airport-related UFPs was determined.

The setup to measure the particle size distribution in a 5 min frequency consisted of a scanning-mobility particle sizer (SMPS; $D = 2.3-82.2$ nm, TSI, model: 3938, Shoreview, MN, USA) equipped with an electrostatic classifier (EC; TSI, model: 3082), an Aerosol Neutralizer (TSI, model 3088) and a nano Differential Mobility Analyser (Nano DMA; TSI, model: 3085A). An ultrafine condensation particle counter (UCPC; TSI, model: 3776) was used to measure particle number concentrations. Pentaerythritol tetrahexanoate was diluted in methanol at ~0.1 g/L to produce nanoparticles with an average electrical mobility diameter of ~50 nm (Figure 20a) using a constant output atomizer (TSI, model: 3076). The mass of the particles formed is more concentrated on the larger particles (Figure 20b).

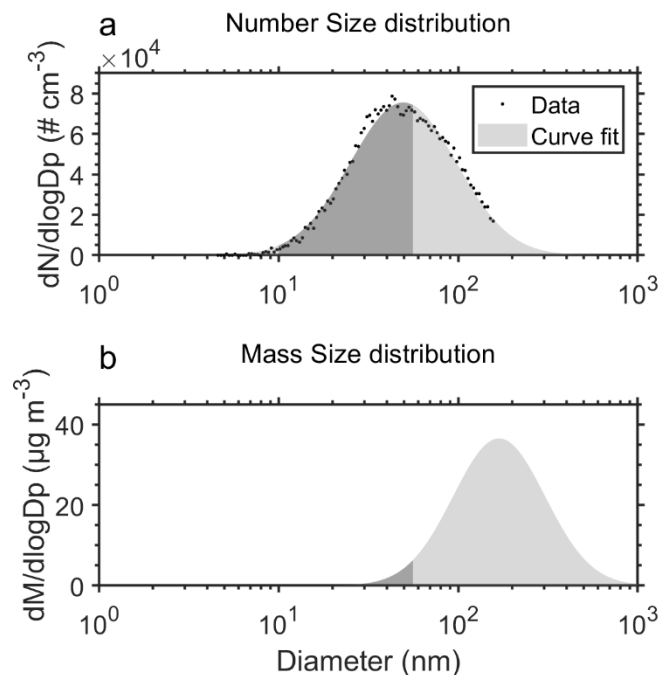


Figure 20. Particle-number size (a) and mass distribution (b) of the formed pentaerythritol tetrahexanoate nanoparticles used to characterize the Nano-MOUDI sampler. Taken from Ungeheuer et al. (2022).

Before entering a mixing chamber (Volume ~2.2 L) the generated nanoparticles pass a diffusion dryer filled with preconditioned silica gel. In order to ensure the flow rate needed for the analysis clean air is directed into the chamber, mixing with the nanoparticle stream. The mixing chamber and the Nano-MOUDI/SMPS system were connected by an aluminium tubing. The connection was designed based on the equation to estimate the laminarisation length for a straight tube (Bird et al., 2007) to ensure a laminar flow (Reynolds number < 2100). The flow was split to the Nano-MOUDI for particle collection and to the SMPS system using a bend bypass at the end of the aluminium tube (ID 1 inch, length 1.5 m). Figure 21 shows the setup and the used flow rates.

a



b

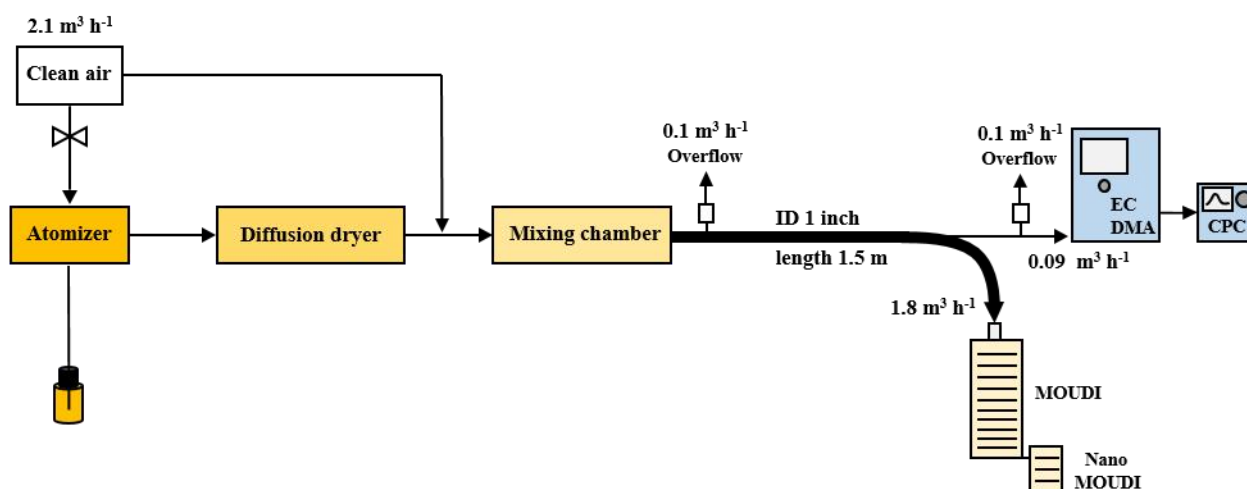


Figure 21. The Nano-MOUDI characterization setup (a) to determine loss factors for the 10-18 nm, 18-32 nm and 32-56 nm size stages. Schematic representation (b) of the Nano-MOUDI characterization setup including the detailed flow rates used. Taken from Ungeheuer et al. (2022).

Three nanoparticle collections were conducted on the last three Nano-MOUDI stages for 7 hours each. Pure methanol was used in two blank measurements carried out equally to correct for a possible formation of nanoparticles from solvent impurities. Integration of the particle-number size distribution, assuming spherical particles, yielded the mass deposited on each of the three nano-stages < 56 nm. In this regard the density of pentaerythritol tetrahexanoate (1.014 g cm^{-3}) and for the blank measurements a unit density of 1 g cm^{-3} was used. The mass of the

three nano-stages was corrected by subtracting the corresponding blank masses averaged stagewise. Furthermore the resulting particle mass was corrected with the purity of the used pentaerythritol tetrahexanoate standard. Next the collected aluminium filter samples were extracted as described previously and measured using the SIM mode. Five concentration points of the pentaerythritol tetrahexanoate standard between 0.1-15 ng μL^{-1} were calibrated to quantify the deposited particle mass by external calibration. Each concentration was measured three times in succession. By averaging the measurements of each concentration a calibration function was determined for quantification. The purity of the pentaerythritol tetrahexanoate standard was used to correct the quantified filter mass.

SMPS measurements nearby Frankfurt Airport

Parallel to the UFP filter sampling the particle-number size distribution was measured using a scanning-mobility particle sizer (SMPS) with a sample flow rate of 1 L min^{-1} . The SMPS consists of an electrostatic classifier (TSI, model: 3082), a Differential Mobility Analyser (DMA, TSI, model: 3081) and a Condensation Particle Counter (CPC, TSI, model: 3772). Airborne particles following the airstream were sampled through a stainless-steel tube (inner diameter: 20 mm, length 1.6 m), equipped with a $\text{PM}_{2.5}$ inlet head. A Nafion dryer (1.2 m length, flow rate of 0.3 $\text{m}^3 \text{h}^{-1}$) was connected upstream the SMPS to stabilize the relative humidity below 40%. In order to minimize residence time and particle losses in the inlet system an additional bypass was used. Corrections regarding particle losses through sedimentation, inertial impaction and diffusion were conducted based on Weiden et al. (2009). The number size distribution of particles between 10 – 500 nm was measured every 5 minutes. The particle mass in the Nano-MOUDI size ranges was determined by integration assuming spherical particles. For mass calculations a unit density of 1 g cm^{-3} was used in accordance to the analysed jet engine oils (see safety data sheets) and aircraft turbine engine studies (Durdina et al., 2014). By using this density a conversion of the measured mobility diameter to aerodynamic diameter is unnecessary (Seinfeld and Pandis, 2016). Furthermore the Nano-MOUDI sampling flow rate of 0.6 $\text{m}^3 \text{h}^{-1}$ was used to calculate the particle mass for each of the seven filter sampling periods during airport operating hours by calculating the volume distribution averaged over the sampling period based on the particle number size distribution. Due to an instrument failure no data was available for one sampling period.

Error estimation of the jet engine oil UFP mass fraction

Several limitations in the analytical process were identified including calibration-, instrumental- and measurement errors. Based on that the uncertainty of the jet engine oil mass fractions regarding UFPs was calculated using error propagation. The coefficient of variation of the standard addition of five pentaerythritol tetrahexanoate calibration curves was used to represent possible uncertainties within the filter quantification process. Calibration errors of the jet oil additives have not been included as the group of pentaerythritol- and trimethylolpropane esters determine most of the quantified jet engine oil mass. By applying the average of the coefficient of variation to the average jet engine oil filter- and blank filter mass of each Nano-MOUDI size fraction yielded the absolute error for the subtractive error propagation. Thereby the absolute error of the blank correction step could be determined. The relative errors for the final error propagation have been obtained by setting the absolute error of each size fraction in ratio to the corresponding average blank corrected jet oil mass. The ambient UFP mass determined by SMPS measurements and subsequent data integration was taken into account with a relative error of 10%. The error of the Nano-MOUDI characterization was determined by taking the coefficient of variation of the external pentaerythritol tetrahexanoate calibration and the SMPS measurements standard deviations into account. The single SMPS scans during the seven hour experiments of filter collection and blank determination were represented by their average absolute standard deviation. For each size fraction the absolute error of the blank corrected SMPS mass per scan was calculated by error propagation. The relative error of the SMPS measurements for each size fraction was determined by referring the absolute values to the average blank corrected mass per scan. Accordingly, the average relative error of each of the three UFP stages within the Nano-MOUDI characterization was obtained by combining the relative error of the external pentaerythritol tetrahexanoate calibration and of the SMPS measurements by error propagation. Finally combining the relative errors of the ambient filter quantification, the Nano-MOUDI characterization and the ambient SMPS measurements by error propagation yielded the error of the UFP jet oil mass fraction for the three size ranges. The determination of errors for each UFP size fraction is based on the equation used to determine the contribution of jet engine oils to the UFP mass. Accordingly, an error of 52%, 53% and 25% for the 10-18 nm, 18-32 nm and 32-56 nm stage was obtained.

Jet engine oil volatility analysis by thermodenuder measurements and modelling

The new international aircraft particulate matter (PM) standard only considers the non-volatile PM number and mass (International Civil Aviation Organization, 2019). Particulate emissions which pass over into the gas phase at certification conditions are not taken into account. The volatility of jet oil UFPs was determined based on thermodenuder measurements and analysis of the particle-number size distribution (PNSD) of Mobil JetTM Oil II generated UFPs at two different temperatures. The particles were formed using an atomizer with $\sim 0.04 \text{ g L}^{-1}$ jet oil in methanol. The PNSD was measured using a SMPS (TSI, model: 3938, Shoreview, MN, USA) after they passed the thermodenuder at $20 \text{ }^\circ\text{C}$ or at $300 \text{ }^\circ\text{C}$. Comparing the SMPS mass at both temperatures revealed the remaining jet engine oil fraction at the elevated temperature.

In this regard the jet oil base stocks were analysed using semi-empirical group contribution methods (SIMPOL.1 model; (Pankow and Asher, 2008)) and a volatility basis set (VBS; (Donahue et al., 2011)). This allows the grouping of the single ester compounds to volatility classes (ULVOC: ultra-low volatility-, ELVOC: extremely-low volatility-, LVOC: low-volatility organic compound) as their volatility strongly determines their gas-to-particle partitioning behaviour. The volatility of compounds can be expressed as the logarithm of the saturation mass concentration ($\log_{10} C_i^*$). The inverse of the gas-to-particle phase partition constant yields the saturation mass concentration (C_i^*) (Donahue et al., 2006). One decade in C_i^* is assumed as uncertainty which is also the scale by which the volatility can be differentiated. Within this approach the individual molecular composition and a parametrization of the oxidation state is taken into account (Donahue et al., 2011).

To take into account changes of the saturation vapour pressure due to different temperatures, the Clausius-Clapeyron equation can be used to describe C_i^* (Epstein et al., 2010). This approach allows an estimate of the temperature dependence although it is burdened by higher uncertainties. Assuming that the base stock ester concentrations quantified in the particle phase have been in the gas phase in the engine exhaust plume, their gas-phase saturation ratio (S_i^*) can be calculated (Donahue et al., 2013). Thereby it is possible to determine whether jet oil constituents reach gas-phase supersaturation. The behaviour of the jet engine oil constituents in a cooling engine exhaust plume was analysed by calculating the approximate temperature at which they reach gas-phase supersaturation ($S_i^* = 1$).

Nucleation of jet engine lubrication oil

Ambient measurements at Frankfurt-Schwanheim (Figure 7) showed a distinct difference between particle number size distributions of UFPs coming from the city centre and the airport (Figure 22a). Air masses emerging from Frankfurt Airport differ compared to air masses from the city centre showing higher particle number concentrations of ~18 nm UFPs by a factor of ~15. Furthermore, these ambient particle-number size distributions (PNSD) were compared with jet engine oil particles generated in the laboratory. Assessment of the volatility and nucleation capability of the jet oil was strived for by studying the PNSD of the jet oil particles passing a thermodenuder at 20 °C and 300 °C. After passing the thermodenuder at 300 °C, newly formed particles show a five-fold increase of the total particle number compared to the experiment at 20 °C and a reduction of the mean diameter from 27 nm to ~12 nm (Figure 22b). Compared to the experiment at 20 °C the 300 °C experiment showed a reduction of the jet oil mass fraction by ~99%, indicating the volatile character of jet engine oils (Figure 22c). The PNSD was measured downstream the heating section at room temperature, with a large fraction of the oil vapours likely lost to the inner surfaces of the connection tubing.

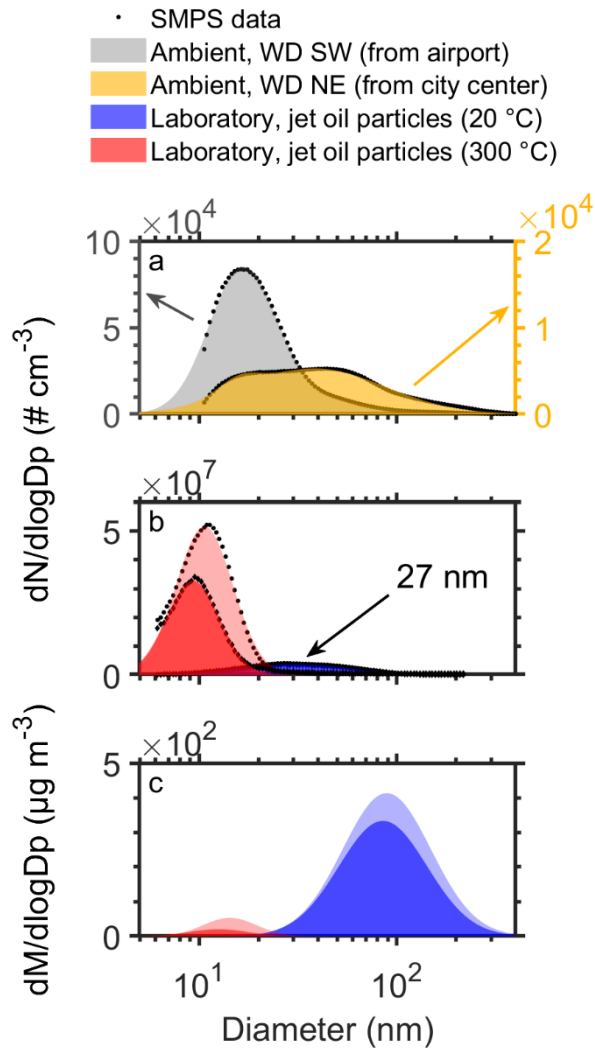


Figure 22. Three days average (05:00–23:00 CET) of the ambient particle size distribution (a) at the monitoring site under airport- (grey) and city (yellow) wind direction (WD). Size (b) and mass distributions (c) from the two thermodenuder experiments using Mobil Jet Oil II nanoparticles at 20 °C (blue/light blue) and 300 °C (red/light red). Black dots display the measured data which were extrapolated using a lognormal distribution. Taken from Ungeheuer et al. (2022).

Nonetheless new-particle formation can be observed downstream of the thermodenuder as a small fraction of the jet oil vapours nucleate within a few seconds. Nucleation occurs when the temperature of the sampling flow cools down and the jet oil vapour becomes supersaturated. To evade scavenging by coagulation, small particles have to grow rapidly to sizes > 10 nm allowing to escape the nucleation “valley of death” (Wang et al., 2020). Hence, jet engine oil particles are volatile UFPs at the thermodenuder temperature of 300 °C, assuming a complete shift to the gas phase at operating temperatures of aircraft turbofan engines ($\gg 300$ °C (El-Sayed, 2017)). The full complexity of jet engine emissions is surely not reflected by the conducted experiments. Nevertheless, the formed oil particles after passing the thermodenuder and the ambient UFPs downwind of Frankfurt Airport can be assigned to the same size region

(particle diameter). Therefore, it is rather likely that nucleation of jet engine oils contributes to the high number concentration of UFPs < 30 nm nearby airports.

Fraction of lubrication oil in ambient UFP samples

In order to determine the oil fraction in UFPs near Frankfurt Airport, the jet engine oil constituents were quantified in the ambient particle samples collected in seven periods during airport operating hours and southerly wind direction (Figure 23a and blue horizontal bars in Figure 23b-d). Furthermore the measured PNSD was used to calculate the mass concentration (oil density = 1 g cm^{-3} , see Durdina et al. (2014)) for the three investigated particle size bins (Figure 23b-d).

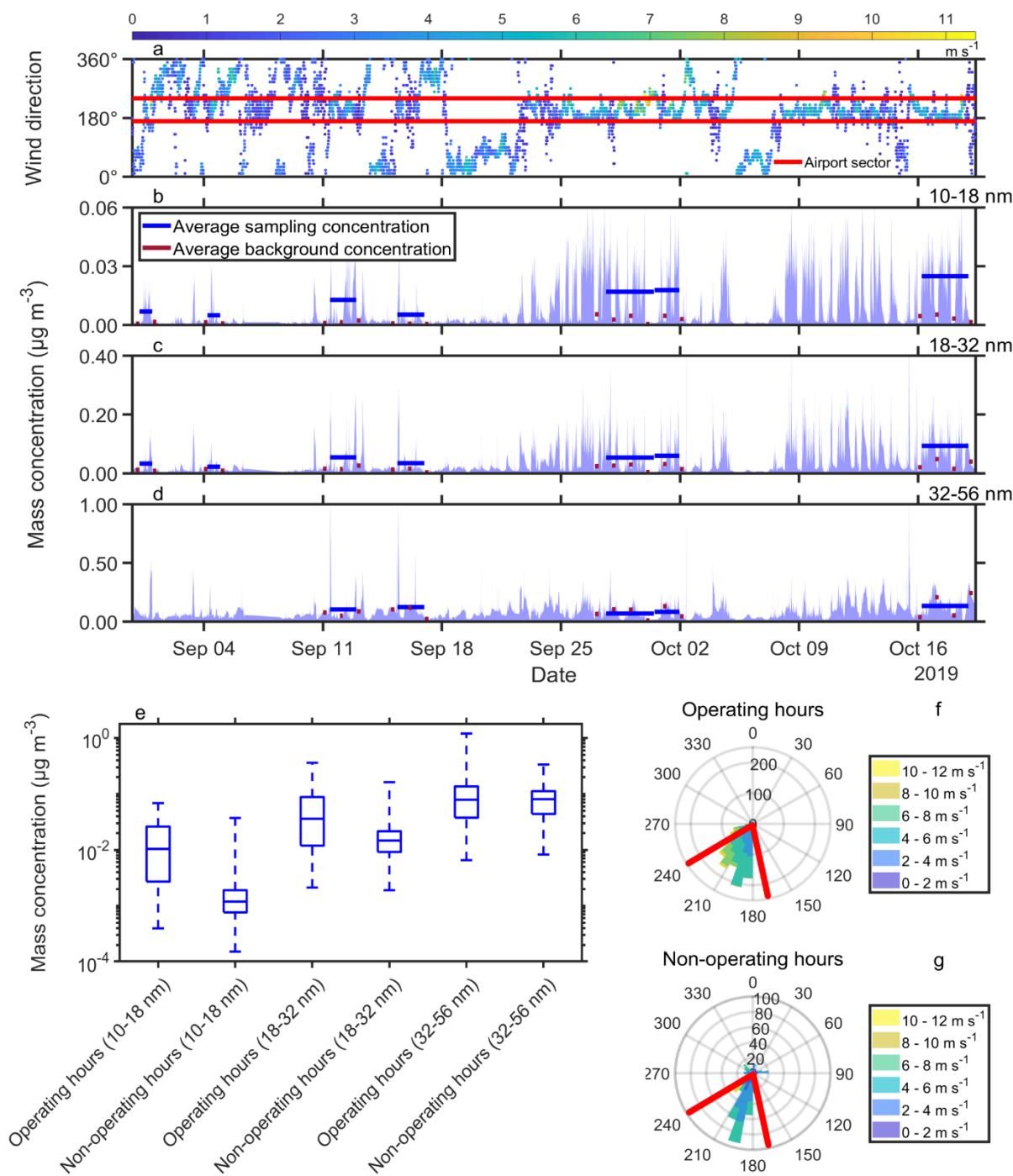


Figure 23. Overview of the size-resolved UFP mass concentration measurements at Frankfurt Airport. Wind direction (a) with wind speed indicated by colour bar. The wind data is provided by the meteorological station at Frankfurt Airport (International Civil Aviation Organization, ICAO, code: EDDF) of the German weather service (DWD). The ambient UFP mass concentration ($\mu\text{g m}^{-3}$) in the size ranges 10-18 nm (b), 18-32 nm (c) and 32-56 nm (d), and the Nano-MOUDI sampling intervals are shown. Horizontal lines of the average mass concentration during sampling hours (blue) and the average background mass concentration (dark red) exhibit the individual filter sampling periods. Mass calculations were conducted assuming a unit density of 1 g cm^{-3} . In (e) the distribution of the total mass concentrations ($\mu\text{g m}^{-3}$) for particles in the 10-18 nm, 18-32 nm and 32-56 nm ranges during airport operating- and non-operating hours are shown. The prevailing wind directions during filter sampling at airport operating hours are depicted in (f). The wind directions during the non-operating hour periods used for SMPS background correction are shown as well (g). Taken from Ungeheuer et al. (2022).

Particles < 32 nm showed a significantly higher UFP mass during airport operating hours (Figure 23e-g), likewise their particle mass concentration increased significantly within the airport wind sector compared to periods of other wind directions (Figure 23a-c). According to other studies, aircraft-related particle emissions are primarily < 30 nm supporting these findings and contrasting particle emissions from on-road vehicles which are dominated by particles > 30 nm (Shirmohammadi et al., 2017; Stacey, 2019; Pirhadi et al., 2020; Keuken et al., 2015). The mean particle mass of the largest size bin (32-56 nm) showed no significant difference between airport operating- and non-operating hours (Figure 23e).

The total accumulated UFP mass on each impactor stage was calculated by subtraction of the mean background mass from the mass during UFP sampling. Therefore, the night-time periods between 00:00 – 05:00 CET adjacent to each sampling day were used to determine the mean rural background particle mass concentration that is largely unaffected by airport UFP emissions (see dark red bars in Figure 23b-d). This is a consequence of the finding that the rural background level of the particle number concentration (< 32 nm) is reached around midnight. As particle mass concentrations during non-operating hours are sometimes higher than during airport operating hours (see Figure 23d) this approach cannot be applied to the largest Nano-MOUDI stage (32-56 nm). Quantification of the jet oil concentration of the collected filter samples, comprising different UFP size fractions, was conducted by adding authentic standards to filter-solvent-extract aliquots (standard addition method). Particle losses in the Nano-MOUDI were corrected using an experimentally determined loss function. Results reveal a $21 \pm 11\%$ contribution of jet engine oils to the total particle mass averaged over seven ambient UFP samples in the 10-18 nm size range. In this size range the individual samples showed jet-oil mass contributions between 10 and 38%, with the higher mass fractions linked to the shorter sampling intervals. The 18-32 nm particles exhibit only a $5 \pm 3\%$ jet engine oil UFP mass fraction on average. As mentioned before the background subtraction could not be applied on the largest size stage, therefore the non-background corrected SMPS mass was used. This results in a mean jet oil contribution of 9% to the largest size bin (32-56 nm) (Table 1).

Table 1. UFP mass fractions of jet engine oil for the three Nano-MOUDI size stages. Taken from Ungeheuer et al. (2022).

Particle diameter (nm)	Range of oil contribution to total UFP mass (%)	Average oil contribution to total UFP mass (%)	Average oil contribution to total UFP mass not background corrected (%)
10-18	10 - 38	21 ± 11	18
18-32	1 - 13	5 ± 3	3
32-56	13 - 49*	33* ± 8	9

* In this size range the values are artificially high due to a high SMPS background correction.

Accordingly, the highest fraction of jet engine lubrication oils was detected in the smallest particle size fraction. Determination of the jet oil contribution to the individual size stages was conducted by taking particle wall losses as well as evaporative losses (pressure in sampling stages < 200 mbar) into account. As the Nano-MOUDI sampling takes place at reduced pressures the observed bias in the molecular composition of jet oil from the ambient samples can be well explained by evaporation of the semi-volatile additives (Table 2).

Table 2. The ambient UFP mass fractions of the single jet engine oil constituents averaged over all size stages are shown. The vapour pressures of the different compounds and compound classes are listed. Taken from Ungeheuer et al. (2022).

Jet oil constituents	C ₁₆ H ₁₃ N	C ₂₁ H ₂₁ O ₄ P	C ₂₈ H ₄₃ N	C ₂₇₋₃₈ H ₄₈₋₇₀ O ₈	C ₂₇₋₃₄ H ₅₀₋₆₄ O ₆
Ambient constituent fraction (%)	0.10	0.34	0.10	94.87	4.58
Mobil II constituent fraction (measured)	2.15	5.22	1.05	91.57	-
Mobil II constituent fraction (MSDS)	1	1 - < 3	-	-	-
Vapour pressure* (Pa)	3.85E-03	1.45E-05	6.73E-06	3.12E-08***	2.37E-06****
Vapour pressure** (Pa)	8.32E-04	1.53E-07	2.21E-08	1.54E-10 - 2.36E-15	2.43E-09 - 2.10E-12

* Calculated with EPI Suite (25 °C)(United States Environmental Protection Agency, 2012).

** Calculated with SIMPOL.1 (20 °C)(Pankow and Asher, 2008).

*** Vapour pressure of C₂₉H₅₂O₈.

**** Vapour pressure of C₂₇H₅₀O₆.

Based on laboratory experiments the sampling efficiency of the Nano-MOUDI toward semi-volatiles was evaluated by generating pure ethyl oleate UFPs (C₂₀H₃₈O₂, CAS: 111-62-6, 98%, Sigma-Aldrich) covering the whole Nano-MOUDI size range. The compound was only detectable on the 32-56 nm stage, with a UFP mass loss of more than 99%. Ethyl oleate has a calculated vapour pressure of 8.10E-03 Pa (EPI Suite; United States Environmental Protection Agency, 2012), similar to the vapour pressure of the N-phenyl-1-naphthylamine additive used in jet engine oils. The other jet oil constituents (additives and base stock esters) exhibit lower

vapour pressures (Table 2). As a consequence, the vapour pressure is most likely the main important factor for sampling losses in the Nano-MOUDI, affecting the volatilization of semi-volatile compounds. Fortunately, volatilization of the synthetic jet oil esters is negligible due to their extremely-low volatility.

Lubrication oil base stock esters in the volatility basis set

The important role of jet engine lubrication oils regarding the formation of airborne UFPs is supported by the fact that the largest mass fraction of lubrication oil is observed in the smallest ambient Nano-MOUDI size fraction, consistent with the size range of the particles formed in the thermodenuder experiment. This hypothesis was further investigated concerning the individual base stock synthetic esters using the volatility basis set (VBS, Donahue et al., 2006, Donahue et al., 2011, Donahue et al., 2012). The vapour pressure of each single ester compound was calculated using the SIMPOL.1 model (Pankow and Asher, 2008). The quantified particle-phase concentration of each individual ester compound attributable to the two different synthetic ester base stocks, pentaerythritol esters ($C_{27-38}H_{48-70}O_8$) and trimethylolpropane esters ($C_{27-34}H_{50-64}O_6$), are shown in Figure 24a. Ester concentrations ranged between 0.01-4 ng m⁻³ in the ambient UFP samples. The volatility of these compounds can be expressed by calculating their saturation mass concentration $\log_{10} C_i^*$ (20 °C) and by this means they can be assigned to known volatility classes (Stolzenburg et al., 2018). Assuming that the ester compounds are in the gas phase at engine exhaust temperatures, their theoretical gas-phase concentration at Frankfurt-Schwanheim can be calculated using the determined particle phase concentrations. Certainly the gas phase concentration near the jet engine exhaust exit is higher than this lower limit gas phase concentration, since dilution between the source and the measurement station was not taken into account. The three pentaerythritol esters attributable to the ultra-low volatility region reach a saturation ratio larger than 1×10^5 (Figure 24b). This finding substantiates the hypothesis that jet oil synthetic esters can initiate rapid nucleation in the exhaust plume of aircraft engines, even if a lower-limit estimate of the gas phase concentration is used. Furthermore the temperature at which gas-phase supersaturation ($S_i^* > 1$) is reached was calculated, using the theoretical gas-phase concentration derived from the ambient samples of each single ester compound (Figure 24c). $C_{36}H_{66}O_8$ - $C_{38}H_{70}O_8$ pentaerythritol esters in the ultra-low volatility region are the first compounds that reach $S_i^* > 1$ at around 60 °C, even though these ester compounds occur at ambient concentrations an order of magnitude or even

lower than the $C_{29}H_{52}O_8$ ester with the highest ambient concentration. Apart from the three most volatile trimethylolpropane esters $C_{27-29}H_{50-54}O_6$ all synthetic esters reach supersaturation.

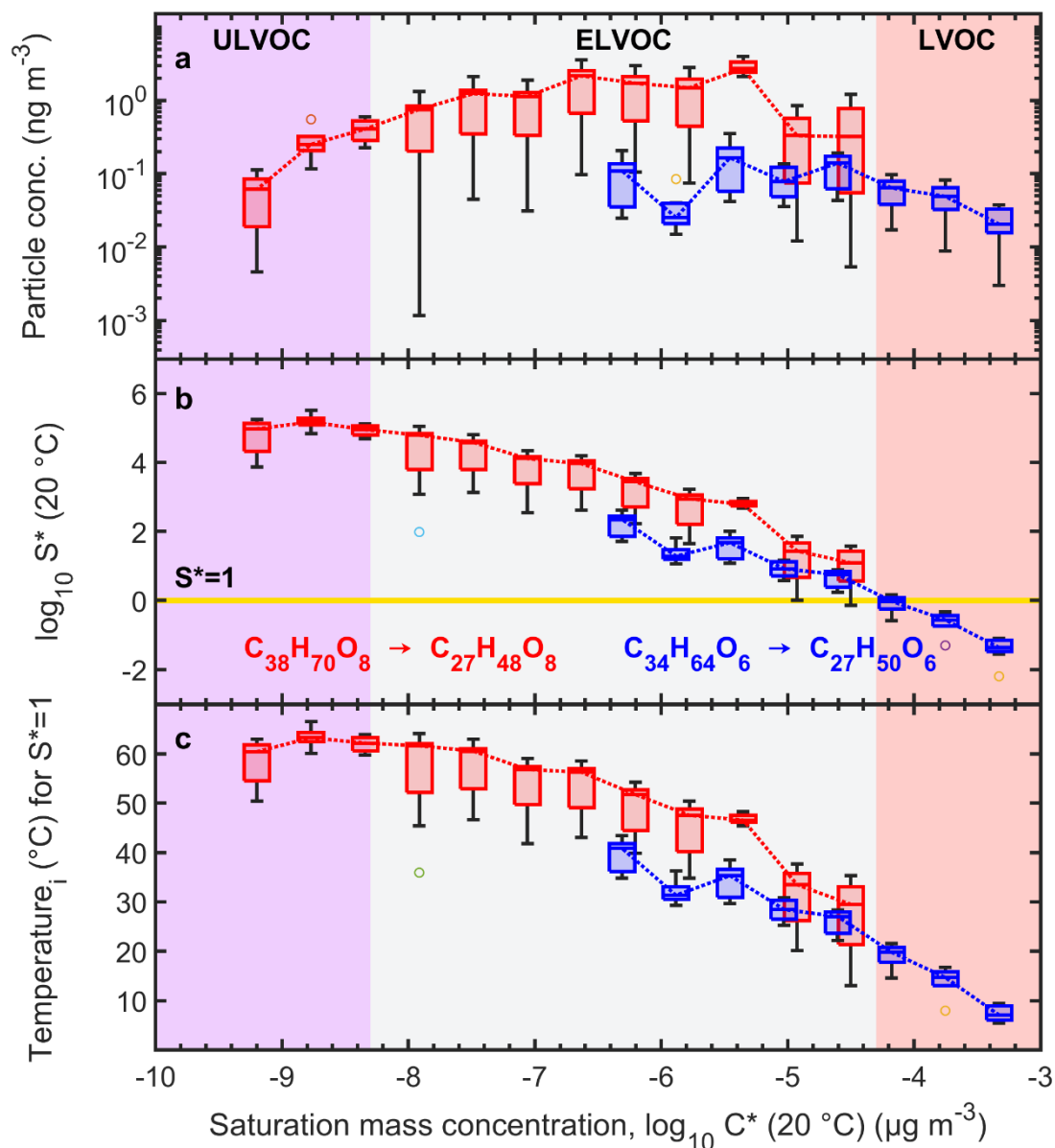


Figure 24. (a) Quantified particle concentration (ng m^{-3}) of the individual synthetic ester compounds ($C_{27-38}H_{48-70}O_8$; $C_{27-34}H_{50-64}O_6$) plotted against the $\log_{10} C_i^*$ at 20 °C (ULVOC: ultra-low volatility-, ELVOC: extremely-low volatility-, LVOC: low-volatility organic compound). The spread of the ambient concentrations is shown by the boxes as interquartile range. (b) Resulting gas-phase saturation ratio S_i^* (20 °C) based on the theoretical gas-phase concentration assuming that all particle-phase compounds of (a) shifted entirely to the gas phase. Reached supersaturation is indicated by values of S_i^* (20 °C) above 1 (yellow line). (c) The approximate temperature at which each individual jet oil ester reaches $S_i^* = 1$. Taken from Ungeheuer et al. (2022).

4.3 Occurrence and in vitro toxicity of organic compounds in urban background PM_{2.5}

This chapter describes the content of the third paper of this study (Wallraff et al., 2022), which focuses on the combination of toxicity testing and non-target screening to analyse urban background PM_{2.5}. To investigate the relationship between toxicity and chemical composition, two in vitro bioassays were performed and a wind direction dependency was also analysed.

The chemical characterization of aviation-related ultrafine particles gave insight into the chemical composition of the smallest analysable particle size fraction. As the collected ultrafine particle samples are not sufficient in mass for toxicity testing we used larger airborne particulate matter < 2.5 µm (PM_{2.5}). Hence, the toxicity of organic compounds in PM_{2.5} was investigated and combined with a non-target screening in order to attribute the toxicological findings to certain compound classes. Air pollution and in this regard PM_{2.5} exposure is seen as a risk factor to human health with the respiratory system as the primary target organ (Yang et al., 2020). Furthermore, it was shown that PM exposure can cause oxidative stress and inflammation damaging the respiratory and cardiovascular system (Arias-Pérez et al., 2020; Bates et al., 2015). An impairment of the brain is considered to be possible, leading to neurodegenerative disorders (Kanninen et al., 2020). However linking specific chemicals and their sources to detrimental health effects remains highly uncertain (Daellenbach et al., 2020). Additionally, the understanding of the chemical composition of urban organic aerosol is still lacking. Only a relatively small number of organic pollutants are monitored including phthalate diesters, polycyclic aromatic hydrocarbons (PAHs) and organophosphorus esters (OPEs) (Kolossa-Gehring et al., 2011).

The Microtox assay (*Aliivibrio fischeri*) used in this study can be applied to investigate the basic toxicity of PM_{2.5}. This test accounts for toxicological effects on the bacterial energy metabolism like narcosis, uncoupling and electrophilicity-based effects (Hermens et al., 1985; Schultz and Cronin, 1997; Cronin and Schultz, 1998; Brack, 2003). In contrast the more specific AChE-inhibition assay accounts for neurotoxic effects induced by for example organophosphates (Hageman et al., 2022). Nevertheless, in vitro bioassays of PM extracts only provide indications of the toxicity of the entire substance mixture, which cannot be traced back to individual substances. Filter sampling was conducted at two different wind directions with air masses emerging from the Frankfurt city centre and airport direction to represent three different sampling conditions. The analysed samples give insight into the emissions of a large

international airport (Frankfurt International Airport, Germany) during normal operations and an airport strike event. Furthermore, they enable a differentiation between airport emissions and urban background emissions from downtown Frankfurt.

Filter sampling, preparation and analysis

Filter sampling was conducted between October and November 2019 at the air-quality monitoring station of the Hessian Agency for Nature Conservation, Environment, and Geology (HLNUG) in Frankfurt-Schwanheim (Figure 7). The city centre of Frankfurt is located in the northeast, the Frankfurt Airport in the south both in a distance of about 4 km to the station. Micro glassfiber filters were used in combination with a High Volume Air Sampler (HVS) (Digitel DHA-80, Digitel Elektronik AG, Volketswil, Switzerland) to sample in 6 h intervals to cover the airport night flight ban period, from 23:00 to 05:00 CET. Sampling was conducted with a flow rate of 500 L min⁻¹ with the filters subsequently stored at -20 °C until analysis. To investigate emissions emerging from the airport, the Frankfurt city centre and from the airport during a Lufthansa strike four samples for each period were used with one sample reflecting the night-time period. One filter, only stored inside the HVS within the sampling periods, served as a field blank.

For the analysis each filter was cut into small pieces and extracted two times with a total of 20 mL distilled dichloromethane. The extraction was conducted on an orbital shaker for 20 min each at 300 rpm. After filtration and pooling of the two extracts, the solvent was evaporated at 35 °C applying a gentle nitrogen stream. A mixture of methanol : water (50:50) (85 µL) was used to resolve the extract residues for *in vitro* testing. The chemical characterization was conducted by diluting 5 µL aliquots with the same solvent mixture by 1:20.

Baseline toxicity was determined by the Microtox assay according to Escher et al. (2008) and the ISO-guideline (ISO 11348-3:2007, 2007). The *A. fischeri* luminescence emission was detected by a microplate reader (Tecan Spark 10 M, Tecan Group, Männedorf, Switzerland). Three experiments with one technical replicate were carried out for each sample. Inhibition by negative controls were used for correction. Final results were calculated as effective concentration (EC₂₀ in m³ air mL⁻¹) reflecting a 20% reduction in light emission.

The more specific acetylcholinesterase (AChE) inhibition assay, originally by Ellman et al. (1961), can be used to examine potential neurotoxic effects induced by AChE inhibitors. This neurotoxicity assay is based on the hydrolysis of acetylthiocholine resulting in the formation of thiocholine which is colorimetrically measurable (Escher et al., 2008). Inhibition of AChE via phosphorylation can lead to headaches, general weakness, emotional lability and confusion

(Eyer, 1995). Four independent experiments including one technical replicate were conducted for each sample. The assay was adapted and the inhibition rate for each sample determined according to Sigma-Aldrich (2018). By pooling the quadruplicates an EC₂₅ value for each sample was calculated.

The chemical characterization of the PM_{2.5} extracts was carried out using the same instrumental setup as for the ultrafine particle studies. Briefly, the gradient for chromatographic separation started with 5% methanol (solvent B). After 1 minute solvent B was increased to 95% within 12 minutes and held for 2 minutes. Thereafter, solvent B was reduced to 5% within 2 minutes to re-establish the starting conditions. Including the equilibration time of 3 min prior the next run, the total method duration was 20 minutes. The sample compounds were ionised using heated electrospray ionisation (HESI) in the positive mode. The Orbitrap mass spectrometer was operated in a range of mass-to-charge ratios (m/z) between 50–750 and in discovery mode to obtain fragmentation spectra of single compounds. The non-target analysis software Compound Discoverer (CD) (version 3.2.0.421, Thermo Fisher Scientific) was utilised for the analysis of the full-scan MS- and fragmentation spectra and Matlab (R2019b, MathWorks, Natick, Massachusetts, USA) for subsequent data evaluation. The applied criteria were identical to the previously described ultrafine particle study (Ungeheuer et al., 2021). For each compound class (CHO, CHN, CHNO, CHOS, CHNOS, CHOP, other) the summed area was calculated to compare the three different sampling conditions.

The summed signal intensities of the detected organic compounds were correlated with PM_{2.5} concentrations ($\mu\text{g m}^{-3}$). These concentrations were continuously measured by a hybrid particulate mass monitor (SHARP 5030, Thermo Fisher Scientific), utilizing nephelometry and β -absorption with the data publicly accessible (HLNUG, 2019). Hourly measured concentrations were averaged according to the 6 hours individual sampling periods. The highest concentrations in the dilution series of each bioassay were examined regarding a linear correlation of AChE inhibition and luminescence emission with the summed signal intensities of the different compound classes. The summed signal intensity of all compounds was also tested equally.

Organic molecular composition and in vitro toxicity

The non-target screening led to the detection of 460 organic compounds with a sample-to-blank ratio larger than five out of ~1600 compounds in total. The overall highest signal intensities and variety of compounds was detectable in the city condition samples with the CHO and CHNO compounds showing the highest summed signal intensities. Only the group of CHOP

compounds were more dominant in the airport samples. The analysis of the appearance of specific compounds was based on a minimum confidence level for identification of two (level 1: confirmed structure by reference standard; level 2: probable structure by library spectrum match) according to Schymanski et al. (2014). In the group of CHOP compounds mostly organophosphorus esters (OPEs) were detected. They are high-production-volume chemicals used as flame retardants, plasticisers or oil additives which are released into the environment by evaporation and leaching (Reemtsma et al., 2008). Tributyl phosphate (TBP, level 1), tricresyl phosphate (TCP, level 1) and dibutyl phosphate (level 2), probably formed by fragmentation of TBP, were identified exhibiting high signal intensities. Furthermore, dicresylphenyl- (DPP, level 1) and cresyldiphenyl phosphate (CDP, level 1) were detected particularly in the city samples. Triethyl phosphate ($C_6H_{15}O_4P$, TEP, level 1) had significantly higher average signal intensities in the city samples compared to the airport samples. TCP, an airport marker compound used as anti-wear agent in jet engine lubrication oils, was detectable in the airport samples and being absent in the city samples (Boer et al., 2015). Compared to the normal airport operation samples a lower average intensity was detected under strike condition. Triphenyl phosphate (TPhP, level 1) was detected with more than sixfold higher intensities in average in the city samples compared to the airport samples. TBP was only detectable in the airport samples which is congruent with its application as additive in aircraft hydraulic fluids (Marklund et al., 2005). Within the class of CHO compounds pentaerythritol esters ($C_{25}H_{44}O_8$, level 1; $C_{27}H_{48}O_8$, level 1), used as jet engine oil base stocks, were identified in the airport $PM_{2.5}$ samples. This class of compounds was also detectable in ultrafine particles collected at the same monitoring site (Ungeheuer et al., 2021). Furthermore, 4-*tert*-octylphenol monoethoxylate ($C_{16}H_{26}O_2$, OP1EO, level 2) was identified particularly in the city samples being an environmental pollutant and potential endocrine disruptor (Bergé et al., 2012). OP1EO belongs to the class of alkylphenol ethoxylates (non-ionic surfactants) utilized for instance as industrial cleaners and solubilisers in agricultural products (Acir and Guenther, 2018; Ying et al., 2002). CHNO compounds, based on summed signal intensities, were most dominant in the city samples. Many of the detected CHNO compounds with high intensity independently of the sampling conditions showed H/C ratios of about 0.8 to 1.5 indicating a cyclic character. The city samples also showed a more than eightfold higher summed signal intensity of CHOS compounds and the highest summed signal intensities regarding the CHNOS class compared to the airport direction samples. In all samples prosulfocarb ($C_{14}H_{21}NOS$, PSC, level 1) a systemic thiocarbamate herbicide was identified, whereas N-butylbenzenesulfonamide ($C_{10}H_{15}NO_2S$, NBBS, level 2) a neurotoxic plasticiser was mainly present in the city samples (Rider et al.,

2012). NBBS has also been detected in brake pad emissions (Plachá et al., 2017). In the class of CHN compounds the samples from the city wind sector exhibited the highest summed signal intensities. Overall, the non-target analysis exposed a strong wind direction dependency regarding the organic chemical composition and a greater heterogeneity in the city samples compared to the airport samples.

The highest applied concentrations in both bioassays revealed a positive correlation between the inhibitory response and the summed signal intensity of the four compound classes CHO, CHN, CHNO and CHNOS with the CHO group correlating strongest with luminescence inhibition. The signal intensity of all detected compounds correlated strongly with both assays and also with the averaged PM_{2.5} mass concentration of the filter sampling periods. Hence, a correlation between the PM_{2.5} mass concentration and both assays could also be observed. No positive correlation between the TCP signal intensities and AChE inhibition was detected, although TCP is described as an AChE inhibitor with different potency depending on the respective isomers (Winder and Balouet, 2002). Possibly this outcome is related to the absence of the tri-*ortho* isomer (TOCP) in jet engine oils and aviation-related ultrafine particles as mentioned in a previous study (Ungeheuer et al., 2021). Positive correlations with both bioassays were obtained for TPhP, CDP, DPP and TEP. TPhP has been described as an AChE inhibitor and endocrine disruptor (Shi et al., 2018). Surprisingly, no distinct correlation between the sum of CHOP compounds and both bioassays was observed. OP1EO as well as PSC showed a positive correlation with the outcome of both assays while NBBS only with the Microtox assay. Hence, OP1EO and the detected OPEs seem to be relevant regarding AChE inhibition effects. PM_{2.5} samples collected under the city wind direction showed the highest luminescence- (Microtox assay) and AChE inhibition and samples of the airport strike event the lowest inhibitions. The two different airport sampling conditions only differed slightly in the AChE inhibition assay. Generally, compared to the Microtox assay the AChE assay showed a higher sensitivity towards the PM_{2.5} filter extracts. Nevertheless, some samples with a high summed signal intensity showed a lower toxicity in the bioassays compared to lower intensity samples, indicating the strong influence of the chemicals composition and individual compound concentrations towards toxicity.

4.4 Nontarget Screening Exhibits a Seasonal Cycle of PM_{2.5} Organic Aerosol Composition in Beijing

This chapter describes the content of the fourth paper of this study (Ma et al., 2022), which focuses on the chemical characterization of Beijing PM_{2.5} organic aerosol by non-target screening. The large data set was analysed for seasonal variation in chemical composition using hierarchical cluster analysis and conclusions were drawn about possible sources.

The identification of organic aerosol (OA) sources is essential in order to reduce emissions by developing mitigation strategies. Therefore, identification of the OA chemical composition and related chemical transformation processes is needed. Several studies applied high-resolution mass spectrometry to investigate haze episodes in Beijing and identified anthropogenic emissions as an influencing factor (Bryant et al., 2020; Wang et al., 2018). Within this study non-target screening and hierarchical cluster analysis (HCA) was applied on 172 (including 10 blank samples) ambient PM_{2.5} filters from Beijing, analysed by ultra-high performance liquid chromatography/heated electrospray ionization/Orbitrap high-resolution mass spectrometry (UHPLC-ESI-HRMS) in order to reduce the complexity of the measured chemical composition. The twenty-four hours integrated samples were collected over a period of 13 months at Beijing University of Chemical Technology (BUCT) (Liu et al., 2020). In parallel OA was measured using a Time-of-Flight Aerosol Chemical Speciation Monitor (ToF-ACSM, more details see Cai et al. (2020)). Mean PM_{2.5} mass concentrations were calculated based on data from the Wanliu, Gucheng, Wanshouxigong, and Guanyuan monitoring stations, as the ToF-ACSM provides only non-refractory PM_{2.5} data. UHPLC-ESI-HRMS measurements in the negative mode were conducted with similar settings as described in the previous studies. For non-target screening Compound Discoverer (CD, version 3.2, Thermo Fisher Scientific) was used to obtain peak features in dependence on retention time and mass-to-charge ratio (m/z) for compound identification. Filtering for duplicates, background correction and applying a signal intensity sample-to-blank ratio of > 3 led to a total of 2136 compounds. The identified compounds were grouped into six classes CHO_a, CHO_n, CHNO, CHNOS, CHOS, and others, based on their elemental composition. To determine whether molecules contain double- and triple-bonds and ring-structures the double bond equivalent can be calculated. This value is used to calculate the aromaticity equivalent (X_c) (Yassine et al., 2014) for identification of (poly)aromatic compounds considering also significant alkylation (Daellenbach et al., 2019). Based on X_c the class of CHO containing compounds is divided into aromatic (CHO_a) and non-aromatic

(CHOn). The HCA was performed using Matlab (Mathworks) in order to merge samples and detected organic compounds (including peak areas) into clusters of similar temporal behaviour and chemical characteristics. Accordingly, the data input comprised of 1323 compounds with 1097 unambiguously identified molecular formulas making up 94% of the non-target screening detected peak area. This reduced set of compounds was utilized as the input of a large number of small peak signals could bias the HCA.

Seasonal variability of the organic aerosol chemical composition

In winter the compound classes CHOa and CHNO contributed 17% and 38% to the overall signal intensity. Emissions of those compounds are presumably attributable to intensified solid fuel burning during winter time (Steimer et al., 2020). In summer, both compound classes only contributed 8% and 6% to the total signal intensity. Generally, the total intensity of organic compounds was largest in the winter period. CHOn, CHOS and CHNOS compounds made up 16%, 14% and 3% of the overall signal intensity in winter. In contrast, CHOn compounds contributed 30% to the summer total signal intensity. This could be the result of increased biogenic emissions in the summer period, which was supported by the identification of certain compounds as oxidation products of volatile biogenic emissions based on MS/MS-spectra and retention time (Vogel et al., 2019). CHOS and CHNOS compounds contributed up to 30% and 9% to the summer overall signal intensity.

Based on the HCA and PM_{2.5} mass concentrations the samples were separated into summer high (SH) and low (SL) PM, and winter high (WH) and low (WL) PM. CHOS compounds contributed with 40% to the SH cluster signal intensity, whereas to cluster SL only with 12%. As most of the detected aliphatic organosulphates were only present in the SH cluster, their formation could enhance the organic aerosol mass in summer Beijing. In the winter clusters the chemical composition was comparable, indicating rather constant emission sources and formation processes. The total signal intensity in WH was much higher than in WL, explainable by the increased wind speed during both periods of low-pollution, therefore the difference in OA could be determined by aerosol accumulation.

Analysing the H/C- and O/C ratio of Cluster A in the Van Krevelen-space pointed out that CHNO and CHO aromatic compounds are prominent in the winter period. Within the two detected homologous series ($C_{5+n}H_{3+2n}NO_3$ ($n = 1-5$), $C_{5+n}H_{3+2n}NO_4$ ($n = 1-4$)) the largest signals were identified as 4-nitrophenol ($C_6H_5NO_3$) and 4-nitrocatechol ($C_6H_5NO_4$) by matching the fragmentation patterns and retention times with the authentic standards. Nitroaromatics are emitted by biomass and coal burning and also by vehicular fuel combustion

(Yuan et al., 2021). Furthermore, a tracer for naphthalene oxidation, monohydroxy benzoic acid ($C_7H_6O_3$), was tentatively identified (Kautzman et al., 2010). CHOa compounds had the highest intensities in cluster B, with the largest peak signal identified as phthalic acid ($C_8H_6O_4$) possibly attributable to anthropogenic emissions (Wang et al., 2021). Alkylorganosulphates tentatively identified in cluster A and B are mentioned as tracers for diesel fuel emissions (Blair et al., 2017). Accordingly, the chemical composition of cluster A and B could be strongly influenced by traffic emissions and solid fuel combustion. Cluster C was dominated by CHOS and CHNOS compounds, their high H/C- and O/C ratios suggest a high aliphatic character and oxidation state, respectively. Some of the observed aliphatic organosulphates are described as transformation products of liquid fossil fuel emissions (Tao et al., 2014). Therefore, this cluster of organosulphates showed distinct contributions of liquid fossil fuel emissions and also of biogenic emissions as monoterpene-derived nitrooxy-organosulphates ($C_{10}H_{17}NO_7S$, (Brüggemann et al., 2020)) and isoprene-derived organosulphates ($C_5H_8SO_7$, (Surratt et al., 2008)) were detected as well. In cluster D mainly CHOn compounds appeared, while the detection of α -pinene tracers like MBTCA ($C_8H_{12}O_6$) and pinic acid ($C_9H_{14}O_4$) indicates contributions of biogenic emission sources (Müller et al., 2012; E. Jenkin et al., 2000). Nevertheless, anthropogenic sources could also have contributed to this cluster.

To gain more insight into the chemical composition of clusters A-D, the average response of eight surrogate standards was determined and used for quantification, although this approach is subject to uncertainty. 4-nitrophenol and 4-nitrocatechol showed the highest signal response, their average was used for quantification of the cluster A and B nitroaromatics. Quantification of the CHOa compounds in cluster A and B was conducted using the average response of 5,7-dihydroxy-4-phenyl-coumarin, phthalic acid and benzoic acid. For the organosulphates in cluster C, camphor-10-sulphonic acid was utilized (Brüggemann et al., 2019) and for cluster D the average response of MBTCA and pinic acid.

During the residential-heating period (cluster A and B), aromatic compounds showed an increasing trend supporting the assumption of OA emissions related to traffic- and solid fuel combustion. Aliphatic organosulphur marker compounds for traffic emissions showed a lower abundance in summer, possibly due to enhanced higher boundary layer mixing and chemical degradation. Clusters C and D showed a strong positive correlation, indicating similar biogenic sources as the compounds are also more abundant in summer. In addition, the influence of sulphate on the secondary formation of organosulphates is shown, since cluster C compounds and the sulphate mass concentration increase in parallel (Wang et al., 2018). At the same time, another indication is given that various compounds from cluster D are likewise affected by

anthropogenic activities, since their occurrence is also relatively high in winter. It is worthwhile to mention that, based on the concentration time series of the compounds of the individual clusters, a distinct seasonal cycle can be observed while the sum concentration of the four clusters does not show this trend. Since, the OA time series measured by ACSM also does not exhibit a seasonal variation and showing a strong correlation with the sum of the quantified clusters, evidence is given that the OA seasonal cycles are well described by the cluster analysis. Although, only ~11-14% of the total OA could be explained, seasonal variations are clearly shown by this study. Traffic and solid fuel combustion emissions are represented by cluster A and B, making up 76% of the combined four clusters in winter and 15% in summer. Cluster D contributed with 60% in summer and 17% in winter. Summer haze periods are characterized by increased organosulphate formation. Overall, by combining non-target screening with HCA, it was possible to seasonally discriminate between high and low PM samples. Furthermore, the variation of the detected aerosol chemical composition was determined. The composition patterns allowed conclusions about the sources of the organic compounds with the applied quantification method enabling the observation of trends.

5. Publications

5.1 Identification and source attribution of organic compounds in ultrafine particles near Frankfurt International Airport



Identification and source attribution of organic compounds in ultrafine particles near Frankfurt International Airport

Florian Ungeheuer¹, Dominik van Pinxteren², and Alexander L. Vogel¹

¹Institute for Atmospheric and Environmental Sciences, Goethe University Frankfurt, 60438 Frankfurt am Main, Germany

²Atmospheric Chemistry Department (ACD), Leibniz Institute for Tropospheric Research (TROPOS), 04318 Leipzig, Germany

Correspondence: Alexander L. Vogel (vogel@iau.uni-frankfurt.de)

Received: 19 October 2020 – Discussion started: 4 November 2020

Revised: 28 January 2021 – Accepted: 30 January 2021 – Published: 12 March 2021

Abstract. Analysing the composition of ambient ultrafine particles (UFPs) is a challenging task due to the low mass and chemical complexity of small particles, yet it is a prerequisite for the identification of particle sources and the assessment of potential health risks. Here, we show the molecular characterization of UFPs, based on cascade impactor (NanoMOUDI) samples that were collected at an air quality monitoring station near one of Europe's largest airports, in Frankfurt, Germany. At this station, particle-size-distribution measurements show an enhanced number concentration of particles smaller than 50 nm during airport operating hours. We sampled the lower UFP fraction (0.010–0.018, 0.018–0.032, 0.032–0.056 μm) when the air masses arrived from the airport. We developed an optimized filter extraction procedure using ultra-high-performance liquid chromatography (UH-PLC) for compound separation and a heated electrospray ionization (HESI) source with an Orbitrap high-resolution mass spectrometer (HRMS) as a detector for organic compounds. A non-target screening detected ~ 200 organic compounds in the UFP fraction with sample-to-blank ratios larger than 5. We identified the largest signals as homologous series of pentaerythritol esters (PEEs) and trimethylolpropane esters (TMPEs), which are base stocks of aircraft lubrication oils. We unambiguously attribute the majority of detected compounds to jet engine lubrication oils by matching retention times, high-resolution and accurate mass measurements, and comparing tandem mass spectrometry (MS^2) fragmentation patterns between both ambient samples and commercially available jet oils. For each UFP stage, we created molecular fingerprints to visualize the complex chemical composition of the organic fraction and their average car-

bon oxidation state. These graphs underline the presence of the homologous series of PEEs and TMPEs and the appearance of jet oil additives (e.g. tricresyl phosphate, TCP). Targeted screening of TCP confirmed the absence of the harmful tri-*ortho* isomer, while we identified a thermal transformation product of TMPE-based lubrication oil (trimethylolpropane phosphate, TMP-P). Even though a quantitative determination of the identified compounds is limited, the presented method enables the qualitative detection of molecular markers for jet engine lubricants in UFPs and thus strongly improves the source apportionment of UFPs near airports.

1 Introduction

Ultrafine particles (UFPs) are particles with a diameter of less than 100 nm that are strongly influenced by primary emissions in the urban environment (Allan et al., 2010). Current observations indicate that airports are major sources of UFPs (Yu et al., 2012; Keuken et al., 2015; Yu et al., 2017; Fushimi et al., 2019), but also road traffic and (biogenic) secondary organic aerosol are possible sources for nanoparticles contributing to the overall ultrafine-particle mass in urban areas (Zhu et al., 2002a, b; Morawska et al., 2008; Paasonen et al., 2016; Rönkkö et al., 2017). Measurements in the vicinity of Schiphol Airport (the Netherlands) concluded that road traffic contributes less to the UFP burden compared to air traffic (Keuken et al., 2015).

With increasing numbers of flight operations worldwide, aircraft emissions will become increasingly relevant regarding the long-term development of local and global air pollu-

tion and its impact on global radiative forcing (Lee et al., 2009; Masiol and Harrison, 2014; Yu et al., 2017). Forecasts indicate an increase in flights in Europe in the range of $1.9\% \text{ yr}^{-1}$, with 16.2 million movements in 2040 (Eurocontrol, 2018). Due to the coronavirus pandemic, however, the European flight traffic in 2020 declined by 55 % compared to 2019 (Eurocontrol, 2021). Current forecasts predict a full recovery of flight movements between 2024 and 2029, depending on the pandemic course (Eurocontrol, 2020). UFPs can be transported over long distances towards urban areas (Keuken et al., 2015; Hudda and Fruin, 2016), and although they have very low mass, they can cause oxidative stress, inflammatory reactions, and other adverse health effects (Jonsdottir et al., 2019; Schraufnagel, 2020). In contrast to larger-sized particles, UFPs are able to penetrate the pulmonary alveoli and can enter the bloodstream (Yang and Omaye, 2009). At the same time, studies indicate that UFPs have an influence on humans via different mechanisms compared to $\text{PM}_{2.5}$ and are also able to create synergetic effects with transition metals (Costa and Dreher, 1997; Campen et al., 2001; World Health Organization, 2013). Still, the molecular composition of ambient UFPs and their effects on human health are only poorly understood, primarily because of a lack of the deployment of specific and sensitive chemical measurement approaches.

Various studies examined the exhaust of aircraft and found dependencies between particle emissions, their chemical composition, engine design, and the engine operating state. It is stated that the volatile organic fraction of the emitted particles is increasing through photochemical ageing (Kılıç et al., 2018), and the oxidized organic fraction tends to condense on nucleation-mode particles (Wey et al., 2007; Yu et al., 2017). The non-volatile fraction is dominated by black carbon. The ratio of volatile organics to non-volatile organics varies mainly depending on the operating state and the used jet fuel (Timko et al., 2010; Timko et al., 2013; Beyersdorf et al., 2014; Keuken et al., 2015). It appears that black carbon is a minor fraction of airport-related particulate emissions (Keuken et al., 2015), and it is often distinguished between the idle and the take-off status of aircraft.

Further studies identified jet engine oil constituents in airport-located UFPs (Yu et al., 2010, 2012, 2019; Timko et al., 2010; Fushimi et al., 2019). This is a consequence of the jet engine design, where rotating parts of the turbines need to be lubricated, and other parts like bearings need to be cooled. Due to a technically required venting system, nanometre-sized oil droplets are released into the atmosphere (Yu et al., 2010). Depending on the seal tightness, the overall consumption of jet engine oil can amount to up to 0.6 L h^{-1} per jet engine (Boyce, 2012), of which a part is emitted into the atmosphere.

The exposure of turbine and hydraulic oils to aircraft crews and ground staff has been linked to health effects such as disorientation, headaches, respiratory problems, and weakness (van Netten and Leung, 2000; Winder and Balouet, 2001,

2002). These symptoms, likely induced through an exposure to organophosphorous compounds, are summarized under the expression organophosphorus-induced delayed neuropathy (OPIDN). One possible etiological factor is the inhibition of the neurotoxic esterase (NTE) by organophosphorous compounds, which are present as additives in aircraft lubrication oil (Freudenthal et al., 1993; Ehrich et al., 1993; Eyer, 1995; O'Callaghan, 2003). However, the understanding of health effects from potentially harmful chemicals formed during aircraft operations requires further elucidation as it has been shown that, for example, tricresyl phosphate exposure from bleed air in aircraft cabins is below effect thresholds and cannot explain observed symptoms (de Boer et al., 2015).

Therefore, it is important to determine the chemical composition of UFPs near airports in order to identify their sources during airport operations, to assess further possible detrimental effects on human health, and finally to mitigate their emission. Due to the low mass of UFPs, the typical sampling and extraction methods need to be refined in order to characterize particles with aerodynamic diameters $< 56 \text{ nm}$, requiring detection limits of low picogram levels of single organic molecules. Here, we describe an offline method combining size-resolved UFP sampling with target and non-target screening by ultra-high-performance liquid chromatography (UHPLC) coupled to high-resolution mass spectrometry (HRMS) in order to shed light on the chemical composition of airport-related UFPs. The overall aim of this study was to develop an analytical routine that allows the identification of as many compounds contributing to the particle mass as possible. Within the scope of this study, we compare the molecular-composition pattern of 22 size-resolved ambient-UFP samples with the composition of five different jet engine lubrication oils. Therefore, our results provide an overview of the chemical composition of UFPs near large international airports, covering various aircraft engine designs, operating conditions, fuels, and jet engine lubrication oils.

2 Methods

2.1 Frankfurt Airport – measuring site

Frankfurt Airport is one of the largest airports in Europe, with more than 500 000 flight operations in 2019, shared over four runways. It is located in the Rhine–Main metropolitan area within a distance of around 12 km to the city centre of Frankfurt. In 2019 more than 70.5 million passengers and $2.1 \times 10^6 \text{ t}$ of cargo were transported, with a kerosine consumption of around $5.5 \times 10^6 \text{ m}^3$ (Fraport AG, 2020). The coronavirus pandemic caused a decline in flight movements by 58.7 % in 2020 compared to 2019. The transported cargo decreased by 8.3 % and passenger numbers by 73.4 % (Fraport AG, 2021).

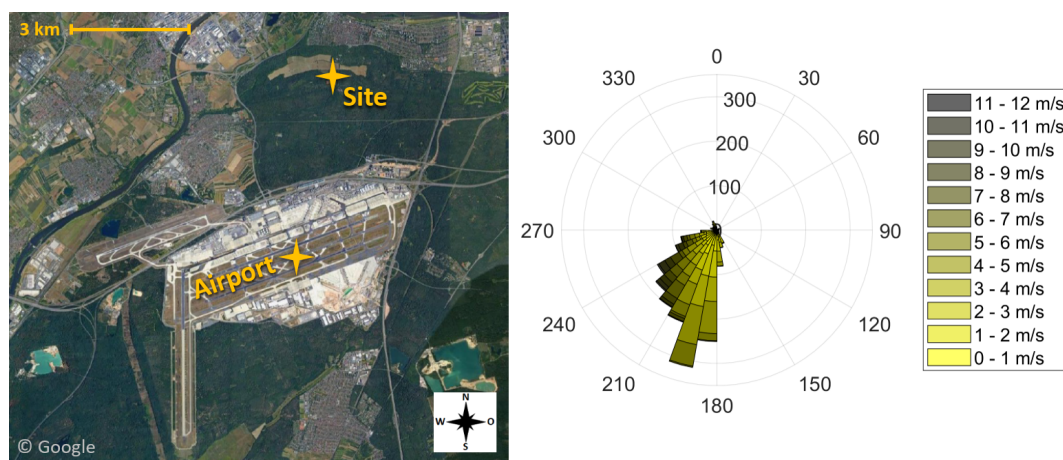


Figure 1. Illustration of the sampling site at a distance of 4 km to Frankfurt Airport (pictures © 2020 AeroWest, GeoBasis-DE/BKG, GeoContent, Landsat/Copernicus, Maxar Technologies; map data © 2020 Google). The wind rose indicates the wind direction during the eight sampling periods of the campaign. Data provided by the meteorological station at Frankfurt Airport (International Civil Aviation Organization, ICAO, code: EDDF) of the Deutscher Wetterdienst (DWD).

Since September 2017 the size distributions of ambient particles, including the ultrafine fraction, have been monitored at an air quality monitoring station of the Hessian Agency for Nature Conservation, Environment and Geology 4 km north of Frankfurt Airport (Fig. 1). It is located in a forested area with no highly frequented streets within 1 km distance. This sampling station is considered representative of the outflow emissions of highly frequented airports.

2.2 Sampling

We used a Micro Orifice Uniform Deposition Impactor (Nano-MOUDI; Model 115, MSP, Minneapolis, MN, USA), which consists of a 13-stage impactor system that is able to collect size-resolved UFPs on the last four stages. However, we only sampled on the last three stages (aerodynamic diameters between 0.010–0.018, 0.018–0.032, and 0.032–0.056 μm) since particle-size-distribution measurements show the highest number concentrations for particles smaller than 50 nm (Rose and Jacobi, 2018). This type of low-pressure cascade impactor was already used by other research groups for analysis of atmospheric and industrial particulate matter (Cena et al., 2014; Chen et al., 2016; Fushimi et al., 2019).

The Nano-MOUDI was installed at the air quality monitoring site in Frankfurt Schwanheim (Fig. 1). We sampled ambient air without a pre-impactor inlet through a stainless-steel tube (ID: 1 in.; length: 2 m) towards the Nano-MOUDI, with a total sampling flow rate of 1.8 $\text{m}^3 \text{h}^{-1}$. The sampling on the last three stages was conducted with a flow rate of 0.6 $\text{m}^3 \text{h}^{-1}$. The deposition of particles $> 0.056 \mu\text{m}$ on the upper 10 stages and the sampling of ambient UFPs on the last three stages were carried out using aluminium foils (TSI; $\text{Ø} \times \text{THK}$: 47 \times 0.015 mm). To limit a bounce-off of larger

particles to the lower stages, the foils for the upper 10 stages were coated with Apiezon[®] L grease. Therefore, after baking out the filters for 30 min at 300 °C, a 1 cm section of the Apiezon[®] grease was dissolved in 100 mL *n*-hexane, and each foil was evenly coated by adding six droplets of the mixture. After drying for 24 h in a fume hood, each single foil was stored in a glass petri dish. The foils for the UFP sampling were heated at 300 °C for 30 min and then stored in metal boxes until sampling.

Sampling took place from August to October 2019 exclusively during a southerly wind direction and during the airport operating hours (05:00–23:00 CET). Sampling times varied between 18 and 54 h (Table S1 in the Supplement) in order to accumulate sufficient mass for analysis. Shortly after sampling, the filters were stored in metal boxes at -20 °C to prevent subsequent evaporation or transformation processes. The final filter loadings depend on sampling time, meteorological conditions, and operating state of the airport. Although the particle emissions of aircraft engines depend on the actual thrust (Timko et al., 2014; Lobo et al., 2015; Yu et al., 2017), we assume that we sampled a mixture of UFPs that represent different aircraft engines under various operating states. Hence, the collected samples reveal the average UFP emissions of the whole airport and not of individual engines or operating conditions. Due to no strict compliance with the night flight ban between 23:00–05:00 CET and further urban and industrial sources in the other wind directions, it was not feasible to collect isolated background samples. We collected field blanks on the last three stages for 115 h without active sampling air flow and processed them analogously to the UFP samples.

2.3 Filter extraction

As a consequence of the low mass of the sampled UFPs (sub-microgram range of total particle mass after 30–50 h of sampling), the extraction method was developed in order to achieve the highest possible extract concentration. Simultaneously, no pre-concentration step through solvent evaporation was conducted in order to prevent volatilization of target compounds. Owing to the strongly adsorptive behaviour of the jet engine oil constituents, no filtration step of the solvent extracts was implemented. Various solvents were tested regarding their ability to dissolve the jet engine oil target compounds and the overall particle mass. Pure organic solvents provided a higher extraction efficiency than mixtures with water and similar efficiencies to mixtures of acetonitrile and methanol. The tests were based on UFP filter extractions with different solvents (100 % methanol; 50 % acetonitrile, 50 % methanol; 60 % methanol, 40 % water; 60 % acetonitrile, 40 % water) and evaluated based on the non-target-analysis-generated identifications and corresponding signal intensities. Due to the use of methanol (Optima[®] LC/MS grade, Thermo Fisher Scientific) and water (Milli-Q, Merck) as the UHPLC solvents, pure methanol was used for the filter extraction.

A circular section with a diameter of 2.5 cm was cut out of each foil sample, which were located below the array of the nozzles of each impactor stage. It is worth mentioning that the region of deposited UFPs on the foil surface was generally not visible. The resulting sections were cut in small pieces (approximately 2.5 mm × 2.5 mm) with ceramic scissors and extracted two times with 100 and 50 μL, respectively, for 20 min each on an orbital shaker (300 rpm). We avoided ultrasonic extraction due to a possible formation of free radicals, which can lead to chemical transformation of the original sample composition (Riesz et al., 1985). The extraction was conducted in glass vials equipped with flat-bottom micro inserts with a maximal volume of 200 μL (LLG Labware; Ø × H: 6 × 31 mm) to ensure a complete filter surface covering and then pipetted into 100 μL micro inserts with conical bottoms (VWR; Ø × H: 6 × 31 mm) to guarantee a complete UHPLC injection of 5 μL in the autosampler. Altogether 22 filter samples and 3 field blanks were analysed.

2.4 Jet engine lubrication oils

Jet engine oils are made of a base stock material like pentaerythritol esters or trimethylolpropane esters and different additives. Organophosphate additives are used as anti-wear agents and metal deactivators (Wyman et al., 1987; Du Han and Masuko, 1998), whereas amine constituents serve as stabilizers (Wu et al., 2013) (Table S2).

In order to characterize UFPs and screen for the molecular composition of jet engine oil, we analysed five different jet engine oils of various brands. The oils were selected regarding the recommended oil brand of engine manufacturers.

The Mobil Jet Oil II (ExxonMobil, Irving, TX, USA) has the highest market share (Winder and Balouet, 2002), whereas the market share of the other oils (Mobil Jet Oil 254 (ExxonMobil, Irving, TX, USA), Aeroshell 500 (Royal Dutch Shell, The Hague, Netherlands), Turbo Oil 2197 and 2380 (Eastman, TN, USA)) is unknown.

2.5 UHPLC–HRMS method

The chemical characterization of the airport filter samples was realized by using ultra-high-performance liquid chromatography (UHPLC) (Vanquish Flex, Thermo Fisher Scientific) and heated electrospray ionization (HESI) coupled to an Orbitrap high-resolution mass spectrometer (HRMS) (Q Exactive Focus Hybrid Quadrupole-Orbitrap, Thermo Fisher Scientific) as a detector. The chromatographic separation was achieved by using a reversed-phase column (Accucore C₁₈, 150 × 2.1 mm, 2.6 μm particle size, Thermo Fisher Scientific), operated in gradient mode and thermostated at 40 °C (still air). Ultrapure water (18.2 MΩ cm; Millipak[®] Express 40: 0.22 μm, Millipore; Milli-Q[®] Reference A+, Merck) with 0.1 % formic acid (by volume; solvent A) and methanol (Optima[®] LC/MS grade, Thermo Fisher Scientific) with 0.1 % formic acid (solvent B) were used as the UHPLC solvents. Formic acid (LiChropur[®], Merck) with a purity of 98 %–100 % was used to improve the chromatographic separation and ionization in the positive mode. Due to the high fraction of nonpolar compounds in the samples, the UHPLC chromatography started with 60 % solvent B (0–0.5 min), was then increased to 90 % (0.5–11 min), and then was ramped up to 99 % (11–16 min). The high-organic-solvent starting conditions allow the injection of large sample volumes of organic solvents without compromising the chromatographic separation. In the end, solvent B was reduced to 60 % (16–17 min), and the system was allowed to equilibrate for the subsequent measurement within 3 min. The overall method duration was 20 min, with a flow rate of 400 μL min⁻¹ and an injection volume of 5 μL. The ionization for the mass spectrometric detection was conducted by HESI in positive and negative mode. The HESI settings in positive mode were 3.5 kV spray voltage, 40 psi sheath gas (nitrogen), 8 psi auxiliary gas (nitrogen), and 350 °C gas temperature. The negative mode was operated with the same settings but with a spray voltage of 2.5 kV. The scan range in the positive mode was from 150 to 750 and in the negative mode from 50 to 700 mass-to-charge ratio (m/z) with a resolution of ~ 70 k at m/z 200. In negative-mode molecular ions ($[M - H]^-$) are produced by deprotonation, whereas in positive-mode molecular ions ($[M + H]^+$, $[M + Na]^+$) are generated by adduct formation. In order to gain structural information of the single molecules, a data-dependent MS² (dd-MS²) method was used with MS data recorded in profile mode.

The limit of detection (LOD) and limit of quantification (LOQ) of tri-*o*-cresyl phosphate (TCP) and pentaery-

thritol tetrahexanoate ($C_{29}H_{52}O_8$) were determined by external calibration according to the standard DIN 32645 of the German Institute for Standardization (DIN). For tri-*o*-cresyl phosphate ($\geq 97.0\%$; Sigma-Aldrich) and for pentaerythritol tetrahexanoate (95%; Carbosynth Ltd), we calibrated with five points in the range of $0.001\text{--}1\text{ ng }\mu\text{L}^{-1}$. Each calibration point was measured three times in succession. We determined the LOD of pentaerythritol tetrahexanoate as $0.007\text{ ng }\mu\text{L}^{-1}$ and the LOQ as $0.018\text{ ng }\mu\text{L}^{-1}$. For tricresyl phosphate we achieved an LOD of $0.021\text{ ng }\mu\text{L}^{-1}$ and an LOQ of $0.060\text{ ng }\mu\text{L}^{-1}$. Both calibration curves show only a small linear-response range, which is likely due to their adsorptive behaviour on glass surfaces. Therefore, we used only three concentrations in the range of $0.001\text{--}0.1\text{ ng }\mu\text{L}^{-1}$ for the determination of the LOD and LOQ. Presumably, all the detected pentaerythritol esters and trimethylolpropane esters show a similar adsorption tendency like the used ester standard. Due to the adsorptive behaviour, quantification of the UFP constituents in ambient samples should preferentially be carried out by standard addition. We translate the results of the calibration into ambient-concentration LODs: an average sampling duration of 40 h with the Nano-MOUDI flow rate of $0.6\text{ m}^3\text{ h}^{-1}$ results in a sampled air volume of 24 m^3 . Reaching the LOD of pentaerythritol tetrahexanoate and tricresyl phosphate in a solvent extraction volume of $150\text{ }\mu\text{L}$ would require ambient-air concentrations of 44 and 131 pg m^{-3} (for each sampled size interval), respectively. However, we can project this calculation on ambient samples only under the assumption that no losses occur during sampling.

2.6 Non-target screening

The full-scan MS spectra analysis was carried out by the non-target-analysis software Compound Discoverer (CD) (version 3.2.0.261, Thermo Fisher Scientific), which was already validated regarding the qualitative and quantitative results by comparison with the non-target-analysis software MZmine2 (Vogel et al., 2019). The Compound Discoverer software identifies substances and determines their molecular formula depending on their exact mass, isotopic signature, and MS^2 fragmentation pattern and by database matching of MS^2 fragmentation spectra (database: <https://www.mzcloud.org/>, last access: 11 July 2020).

We iteratively optimized the non-target-analysis workflow (see Supplement Fig. S1 and Table S3 for the detailed settings of the CD workflow) in order to achieve the best possible characterization of the particles' chemical composition. The described jet engine oils were diluted to a concentration of $1\text{ }\mu\text{g mL}^{-1}$ in methanol (Optima[®] LC/MS grade, Thermo Fisher Scientific) and analysed with an identical non-target approach. The chromatograms of the jet engine oils, the UFP samples, and the field blanks were processed in one experiment in order to improve the software-based identification procedure. We filtered the non-target-analysis results with the following criteria: the sample signal must

be more than 5 times larger than the blank signal, the minimum area is 1.0×10^5 , and the minimum retention time is 0.7 min (column dead time peak at 0.6 min). A large signal at $m/z\ 399.2506 \pm 4\text{ ppm}$ ($[M + H]^+$ of tris(2-butoxyethyl) phosphate, $C_{18}H_{39}O_7P$) was manually filtered out prior to the graphical illustration because of its ubiquitous use as a plasticizer, flame retardant, and floor finish (Lewis et al., 2016). The peak areas of the compounds in the samples were background-corrected by subtracting the corresponding peak areas of the field blank. For the detection of the compounds, a mass tolerance of 5 ppm was allowed, whereas we reduced the mass tolerance for the molecular-formula prediction to 2 ppm. The allowed elemental combinations for the molecular formulae assignments were constrained to the limits of $C_{1\text{--}90}$, $H_{1\text{--}190}$, $O_{0\text{--}20}$, $N_{0\text{--}4}$, $S_{0\text{--}3}$, $P_{0\text{--}1}$, $Cl_{0\text{--}4}$, and $Br_{0\text{--}3}$. Finally, we classified the assigned molecular formulas into composition groups (CHO, CHN, CHNO, CHOS, CHNOS, CHOP, other), which helped to graphically illustrate the complex chemical composition of UFPs.

2.7 Fragmentation experiments

In order to gain structural information of the chemical species found by the non-target analysis, we conducted successive data-dependent full-scan and dd- MS^2 measurements in the discovery and confirmation mode, respectively. In a first measurement, we used the discovery mode to obtain the exact mass and possibly MS^2 spectra of abundant signals. In this mode, the mass spectrometer estimates a peak apex during acquisition of the chromatogram and triggers the recording of a fragmentation spectrum by higher-energy collisional dissociation (HCD) of the highly abundant signals. Subsequently, we analysed the discovery-mode data with CD, and we obtained a list of compounds that are significantly different from the blank. This list was loaded as an inclusion list for a second measurement of the samples. By this approach, we recorded high-quality MS^2 fragmentation spectra of the listed compounds of interest (even of the low-intensity compounds), allowing us to confirm the molecular structure and improve the accuracy of the database identification process. The MS^2 experiments were conducted with a normalized collision energy (NCE) of 30.

We used the different jet engine lubrication oils as qualitative identification standards with regard to the material safety data sheets (MSDSs) declaring the composition of the oils. With the help of the exact mass, retention time, and MS^2 fragmentation pattern of the jet oil constituents, we were able to unambiguously identify the oil-related compounds in ambient-UFP samples. In the case of TCP, the different structural isomers do not show different MS^2 fragmentation patterns. Here, we make use of different retention times for the unambiguous identification of tri-*o*-cresyl phosphate, enabling us to examine whether the *ortho*-isomer can be found in the jet oils and the ambient-UFP samples.

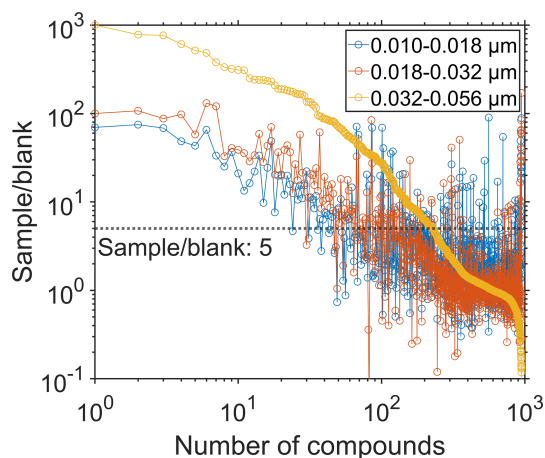


Figure 2. The sample-to-blank ratios of the detected compounds, averaged over all samples belonging to a certain size fraction (0.010–0.018, 0.018–0.032, 0.032–0.056 μm). Detection of the compounds was accomplished in positive-ionization mode. The sample-to-blank ratio of 5 was specified for data filtering and is displayed as a dashed horizontal line.

3 Results

3.1 Non-target screening and molecular fingerprints of UFPs

The non-target screening detected almost 1000 compounds in the positive-ionization mode. However, we observed the majority of these compounds at similar intensities also in the field blanks and hence excluded from the dataset. We find approximately 200 organic compounds at a sample-to-blank ratio > 5 in the largest size fraction (0.032–0.056 μm) based on the average of six samples. For the two smaller size fractions, we determined the sample-to-blank ratios based on the average of 2×8 samples (see Table S1). The two smaller size fractions yielded more than 100 organic compounds with a sample-to-blank ratio > 5 (Fig. 2). Averaged over all filters of the largest size fraction, we obtained sample-to-blank ratios > 100 for approximately 30 compounds in the positive-ionization mode. The particles in the size fraction 0.032–0.056 μm show a 5- to 10-times-higher signal intensity of the most abundant compounds as well as a larger number of compounds due to the larger mass concentration compared to the smaller size bins. The negative-ionization mode revealed only 16 compounds with the same data processing filter criteria.

For each size fraction, we use the molecular fingerprints (retention time vs. molecular weight (MW), Van Krevelen diagram, Kroll diagram, and Kendrick mass defect vs. MW) for illustration of the chemical composition of the organic fraction, which is shown in Fig. 3 for 0.032–0.056 μm particles. Molecular fingerprints of the size stages 0.010–0.018 and 0.018–0.032 μm are shown in Figs. S2 and S3, respectively.

Each circle represents a compound, and the colouring describes the molecular-composition group. Signals to which a molecular formula could not be assigned are classified as “other”. The area of the circles is proportional to the measured signal intensity. The measured mass-to-charge ratios (m/z) are converted into MW.

Figure 3a (retention time vs. MW) shows primarily CHO compounds. Group 1 represents mainly the homologous series of pentaerythritol esters ($\text{C}_{27-38}\text{H}_{48-70}\text{O}_8$). We found that Compound Discoverer falsely interprets ion signals as $[\text{M} + \text{H}]^+$ of the measured ions $[\text{M} + \text{Na}]^+$, $[\text{M} + \text{K}]^+$, and $[\text{M} + \text{NH}_4]^+$ of the pentaerythritol esters and hence suggests up to three likely false molecular formulas per ester molecule. These artefacts were manually removed based on the same retention time and exact mass difference to the molecular ions of the pentaerythritol esters. The native molecular fingerprint is displayed for comparison in Fig. S4. Pentaerythritol esters are used as a common base stock material for synthetic jet engine lubrication oils (Winder and Balouet, 2002) and therefore can be attributed to jet engine oil emissions. These synthetic oils are particularly used in aviation, while the base stock of automotive oils is made of a crude-oil fraction that consists mostly of petroleum hydrocarbons (Vazquez-Duhalt, 1989). Another jet engine oil base stock material of trimethylolpropane esters ($\text{C}_{27-34}\text{H}_{50-64}\text{O}_6$) (Wright, 1996) forms a homologous series in group 2. Group 3 can be mainly attributed to fragmentation, probably formed during the ionization of the pentaerythritol esters in the HESI source. The compounds in group 3 have the same retention times as the original pentaerythritol esters of group 1 but differ in their molecular weight, which can be explained by the neutral loss of fatty-acid fragments (e.g. $\text{C}_5\text{H}_{10}\text{O}_2$, $\text{C}_7\text{H}_{14}\text{O}_2$, $\text{C}_8\text{H}_{16}\text{O}_2$, and $\text{C}_{10}\text{H}_{20}\text{O}_2$). Although electrospray ionization is known as a very soft ionization technique, we observe different fragmentation products of the pentaerythritol esters, depending on the side chain length. In order to minimize fragmentation of the pentaerythritol esters, we tested different settings of the HESI source: the auxiliary gas heater temperature was reduced from 350 to 200 $^\circ\text{C}$ in 50 $^\circ\text{C}$ steps, and the spray voltage was reduced from 3.5 to 2.0 kV in 0.5 kV steps. Variation in both parameters, which were identified as the most important drivers of the ionization process, did not reduce fragmentation of the pentaerythritol esters. Besides the large CHO compounds at 5.2 min, which can likely be attributed to decanedioic acid-1,10-diethyl ester ($\text{C}_{14}\text{H}_{26}\text{O}_4$) and its fragments, we do not detect large contributions of other organic species in this size fraction. Only a small number of signals remain unidentified, appearing in the “other” composition group. Hence, the results of the non-target analysis suggest that the sampled UFPs are mainly composed of lubrication oils. However, other techniques might reveal the presence of additional compounds (e.g. metals, black carbon, inorganic compounds) which are not detected by the presented technique.

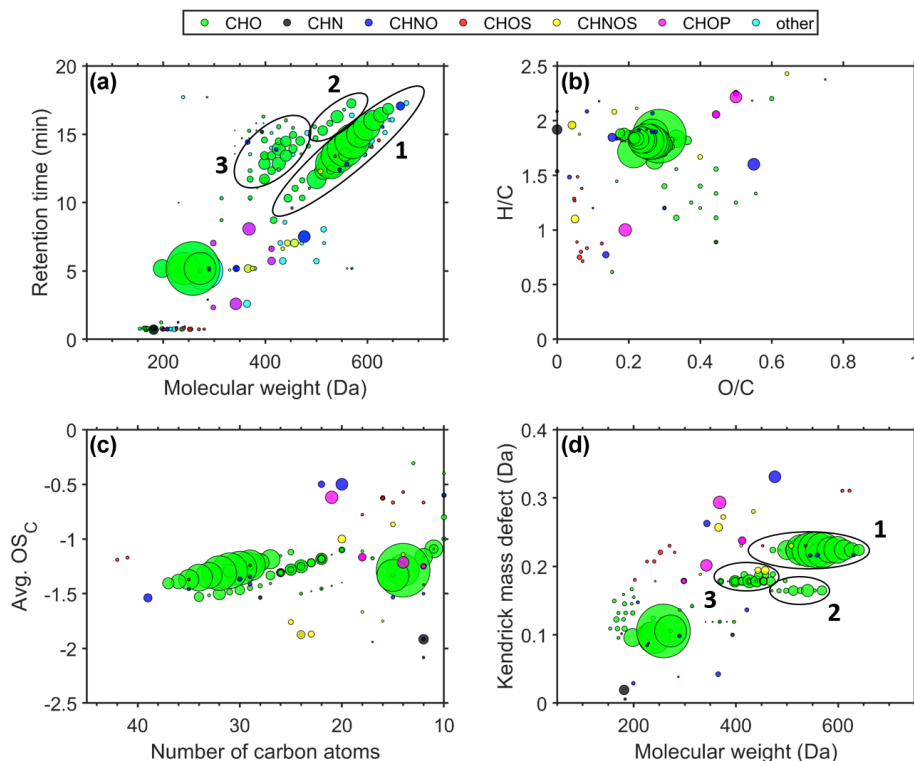


Figure 3. Molecular fingerprints – retention time vs. MW (a), Van Krevelen diagram (b), Kroll diagram (c), Kendrick mass defect vs. MW (d) – of six averaged airport-related ultrafine-particle samples in the size range of 0.032–0.056 μm .

The Van Krevelen diagram describes the different compounds regarding their hydrogen-to-carbon (H/C) and oxygen-to-carbon (O/C) ratios (Fig. 3b). Compounds that consist mainly of single-ring aromatic moieties have an H/C ratio around 1. Tricresyl phosphate, an anti-wear additive in synthetic jet oil, contains three single-ring aromatic (cresol) moieties. TCP appears in Fig. 3b as a magenta circle at H/C = 1 and O/C = 0.2. The majority of the detected compounds, however, are located in the upper part of the diagram (H/C > 1.5), which implies that most of the airport-related UFP constituents do not have an aromatic character. With O/C ratios below 0.6, it can also be stated that the UFPs do not become oxidized during the 4 km transport distance between the emission source and the monitoring station. The analysed jet engine lubrication oils show O/C ratios within the same range (0.2–0.4; Figs. S6–S10).

The average carbon oxidation state (avg. OS_C) versus the number of carbon atoms (Fig. 3c) is a way of characterizing the oxidation state of complex organic-compound compositions and is calculated according to Kroll et al. (2011). The diagram shows that the synthetic esters (CHO) are large molecules containing 27–37 carbon atoms, which implies a low vapour pressure and supposedly the ability to reside in the UFP fraction. The average carbon oxidation state was not corrected for oxygen atoms that are attached to non-carbon atoms. Thus, compounds with oxygen-containing functional

groups (e.g. oxygen atoms of the phosphate group in tricresyl phosphate) are shifted in the diagram towards seemingly higher OS_C values, but in fact the carbon atoms exhibit a lower average oxidation state. Also in this illustration, we find no evidence for oxidation products of airport-related lubrication oil emissions. These results are consistent with the objective to design lubrication oils with a stability against oxidation. For this purpose antioxidants such as N-phenyl-1-naphthylamine (C₁₆H₁₃N) and alkylated diphenyl amine (C₂₈H₄₃N) are added, which serve as radical scavengers (Wu et al., 2013). Even though tricresyl phosphate serves as an anti-wear agent in lubrication oils, it is also reported that this additive is able to enhance the oxidation inhibition ability of antioxidant mixtures (Duangkaewmanee and Petsom, 2011).

We illustrate the Kendrick mass defect (CH₂ base) vs. MW in order to identify homologous series of hydrocarbons (Fig. 3d). The Kendrick mass defect (KMD) is calculated by subtracting the Kendrick mass of the nominal mass (Equation 1). The Kendrick mass is defined as the IUPAC mass standardized on ¹²CH₂ with an exact mass of 14 Da (Kendrick, 1963).

$$\text{KMD} = \text{nominal mass} - \left(\text{IUPAC mass} \cdot \frac{14.00000}{14.01565} \right) \quad (1)$$

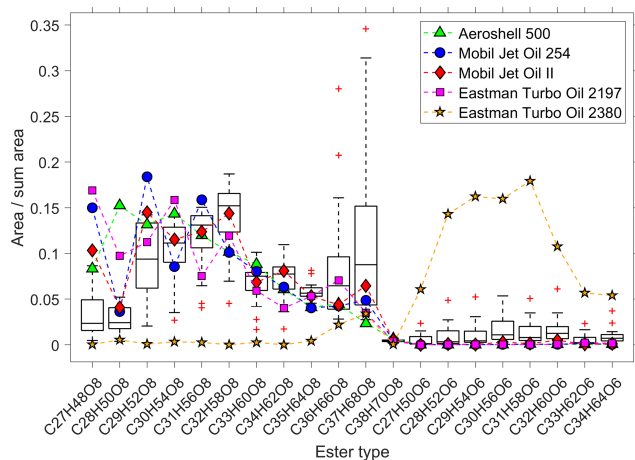


Figure 4. Comparison of the pentaerythritol- and the trimethylolpropane ester ratios of five different jet engine oils (coloured symbols) with the observed spread in 22 ambient-UFP samples (box plots). The y axis is the ratio of the peak area of each individual ester to the summed area of all esters. The horizontal line within the box indicates the median, and the bottom and top edges of the box indicate the interquartile range. The whiskers show the spread to the most extreme values, and outliers (outside $\pm 2.7\sigma$) are shown as red “+” symbols.

Thereby, compounds of a homologous series differing in the number of CH_2 groups align on a horizontal line. We observe the homologous series of pentaerythritol- and trimethylolpropane esters and their fragments as horizontal lines in Fig. 3d.

3.2 Composition pattern of synthetic esters

We analysed the molecular pattern of the synthetic esters by comparison between the UFP samples and the five different jet engine oils. Figure 4 shows the contribution of each individual ester molecule to the sum of all esters. The boxes illustrate the spread of the ester fraction in all 22 measured ambient-UFP samples, and the coloured symbols indicate the composition of the oil standards. We observe that the ester composition of four out of the five jet engine lubrication oils matches the ester composition in the UFP samples well, which confirms that these esters can be attributed to the specific source of jet engine oils. Furthermore, the Mobil Jet Oil II follows most closely the ambient pattern of the median level of the pentaerythritol esters (eight oxygen atoms), which is in line with the highest market share of this oil. The Eastman Turbo Oil 2380 consists of trimethylolpropane esters (six oxygen atoms) as the base stock, which are not a constituent of the other four jet engine oils. We observe a small but significant fraction of the trimethylolpropane esters in the ambient UFPs, indicated by the consistently higher values of the boxes (and the median) compared to the pentaerythritol-ester-based oils. This is presumably a result of a minor utilization of trimethylolpropane ester containing

jet engine lubrication oils in air traffic. Chromatograms of the various jet engine lubrication oils are shown in Fig. S5 and the individual molecular fingerprints as in Figs. S6–S10, showing the different base stock materials.

3.3 MS² fragmentation experiments

We used fragmentation experiments of the homologous series of pentaerythritol esters ($\text{C}_{27-38}\text{H}_{48-70}\text{O}_8$), N-phenyl-1-naphthylamine ($\text{C}_{16}\text{H}_{13}\text{N}$), alkylated diphenyl amine (bis(4-(1,1,3,3-tetramethylbutyl)phenyl)amine; $\text{C}_{28}\text{H}_{43}\text{N}$), tricresyl phosphate ($\text{C}_{21}\text{H}_{21}\text{O}_4\text{P}$), and the homologous series of trimethylolpropane esters ($\text{C}_{27-34}\text{H}_{50-64}\text{O}_6$) in order to verify the identity of the molecules in the ambient-UFP samples. These compounds have been described as molecular markers for jet engine lubrication oil emissions and are not present in automotive lubrication oils (Fushimi et al., 2019). Figure 5 shows the comparison between the fragmentation patterns of tricresyl phosphate (Fig. 5a), the alkylated diphenyl amine (Fig. 5b), and one of the pentaerythritol esters (Fig. 5c) in the UFP samples and the Mobil Jet Oil II by ExxonMobil, respectively.

The fragment at m/z 261.0674 ($\text{C}_{14}\text{H}_{14}\text{O}_3\text{P}$) is a fragment ion of tricresyl phosphate with only two aromatic moieties, whereas the fragment at m/z 91.0543 (C_7H_7) is the corresponding aromatic structure without the oxygen atom related to the phosphate group. Fragmentation of the alkylated diphenyl amine leads only to a slight formation of fragment ions, e.g. m/z 134.0964 ($\text{C}_9\text{H}_{12}\text{N}$), which is one of the two aromatic rings connected to the nitrogen atom and parts of one alkyl side chain. Hence it seems that the alkylated diphenyl amine additive features a higher stability compared to the other oil constituents with the used fragmentation settings. The pentaerythritol ester ($\text{C}_{29}\text{H}_{52}\text{O}_8$), exemplary of the ester base stock material, shows a characteristic fragmentation pattern. The fragment ion at m/z 399.2737 ($\text{C}_{22}\text{H}_{39}\text{O}_6$) is an ester molecule after the loss of one side chain ($\text{C}_7\text{H}_{13}\text{O}_2$), and the fragment ion at m/z 113.0960 ($\text{C}_7\text{H}_{13}\text{O}$) is an aliphatic side chain after ester bond cleavage. We were not able to obtain a clear fragmentation spectrum of N-phenyl-1-naphthylamine in the UFP samples as the detected signal intensity was not sufficient. This could be due to a minor usage of the additive in jet engine lubrication oils and a faster atmospheric degradation rate as it is utilized as a radical scavenger (Wu et al., 2013). Furthermore, the screening of the jet oils showed a matching MS² pattern of tricresyl phosphate and N-phenyl-1-naphthylamine with the mzcloud database.

3.4 TCP isomer characterization

Recent studies have reported that tricresyl phosphate exposure provokes detrimental health effects as it exhibits a neurotoxic potential functioning as an acetylcholinesterase inhibitor and also by acting as an endocrine disruptor (Chang

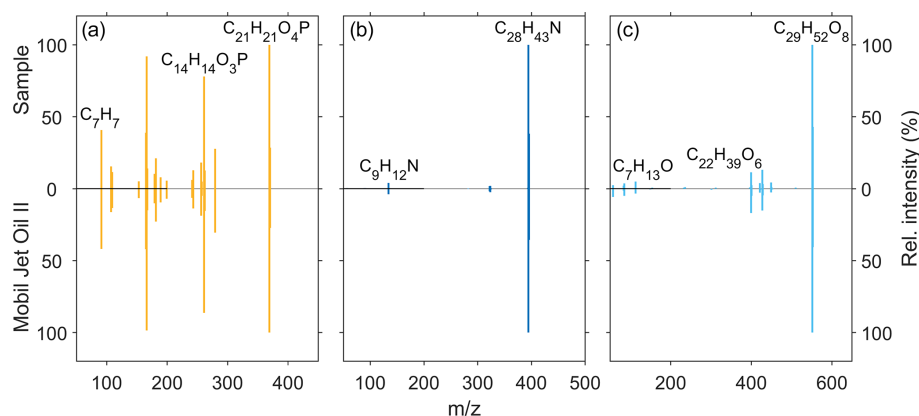


Figure 5. Comparison of the MS² fragmentation patterns of (a) tricresyl phosphate (C₂₁H₂₁O₄P), (b) alkylated diphenyl amine (C₂₈H₄₃N), and one (c) pentaerythritol ester (C₂₉H₅₂O₈) measured in an ambient-UFP sample (0.032–0.056 μm) (upward spectra) and the Mobil Jet Oil II by ExxonMobil (downward spectra).

et al., 2020; Ji et al., 2020). Different TCP isomers vary regarding their potential health effects, for which reason it is important to gain information about the isomer composition of tricresyl phosphate in UFPs. Therefore, we performed a targeted screening on tricresyl phosphate isomers using selected-ion monitoring (SIM). The tri-*ortho* isomer shows a peak at 7.82 min, whereas the TCP peak of the UFP sample elutes after 8.06 min, likely an overlapping peak of a mix of different *meta*- and *para*-isomers. The tri-*ortho*-isomer of tricresyl phosphate was not detected in the airport samples. This is in accordance with the reduction in the *ortho*-isomer fraction of tricresyl phosphate used as an additive for lubrication oils (Winder and Balouet, 2002; de Nola et al., 2008). Other studies have also reported that they were not able to identify the tri-*ortho* isomer of TCP in various sample types (Solbu et al., 2010, 2011). Although no tri-*ortho* isomer of TCP was detected, it is still worthwhile to consider that isomers with only one *ortho*-methyl group feature possibly a higher toxicity than isomers having methyl groups only in *meta*- and *para*-position (Hanhela et al., 2005).

We detect further organophosphate compounds like triphenyl phosphate (TPP) in the UFP samples, which likely originate from hydraulic oils. TPP is a high-production-volume chemical used as a flame retardant and likely has further sources other than airport operations. However, Solbu et al. (2010) have reported that ground maintenance of aircraft is also a possible source of organophosphates in the environment.

3.5 TMP-P formation from thermal decomposition of TMPE oils

Besides the common use of pentaerythritol esters as the base stock of lubrication oils, also trimethylolpropane esters (TMPEs) are in use. It is known that a combination of TMPEs with a phosphate additive proportion of only 2 % can result in the formation of the neurotoxin trimethylolpropane phos-

phate (TMP-P) (Callahan et al., 1989; Centers, 1992). The combination of pentaerythritol esters with phosphate additives does not lead to the formation of TMP-P (Wyman et al., 1987). Studies have shown that the formation of TMP-P occurs possibly with all phosphates, regardless of the structure, at temperatures between 250–750 °C. The reaction is probably not highly temperature-dependent due to the low activation energy (Wright, 1996). At the upper temperature limit, the formed TMP-P starts to decompose, implying that the actual yield of TMP-P depends on the balance between formation and degradation reactions (Callahan et al., 1989). TMP-P affects the nervous system by binding to γ -aminobutyric acid (GABA) receptors, especially at the picrotoxinin site, and therefore affects neurotransmission processes (Bowery et al., 1976, 1977; Mattsson, 1980; Simmonds, 1982; Ticku and Ramanjaneyulu, 1984).

In contrast to other studies (van Netten and Leung, 2000; Solbu et al., 2011), we detected TMP-P in the UFP samples, which could be the result of the continued use of TMPE-based lubrication oils. TMP-P was identified via fragmentation leading to a characteristic phosphate fragment. The analysed Eastman Turbo Oil 2380 shows a different pattern regarding the jet engine oil marker compounds compared to the other tested oils (Fig. 4). This oil is not based on a pentaerythritol but on a trimethylolpropane ester formulation. Callahan et al. (1989) identified the Exxon 2380 oil as a source of TMP-P formation, which is possibly the forerunner oil of the Eastman Turbo Oil 2380 tested here. In order to confirm the identified TMP-P, we simulated the thermal decomposition in a temperature experiment using the Eastman Turbo Oil 2380. The jet engine oil was heated to temperatures of 250–450 °C in 50 °C steps for 4 h. Analysing the oil after the temperature treatment, we were able to detect an emerging signal at m/z 179.0467 ($[M + H]^+$, TMP-P, C₆H₁₁O₄P) at temperatures starting from 400 °C. The appearing compound features the same retention time as de-

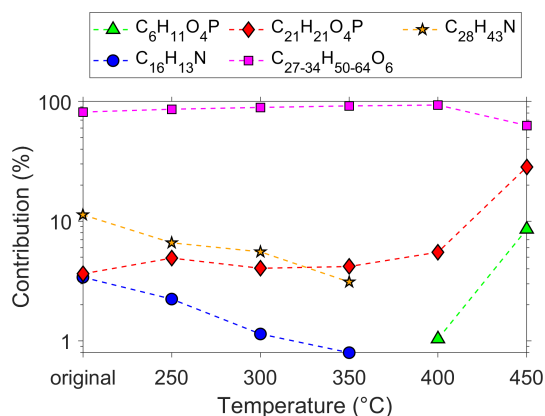


Figure 6. Development of the different constituents of the Eastman Turbo Oil 2380 during the temperature experiment. The contribution (%) is defined as the ratio of the area of one single compound relative to the total area of all jet oil constituents.

tected in the UFP samples, which speaks for the unambiguous identification of TMP-P. To our knowledge, this is the first detection of TMP-P in ambient UFPs. With increasing temperature, we observe the fraction of trimethylolpropane esters decreasing, whereas the fraction of TMP-P rises. The relative fraction of tricresyl phosphate also increases as it is temperature-stable in contrast to the esters. The fraction of the two amines (C₁₆H₁₃N, C₂₈H₄₃N) decreases between 250–350 °C, and from 400 °C onwards both compounds are not detectable anymore (Fig. 6).

4 Conclusions

In this study, we demonstrate a novel analytical approach (non-target analysis) that reveals the chemical composition of UFPs down to the size range of 10–18 nm. We find that jet oil emissions contribute to the non-refractory fraction of particles < 56 nm near Frankfurt Airport, with all specified constituents detectable by HESI in the positive-ionization mode. The analysis of the individual pattern of ester molecules and the comparison to jet oil standards revealed the presence of two different oil base stocks that emerge in the UFPs at Frankfurt Airport. Due to the identification of health-relevant organophosphorous compounds, future studies should perform toxicity testing and effect-directed chemical analysis in order to evaluate the health effects of UFPs from large airports. In this context, it is essential to quantify the contribution of potentially harmful compounds that are present in airport-related UFPs in future studies.

Data availability. The data shown in this study are available by request to the corresponding author (vogel@iau.uni-frankfurt.de).

Supplement. The supplement related to this article is available online at: <https://doi.org/10.5194/acp-21-3763-2021-supplement>.

Author contributions. FU wrote the paper; performed the field sampling, sample preparation, and measurement; and did the bulk of the data analysis. DvP provided the Nano-MOUDI and advised on particle sampling, data interpretation, and manuscript writing. ALV advised on data analysis, data interpretation, and manuscript writing; edited the manuscript; and directed the project administration.

Competing interests. The authors declare that they have no conflict of interest.

Acknowledgements. We thank Diana Rose, Florian Ditas, and Stefan Jacobi of the Hessian Agency for Nature Conservation, Environment and Geology for providing access to the air quality monitoring station. We also thank Anett Dietze of the Leibniz Institute for Tropospheric Research (TROPOS) for the filter preparation.

Financial support. This research has been supported by the Deutsche Forschungsgemeinschaft (DFG; German Research Foundation) (grant no. 410009325).

This open-access publication was funded by the Goethe University Frankfurt.

Review statement. This paper was edited by Drew Gentner and reviewed by two anonymous referees.

References

- Allan, J. D., Williams, P. I., Morgan, W. T., Martin, C. L., Flynn, M. J., Lee, J., Nemitz, E., Phillips, G. J., Gallagher, M. W., and Coe, H.: Contributions from transport, solid fuel burning and cooking to primary organic aerosols in two UK cities, *Atmos. Chem. Phys.*, 10, 647–668, <https://doi.org/10.5194/acp-10-647-2010>, 2010.
- Beyersdorf, A. J., Timko, M. T., Ziemba, L. D., Bulzan, D., Corporan, E., Herndon, S. C., Howard, R., Miake-Lye, R., Thornhill, K. L., Winstead, E., Wey, C., Yu, Z., and Anderson, B. E.: Reductions in aircraft particulate emissions due to the use of Fischer-Tropsch fuels, *Atmos. Chem. Phys.*, 14, 11–23, <https://doi.org/10.5194/acp-14-11-2014>, 2014.
- Bowery, N. G., Collins, J. F., Hill, R. G., and Pearson, S.: GABA antagonism as a possible basis for the convulsant action of a series of bicyclic phosphorus esters, *Br. J. Pharmacol.*, 57, P435–P436, 1976.
- Bowery, N. G., Collins, J. F., Hill, R. G., and Pearson, S.: t-Butyl bicyclo phosphate: a convulsant and GABA antagonist more potent than bicuculline, *Br. J. Pharmacol.*, 60, 275–276, 1977.

- Boyce, M. P.: Gas turbine engineering handbook, 4th Edn., Butterworth-Heinemann, Waltham, Mass., Elsevier, Amsterdam, 956 pp., 2012.
- Callahan, A. B., Tappan, D. V., Mooney, L. W., and Heyder, E.: Analysis of Hydraulic Fluids and Lubricating Oils for the Formation of Trimethylolpropane Phosphate (TMP-P), Naval Submarine Medical Research Lab, Groton, CT, 98 pp., 1989.
- Campen, M. J., Nolan, J. P., Schladweiler, M. C., Kodavanti, U. P., Evansky, P. A., Costa, D. L., and Watkinson, W. P.: Cardiovascular and thermoregulatory effects of inhaled PM-associated transition metals: a potential interaction between nickel and vanadium sulfate, *Toxicol. Sci.*, 64, 243–252, <https://doi.org/10.1093/toxsci/64.2.243>, 2001.
- Cena, L. G., Chisholm, W. P., Keane, M. J., Cumpston, A., and Chen, B. T.: Size Distribution and Estimated Respiratory Deposition of Total Chromium, Hexavalent Chromium, Manganese, and Nickel in Gas Metal Arc Welding Fume Aerosols, *Aerosol Sci. Tech.*, 48, 1254–1263, <https://doi.org/10.1080/02786826.2014.980883>, 2014.
- Centers, P. W.: Potential neurotoxin formation in thermally degraded synthetic ester turbine lubricants, *Arch. Toxicol.*, 66, 679–680, <https://doi.org/10.1007/BF01981509>, 1992.
- Chang, Y., Cui, H., Jiang, X., and Li, M.: Comparative assessment of neurotoxicity impacts induced by alkyl tri-n-butyl phosphate and aromatic tricresyl phosphate in PC12 cells, *Environ. Toxicol.*, 35, 1326–1333, <https://doi.org/10.1002/tox.22997>, 2020.
- Chen, X., Balasubramanian, R., Zhu, Q., Behera, S. N., Bo, D., Huang, X., Xie, H., and Cheng, J.: Characteristics of atmospheric particulate mercury in size-fractionated particles during haze days in Shanghai, *Atmos. Environ.*, 131, 400–408, <https://doi.org/10.1016/j.atmosenv.2016.02.019>, 2016.
- Costa, D. L. and Dreher, K. L.: Bioavailable Transition Metals in Particulate Matter Mediate Cardiopulmonary Injury in Healthy and Compromised Animal Models, *Environ. Health Persp.*, 105, 1053, <https://doi.org/10.2307/3433509>, 1997.
- de Boer, J., Antelo, A., van der Veen, I., Brandsma, S., and Lammermse, N.: Tricresyl phosphate and the aerotoxic syndrome of flight crew members – current gaps in knowledge, *Chemosphere*, 119, 58–61, <https://doi.org/10.1016/j.chemosphere.2014.05.015>, 2015.
- de Nola, G., Kibby, J., and Mazurek, W.: Determination of ortho-cresyl phosphate isomers of tricresyl phosphate used in aircraft turbine engine oils by gas chromatography and mass spectrometry, *J. Chromatogr. A*, 1200, 211–216, <https://doi.org/10.1016/j.chroma.2008.05.035>, 2008.
- Duangkaewmanee, S. and Petsom, A.: Synergistic and antagonistic effects on oxidation stability of antioxidants in a synthetic ester based oil, *Tribol. Int.*, 44, 266–271, <https://doi.org/10.1016/j.triboint.2010.10.028>, 2011.
- Du Han, H. and Masuko, M.: Elucidation of the Antiwear Performance of Several Organic Phosphates Used with Different Polyol Ester Base Oils from the Aspect of Interaction between Additive and Base Oil, *Tribol. T.*, 41, 600–604, <https://doi.org/10.1080/10402009808983788>, 1998.
- Ehrich, M., Jortner, B. S., and Padilla, S.: Relationship of neuropathy target esterase inhibition to neuropathology and ataxia in hens given organophosphorus esters, *Chem.-Biol. Interact.*, 87, 431–437, [https://doi.org/10.1016/0009-2797\(93\)90071-6](https://doi.org/10.1016/0009-2797(93)90071-6), 1993.
- Eurocontrol: European Aviation in 2040: Challenges of Growth, Annex1 Flight Forecast to 2040, European Organisation for the Safety of Air Navigation, 92 pp., available at: https://www.eurocontrol.int/sites/default/files/2019-07/challenges-of-growth-2018-annex1_0.pdf (last access: 5 March 2021), 2018.
- Eurocontrol: Five-Year Forecast 2020–2024 European Flight Movements and Service Units: Three Scenarios for Recovery from COVID-19, Brussels, 15 pp., 2020.
- Eurocontrol: What COVID-19 did to European Aviation in 2020, and Outlook 2021: Think Paper #8 – 1 January 2021, Brussels, 12 pp., 2021.
- Eyer, P.: Neuropsychopathological changes by organophosphorus compounds – a review, *Hum. Exp. Toxicol.*, 14, 857–864, <https://doi.org/10.1177/096032719501401101>, 1995.
- Fraport AG: Fraport-Verkehrszahlen 2019: Über 70,5 Millionen Passagiere am Flughafen Frankfurt, available at: <https://www.fraport.com/de/newsroom/pressemitteilungen/2020/q1-2020/fraport-verkehrszahlen-2019--ueber-70-5-millionen-passagiere-am-> html, last access: 14 July 2020.
- Fraport AG: Fraport-Verkehrszahlen 2020: Passagieraufkommen infolge der COVID-19-Pandemie auf historisch niedrigem Niveau, available at: <https://www.fraport.com/de/newsroom/pressemitteilungen/2021/q1-2021/fraport-verkehrszahlen-2020--passagieraufkommen-infolge-der-covi-> html, last access: 18 January 2021.
- Freudenthal, R. I., Rausch, L., Gerhart, J. M., Barth, M. L., Mackerer, C. R., and Bisinger, E. C.: Subchronic Neurotoxicity of Oil Formulations Containing Either Tricresyl Phosphate or Tri-Orthocresyl Phosphate, *J. Am. Coll. Toxicol.*, 12, 409–416, <https://doi.org/10.1177/109158189301200410>, 1993.
- Fushimi, A., Saitoh, K., Fujitani, Y., and Takegawa, N.: Identification of jet lubrication oil as a major component of aircraft exhaust nanoparticles, *Atmos. Chem. Phys.*, 19, 6389–6399, <https://doi.org/10.5194/acp-19-6389-2019>, 2019.
- Hanhela, P. J., Kibby, J., DeNola, G., and Mazurek, W.: Organophosphate and Amine Contamination of Cockpit Air in the Hawk, F-111 and Hercules C-130 Aircraft, Maritime Platforms Division Platforms Sciences Laboratory, Victoria, Australia, 31 pp., 2005.
- Hudda, N. and Fruin, S. A.: International Airport Impacts to Air Quality: Size and Related Properties of Large Increases in Ultrafine Particle Number Concentrations, *Environ. Sci. Technol.*, 50, 3362–3370, <https://doi.org/10.1021/acs.est.5b05313>, 2016.
- Ji, X., Li, N., Ma, M., Rao, K., Yang, R., and Wang, Z.: Tricresyl phosphate isomers exert estrogenic effects via G protein-coupled estrogen receptor-mediated pathways, *Environ. Pollut.*, 264, 114747, <https://doi.org/10.1016/j.envpol.2020.114747>, 2020.
- Jonsdottir, H. R., Delaval, M., Leni, Z., Keller, A., Brem, B. T., Siegerist, F., Schönenberger, D., Durdina, L., Elser, M., Burtcher, H., Liati, A., and Geiser, M.: Non-volatile particle emissions from aircraft turbine engines at ground-idle induce oxidative stress in bronchial cells, *Commun. Biol.*, 2, 90, <https://doi.org/10.1038/s42003-019-0332-7>, 2019.
- Kendrick, E.: A Mass Scale Based on CH₂ = 14.0000 for High Resolution Mass Spectrometry of Organic Compounds, *Anal. Chem.*, 35, 2146–2154, <https://doi.org/10.1021/ac60206a048>, 1963.

- Keuken, M. P., Moerman, M., Zandveld, P., Henzing, J. S., and Hoek, G.: Total and size-resolved particle number and black carbon concentrations in urban areas near Schiphol airport (the Netherlands), *Atmos. Environ.*, 104, 132–142, <https://doi.org/10.1016/j.atmosenv.2015.01.015>, 2015.
- Kılıç, D., El Haddad, I., Brem, B. T., Bruns, E., Bozetti, C., Corbin, J., Durdina, L., Huang, R.-J., Jiang, J., Klein, F., Lavi, A., Pieber, S. M., Rindlisbacher, T., Rudich, Y., Slowik, J. G., Wang, J., Baltensperger, U., and Prévôt, A. S. H.: Identification of secondary aerosol precursors emitted by an aircraft turbofan, *Atmos. Chem. Phys.*, 18, 7379–7391, <https://doi.org/10.5194/acp-18-7379-2018>, 2018.
- Kroll, J. H., Donahue, N. M., Jimenez, J. L., Kessler, S. H., Canagaratna, M. R., Wilson, K. R., Altieri, K. E., Mazzoleni, L. R., Wozniak, A. S., Bluhm, H., Mysak, E. R., Smith, J. D., Kolb, C. E., and Worsnop, D. R.: Carbon oxidation state as a metric for describing the chemistry of atmospheric organic aerosol, *Nat. Chem.*, 3, 133–139, <https://doi.org/10.1038/nchem.948>, 2011.
- Lee, D. S., Fahey, D. W., Forster, P. M., Newton, P. J., Wit, R. C. N., Lim, L. L., Owen, B., and Sausen, R.: Aviation and global climate change in the 21st century, *Atmos. Environ.*, 43, 3520–3537, <https://doi.org/10.1016/j.atmosenv.2009.04.024>, 2009.
- Lewis Sr., R. J., Larrañaga, M. D., and Lewis, R. A.: *Hawley's Condensed Chemical Dictionary*, John Wiley & Sons, Incorporated, Hoboken, USA, 2016.
- Lobo, P., Durdina, L., Smallwood, G. J., Rindlisbacher, T., Siegerist, F., Black, E. A., Yu, Z., Mensah, A. A., Hagen, D. E., Miake-Lye, R. C., Thomson, K. A., Brem, B. T., Corbin, J. C., Abegglen, M., Sierau, B., Whitefield, P. D., and Wang, J.: Measurement of Aircraft Engine Non-Volatile PM Emissions: Results of the Aviation-Particle Regulatory Instrumentation Demonstration Experiment (A-PRIDE) 4 Campaign, *Aerosol Sci. Tech.*, 49, 472–484, <https://doi.org/10.1080/02786826.2015.1047012>, 2015.
- Masiol, M. and Harrison, R. M.: Aircraft engine exhaust emissions and other airport-related contributions to ambient air pollution: A review, *Atmos. Environ.*, 95, 409–455, <https://doi.org/10.1016/j.atmosenv.2014.05.070>, 2014.
- Mattsson, H.: Bicyclic phosphates increase the cyclic GMP level in rat cerebellum, presumably due to reduced GABA inhibition, *Brain Res.*, 181, 175–184, [https://doi.org/10.1016/0006-8993\(80\)91267-6](https://doi.org/10.1016/0006-8993(80)91267-6), 1980.
- Morawska, L., Ristovski, Z., Jayaratne, E. R., Keogh, D. U., and Ling, X.: Ambient nano and ultrafine particles from motor vehicle emissions: Characteristics, ambient processing and implications on human exposure, *Atmos. Environ.*, 42, 8113–8138, <https://doi.org/10.1016/j.atmosenv.2008.07.050>, 2008.
- O'Callaghan, J. P.: Neurotoxic esterase: not so toxic?, *Nat. Genet.*, 33, 437–438, <https://doi.org/10.1038/ng1135>, 2003.
- Paasonen, P., Kupiainen, K., Klimont, Z., Visschedijk, A., van der Denier Gon, H. A. C., and Amann, M.: Continental anthropogenic primary particle number emissions, *Atmos. Chem. Phys.*, 16, 6823–6840, <https://doi.org/10.5194/acp-16-6823-2016>, 2016.
- Riesz, P., Berdahl, D., and Christman, C. L.: Free radical generation by ultrasound in aqueous and nonaqueous solutions, *Environ. Health. Persp.*, 64, 233–252, <https://doi.org/10.1289/ehp.8564233>, 1985.
- Rönkkö, T., Kuuluvainen, H., Karjalainen, P., Keskinen, J., Hillamo, R., Niemi, J. V., Pirjola, L., Timonen, H. J., Saarikoski, S., Saukko, E., Järvinen, A., Silvennoinen, H., Rostedt, A., Olin, M., Yli-Ojanperä, J., Nousiainen, P., Kousa, A., and Dal Maso, M.: Traffic is a major source of atmospheric nanocluster aerosol, *P. Natl. Acad. Sci. USA*, 114, 7549–7554, <https://doi.org/10.1073/pnas.1700830114>, 2017.
- Rose, D. and Jacobi, S.: 1. Zwischenbericht zur Untersuchung der regionalen Luftqualität auf ultrafeine Partikel im Bereich des Flughafens Frankfurt, Hessisches Landesamt für Naturschutz, Umwelt und Geologie, Wiesbaden, 24 pp., 2018.
- Schraufnagel, D. E.: The health effects of ultrafine particles, *Exp. Mol. Med.*, 52, 311–317, <https://doi.org/10.1038/s12276-020-0403-3>, 2020.
- Simmonds, M. A.: Classification of Some GABA Antagonists With Regard to Site of Action and Potency in Slices of Rat Cuneate Nucleus, *Eur. J. Pharmacol.*, 80, 347–358, 1982.
- Solbu, K., Daae, H. L., Thorud, S., Ellingsen, D. G., Lundanes, E., and Molander, P.: Exposure to airborne organophosphates originating from hydraulic and turbine oils among aviation technicians and loaders, *J. Environ. Monit.*, 12, 2259–2268, <https://doi.org/10.1039/c0em00273a>, 2010.
- Solbu, K., Daae, H. L., Olsen, R., Thorud, S., Ellingsen, D. G., Lindgren, T., Bakke, B., Lundanes, E., and Molander, P.: Organophosphates in aircraft cabin and cockpit air – method development and measurements of contaminants, *J. Environ. Monit.*, 13, 1393–1403, <https://doi.org/10.1039/c0em00763c>, 2011.
- Ticku, M. K. and Ramanjaneyulu, R.: Differential interactions of GABA agonists, depressant and convulsant drugs with [35S]-t-butylbicyclophosphorothionate binding sites in cortex and cerebellum, *Pharmacol. Biochem. Be.*, 21, 151–158, [https://doi.org/10.1016/0091-3057\(84\)90145-X](https://doi.org/10.1016/0091-3057(84)90145-X), 1984.
- Timko, M. T., Yu, Z., Onasch, T. B., Wong, H.-W., Miake-Lye, R. C., Beyersdorf, A. J., Anderson, B. E., Thornhill, K. L., Winstead, E. L., Corporan, E., DeWitt, M. J., Klingshirn, C. D., Wey, C., Tacina, K., Liscinsky, D. S., Howard, R., and Bhargava, A.: Particulate Emissions of Gas Turbine Engine Combustion of a Fischer–Tropsch Synthetic Fuel, *Energ. Fuel.*, 24, 5883–5896, <https://doi.org/10.1021/ef100727t>, 2010.
- Timko, M. T., Fortner, E., Franklin, J., Yu, Z., Wong, H.-W., Onasch, T. B., Miake-Lye, R. C., and Herndon, S. C.: Atmospheric measurements of the physical evolution of aircraft exhaust plumes, *Environ. Sci. Technol.*, 47, 3513–3520, <https://doi.org/10.1021/es304349c>, 2013.
- Timko, M. T., Albo, S. E., Onasch, T. B., Fortner, E. C., Yu, Z., Miake-Lye, R. C., Canagaratna, M. R., Ng, N. L., and Worsnop, D. R.: Composition and Sources of the Organic Particle Emissions from Aircraft Engines, *Aerosol Sci. Tech.*, 48, 61–73, <https://doi.org/10.1080/02786826.2013.857758>, 2014.
- van Netten, C. and Leung, V.: Comparison of the constituents of two jet engine lubricating oils and their volatile pyrolytic degradation products, *Appl. Occup. Environ. Hyg.*, 15, 277–283, <https://doi.org/10.1080/104732200301593>, 2000.
- Vazquez-Duhalt, R.: Environmental impact of used motor oil, *Sci. Total Environ.*, 79, 1–23, [https://doi.org/10.1016/0048-9697\(89\)90049-1](https://doi.org/10.1016/0048-9697(89)90049-1), 1989.
- Vogel, A. L., Lauer, A., Fang, L., Arturi, K., Bachmeier, F., Daelenbach, K. R., Käser, T., Vlachou, A., Pospisilova, V., Baltensperger, U., Haddad, I. E., Schwikowski, M., and Bjelić, S.: A Comprehensive Nontarget Analysis for the Molec-

- ular Reconstruction of Organic Aerosol Composition from Glacier Ice Cores, *Environ. Sci. Technol.*, 53, 12565–12575, <https://doi.org/10.1021/acs.est.9b03091>, 2019.
- Wey, C. C., Anderson, B. E., Wey, C., Miake-Lye, R. C., Whitefield, P., and Howard, R.: Overview on the Aircraft Particle Emissions Experiment (APEX), *J. Propul. Power*, 23, 898–905, <https://doi.org/10.2514/1.26406>, 2007.
- Winder, C. and Balouet, J.-C.: Aircrew Exposure to Chemicals in Aircraft: Symptoms of Irritation and Toxicity, *J. Occup. Health Safe.*, 17, 471–483, 2001.
- Winder, C. and Balouet, J.-C.: The toxicity of commercial jet oils, *Environ. Res.*, 89, 146–164, <https://doi.org/10.1006/enrs.2002.4346>, 2002.
- World Health Organization: Review of evidence on health aspects of air pollution – REVIHAAP, World Health Organization, Copenhagen Ø, Denmark, 33 pp., 2013.
- Wright, R. L.: Formation of the Neurotoxin TMPP from TMPE-Phosphate Formulations, *Tribol. T.*, 39, 827–834, <https://doi.org/10.1080/10402009608983601>, 1996.
- Wu, Y., Li, W., Zhang, M., and Wang, X.: Improvement of oxidative stability of trimethylolpropane trioleate lubricant, *Thermochim. Acta*, 569, 112–118, <https://doi.org/10.1016/j.tca.2013.05.033>, 2013.
- Wyman, J. F., Porvaznik, M., Serve, P., Hobson, D., and Uddin, D. E.: High Temperature Decomposition of Military Specification L-23699 Synthetic Aircraft Lubricants, *J. Fire Sci.*, 5, 162–177, <https://doi.org/10.1177/073490418700500303>, 1987.
- Yang, W. and Omaye, S. T.: Air pollutants, oxidative stress and human health, *Mutat. Res.*, 674, 45–54, <https://doi.org/10.1016/j.mrgentox.2008.10.005>, 2009.
- Yu, Z., Liscinsky, D. S., Winstead, E. L., True, B. S., Timko, M. T., Bhargava, A., Herndon, S. C., Miake-Lye, R. C., and Anderson, B. E.: Characterization of lubrication oil emissions from aircraft engines, *Environ. Sci. Technol.*, 44, 9530–9534, <https://doi.org/10.1021/es102145z>, 2010.
- Yu, Z., Herndon, S. C., Ziemba, L. D., Timko, M. T., Liscinsky, D. S., Anderson, B. E., and Miake-Lye, R. C.: Identification of lubrication oil in the particulate matter emissions from engine exhaust of in-service commercial aircraft, *Environ. Sci. Technol.*, 46, 9630–9637, <https://doi.org/10.1021/es301692t>, 2012.
- Yu, Z., Liscinsky, D. S., Fortner, E. C., Yacovitch, T. I., Croteau, P., Herndon, S. C., and Miake-Lye, R. C.: Evaluation of PM emissions from two in-service gas turbine general aviation aircraft engines, *Atmos. Environ.*, 160, 9–18, <https://doi.org/10.1016/j.atmosenv.2017.04.007>, 2017.
- Yu, Z., Timko, M. T., Herndon, S. C., Miake-Lye, R. C., Beyersdorf, A. J., Ziemba, L. D., Winstead, E. L., and Anderson, B. E.: Mode-specific, semi-volatile chemical composition of particulate matter emissions from a commercial gas turbine aircraft engine, *Atmos. Environ.*, 218, 116974, <https://doi.org/10.1016/j.atmosenv.2019.116974>, 2019.
- Zhu, Y., Hinds, W. C., Kim, S., Shen, S., and Sioutas, C.: Study of ultrafine particles near a major highway with heavy-duty diesel traffic, *Atmos. Environ.*, 36, 4323–4335, [https://doi.org/10.1016/S1352-2310\(02\)00354-0](https://doi.org/10.1016/S1352-2310(02)00354-0), 2002a.
- Zhu, Y., Hinds, W. C., Kim, S., and Sioutas, C.: Concentration and size distribution of ultrafine particles near a major highway, *J. Air Waste Manage. Assoc.*, 52, 1032–1042, <https://doi.org/10.1080/10473289.2002.10470842>, 2002b.



Supplement of

Identification and source attribution of organic compounds in ultrafine particles near Frankfurt International Airport

Florian Ungeheuer et al.

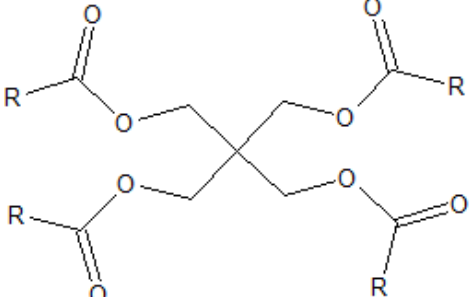
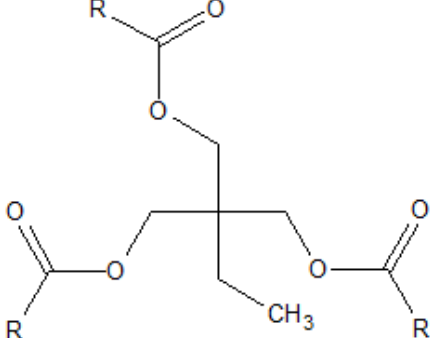
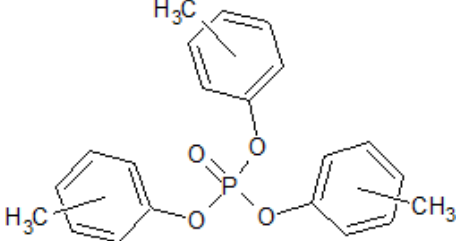
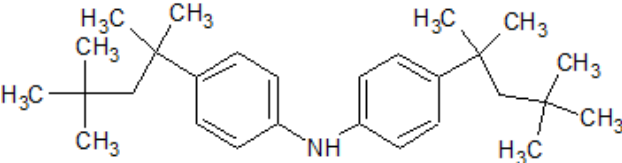
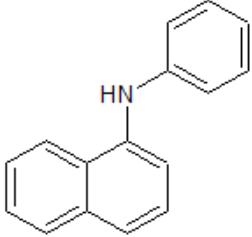
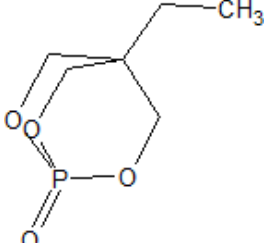
Correspondence to: Alexander L. Vogel (vogel@iau.uni-frankfurt.de)

The copyright of individual parts of the supplement might differ from the article licence.

Table S1. Overview of the sampling times (only during Frankfurt Airport operating hours between 5 AM and 11 PM).

Sample	Start	Stop	Collection time [h]	Dp(aer) [μm]
FF7	8/31/2019 5:00	8/31/2019 23:00	18	0.01 - 0.018
FF8	8/31/2019 5:00	8/31/2019 23:00	18	0.018 - 0.032
FF10	9/4/2019 5:00	9/4/2019 23:00	18	0.01 - 0.018
FF11	9/4/2019 5:00	9/4/2019 23:00	18	0.018 - 0.032
FF13	9/6/2019 12:00	9/7/2019 23:00	29	0.01 - 0.018
FF14	9/6/2019 12:00	9/7/2019 23:00	29	0.018 - 0.032
FF15	9/6/2019 12:00	9/7/2019 23:00	29	0.032 - 0.056
FF16	9/11/2019 10:00	9/12/2019 23:00	31	0.01 - 0.018
FF17	9/11/2019 10:00	9/12/2019 23:00	31	0.018 - 0.032
FF18	9/11/2019 10:00	9/12/2019 23:00	31	0.032 - 0.056
FF19	9/15/2019 9:00	9/16/2019 23:00	32	0.01 - 0.018
FF20	9/15/2019 9:00	9/16/2019 23:00	32	0.018 - 0.032
FF21	9/15/2019 9:00	9/16/2019 23:00	32	0.032 - 0.056
Blank	9/18/2019 17:00	9/23/2019 11:30	-	0.01 - 0.018
Blank	9/18/2019 17:00	9/23/2019 11:30	-	0.018 - 0.032
Blank	9/18/2019 17:00	9/23/2019 11:30	-	0.032 - 0.056
FF28	9/27/2019 15:40	9/30/2019 11:00	49	0.01 - 0.018
FF29	9/27/2019 15:40	9/30/2019 11:00	49	0.018 - 0.032
FF30	9/27/2019 15:40	9/30/2019 11:00	49	0.032 - 0.056
FF31	9/30/2019 12:05	10/1/2019 23:00	29	0.01 - 0.018
FF32	9/30/2019 12:05	10/1/2019 23:00	29	0.018 - 0.032
FF33	9/30/2019 12:05	10/1/2019 23:00	29	0.032 - 0.056
FF43	10/16/2019 5:00	10/18/2019 23:00	54	0.01 - 0.018
FF44	10/16/2019 5:00	10/18/2019 23:00	54	0.018 - 0.032
FF45	10/16/2019 5:00	10/18/2019 23:00	54	0.032 - 0.056

Table S2. Most prominent jet engine lubrication oil constituents and the thermal decomposition product TMP-P.

Name	Molecular formula	Structure
Pentaerythritol ester	$C_{27-38}H_{48-70}O_8$	
Trimethylolpropane ester	$C_{27-34}H_{50-64}O_6$	
Tricresyl phosphate	$C_{21}H_{21}O_4P$	
Bis(4-(1,1,3,3-tetramethylbutyl)phenyl) amine	$C_{28}H_{43}N$	
N-phenyl-1-naphthylamine	$C_{16}H_{13}N$	
Trimethylolpropane phosphate (TMP-P)	$C_6H_{11}O_4P$	

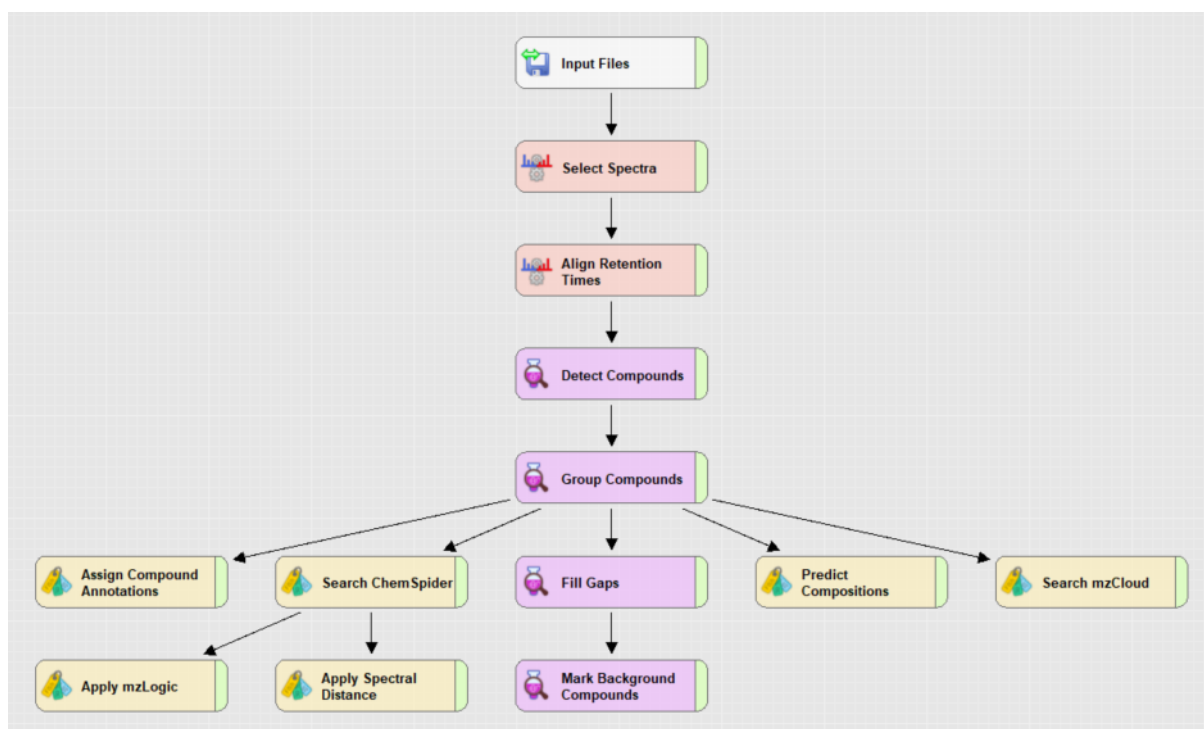


Figure S1. Workflow of the Compound Discoverer (CD) non-target screening.

Table S3. Detailed settings of the CD-workflow.

Processing node 0: Input Files

Processing node 1: Select Spectra

1. Spectrum Properties Filter:

- Lower RT Limit: 0
- Upper RT Limit: 0
- First Scan: 0
- Last Scan: 0
- Ignore Specified Scans: (not specified)
- Lowest Charge State: 0
- Highest Charge State: 0
- Min. Precursor Mass: 0 Da
- Max. Precursor Mass: 5000 Da
- Total Intensity Threshold: 1000000
- Minimum Peak Count: 1

2. Scan Event Filters:

- Mass Analyzer: Is FTMS
- MS Order: Is MS2; MS1
- Activation Type: (not specified)
- Min. Collision Energy: 0
- Max. Collision Energy: 1000
- Scan Type: Any
- Polarity Mode: Is +

3. Peak Filters:

- S/N Threshold (FT-only): 1.5

4. Replacements for Unrecognized Properties:

- Unrecognized Charge Replacements: 1
- Unrecognized Mass Analyzer Replacements: ITMS
- Unrecognized MS Order Replacements: MS2
- Unrecognized Activation Type Replacements: CID
- Unrecognized Polarity Replacements: +

- Unrecognized MS Resolution@200 Replacements: 60000
- Unrecognized MSn Resolution@200 Replacements: 30000

5. General Settings:

- Precursor Selection: Use MS1 Precursor
- Use Isotope Pattern in Precursor Reevaluation: True
- Provide Profile Spectra: Automatic
- Store Chromatograms: False

Processing node 2: Align Retention Times

1. General Settings:

- Alignment Model: Adaptive curve
- Alignment Fallback: Use Linear Model
- Maximum Shift [min]: 0.3
- Shift Reference File: True
- Mass Tolerance: 5 ppm
- Remove Outlier: True

Processing node 3: Detect Compounds

1. General Settings:

- Mass Tolerance [ppm]: 5 ppm
- Intensity Tolerance [%]: 10
- S/N Threshold: 3
- Min. Peak Intensity: 500000
- Ions:

[2M+H]⁺

[2M+K]⁺

[2M+Na]⁺

[2M+NH₄]⁺

[M+H]⁺

[M+H+MeOH]⁺

[M+K]⁺

[M+Na]⁺

[M+NH₄]⁺

- Base Ions: [M+H]⁺; [M+Na]⁺
- Min. Element Counts: C H
- Max. Element Counts: C90 H190 Br3 Cl4 N4 O20 P S3

2. Peak Detection:

- Filter Peaks: True
- Max. Peak Width [min]: 0.5
- Remove Singlets: True
- Min. # Scans per Peak: 5
- Min. # Isotopes: 2

Processing node 5: Group Compounds

1. Compound Consolidation:

- Mass Tolerance: 2 ppm
- RT Tolerance [min]: 0.3

2. Fragment Data Selection:

- Preferred Ions: [M+H]⁺

Processing node 6: Fill Gaps

1. General Settings:

- Mass Tolerance: 2 ppm
- S/N Threshold: 1.5
- Use Real Peak Detection: True

Processing node 7: Mark Background Compounds

1. General Settings:

- Max. Sample/Blank: 3
- Max. Blank/Sample: 0
- Hide Background: False

Processing node 9: Assign Compound Annotations

1. General Settings:

- Mass Tolerance: 2 ppm

2. Data Sources:

- Data Source #1: mzCloud Search

- Data Source #2: Predicted Compositions

- Data Source #3: (not specified)

- Data Source #4: ChemSpider Search

- Data Source #5: (not specified)

- Data Source #6: (not specified)

- Data Source #7: (not specified)

3. Scoring Rules:

- Use mzLogic: True

- Use Spectral Distance: True

- SFit Threshold: 20

- SFit Range: 20

Processing node 10: Search mzCloud

1. General Settings:

- Compound Classes: All

- Precursor Mass Tolerance: 5 ppm

- FT Fragment Mass Tolerance: 5 ppm

- IT Fragment Mass Tolerance: 0.4 Da

- Library: Autoprocessed; Reference

- Post Processing: Recalibrated

- Max. # Results: 10

- Annotate Matching Fragments: False

2. DDA Search:

- Identity Search: HighChem HighRes

- Match Activation Type: True

- Match Activation Energy: Match with Tolerance

- Activation Energy Tolerance: 20

- Apply Intensity Threshold: True

- Similarity Search: Similarity Forward

- Match Factor Threshold: 60

3. DIA Search:

- Use DIA Scans for Search: False
- Max. Isolation Width [Da]: 500
- Match Activation Type: False
- Match Activation Energy: Any
- Activation Energy Tolerance: 100
- Apply Intensity Threshold: False
- Match Factor Threshold: 20

Processing node 8: Predict Compositions

1. Prediction Settings:

- Mass Tolerance: 2 ppm
- Min. Element Counts: C H
- Max. Element Counts: C90 H190 Br3 Cl4 N4 O20 P S3
- Min. RDBE: 0
- Max. RDBE: 40
- Min. H/C: 0.1
- Max. H/C: 3.5
- Max. # Candidates: 10
- Max. # Internal Candidates: 200

2. Pattern Matching:

- Intensity Tolerance [%]: 10
- Intensity Threshold [%]: 0.1
- S/N Threshold: 3
- Min. Spectral Fit [%]: 30
- Min. Pattern Cov. [%]: 90
- Use Dynamic Recalibration: True

3. Fragments Matching:

- Use Fragments Matching: True
- Mass Tolerance: 5 ppm
- S/N Threshold: 3

Processing node 11: Search ChemSpider

1. Search Settings:

- Database(s):

EAWAG Biocatalysis/Biodegradation Database

Nature Chemistry

Sigma-Aldrich

- Search Mode: By Formula Only

- Mass Tolerance: 5 ppm

- Max. # of results per compound: 100

- Max. # of Predicted Compositions to be searched per Compound: 3

- Result Order (for Max. # of results per compound): Order By Reference Count (DESC)

2. Predicted Composition Annotation:

- Check All Predicted Compositions: False

Processing node 12: Apply mzLogic

1. Search Settings:

- FT Fragment Mass Tolerance: 10 ppm

- IT Fragment Mass Tolerance: 0.4 Da

- Max. # Compounds: 0

- Max. # mzCloud Similarity Results to consider per Compound: 10

- Match Factor Threshold: 30

Processing node 13: Apply Spectral Distance

1. Pattern Matching:

- Mass Tolerance: 5 ppm

- Intensity Tolerance [%]: 30

- Intensity Threshold [%]: 0.1

- S/N Threshold: 3

- Use Dynamic Recalibration: True

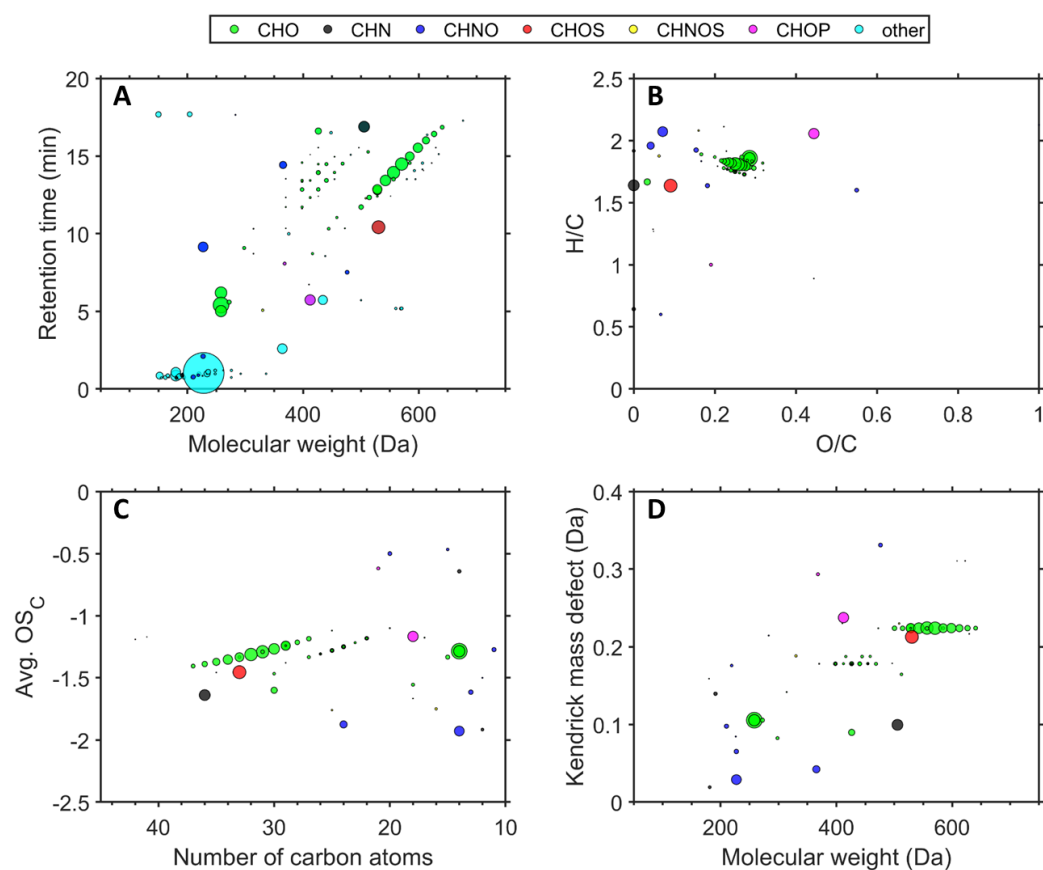


Figure S2. Molecular fingerprints (Retention time vs. MW [A], Van-Krevelen-diagram [B], Kroll-diagram [C], Kendrick mass defect vs. MW [D]) of eight averaged airport-related ultrafine particle samples in the size range of 0.010-0.018 μm (corrected).

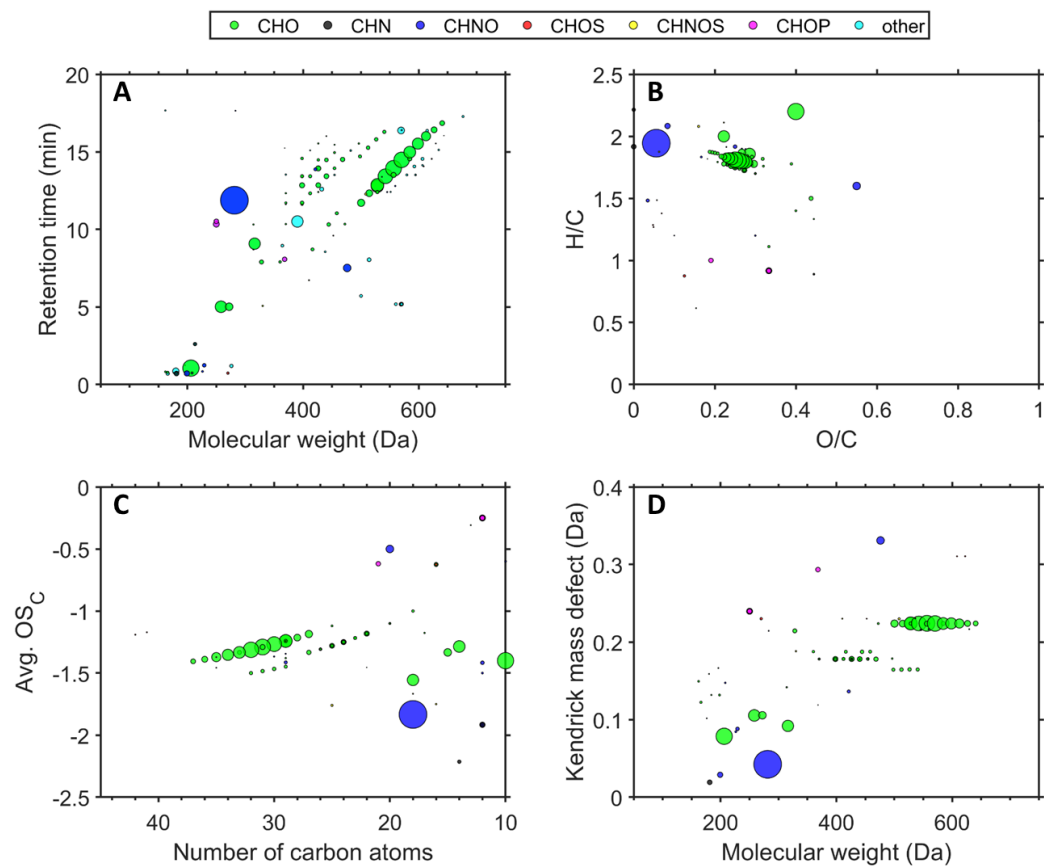


Figure S3. Molecular fingerprints (Retention time vs. MW [A], Van-Krevelen-diagram [B], Kroll-diagram [C], Kendrick mass defect vs. MW [D]) of eight averaged airport-related ultrafine particle samples in the size range of 0.018-0.032 μm (corrected).

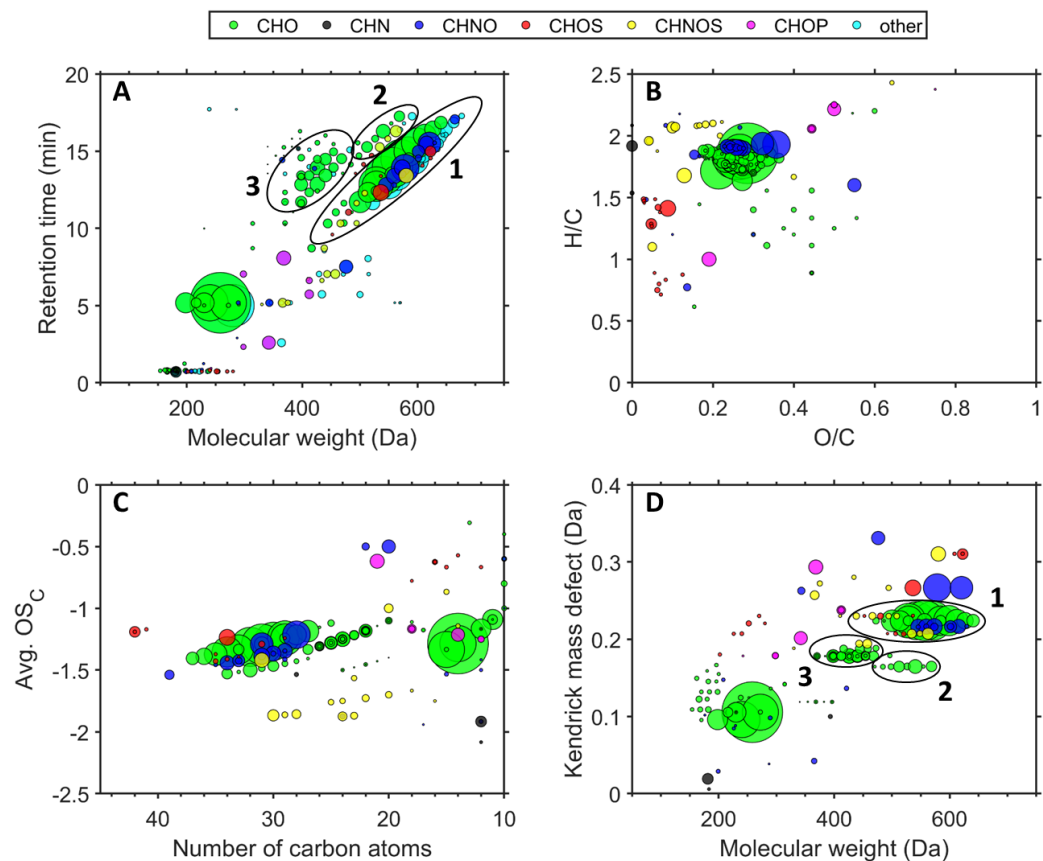


Figure S4. Native (not corrected) molecular fingerprints after non-target analysis (Retention time vs. MW [A], Van-Krevelen-diagram [B], Kroll-diagram [C], Kendrick mass defect vs. MW [D]) of six averaged airport-related ultrafine particle samples in the size range of 0.032-0.056 μm (for comparison with Figure 3).

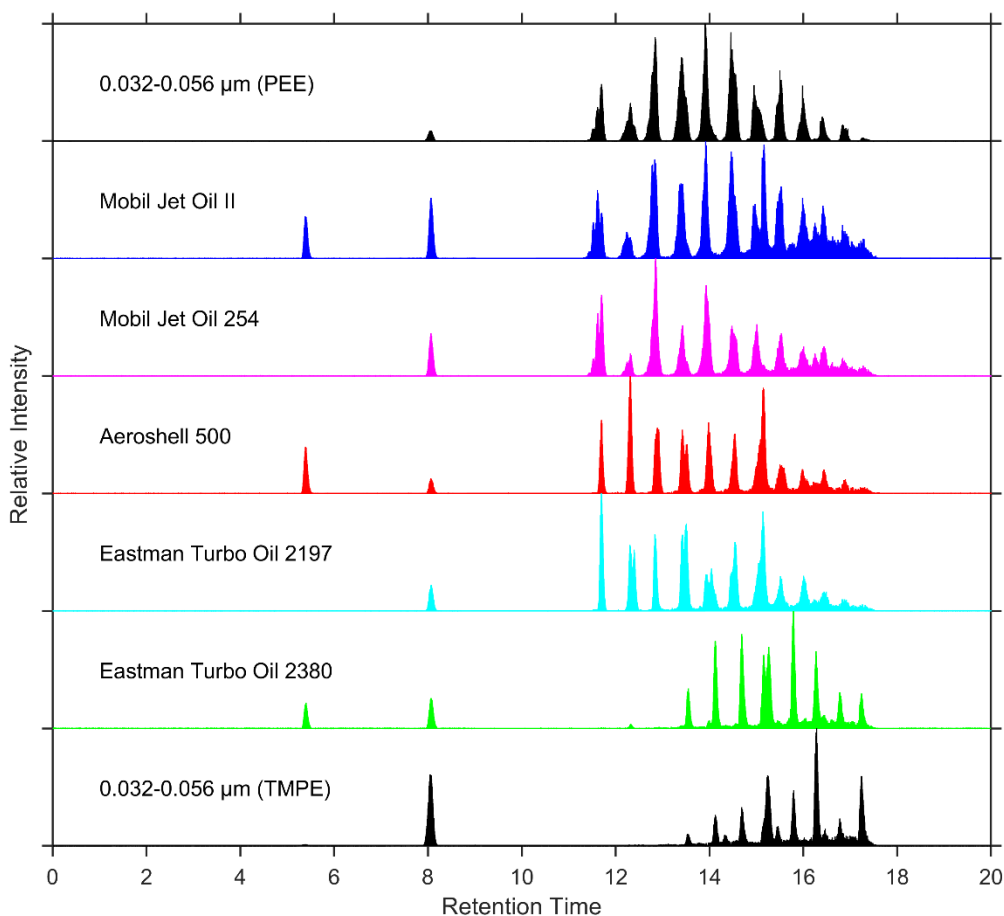


Figure S5. Extracted ion chromatograms (XIC) of an airport-sample (UFP size: 0.032-0.056 μm) and five different jet oils, showing a matching pattern of the major compounds $m/z \pm 4$ ppm 220.1120 (RT: 5.40 min, $[\text{M}+\text{H}]^+$, N-phenyl-1-naphthylamine, $\text{C}_{16}\text{H}_{13}\text{N}$), $m/z \pm 4$ ppm 394.3468 (RT: 15.16 min, $[\text{M}+\text{H}]^+$, alkylated diphenyl amine, $\text{C}_{28}\text{H}_{43}\text{N}$), $m/z \pm 4$ ppm 391.1069 (RT: 8.05 min, $[\text{M}+\text{Na}]^+$, tricresyl phosphate, $\text{C}_{21}\text{H}_{21}\text{O}_4\text{P}$) and homologous series of $m/z \pm 4$ ppm 523.3241 - 677.4962 (RT: 11.70 - 17.27 min, $[\text{M}+\text{Na}]^+$, pentaerythritol esters, $\text{C}_{27-38}\text{H}_{48-70}\text{O}_8$, PEE) and $m/z \pm 4$ ppm 493.3499 - 591.4595 (RT: 13.53 - 17.24 min, $[\text{M}+\text{Na}]^+$, trimethylolpropane esters, $\text{C}_{27-34}\text{H}_{50-64}\text{O}_6$, TMPE). The same sample (0.032-0.056 μm) was depicted once with the focus on the pentaerythritol esters (PEE) and once with the focus on the trimethylolpropane esters (TMPE) to illustrate the different influence of diverse jet engine lubrication oil base stock materials on ultrafine particles.

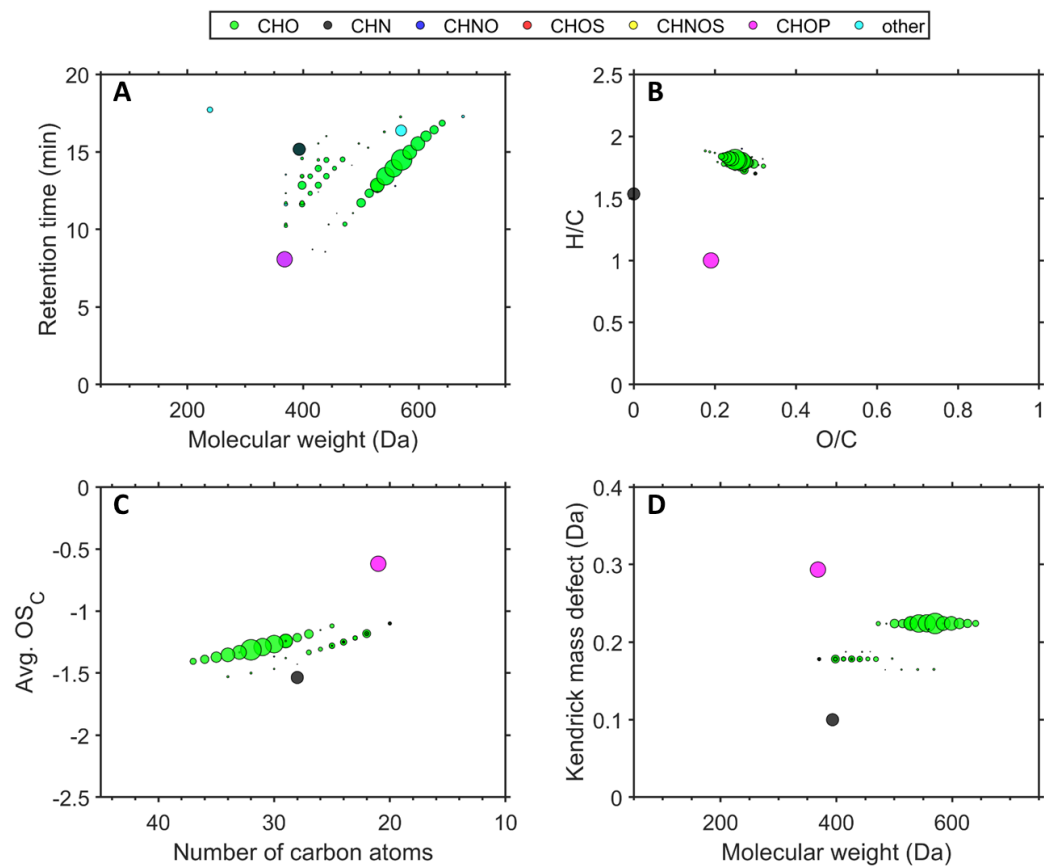


Figure S6. Molecular fingerprints (Retention time vs. MW [A], Van-Krevelen-diagram [B], Kroll-diagram [C], Kendrick mass defect vs. MW [D]) of the jet engine lubrication oil Mobil Jet Oil II by ExxonMobil.

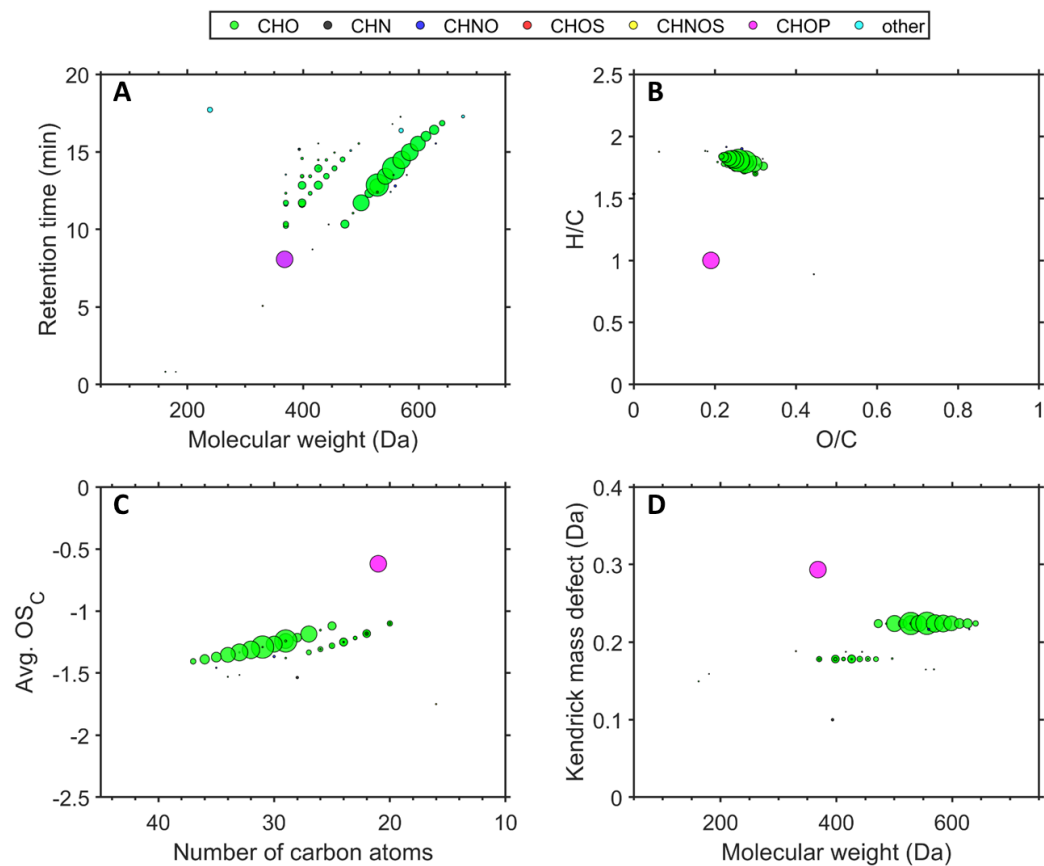


Figure S7. Molecular fingerprints (Retention time vs. MW [A], Van-Krevelen-diagram [B], Kroll-diagram [C], Kendrick mass defect vs. MW [D]) of the jet engine lubrication oil Mobil Jet Oil 254 by ExxonMobil.

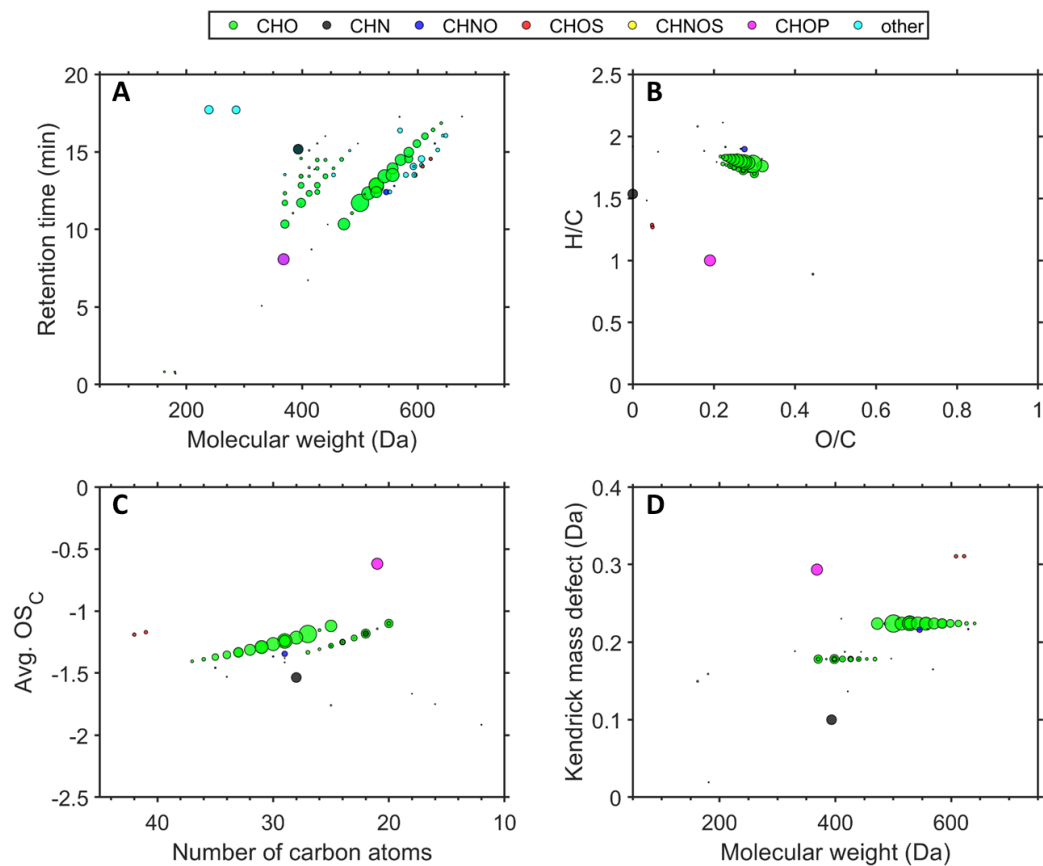


Figure S8. Molecular fingerprints (Retention time vs. MW [A], Van-Krevelen-diagram [B], Kroll-diagram [C], Kendrick mass defect vs. MW [D]) of the jet engine lubrication oil Turbo Oil 2197 by Eastman.

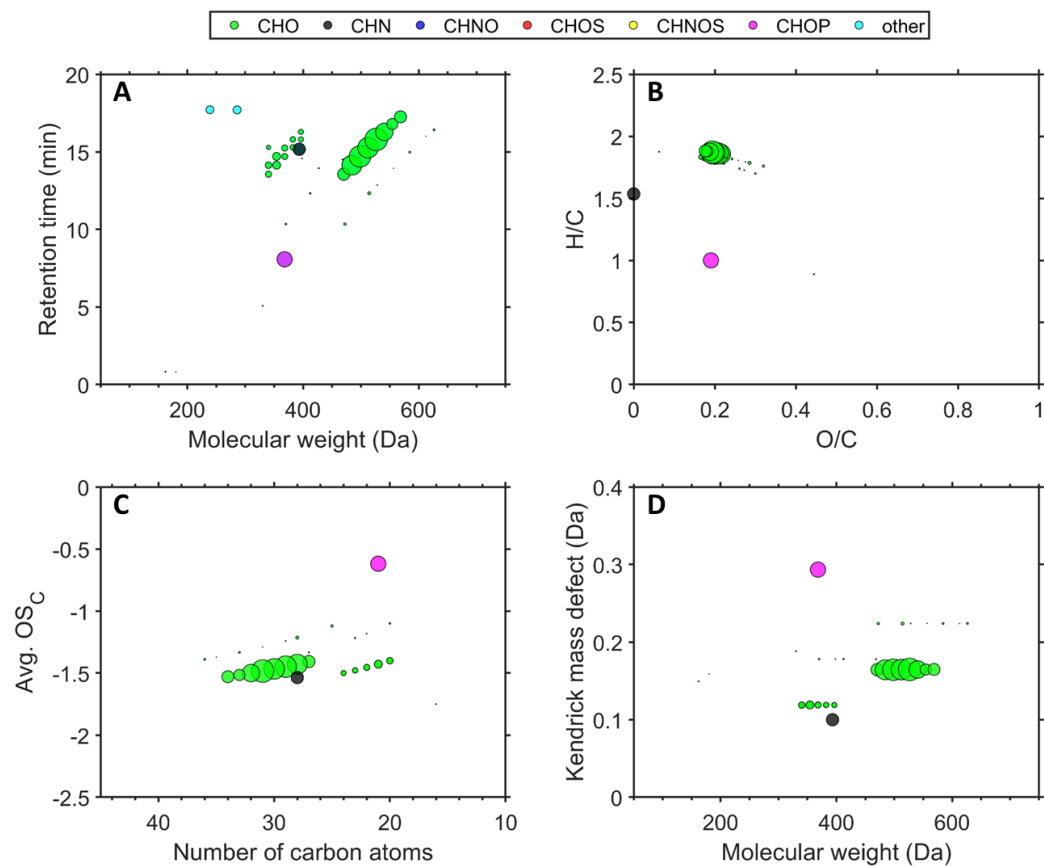


Figure S9. Molecular fingerprints (Retention time vs. MW [A], Van-Krevelen-diagram [B], Kroll-diagram [C], Kendrick mass defect vs. MW [D]) of the jet engine lubrication oil Turbo Oil 2380 by Eastman.

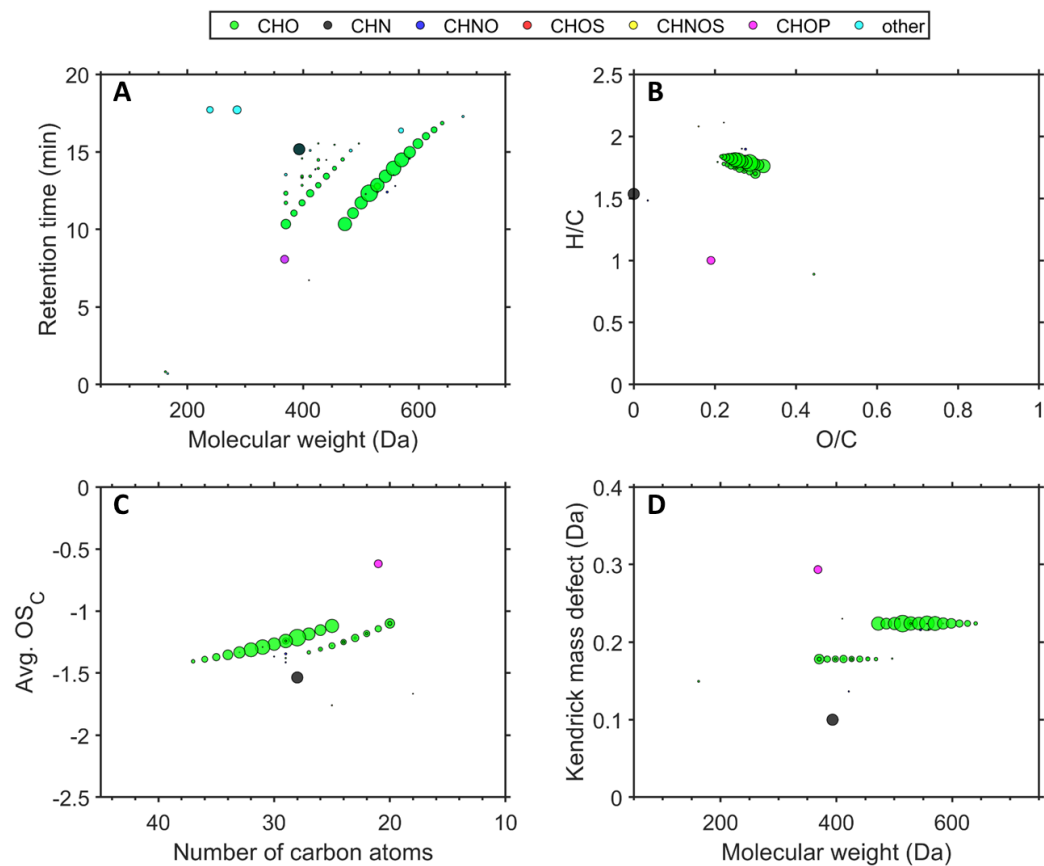






Figure S10. Molecular fingerprints (Retention time vs. MW [A], Van-Krevelen-diagram [B], Kroll-diagram [C], Kendrick mass defect vs. MW [D]) of the jet engine lubrication oil Aeroshell 500 by Royal Dutch Shell.

5.2 Nucleation of jet engine oil vapours is a large source of aviation-related ultrafine particles

Nucleation of jet engine oil vapours is a large source of aviation-related ultrafine particles

Florian Ungeheuer ¹, Lucía Caudillo¹, Florian Ditas ², Mario Simon¹, Dominik van Pinxteren³, Doğuşhan Kılıç^{4,5}, Diana Rose², Stefan Jacobi², Andreas Kürten¹, Joachim Curtius ¹ & Alexander L. Vogel ¹✉

Large airports are a major source of ultrafine particles, which spread across densely populated residential areas, affecting air quality and human health. Jet engine lubrication oils are detectable in aviation-related ultrafine particles, however, their role in particle formation and growth remains unclear. Here we show the volatility and new-particle-formation ability of a common synthetic jet oil, and the quantified oil fraction in ambient ultrafine particles downwind of Frankfurt International Airport, Germany. We find that the oil mass fraction is largest in the smallest particles (10–18 nm) with 21% on average. Combining ambient particle-phase concentration and volatility of the jet oil compounds, we determine a lower-limit saturation ratio larger than 1×10^5 for ultra-low volatility organic compounds. This indicates that the oil is an efficient nucleation agent. Our results demonstrate that jet oil nucleation is an important mechanism that can explain the abundant observations of high number concentrations of non-refractory ultrafine particles near airports.

¹Institute for Atmospheric and Environmental Sciences, Goethe-University Frankfurt, Frankfurt am Main 60438, Germany. ²Department for Ambient Air Quality, Hessian Agency for Nature Conservation, Environment and Geology, Wiesbaden 65203, Germany. ³Atmospheric Chemistry Department (ACD), Leibniz Institute for Tropospheric Research (TROPOS), Leipzig 04318, Germany. ⁴The Department of Earth and Environmental Sciences, the Faculty of Science and Engineering, the University of Manchester, Manchester M13 9PS, UK. ⁵National Centre for Atmospheric Science, Manchester M13 9PS, UK. ✉email: vogel@iau.uni-frankfurt.de

Several studies identified airports as a major source of ultrafine particles (UFPs)^{1–8}. Among different engine operation conditions at the airports, take-off is often associated with the highest UFP emissions^{3,9–12}. These particles are typically formed via gas-to-particle conversion after combustion¹³. Transmission electron microscopy analysis of UFPs from aviation shows spherical particles with a volatile character under high vacuum¹⁴. They can be transported large distances from the source reaching densely populated residential areas, as large airports are usually located in the close vicinity of metropolitan areas^{3,15,16}. UFP emissions from airport operations lead to a higher ambient particle number concentration (PNC) in the surrounding of airports, with a limited knowledge of their chemical composition^{17,18}. UFP transport and subsequent infiltration to the indoor environment seems to be more relevant than infiltration of PM_{2.5} and PM₁₀^{18,19}. The number-size distributions of particles emitted by jet engines are dominated by a mode diameter smaller than ~30 nm, which is significantly smaller compared to particles from road traffic emissions^{12,20–23}. Jet engine oil constituents (Supplementary Fig. 1) have been identified in UFPs near airports^{2,7,24–26}. Lubrication oils are emitted from aircraft engines through a breather vent and unintentionally as leaks of the oil circulating system (i.e., due to worn seals)²⁴.

Due to the small size of UFPs, exposure-related health effects are of importance as they potentially reach the alveoli, penetrate

through the pulmonary epithelium in the lower respiratory tract, and translocate the air-blood barrier^{27–30}. Animal tests also showed that they can reach the central nervous system via the olfactory nerve circumventing the blood-brain barrier³¹. UFPs can permeate into the respiratory and cardiovascular system within minutes to hours and are still detectable for months after the exposure³². Depending on their chemical composition, UFPs can induce oxidative stress, inflammatory reactions, and cell membrane damages^{33–35}. Health effects depend on their particle size, mass and number concentration⁵, and additionally on individual properties such as surface area, solubility, oxidative potential and the ability to counteract macrophage phagocytosis³⁶. Several studies investigated the UFP exposure of airport ground personnel and passengers^{37,38} and health effects due to UFP exposure near the airport⁶. A recent cohort study reported a 12% increased risk of developing a malignant brain tumour in the Los Angeles airport area for each increase of UFP exposure by 6,700 particles cm⁻³³⁹. This finding is supported by a study from Toronto, which reports a hazard ratio of 1.112 in developing a malignant brain tumour per UFP increase of 10,000 particles cm⁻³, adjusted for other air pollutants and socio-demographic factors⁴⁰. A study of the health effects from long-term UFP exposure of airport workers reported no association to cardiovascular disease⁴¹.

Ultrafine and fine particle emissions by jet engines during flight have also been investigated^{42,43}. Here the focus has been put on determining emission indices for particle emissions at cruise and their role for contrail and cirrus formation⁴⁴. Black carbon (soot) emissions have been discussed to dominate the formation of ice crystals in contrails, especially in the soot-rich regime characterised by soot particle number emission indices, EIs, in excess of ~10¹⁴ (kg-fuel)⁻¹⁴⁴. Recent studies have shown that soot formation by aircraft engines burning plant-based bio-fuels blended with petroleum-based conventional kerosene (Jet A) or blends of synthetic fuels (Fischer-Tropsch) with Jet A fuel, both significantly reduces the soot formation^{43,45}, which is likely explained by the near zero aromatic contents of the bio and synthetic fuels. Ultrafine volatile particles were assumed to be mostly composed of sulphuric acid and organic fuel components that nucleate in the young exhaust plume^{46,47}, but jet lubrication oil has so far not been suggested as an important source of the freshly formed particles in the exhaust plume in flight.

In our previous study on airport-related UFPs, we showed that jet engine lubrication oils dominate the spectrum of detected organic compounds after a non-target analysis²⁶. Following this non-target study, here we describe the nucleation ability of jet oil vapours in laboratory experiments and by quantification of jet engine oil constituents in three ambient UFP size fractions (<56 nm) downwind Frankfurt International Airport.

Results

Volatility and new-particle formation of jet engine lubrication oil.

We compared particle-number size distributions (PNSD) of ambient UFPs with laboratory-generated jet oil particles. In the ambient measurements at Frankfurt-Schwanheim (Supplementary Fig. 2) we observe a distinct difference between UFPs from the airport and the city centre (Fig. 1a). Air masses transported from Frankfurt Airport show a ~15-times higher PNC of UFPs at ~18 nm compared to air masses from the city centre (wind roses are shown in Supplementary Fig. 3). For larger UFPs, this difference becomes less pronounced. In the laboratory, we studied the PNSD of atomised lubrication oil passing a thermodenuder at 20 °C and 300 °C to investigate the volatility and nucleation capability of the jet oil compounds. When the jet oil particles (mean diameter of 27 nm) pass the thermodenuder at 300 °C, we observe a more than fivefold increase of the particle number concentration compared to the experiment at 20 °C, and a reduction of the mean diameter

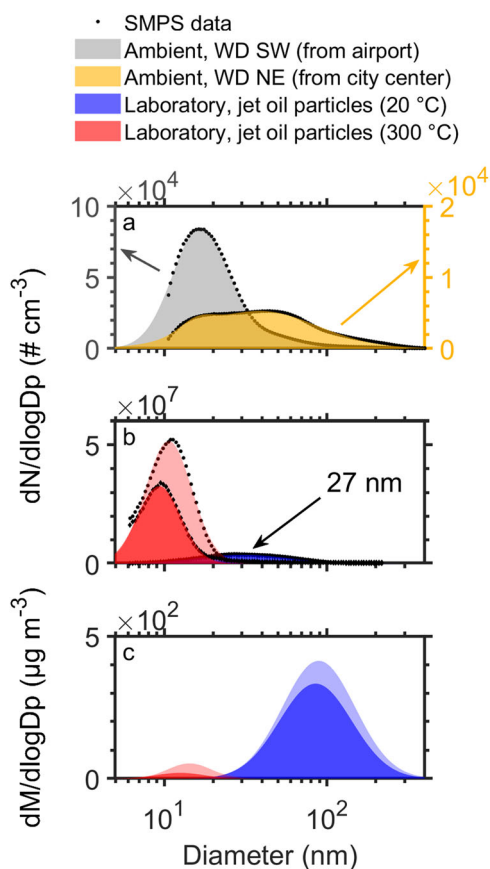


Fig. 1 Particle size distributions of ambient and laboratory-generated ultrafine particles. Ambient particle size distribution (a) at the monitoring site during wind direction (WD) from the airport (grey) and the city (yellow), averaged over three days (05:00–23:00 CET). Number-size (b) and mass-size distribution (c) from two laboratory experiments, each with jet oil nanoparticles generated from a methanolic solution, native at 20 °C (blue & light blue) and after heating to 300 °C (red & light red).

Measurement data (black dots) were fitted using a lognormal distribution.

down to ~10 nm of the measured particles (Fig. 1b). Although the particles passed the thermodenuder, it is important to mention that the PNSD measurement was conducted downstream the heating section at room temperature. The volatility of the jet oil at 300 °C is evident as the mass fraction of jet oil is reduced by ~99% compared to the 20 °C control experiment (Fig. 1c). Downstream the heating section of the thermodenuder the majority of oil vapours in the gas phase is likely lost to the surfaces of the tubing. However, a small fraction of the oil vapours nucleates and forms new particles downstream of the thermodenuder within a few seconds, when the temperature of the sampling flow reaches a point at which the oil vapour becomes supersaturated. Rapid growth of particles to sizes >10 nm allows escaping the “valley of death” in the nucleation mode⁴⁸, in which small particles are efficiently scavenged by coagulation. The thermodenuder experiment demonstrates that jet engine oil particles are volatile UFPs at 300 °C, and it can be assumed that the oil partitions entirely to the gas phase if exposed to operating temperatures of aircraft turbofan engines ($\gg 300$ °C⁴⁹).

Fraction of lubrication oil in ambient UFP samples. We quantified jet engine oil constituents (Supplementary Fig. 1 and Supplementary Note 1) from ambient particle samples to determine the oil fraction in UFPs near Frankfurt Airport. Therefore, we collected UFP samples downwind the airport at Frankfurt-Schwanheim when air masses arrived from the airport (Fig. 2a–d). Using a cascade impactor (Nano-MOUDI), we sampled UFPs during seven periods (18–54 h) in three different UFP size bins (10–18 nm, 18–32 nm, 32–56 nm) for subsequent chemical analysis. From the continuous measurements of the PNSD we calculated the mass concentration (oil density = 1 g cm⁻³, see Durдина et al.⁵⁰) for the three investigated particle size bins (Fig. 2b–d). The corresponding UFP number concentration is shown in Supplementary Fig. 4. Particle mass concentration of the two smallest size bins (<32 nm) increased significantly (two-tailed *t*-test, *p* < 0.001) when the wind direction falls within the airport sector during its operating hours, compared to periods of other wind directions or non-operating hours. The variability of larger UFPs (>32 nm) does not show this behaviour (Fig. 2d–g). This is in accordance with previous studies, which state that the mode diameter of aircraft-related particle emissions is smaller than 30 nm, while the mode diameter of particles from on-road vehicles is predominantly larger than 30 nm^{3,12,22,23}. The particle number concentration (<32 nm) reaches the rural background level around midnight. Hence, we consider the night-time periods between 00:00–05:00 CET adjacent to each sampling day as the mean rural background particle mass concentration that is largely unaffected by UFPs from the airport (dark red bars in Fig. 2b–d). Subtraction of the mean background mass from the mass during UFP sampling results in the total accumulated UFP mass on each impactor stage that can be attributed to the airport (Supplementary Figure 5 & Supplementary Table 1). This approach of mass closure cannot be applied to the largest stage (32–56 nm), because the particle mass concentration reaches sometimes higher values during non-operating than during operating hours (Fig. 2d).

We quantified the jet oil concentration of the individual impactor stages by adding authentic standards to aliquots of the filter extracts (standard addition method). Furthermore, we corrected for particle losses in the Nano-MOUDI based on an experimentally determined loss function of the three nano-stages (see Methods section). We find that jet engine oils contribute on average $21 \pm 11\%$ to the UFP mass in the 10–18 nm size bin. The jet-oil mass fraction of individual samples in the 10–18 nm size bin varies between 10 and 38%, with generally higher values for short sampling intervals. The contribution of jet engine oil to the total mass of the 18–32 nm particles is only $5 \pm 3\%$ on average

(Error estimation see Supplementary Note 2). Because the background subtraction could not be applied on the largest stage, we used the non-background corrected SMPS mass of the 32–56 nm stage and find a mean of 9% for the oil fraction of this size bin. Hence, the smallest particle stage shows consistently the highest mass fraction of jet engine lubrication oils (Supplementary Table 1 and Supplementary Fig. 6).

The calculation of the fractional oil contribution on all three stages did take into account experimentally determined particle losses. Regarding evaporative losses, we observe a bias in the molecular composition of jet oil from the ambient samples, which can be well explained by evaporation of the semi-volatile additives during Nano-MOUDI sampling (Supplementary Table 2). We evaluated the sampling efficiency of the Nano-MOUDI toward semi-volatiles based on pure ethyl oleate UFPs (C₂₀H₃₈O₂, 98%, Sigma-Aldrich) from an atomised solution. Although the generated PNSD covered the whole Nano-MOUDI range, we only detected the compound on the 32–56 nm stage (with the lowest pressure difference of the three Nano-MOUDI stages), and even on this stage we observed a loss of >99% of mass of the ethyl-oleate-UFPs. The vapour pressure of ethyl oleate is 8.10×10^{-3} Pa (EPI Suite⁵¹), which is similar to the vapour pressure of the N-phenyl-1-naphthylamine jet oil additive. The other additives and the jet oil esters exhibit lower vapour pressures (Supplementary Table 2). Therefore, it can be stated that the vapour pressure, and with this regard the volatilisation of semi-volatile compounds is the most important sampling loss process in the Nano-MOUDI. Fortunately, the jet oil esters are extremely low-volatile, and therefore evaporation of this compound class during sampling is negligible.

Lubrication oil base stock esters in the volatility basis set. The observed new-particle formation downstream the thermodenuder and the largest mass fraction of lubrication oil in the smallest ambient UFPs suggests that lubrication oil emissions from jet engines play a pivotal role in nucleation and early growth of new particles. We further evaluated this hypothesis by classifying the oils' synthetic esters into the volatility basis set (VBS^{52–54}). Figure 3a shows the quantified ambient particle-phase concentration of single esters from two different jet oil base stocks: pentaerythritol esters (C_{27–38}H_{48–70}O₈) and trimethylolpropane esters (C_{27–34}H_{50–64}O₆). We used the SIMPOL.1 model⁵⁵ to estimate the vapour pressures of the different esters. We then calculated their saturation mass concentration C_i^* (at 293.15 K), which is the inverse of the gas-to-particle partitioning constant [Eq. 1], and assigned them to volatility classes⁵⁶. In the ambient UFP samples, we measured particle-phase concentrations of the esters between 0.01 and 4 ng m⁻³. Following, we calculated the theoretical gas-phase concentration, assuming that the esters' partitioning would shift entirely to the gas phase at ambient temperatures [Eq. 2]. As the lubrication oil concentration is not corrected for atmospheric dilution between the airport and the measurement station at Frankfurt-Schwanheim, the gas-phase concentration in the engine exhaust plumes at high temperatures (>300 °C) is certainly higher than this lower-limit estimate downwind of the airport. However, we still observe a large saturation ratio of the theoretical gas-phase concentration [Eq. 3], which we derived from ambient particle-phase concentrations (Fig. 3b). The three largest pentaerythritol esters, which fall into the region of ultra-low volatility, reach a saturation ratio of up to 3×10^5 . Although this calculation is a lower-limit estimate, it supports the hypothesis that the synthetic esters from lubrication oils can initiate rapid nucleation in the exhaust plume of aircraft engines. Based on the theoretical gas-phase concentration, we

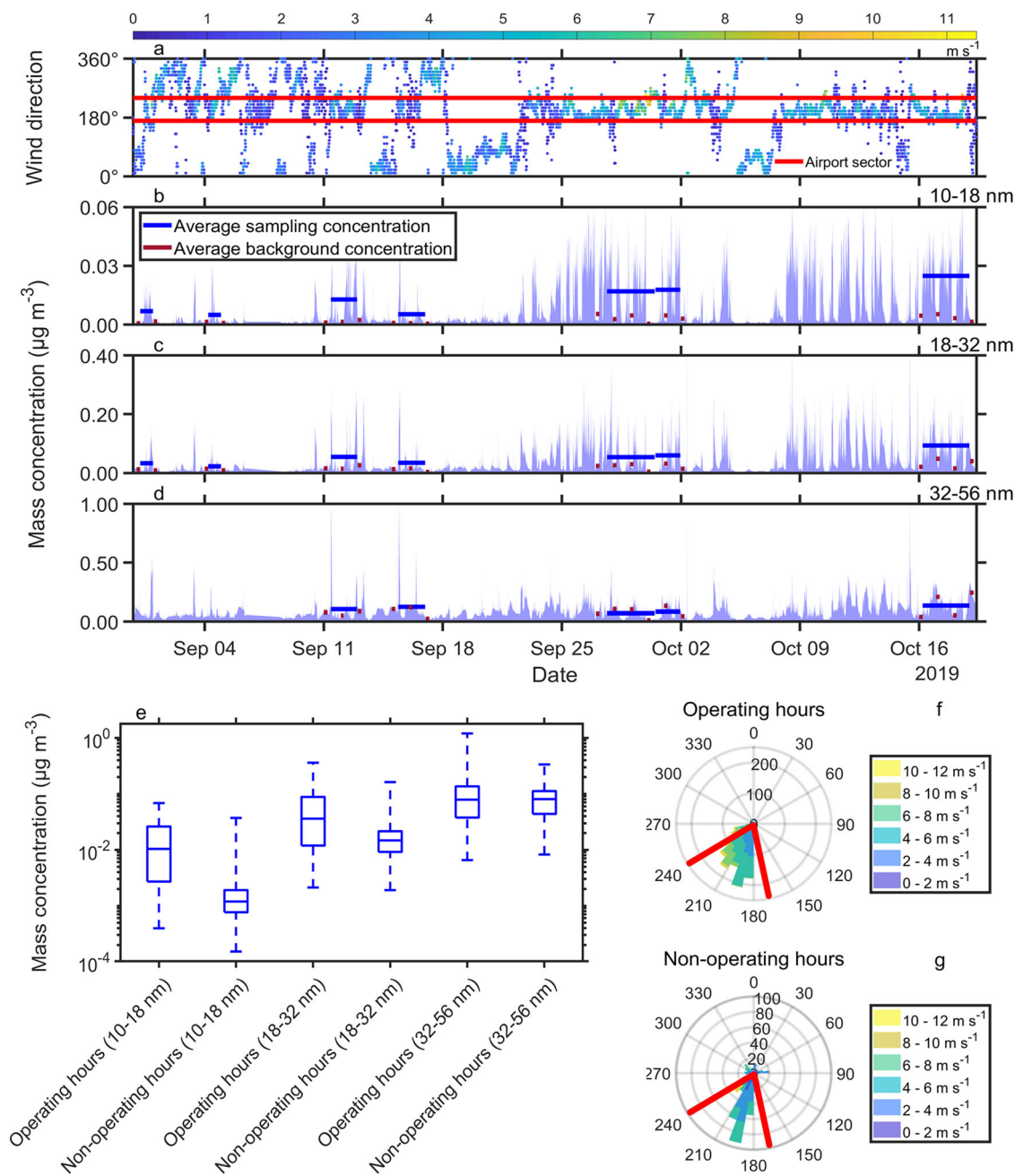


Fig. 2 Overview of the UFP mass concentrations derived from PNSD measurements and wind direction at Frankfurt Airport. Wind direction (a) with wind speed indicated by the colour code. The wind data is provided by the meteorological station at Frankfurt Airport (International Civil Aviation Organization, ICAO, code: EDDF) of the German weather service (DWD). The ambient UFP mass concentration ($\mu\text{g m}^{-3}$) in the size ranges 10–18 nm (b), 18–32 nm (c) and 32–56 nm (d), and the Nano-MOUDI sampling intervals (horizontal lines), indicating the average mass concentration during sampling hours (blue) and the average background mass concentration (dark red). Boxplots in (e) show the spread of the total mass concentrations ($\mu\text{g m}^{-3}$) for 10–18 nm, 18–32 nm and 32–56 nm particles during airport operating- and non-operating hours (based on SMPS data of the sampling- and background correction periods). The bottom and top of the boxes indicate the interquartile range and the horizontal line inside the boxes indicates the median. The whiskers show the scatter towards the most extreme values. The wind roses depict the prevailing wind directions during filter sampling at airport operating hours (f). Furthermore, the wind directions during the non-operating hour periods used for SMPS background correction are shown (g).

also determined the temperature at which each single ester compound reaches gas-phase supersaturation ($S_i^* > 1$) during cool-down of the exhaust plume [Eq. 6] (Fig. 3c). At $\sim 60^\circ\text{C}$, the ultra-low volatility pentaerythritol esters ($\text{C}_{36}\text{H}_{66}\text{O}_8$ – $\text{C}_{38}\text{H}_{70}\text{O}_8$) are the first compounds that reach $S_i^* > 1$, although their ambient concentration is an order of magnitude lower than the extremely-low volatility ester $\text{C}_{29}\text{H}_{52}\text{O}_8$. Based on our measurements we observe that all synthetic esters reach

supersaturation at ambient temperature, except the three most volatile trimethylolpropane esters $\text{C}_{27-29}\text{H}_{50-54}\text{O}_6$.

Discussion

We interpret our laboratory thermodenuder experiment in such way that heated oil particles from an atomised solution generate gaseous oil vapours, which nucleate and form new ~ 10 nm

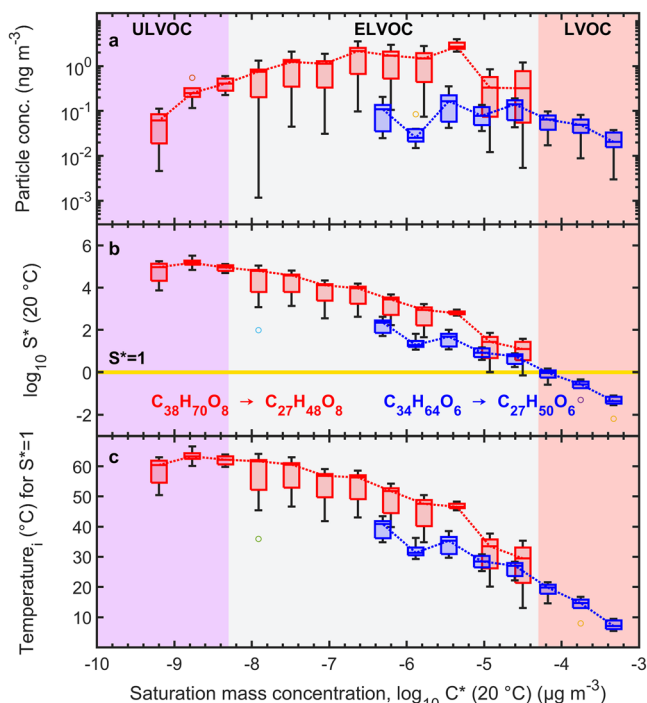


Fig. 3 Ambient concentrations of jet oil esters in the volatility basis set.

a Quantified ambient particle concentration (ng m^{-3}) of each synthetic ester compound ($\text{C}_{27-38}\text{H}_{48-70}\text{O}_8$ (red boxes); $\text{C}_{27-34}\text{H}_{50-64}\text{O}_6$ (blue boxes)) plotted against the $\log_{10} C^*$ at 20 °C (ULVOC: ultra-low volatility-, ELVOC: extremely-low volatility-, LVOC: low-volatility organic compound). The boxes show the spread of the quantified mass concentrations (10–56 nm) as interquartile range during airport operating hours. The horizontal line within the boxes shows the median and the whiskers show the spread to the most extreme values. Values outside $\pm 2.7 \sigma$ are marked as outliers by “o” symbols. **b** Resulting gas-phase saturation ratio S^* (20 °C) of the theoretical gas-phase concentration when all particle-phase compounds of (a) would partition to the gas phase. Values of S^* (20 °C) above 1 (yellow line) indicate supersaturation. **c** The approximate temperature at which the different jet oil esters reach $S^*=1$.

particles right behind the heated section. This experiment demonstrates that the jet oil compounds are volatile at 300 °C, but also efficient nucleators at room or ambient temperature. The particle diameter of the freshly nucleated particles in our laboratory experiment appears in the same size region as the ambient UFPs downwind of Frankfurt Airport. Certainly, these laboratory experiments do not reflect the full complexity of jet engine emissions in the atmosphere. In real emission plumes, non-volatile particulate matter (nvPM) could scavenge nucleation by providing surface for condensation of oil vapours. However, earlier studies describe aviation-related UFPs as volatile under high vacuum¹⁴, therefore, it appears likely that a large number of these particles, which are observed downwind of airports^{12,23}, are formed via nucleation of gaseous jet oil emissions.

Efficient nucleation and growth by organic compounds requires both (ultra-low) volatility compounds and sufficient high gas-phase concentrations for growing the particles fast enough. The lower concentration of the three ultra-low volatility organic compounds (ULVOCs) and higher concentrations of extremely-low volatility organic compounds (ELVOCs) create ideal conditions for initial nucleation by the jet oil ULVOCs, followed by rapid growth due to condensation from a large gas-phase reservoir of jet oil ELVOCs. The range of critical temperatures at which the compounds reach supersaturation suggests that nucleation and particle growth occurs in the near-field during

cool down of hot exhaust behind the turbofan (Fig. 4), and can explain the large volatile fraction (at elevated temperatures) of UFPs from aviation. To which extent the emission of nvPM from turbofan engines can scavenge this nucleation and growth needs further evaluation.

In fact, the reduction of nvPM emissions (e.g. soot) from aircraft engines in the last decades⁵⁷—and with this the reduction of the condensational sink—might have led to an increase of the number concentration of volatile UFPs that are formed via nucleation of gaseous oil vapours or sulphuric acid. Nevertheless, the determined high gas-phase saturation ratios of the ULVOC synthetic esters suggest that nucleation can occur despite the presence of the condensation sink from nvPM. The dynamics of formation and condensation of semi-volatile oxidation products (e.g. from incomplete combustion) are not investigated in this study, but are complementary for understanding the UFP composition. Hence, the above-mentioned Nano-MOUDI sampling artefacts are critical, as low- and semi-volatile oxidation products, which can contribute to UFP mass, are lost during sampling. Despite these uncertainties and considering that our results are lower-limit estimates, they substantiate the main finding that jet-oil vapours reach gas-phase supersaturation in cooling emission plumes leading to rapid nucleation and formation of UFPs in the range of ~10–20 nm.

Our observations of lubrication oil emissions being an important source for UFPs implies that this source will not be addressed by replacing traditional jet fuels with sustainable aviation fuels (SAF)⁴⁵, and should therefore also be taken into account in the current endeavour to eliminate UFP emissions from aviation. Accordingly, the air/oil separator should be optimised with regard to an improved jet oil recovery, and thus preventing oil emissions. In addition, developing advanced maintenance routines and reducing the total uptime of jet engines at airports (e.g. through electrification of ground handling) could also reduce oil emissions. Furthermore, evaluation of the toxicological properties of jet oil UFPs should be conducted to assess their health effects, also considering detrimental and potentially neurotoxic substances that are either directly emitted (e.g. organophosphates as lubrication oil additives^{58,59}), or which are formed through thermal transformation of the utilised trimethylpropane esters (e.g. trimethylpropane phosphate)^{26,60}. Furthermore, lubricant oil emissions during cruise and their possible effects on cirrus cloud formation needs further investigation, as the oil effect (e.g. as an organic coating on soot particles) has not been studied, yet.

Materials and methods

Jet engine oil thermodesuder measurements. We used thermodesuder measurements to determine the volatility of jet oil UFPs, as the new international aircraft particulate matter standard only considers the number and mass concentration of nvPM⁶¹. We determined the particle-number size distribution of Mobil Jet™ Oil II UFPs, formed using an atomizer (replica of TSI model 3076) with 0.04 g L^{-1} jet oil solved in ultra-pure methanol. The resulting PNSD downstream of the thermodesuder (operated at 20 °C and 300 °C) was measured using a scanning-mobility particle sizer (SMPS, TSI, model: 3938, Shoreview, MN, USA). The remaining jet engine oil fraction after the heating section was determined by comparing the particle mass derived from the PNSD measurements at both temperatures.

Impactor sampling and molecular characterisation. Detailed information on sampling technique, sample preparation and extraction procedure can be found elsewhere²⁶. Briefly, we used a Micro Orifice Uniform Deposition Impactor (Nano-MOUDI, Model 115, MSP, Minneapolis, MN, USA) at an air-quality monitoring site in Frankfurt-Schwanheim and sampled particles on the three nano-stages <56 nm. All stages were equipped with aluminium foils (TSI, diameter 47 mm and thickness 0.015 mm), and the upper ten stages were coated with Apiezon® grease to minimise the bounce-off of larger particles.

In the period of August to October 2019, we sampled UFPs for 18–54 h during airport operating hours (5:00–23:00 CET) and during southerly wind direction.

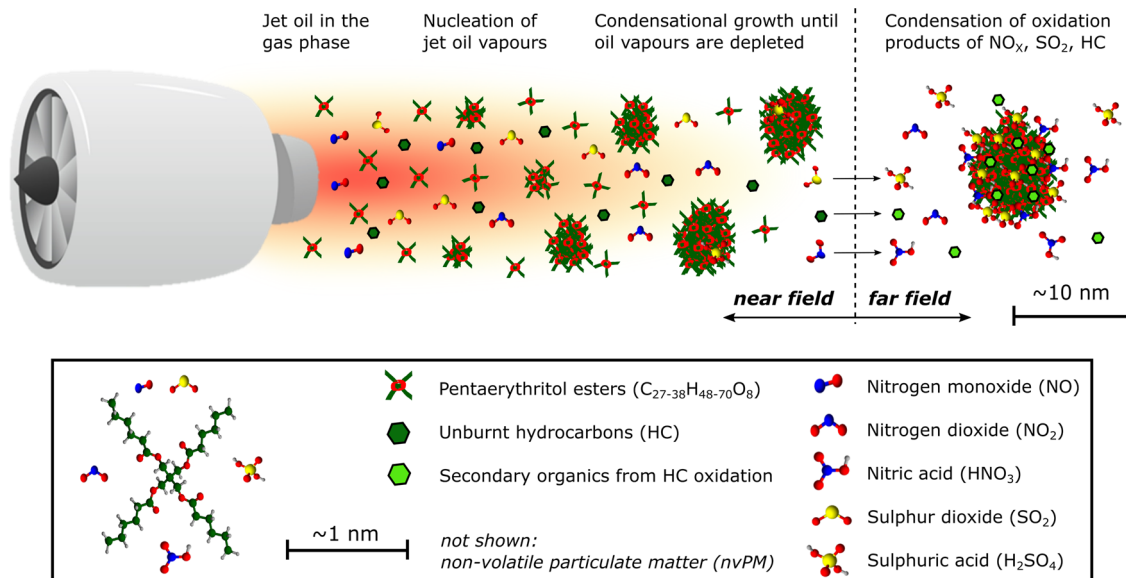


Fig. 4 Conceptual illustration of the UFP formation. Emissions of aircraft turbofan engines result in fast nucleation and growth of jet oil vapours in the near field. Non-volatile emissions (nvPM) are not shown. Dimensions are not true to scale.

Without an active sampling airflow, we collected field blanks for 115 h on the three nano-stages to estimate possible background concentrations regarding the target compounds. We stored the filters until analysis at -20°C . Due to the extensive sampling time span, we assume that our UFP samples represent aircraft engines of several types under various operating states. This is essential for covering the average UFP emission of the whole airport and not of individual engines or certain engine operating states.

We quantified the additives and jet oil esters using standard addition with authentic and surrogate standards, respectively (Supplementary Figs. 7 and 8). Targeted measurements of the jet engine oil constituents were carried out by using ultra-high performance liquid chromatography (UHPLC)/heated electrospray ionisation (HESI) coupled to an Orbitrap high-resolution mass spectrometer (HRMS). Chromatographic separation of the jet engine oil constituents was accomplished using a C_{18} -reversed phase column (Details see Supplementary Note 3). Using the standard addition method, we quantified 23 compounds in 25 ambient filter samples including 3 blank samples (Details see Supplementary Note 4). Most of these compounds belong to the group of pentaerythritol- or trimethylolpropane esters, which are utilised as jet engine oil base stocks (Supplementary Table 2). Finally, we determined the jet engine oil mass of the deposited UFPs after field blank correction.

Experimental loss determination in the Nano-MOUDI. Since sampling UFPs with a Nano-MOUDI is accompanied by particle losses, we determined a loss factor for each Nano-MOUDI stage (Details see Supplementary Note 5, Supplementary Figs. 9–11, and Supplementary Table 3). The loss of particles with an aerodynamic diameter between 32–56 nm is 28% and for 18–32 nm particles 40%, respectively. We were not able to experimentally determine a loss factor for the smallest size bin of 10–18 nm particles, due to insufficient deposited mass. We calculated the loss under the assumption that particle diffusivity is the main driving force for sampling losses of extremely low-volatile compounds in the UFP size range. We determined the dependency between particle diameter and diffusion coefficient at 17.2 kPa and 20°C (sampling condition of the 18–32 nm stage). To fit the experimentally determined particle losses of the two larger stages, we applied a damping term on the diffusion coefficient equation (Supplementary Fig. 11). Based on the experimentally determined losses of the two upper nano-stages, we calculated a loss of $\sim 58\%$ for the smallest stage. This loss factor can be considered as a conservative estimate, as it is only based on particle diffusive losses and not including losses due to evaporation after impaction (see main text). By implementing these loss factors, we corrected the quantified jet oil filter mass and determined the mass fraction of jet engine lubrication oils in airport-related UFPs.

Ambient SMPS measurements. The PNSD at the sampling site was determined using a SMPS including an electrostatic classifier (TSI, model: 3082), a Differential Mobility Analyser (DMA, TSI, model: 3081) and a Condensation Particle Counter (CPC, TSI, model: 3772). Ambient air was sampled through a stainless-steel tube (inner diameter: 20 mm, length 1.6 m), using a $\text{PM}_{2.5}$ inlet head at a flow rate of $1\text{ m}^3\text{ h}^{-1}$. Prior entering the SMPS, the aerosol passes a Nafion dryer (1.2 m length, flow rate of $0.3\text{ m}^3\text{ h}^{-1}$) to stabilise the relative humidity below 40%. The actual sample flow of the SMPS was 1 L min^{-1} , the additional bypass is used to minimise

residence time and particle losses in the inlet system. The PNSD was measured in the size range of 10–500 nm at a temporal resolution of 5 min. Particle losses due to sedimentation, inertial impaction and diffusion have been calculated and corrected accordingly⁶². The UFP mass was determined by integration assuming spherical particles. We calculated the particle mass for each filter collection interval exclusively during airport operating hours by converting the PNSD into a volume distribution averaged over the sampling period using a unit density of 1 g cm^{-3} and the Nano-MOUDI sampling flow rate of $0.6\text{ m}^3\text{ h}^{-1}$. The particle density was chosen according to the analysed jet engine oil densities (see safety data sheets) and aircraft turbine engine studies⁵⁰. Consequently, conversion of the measured mobility diameter to aerodynamic diameter is not necessary⁶³. We analysed the SMPS data of seven filter sampling periods as no data is available for one sampling period due to an instrument failure.

Volatility and saturation ratio of jet oil esters. The volatility of compounds strongly determines their gas-to-particle partitioning behaviour. Hence, evaluation of the jet oil base stocks using semi-empirical group contribution methods (SIMPOL.1 model⁵⁵) and the volatility basis set (VBS^{52,53}) enables the grouping of the single ester compounds to volatility classes (ULVOC: ultra-low volatility-, ELVOC: extremely-low volatility-, LVOC: low-volatility organic compound). Compound classification is based on their volatility expressed as the logarithm of the saturation mass concentration ($\log_{10} C_i^*$), where the volatility is differentiated by one decade in C_i^* , which is also assumed as uncertainty. The saturation mass concentration (C_i^* ($\mu\text{g m}^{-3}$)) is calculated as the inverse of the gas-to-particle phase partitioning constant (K_p)⁵² taking into account the weight fraction of the absorbing organic material (om) phase (f_{om}), its average molecular weight (MW_{om} , g mol^{-1}), and the activity coefficient (ζ_i) and vapour pressure ($p_{L,i}^0$, Torr)^{52,64} of compound i :

$$\frac{1}{\zeta_i * C_i^*} = K_p = \frac{f_{om} * 760 * R * T}{MW_{om} * \zeta_i * p_{L,i}^0 * 10^6} \quad (1)$$

We calculated K_p assuming the absorbing organic phase consists only of the respective substance ($f_{om} = 1$), which leads to an ideal absorption affinity of the molecules passing from the gas phase to the particle phase ($\zeta_i = 1$). The compound's affinity to the particle phase inversely correlates with ζ_i ⁶⁵. R is the gas constant ($8.2 \times 10^{-5}\text{ m}^3\text{ atm mol}^{-1}\text{ K}^{-1}$) and T (K) the temperature.

We converted the quantified base stock ester concentrations in the particle phase ($\frac{m_i}{V}$ (g m^{-3})) to gas phase number concentrations (c_i^g (m^{-3})) using the ideal gas law (m_i : quantified ester mass; M_i : molecular mass in g mol^{-1}):

$$c_i^g = \frac{m_i * N_A}{V * M_i} \quad (2)$$

To determine whether jet oil constituents reach gas-phase supersaturation, we calculated their gas-phase saturation ratio (S_i^g)⁶⁶:

$$S_i^g = \frac{c_i^g * M_i * 10^6}{C_i^* * N_A} \quad (3)$$

Accounting for the temperature dependence of the saturation vapour pressure, C_i^* can be described according to the Clausius-Clapeyron equation:

$$\log_{10} C_i^*(T) = \log_{10} C_i^*(293.15 \text{ K}) + \frac{\Delta H_i^{vap}}{R * \ln(10)} * \left(\frac{1}{293.15 \text{ K}} - \frac{1}{T} \right) \quad (4)$$

where $R = 8.314 \times 10^{-3} \text{ kJ K}^{-1} \text{ mol}^{-1}$. The evaporation enthalpy ΔH_i^{vap} (kJ mol^{-1}) can be approximated by:

$$\Delta H_i^{vap} = -11 * \log_{10} C_i^*(293.15 \text{ K}) + 129 \quad (5)$$

Despite the large uncertainties of this approach⁶⁷, it still can be used to describe a simple estimate of the temperature dependence of the oil partitioning. Finally, we combined [Eq. 3] and [Eq. 4] to calculate the approximate temperature at which the jet oil esters reach gas-phase supersaturation ($S_i^* = 1$) in a cooling engine exhaust plume [Eq. 6].

$$T_i^{S^*=1} = - \frac{1}{\log_{10} \left(\frac{C_i^* * M_i * 10^6}{N_A * C_i^*(293.15 \text{ K})} \right) * \frac{R * \ln(10)}{\Delta H_i^{vap}} - \frac{1}{293.15 \text{ K}}} \quad (6)$$

Reporting summary. Further information on research design is available in the Nature Portfolio Reporting Summary linked to this article.

Data availability

The data shown in this study is available at <https://doi.org/10.5281/zenodo.6876277>.

Received: 22 October 2022; Accepted: 1 December 2022;

Published online: 21 December 2022

References

- Hu, S. et al. Aircraft emission impacts in a neighborhood adjacent to a general aviation airport in southern California. *Environ. Sci. Technol.* **43**, 8039–8045 (2009).
- Yu, Z. et al. Identification of lubrication oil in the particulate matter emissions from engine exhaust of in-service commercial aircraft. *Environ. Sci. Technol.* **46**, 9630–9637 (2012).
- Keuken, M. P., Moerman, M., Zandveld, P., Henzing, J. S. & Hoek, G. Total and size-resolved particle number and black carbon concentrations in urban areas near Schiphol airport (the Netherlands). *Atmos. Environ.* **104**, 132–142 (2015).
- Stafoggia, M. et al. Particle number concentrations near the Rome-Ciampino city airport. *Atmos. Environ.* **147**, 264–273 (2016).
- Yu, Z. et al. Evaluation of PM emissions from two in-service gas turbine general aviation aircraft engines. *Atmos. Environ.* **160**, 9–18 (2017).
- Habre, R. et al. Short-term effects of airport-associated ultrafine particle exposure on lung function and inflammation in adults with asthma. *Environ. Int.* **118**, 48–59 (2018).
- Fushimi, A., Saitoh, K., Fujitani, Y. & Takegawa, N. Identification of jet lubrication oil as a major component of aircraft exhaust nanoparticles. *Atmos. Chem. Phys.* **19**, 6389–6399 (2019).
- Rivas, I. et al. Source apportionment of particle number size distribution in urban background and traffic stations in four European cities. *Environ. Int.* **135**, 105345 (2020).
- Zhu, Y., Fanning, E., Yu, R. C., Zhang, Q. & Froines, J. R. Aircraft emissions and local air quality impacts from takeoff activities at a large International Airport. *Atmos. Environ.* **45**, 6526–6533 (2011).
- Hsu, H.-H. et al. The relationship between aviation activities and ultrafine particulate matter concentrations near a mid-sized airport. *Atmos. Environ.* **50**, 328–337 (2012).
- Hsu, H.-H. et al. Contributions of aircraft arrivals and departures to ultrafine particle counts near Los Angeles International Airport. *Sci. Total Environ.* **444**, 347–355 (2013).
- Pirhadi, M. et al. Relative contributions of a major international airport activities and other urban sources to the particle number concentrations (PNCs) at a nearby monitoring site. *Environ. Pollut.* **260**, 114027 (2020).
- Pekkanen, J. & Kulmala, M. Exposure assessment of ultrafine particles in epidemiologic time-series studies. *Scand. J. Work Environ. Health* **30**, 9–18 (2004).
- Mazaheri, M., Bostrom, T. E., Johnson, G. R. & Morawska, L. Composition and morphology of particle emissions from in-use aircraft during takeoff and landing. *Environ. Sci. Technol.* **47**, 5235–5242 (2013).
- Hudda, N. & Fruin, S. A. International airport impacts to air quality: size and related properties of large increases in ultrafine particle number concentrations. *Environ. Sci. Technol.* **50**, 3362–3370 (2016).
- Zhang, X., Karl, M., Zhang, L. & Wang, J. Influence of aviation emission on the particle number concentration near zurich airport. *Environ. Sci. Technol.* **54**, 14161–14171 (2020).
- Hudda, N., Simon, M. C., Zamore, W. & Durant, J. L. Aviation-related impacts on ultrafine particle number concentrations outside and inside residences near an airport. *Environ. Sci. Technol.* **52**, 1765–1772 (2018).
- Hudda, N., Durant, L. W., Fruin, S. A. & Durant, J. L. Impacts of aviation emissions on near-airport residential air quality. *Environ. Sci. Technol.* **54**, 8580–8588 (2020).
- Chen, C. et al. Outdoor-to-indoor transport of ultrafine particles: measurement and model development of infiltration factor. *Environ. Pollut.* **267**, 115402 (2020).
- Riley, E. A. et al. Ultrafine particle size as a tracer for aircraft turbine emissions. *Atmos. Environ.* **139**, 20–29 (2016).
- Masiol, M., Harrison, R. M., Vu, T. V. & Beddows, D. C. S. Sources of sub-micrometre particles near a major international airport. *Atmos. Chem. Phys.* **17**, 12379–12403 (2017).
- Shirmohammadi, F. et al. Emission rates of particle number, mass and black carbon by the Los Angeles International Airport (LAX) and its impact on air quality in Los Angeles. *Atmos. Environ.* **151**, 82–93 (2017).
- Stacey, B. Measurement of ultrafine particles at airports: a review. *Atmos. Environ.* **198**, 463–477 (2019).
- Yu, Z. et al. Characterization of lubrication oil emissions from aircraft engines. *Environ. Sci. Technol.* **44**, 9530–9534 (2010).
- Timko, M. T. et al. Particulate emissions of gas turbine engine combustion of a fischer-tropsch synthetic fuel. *Energy Fuel.* **24**, 5883–5896 (2010).
- Ungeheuer, F., van Pinxteren, D. & Vogel, A. L. Identification and source attribution of organic compounds in ultrafine particles near Frankfurt International Airport. *Atmos. Chem. Phys.* **21**, 3763–3775 (2021).
- Oberdörster, G. et al. Extrapulmonary translocation of ultrafine carbon particles following whole-body inhalation exposure of rats. *J. Toxicol. Environ. Health Part A* **65**, 1531–1543 (2002).
- Oberdörster, G., Oberdörster, E. & Oberdörster, J. Nanotoxicology: an emerging discipline evolving from studies of ultrafine particles. *Environ. Health Persp.* **113**, 823–839 (2005).
- Kreyling, W. G. et al. Air-blood barrier translocation of tracheally instilled gold nanoparticles inversely depends on particle size. *ACS Nano* **8**, 222–233 (2014).
- Lu, D. et al. Chemical multi-fingerprinting of exogenous ultrafine particles in human serum and pleural effusion. *Nat. Commun.* **11**, 2567 (2020).
- Oberdörster, G. et al. Translocation of inhaled ultrafine particles to the brain. *Inhal. Toxicol.* **16**, 437–445 (2004).
- Miller, M. R. et al. Inhaled nanoparticles accumulate at sites of vascular disease. *ACS Nano* **11**, 4542–4552 (2017).
- Nel, A., Xia, T., Mädler, L. & Li, N. Toxic potential of materials at the nanolevel. *Science* **311**, 622–627 (2006).
- Jonsdottir, H. R. et al. Non-volatile particle emissions from aircraft turbine engines at ground-idle induce oxidative stress in bronchial cells. *Commun. Biol.* **2**, 90 (2019).
- Ohlwein, S., Kappeler, R., Kutlar Joss, M., Künzli, N. & Hoffmann, B. Health effects of ultrafine particles: a systematic literature review update of epidemiological evidence. *Int. J. Public Health* **64**, 547–559 (2019).
- Chalupa, D. C., Morrow, P. E., Oberdörster, G., Utell, M. J. & Frampton, M. W. Ultrafine particle deposition in subjects with asthma. *Environ. Health Persp.* **112**, 879–882 (2004).
- Møller, K. L. et al. Occupational exposure to ultrafine particles among airport employees-combining personal monitoring and global positioning system. *PLoS ONE* **9**, e106671 (2014).
- Ren, J., Cao, X. & Liu, J. Impact of atmospheric particulate matter pollutants to IAQ of airport terminal buildings: a first field study at Tianjin Airport, China. *Atmos. Environ.* **179**, 222–226 (2018).
- Wu, A. H. et al. Association between airport-related ultrafine particles and risk of malignant brain cancer: A Multiethnic Cohort Study. *Cancer Res.* **81**, 4360–4369 (2021).
- Weichenthal, S. et al. Within-city spatial variations in ambient ultrafine particle concentrations and incident brain tumors in adults. *Epidemiology* **31**, 177–183 (2020).
- Møller, K. L. et al. Cardiovascular disease and long-term occupational exposure to ultrafine particles: a cohort study of airport workers. *Int. J. Hyg. Environ. Health* **223**, 214–219 (2020).
- Brock, C. A. et al. Ultrafine particle size distributions measured in aircraft exhaust plumes. *J. Geophys. Res.* **105**, 26555–26567 (2000).
- Voigt, C. et al. Cleaner burning aviation fuels can reduce contrail cloudiness. *Commun. Earth Environ.* <https://doi.org/10.1038/s43247-021-00174-y> (2021).

44. Kärcher, B., Burkhardt, U., Bier, A., Bock, L. & Ford, I. J. The microphysical pathway to contrail formation. *J. Geophys. Res. Atmos.* **120**, 7893–7927 (2015).
45. Moore, R. H. et al. Biofuel blending reduces particle emissions from aircraft engines at cruise conditions. *Nature* **543**, 411–415 (2017).
46. Anderson, B. E., Cofer, W. R., Barrick, J. D., Bagwell, D. R. & Hudgins, C. H. Airborne observations of aircraft aerosol emissions II: Factors controlling volatile particle production. *Geophys. Res. Lett.* **25**, 1693–1696 (1998).
47. Curtius, J. et al. First direct sulfuric acid detection in the exhaust plume of a jet aircraft in flight. *Geophys. Res. Lett.* **25**, 923–926 (1998).
48. Wang, M. et al. Rapid growth of new atmospheric particles by nitric acid and ammonia condensation. *Nature* **581**, 184–189 (2020).
49. El-Sayed, A. F. *Aircraft Propulsion And Gas Turbine Engines* (CRC Press Taylor & Francis Group, 2017).
50. Durдина, L. et al. Determination of PM mass emissions from an aircraft turbine engine using particle effective density. *Atmos. Environ.* **99**, 500–507 (2014).
51. United States Environmental Protection Agency. *US EPA. [2021]. Estimation Programs Interface Suite™ v 4.11* (Washington, DC, USA, 2012).
52. Donahue, N. M., Robinson, A. L., Stanier, C. O. & Pandis, S. N. Coupled partitioning, dilution, and chemical aging of semivolatile organics. *Environ. Sci. Technol.* **40**, 2635–2643 (2006).
53. Donahue, N. M., Epstein, S. A., Pandis, S. N. & Robinson, A. L. A two-dimensional volatility basis set: 1. organic-aerosol mixing thermodynamics. *Atmos. Chem. Phys.* **11**, 3303–3318 (2011).
54. Donahue, N. M., Kroll, J. H., Pandis, S. N. & Robinson, A. L. A two-dimensional volatility basis set—Part 2: diagnostics of organic-aerosol evolution. *Atmos. Chem. Phys.* **12**, 615–634 (2012).
55. Pankow, J. F. & Asher, W. E. SIMPOL.1: a simple group contribution method for predicting vapor pressures and enthalpies of vaporization of multifunctional organic compounds. *Atmos. Chem. Phys.* **8**, 2773–2796 (2008).
56. Stolzenburg, D. et al. Rapid growth of organic aerosol nanoparticles over a wide tropospheric temperature range. *Proc. Natl. Acad. Sci. USA* **115**, 9122–9127 (2018).
57. Lee, D. S. et al. Transport impacts on atmosphere and climate: aviation. *Atmos. Environ.* **44**, 4678–4734 (2010).
58. Duarte, D. J., Rutten, J. M. M., van den Berg, M. & Westerink, R. H. S. In vitro neurotoxic hazard characterization of different tricresyl phosphate (TCP) isomers and mixtures. *Neurotoxicology* **59**, 222–230 (2017).
59. Hageman, G., Mackenzie Ross, S. J., Nihom, J. & van der Laan, G. *Occupational Neurotoxicology*, edited by M. Aschner (Elsevier Science & Technology, San Diego, 2022), Vol. 7, p. 77–132.
60. Keefer, E. W., Gramowski, A., Stenger, D. A., Pancrazio, J. J. & Gross, G. W. Characterization of acute neurotoxic effects of trimethylolpropane phosphate via neuronal network biosensors. *Biosens. Bioelectron.* **16**, 513–525 (2001).
61. International Civil Aviation Organization (ICAO). *Environmental Report Aviation And Environment. Destination Green The Next Chapter. International Civil Aviation Organization (ICAO)* (2019).
62. Weiden, S.-L., von der Drevnick, F. & Borrmann, S. Particle Loss Calculator—a new software tool for the assessment of the performance of aerosol inlet systems. *Atmos. Meas. Tech.* **2**, 479–494 (2009).
63. Seinfeld, J. H. & Pandis, S. N. *Atmospheric Chemistry and Physics. From Air Pollution to Climate Change*. 3rd ed. (Wiley, s.l., 2016).
64. Pankow, J. F. An absorption model of gas/particle partitioning of organic compounds in the atmosphere. *Atmos. Environ.* **28**, 185–188 (1994).
65. Williams, B. J., Goldstein, A. H., Kreisberg, N. M. & Hering, S. V. In situ measurements of gas/particle-phase transitions for atmospheric semivolatile organic compounds. *Proc. Natl. Acad. Sci. USA* **107**, 6676–6681 (2010).
66. Donahue, N. M. et al. How do organic vapors contribute to new-particle formation. *Faraday Discuss.* **165**, 91–104 (2013).
67. Epstein, S. A., Riipinen, I. & Donahue, N. M. A semiempirical correlation between enthalpy of vaporization and saturation concentration for organic aerosol. *Environ. Sci. Technol.* **44**, 743–748 (2010).

Acknowledgements

We thank Anett Dietze of the Leibniz Institute for Tropospheric Research (TROPOS) for filter preparation and weighing. This research has been supported by the Deutsche Forschungsgemeinschaft (DFG; German Research Foundation) (grant no. 410009325 and 428312742 (TRR 301)).

Author contributions

F.U. wrote the paper; designed research, performed the field sampling, sample preparation, measurements, lab experiments and majority of data analysis; L.C. performed lab experiments and analysed data; F.D. and D.R. performed SMPS measurements; M.S., D.v.P., S.J., D.K., A.K. and J.C. advised on data interpretation; A.L.V. designed research, advised on data analysis, data interpretation and manuscript writing; edited and revised the manuscript; and directed the project administration. All authors commented on the manuscript and contributed to the scientific discussion.

Funding

Open Access funding enabled and organized by Projekt DEAL.

Competing interests

The authors declare no competing interests.

Additional information

Supplementary information The online version contains supplementary material available at <https://doi.org/10.1038/s43247-022-00653-w>.

Correspondence and requests for materials should be addressed to Alexander L. Vogel.

Peer review information *Communications Earth & Environment* thanks the anonymous reviewers for their contribution to the peer review of this work. Primary Handling Editors: Clare Davis. The peer reviewer reports are only from the second round of peer-review.

Reprints and permission information is available at <http://www.nature.com/reprints>

Publisher's note Springer Nature remains neutral with regard to jurisdictional claims in published maps and institutional affiliations.



Open Access This article is licensed under a Creative Commons Attribution 4.0 International License, which permits use, sharing, adaptation, distribution and reproduction in any medium or format, as long as you give appropriate credit to the original author(s) and the source, provide a link to the Creative Commons license, and indicate if changes were made. The images or other third party material in this article are included in the article's Creative Commons license, unless indicated otherwise in a credit line to the material. If material is not included in the article's Creative Commons license and your intended use is not permitted by statutory regulation or exceeds the permitted use, you will need to obtain permission directly from the copyright holder. To view a copy of this license, visit <http://creativecommons.org/licenses/by/4.0/>.

© The Author(s) 2022

Supplementary Information for:

Nucleation of jet engine oil vapours is a large source of aviation-related ultrafine particles

Florian Ungeheuer¹, Lucía Caudillo¹, Florian Ditas², Mario Simon¹, Dominik van Pinxteren³, Dogushan Kilic^{4,5}, Diana Rose², Stefan Jacobi², Andreas Kürten¹, Joachim Curtius¹, Alexander L. Vogel^{1,*}

¹Institute for Atmospheric and Environmental Sciences, Goethe-University Frankfurt, Frankfurt am Main, 60438, Germany

²Department for Ambient Air Quality, Hessian Agency for Nature Conservation, Environment and Geology, Wiesbaden, 65203, Germany

³Atmospheric Chemistry Department (ACD), Leibniz Institute for Tropospheric Research (TROPOS), Leipzig, 04318, Germany

⁴The Department of Earth and Environmental Sciences, the Faculty of Science and Engineering, the University of Manchester, Manchester, UK

⁵National Centre for Atmospheric Science, Manchester, UK

*Correspondence to: vogel@iau.uni-frankfurt.de

This PDF file includes:

Supplementary Note 1 to 5

Supplementary Figure 1 to 11

Supplementary Table 1 to 3

Supplementary References

Supplementary Note 1.

Jet engine oil constituents

Jet engine oils are mainly composed of only a few constituents selected in terms of their lubricating, cooling and stability characteristics¹. Base stock materials like pentaerythritol esters or trimethylolpropane esters are combined with organophosphates functioning as anti-wear agents and metal deactivators^{2,3}. Amine additives act as antioxidants⁴. In aircraft engines, the oil is circulating and a lubrication oil recovery system ensures the cleaning and reuse of the oil. Although it is a closed system, oil can be released to the atmosphere depending on seal tightness and the venting system^{1,5}. These emissions depend on the engine model, the engine design⁵ and the operational state¹.

We analysed commonly used oils like the Mobil Jet™ Oil II⁶ and Mobil Jet™ Oil 254 (Exxon Mobil, Irving, TX, USA), the Turbo Oil 2197 and 2380 (Eastman, Tennessee, USA) and the AeroShell Turbine Oil 500 (Royal Dutch Shell, The Hague, Netherlands). The composition of these oils can be described in accordance to the safety data sheets mainly by five different compounds: pentaerythritol esters ($C_{27-38}H_{48-70}O_8$), trimethylolpropane esters ($C_{27-34}H_{50-64}O_6$), N-phenyl-1-naphthylamine ($C_{16}H_{13}N$), alkylated diphenylamine (Bis(4-(1,1,3,3-tetramethylbutyl)phenyl)amine; $C_{28}H_{43}N$) and tricresyl phosphate ($C_{21}H_{21}O_4P$) (Supplementary Figure 1). These compounds have been described as molecular markers for jet engine oil emissions during aircraft operations⁷. We confirmed that finding and, furthermore, detected that trimethylolpropane esters are still in use at Frankfurt International Airport, although it is known that the neurotoxin trimethylolpropane phosphate is formed upon pyrolysis of this oil⁸. Although the safety data sheet of Jet Oil II lists 1,4-Dihydroxyanthraquinone (CAS: 81-64-1), we were not able to detect this compound in either ionization polarity.

Supplementary Note 2.

Error estimation of the jet engine oil UFP mass fraction

We determined the uncertainty of the UFP jet engine oil mass fractions based on calibration-, instrumental- and measurement errors. To ensure a conclusive error calculation we identified several limitations in our analytical process taking them into account by error propagation. For the ambient filter quantification, we used the coefficient of variation of the standard addition of a sample of five pentaerythritol tetrahexanoate calibration curves. We did not consider the calibration errors of the jet oil additives as most of the quantified jet engine oil mass is determined by the group of pentaerythritol- and trimethylolpropane esters with concurrently higher uncertainties (see Supplementary Table 2). Averaging the coefficient of variation and applying it to the average jet engine oil filter- and blank filter mass of each size fraction gave us the absolute error for the

subtractive error propagation yielding the absolute error of the blank correction step. We set the absolute error of each size fraction in ratio to the size respective average blank corrected jet oil mass to obtain the relative errors for the final error propagation. For determination of the ambient UFP mass by SMPS measurements and data integration we considered a relative error of 10%. In order to determine the error of the Nano-MOUDI characterization we made use of the coefficient of variation of the external pentaerythritol tetrahexanoate calibration and the SMPS measurements standard deviations. We used the average absolute standard deviation of the single SMPS scans during the seven hour experiments of filter collection and blank determination. We calculated the absolute error of the blank corrected SMPS mass per scan by error propagation for each size fraction. Referring these values to the average blank corrected mass per scan yielded the relative error of the SMPS measurements for each size fraction. Combination of the relative error of the SMPS measurements and of the external pentaerythritol tetrahexanoate calibration by error propagation yielded the average relative error for the three size fractions of the Nano-MOUDI characterization. Including the relative errors of the Nano-MOUDI characterization, the ambient SMPS measurements and the ambient filter quantification in a final error propagation step yielded an error of the UFP jet oil mass fraction for the three size ranges. The error analysis follows the equation used to determine the contribution of jet engine oil to the UFP mass giving an error of 52%, 53% and 25% for the 10-18 nm, 18-32 nm and 32-56 nm stage, respectively.

Supplementary Note 3.

UHPLC-HRMS method

Targeted measurements of the jet engine oil constituents in the UFP samples were carried out by using ultra-high performance liquid chromatography (UHPLC) (Vanquish Flex, Thermo Fisher Scientific)/heated electrospray ionization (HESI) combined with an Orbitrap high-resolution mass spectrometer (HRMS) (Q Exactive Focus Hybrid-Quadrupol-Orbitrap, Thermo Fisher Scientific). Chromatographic separation of the jet engine oil constituents was accomplished using a reversed phase column (Accucore C₁₈, 150 x 2.1 mm, 2.6 µm particle size, Thermo Fisher Scientific), thermostated at 40 °C (still air) operated in gradient mode. As mobile phase we used ultrapure water (18.2 MΩ·cm, Millipak® Express 40: 0.22 µm, Millipore; Milli-Q® Reference A+, Merck) with 0.1% formic acid (v/v, solvent A) and methanol (Optima™ LC/MS grade, Fisher scientific) with 0.1% formic acid (v/v, solvent B). Both UHPLC solvents were spiked with formic acid (LiChropur®, Merck, 98-100%) functioning as an acidifier/proton donor. This leads to an enhanced ionization in the positive mode and improves the chromatographic separation.

The total method duration was 20 minutes with a flow rate of 400 µL/min and an injection volume of 5 µL. We started the UHPLC chromatography with 60% solvent B (0-0.5 min). Then we increased solvent B to 90% (0.5-11 min) and then raised up to 99% (11-16 min). In the end, solvent B was

reduced to 60% (16-17 min) to equilibrate the starting conditions for the following measurement within three minutes.

Due to the chemical composition and molecular structure, the jet engine oil constituents form positively charged molecular ions ($[M+H]^+$, $[M+Na]^+$) by adduct formation. Hence, the mass spectrometric detection was conducted by HESI in positive mode. The applied HESI settings were: 350 °C gas temperature, 40 psi sheath gas (nitrogen), 8 psi auxiliary gas (nitrogen) and a spray voltage of 3.5 kV. The measurement for quantification was realised by selected ion monitoring (SIM) with a resolution of $\sim 35k$ using an inclusion list based on prior measurements of the purchased jet engine oils and ambient samples. At maximum only four compounds were detected simultaneously in a SIM time window to attain highest possible detection sensitivity. Mass spectrometry (MS) data was recorded in profile mode. The target compounds were N-phenyl-1-naphthylamine ($C_{16}H_{13}N$, CAS: 90-30-2), 1,4-Dihydroxyanthraquinone ($C_{14}H_8O_4$, CAS: 81-64-1), tri-*o*-cresyl phosphate ($C_{21}H_{21}O_4P$, CAS: 78-30-8), pentaerythritol esters ($C_{27-38}H_{48-70}O_8$), trimethylolpropane esters ($C_{27-34}H_{50-64}O_6$) and Bis(4-(2,4,4-trimethylpentan-2-yl)phenyl)amine ($C_{28}H_{43}N$, CAS: 15721-78-5).

Supplementary Note 4.

Quantification method of jet engine oil constituents

Quantification of the jet engine oil constituents was achieved by the use of a standard addition method with authentic standards. For the analysis, we extracted a centred circular punch of the samples with a diameter of 2.5 cm two times, 20 minutes each on a shaker with 100 and 50 μ L pure methanol (Optima™ LC/MS grade, Fisher scientific). Glass vials with 200 μ L flat bottom micro inserts (LLG Labware, $\varnothing \times H$: 6 \times 31 mm) were used for the extraction to ensure a covering of the entire filter surface. After the combination of the two extracts, the solvent extracts were then aliquoted onto three glass vials by pipetting 20 μ L into 100 μ L micro inserts with conical bottoms (VWR, $\varnothing \times H$: 6 \times 31 mm). One vial was used for the measurement of the native sample and two for the standard addition. The sample extracts were measured directly after extraction. We used pentaerythritol tetrahexanoate (95%, Carbosynth Ltd) for the oil base stock and the oil additives N-phenyl-1-naphthylamine ($\geq 98.0\%$, Sigma-Aldrich), tri-*o*-cresyl phosphate ($\geq 97.0\%$, Sigma-Aldrich), Bis(4-(2,4,4-trimethylpentan-2-yl)phenyl)amine (90%, Fluorochem) and 1,4-Dihydroxyanthraquinone ($\geq 98.0\%$, Sigma-Aldrich). The jet oil base stock is composed of a mixture of pentaerythritol esters with different total carbon chain length of $C_{27} - C_{38}$ attached to the ester groups. As the ionization efficiency of HESI and therefore the resulting signal intensity is mainly dependent on functional groups, we used pentaerythritol tetrahexanoate to quantify all pentaerythritol ester compounds. Standard addition method was chosen to overcome matrix effects because of the strong tendency of the target compounds to adsorb on surfaces.

Two dilutions of the jet engine oil constituents in methanol were prepared, one contained the four additives at $0.08 \text{ ng } \mu\text{L}^{-1}$ and pentaerythritol tetrahexanoate at $1.5 \text{ ng } \mu\text{L}^{-1}$. The second dilution was four times higher in concentrations. The concentrations of the different dilutions were set based on single UFP filter measurements and quantification by external calibrations to cover the ambient filter concentration ranges.

After separating the solvent extracts onto three vials $20 \mu\text{L}$ each, we added $3 \mu\text{L}$ of each dilution to a respective vial. The degree of dilution of the native sample was adjusted by adding $3 \mu\text{L}$ of pure methanol. The nominal final concentrations were $0.010 \text{ ng } \mu\text{L}^{-1}$ for each additive (N-phenyl-1-naphthylamine, 1,4-Dihydroxyanthraquinone, Bis(4-(2,4,4-trimethylpentan-2-yl)phenyl)amine, tri-*o*-cresyl phosphate) and $0.196 \text{ ng } \mu\text{L}^{-1}$ for pentaerythritol tetrahexanoate in the first spiking series and four times higher in the second, respectively. This led to a total of 75 measurements with 3 measurements per UFP filter. Signal integration was automatically carried out by the software Xcalibur (version 4.2.47, Thermo Fisher Scientific), and checked manually. For each compound in every UFP sample a linear regression was accomplished based on the spiked samples allowing to quantify the jet engine oil constituents in the native samples (Supplementary Figure 8). The quantification results were field blank corrected and adjusted with the individual purity of the used calibration standards.

As the ester base stock of trimethylolpropane esters was detected in the course of the data analysis, we used previously measured full scan MS-spectra for quantification of these esters. Therefore, we applied a correction factor between full-MS and SIM mode of 1.95 that was determined using the surrogate standard pentaerythritol tetrahexanoate.

Supplementary Note 5.

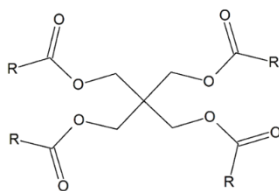
Characterization of the Nano-MOUDI sampler

Various groups used MOUDI and Nano-MOUDI samplers for the collection and subsequent analysis of UFPs⁹⁻¹². However, the quantitative determination is not only challenging because of the very low mass of UFPs (sub-microgram of total particle mass collected after 30-50 hours of sampling), but it is also difficult to account for sampling artefacts while quantifying UFP mass in the Nano-MOUDI sampler. Therefore, we characterized the cascade impactor in the lab using a variety of compounds with different chemical functional groups as surrogates. Finally, we used pentaerythritol tetrahexanoate as representative for jet oil basestocks to attain a loss correction factor for each size distribution stage.

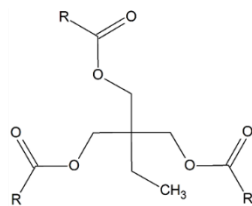
The Nano-MOUDI loss factors were determined based on the quantified filter mass compared to the mass based on the measured particle number size distributions. The loss of particles $< 100 \text{ nm}$ is dominated by diffusional wall losses¹³. In addition, sampling on the last three Nano-MOUDI stages takes place at reduced pressures down to approximately 1/6 of the ambient pressure

(~17.2 kPa; 18-32 nm stage) and therefore evaporation of semi-volatile compounds is expected to be relevant. In order to determine possible losses of jet engine oil constituents during sampling, we characterized the Nano-MOUDI sampler in a lab experiment by generating nanoparticles of pentaerythritol tetrahexanoate ($C_{29}H_{52}O_8$) and quantification of the collected particle mass. This single ester compound was chosen as a suitable surrogate as the jet engine oils are mainly composed of these synthetic esters. The particle size distribution was measured every 5 min using a scanning-mobility particle sizer (SMPS; $D = 2.3-82.2$ nm, TSI, model: 3938, Shoreview, MN, USA) containing an electrostatic classifier (EC; TSI, model: 3082) equipped with an Aerosol Neutralizer (TSI, model 3088) and a nano Differential Mobility Analyzer (Nano DMA; TSI, model: 3085A). Particle number concentrations were recorded using an ultrafine condensation particle counter (UCPC; TSI, model: 3776). We used a Constant Output Atomizer (home-built replica of TSI model: 3076) to produce nanoparticles with an average electrical mobility diameter of ~50 nm (Supplementary Figure 9) by using ~0.1 g/L pentaerythritol tetrahexanoate in methanol. The formed nanoparticles pass a diffusion dryer filled with preconditioned silica gel. Subsequently they enter a mixing chamber (Volume ~2.2 L) where mixing with clean air provides the flow rate needed for the analysis. The particles follow the airstream to the Nano-MOUDI for particle collection and to the SMPS system. In order to guarantee a laminar flow (Reynolds number < 2100) the aluminium tube connection between the mixing chamber and the Nano-MOUDI/SMPS system was designed based on the equation to estimate the laminarisation length for a straight tube¹⁴. At the end of the aluminium tube (ID 1 inch, length 1.5 m) a bend bypass was used to split the flow for the respective analysis. The flow rates were adjusted according to the instruments used, the setup with the detailed flow rates is shown in Supplementary Figure 10.

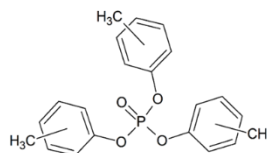
We collected nanoparticles on the last three Nano-MOUDI stages for 7 hours in triplicate experiments. Two blank measurements with pure methanol were conducted equally to correct for nanoparticle formation from solvent impurities. We determined the deposited mass on each Nano-MOUDI size distribution stage by integration of the particle size number distribution assuming spherical particles and using the pentaerythritol tetrahexanoate density (1.014 g cm^{-3}). The mass of the blank measurements was determined equally using a unit density of 1 g cm^{-3} (Details see Supplementary Table 3). Averaging the blank masses stage wise and subtracting of the corresponding masses provided the corrected mass, based on the measured particle number size distribution. The resulting mass was adjusted with the purity of the used pentaerythritol tetrahexanoate standard. The aluminium filter extraction was conducted as described above. Mass spectrometric analysis was carried out in SIM mode and quantification by external calibration using the pentaerythritol tetrahexanoate standard. We calibrated five points in the range of $0.1-15$ ng μL^{-1} and measured each calibration point three times in succession. The calibration function was determined based on the average of the measurements of each concentration. The quantified filter mass was adjusted with the purity of the pentaerythritol tetrahexanoate standard.



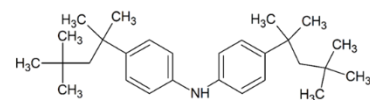
Pentaerythritol ester
($C_{27-38}H_{48-70}O_8$)



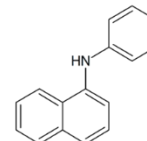
Trimethylolpropane ester
($C_{27-34}H_{50-64}O_6$)



Tris(2-methylphenyl) phosphate
($C_{21}H_{21}O_4P$)



Bis(4-(2,4,4-trimethylpentan-2-yl)phenyl)amine
($C_{28}H_{43}N$)

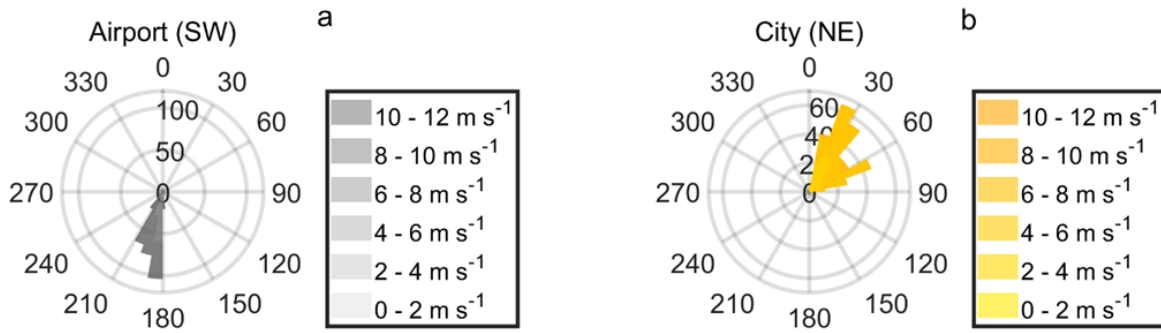


N-Phenyl-1-naphthylamine
($C_{16}H_{13}N$)

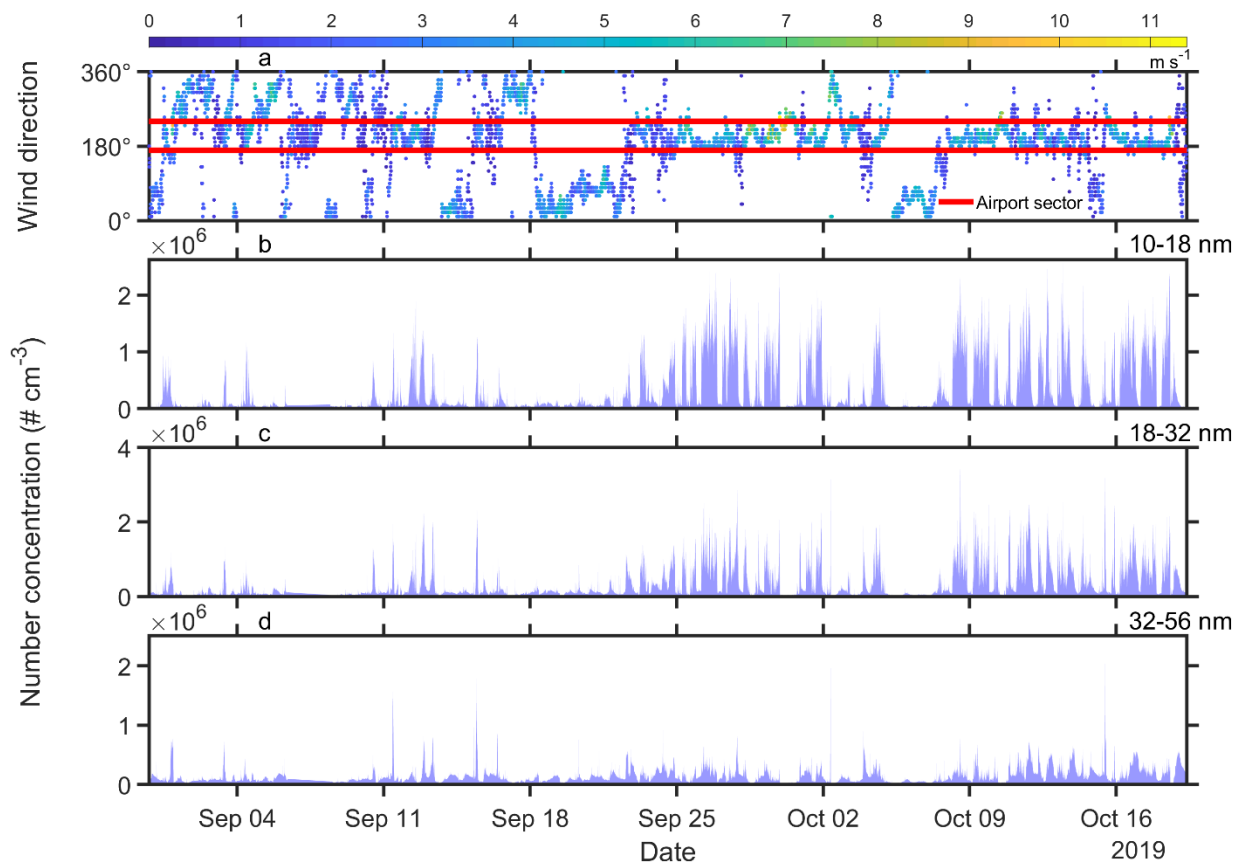
Supplementary Figure 1. Most prominent jet engine lubrication oil constituents.



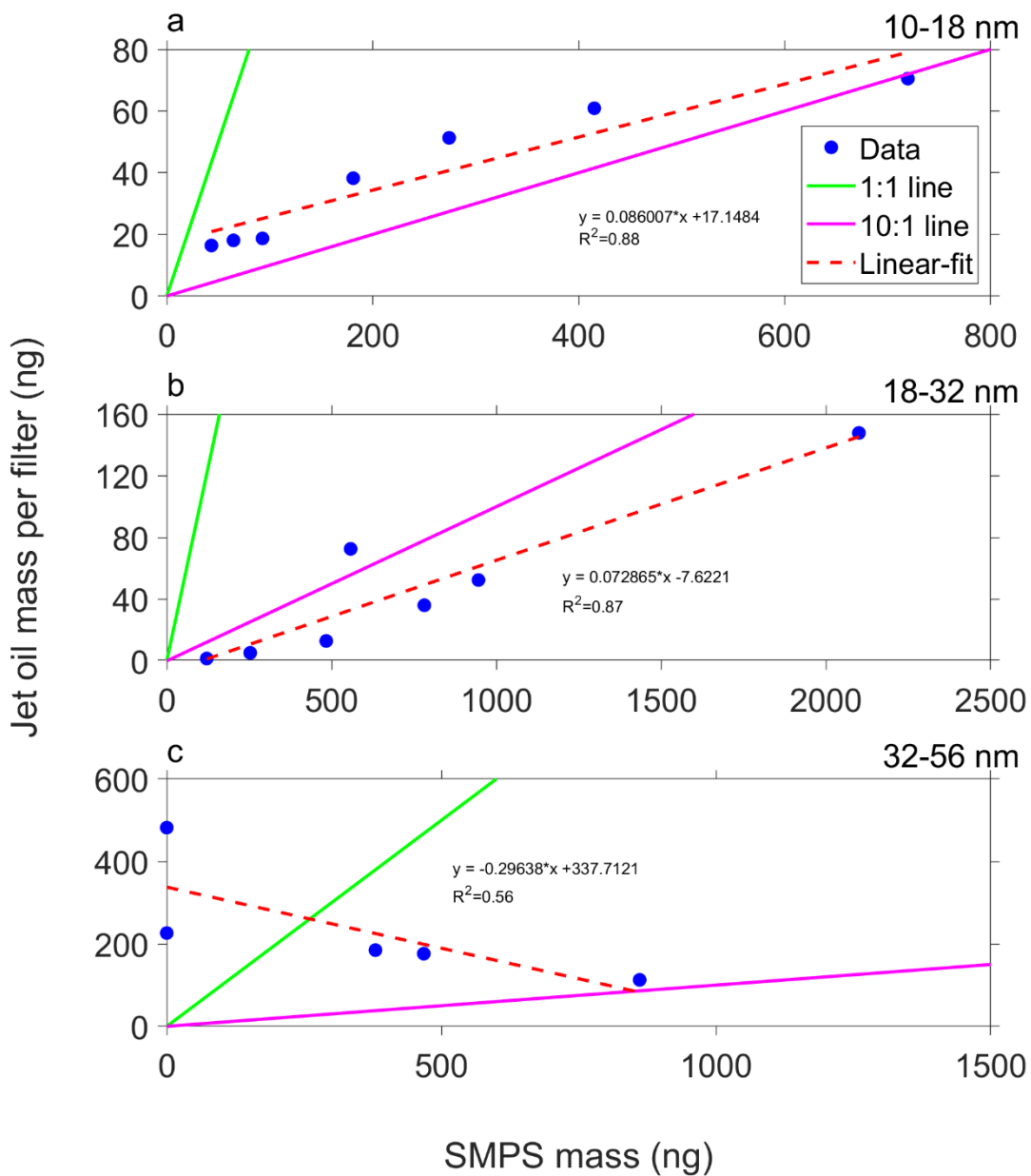
Supplementary Figure 2. Map showing the sampling site in a distance of 4 km to Frankfurt Airport (www.openstreetmap.org/copyright).



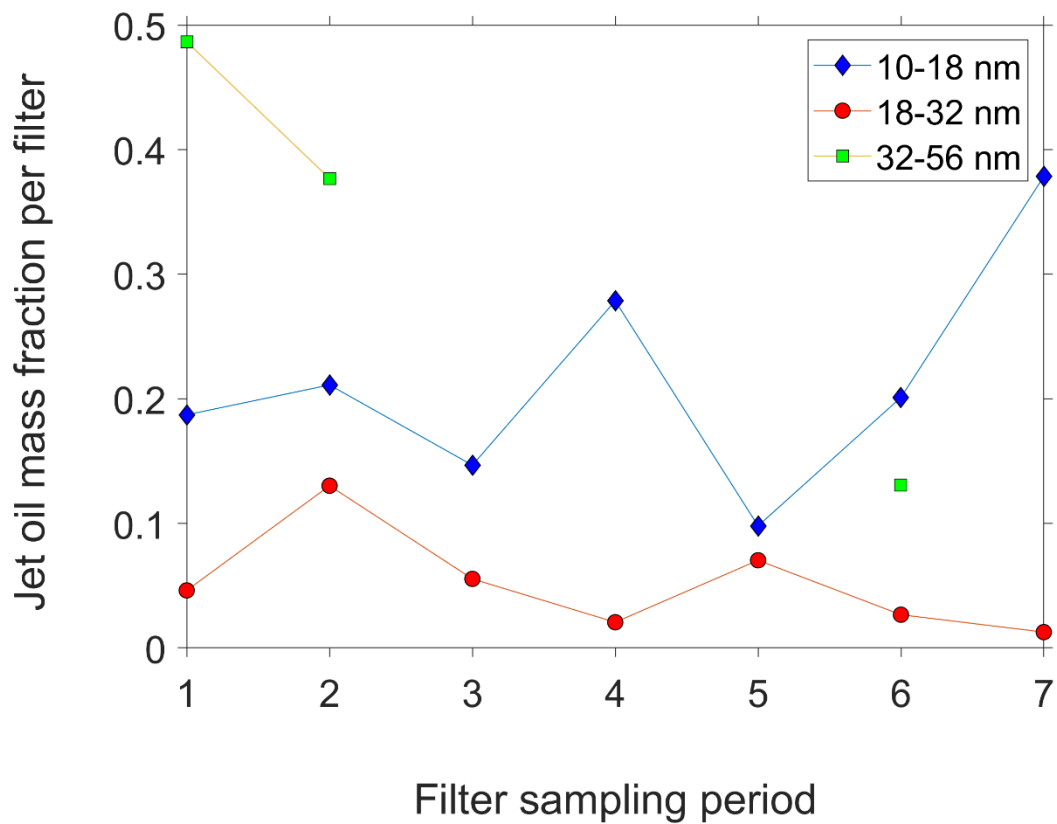
Supplementary Figure 3. Wind roses related to figure 1a showing the wind direction of the ambient SMPS data (Airport (a)- and city (b) direction) averaged over three days (05:00–23:00 CET).



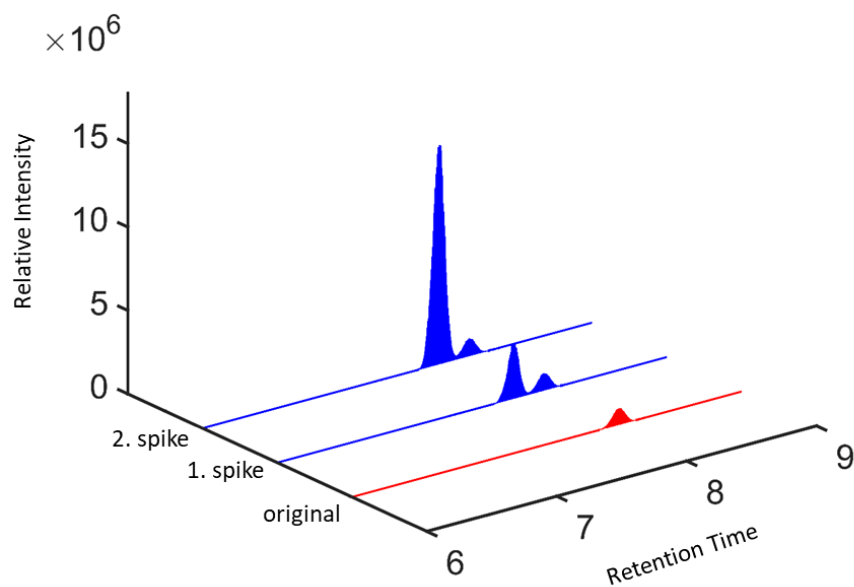
Supplementary Figure 4. Overview of the size-resolved UFP number concentration ($\# \text{ cm}^{-3}$) measurements at Frankfurt Airport. Wind direction (a) with wind speed indicated by colour bar. The wind data is provided by the meteorological station at Frankfurt Airport (International Civil Aviation Organization, ICAO, code: EDDF) of the German weather service (DWD). The ambient UFP number concentration ($\# \text{ cm}^{-3}$) in the size ranges (b) 10-18 nm, (c) 18-32 nm and (d) 32-56 nm are shown.



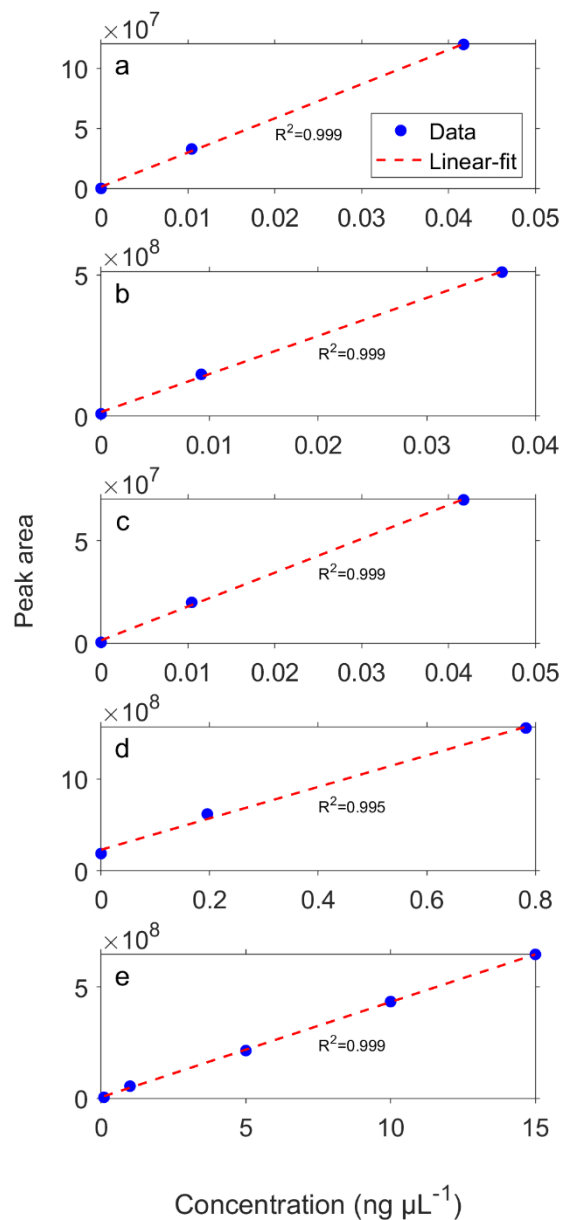
Supplementary Figure 5. Correlation between the corrected jet oil mass per filter and the ambient SMPS mass showing a distinct correlation for the 10-18 nm (a) and 18-32 nm (b) size range. For the 32-56 nm (c) size range no correlation can be observed.



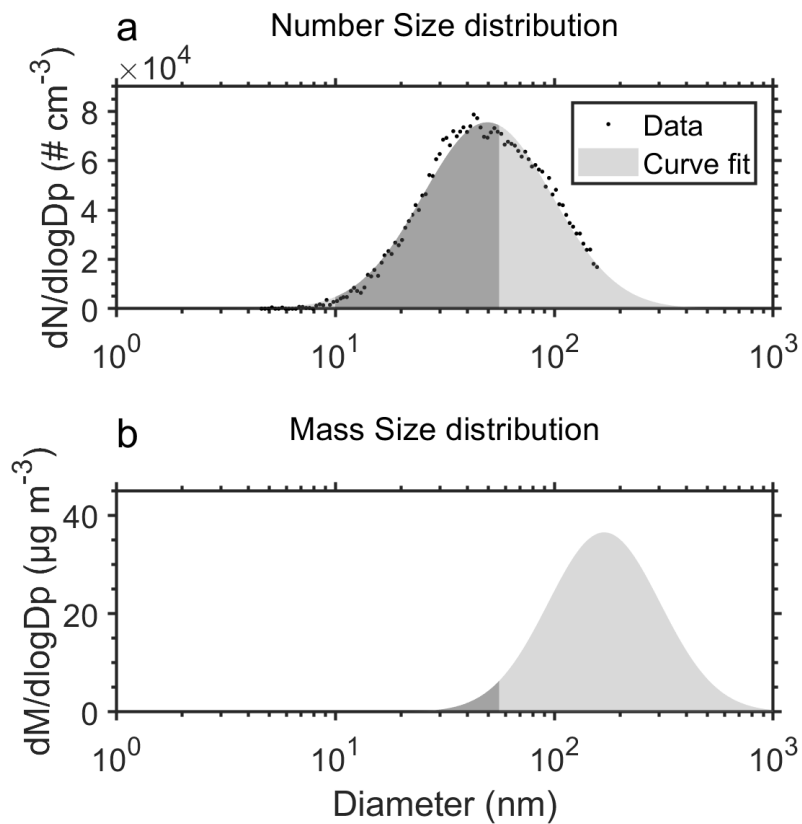
Supplementary Figure 6. Jet oil mass fractions of the collected filter samples for the three Nano-MOUDI size stages (10-18 nm, 18-32 nm, 32-56 nm). The values of the 32-56 nm stage are limited and artificially high due to a high SMPS background correction.



Supplementary Figure 7. Development of the extracted ion chromatogram (XIC) of tricresyl phosphate ($[M+Na]^+$: 391.1069) during the add-on steps. The added tri-*o*-cresyl phosphate ($C_{21}H_{21}O_4P$) forms a peak signal left of the original sample signal, which indicates no high *ortho*-isomer concentrations in the airport samples.



Supplementary Figure 8. Standard addition calibration curves of (a) N-phenyl-1-naphthylamine, (b) alkylated diphenylamine, (c) tricresyl phosphate and (d) pentaerythritol tetrahexanoate. Plot (e) shows the pentaerythritol tetrahexanoate external calibration curve for the Nano-MOUDI characterization.

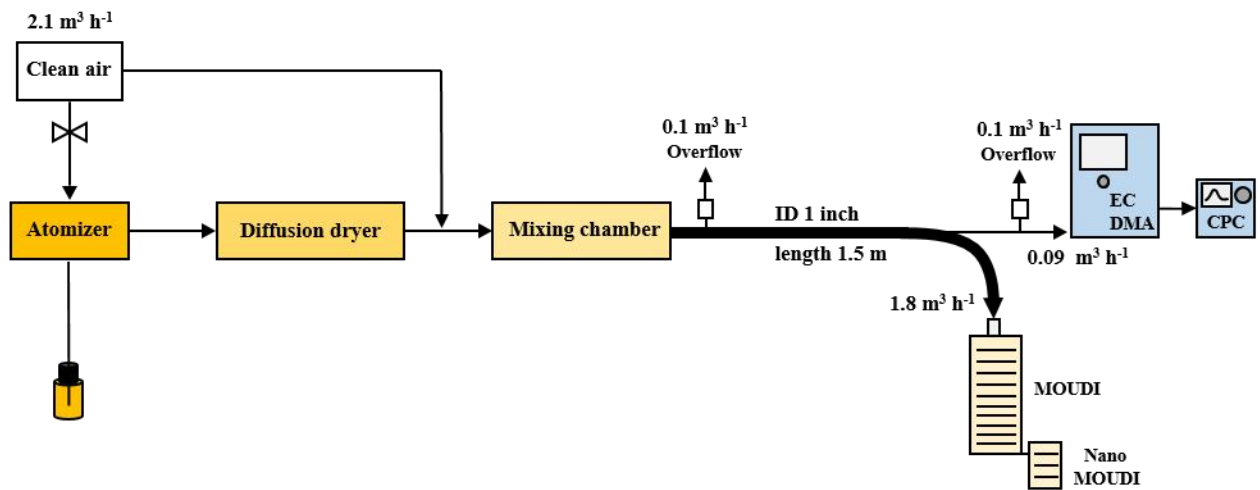


Supplementary Figure 9. Particle number size and mass distribution (a, b) of the pentaerythritol tetrahexanoate nanoparticles formed for the Nano-MOUDI sampler characterization. The dark shading indicates the size range of particle deposition in the Nano-MOUDI stages.

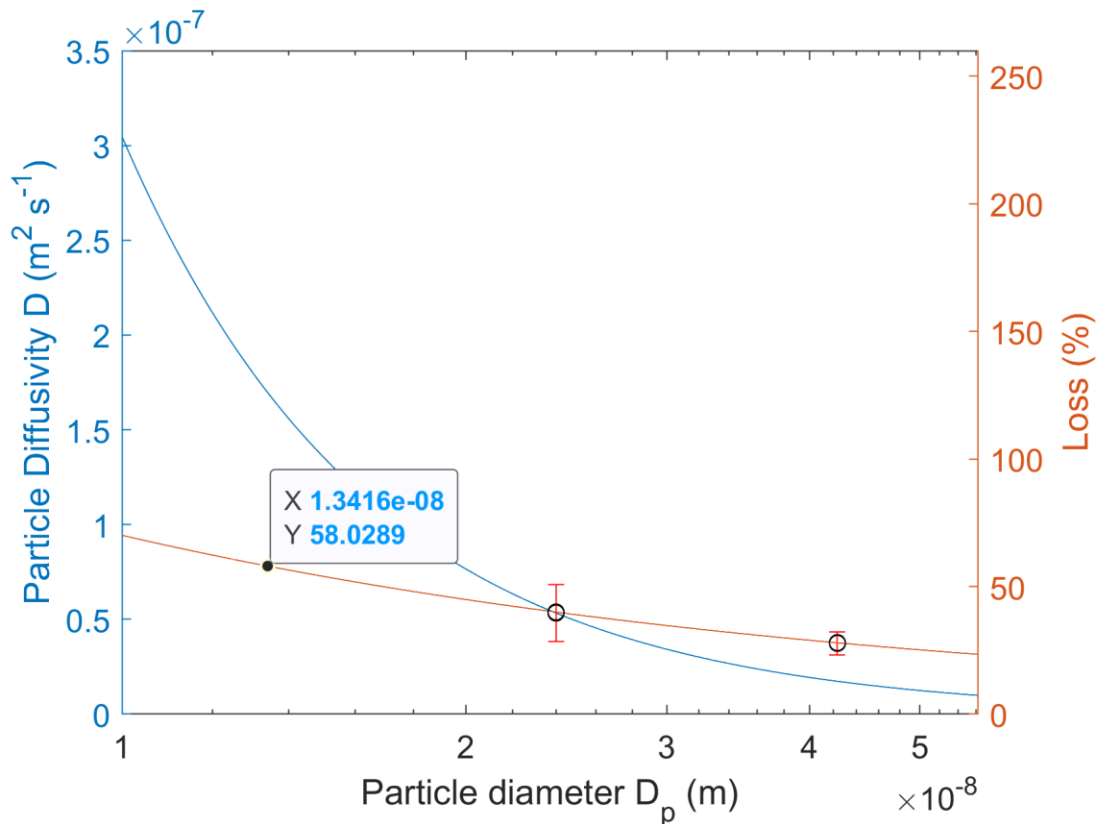
a



b



Supplementary Figure 10. (a) Photo of the setup to characterize the Nano-MOUDI regarding possible sampling artefacts and to determine loss factors for the 10-18 nm, 18-32 nm and 32-56 nm size stages. (b) Schematic representation of the Nano-MOUDI characterization setup including the detailed flow rates used.



Supplementary Figure 11. Dependency between particle diffusivity, particle diameter and the experimental Nano-MOUDI loss factors. Using an exponential damping term to calculate the particle loss of 58% on the smallest Nano-MOUDI stage (10-18 nm). This term fits the particle loss factors and diffusion coefficients and is based on the particle diffusivity equation.

Supplementary Table 1. UFP mass fractions of jet engine oil with lowest to highest and average contributions for the three Nano-MOUDI size stages.

Particle diameter (nm)	Range of oil contribution to total UFP mass (%)	Average oil contribution to total UFP mass (%)	Average oil contribution to total UFP mass not background corrected (%)
10-18	10 - 38	21 ± 11	18
18-32	1 - 13	5 ± 3	3
32-56	13 - 49*	33* ± 8	9

* These values are artificially high due to a high SMPS background correction in this size range.

Supplementary Table 2. The ambient UFP mass fractions of the single jet engine oil constituents averaged over all size stages are shown. The vapour pressures of the different compounds and compound classes are listed.

Jet oil constituents	C₁₆H₁₃N	C₂₁H₂₁O₄P	C₂₈H₄₃N	C₂₇₋₃₈H₄₈₋₇₀O₈	C₂₇₋₃₄H₅₀₋₆₄O₆
Ambient constituent fraction (%)	0.10	0.34	0.10	94.87	4.58
Mobil II constituent fraction (measured)	2.15	5.22	1.05	91.57	-
Mobil II constituent fraction (MSDS)	1	1 - < 3	-	-	-
Vapour pressure* (Pa)	3.85E-03	1.45E-05	6.73E-06	3.12E-08***	2.37E-06****
Vapour pressure** (Pa)	8.32E-04	1.53E-07	2.21E-08	1.54E-10 - 2.36E-15	2.43E-09 - 2.10E-12

* Calculated with EPI Suite (25 °C)¹⁵.

** Calculated with SIMPOL.1 (20 °C)¹⁶.

*** Vapour pressure of C₂₉H₅₂O₈.

**** Vapour pressure of C₂₇H₅₀O₆.

Supplementary Table 3. SMPS masses of the individual Nano-MOUDI characterization experiments. The collected pentaerythritol tetrahexanoate mass was determined using the density of 1.014 g cm⁻³. For the blank mass a unit density of 1 g cm⁻³ was used.

Collection 1	
Nano MOUDI stage	Total collected mass [ng]
32 - 56 nm	2574.0
18 - 32 nm	249.7
10 - 18 nm	8.4
10 - 56 nm	2832.1
Collection 2	
Nano MOUDI stage	Total collected mass [ng]
32 - 56 nm	3641.0
18 - 32 nm	368.5
10 - 18 nm	14.5
10 - 56 nm	4024.0
Collection 3	
Nano MOUDI stage	Total collected mass [ng]
32 - 56 nm	3643.5
18 - 32 nm	388.4
10 - 18 nm	16.2
10 - 56 nm	4048.1
Blank 1	
Nano MOUDI stage	Total collected mass [ng]
32 - 56 nm	974.2
18 - 32 nm	173.7
10 - 18 nm	14.7
10 - 56 nm	1162.6
Blank 2	
Nano MOUDI stage	Total collected mass [ng]
32 - 56 nm	1245.1
18 - 32 nm	215.4
10 - 18 nm	14.3
10 - 56 nm	1474.9

Supplementary References

1. Yu, Z. *et al.* Characterization of lubrication oil emissions from aircraft engines. *Environ. Sci. Technol.* **44**, 9530–9534; 10.1021/es102145z (2010).
2. Wyman, J. F., Porvaznik, M., Serve, P., Hobson, D. & Uddin, D. E. High Temperature Decomposition of Military Specification L-23699 Synthetic Aircraft Lubricants. *J. Fire Sci.* **5**, 162–177; 10.1177/073490418700500303 (1987).
3. Du Han, H. & Masuko, M. Elucidation of the Antiwear Performance of Several Organic Phosphates Used with Different Polyol Ester Base Oils from the Aspect of Interaction between Additive and Base Oil. *Tribol. T.* **41**, 600–604; 10.1080/10402009808983788 (1998).
4. Wu, Y., Li, W., Zhang, M. & Wang, X. Improvement of oxidative stability of trimethylolpropane trioleate lubricant. *Thermochim. Acta* **569**, 112–118; 10.1016/j.tca.2013.05.033 (2013).
5. Timko, M. T. *et al.* Composition and Sources of the Organic Particle Emissions from Aircraft Engines. *Aerosol Sci. Technol.* **48**, 61–73; 10.1080/02786826.2013.857758 (2014).
6. Winder, C. & Balouet, J.-C. The toxicity of commercial jet oils. *Environ. Res.* **89**, 146–164; 10.1006/enrs.2002.4346 (2002).
7. Fushimi, A., Saitoh, K., Fujitani, Y. & Takegawa, N. Identification of jet lubrication oil as a major component of aircraft exhaust nanoparticles. *Atmos. Chem. Phys.* **19**, 6389–6399; 10.5194/acp-19-6389-2019 (2019).
8. Ungeheuer, F., van Pinxteren, D. & Vogel, A. L. Identification and source attribution of organic compounds in ultrafine particles near Frankfurt International Airport. *Atmos. Chem. Phys.* **21**, 3763–3775; 10.5194/acp-21-3763-2021 (2021).
9. Díaz-Robles, L. A. *et al.* Health risks caused by short term exposure to ultrafine particles generated by residential wood combustion: a case study of Temuco, Chile. *Environ. Int.* **66**, 174–181; 10.1016/j.envint.2014.01.017 (2014).
10. Andrade-Oliva, M.-A. *et al.* In vitro exposure to ambient fine and ultrafine particles alters dopamine uptake and release, and D2 receptor affinity and signaling. *Environ. Toxicol. Pharmacol.* **80**, 103484; 10.1016/j.etap.2020.103484 (2020).
11. Focsa, C. *et al.* Multi-technique physico-chemical characterization of particles generated by a gasoline engine: Towards measuring tailpipe emissions below 23 nm. *Atmos. Environ.* **235**, 117642; 10.1016/j.atmosenv.2020.117642 (2020).
12. Takegawa, N. *et al.* Characteristics of sub-10 nm particle emissions from in-use commercial aircraft observed at Narita International Airport. *Atmos. Chem. Phys.* **21**, 1085–1104; 10.5194/acp-21-1085-2021 (2021).
13. Weiden, S.-L. von der, Drewnick, F. & Borrmann, S. Particle Loss Calculator – a new software tool for the assessment of the performance of aerosol inlet systems. *Atmos. Meas. Tech.* **2**, 479–494; 10.5194/amt-2-479-2009 (2009).

14. Bird, R. B., Stewart, W. E. & Lightfoot, E. N. *Transport phenomena*. 2nd ed. (Wiley, New York, 2007).
15. United States Environmental Protection Agency. *US EPA. [2021]. Estimation Programs Interface Suite™ v 4.11* (Washington, DC, USA,).
16. Pankow, J. F. & Asher, W. E. SIMPOL.1: a simple group contribution method for predicting vapor pressures and enthalpies of vaporization of multifunctional organic compounds. *Atmos. Chem. Phys.* **8**, 2773–2796; 10.5194/acp-8-2773-2008 (2008).

5.3 Occurrence and in vitro toxicity of organic compounds in urban background PM_{2.5}



Occurrence and *in vitro* toxicity of organic compounds in urban background PM_{2.5}



Jonas P. Wallraff^{a,1}, Florian Ungeheuer^{a,1}, Andrea Dombrowski^b, Jörg Oehlmann^b, Alexander L. Vogel^{a,*}

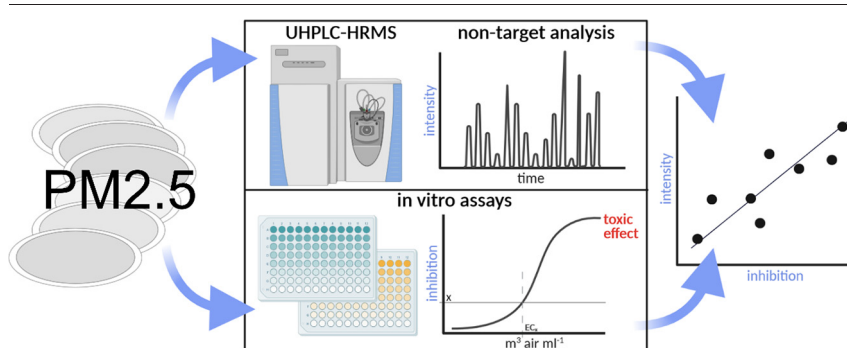
^a Institute for Atmospheric and Environmental Sciences, Goethe-University Frankfurt, Altenhöferallee 1, 60438 Frankfurt am Main, Germany

^b Institute of Ecology, Evolution and Diversity, Goethe-University Frankfurt, Max-von-Laue-Str. 9, 60438 Frankfurt am Main, Germany

HIGHLIGHTS

- High-resolution mass spectrometry and *in vitro* toxicity assays applied on PM_{2.5}.
- The chemical composition of urban background PM_{2.5} has a strong source dependency.
- Urban PM_{2.5} exerts higher *in vitro* toxicity than PM_{2.5} advected from an airport.
- Unspecific and specific toxicity correlate well with PM_{2.5} mass concentration.
- Future work needs to identify the drivers for toxicity in urban PM.

GRAPHICAL ABSTRACT



ARTICLE INFO

Article history:

Received 29 October 2021

Received in revised form 12 December 2021

Accepted 25 December 2021

Available online 8 January 2022

Editor: Jianmin Chen

Keywords:

Non-target analysis
Baseline toxicity
Microtox
AChE inhibition
Particulate matter
Aerosol

ABSTRACT

This study describes the chemical composition and *in vitro* toxicity of the organic fraction of fine particulate matter (PM_{2.5}) at an urban background site, which receives emissions either from Frankfurt international airport or the city centre, respectively. We analysed the chemical composition of filter extracts (PM_{2.5}) using ultrahigh-performance liquid chromatography coupled to a high-resolution mass spectrometer, followed by a non-target analysis. In parallel, we applied the bulk of the filter extracts to a Microtox and acetylcholinesterase-inhibition assay for *in vitro* toxicity testing. We find that both the chemical composition and toxicity depend on the prevailing wind directions, and the airport operating condition, respectively. The occurrence of the airport marker compounds tricresyl phosphate and pentaerythritol esters depends on the time of the day, reflecting the night flight ban as well as an airport strike event during November 2019. We compared the organic aerosol composition and toxicity from the airport wind-sector against the city centre wind-sector. We find that urban background aerosol shows a higher baseline toxicity and acetylcholinesterase inhibition compared to rural PM_{2.5} that is advected over the airport. Our results indicate that the concentration and individual composition of PM_{2.5} influence the toxicity. Suspected drivers of the acetylcholinesterase inhibition are i.e. organophosphorus esters like triphenyl phosphate and cresyldiphenyl phosphate, and the non-ionic surfactant 4-tert-octylphenol ethoxylate. However, further research is necessary to unambiguously identify harmful organic air pollutants and their sources and quantify concentration levels at which adverse effects in humans and the environment can occur.

1. Introduction

Air pollution is a significant worldwide environmental risk with adverse effects on human health, which are largely determined by fine particulate matter (PM_{2.5}, aerodynamic diameter < 2.5 μm) (Landrigan et al., 2018; Lelieveld et al., 2015; Lim et al., 2012). PM_{2.5} enters the respiratory system

* Corresponding author.

E-mail address: vogel@iau.uni-frankfurt.de (A.L. Vogel).

¹ These authors contributed equally.

via airways and can penetrate deep into the lung (Xing et al., 2016). Chronic exposure can lead to negative influences on mostly any organ (Schraufnagel, 2020; Schraufnagel et al., 2019). Lelieveld et al. (2019) estimate an annual excess mortality rate of 659,000 per year from air pollution in the European Union (EU-28), which largely can be attributed to PM_{2.5} exposure. In the new air quality guidelines of the World Health Organization (WHO) the PM_{2.5} limit has been reduced from 10 down to 5 µg m⁻³ (WHO, 2021). This limit is exceeded in many European regions (European Environment Agency (EEA), 2019).

In order to assess the health effects of ambient PM, a small fraction of anthropogenic organic pollutants is monitored in urban areas. These are usually polycyclic aromatic hydrocarbons (PAHs), and more rarely phthalate diesters and organophosphorus esters (OPEs). Both PAHs, as well as their transformation products, nitro-PAHs, are mutagenic and carcinogenic substances (Bandowe and Meusel, 2017; Guo et al., 2011; Kim et al., 2013). Phthalate diesters, mostly used as plasticisers, are suspected to exert a variety of toxic effects (e.g., endocrine disrupting effects) in humans and animals (UBA (Umweltbundesamt), 2004, 2017). OPEs, such as triphenyl phosphate (TPhP) or tributyl phosphate (TBP) have numerous use cases e.g., as flame retardants, plasticisers, or additives in lubrication and hydraulic oils, why they are found in both indoor and outdoor air (Reemtsma et al., 2008; Wong et al., 2018; Zhou et al., 2017). Many OPEs are hazardous. The specific mechanism of intoxication is the inhibition of the acetylcholinesterase (AChE) via phosphorylation, which can lead to cholinergic overstimulation resulting in headaches, emotional instability, confusion, as well as chronic diseases (Abou-Donia, 1981; Winder and Balouet, 2002).

However, there is still a lack of a holistic understanding of the chemical composition of urban organic aerosol (OA), and the number and identity of harmful chemicals that remain undetected is highly uncertain. In contrast, *in vitro* biotests of PM extracts always respond to the complex mixtures that are tested. Various studies show that particulate matter can induce oxidative stress, genotoxicity, DNA degradation, inflammation, and apoptosis, with harmful consequences on the respiratory and cardiovascular system (Arias-Pérez et al., 2020). The oxidative potential of airborne PM, as a metric for acute PM health effects (Bates et al., 2019), led to the recognition that anthropogenic emissions from residential wood burning and non-exhaust vehicular emissions are mostly associated with the oxidative potential concentration (Daellenbach et al., 2020). Further studies show that air pollution also exhibits detrimental effects on the central nervous system and increases the risk of dementia and neurodegeneration (Chew et al., 2020; Kanninen et al., 2020; Peters et al., 2019). Still, the molecular link to specific chemicals or chemical classes as toxicity drivers remains elusive, while there is evidence that the mass of PM alone cannot explain the variability of toxicological effects (Cassee et al., 2013; Rönkkö et al., 2021; Daellenbach et al., 2020).

In earlier studies, the Microtox assay with the autoluminescent bacterium *Aliivibrio fischeri* was used to examine the baseline toxicity of PM_{2.5}. The Microtox assay considers multiple toxicological effects that take place at the cellular level, such as log *K_{OW}*-dependent unspecific effects that include narcosis, uncoupling (disruption of the oxidative phosphorylation), and electrophilicity-based effects (Brack, 2003; Cronin and Schultz, 1998; Hermens et al., 1985; Lionetto et al., 2019; Schultz and Cronin, 1997). The assay is widespread in aquatic ecotoxicology and has previously been used for the examination of airborne particles (Lionetto et al., 2019; Roig et al., 2013). Lionetto et al. (2019) found a strong correlation between the bioluminescence inhibition in the Microtox assay and PM₁₀ (aerodynamic diameter < 10 µm) concentration at an urban background in Southern Italy. They report a weak correlation between the baseline toxicity and the oxidative potential of PM₁₀, making it a valuable test system for airborne particles (Lionetto et al., 2019). In contrast, Roig et al. (2013) found no correlation between PM₁₀ concentrations and the results obtained with the Microtox assay, concluding that only a few substances drive the toxicity.

The AChE inhibition of single chemicals or complex mixtures can be determined using the Ellman assay, in which acetylthiocholine, as an alternative enzyme substrate, is hydrolysed by AChE into thiocholine and acetate. The formed thiocholine can be photometrically determined using Ellman's reagent (Ellman 1961). To our knowledge, the AChE-inhibition assay has not yet been applied on organic extracts of atmospheric PM in order to determine the potential neurotoxic effects of organophosphates or other neurotoxic compounds.

To gain further insight about a potential composition-dependent toxicity, in this study we comprehensively characterised the chemical composition of organic PM_{2.5} extracts and determined their toxic potential with the two *in vitro* assays; Microtox and AChE inhibition. The investigated samples were chosen to reflect the emissions of a large airport in contrast to air masses from a large city centre (urban background), which both can be considered as a source of different organophosphates. PM_{2.5} in airport direction was sampled during normal operation and during an airport strike event and before the Covid-19 pandemic.

2. Material and methods

2.1. Sampling site

Field sampling was conducted at the air quality monitoring station Frankfurt-Schwanheim, located 4 km north of the Frankfurt International Airport, Germany (Fig. 1). Frankfurt airport is the largest German commercial airport and counted over 70 million passengers in 2019 (Fraport, 2020). It is located 100 m above sea level at 50° 3' 40" N, 8° 33' 51" E.

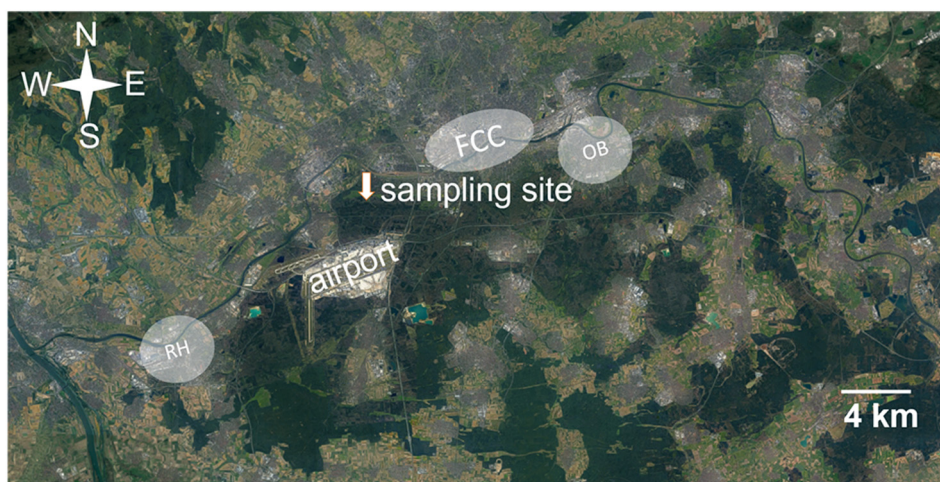


Fig. 1. Location of the air quality monitoring station Frankfurt-Schwanheim. It is located 4 km north of the Frankfurt International Airport. FCC – Frankfurt city centre, OB – city of Offenbach, Main, RH – city of Rüsselsheim (Bilder © 2021, Google, Bilder © 2021 TerraMetrics, Kartendaten © 2021 GeoBasis-DE/BKG (©2009)).

The main wind directions at the airport are south-southwest and northeast (HLNUG, 2018). South-southwest is the predominant direction. The monitoring station is located on a sports ground, the nearest street is in approximately 100 m distance. It is surrounded by the Frankfurt forest. The city centre of Frankfurt (FCC) is located roughly 4 km northeast of the station (Fig. 1). The district Niederrad and the residential area of Schwanheim are located 4 km east-northeast, and 2 km north-northeast, respectively. The city Offenbach (OB) lies 14 km east-northeast of the station, the city Rüsselsheim (RH) in a distance of 15 km southwest (Fig. 1). According to the Hessian Agency for Nature Conservation, Environment, and Geology (HLNUG) the air quality monitoring station Schwanheim has urban background characteristics (HLNUG, 2018). This is excepted by the lower burden with airborne pollutants due to the distance to inhabited areas (HLNUG, 2018). At south-southwesterly wind direction there is a rural emission background with low anthropogenic influence, with the exception of the airport. The station is representative for the emissions of highly frequented airports, overflights do not take place (HLNUG, 2018).

2.2. Sampling procedure

PM_{2.5} was sampled during the 30th of October 2019 to the 9th of November 2019 using a High Volume Air Sampler (HVS) (Digital DHA-80, Digital Elektronik AG, Volketswil, Switzerland) loaded with baked-out (6 h at 450 °C) micro glassfiber filters with a diameter of 150 mm (Munktel MG 160, Ahlstrom-Munksjö, Helsinki, Finland). A sampling interval of 6 h per filter was chosen to illustrate the night flight ban at Frankfurt Airport, which applies from 23:00 to 05:00. The HVS was operated with a flow of 500 l min⁻¹.

After sampling, the filters were stored at -20 °C until further analysis. Three different sampling conditions were chosen, each reflecting specific wind directions. Filters that were taken during normal airport operation and main wind direction from south-southwest are marked as AN (Fig. 2). Filters assigned to condition AS were sampled during a Deutsche Lufthansa strike in November 2019 with comparable wind conditions as AN (Fig. 2). The city condition (C) includes filters that were taken during the main wind directions from north-northeast to east-northeast, reflecting an urban background from the city centre (Fig. 2). For every condition four filters were analysed, one assigned to nighttime (23:00–05:00) and three sampled at daytime (Table 1). An unsampled filter, which was treated just as the samples, was stored inside the HVS for a couple of days and served as field blank for both chemical analysis and toxicity testing.

2.3. Sample preparation

The sampled filter area used for analysis was 154 cm². A whole filter was cut into small pieces using pre-cleaned ceramic scissors. The pieces were transferred into a 30 ml glass vial. For the extraction of organic compounds, a total of 20 ml distilled dichloromethane (DCM) was used in a two-step extraction. In the first step, filters were covered with 15 ml DCM and extracted on an orbital shaker (KS 15-A, Edmund Bühler GmbH, Bodelshausen, Germany) for 20 min at 300 rpm. Afterwards, the solvent

Table 1

List of analysed samples.

	Normal airport operation (AN)		Airport strike (AS)		City (C)	
	Sample #	Time	Sample #	Time	Sample #	Time
Nighttime	AN27	23:00–05:00	AS31	23:00–05:00	C5	23:00–05:00
Daytime	AN19	11:00–17:00	AS29	11:00–17:00	C7	11:00–17:00
	AN24	17:00–23:00	AS30	17:00–23:00	C4	17:00–23:00
	AN26	17:00–23:00	AS28	05:00–11:00	C3	11:00–17:00

extract was filtered using a solid phase extraction (SPE) cartridge made of glass. It was loaded with a filter punch that retained particles of $\geq 1.2 \mu\text{m}$ (Munktel MG 160) and fitted with a steel pin. The second extraction step consisted of the same procedure but was carried out using only 5 ml of DCM. Thereupon, the pooled extract of about 15 ml was evaporated near dryness under a gentle nitrogen stream and at 35 °C. The remaining extract was transferred into a 1 ml glass vial. The extraction glass was rinsed with a small amount of DCM, which was pooled with the extract. The extract was then evaporated to dryness. The residue was taken up in 85 μl of MeOH:H₂O (50:50) (see 2.5 Chemical analysis for used chemicals) and used for *in vitro* testing. All analyses were carried out within 3 weeks after sample preparation. For the chemical analysis of PM_{2.5}, aliquots of 5 μl from the *in vitro* extracts were taken and diluted 1:20 by MeOH:H₂O (50:50). The remaining *in vitro* extract (80 μl) was further diluted for triplicate and quadruplicate *in vitro* analysis. Hence, the procedure ensures identical sample extraction conditions for both the *in vitro* and organic-chemical analysis.

2.4. In vitro testing

The sample-extracts (four per sampling condition) were tested for baseline toxicity, applying the Microtox assay according to Escher et al. (2008) and neurotoxic effects using an AChE inhibition assay. Microtox assays with *A. fischeri* cover effects altering the bacterial energy metabolism (Brack, 2003). The assay provides insight about the unspecific toxicity as multiple stressors may inhibit the metabolism of *A. fischeri* leading to decreased bioluminescence (Escher et al., 2014; Völker et al., 2017). The decrease in bioluminescence reflects the cellular metabolic status as determinant for the toxicity (Abbas et al., 2018). As a specific assay targeting neurotoxicity, the AChE inhibition assay originally described by Ellman et al. (1961) was used. The assay aims to examine potential neurotoxic effects caused by AChE inhibitors such as organophosphorus compounds (Eyer, 1995; Winder and Balouet, 2002).

2.4.1. Baseline toxicity

The baseline toxicity was determined using the bioluminescent bacterium *A. fischeri* following the procedure described in Escher et al. (2008) and was based on the ISO-guideline (ISO 11348-3:2007). PM_{2.5} extracts and controls including 3,5-dichlorophenol as positive control were serially diluted (1:2) obtaining eight concentrations for each sample. For the

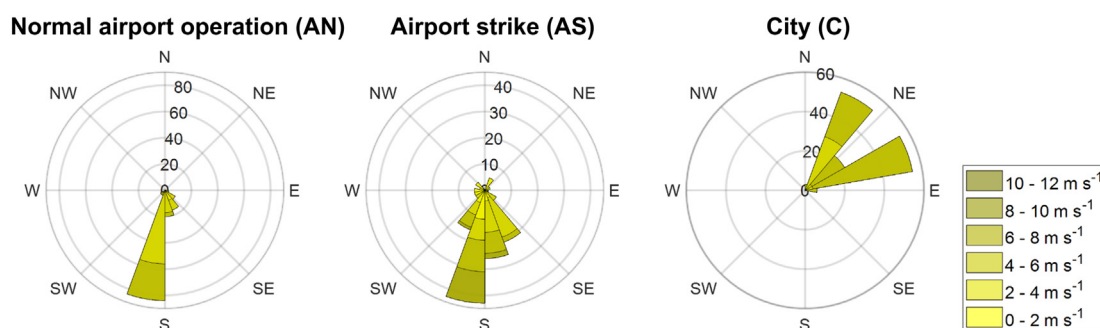


Fig. 2. Wind roses indicating the wind directions and speed of the examined filters assigned to the three sampling conditions. All filter samples were taken during 30.10.2019 to 09.11.2019. Data provided by the meteorological station at Frankfurt airport (ICAO-Code: EDDF) of the Deutscher Wetterdienst (DWD).

extracts these dilutions refer to 0.35 to 47 m³ air ml⁻¹. The diluted sample solutions (100 µl) were added to 50 µl of bacterial suspension. The luminescence emitted by *A. fischeri* was measured prior to and 30 min after sample addition using a microplate reader (Tecan Spark 10 M, Tecan Group, Männedorf, Switzerland). Each sample was tested in three independent experiments including one technical replicate. The results were corrected for the inhibition caused by the negative controls (bacterial solution without any present inhibitor) resulting in a relative inhibition rate (%). By pooling the triplicates, a mean relative inhibition was derived for each sample. Based on this, an effective concentration (EC₂₀ ± confidence intervals (CI) in m³ air ml⁻¹ reflecting a decrease in light emission of 20%) was calculated using a nonlinear regression model. The upper plateau was constrained to 100% luminescence inhibition, the lower plateau to the inhibition caused by the field blank, respectively.

2.4.2. AChE inhibition

The assay according to the protocol by Ellman et al. (1961) was used. Further alterations were made to adapt the assay to 96-well plates as described by Sigma-Aldrich (2018). 10 µl positive control (0.1 mM paraoxon-methyl, PESTANAL®, ≥ 98% purity, Sigma-Aldrich, St. Louis, Missouri, USA), negative control (0.4 units ml⁻¹ AChE from *Electrophorus electricus*, Sigma-Aldrich) or sample, and 90 µl AChE (0.4 units ml⁻¹) were added to a 96-well plate and diluted 1:2 column-wise, obtaining eight concentrations for each sample. For the extracts these dilutions refer to 0.4 to 53 m³ air ml⁻¹. After incubation on a platform shaker (Titramax 1000, Heidolph Instruments GmbH & Co. KG, Schwabach, Germany) for 5 min at 450 rpm the reaction was started by adding 150 µl of the reaction mix consisting of 5,5'-dithio-bis-(2-nitrobenzoic acid) (30 µM, ≥ 98% purity, Sigma-Aldrich) and acetylthiocholine iodide (600 µM, ≥ 98% purity, Sigma-Aldrich) dissolved in phosphate buffer (1.5 M, pH 7.2) (see Supplementary Information (SI), Table S1). The increase in absorbance was immediately measured at 412 nm over 6 min in intervals of 15 s using a microplate reader (Tecan Spark 10 M, Tecan Group). Each sample was tested in four independent experiments including one technical replicate. Only samples showing a linear absorbance increase ($r^2 \geq 0.9$) in the initial reaction phase of the kinetic were used for further data evaluation. The inhibition rate was calculated as described by Sigma-Aldrich (2018) where ΔA_{sample} is the increase in absorption for each individual sample and $\Delta A_{\text{NCpooled}}$ reflects the averaged increase in the negative controls without a present inhibitor (Eq. (1)). Based on the inhibition rate an EC₂₅ pooling the quadruplicates was calculated for each sample using a nonlinear regression model. The upper plateau was constrained to 100% AChE inhibition, the lower one to 0%, respectively.

$$\text{Inhibition [\%]} = \frac{1 - \Delta A_{\text{sample}}}{\Delta A_{\text{NCpooled}}} \times 100 \quad (1)$$

2.5. Chemical analysis of organic PM fraction

The chemical composition of PM_{2.5} was examined using an ultra-high performance liquid chromatograph (UHPLC; Vanquish Flex, Thermo Fisher Scientific, Waltham, Massachusetts, USA) coupled to a quadrupole-Orbitrap hybrid mass spectrometer (Q Exactive Focus, Thermo Fisher Scientific). The chromatographic separation of compounds was carried out on an Accucore™ C₁₈ column (150 mm × 2.1 mm; 2.6 µm solid-core particles, Thermo Fisher Scientific) operated in gradient mode with a constant flow of 400 µl min⁻¹ and heated to 40 °C (still air). Ultrapure water (solvent A) (Millipak® Express 40: 0.22 µm, Millipore; Milli-Q® Reference A+, Merck, Darmstadt, Germany) and Methanol (solvent B) (Optima™ LC/MS grade, Thermo Fisher Scientific), both acidified (v/v 0.1%) with formic acid (LiChropur® ≥ 98% purity, Merck), were used as mobile phase. The chromatographic separation started with 5% solvent B, maintained for 1 min. Within 12 min the amount of solvent B was increased to 95% and held for 2 min. Subsequently, the starting conditions were restored by decreasing solvent B to 5% within 2 min, allowing the system to equilibrate

for 3 min before the next run. Altogether, one chromatographic run lasted 20 min. The sample (5 µl) was injected using an autosampler thermostated at 15 °C. Samples were ionised via heated electrospray ionisation (HESI) and measured in the positive ionisation mode over a range of mass-to-charge ratio (m/z) 50–750. The mass resolving power was ~70 k at m/z 200. The capillary voltage was set to 3.5 kV, the capillary temperature was at 300 °C. The sheath gas was set to a flow of 50 psi (nitrogen), the aux gas flow rate was set to 10 psi (nitrogen) with an aux gas temperature of 350 °C. The Orbitrap instrument was operated in discovery mode to gain further insight into the fragmentation of single compounds. In this mode, fragmentation spectra of the highly abundant signals are recorded by estimating a peak apex during acquisition of the chromatogram. Prior to the measurements, the MS was calibrated using an external calibration solution (Pierce™ LTQ Velos ESI positive ion, Thermo Fisher Scientific) obtaining a mass accuracy of better than 2 ppm.

2.6. Non-target analysis and data filtering

The full-scan MS spectra were analysed by the non-target analysis software Compound Discoverer (CD) (version 3.2.0.421, Thermo Fisher Scientific) as described by Ungeheuer et al. (2021). CD was already tested against the non-target analysis software MZmine2 (Vogel et al., 2019). Briefly, CD identifies compounds and determines the molecular composition based on the measured exact mass, isotopic signature, MS/MS fragmentation patterns and compares measured MS/MS fragmentation spectra with a MS/MS database (mzcloud.org, last access: 12th January 2021). For the detection of compounds, a mass tolerance of 5 ppm was used, and further constrained to 2 ppm for the formula prediction. The analysis results were filtered with Matlab (R2019b, MathWorks, Natick, Massachusetts, USA) by the following requirements: the minimum sample-to-blank ratio (s/b) of a compound had to be five, the minimum area 1×10^5 counts and the minimum retention time 0.7 min (deadtime of the used column was 0.6 min). The peak areas of each sample were background corrected by subtracting the related peak area of the field blank. Minimum element counts of C₁, H₁ and maximum counts of C₉₀, H₁₉₀, Br₃, Cl₄, N₄, O₂₀, P₁, S₃ were used. The obtained molecular formulae of the organic molecules were categorised into compound classes according to their elemental composition (CHO, CHN, CHNO, CHOS, CHNOS, or CHOP). Compounds to which a molecular formula could not be assigned were classified as 'other'. To compare the different sampling conditions, the summed area of each compound class was calculated. For the comparison of two conditions, an unpaired *t*-test with Welch's correction using the software GraphPad Prism (Version 5.01, GraphPad Software, San Diego, California, USA) was performed. A *p*-value <0.05 was considered as statistically significant and is indicated by ★.

2.7. Measurement of PM_{2.5} concentrations

The PM_{2.5} concentrations (in µg m⁻³) were continuously measured using a hybrid particulate mass monitor (SHARP 5030, Thermo Fisher Scientific) that utilizes nephelometry and β-absorption for real-time measurements of PM_{2.5}. For each sampling interval referring to one sample and 6 h, we averaged the PM_{2.5} concentrations based on hourly PM_{2.5} concentration values. The data was provided by the HLNUG and is available to the public (HLNUG (2019), last access: 7th July 2021). We correlated the averages with the summed signal intensity of the detected organic molecules using the software GraphPad Prism. For the linear correlation a *p*-level of <0.01 was considered as a statistically significant correlation.

2.8. Statistical analysis of bioassay data

The software GraphPad Prism was used for nonlinear regression and statistical analyses of the *in vitro* assay data. Statistical differences between the EC-values were obtained by comparison of the 95% confidence intervals. Non-overlapping CIs were considered statistically significant at a *p*-level of 0.05. We used the Pearson correlation coefficient to gain insight

about statistical relationships between the chemical composition and *in vitro* toxicity. Each samples' luminescence and AChE inhibition (%) caused by the highest analysed concentration in the dilution series of the corresponding assay was tested for linear correlations with the summed signal intensities of each compound class. Further, it was tested with the overall signal intensities for all detected compounds. A p -level < 0.01 was considered as a statistically significant correlation. The correlations were compared by their coefficient of determination (r^2).

3. Results

3.1. *In vitro* toxicity

3.1.1. Baseline toxicity

The baseline toxicity of the organic PM_{2.5} extracts was evaluated by the Microtox test. For 75% of the examined samples an effect concentration of EC₂₀, which reflects a luminescence inhibition of 20%, could be calculated. The remaining samples exerted too low toxicity on *A. fischeri* to calculate an EC₂₀. The obtained EC₂₀ values ranged from 24.7 to 57.1 m³ air ml⁻¹. Individual values with corresponding 95%-CIs are given in Fig. 3A and the SI, Table S2. The highest luminescence inhibition was found in the samples from group C (C5 and C4) (Fig. 3). In this group, C4 had the lowest EC₂₀ (24.7 (20.2 to 30.3) m³ air ml⁻¹). This was significantly lower than AN27, AN26, AS28 and C3 ($p < 0.05$). Notably, samples with no calculable EC₂₀, and therefore no observed baseline toxicity, stemmed from groups AN and AS, while the highest inhibiting samples were all from group C. City samples excluding C3 had an EC₂₀ of approximately 30 m³ air ml⁻¹, whereas for samples taken during normal airport operation and strike, the values were about twice as high indicating a considerably lower baseline toxicity.

3.1.2. AChE inhibition

The neurotoxicity of the organic PM_{2.5} extracts was examined by the evaluation of their AChE inhibition. The two highest test concentrations of each quadruplicate had to be excluded from the EC calculation due to high activity in the field blank (see SI, Fig. S1). The quadruplicate inhibition (%) for each concentration were tested for outliers with Grubb's outlier test according to Barnett and Lewis (1994). Outliers were excluded from the analysis. An EC₂₅ was obtained for all but one sample, individual values and their 95% CIs are given in Fig. 3B and the SI, Table S2. The highest inhibition was obtained in samples of group C (Fig. 3). Samples from AN had lower values than those from AS. One sample that showed no AChE inhibition stemmed from group AN (AN19). The calculated EC₂₅ values ranged from 1.39 to 11.2 m³ air ml⁻¹. The highest inhibition of AChE was observed in samples that were taken during wind from north-northeast to east-northeast and daytime (C3 and C4), the lowest during airport strike and daytime (AS29 and AS30). AS29 had an EC₂₅ of

11.2 m³ air ml⁻¹. The value was significantly higher than all other obtained values ($p < 0.05$). The highest overall AChE inhibition was observed in the daytime sample C4. It had an EC₂₅ of 1.39 m³ air ml⁻¹, no overlapping CI with all samples but C3, and about a ten times lower EC₂₅ than that of the least inhibiting sample AS29. Under normal airport operation, the largest inhibition was obtained for AN27. It had overlapping CIs with the other samples from AN and AS28, AS31, C5, C3, and C7. EC₂₅ values of AS28 and AS31 were significantly lower than those of AS29 and AS30 ($p < 0.05$). Notably, the lowest EC₂₅ and therefore highest inhibition for samples taken during the strike is reflected by the night-time sample AS31.

3.2. Organic aerosol molecular composition

The non-target screening detected a total of ~1600 different organic compounds within all analysed samples in the positive electrospray ionisation mode. Thereof, approximately 460 compounds showed at least fivefold higher signal intensities than the field blank. Airport marker compounds were detected in samples of both airport operation conditions and during day- and night-time. For a better graphical comparison between the sampling conditions, all samples of each condition were averaged (AN, AS, and C), and the organic molecular pattern is displayed by retention time against molecular weight (MW) (Fig. 4), Kroll-diagram (SI, Fig. S2), and Kendrick mass defect (KMD) against MW (Fig. 4). The KMD was calculated as described by Kendrick (1963) to identify homologous series of hydrocarbons with all homologues appearing plotted on a horizontal line. Every circle represents a single compound assigned to one of the seven compound classes. Their colouration depends on the assignment to one of the individual compound classes. The area of each circle is proportional to the signal intensity of the detected compound. We use the compound identification levels for HR-MS as suggested by Schymanski et al. (2014). All namely mentioned compounds are determined based on a minimum confidence level of two and marked accordingly (level 1: confirmed structure by reference standard; level 2: probable structure by library spectrum match) (Schymanski et al., 2014). The corresponding MS/MS spectra and chromatograms can be obtained from the SI. The compound dibutyl phthalate and its fragmentation product were excluded from the fingerprints due to their high signals in the field blank and its ubiquitous use as a plasticiser and cosmetic product (Benson, 2009). For some compounds, CD falsely interpreted ion signals of the measured ion [M + Na]⁺ as [M + H]⁺. This led to an overestimation of detected compounds since two to three additional false formulas with higher m/z than their parent molecular ion were suggested for each affected compound. These artifacts were filtered out based on the same retention time and exact mass difference between sodium and hydrogen.

Both scatter plots for normal airport operation (AN) and airport during strike (AS) show a similar molecular fingerprint, while the city condition

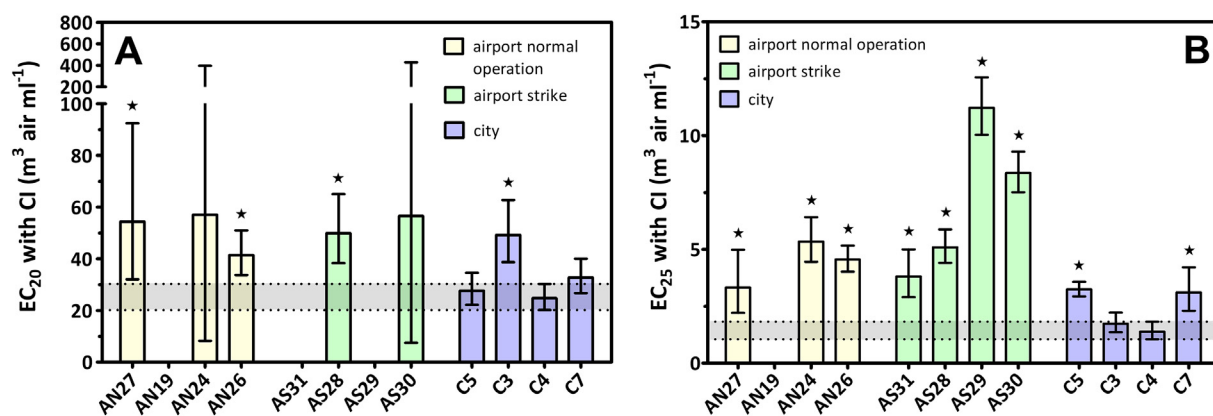


Fig. 3. Results of the Microtox and AChE inhibition assay. EC values are given with 95% confidence interval (CI) for baseline toxicity assessed via Microtox test (A, $n = 3$) and AChE inhibition (B, $n = 4$). In cases where a corresponding EC could not be calculated, the column is left out blank. The grey area indicates the interval of confidence of the sample with the highest activity, C4. Significant differences between C4 and the other samples at a p -value of < 0.05 are indicated by \star (CI comparison).

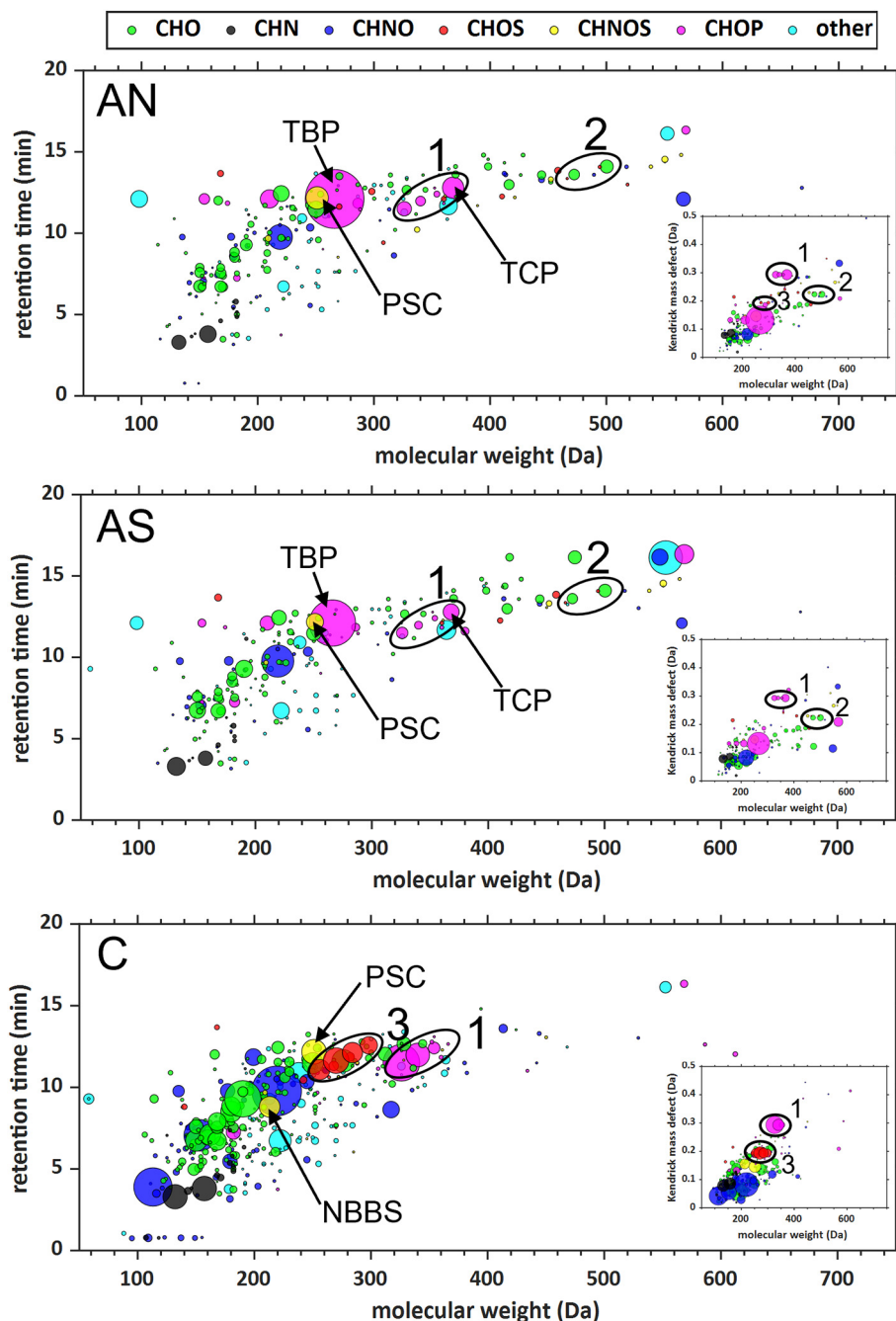


Fig. 4. Retention time against molecular weight (MW) and Kendrick mass defect plots based on the average of all samples belonging to a certain sampling condition. Three homologous rows were identified: 1 Homologues of organophosphate ($C_{18}H_{15}O_4P$ to $C_{21}H_{21}O_4P$), TCP is absent in C. 2 Pentaerythritol esters $C_{25}H_{44}O_8$ and $C_{27}H_{48}O_8$, 3 Homologous row of CHOS compounds present in C ($C_{16}H_{16}OS$ to $C_{19}H_{22}OS$) and AN ($C_{17}H_{18}OS$ and $C_{19}H_{22}OS$). Prosulfocarb (PSC) was present in all groups, N-butylbenzenesulfonamide (NBBS) only in C. AN – normal airport operation, AS – airport strike, C – city.

(C) clearly shows a distinct pattern (Fig. 4). We observed the highest number of different compounds and overall signal intensities in the city-condition samples. The summed intensities for all compounds detected in C were significantly higher than in AN (Welch's *t*-test, $p = 0.0251$) and AS ($p = 0.0257$) (Fig. 5). The samples C4 and C5 had the largest signal intensity of all detected compounds in total, AN19 and AS31 the lowest. The airport samples consisted mostly of CHO, CHNO, and CHOP compounds with CHO and CHOP showing the highest intensities. Under city-condition, the highest summed signal intensities were observed in the classes CHO and CHNO. The summed signals of these compound classes were two to four times higher than under both airport conditions. Compared to the city samples, we found higher summed intensities of phosphorus-

containing (CHOP) organic compounds in the airport samples. Among the highest signals we identified the organophosphorus compounds tributyl phosphate (TBP, level 1), tricresyl phosphate (TCP, level 1), and dibutyl phosphate (level 2), which is likely generated in the ion source *via* fragmentation of tributyl phosphate. During the airport strike period, a greater heterogeneity in the largest detected compound-signals was observed. Two of them were assigned to the CHOP (tributyl phosphate and $C_{33}H_{61}O_5P$) and one to the CHNO class ($C_{14}H_{21}NO$). Among the highest signals in the city samples, we observed nitrogen-containing compounds (e.g. $C_6H_{11}NO$, $C_{19}H_{15}NO$, and $C_{14}H_{21}NO$), which are no organonitrates but rather secondary and tertiary amines that are likely directly emitted and not formed *via* secondary formation.

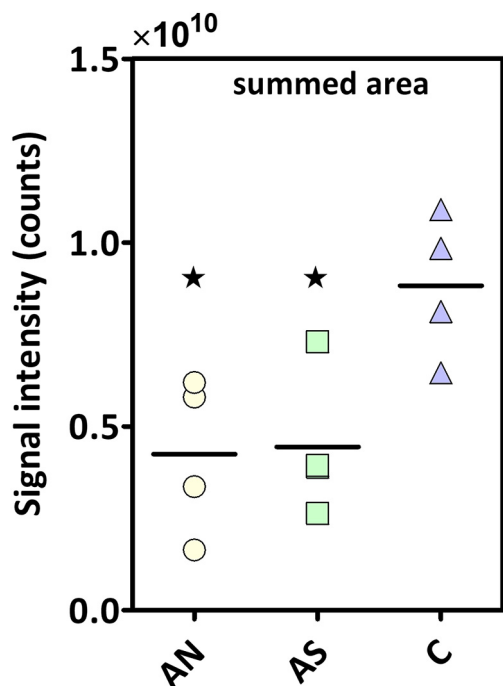


Fig. 5. Comparison between the summed signal intensities of all compounds with a signal to blank ratio higher than five. There is no significant difference between the summed intensity of AN and AS. Samples from C have significantly higher summed areas than AN and AS. Significant differences of $p < 0.05$ are indicated by \star (unpaired t -test with Welch's correction).

Across all samples we detected 195 compounds of the CHO class. Thereof, 95 were found in AN, 100 in AS and 170 in C. The summed signal intensities of CHO for AN and AS were approximately the same, whereas C had at least twofold and significantly higher intensities than AN ($p = 0.0406$) and AS ($p = 0.0499$) (Fig. 6). The samples C4 and C5 had the largest summed signal intensity, sample AN19 and AS31 the lowest (Fig. 7). The CHO class of C predominantly consisted of molecules with an MW < 350 Da (Fig. 4). CHO compounds with an MW > 500 Da were only detected in AS and AN (Fig. 4). Their carbon number was mostly below 20 in city samples, while compounds with $\geq C_{25}$ were detected under both airport conditions (see SI, Fig. S2). In the airport PM_{2.5} samples we identified specific airport marker compounds which stem from pentaerythritol-based lubrication oils that have earlier been detected in ultrafine particles at the same site (e.g. C₂₅H₄₄O₈, level 1 and C₂₇H₄₈O₈, level 1) (Ungeheuer et al., 2021) (Fig. 4, circle 2). C₂₅H₄₄O₈ exhibited high sample-to-blank (s/b) ratios of up to 100 in AN and 68 in AS, while

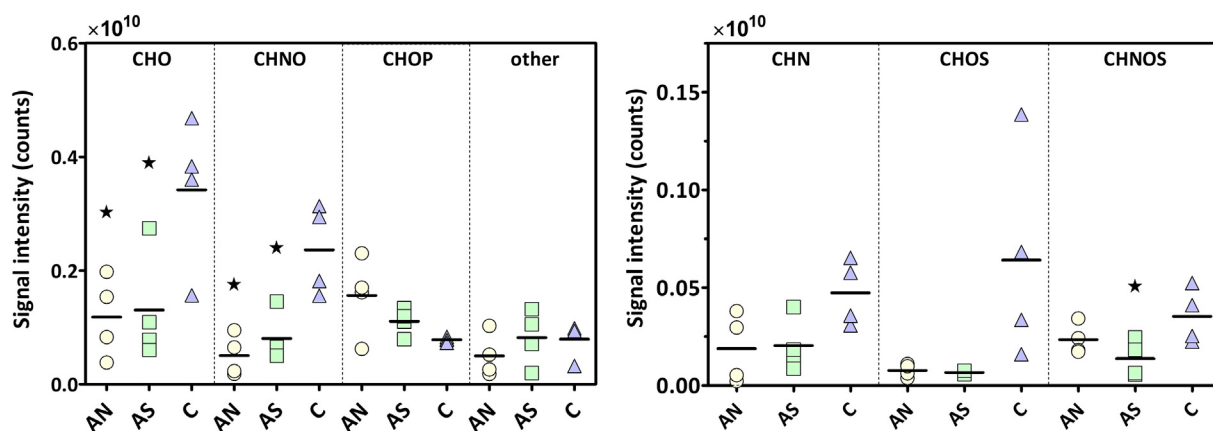


Fig. 6. Comparison between the summed signal intensities of the different compound classes. There were no significant differences between AN and AS. Significant differences between AN and AS against C with $p < 0.05$ are indicated by \star (unpaired t -test with Welch's correction).

C₂₇H₄₈O₈ had s/b ratios of up to 40 in both AN and AS. Their occurrence during night-time was at the blank level for normal airport operation (AN27). Furthermore, we identified the compound C₁₆H₂₆O₂ in all samples as 4-*tert*-octylphenol monoethoxylate (OP1EO, level 2), a common environmental pollutant (Bergé et al., 2012; Renner, 1997; Ying et al., 2002). Its abundance was the highest in samples from the city condition (C4 and C5) and lowest in sample AN19. Moreover, caryophyllene oxide (C₁₅H₂₄O, level 2) was identified in AN, AS, and C with approximately the same averaged signal intensities.

In the class of CHN compounds, which largely represents amines and heterocyclic compounds, we observed 18 compounds across all samples. Thereof, 10 were found in AN, 11 in AS, and 17 in C. The summed signal intensity for all CHN compounds within AN and AS was at least twofold lower than in C but showed no significant differences between the sampling conditions. The predominant CHN compounds were similar within groups AN and AS and consisted mostly of cyclic amines, e.g., norharmane (C₁₁H₈N₂, level 2), which was also found in C. Norharmane was most abundant in the samples C4 and AS31 (night). AN19 had the smallest signal and was approximately 20 times lower than C4.

The class of CHNO compounds consisted of 88 different compounds across all analysed samples whereof 76 were detected in the city group. In the groups AN and AS we detected 45 and 39 compounds, respectively. The summed signal intensities for C were significantly higher than those in AN ($p = 0.0130$) and AS ($p = 0.0261$), while AN and AS showed no significant difference (Fig. 6). The samples C4 and C5 had the largest overall signal intensity of CHNO compounds (Fig. 7). The lowest intensities were found in AN19 and AN24 (Fig. 7). The highest signals showed great heterogeneity among the sampling conditions, but none could be identified. However, many of the molecules were cyclic based on their H/C ratios of about 0.8 to 1.5. The largest measured CHNO signal was C₁₄H₂₁NO, which exhibited a fragment through the loss of C₃H₆. C₁₄H₂₁NO was found in all groups and had about two- to threefold higher intensities in samples from the city wind-sector.

The class of CHOS compounds consisted of 19 different compounds across all samples. Thereof 11 were detected in C, 6 in AS, and 10 in AN. The largest signal areas of CHOS compounds were found in C3 and C7, the lowest in the night sample AN27. Notably, the highest CHOS signals for C consisted of smaller molecules with an MW < 300 Da while for AN and AS compounds with an MW > 450 Da were detected (Fig. 4). Their summed signal intensity was at least eightfold higher in C than in AN and AS. This could be traced back to a homologous row of four CHOS compounds (C₁₆H₁₆OS to C₁₉H₂₂OS) present in C but absent in AS (Fig. 4, circle 3). Two of them (C₁₇H₁₈OS and C₁₉H₂₂OS) were also found in AN but had at least sevenfold lower averaged signal intensities than in C. The homologues were characterised by their identical KMD of 0.19 Da and differed by a CH₂-unit (Fig. 4). The compounds could not be further identified with the mzcloud database, however, based on their H/C ratios of ~ 1 we can state that they likely contain a cyclic or unsaturated carbon skeleton.

For the CHNOS class, 18 different signals were detected. Thereof, 11 were found in AN, 8 in AS, and 10 in C. Their summed signal intensity for C was significantly higher than for AS ($p = 0.0498$) (Fig. 6). Again, we observed the lowest summed signal intensities in the airport wind-sector (AN24 and AS29), and the highest for the city wind-sector (C5 and C4) (Fig. 7). One of the detected molecules was identified as the systemic herbicide prosulfocarb (PSC, $C_{14}H_{21}NO_5$, level 1). PSC was present in all groups with the highest intensity in AN26 and C4 (Fig. 4). The night-time sample AS31 exhibited the lowest signal. Furthermore, the neurotoxic plasticiser N-butylbenzenesulfonamide ($C_{10}H_{15}NO_2S$, NBBS, level 2) (Rider et al., 2012) was identified in all samples from C, but it was largely absent in samples from the airport wind-sector (Fig. 4).

The class of CHOP compounds consisted of 29 different compounds across all samples. Thereof 17 compounds were detected in each AN and AS, and 21 compounds were found in C. We found that the CHOP-group is the only elemental composition group that exhibited the lowest summed intensity for samples from the city-sector. The AN samples were twofold higher than in C, and a third higher than in AS, indicating a strong emission of this class during normal airport operation. The compound $C_{12}H_{27}O_4P$ was identified as tributyl phosphate (TBP, level 1), which was absent in the city-sector and largely present in air masses from the airport during daytime with higher values under normal operating conditions and lower during the strike event (Fig. 4). Furthermore, we identified a homologous row of aromatic organophosphorus compounds ($C_{18}H_{15}O_4P$ to $C_{21}H_{21}O_4P$) based on a CH_2 -based KMD, caused by the varying number of methylated phenyl groups (Fig. 4). The largest homologue was identified as tricresyl phosphate (TCP, level 1), which was absent in samples from the city sector and showed a lower averaged intensity under airport strike condition compared to the normal airport operation (Fig. 4). The highest signal of TCP

was obtained during daytime and normal airport operation. The smallest homologue was identified as triphenyl phosphate (TPHP, level 1) and detected among all groups being at least sixfold higher on average in C than in AN and AS, indicating that this compound has other sources than the airport operation. The remaining two homologues $C_{20}H_{19}O_4P$ and $C_{19}H_{17}O_4P$ were also detected under all sampling conditions and were identified as dicresylphenyl- (DPP, level 1) and cresyldiphenyl phosphate (CDP, level 1). Both compounds were predominant in samples from the city condition. The compound $C_6H_{15}O_4P$ was identified as triethyl phosphate (TEP, level 1). TEP had the highest signal in C4 and had approximately two- to fivefold greater averaged signal intensities than in samples from AS and AN.

Contrasting the results of all sampling conditions, the non-target analysis revealed a greater heterogeneity regarding the organic aerosol composition for samples from the city centre wind-sector. We found a significantly larger signal intensity in samples from the city for the composition classes CHO, CHNO and CHNOS (Fig. 6). The CHOP class had the lowest signal intensity regarding samples from the city wind-sector. High molecular CHO compounds were only found in airport samples, while lower molecular compounds dominated in samples from C. Individual airport marker compounds, such as $C_{25}H_{44}O_8$, $C_{27}H_{48}O_8$, TCP, and TBP, were completely absent in the urban background aerosol under C-condition. Differences between both airport conditions were observable by the signal intensity of single compounds.

3.3. Correlation between *in vitro* inhibition, compound intensities and $PM_{2.5}$ mass concentration

We found a significant ($p < 0.01$) positive correlation between the inhibition of the highest used concentration in both *in vitro* assays (see 3.1.2

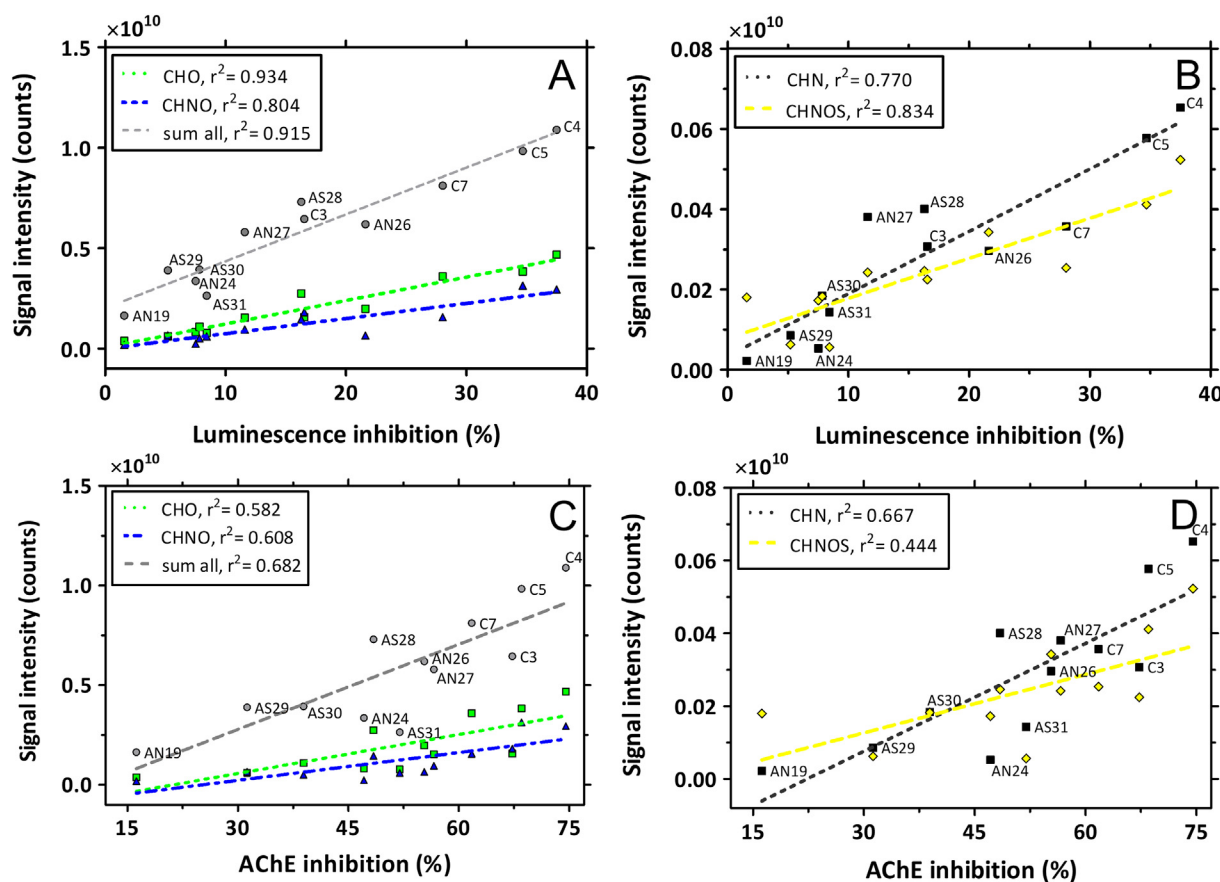


Fig. 7. Linear regression lines and coefficients of determination (r^2) for the correlation between the *in vitro* inhibition of the highest tested concentration and different compound classes. A – Linear regression lines and r^2 for CHO, CHNO and the sum of all compounds in the Microtox assay. B – Linear regression lines and r^2 for CHN and CHNOS compounds in the Microtox assay. C – Linear regression lines and r^2 for CHO, CHNO and the sum of all compounds in the AChE inhibition assay. D – Linear regression lines and r^2 for CHN and CHNOS compounds in the AChE inhibition assay.

AChE inhibition and SI, Fig. S3) and the summed signal intensity of organic aerosol compounds for four compound classes (CHO, CHN, CHNO, CHNOS) (Fig. 7). The highest coefficients of determination were found for the Microtox assay. The strongest correlation was found between the luminescence inhibition and signal intensity of the CHO compounds ($r^2 = 0.934$). This was followed by the correlation with the sum of all compounds ($r^2 = 0.915$), CHNOS ($r^2 = 0.834$), CHNO ($r^2 = 0.804$), and CHN compounds ($r^2 = 0.770$). The coefficients of determination were slightly lower for the comparison between AChE inhibition and different compound classes (Fig. 7). The sum of all compounds had the strongest correlation with AChE inhibition ($r^2 = 0.682$), CHNOS compounds the lowest ($r^2 = 0.444$).

We observed different organic composition classes, but certainly, a large fraction of PM_{2.5} is not represented by our non-target analysis due to a specific extraction and ionisation method. However, we observed a strong correlation between the summed signal intensities of the detected organic molecules and averaged PM_{2.5} mass concentration during the filter sampling periods (see SI, Fig. S4). Hence, we observe *in vitro* effects even at mass concentrations of 10 µg m⁻³ and less, as can be seen at sample C4, which exhibited the highest activity in both assays, although the average PM_{2.5} mass concentration during this sampling interval was below 10 µg m⁻³. Certainly, the transferability of these biological outcomes on human health effects is limited, but they can help identifying causal relationships between PM pollution and adverse health effects.

4. Discussion

4.1. Source attribution of single organic compounds

The chemical composition of the organic fraction in PM_{2.5} determined by the non-target approach had a strong wind direction dependency. Possible emission sources of selected compounds are discussed in the following. The class of CHO compounds consisted of compounds with a molecular weight below 350 Da for samples from the city wind-sector, while compounds with a higher molecular weight were found in the airport wind-sector. The large CHO compounds C₂₅H₄₄O₈ and C₂₇H₄₈O₈ were only detected in airport samples (AN and AS). In an earlier work we examined ultrafine particles from the Frankfurt airport sampled at the same monitoring site and identified these compounds as pentaerythritol esters (PEEs) that are used in jet engine lubrication oils (Timko et al., 2010; Ungeheuer et al., 2021; Yu et al., 2012). This finding is supported by their absence under the city wind-sector condition and their high occurrence at the airport during the daytime. It remains ambiguous why we detect these compounds also in the night-time strike sample AS31. The emission of such jet oil constituents has previously been reported at other airports (Fushimi et al., 2019; Yu et al., 2012). The use of high molecular PEEs is especially reported for synthetic aviation oils, while oils used in automotive have an average MW of 340 Da (fresh) and 293 Da (used) (Chen et al., 1994; Vazquez-Duhalt, 1989). The substance 4-*tert*-octylphenol monoethoxylate (OP1EO) belongs to the class of alkylphenol ethoxylates (APEO). APEOs are the major group of non-ionic surfactants and have wide use as industrial cleaners, dispersing agents and emulsifiers, demulsifiers and solubilisers in agricultural products (Acir and Guenther, 2018; Ying et al., 2002). OP1EO is an environmental pollutant with endocrine disruption potential (Bergé et al., 2012; European Chemicals Agency (ECHA), 2020) and was predominantly detected in samples from the city wind-sector. The wide use of APEOs in cleaning and agricultural products makes them prone to high emissions from such environments as the city or nearby agricultural fields, which is why they are found ubiquitously in the environment, including the air (Bergé et al., 2012). This would explain the high occurrence of OP1EO in samples from the city condition. However, the compound also had high signal values in some airport samples.

The occurrence of the epoxide caryophyllene oxide showed no dependency of the wind-sector, yet airport samples tended to have higher signal intensities than city samples. Caryophyllene oxide is an oxidation product of β-caryophyllene that is naturally emitted by several plant families such

as Pinaceae (Helmig et al., 2007; Pokorska et al., 2012; Sköld et al., 2006). Higher occurrences of caryophyllene oxide in samples from the south (airport wind-sector) can be explained by the biogenic emissions from the surrounding forest. Caryophyllene oxide is considered as an inhibitor of the mitochondrial electron transport chain (Monzote et al., 2009), however, its metabolites might exhibit different properties (Choudhary et al., 2006).

The cyclic amine norharmane had the highest abundance in C4, yet it was equally distributed among the remaining samples. Norharmane is a β-carboline and formed as a pyrolysis product in cooking and can be found in tobacco or marijuana smoke (Pfau and Skog, 2004; Rommelspacher et al., 2002). Pfau and Skog (2004) identified tobacco smoke as a major emission source. Reported emission index is ~12 µg norharmane g⁻¹ tobacco (Poindexter and Carpenter, 1962; Rommelspacher et al., 2002). Therefore, high emissions around urban areas seem plausible. Nevertheless, this is contrasted by the further mentioned equal distribution between all samples except C4. A possible explanation is the sheer size of the Frankfurt Airport with plenty of restaurants and its large passenger numbers (potential smokers). Norharmane can induce neurodegeneration and motoric impairment (Östergren et al., 2006). It is further known as an inhibitor for the monoaminoxidase B and AChE (Rommelspacher et al., 2002; Skup et al., 1983).

NBBS is a neurotoxic plasticiser that is frequently used in polyacetals and polyamides (Rider et al., 2012). It is also naturally formed in greenhouse soil by the bacterium *Pseudomonas sp.* (Kim et al., 2000). Its abundance was high in the city samples C4 and C5 and low in samples taken under airport strike condition. This might be explained by the abrasion of brake pads. Polyamides such as Kevlar are used in brake and clutch pads due to their high-temperature resistance and solidity (Bin Kabir and Ferdous, 2012; Kankanala and Sarkar, 2020; Loken, 1980; Unaldi and Kus, 2014). Correspondingly, NBBS has already been described in particulate matter emissions from brake pads (Plachá et al., 2017). The city samples reflect an urban background with lots of motor traffic. Furthermore, its occurrence was slightly higher in samples taken during normal airport operation than during airport strike. This possibly reflects fewer breaking events due to the decreased airplane, shuttle, and passenger traffic.

PSC is a thiocarbamate herbicide and a relevant aerosol constituent with the potential to induce acute toxicity (Bo et al., 2020; Devault et al., 2019). Its wind-driven atmospheric dispersion is especially relevant in autumn with the highest described concentrations in November (Devault et al., 2019). Furthermore, the potential of long-range transport is described (Van Dijk and Guicherit, 1999). This corresponds with our unambiguous finding of PSC in PM_{2.5} as the examined samples were sampled during November. Its occurrence could not be clearly assigned to a specific wind direction, which might be explained by its use. Agricultural fields are equally distributed among the sampled wind directions, so its abundance may rather depend on the seasonal application of PSC.

Most detected CHOP compounds can be attributed to the class of organophosphorus esters (OPEs). The OPEs identified on an identification confidence level of 1 included TCP, TBP, TPhP, CDP, DPP and TEP. OPEs are high-production-volume chemicals that are emitted into the environment by leaching and volatilisation (Marklund et al., 2003; Reemtsma et al., 2008). TBP was exclusively detected in samples from the airport. It is used as a plasticiser, anti-foaming agent, and additive in lubricants and hydraulic fluids (Marklund et al., 2005; Reemtsma et al., 2008). Marklund et al. (2005) examined OPE concentrations at the Umeå airport in Sweden and at a road intersection. They found TBP to be the most abundant of all measured OPEs at the airport. Its main source was identified as aircraft hydraulic fluids. Further, they did not find a strong correlation between TBP levels and road traffic (Marklund et al., 2005). This coincides with the finding that TBP had the highest signal intensity of all detected compounds and was only present in airport samples. The high abundance of TCP in airport samples can be explained by its distinctive use as an anti-wear agent in aircraft engine lubrication oils (de Boer et al., 2015; De Nola et al., 2008). Therefore, the TCP signals during the night-time flight ban at normal airport operation were remarkably lower than at daytime

and for the city condition, respectively. It further explained the lower average TCP signals during the airport strike. This is in accordance with previous examinations that described TCP as an airport marker compound (Fushimi et al., 2019; Ungeheuer et al., 2021). However, its high abundance during nighttime and strike (AS31) remains unclear. TCP acts as an inhibitor of acetylcholinesterase, its toxicity is dependent on the present isomers (Abou-Donia, 1981; Winder and Balouet, 2002). CDP, DPP, and TPhP had the highest abundances at wind directions from north-northeast to east-northeast (city). Because OPEs are not chemically bonded to the products they are used in, outgassing is likely to happen (Marklund et al., 2003; Rodríguez et al., 2006). Due to their ubiquitous use, large cities may have a higher burden than remote areas, thus explaining the lower occurrence of these compounds in airport samples. In contrast, Ren et al. (2016) reported significantly higher OPE concentrations in sub-urban air than in urban air. CDP and TPhP are used as flame retardants and plasticisers in PVC, hydraulic fluids, lubricants, electrical components, and the automobile industry (Esch et al., 1997; WHO & IPCS, 1991). CDP has already been found in indoor dust and soils (Björnsdotter et al., 2018; Huang et al., 2020; Wang et al., 2019). TPhP is a described endocrine disruptor and inhibits the acetylcholinesterase (Shi et al., 2018). TEP had a similar distribution behaviour between the sampling conditions as CDP and TPhP. It is also used as a flame retardant but does not inhibit the acetylcholinesterase (Gumbmann and Williams, 1970; Salthammer et al., 2003).

4.2. PM_{2.5} composition and *in vitro* toxicity

The observed *in vitro* toxicity of the PM_{2.5} filter extracts showed a strong wind direction dependency. Samples of the city wind-sector exhibited the highest toxicity, samples obtained during the airport strike event showed the lowest. The AChE assay assesses a characteristic mechanism for neurotoxicity from *i.e.*, organophosphorus compounds (Baron, 1981; Winder and Balouet, 2002) and revealed a higher sensitivity to the PM_{2.5} extracts than the Microtox assay thus resulting in lower EC values. However, the inhibition of bioluminescence is a more sensitive indicator for unspecific toxicity than other assays such as mammalian cell viability assays (Neale et al., 2012). Both assays had a strong correlation with the total signal intensity of all detected organic compounds. The total signal intensities of the organic fraction also showed a strong correlation with the PM_{2.5} mass concentration (SI, Fig. S4). Therefore, we also observe an apparent correlation between baseline toxicity/AChE inhibition and PM_{2.5} mass concentration. This supports the need for low ambient PM_{2.5} concentrations. Studies on the baseline toxicity of PM_{2.5} are scarce. However, this explanation is following Lionetto et al. (2019) who examined the water-soluble fraction of urban PM₁₀ with the Microtox assay. They found a positive correlation between the increase of luminescence inhibition and PM₁₀ concentrations (Lionetto et al., 2019). Nonetheless, this contrasts with the findings of Roig et al. (2013). They found no correlation between the water-soluble fraction of PM₁₀ and Microtox results. This was explained by varying PM₁₀ compositions of which only a few compounds might induce toxicity (Roig et al., 2013). Considering that some samples had a high summed signal intensity but lower toxicity than samples with lower signal intensity, the chemical composition of PM_{2.5} seems to play an important role. Further, both mentioned studies tested the water-soluble fraction of the coarse PM₁₀ and measured its concentration. In contrast, the filters that we examined were extracted with an organic solvent, thus leading to a different extraction result. It can be assumed that highly lipophilic compounds have a higher extraction rate with an organic solvent such as the used DCM. Those differences make the comparison of different studies difficult. Yet PM_{2.5} is reported to induce lower toxicity to *A. fischeri* than PM₁₀ (Papadimitriou et al., 2006). This corresponds with the present results as reported Microtox EC₅₀ values of PM₁₀ (<20 m³ air ml⁻¹) are lower than the obtained EC₂₀ values of PM_{2.5} (Roig et al., 2013). Roig et al. (2013) used acidified water, thus extracting a large amount of metals that might be more toxic and were not examined in this study. This suggests that the toxicity of PM depends on the specific sample composition and extracted compounds. To gain further insight on the effect of specific substances,

substances with high signal intensities and described adverse effects were also tested for their correlation with the assay results (see SI, Table S3). OP1EO had a significant positive correlation with the results of both assays. Hence, it is a suspected driver of the found CHO compound dependent toxicity. The neurotoxicant norharmene also had a weak positive correlation with both assays, while NBBS only correlated with luminescence inhibition. The herbicide proflumofen had a significant positive correlation with both assays. Notably, no significant correlation between the sum of CHOP compounds and both assays was obtained. The CHOP class consisted of many OPEs that had the largest signals. As AChE inhibition is a specific mechanism of OPE toxicity (Eyer, 1995; Winder and Balouet, 2002), this finding was unexpected (see 4.3 Limitations). Therefore, the predominant OPEs were correlated with both assays, obtaining a positive correlation for TPhP, CDP, DPP and TEP (see SI, Table S3). TPhP is described as an AChE inhibitor (Shi et al., 2018). Therefore, a positive correlation between its abundance and the assay result is plausible. Interestingly, the signal intensities of TCP had no positive correlation with the inhibition of AChE. This might be an indicator for the use of nontoxic isomers in aircraft engine oils as the TCP-toxicity is strongly isomer-dependent (Eto et al., 1962; Winder and Balouet, 2002). This finding is in accordance with Ungeheuer et al. (2021) who reported the absence of the harmful tri-*ortho* isomer (TOCP) in aircraft engine lubrication oils and airport-related ultrafine particles.

4.3. Limitations

The toxicity of TOCP is described as dependent on its metabolic activation by the cytochrome P450 system (Eto et al., 1962), and might therefore be underestimated in this study. The activation leads to the formation of cyclic saligenin phosphate esters, which induce the toxic effect of TOCP (Eto et al., 1962; Lorke et al., 2016). This metabolic activation is also described for phosphorothioates and takes place in the brain, having a major role in acute toxicity (Sanchez-Hernandez and Walker, 2000). To address the metabolite-dependent toxicity of TCP, future studies with S9 liver extract, which mimics the hepatic metabolism by P450 enzymes, are conceivable. We also observed a positive correlation between TEP and AChE inhibition, although it can be concluded that TEP is not responsible for the AChE inhibition as it has been evaluated as non-AChE inhibiting (Gumbmann and Williams, 1970). In contrast, TBP, which is described as AChE inhibitor had no significant correlation with the assay results. This might be explained by the exceeding effect of other neurotoxicants in the air masses from the city center. Therefore, these cases (TCP and TEP) point out the limitation of the correlation analysis. Based on the correlation analysis, we can only observe indications for potential drivers of toxicity, but cannot attribute the observed effects to individual compound classes or single compounds. An underlying hidden effect cannot be avoided when considering individual compound classes as only the whole filter extracts were analysed for *in vitro* toxicity. To overcome this limitation, future investigations shall apply fractionation of filter sample extracts before biotesting in order to clearly identify the key drivers of toxicity.

In our non-target analysis approach many detected compounds remain unidentified, and a part of the described compounds are only identified with an identification confidence of level 2 that is based on exact mass and fragmentation pattern comparison with a database. Future work is needed to unambiguously identify the suspected drivers of toxicity using authentic standards. However, the non-target analysis is a promising tool for holistic chemical characterisation of extracts of ambient PM.

The use of high-volume air samplers also holds the potential for sampling artifacts. The gas-particle partitioning of compounds is dependent on the temperature and the total suspended particles (Pankow, 1994). Volatile compounds can desorb from the filter depending on their physicochemical properties (Peters et al., 2000). This so-called 'blow-off' can take place during and after sampling. The potential desorption after sampling was addressed by the filter storage at -20 °C. The high volume flux of a high-volume air sampler may also lead to 'blow-on' events that increase the particle phase concentration (Peters et al., 2000). This is critical for organophosphorus compounds for which the gas-particle partitioning

- treatment plants and surface waters using a mode-of-action based test battery. *J. Environ. Monit.* 10, 622–631. <https://doi.org/10.1039/b800951a>.
- Escher, B.I., Allinson, M., Altenburger, R., Bain, P.A., Balaguer, P., Busch, W., Crago, J., Denslow, N.D., Dopp, E., Hilscherova, K., Humpage, A.R., Kumar, A., Grimaldi, M., Jayasinghe, B.S., Jarosova, B., Jia, A., Makarov, S., Maruya, K.A., Medvedev, A., Mehinto, A.C., Mendez, J.E., Poulsen, A., Prochazka, E., Richard, J., Schifferli, A., Schlenk, D., Scholz, S., Shiraiishi, F., Snyder, S., Su, G., Tang, J.Y.M., Burg, B.Van, Der, Linden, Der, S.C.V., Werner, I., Westerheide, S.D., Wong, C.K.C., Yang, M., Yeung, B.H.Y., Zhang, X., Leusch, F.D.L., 2014. Benchmarking organic micropollutants in wastewater, recycled water and drinking water with in vitro bioassays. *Environ. Sci. Technol.* 48, 1940–1956. <https://doi.org/10.1021/es403899t>.
- Eto, M., Casida, J.E., Eto, T., 1962. Hydroxylation and cyclization reactions involved in the metabolism of tri-*o*-cresyl phosphate. *Biochem. Pharmacol.* 11, 337–352. [https://doi.org/10.1016/0006-2952\(62\)90056-4](https://doi.org/10.1016/0006-2952(62)90056-4).
- European Chemicals Agency (ECHA), 2020. 2-[4-(1,1,3,3-Tetramethylbutyl)phenoxy]ethanol [WWW Document]. <https://echa.europa.eu/substance-information/-/substanceinfo/100.150.206>. (Accessed 26 February 2021).
- European Environment Agency (EEA), 2019. Healthy Environment, Healthy Lives: How the Environment Influences Health and Well-being in Europe. <https://doi.org/10.2800/53670> Denmark.
- Eyer, P., 1995. Neuropsychopathological changes by organophosphorus compounds - a review. *Hum. Exp. Toxicol.* 14, 857–864. <https://doi.org/10.1177/096032719501401101>.
- Fraport, 2020. Fraport-Verkehrszahlen 2019: Über 70,5 Millionen Passagiere am Flughafen Frankfurt [WWW Document]. <https://www.fraport.com/de/newsroom/pressemittelungen/2020/q1-2020/fraport-verkehrszahlen-2019-ueber-70-5-millionen-passagiere-am.html>. (Accessed 7 July 2021).
- Fushimi, A., Saitoh, K., Fujitani, Y., Takegawa, N., 2019. Identification of jet lubrication oil as a major component of aircraft exhaust nanoparticles. *Atmos. Chem. Phys.* 19, 6389–6399. <https://doi.org/10.5194/acp-19-6389-2019>.
- Gumbmann, M.R., Williams, S.N., 1970. Anticholinesterase activity of triethyl phosphate resulting from an impurity. *J. Agric. Food Chem.* 18, 76–77. <https://doi.org/10.1021/jf60167a009>.
- Guo, Y., Wu, K., Huo, X., Xu, X., 2011. Sources, distribution, and toxicity of polycyclic aromatic hydrocarbons. *J. Environ. Health* 73, 22–25. <https://doi.org/10.5772/10045>.
- Helmig, D., Ortega, J., Duhl, T., Tanner, D., Guenther, A., Harley, P., Wiedinmyer, C., Milford, J., Sakulyanontvittaya, T., 2007. Sesquiterpene emissions from pine trees - identifications, emission rates and flux estimates for the contiguous United States. *Environ. Sci. Technol.* 41, 1545–1553. <https://doi.org/10.1021/es0618907>.
- Hermens, J., Busser, F., Leeuwangh, P., Musch, A., 1985. Quantitative structure-activity relationships and mixture toxicity of organic chemicals in photobacterium phosphoreum: the microtox test. *Ecotoxicol. Environ. Saf.* 9, 17–25. [https://doi.org/10.1016/0147-6513\(85\)90030-2](https://doi.org/10.1016/0147-6513(85)90030-2).
- HLNUG, 2018. 1. Zwischenbericht zur Untersuchung der regionalen Luftqualität auf ultrafeine Partikel im Bereich des Flughafens Frankfurt. Wiesbaden.
- HLNUG, 2019. Measurement Data Portal [WWW Document]. <https://www.hlnug.de/messwerte/datenportal/messstelle/2/1/0619>. (Accessed 7 July 2021).
- Huang, Y., Tan, H., Li, L., Yang, L., Sun, F., Li, J., Gong, X., Chen, D., 2020. A broad range of organophosphate tri- and di-esters in house dust from Adelaide, South Australia: concentrations, compositions, and human exposure risks. *Environ. Int.* 142, 105872. <https://doi.org/10.1016/j.envint.2020.105872>.
- ISO-Guideline 11348-3:2007, 2007. Water quality - determination of the inhibitory effect of water samples on the light emission of *Vibrio fischeri* (Luminescent bacteria test) - part 3: method using freeze-dried bacteria. <https://doi.org/10.31030/1495363>.
- Kankanala, A.K., Sarkar, M., 2020. A review on material and wear analysis of automotive break pad. *Int. Res. J. Eng. Technol.* 7, 2537–2543. <https://doi.org/10.1016/j.matpr.2018.10.114>.
- Kanninen, K.M., Lampinen, R., Rantanen, L.M., Odendaal, L., Jalava, P., Chew, S., White, A.R., 2020. Olfactory cell cultures to investigate health effects of air pollution exposure: implications for neurodegeneration. *Neurochem. Int.* 136, 104729. <https://doi.org/10.1016/j.neuint.2020.104729>.
- Kendrick, E., 1963. A mass scale based on CH₂ = 14.0000 for high resolution mass spectrometry of organic compounds. *Anal. Chem.* 35, 2146–2154. <https://doi.org/10.1021/ac60206a048>.
- Kim, K.H., Jahan, S.A., Kabir, E., Brown, R.J.C., 2013. A review of airborne polycyclic aromatic hydrocarbons (PAHs) and their human health effects. *Environ. Int.* 60, 71–80. <https://doi.org/10.1016/j.envint.2013.07.019>.
- Kim, K.K., Kang, J.G., Moon, S.S., Kang, K.Y., 2000. Isolation and identification of antifungal *N*-butylbenzenesulphonamide produced by *Pseudomonas* sp. AB2. *J. Antibiot. (Tokyo)* 53, 131–136. <https://doi.org/10.7164/antibiotics.53.131>.
- Landrign, P.J., Fuller, R., Acosta, N.J.R., Adeyi, O., Arnold, R., Basu, N.N., Baldé, A.B., Bertolini, R., Bose-O'Reilly, S., Boufford, J.I., Breyse, P.N., Chiles, T., Mahidol, C., Coll-Seck, A.M., Cropper, M.L., Fobil, J., Fuster, V., Greenstone, M., Haines, A., Hanrahan, D., Hunter, D., Khare, M., Krupnick, A., Lanphear, B., Lohani, B., Martin, K., Mathiasen, K.V., McTeer, M.A., Murray, C.J.L., Ndahimananjara, J.D., Perera, F., Potočník, J., Preker, A.S., Ramesh, J., Rockström, J., Salinas, C., Samson, L.D., Sandilya, K., Sly, P.D., Smith, K.R., Steiner, A., Stewart, R.B., Suk, W.A., van Schayck, O.C.P., Yada, G.N., Yumkella, K., Zhong, M., 2018. The Lancet commission on pollution and health. *Lancet* 391, 462–512. [https://doi.org/10.1016/S0140-6736\(17\)32345-0](https://doi.org/10.1016/S0140-6736(17)32345-0).
- Lelieveld, J., Evans, J.S., Fnais, M., Giannadaki, D., Pozzer, A., 2015. The contribution of outdoor air pollution sources to premature mortality on a global scale. *Nature* 525, 367–371. <https://doi.org/10.1038/nature15371>.
- Lelieveld, J., Klingmüller, K., Pozzer, A., Pöschl, U., Fnais, M., Daiber, A., Münzel, T., 2019. Cardiovascular disease burden from ambient air pollution in Europe reassessed using novel hazard ratio functions. *Eur. Heart J.* 40, 1590–1596. <https://doi.org/10.1093/eurheartj/ehz135>.
- Lim, S.S., Vos, T., Flaxman, A.D., Danaei, G., Shibuya, K., Adair-Rohani, H., Amann, M., Anderson, H.R., Andrews, K.G., Aryee, M., Atkinson, C., Bacchus, L.J., Bahalim, A.N., Balakrishnan, K., Balmes, J., Barker-Collo, S., Baxter, A., Bell, M.L., Blore, J.D., Blyth, F., Bonner, C., Borges, G., Bourne, R., Boussinesq, M., Brauer, B., Brooks, P., Bruce, N.G., Brunekeerf, B., Bryan-Hancock, C., Bucello, C., Buchbinder, R., Bull, F., Burnett, R.T., Byers, T.E., Calabria, B., Carapetis, J., Carnahan, E., Chafe, Z., Charlson, F., Chen, H., Chen, J.S., Cheng, A.T.A., Child, J.C., Cohen, A., Colson, K.E., Cowie, B.C., Darby, S., Darling, S., Davis, A., Degenhardt, L., Dentener, F., Des Jarlais, D.C., Devries, K., Dherani, M., Ding, E.L., Dorsey, E.R., Driscoll, T., Edmond, K., Ali, S.E., Engell, R.E., Erwin, P.J., Fahimi, S., Falder, G., Farzadfar, F., Ferrari, A., Finucane, M.M., Flaxman, S., Fowkes, F.G.R., Freedman, G., Freeman, M.K., Gakidou, E., Ghosh, S., Giovannucci, E., Gmel, G., Graham, K., Grainger, R., Grant, B., Gunnell, D., Gutierrez, H.R., Hall, W., Hoek, H.W., Hogan, A., Hosgood, H.D., Hoy, D., Hu, H., Hubbell, B.J., Hutchings, S.J., Ibeanusi, S.E., Jacklyn, G.L., Jasrasaria, R., Jonas, J.B., Kan, H., Kanis, J.A., Kassebaum, N., Kawakami, N., Khang, Y.H., Khatibzadeh, S., Khoo, J.P., Kok, C., Laden, F., Lalloo, R., Lan, Q., Lathlean, T., Leasher, J.L., Leigh, J., Li, Y., Lin, J.K., Lipschultz, S.E., London, S., Lozano, R., Lu, Y., Mak, J., Malekzadeh, R., Mallinger, L., Marceson, M., March, L., Marks, R., Martin, R., McGale, P., McGrath, J., Mehta, S., Mensah, G.A., Merriman, T.R., Micha, R., Michaud, C., Mishra, V., Hanafiah, K.M., Mokdad, A.A., Morawska, L., Mozaffarian, D., Murphy, T., Naghavi, M., Neal, B., Nelson, P.K., Nolla, J.M., Norman, S., Omer, S.B., Orchard, J., Osborne, R., Ostro, B., Page, A., Pandey, K.D., Parry, C.D.H., Passmore, E., Patra, J., Pearce, N., Pelizzari, P.M., Petzold, M., Phillips, M.R., Pope, D., Pope, C.A., Powles, J., Rao, M., Razavi, H., Rehfues, E.A., Rehm, J.T., Ritz, B., Rivara, F.P., Roberts, T., Robinson, C., Rodriguez-Portales, J.A., Romieu, I., Room, R., Rosenfeld, L.C., Roy, A., Rushton, L., Salomon, J.A., Sampson, U., Sanchez-Griera, L., Sanman, E., Sapkota, A., Seedat, S., Shi, P., Shield, K., Shivakoti, R., Singh, G.M., Sleet, D.A., Smith, E., Smith, K.R., Stapelberg, N.J.C., Steenland, K., Stöckl, H., Stovner, L.J., Straif, K., Straney, L., Thurston, G.D., Tran, J.H., Van Dingenen, R., Van Donkelaar, A., Veerman, J.L., Vijayakumar, L., Weintraub, R., Weissman, M.M., White, R.A., Whiteford, H., Wiersma, S.T., Wilkinson, J.D., Williams, H.C., Williams, W., Wilson, N., Woolf, A.D., Yip, P., Zielinski, J.M., Lopez, A.D., Murray, C.J.L., Ezzati, M., 2012. A comparative risk assessment of burden of disease and injury attributable to 67 risk factors and risk factor clusters in 21 regions, 1990–2010: a systematic analysis for the global burden of disease study 2010. *Lancet* 380, 2224–2260. [https://doi.org/10.1016/S0140-6736\(12\)61766-8](https://doi.org/10.1016/S0140-6736(12)61766-8).
- Lionetto, M.G., Guascito, M.R., Caricato, R., Giordano, M.E., De Bartolomeo, A.R., Romano, M.P., Conte, M., Dinoi, A., Contini, D., 2019. Correlation of oxidative potential with ecotoxicological and cytotoxicological potential of PM10 at an urban background site in Italy. *Atmosphere (Basel)*. 10. <https://doi.org/10.3390/ATMOS10120733>.
- Loken, H.Y., 1980. Asbestos free brakes and dry clutches reinforced with Kevlar® aramid fiber. *SAE Tech. Pap.* 89, 2202–2208. <https://doi.org/10.4271/800667>.
- Lorke, D.E., Stegmeier-Petroianu, A., Petroianu, G.A., 2016. Biologic activity of cyclic and caged phosphates: a review. *J. Appl. Toxicol.* 37, 13–22. <https://doi.org/10.1002/jat.3369>.
- Marklund, A., Andersson, B., Haglund, P., 2003. Screening of organophosphorus compounds and their distribution in various indoor environments. *Chemosphere* 53, 1137–1146. [https://doi.org/10.1016/S0045-6535\(03\)00666-0](https://doi.org/10.1016/S0045-6535(03)00666-0).
- Marklund, A., Andersson, B., Haglund, P., 2005. Traffic as a source of organophosphorus flame retardants and plasticizers in snow. *Environ. Sci. Technol.* 39, 3555–3562. <https://doi.org/10.1021/es0482177>.
- Monzote, L., Stamberg, W., Staniek, K., Gille, L., 2009. Toxic effects of carvacrol, caryophyllene oxide, and ascaridole from essential oil of *Chenopodium ambrosioides* on mitochondria. *Toxicol. Appl. Pharmacol.* 240, 337–347. <https://doi.org/10.1016/j.taap.2009.08.001>.
- Neale, P.A., Antony, A., Bartkow, M.E., Farré, M.J., Heitz, A., Kristiana, I., Tang, J.Y.M., Escher, B.I., 2012. Bioanalytical assessment of the formation of disinfection byproducts in a drinking water treatment plant. *Environ. Sci. Technol.* 46, 10317–10325. <https://doi.org/10.1021/es302126t>.
- Okeme, J.O., Rodgers, T.F.M., Jantunen, L.M., Diamond, M.L., 2018. Examining the gas-particle partitioning of organophosphate esters: how reliable are air measurements? *Environ. Sci. Technol.* 52, 13834–13844. <https://doi.org/10.1021/acs.est.8b04588>.
- Östergren, A., Fredriksson, A., Brittebo, E.B., 2006. Norharman-induced motoric impairment in mice: neurodegeneration and glial activation in substantia nigra. *J. Neural Transm.* 113, 313–329. <https://doi.org/10.1007/s00702-005-0334-0>.
- Pankow, J.F., 1994. An absorption model of gas/particle partitioning of organic compounds in the atmosphere. *Atmos. Environ.* 28, 185–188. [https://doi.org/10.1016/1352-2310\(94\)90093-0](https://doi.org/10.1016/1352-2310(94)90093-0).
- Papadimitriou, C., Evagelopoulou, V., Samaras, P., Triantafyllou, A.G., Zoras, S., Albanis, T.A., 2006. Toxicity of atmospheric particulate matter using aquatic bioassays. *WIT Trans. Biomed. Health* 10, 31–39. <https://doi.org/10.2495/ETOX0600041>.
- Peters, A.J., Lane, D.A., Gundel, L.A., Northcott, G.L., Jones, K.C., 2000. A comparison of high volume and diffusion denuder samplers for measuring semivolatile organic compounds in the atmosphere. *Environ. Sci. Technol.* 34, 5001–5006. <https://doi.org/10.1021/es000056t>.
- Peters, R., Ee, N., Peters, J., Booth, A., Mudway, I., Anstey, K.J., 2019. Air pollution and dementia: a systematic review. *J. Alzheimers Dis.* 70, S145–S163. <https://doi.org/10.3233/JAD-180631>.
- Pfau, W., Skog, K., 2004. Exposure to β -carbolines norharman and harman. *JChromatogr. B Anal. Technol. Biomed. Life Sci.* 802, 115–126. <https://doi.org/10.1016/j.jchromb.2003.10.044>.
- Plachá, D., Vaculík, M., Mikeska, M., Dutko, O., Peikertová, P., Kukutschová, J., Mamulová Kutláková, K., Růžičková, J., Tomášek, V., Filip, P., 2017. Release of volatile organic compounds by oxidative wear of automotive friction materials. *Wear* 376–377, 705–716. <https://doi.org/10.1016/j.wear.2016.12.016>.

- Poindexter, E.H., Carpenter, R.D., 1962. The isolation of harmaline and norharmaline from tobacco and cigarette smoke. *Phytochemistry* 1, 215–221. [https://doi.org/10.1016/S0031-9422\(00\)82825-3](https://doi.org/10.1016/S0031-9422(00)82825-3).
- Pokorska, O., Dewulf, J., Amelynck, C., Schoon, N., Šimpraga, M., Steppe, K., Van Langenhove, H., 2012. Isoprene and terpenoid emissions from *Abies alba*: identification and emission rates under ambient conditions. *Atmos. Environ.* 59, 501–508. <https://doi.org/10.1016/j.atmosenv.2012.04.061>.
- Reemtsma, T., García-López, M., Rodríguez, L., Quintana, J.B., Rodil, R., 2008. Organophosphorus flame retardants and plasticizers in water and air: Occurrence and fate. *Trends Anal. Chem.* 27, 727–737. <https://doi.org/10.1016/j.trac.2008.07.002>.
- Ren, G., Chen, Z., Feng, J., Ji, W., Zhang, J., Zheng, K., Yu, Z., Zeng, X., 2016. Organophosphate esters in total suspended particulates of an urban city in East China. *Chemosphere* 164, 75–83. <https://doi.org/10.1016/j.chemosphere.2016.08.090>.
- Renner, R., 1997. European bans on surfactant trigger transatlantic debate. *Environ. Sci. Technol.* 31. <https://doi.org/10.1021/es972366q>.
- Rider, C.V., Janardhan, K.S., Rao, D., Morrison, J.P., McPherson, C.A., Harry, G.J., 2012. Evaluation of *N*-butylbenzenesulfonamide (NBBS) neurotoxicity in Sprague-dawley male rats following 27-day oral exposure. *Neurotoxicology* 33, 1528–1535. <https://doi.org/10.1016/j.neuro.2012.07.002>.
- Rodríguez, I., Calvo, F., Quintana, J.B., Rubí, E., Rodil, R., Cela, R., 2006. Suitability of solid-phase microextraction for the determination of organophosphate flame retardants and plasticizers in water samples. *J. Chromatogr. A* 1108, 158–165. <https://doi.org/10.1016/j.chroma.2006.01.008>.
- Roig, N., Sierra, J., Rovira, J., Schuhmacher, M., Domingo, J.L., Nadal, M., 2013. In vitro tests to assess toxic effects of airborne PM10 samples. Correlation with metals and chlorinated dioxins and furans. *Sci. Total Environ.* 443, 791–797. <https://doi.org/10.1016/j.scitotenv.2012.11.022>.
- Rommelspacher, H., Meier-Henco, M., Smolka, M., Kloft, C., 2002. The levels of norharman are high enough after smoking to affect monoamine oxidase B in platelets. *Eur. J. Pharmacol.* 441, 115–125. [https://doi.org/10.1016/S0014-2999\(02\)01452-8](https://doi.org/10.1016/S0014-2999(02)01452-8).
- Rönkkö, T.J., Hirvonen, M.-R., Happonen, M.S., Ihantola, T., Hakkarainen, H., Martikainen, M.-V., Gu, C., Jokiniemi, J., Komppula, M., Jalava, P.I., Wang, Q.-G., 2021. Inflammatory responses of urban air PM modulated by chemical composition and different air quality situations in Nanjing, China. *Environ. Res.* 192, 110382. <https://doi.org/10.1016/j.envres.2020.110382>.
- Salthammer, T., Fuhrmann, F., Uhde, E., 2003. Flame retardants in the indoor environment - part II: release of VOCs (triethylphosphate and halogenated degradation products) from polyurethane. *Indoor Air* 13, 49–52. <https://doi.org/10.1034/j.1600-0668.2003.01150.x>.
- Sanchez-Hernandez, J.C., Walker, C.H., 2000. In vitro and in vivo cholinesterase inhibition in lacertides by phosphonate- and phosphorothioate-type organophosphates. *Pestic. Biochem. Physiol.* 67, 1–12. <https://doi.org/10.1006/pest.1999.2471>.
- Schraufnagel, D.E., 2020. The health effects of ultrafine particles. *Exp. Mol. Med.* 52, 311–317. <https://doi.org/10.1038/s12276-020-0403-3>.
- Schraufnagel, D.E., Balmes, J.R., de Matteis, S., Hoffman, B., Kim, W.J., Perez-Padilla, R., Rice, M., Sood, A., Vanker, A., Wuebbles, D.J., 2019. Health benefits of air pollution reduction. *Ann. Am. Thorac. Soc.* 16, 1478–1487. <https://doi.org/10.1513/AnnalsATS.201907-538CME>.
- Schultz, T.W., Cronin, M.T.D., 1997. Quantitative structure-activity relationships for weak acid respiratory uncouplers to *Vibrio fischeri*. *Environ. Toxicol. Chem.* 16, 357–360. [https://doi.org/10.1897/1551-5028\(1997\)016<0357:QSARFW>2.3.CO;2](https://doi.org/10.1897/1551-5028(1997)016<0357:QSARFW>2.3.CO;2).
- Schymanski, E.L., Jeon, J., Gulde, R., Fenner, K., Ruff, M., Singer, H.P., Hollender, J., 2014. Identifying small molecules via high resolution mass spectrometry: communicating confidence. *Environ. Sci. Technol.* 48, 2097–2098. <https://doi.org/10.1021/es5002105>.
- Shi, Q., Wang, M., Shi, F., Yang, L., Guo, Y., Feng, C., Liu, J., Zhou, B., 2018. Developmental neurotoxicity of triphenyl phosphate in zebrafish larvae. *Aquat. Toxicol.* 203, 80–87. <https://doi.org/10.1016/j.aquatox.2018.08.001>.
- Sigma-Aldrich, 2018. Acetylcholinesterase Inhibitor Screening Kit MAK324 - Technical Bulletin [WWW Document]. <https://www.sigmaaldrich.com/deepweb/assets/sigmaaldrich/product/documents/370/429/mak324bul.pdf>. (Accessed 6 June 2020).
- Sköld, M., Karlberg, A.T., Matura, M., Börje, A., 2006. The fragrance chemical β -caryophyllene - air oxidation and skin sensitization. *Food Chem. Toxicol.* 44, 538–545. <https://doi.org/10.1016/j.fct.2005.08.028>.
- Skup, M., Oderfeld-Nowak, B., Rommelspacher, H., 1983. In vitro studies on the effect of β -carbolines on the activities of acetylcholinesterase and choline acetyltransferase and on the muscarinic receptor binding of the rat brain. *J. Neurochem.* 41, 62–68. <https://doi.org/10.1111/j.1471-4159.1983.tb11814.x>.
- Timko, M.T., Onash, T.B., Northway, M.J., Jayne, J.T., Canagaratna, M.R., Herndon, S.C., Wood, E.C., Miake-Lye, R.C., 2010. Gas turbine engine emissions — part II: chemical properties of particulate matter. *J. Eng. Gas Turbines Power* 132, 1–15. <https://doi.org/10.1115/1.4000132>.
- UBA (Umweltbundesamt), 2004. *Umwelt-Survey 1998 Band V: Hausstaub*. Berlin.
- UBA (Umweltbundesamt), 2017. Frequently Asked Questions About Phthalates and Plasticisers [WWW Document]. <https://bit.ly/3jrDejq>. (Accessed 8 May 2021).
- Unaldi, M., Kus, R., 2014. Effect of pressing pressure on density and hardness of powder miscanthus reinforced brake pads. *Appl. Mech. Mater.* 680, 237–240. <https://doi.org/10.4028/www.scientific.net/AMM.680.237>.
- Ungeheuer, F., van Pinxteren, D., Vogel, A.L., 2021. Identification and source attribution of organic compounds in ultrafine particles near Frankfurt international airport. *Atmos. Chem. Phys.* 21, 3763–3775. <https://doi.org/10.5194/acp-21-3763-2021>.
- Van Dijk, H.F.G., Guicherit, R., 1999. Atmospheric dispersion of current-use pesticides: A review of the evidence from monitoring studies. *Air. Soil Pollut. Water* <https://doi.org/10.1023/A:1005293020536>.
- Vazquez-Duhalt, R., 1989. Environmental impact of used motor oil. *Sci. Total Environ.* 79, 1–23. [https://doi.org/10.1016/0048-9697\(89\)90049-1](https://doi.org/10.1016/0048-9697(89)90049-1).
- Vogel, A.L., Lauer, A., Fang, L., Arturi, K.R., Bachmeier, F., Dällenbach, K.R., Käser, T., Vlachou, A., Pospisilova, V., Baltensperger, U., El Haddad, I., Schwikowski, M., Bjelčić, S., 2019. A comprehensive nontarget analysis for the molecular reconstruction of organic aerosol composition from glacier ice cores. *Environ. Sci. Technol.* 53, 12565–12575. <https://doi.org/10.1021/acs.est.9b03091>.
- Völker, J., Vogt, T., Castronovo, S., Wick, A., Ternes, T.A., Joss, A., Oehlmann, J., Wagner, M., 2017. Extended anaerobic conditions in the biological wastewater treatment: higher reduction of toxicity compared to target organic micropollutants. *Water Res.* 116, 220–230. <https://doi.org/10.1016/j.watres.2017.03.030>.
- Wang, Y., Yao, Y., Li, W., Zhu, H., Wang, L., Sun, H., Kannan, K., 2019. A nationwide survey of 19 organophosphate esters in soils from China: spatial distribution and hazard assessment. *Sci. Total Environ.* 671, 528–535. <https://doi.org/10.1016/j.scitotenv.2019.03.335>.
- WHO, 2021. WHO global air quality guidelines. Particulate matter (PM2.5 and PM10), ozone, nitrogen dioxide, sulfur dioxide and carbon monoxide. 2021. World Health Organization, Geneva Licence: CC BY-NC-SA 3.0 IGO.
- WHO & IPCS, 1991. Environmental Health Criteria 111: Triphenyl Phosphate. World Health Organization (WHO), Vammala.
- Winder, C., Balouet, J.C., 2002. The toxicity of commercial jet oils. *Environ. Res.* 89, 146–164. <https://doi.org/10.1006/enrs.2002.4346>.
- Wong, F., de Wit, C.A., Newton, S.R., 2018. Concentrations and variability of organophosphate esters, halogenated flame retardants, and polybrominated diphenyl ethers in indoor and outdoor air in Stockholm, Sweden. *Environ. Pollut.* 240, 514–522. <https://doi.org/10.1016/j.envpol.2018.04.086>.
- Xing, Y.F., Xu, Y.H., Shi, M.H., Lian, Y.X., 2016. The impact of PM2.5 on the human respiratory system. *J. Thorac. Dis.* 8, 69–74. <https://doi.org/10.3978/j.issn.2072-1439.2016.01.19>.
- Ying, G.G., Williams, B., Kookana, R., 2002. Environmental fate of alkylphenols and alkylphenol ethoxylates - a review. *Environ. Int.* 28, 215–226. [https://doi.org/10.1016/S0160-4120\(02\)00017-X](https://doi.org/10.1016/S0160-4120(02)00017-X).
- Yu, Z., Herndon, S.C., Ziemba, L.D., Timko, M.T., Liscinsky, D.S., Anderson, B.E., Miake-Lye, R.C., 2012. Identification of lubrication oil in the particulate matter emissions from engine exhaust of in-service commercial aircraft. *Environ. Sci. Technol.* 46, 9630–9637. <https://doi.org/10.1021/es301692t>.
- Zhou, L., Hiltcher, M., Gruber, D., Püttmann, W., 2017. Organophosphate flame retardants (OPFRs) in indoor and outdoor air in the Rhine/Main area, Germany: comparison of concentrations and distribution profiles in different microenvironments. *Environ. Sci. Pollut. Res.* 24, 10992–11005. <https://doi.org/10.1007/s11356-016-6902-z>.

Supplementary Information (SI) to:

Occurrence and *in vitro* toxicity of organic compounds in urban background PM_{2.5}

Jonas P. Wallraff^{a*}, Florian Ungeheuer^{a*}, Andrea Dombrowski^b, Jörg Oehlmann^b, Alexander L. Vogel^a

^aInstitute for Atmospheric and Environmental Sciences, Goethe-University Frankfurt, Altenhöferallee 1, 60438 Frankfurt am Main, Germany

^bInstitute of Ecology, Evolution and Diversity, Goethe-University Frankfurt, Max-von-Laue-Str. 9, 60438 Frankfurt am Main, Germany

*These authors contributed equally

Correspondence to: Alexander L. Vogel (vogel@iau.uni-frankfurt.de)

Table S1. AChE phosphate buffer.

	Solution	M (mol l ⁻¹)	Mass concentration (g l ⁻¹)
K ₂ HPO ₄	A	1.5	342.34
KH ₂ PO ₄	B	1.5	204.14
100 ml solution A and 48.5 ml solution B were mixed. If necessary, the pH was adjusted to 7.2			

Table S2. EC₂₀ and EC₂₅ values with 95 % confidence interval (CI) for the Microtox- and AChE inhibition assay.

	Sample	Microtox, EC ₂₀ with CI (m ³ air ml ⁻¹)	AChE, EC ₂₅ with CI (m ³ air ml ⁻¹)
Airport, normal operation	AN27	54.5 (7.48 to 427)	3.32 (2.21 to 4.98)
	AN19		
	AN24	57.1 (8.25 to 395)	5.34 (4.45 to 6.41)
	AN26	41.4 (33.7 to 51.0)	4.553 (4.01 to 5.17)
Airport strike	AS31		3.81 (2.90 to 5.00)
	AS28	49.9 (38.3 to 65.0)	5.09 (4.41 to 5.88)
	AS29		11.2 (10.0 to 12.6)
	AS30	56.6 (7.48 to 427)	8.353 (7.51 to 9.30)
City	C5	27.7 (22.2 to 34.6)	3.24 (2.94 to 3.57)
	C3	49.3 (38.7 to 62.7)	1.74 (1.36 to 2.22)
	C4	24.7 (20.2 to 30.3)	1.39 (1.05 to 1.83)
	C7	32.7 (26.8 to 40.0)	3.11 (2.30 to 4.21)

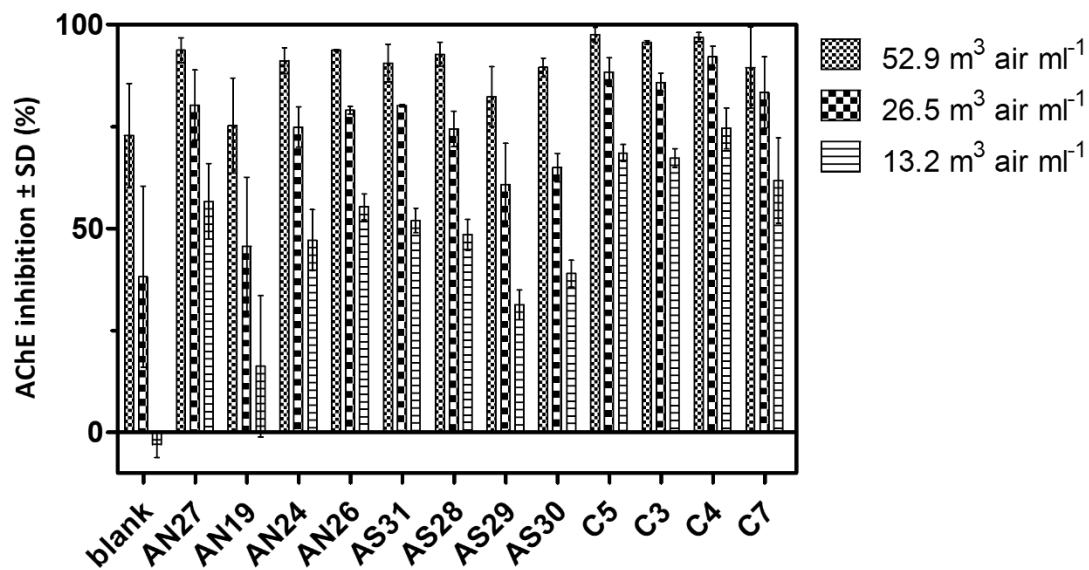


Fig. S1. AChE inhibition of the three highest tested concentrations in $\text{m}^3 \text{air ml}^{-1}$. The field blank showed high activity in the two highest concentrations of 52.9 and $26.5 \text{ m}^3 \text{air ml}^{-1}$. Therefore, these concentrations were excluded from the EC_{25} calculation. In the remaining six dilutions from $13.2 \text{ m}^3 \text{air ml}^{-1}$ downwards, the field blank shows no inhibition to AChE.

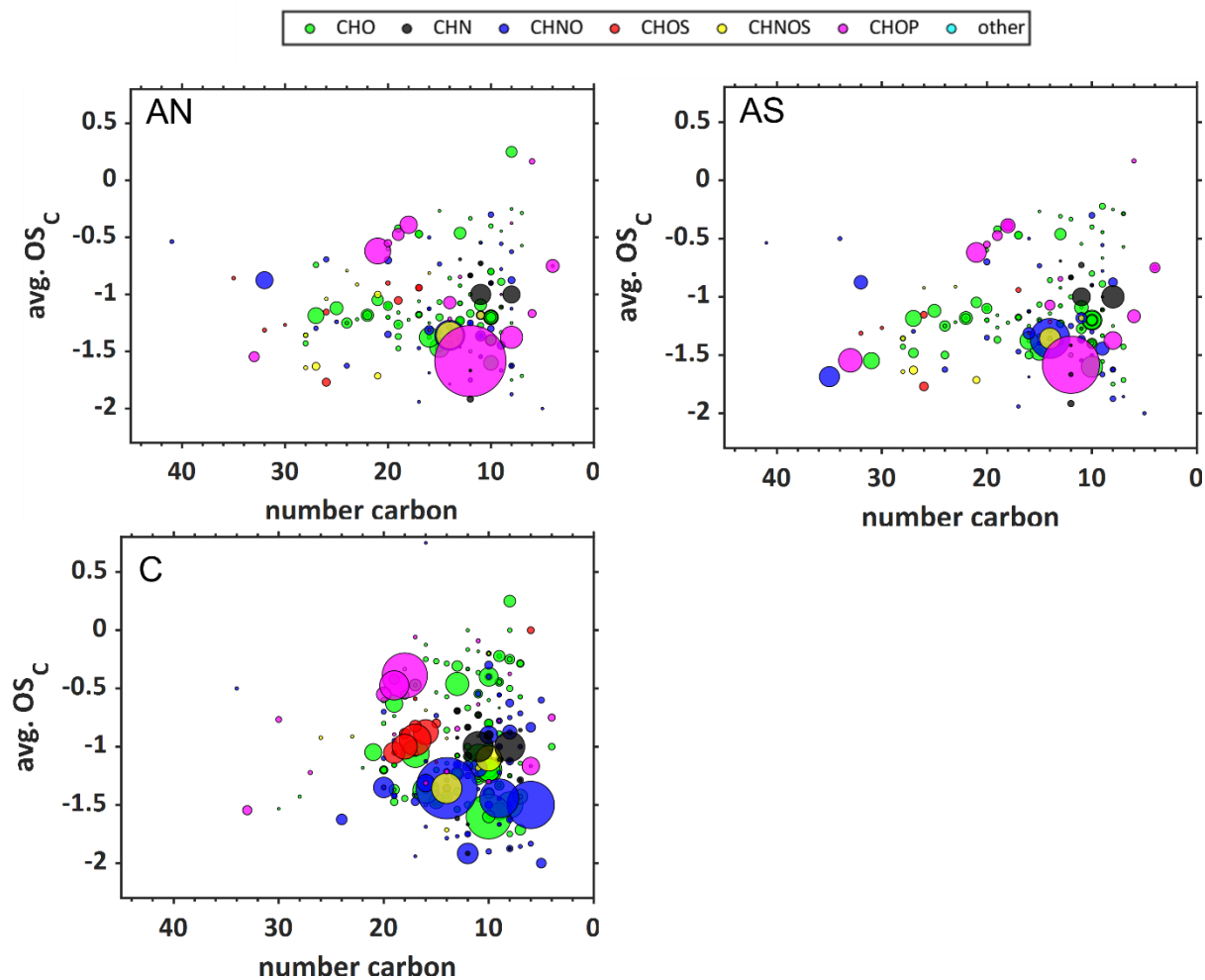


Fig. S2. Krill plot of the filter averages for each sampling condition. The plot shows the average carbon oxidation state (avg. OS_C) against the number of carbon atoms. It is a way of characterizing complex organic fractions based on their oxidation state and was calculated according to Kroll et al. (2011). Notably, CHO compounds from AN and AS have higher carbon numbers than samples from C. **AN** – normal airport operation, **AS** – airport strike, **C** – city.

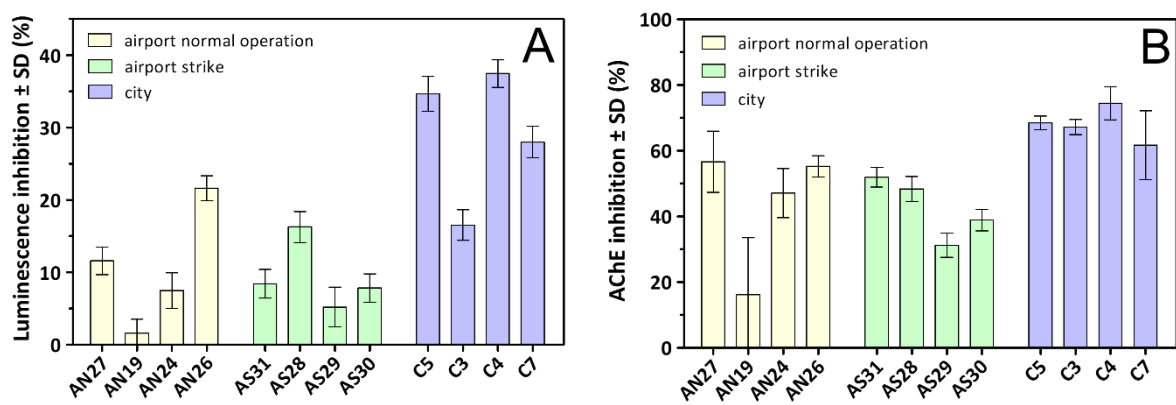


Fig. S3. Luminescence inhibition and AChE inhibition of the highest used test concentrations. A represents the luminescence inhibition (%) in the Microtox assay caused by extracts with a concentration of $47.1 \text{ m}^3 \text{ air ml}^{-1}$, B represents the AChE inhibition caused by extracts with a concentration of $13.2 \text{ m}^3 \text{ air ml}^{-1}$.

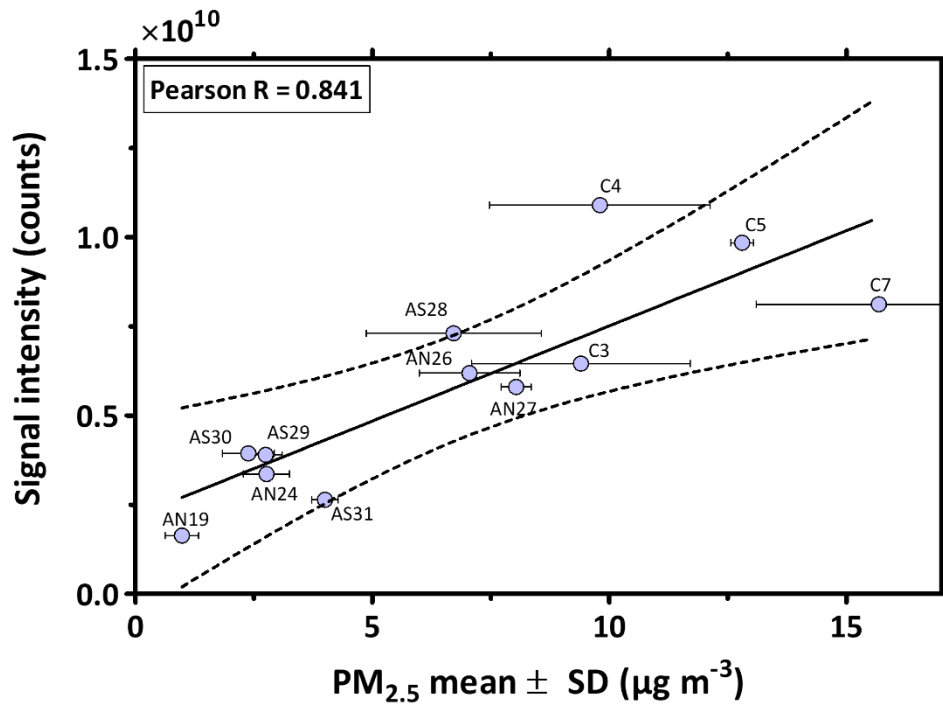


Fig. S4. Pearson correlation between the summed signal intensity of all detected compounds with a $s/b \geq 5$ and the ambient PM_{2.5} concentrations. $P=0.0006$, Pearson $r=0.841$ (0.352 to 0.970), confidence interval 99 %.

Table S3. Coefficients of determination (r^2) for the linear regression analyses (Pearson) at a p-level of 0.01 for single compounds. ns = not significant.

	AChE (r^2)	Microtox (r^2)
TPhP	0.616	0.616
CDP	0.674	0.659
DPP	0.704	0.703
TCP	ns	ns
TBP	ns	ns
TEP	0.341	0.523
Norharman	0.396	0.364
NBBS	ns	0.558
Caryophyllene oxide	ns	ns
OP1EO	0.575	0.693
Prosulfocarb	0.360	0.542

Table S4. Detailed settings of the CD-workflow.

Processing node 0: Input Files

Processing node 1: Select Spectra

1. Spectrum Properties Filter:

- Lower RT Limit: 0
- Upper RT Limit: 0
- First Scan: 0
- Last Scan: 0
- Ignore Specified Scans: (not specified)
- Lowest Charge State: 0
- Highest Charge State: 0
- Min. Precursor Mass: 0 Da
- Max. Precursor Mass: 5000 Da
- Total Intensity Threshold: 1000000
- Minimum Peak Count: 1

2. Scan Event Filters:

- Mass Analyzer: Is FTMS
- MS Order: Is MS2; MS1
- Activation Type: (not specified)
- Min. Collision Energy: 0
- Max. Collision Energy: 1000
- Scan Type: Any
- Polarity Mode: Is +

3. Peak Filters:

- S/N Threshold (FT-only): 1.5

4. Replacements for Unrecognized Properties:

- Unrecognized Charge Replacements: 1
- Unrecognized Mass Analyzer Replacements: ITMS
- Unrecognized MS Order Replacements: MS2
- Unrecognized Activation Type Replacements: CID
- Unrecognized Polarity Replacements: +
- Unrecognized MS Resolution@200 Replacements: 60000
- Unrecognized MSn Resolution@200 Replacements: 30000

5. General Settings:

- Precursor Selection: Use MS1 Precursor
- Use Isotope Pattern in Precursor Reevaluation: True
- Provide Profile Spectra: Automatic
- Store Chromatograms: False

Processing node 2: Align Retention Times

1. General Settings:

- Alignment Model: Adaptive curve
- Alignment Fallback: Use Linear Model
- Maximum Shift [min]: 0.3
- Shift Reference File: True
- Mass Tolerance: 5 ppm
- Remove Outlier: True

Processing node 3: Detect Compounds

1. General Settings:

- Mass Tolerance [ppm]: 5 ppm

- Intensity Tolerance [%]: 10

- S/N Threshold: 3

- Min. Peak Intensity: 500000

- Ions:

[2M+H]⁺

[2M+K]⁺

[2M+Na]⁺

[2M+NH₄]⁺

[M+H]⁺

[M+H+MeOH]⁺

[M+K]⁺

[M+Na]⁺

[M+NH₄]⁺

- Base Ions: [M+H]⁺; [M+Na]⁺

- Min. Element Counts: C H

- Max. Element Counts: C90 H190 Br3 Cl4 N4 O20 P S3

2. Peak Detection:

- Filter Peaks: True

- Max. Peak Width [min]: 0.5

- Remove Singlets: True

- Min. # Scans per Peak: 5

- Min. # Isotopes: 2

Processing node 5: Group Compounds

1. Compound Consolidation:

- Mass Tolerance: 2 ppm

- RT Tolerance [min]: 0.3

2. Fragment Data Selection:

- Preferred Ions: [M+H]⁺

Processing node 6: Fill Gaps

1. General Settings:

- Mass Tolerance: 2 ppm

- S/N Threshold: 1.5

- Use Real Peak Detection: True

Processing node 7: Mark Background Compounds

1. General Settings:

- Max. Sample/Blank: 3

- Max. Blank/Sample: 0

- Hide Background: False

Processing node 9: Assign Compound Annotations

1. General Settings:

- Mass Tolerance: 2 ppm

2. Data Sources:

- Data Source #1: mzCloud Search

- Data Source #2: Predicted Compositions

- Data Source #3: (not specified)

- Data Source #4: ChemSpider Search

- Data Source #5: (not specified)

- Data Source #6: (not specified)

- Data Source #7: (not specified)

3. Scoring Rules:

- Use mzLogic: True

- Use Spectral Distance: True

- SFit Threshold: 20

- SFit Range: 20

Processing node 10: Search mzCloud

1. General Settings:

- Compound Classes: All

- Precursor Mass Tolerance: 5 ppm

- FT Fragment Mass Tolerance: 5 ppm

- IT Fragment Mass Tolerance: 0.4 Da

- Library: Autoprocessed; Reference

- Post Processing: Recalibrated

- Max. # Results: 10
- Annotate Matching Fragments: False

2. DDA Search:

- Identity Search: HighChem HighRes
- Match Activation Type: True
- Match Activation Energy: Match with Tolerance
- Activation Energy Tolerance: 20
- Apply Intensity Threshold: True
- Similarity Search: Similarity Forward
- Match Factor Threshold: 60

3. DIA Search:

- Use DIA Scans for Search: False
- Max. Isolation Width [Da]: 500
- Match Activation Type: False
- Match Activation Energy: Any
- Activation Energy Tolerance: 100
- Apply Intensity Threshold: False
- Match Factor Threshold: 20

Processing node 8: Predict Compositions

1. Prediction Settings:

- Mass Tolerance: 2 ppm
- Min. Element Counts: C H
- Max. Element Counts: C90 H190 Br3 Cl4 N4 O20 P S3

- Min. RDBE: 0
- Max. RDBE: 40
- Min. H/C: 0.1
- Max. H/C: 3.5
- Max. # Candidates: 10
- Max. # Internal Candidates: 200

2. Pattern Matching:

- Intensity Tolerance [%]: 10
- Intensity Threshold [%]: 0.1
- S/N Threshold: 3
- Min. Spectral Fit [%]: 30
- Min. Pattern Cov. [%]: 90
- Use Dynamic Recalibration: True

3. Fragments Matching:

- Use Fragments Matching: True
- Mass Tolerance: 5 ppm
- S/N Threshold: 3

Processing node 11: Search ChemSpider

1. Search Settings:

- Database(s):
 - EAWAG Biocatalysis/Biodegradation Database
 - Nature Chemistry
 - Sigma-Aldrich

- Search Mode: By Formula Only
- Mass Tolerance: 5 ppm
- Max. # of results per compound: 100
- Max. # of Predicted Compositions to be searched per Compound: 3
- Result Order (for Max. # of results per compound): Order By Reference Count (DESC)

2. Predicted Composition Annotation:

- Check All Predicted Compositions: False

Processing node 12: Apply mzLogic

1. Search Settings:

- FT Fragment Mass Tolerance: 10 ppm
- IT Fragment Mass Tolerance: 0.4 Da
- Max. # Compounds: 0
- Max. # mzCloud Similarity Results to consider per Compound: 10
- Match Factor Threshold: 30

Processing node 13: Apply Spectral Distance

1. Pattern Matching:

- Mass Tolerance: 5 ppm
- Intensity Tolerance [%]: 30
- Intensity Threshold [%]: 0.1
- S/N Threshold: 3
- Use Dynamic Recalibration: True

RT :10.78-16.31

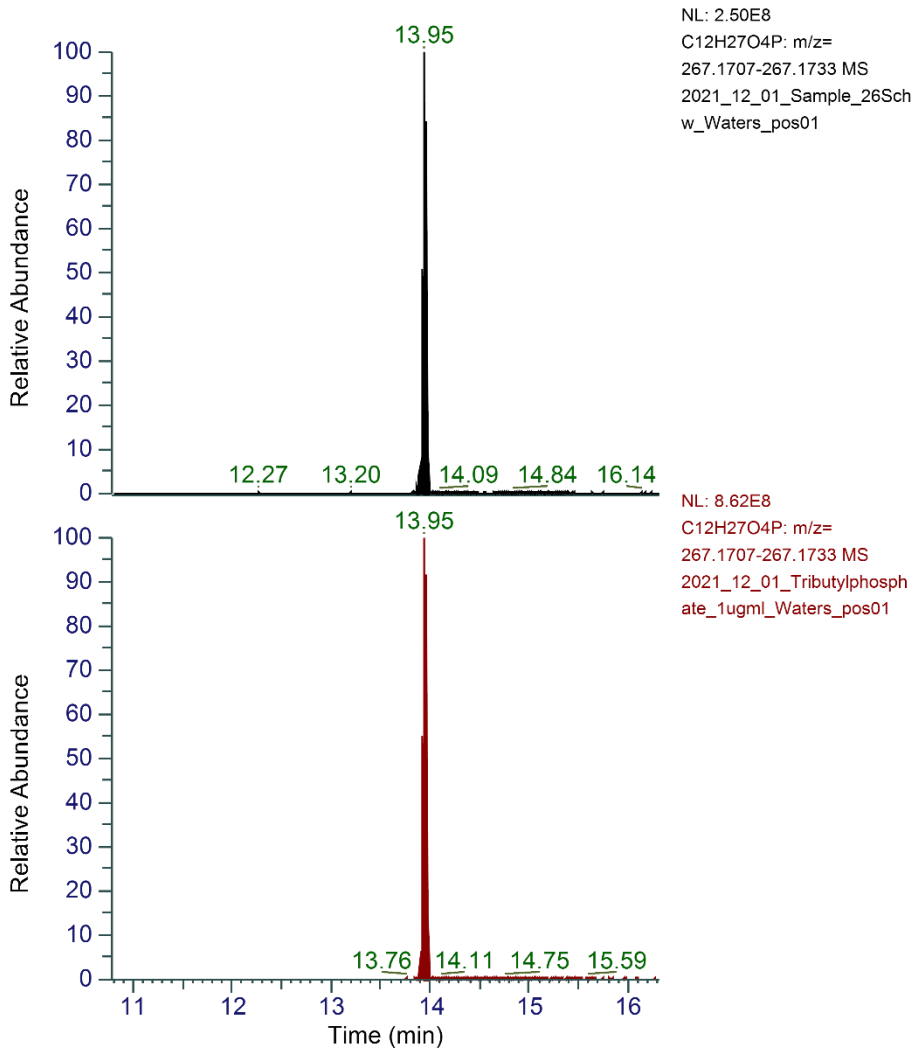


Fig. S5. Chromatograms of tributyl phosphate (TBP) signals in the sample AN26 (top) and the authentic standard ($\geq 99\%$, Sigma Aldrich) (bottom).

RT :13.07-16.52

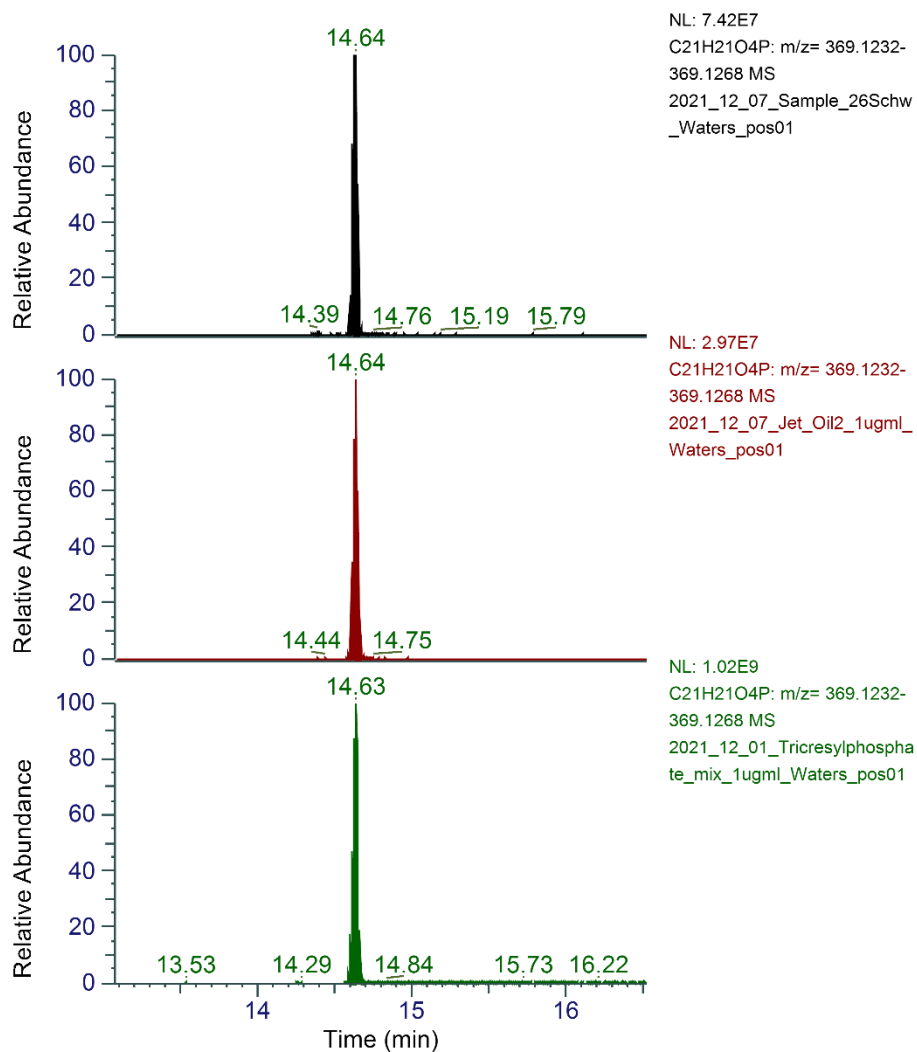


Fig. S6. Chromatograms of tricesyl phosphate (TCP) signals in the sample AN26 (top), in Mobil Jet Oil II (middle) and in the authentic standard (mixture of TCP isomers 63-85 %, residue of other tolyl phosphate isomers, Acros Organics) (bottom).

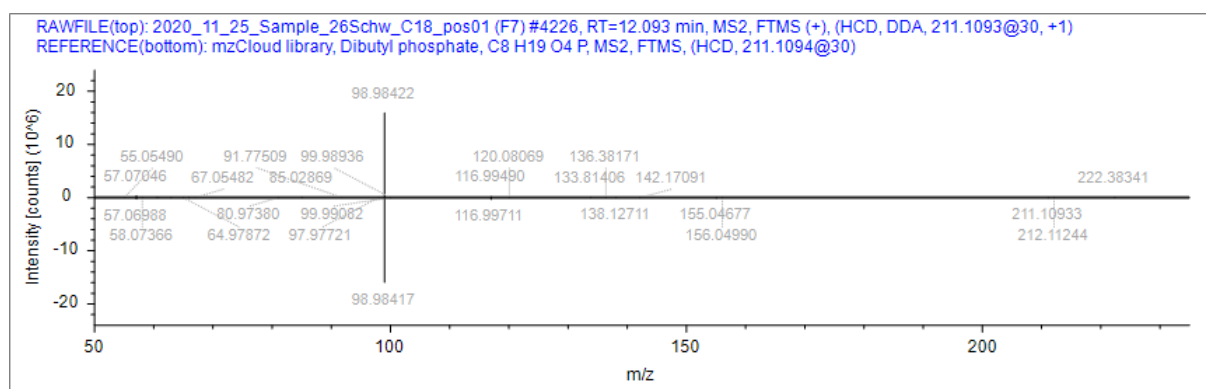


Fig. S7. MS/MS mirror plot of the compound dibutyl phosphate in sample AN26 (top) and the mzcloud library spectrum (bottom).

RT :10.43-16.59

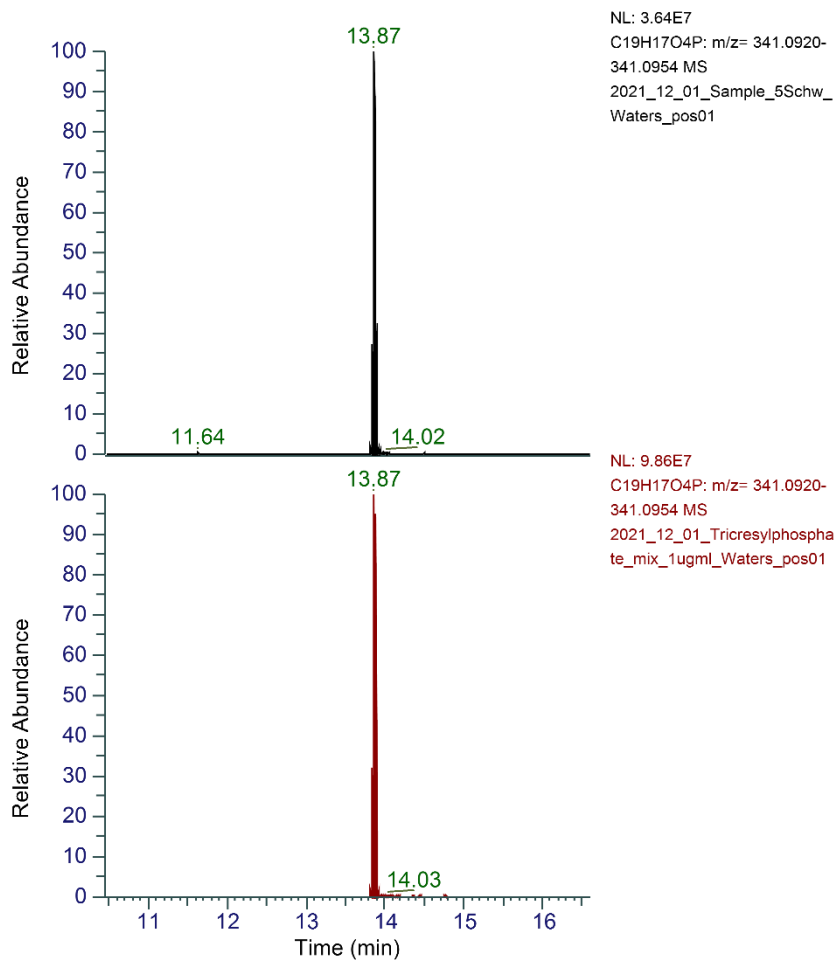


Fig. S8. Chromatograms of cresyldiphenyl phosphate (CDP) signals in the sample C5 (top) and the authentic standard (mixture of TCP isomers 63-85 %, residue of other tolyl phosphate isomers, Acros Organics) (bottom).

RT :10.43-16.59

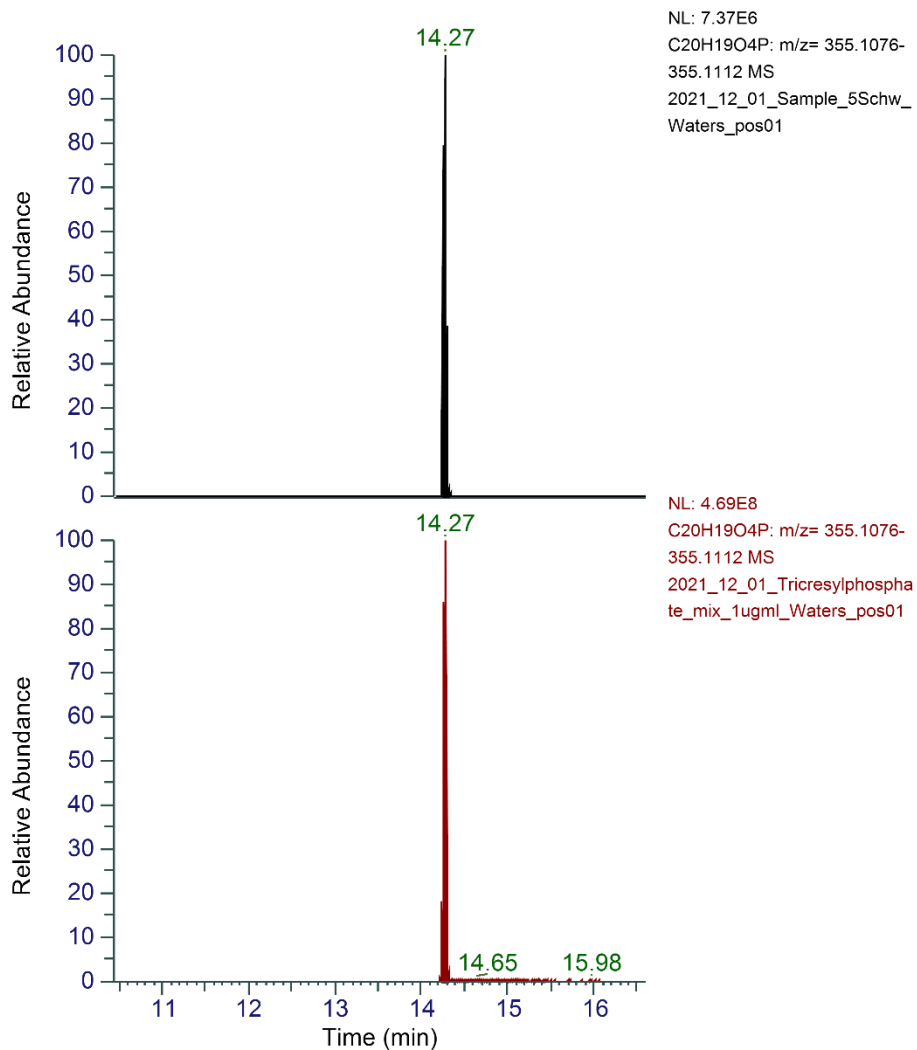


Fig. S9. Chromatograms of dicresylphenyl phosphate (DPP) signals in the sample C5 (top) and the authentic standard (mixture of TCP isomers 63-85 %, residue of other tolyl phosphate isomers, Acros Organics) (bottom).

RT :7.87-11.03



Fig. S10. Chromatograms of triethyl phosphate (TEP) signals in the sample C5 (top) and the authentic standard ($\geq 99.8\%$, Sigma Aldrich) (bottom).

RT :9.60-16.31

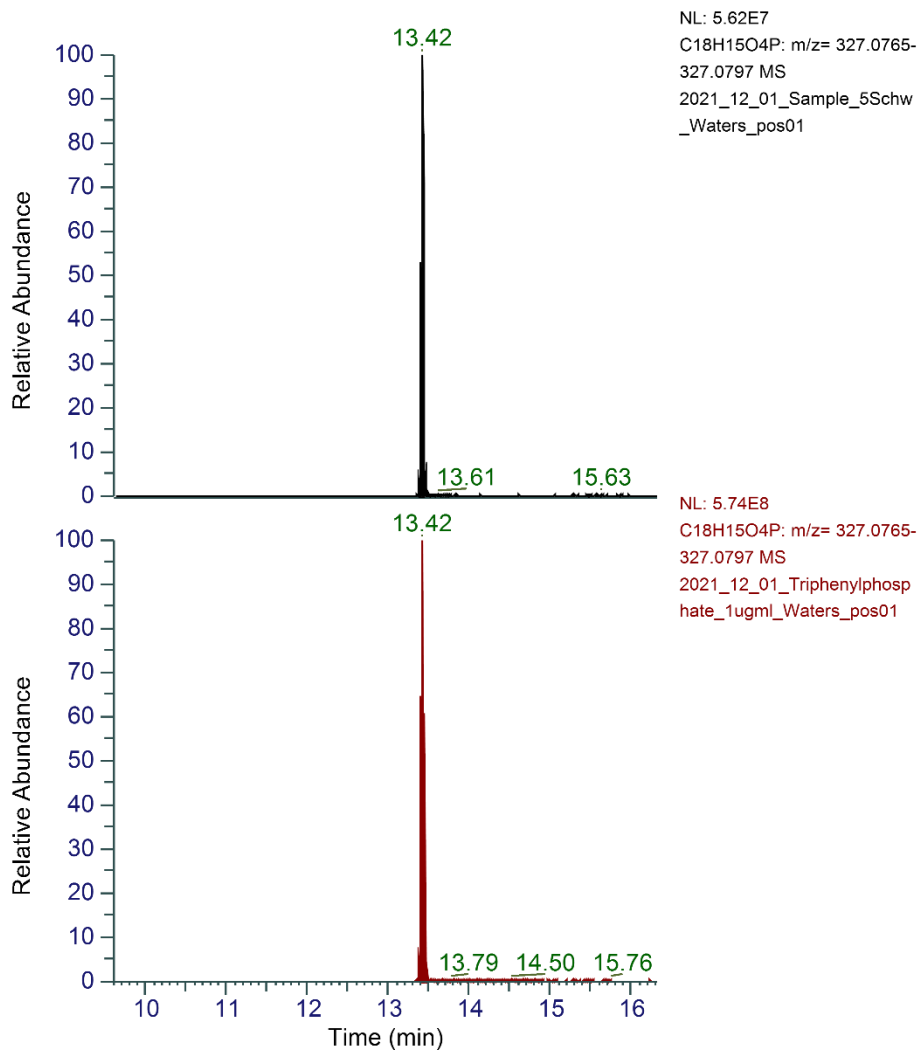


Fig. S11. Chromatograms of triphenyl phosphate (TPhP) signals in the sample C5 (top) and the authentic standard ($\geq 99\%$, Sigma Aldrich) (bottom).

RT :12.76-14.99

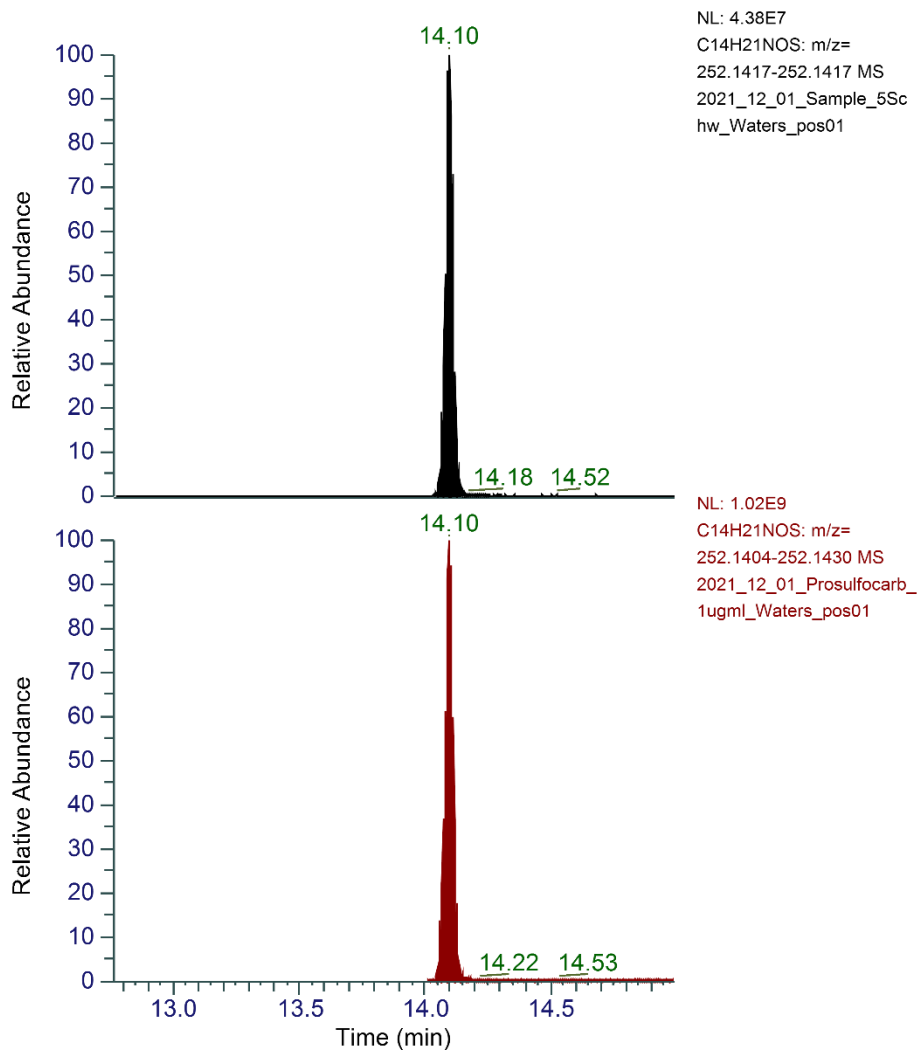


Fig. S12. Chromatograms of prosulfocarb (PSC) signals in the sample C5 (top) and the authentic standard ($\geq 98\%$, Sigma Aldrich) (bottom).

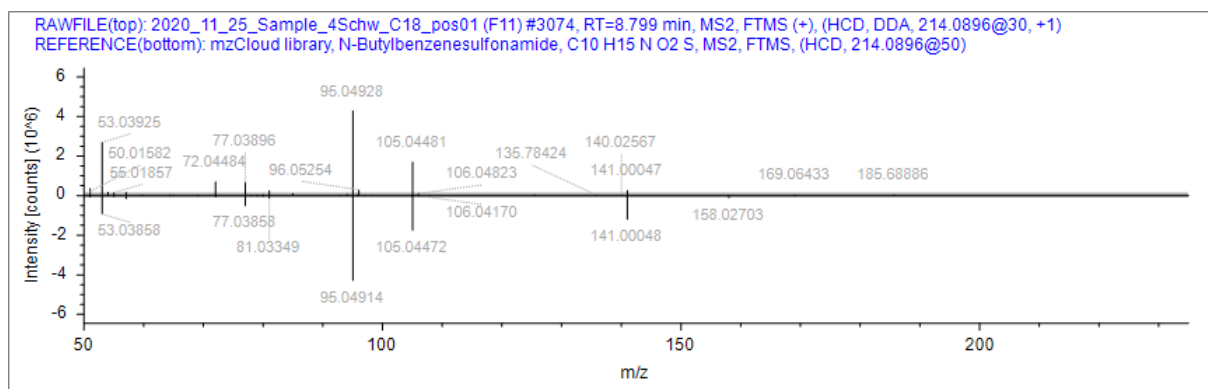


Fig. S13. MS/MS mirror plot for N-butylbenzenesulfonamide (NBBS) in sample C4 (top) and the mzcloud library spectrum (bottom).

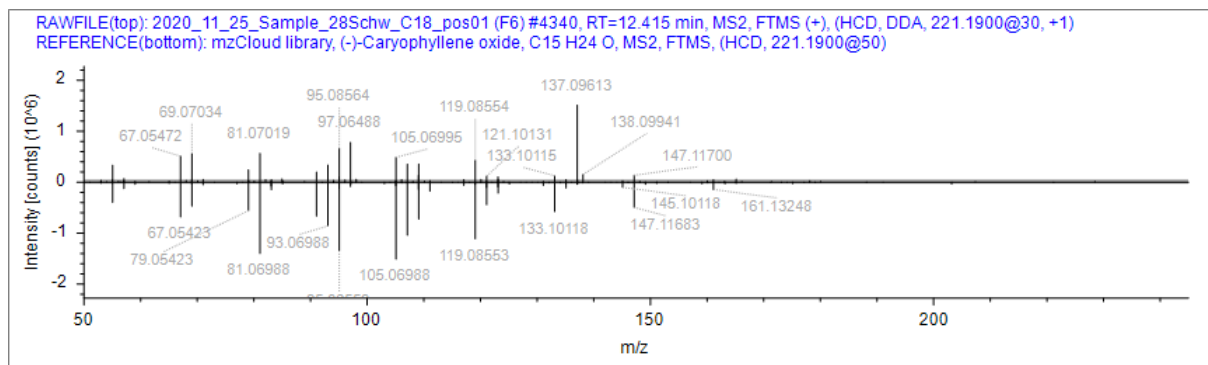


Fig. S14. MS/MS mirror plot for caryophyllene oxide in sample AS28 (top) and the mzcloud library spectrum (bottom).

RT :11.60-19.26

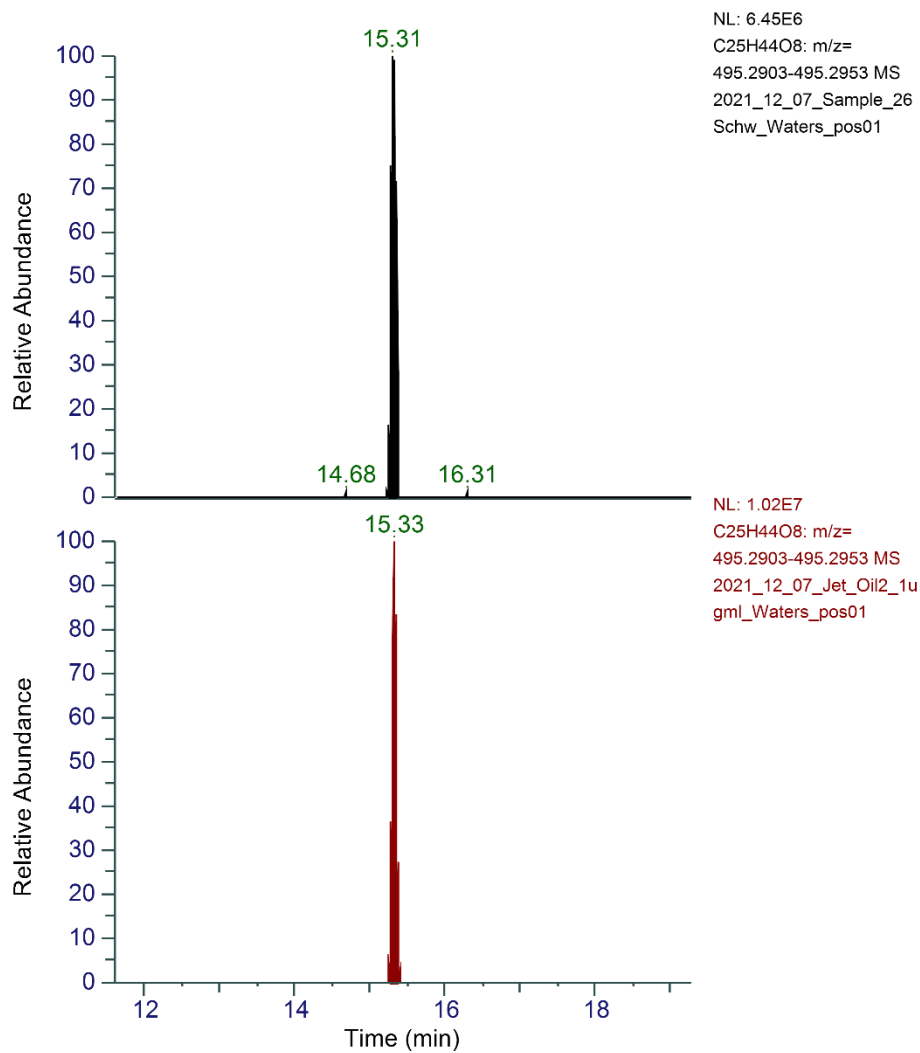


Fig. S15. Chromatograms for the signals of the synthetic ester $C_{25}H_{44}O_8$ in the sample AN26 (top) and in Mobil Jet Oil II (bottom).

RT :11.60-19.26

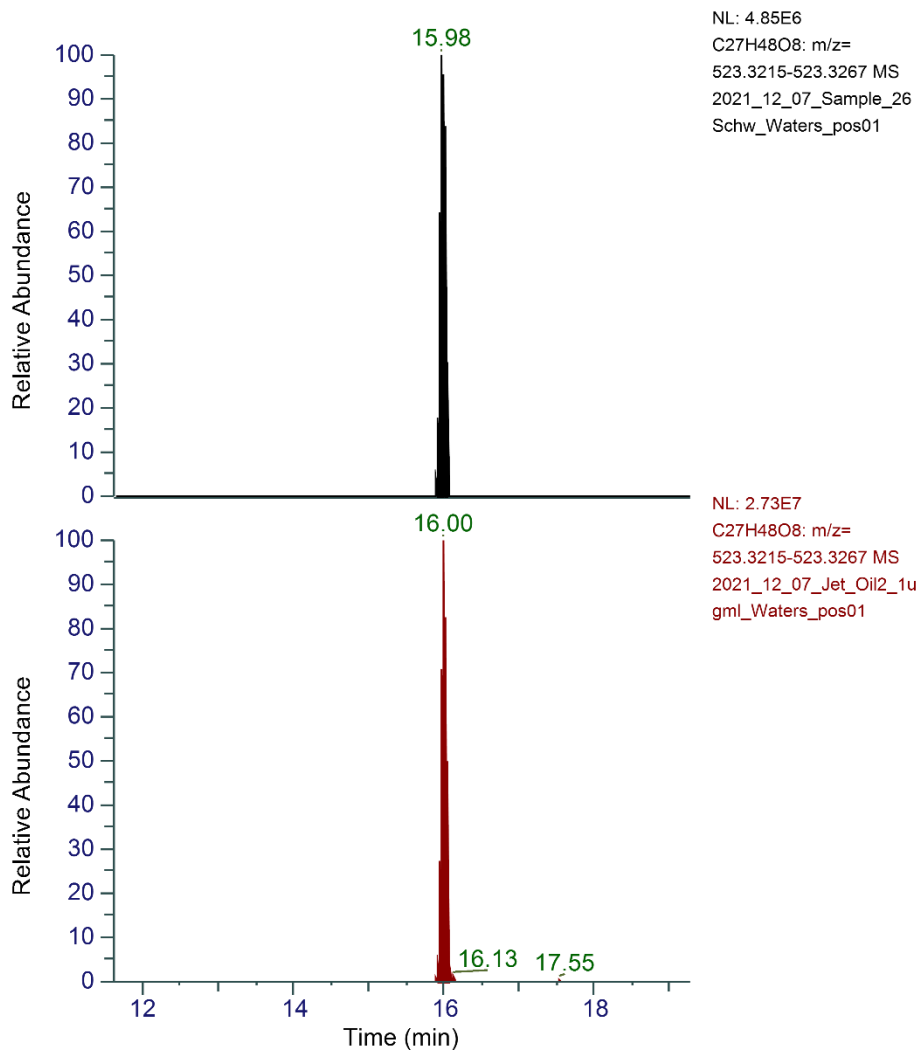


Fig. S16. Chromatograms for the signals of the synthetic ester $C_{27}H_{48}O_8$ in the sample AN26 (top) and in Mobil Jet Oil II (bottom).

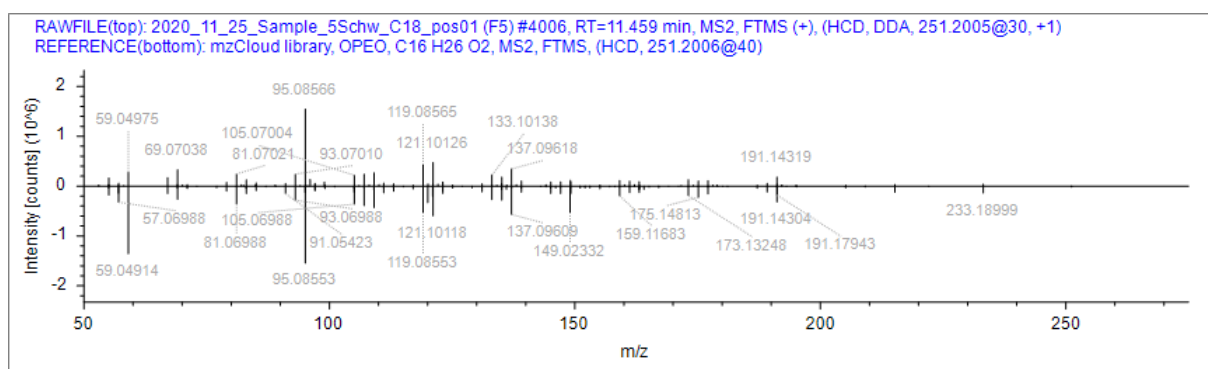
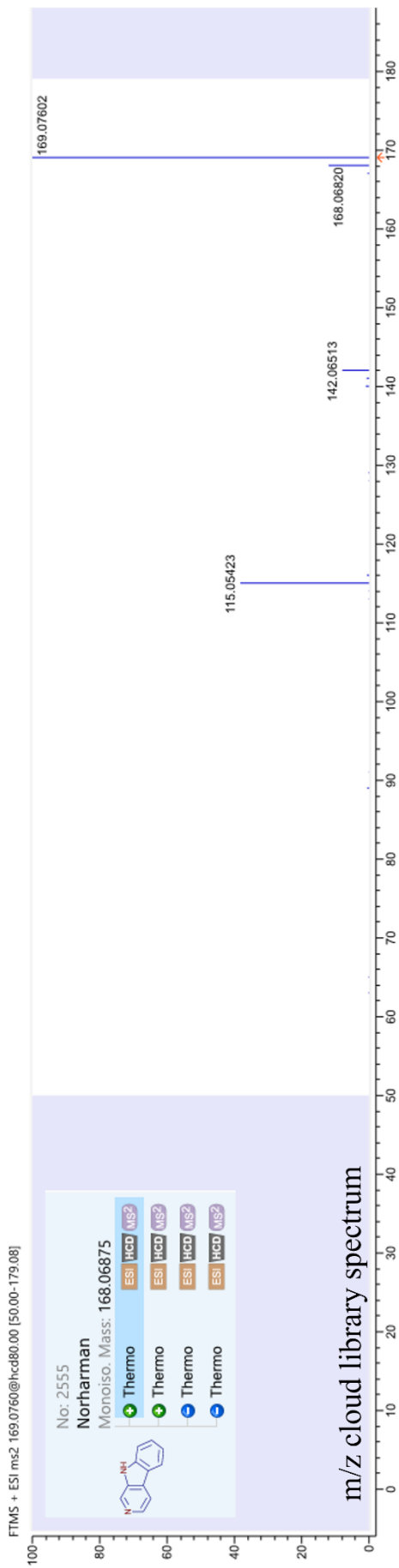


Fig. S17. MS/MS mirror plot for OP1EO in sample C5 (top) and the mzcloud library spectrum (bottom).



RAWFILE(top): 2020_11_25_Sample_4Schw_C18_pos01 (F11) #1606, RT=4.605 min, MS2, FTMS (+), (HCD, DDA, 169.0761@30, +1)
 REFERENCE(bottom): spectrum missing

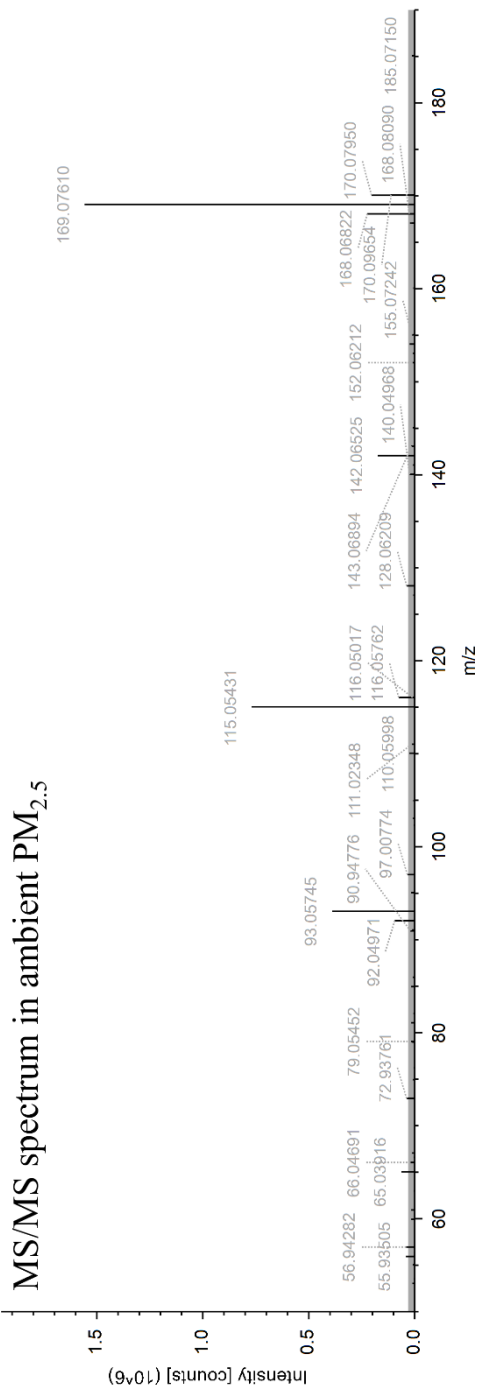


Fig. S18. Mzcloud library spectrum for norharmane with the characteristic fragments of m/z 115.05423; 142.06513; 168.06820; and 169.07602 (top) and the MS/MS spectrum for sample C4 at m/z 169.0761, where we observe the according fragments and therefore identify the compound as norharmane (level 2).

References

- Kroll, J.H., Donahue, N.M., Jimenez, J.L., Kessler, S.H., Canagaratna, M.R., Wilson, K.R., Altieri, K.E., Mazzoleni, L.R., Wozniak, A.S., Bluhm, H., Mysak, E.R., Smith, J.D., Kolb, C.E., Worsnop, D.R., 2011. Carbon oxidation state as a metric for describing the chemistry of atmospheric organic aerosol. *Nat. Chem.* 3, 133–139. <https://doi.org/10.1038/nchem.948>

5.4 Nontarget Screening Exhibits a Seasonal Cycle of PM_{2.5} Organic Aerosol Composition in Beijing

Nontarget Screening Exhibits a Seasonal Cycle of PM_{2.5} Organic Aerosol Composition in Beijing

Jialiing Ma, Florian Ungeheuer, Feixue Zheng, Wei Du, Yonghong Wang, Jing Cai, Ying Zhou, Chao Yan, Yongchun Liu, Markku Kulmala, Kaspar R. Daellenbach,* and Alexander L. Vogel*



Cite This: *Environ. Sci. Technol.* 2022, 56, 7017–7028



Read Online

ACCESS |

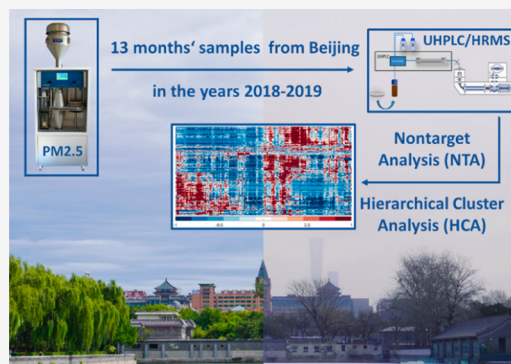
Metrics & More

Article Recommendations

Supporting Information

ABSTRACT: The molecular composition of atmospheric particulate matter (PM) in the urban environment is complex, and it remains a challenge to identify its sources and formation pathways. Here, we report the seasonal variation of the molecular composition of organic aerosols (OA), based on 172 PM_{2.5} filter samples collected in Beijing, China, from February 2018 to March 2019. We applied a hierarchical cluster analysis (HCA) on a large nontarget-screening data set and found a strong seasonal difference in the OA chemical composition. Molecular fingerprints of the major compound clusters exhibit a unique molecular pattern in the Van Krevelen-space. We found that summer OA in Beijing features a higher degree of oxidation and a higher proportion of organosulfates (OSs) in comparison to OA during wintertime, which exhibits a high contribution from (nitro-)aromatic compounds. OSs appeared with a high intensity in summer-haze conditions, indicating the importance of anthropogenic enhancement of secondary OA in summer Beijing. Furthermore, we quantified the contribution of the four main compound clusters to total OA using surrogate standards. With this approach, we are able to explain a small fraction of the OA (~11–14%) monitored by the Time-of-Flight Aerosol Chemical Speciation Monitor (ToF-ACSM). However, we observe a strong correlation between the sum of the quantified clusters and OA measured by the ToF-ACSM, indicating that the identified clusters represent the major variability of OA seasonal cycles. This study highlights the potential of using nontarget screening in combination with HCA for gaining a better understanding of the molecular composition and the origin of OA in the urban environment.

KEYWORDS: *particulate matter, urban aerosol, molecular composition, mass spectrometry, hierarchical cluster analysis*



1. INTRODUCTION

Atmospheric particulate matter (PM), in the form of liquid or solid particles suspended in air, can cause detrimental effects on human health depending on the particles chemical composition and their sources.^{1,2} Furthermore, PM affects Earth's radiative balance through direct interaction with radiation and the formation of cloud condensation nuclei (CCN).³ Organic aerosol (OA) represents a large proportion (20–90%) of the fine aerosol mass in the lower troposphere.^{4–8} Thus, understanding the chemical composition and atmospheric transformation of OA is essential for understanding the sources and enables the identification of effective mitigation strategies. Among various aerosol components, OA typically represents ~30%–50% of the PM_{2.5} mass concentration in China,^{9,10} formed from a variety of natural and anthropogenic sources. Determining the chemical composition of urban OA at the molecular level is challenging due to the highly complex composition, represented by several thousands of compounds present at trace-level concentrations in a complex matrix. Therefore, the molecular-resolved character-

ization of OA requires the application of robust state-of-the-art analytical strategies.¹¹

High-resolution mass spectrometry (HRMS) combined with electrospray ionization (ESI) has been widely applied to identify various organic compound classes.^{12–14} The “soft” ESI technique, which converts the precursor molecules to molecular ions with minor fragmentation reactions, is advantageous for the determination of the molecular formulas of native organic compounds. High-resolution and accurate mass (HR/AM) measurement of the molecular ions and their isotopic patterns allow the determination of the molecular formulas of unknown compounds. Moreover, several studies have introduced the use of ESI-HRMS coupled with high-performance liquid chromatography (HPLC).^{11,15–18} The separation of

Special Issue: Urban Air Pollution and Human Health

Received: October 13, 2021

Revised: March 9, 2022

Accepted: March 9, 2022

Published: March 18, 2022



individual compounds by HPLC provides an additional dimension of information (e.g., on the polarity of the compounds), compared to HRMS studies using direct infusion. Furthermore, HPLC separation minimizes the variation arising from matrix ion suppression. For example, a previous study found a larger number of determined molecular formulas using HPLC combined with ESI-HRMS¹⁹ than studies solely using direct infusion ESI-HRMS;^{13,20–22} possibly caused by ion suppression reactions in the direct infusion technique. Moreover, separation by HPLC is a prerequisite for nontarget analysis (NTA) since algorithms use the information on retention time to attribute ions from fragmentation reactions, adduct and cluster formation reactions to their parent molecule.^{23,24} However, care must be taken in setting up the individual NTA steps such as the detection and merging of features, filtering, and background correction.²⁵ In a recent NTA study of atmospheric PM preserved in an ice core, we demonstrated that applying different analysis software results in almost identical molecular fingerprints using HPLC-(–)ESI-HRMS.²⁶

Haze episodes in Beijing attract worldwide attention and many studies using an HRMS approach have been conducted in Beijing.^{19,27–32} For example, previous studies have revealed OA in winter Beijing is dominated by aromatics, which suggests a high contribution of combustion aerosols to the total OA.^{19,27,33} Bryant et al.²⁹ discovered that the formation of isoprene-derived secondary organic aerosol (SOA) in urban Beijing is strongly influenced by anthropogenic emissions. Xie et al.³⁰ found that the number of detected compounds (especially for high molecular weight compounds) in aqueous PM extracts decreased with larger particle sizes. In this study, we applied NTA to HPLC-ESI-HRMS measurements of 172 ambient PM_{2.5} filters from Beijing that cover a period of 13 months, and represent all detected compounds in comprehensive molecular fingerprints. Moreover, we used a hierarchical cluster analysis (HCA) for complexity reduction of the large data set that enabled the identification of compound classes that were likely to originate from similar sources and/or processes. Finally, we estimated the quantitative contribution of the four largest compound clusters to total OA based on calibrations using selected surrogate standards.

2. METHODS

2.1. Sampling, Filter Extraction, and Online Measurements. The ambient filters were collected at Beijing University of Chemical Technology (BUCT, 39°58'N, 116°25'E), which is an urban site located in the North-East of Beijing.³⁴ 24 h integrated samples were collected during the period from 27 February 2018 to 30 March 2019 on preheated quartz-fiber filters (Ø150 mm, TISSUQUARTZ-2500QAT-UP, Pall Life Science, U.S.A.) by using a high-volume sampler (CAV-A/mb, MCV, Spain). We set the flow rate of the sampler to 30 m³/h and collected samples every second or third day. In total, we collected 172 samples including 10 blank samples. Filter samples were sealed by aluminum foil and stored at –20 °C until analysis. For analysis, we punched 2 cm diameter circular sections from each filter and cut these sections into small pieces using ceramic scissors. Then we extracted the filters in an orbital shaker, twice for 20 min, consecutively, using 250 and 150 µL of an acetonitrile/water mixture (50/50 (v/v), acetonitrile: Optima LC/MS grade, Fisher scientific; water: 18.2 MΩ·cm, Millipak Express 40:0.22 µm, Millipore; Milli-Q Reference A+, Merck). After

each extraction, we used a 0.22 µm polytetrafluoroethylene (PTFE) syringe filter (Fisher Scientific) and then combined the extracts in a sharp bottom vial (CS Chromatographie Service GmbH) for subsequent analysis.

At the same site, OA was simultaneously measured by a Time-of-Flight Aerosol Chemical Speciation Monitor (ToF-ACSM, details see Cai et al.³⁵ and Supporting Information, SI). Since the ToF-ACSM only measures nonrefractory PM_{2.5} constituents, the PM_{2.5} mass concentration used in this paper is the mean value of the Wanliu, Gucheng, Wanshouxigong, and Guanyuan monitoring stations, which are the nearest monitor sites operated by China National Environmental Monitoring Center (CNEMC). However, we note that the PM_{2.5} mass concentrations measured by ToF-ACSM correlate well with the mean PM_{2.5} values from these four monitoring stations ($R = 0.89$, SI Figure S1).

2.2. UHPLC-HRMS Analysis. The analysis of the filter extracts was conducted with an Orbitrap HRMS (Q Exactive Focus Hybrid-Quadrupole-Orbitrap, Thermo Scientific) coupled with an ultrahigh performance liquid chromatography (UHPLC) system (Vanquish Flex, Thermo Fisher Scientific). The chromatographic separation was performed on a reversed phase column (Accucore C₁₈, 150 × 2.1 mm, 2.6 µm particle size, Thermo Scientific), at 40 °C (still air). As mobile phases we used eluent A (ultrapure water with 0.1% formic acid (LiChropur, Merck), v/v) and eluent B (acetonitrile with 0.1% formic acid, v/v). The gradient was set as follows: starting with 1% B for 2.0 min, increased to 99% B within 13 min, held for 2 min, decreased to 1% B within 1 min and finally held for 2 min for re-equilibration. The flow rate was 0.4 mL/min, and the injection volume was 2 µL. It is worth mentioning that due to the large set of samples, the UHPLC-HRMS measured continuously for 6 days to complete the measurements. Consequently, we repeated the measurement of one sample on a daily basis to monitor the performance of the instrument. We observe a highly reproducible instrumental performance in terms of intensity variation and mass accuracy of the five quantified compounds (4-Nitrophenol, 4-Nitrocatechol, Phthalic acid, 3-methyl-1,2,3-butanetricarboxylic acid (MBTCA), and Pinic acid) during the measurement period (see Figures S2 and S3). The mass spectra (m/z 50–750) with a resolving power of 70 000@ m/z 200 were obtained by using (–)ESI. Ion source settings were as follows: 8 psi auxiliary gas (nitrogen), 40 psi sheath gas (nitrogen), 3.5 kV spray voltage, and 350 °C gas temperature.

2.3. UHPLC-HRMS Data Processing. We used the NTA software (Compound Discoverer (CD), version 3.2, Thermo Fisher Scientific) to identify chromatographic peak features in the two-dimensional space of retention time and m/z . These features are combined to compounds when eluting at the same retention time and appearing at a m/z that corresponds to the exact mass differences from either isotopes, adducts, clusters or fragments. On the basis of the HR/AM-measurement and the isotopic pattern, molecular formulas for the detected compounds were calculated. The detailed settings of the CD-workflow are provided in Table S1.

A brief description of the NTA-workflow: a threshold intensity of 1E6 was applied to the two-dimensional coordinate system (RT: 0–20 min, m/z : 50–750) for all 172 measurements. CD automatically filtered out ions with peak abundance below the threshold intensity, as well as the ions that appeared in blank samples at intensities of >1/3 of the maximum values of the ambient samples. For the remaining ions, the molecular

formulas were calculated with elemental combinations of $C_{n1}H_{n2}Br_{n3}Cl_{n4}N_{n5}O_{n6}P_{n7}S_{n8}$ ($n1 = 1-90$, $n2 = 1-190$, $n3 = 0-3$, $n4 = 0-4$, $n5 = 0-4$, $n6 = 0-20$, $n7 = 0-1$, and $n8 = 0-3$) and with a mass tolerance of 2 ppm. To filter out chemically unreasonable formulas, the minimum H/C and maximum H/C were set as 0.1 and 3.5, respectively.

2.4. Calculation of Molecular Characteristics. The double bond equivalent (DBE) of a molecular formula containing C, H, N, O, and S indicates the number of rings, double and triple bonds. The value of the DBE is calculated based on the number of the individual elements as follows:³⁶

$$DBE = \#C - \frac{\#H}{2} + \frac{\#N}{2} + 1 \quad (1)$$

Both the aromaticity equivalent³⁷ (X_c) and aromaticity index³⁸ (AI) can be applied to estimate the aromaticity of the organic compounds. Here we used X_c as it classifies (poly)aromatic compounds with significant alkylation as aromatic compounds.³⁹ Thus, X_c was applied in this study to estimate the aromaticity of the compounds, expressed as follows:

$$X_c = \frac{3*[DBE - (m*\#O + n*\#S)] - 2}{DBE - (m*\#O + n*\#S)} \quad (0 \text{ if } < 0) \quad (2)$$

Here “ m ” and “ n ” are the fractions of oxygen and sulfur atoms in the π -bond structures of a compound (both “ m ” and “ n ” are presumed to be 0.5³⁷), respectively. If the $DBE \leq m*\#O + n*\#S$, then $X_c = 0$, showing no aromaticity as Yassine et al.³⁷ suggested that compounds with $X_c < 2.5000$ correspond to nonaromatic compounds, for aromatics $2.5000 \leq X_c < 2.7143$ and for condensed aromatics $X_c \geq 2.7143$.

All the observed formulas were classified into six categories based on their elemental compositions, including CHOa, CHOn, CHNO, CHNOS, CHOS, and others. As an example, CHOS refers to compounds that contain the elements carbon, hydrogen, oxygen, and sulfur. The compound categories CHOa represent aromatics ($X_c \geq 2.5$), while CHOn are nonaromatic ($X_c < 2.5$) compounds (e.g., terpene oxidation products). “Others” (e.g., CH, CHS, CHNS, and signals to which no elemental formulas were calculated) refers to the compounds excluded from the above major compound categories.

2.5. Hierarchical Cluster Analysis. HCA is a data mining method that merges individual observations into clusters of similar behavior through the determination of the similarity between every pair of objects in a data matrix. Previous studies have described the principle of HCA in detail^{40,41} and discuss its difference to other methods, such as the widely used positive matrix factorization (PMF). In brief, HCA groups compounds in a stepwise process in contrast to PMF that defines components (termed factors) that explain the compounds’ variability. In this work, we use Matlab (Mathworks) to perform the HCA. The observation used as input for the HCA was a matrix of organic compounds and their peak area in the 172 samples covering a time span of 13 months. As a first step, the peak areas were standardized based on z-transformation. The proximity between the observation pairs was determined by Euclidean distance for both compound rows and sample columns. We note that it is also possible to use other metrics of distance, for example, correlation or cosine distance, however, the Euclidean distance made our data set the most understandable and reproducible. We used the Ward

linkage method for merging different compounds and samples into compound clusters and sample clusters, respectively. The hierarchical clustering in this study was performed twice, on both compound rows and sample columns. Moreover, the two clusterings were independent from each other since the order of components does not matter when one computes the distance between two vectors.

The outcome of the NTA resulted in 2136 compounds after background correction, filtering for duplicates, and applying an intensity threshold for the sample-to-blank ratio of >3 . In order to avoid a bias in the HCA introduced by a large number of small signals, we used, as input, only the major compounds that were responsible for 94% of the total peak area (SI Figure S4). Variation of this threshold does not affect the compound clustering. However, with 95% as input we observe a slight difference of the sample clustering, but with 94% as input we observe a better separation between summer samples into clean and haze conditions. With using 94% as input, there were 1323 compounds remaining, of which 1097 had unambiguous molecular formulas.

3. RESULTS AND DISCUSSION

3.1. Seasonal Differences of the OA Chemical Composition in Beijing. Figure 1 indicates a clear seasonal variation in the intensities and the relative contribution of different compound categories (Figure 1A and B). We observed an enhanced absolute intensity of organic compounds (Figure 1C), especially for the intensity of the compound groups CHNO (e.g., nitroaromatics) and CHOa (e.g., oxidized aromatics), which contribute 38% and 17%, respectively, to the total peak intensity during winter. These specific compound groups are likely attributed to the increased solid fuel combustion activities in winter.³³ Moreover,

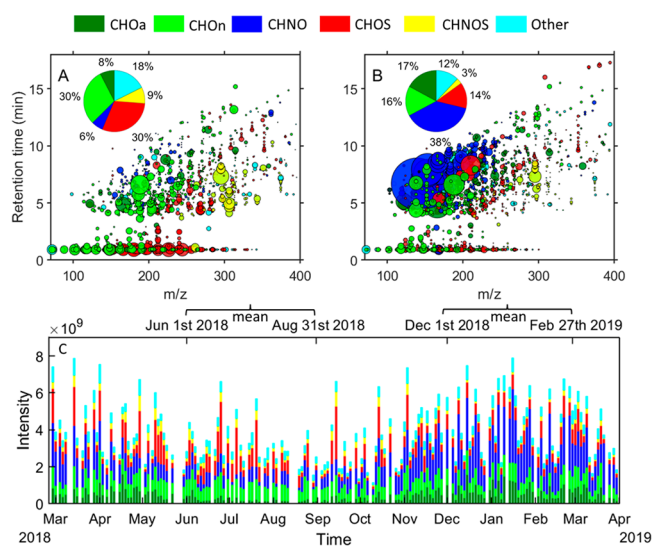


Figure 1. Seasonal differences and time series for the intensity of OA chemical composition. (A, B) The m/z vs retention time (RT) plots represent a three-month mean value of summer (A) and winter (B) samples. Individual detected compounds are displayed as circles with the area representing the signal intensity, and the color indicates the molecular composition. The x -axes show the mass-to-charge ratio (m/z) of the compounds, and the measured retention time (y -axis) indicates the polarity of the single molecules. (C) Time series of the different compound categories (CHOn, CHOa, CHNO, CHOS, CHNOS, and others).

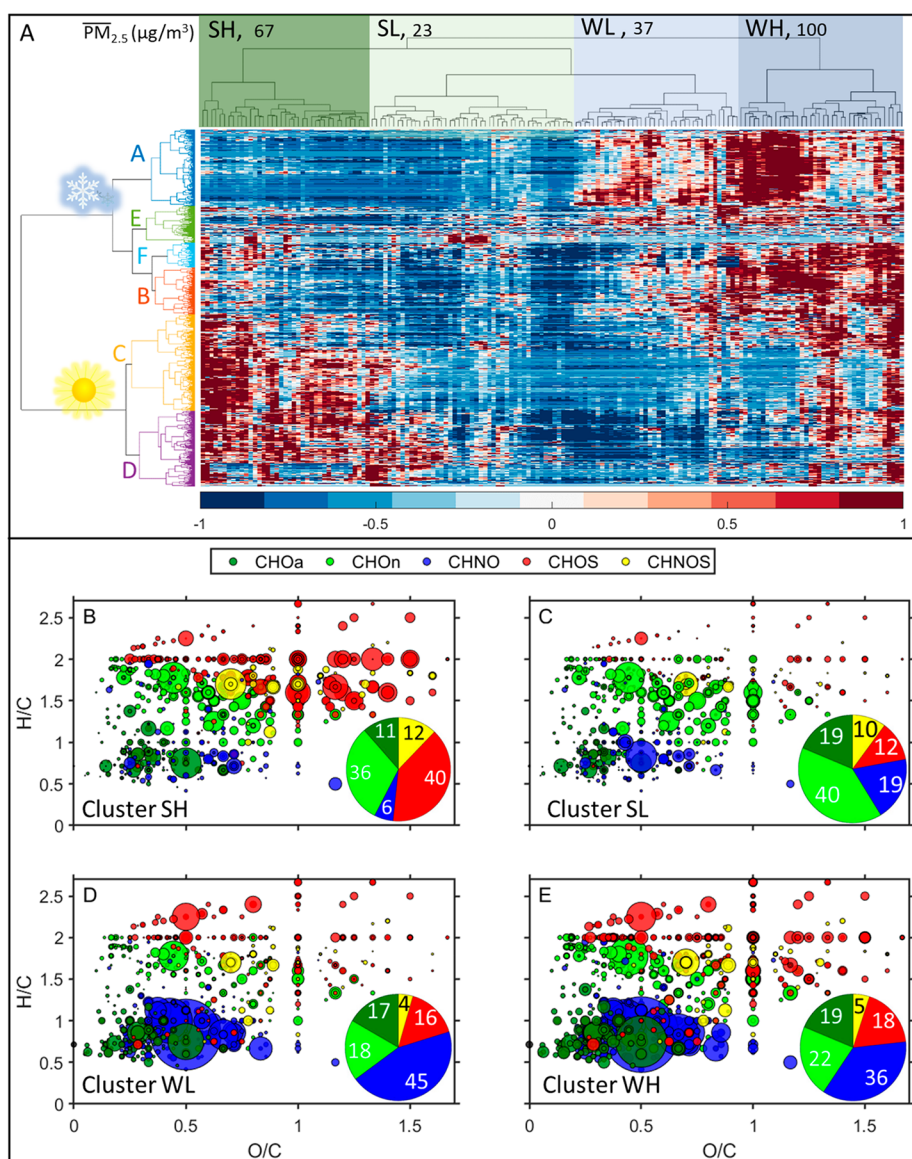


Figure 2. HCA and molecular fingerprints. (A) Hierarchical clustergram: the *x*-axis and *y*-axis represent the sample cluster and compound cluster, respectively. The letters A–F in the *y*-axis represent the respective compound clusters. Sun: compound clusters high in summer, snowflake: compound clusters high in winter. (B–E) show the average intensities for samples from the summer high PM (SH), summer low PM (SL), winter low PM (WL), and winter high PM (WH) days, respectively, in a Van Krevelen-diagram. The numbers inside the pie chart represent the intensity contribution (%) of each compound category to the total detected compound intensity.

unfavorable meteorological conditions (e.g., low wind speed, stagnation of air, and a shallow and stable inversion layer) may promote OA accumulation in Beijing during winter.⁴² In contrast, the relative contribution of these two groups to the total intensity in summer are 6% and 8%, respectively. The major compounds in these two groups have an RT > 4.5 min, indicating their relatively low polarity. Contrary to the enhancement of the CHNO and CHOa compounds, the CHOn, CHOS, and CHNOS compounds show decreased abundance in winter, accounting for 16%, 14%, and 3% of the total intensity, respectively. The relative contribution of the CHOn compounds to the total intensity in summer is 30%, which can partly be explained by enhanced biogenic emissions in summer. On the basis of MS²-spectra and retention time, we are able to unambiguously identify CHON compounds as oxidation products of certain biogenic VOCs.²⁶ Moreover, low temperatures during winter may lead to lower evaporation of

anthropogenic CHON compounds. A clear decrease of CHON with short retention times was observed for the winter season, similar to the trend for CHOS compounds (e.g., isoprene-organosulfates (OSs)), which contribute up to 30% of the total intensity in summer. The CHOS compounds display a wide spectrum in polarity, ranging from polar (short RT) to nonpolar (long RT) compounds. Due to more oxygen- and heteroatoms, the CHNOS compounds tend to have higher mass-to-charge ratios (*m/z*) than most of the other compounds. The relative contribution of CHNOS compounds in summer is 9%. The formation of OSs can enhance PM mass, since the sulfate-functionalization of small organic compounds (e.g., from isoprene oxidation) changes the gas-to-particle partitioning of these small organic molecules toward the particle phase. Furthermore, some of the OSs are hygroscopic and light-absorbing,^{43–45} hence this class of compounds may enhance haze in summer. However, further research on the

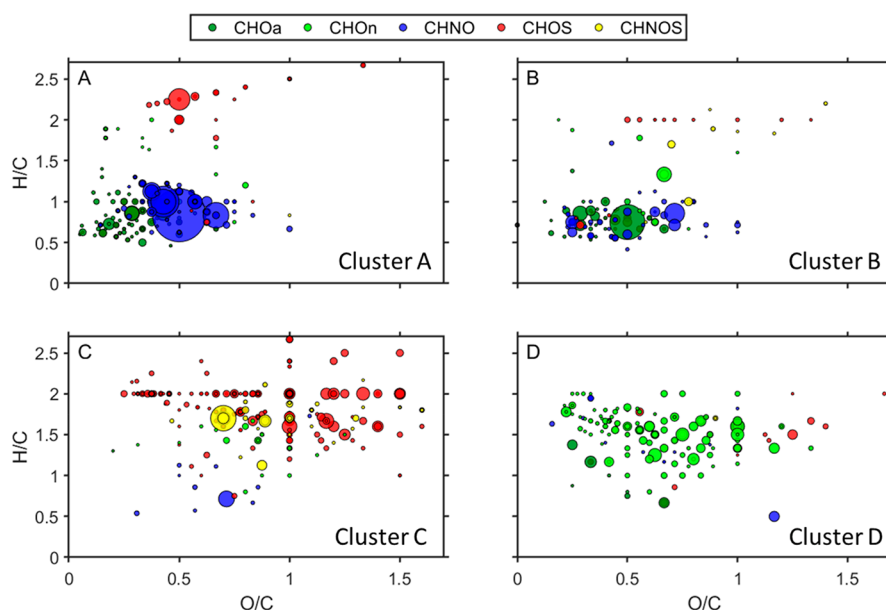


Figure 3. Comparison of compounds that originate from different sources, illustrated in the Van Krevelen space (peak area shows the mean intensity of all 172 samples). (A–D) Van Krevelen diagram of clusters A–D from HCA (see Figure 2).

quantification of the organosulfate effect on urban haze is needed. Finally, we like to emphasize that the peak intensities in Figure 1 are not directly linked to the concentration of the individual compounds, however, differences of peak intensities of the same compound (category) throughout the time series can be interpreted.

3.2. Application of Hierarchical Cluster Analysis on 172 PM Samples. We used the filtered data matrix to (1) display molecular fingerprints of the average intensity (Figure S5A,B), (2) perform a HCA (Figure 2A), and (3) identify groups of samples (Figure 2B–E) and compounds that exhibit similar temporal patterns (Figure 3A–D).

The horizontal and vertical dendrograms in Figure 2A visualize the distance between different samples and different compounds, respectively. Interestingly, we found that the horizontal dendrogram clearly separated the samples into summer high PM (SH, haze episodes), summer low PM (SL), winter low PM (WL), and winter high PM (WH, haze episodes) clusters by comparison with $\text{PM}_{2.5}$ mass concentration (Figure 2A). The mean $\text{PM}_{2.5}$ mass of clusters SH, SL, WL, and WH was $67 \mu\text{g}/\text{m}^3$, $23 \mu\text{g}/\text{m}^3$, $37 \mu\text{g}/\text{m}^3$, and $100 \mu\text{g}/\text{m}^3$, respectively (the distribution of $\text{PM}_{2.5}$ mass of these four clusters is shown in Figure S6). We observed a strong variation of the organic aerosol composition by plotting the molecular fingerprints of clusters SH, SL, WL, and WH (average intensity, Figure 2B–E). Most clearly, the majority aliphatic OSs, which appeared in the SH samples, are not detected in the SL samples. The relative contribution of the CHOS compounds to the total intensity in cluster SH is 40%, which is much higher than in cluster SL (12%, Figure 2B and C). This observation indicates that the formation of aliphatic OSs (at high particulate sulfate concentration and high relative humidity⁴⁶) can be an important factor for the increase of organic aerosol mass in summer Beijing. The organic aerosol composition was similar in the clusters WL and WH, however, the compound intensity of cluster WH was much higher than that of cluster WL. This may indicate that the emission sources and chemical processes in winter are relatively constant, and OA pollution accumulates when wind speed is low. In fact, we

observe that both low-pollution episodes experienced higher wind speed, and the backward trajectories show that the air masses were coming from the northwest to north sector (see Figure S7A,B).

Regarding the clustering result of the compounds (vertical dendrogram), we observed two separate clusters: the compounds in the upper cluster were abundant in winter, while the lower cluster's compounds had a higher intensity in summer. In order to elucidate this seasonal variation in the chemical properties of the compounds (e.g., molecular formula, oxidation state, aromaticity), we divided them into smaller clusters. The Van Krevelen diagrams in Figure 3 display the compound clusters A–D. It becomes evident that the HCA is a powerful tool that reduces the chemical complexity by aggregating compounds of similar chemical characteristics into the same clusters (clusters A, B, C, and D, Figure 3). Clusters E and F either have no clear chemical patterns in the Van Krevelen-space (Figure S8A) or contain very small amounts of aliphatic compounds (Figure S8B), therefore, these two clusters will not be discussed further.

Figure 3A shows that this cluster is dominated by the CHNO compounds, followed by the CHOa compounds. The majority of the compounds appear at the region of $0.2 < \text{H}/\text{C} < 1.2$ and $0.3 < \text{O}/\text{C} < 0.6$, indicating that CHNO and CHO aromatics are important compound classes in wintertime Beijing. We found the homologous series of $\text{C}_{5+n}\text{H}_{3+2n}\text{NO}_3$ ($n = 1-5$) and $\text{C}_{5+n}\text{H}_{3+2n}\text{NO}_4$ ($n = 1-4$) in this cluster with slopes of -2.33 and -1.75 , respectively (y -intercept at $\text{H}/\text{C} = 2$). The largest signals of the two series corresponded to $\text{C}_6\text{H}_5\text{NO}_3$ and $\text{C}_6\text{H}_5\text{NO}_4$, which were identified (by comparing the retention time and fragmentation pattern with the authentic standards, Figure S9A,B) as 4-nitrophenol and 4-nitrocatechol, respectively. Previous studies have identified nitroaromatics as oxidation products of coal burning,^{47,48} biomass burning,⁴⁹⁻⁵¹ and vehicle emissions.⁵²⁻⁵⁵ A recent study by Yuan et al. suggests that coal and biomass burning in winter are the major sources for nitroaromatics.⁵⁶ Furthermore, previous studies have also revealed that in winter, nitrophenol and nitrocatechol are likely arising from biomass

and coal burning emissions.^{55,57,58} In addition, we observed C₇H₆O₃ as a major compound in this cluster, being tentatively identified as monohydroxy benzoic acid, which is a tracer compound for naphthalene oxidation.^{59,60}

In cluster B, CHOa compounds were the most abundant compounds (according to the intensities of the compounds), followed by CHNO compounds (Figure 3B). Most of the compounds appear in the area of 0.5 < H/C < 1.2 and 0.25 < O/C < 0.8, which indicates an aromatic character. The largest signal of this cluster was identified as phthalic acid (C₈H₆O₄, Figure S9C), which is a product of naphthalene photo-oxidation.^{61,62} Similarly, phthalic acid has also been reported as a product of vehicle exhaust and biomass burning.^{39,60,63,64} We observed that the most abundant compounds in this cluster have a carbon number between 6 and 10 (Figure S10A). In this range, these compounds could be associated with the oxidation products of benzene, toluene, ethylbenzene, xylene (BTEX), C3- and C4-benzenes, all of which were previously observed in emissions from traffic and coal burning in north China.^{65–69} Simultaneously, the homologous series of aliphatic organosulfates in both clusters A and B are tentatively classified as alkylorganosulfates (cluster A: C_nH_{2n+2}SO₄, n = 3–11, cluster B: C_nH_{2n}SO₅, n = 7–10), which are described as markers for secondary traffic OA.¹⁴ As consequence, we infer that the compounds in clusters A and B originate mainly from solid fuel combustion and traffic emissions.

As Figure 3C indicates, almost all compounds in cluster C are sulfur-containing compounds (CHOS and CHNOS). Interestingly, most of the sulfur-containing compounds fall into the area of 1.5 < H/C < 2 and 0.3 < O/C < 1.5. The high H/C ratio indicates that the S-containing compounds are affected by more aliphatic precursors, while the high O/C ratio suggests that they also have a high oxidation state. As previous studies indicate, the CHOS compounds which fulfill O/S ≥ 4 can be tentatively classified as OSs.^{19,31,60,70} Thus, a large majority (>99%) of CHOS compounds in this cluster could be assigned as OSs (by peak intensity). We also found the homologues of C_nH_{2n}SO₅ (n = 4–17) and C_nH_{2n}SO₆ (n = 4–16) appearing in the diagram at H/C = 2; such aliphatic OSs were reported as products from the reaction of SO₂ with emissions from liquid fossil fuel.^{12,26,60} However, there are also plenty of very polar OSs with extremely short retention times (Figure S5A); most of these have less than 10 carbon atoms (Figure S10B). In this range, one can expect OSs from biogenic emissions; for example, we find C₅H₈SO₇ that has been reported as an isoprene-derived organosulfate,^{71,72} while C₆H₁₀SO₆ and C₆H₁₀SO₇ have been reported as OSs formed from the OH-initiated oxidation from green leaf volatiles.⁷³ Furthermore, six isomers of the monoterpene-derived nitrooxy-OS (C₁₀H₁₇NO₇S),^{46,74} were also observed in this cluster. These compounds have relatively high intensities during summertime, when biogenic emissions are high and radiation can accelerate the formation of sulfate and OSs from SO₂ emissions.^{74–76} Overall, this organosulfate cluster has diverse sources with clear contributions from liquid fossil fuel and biogenic emissions.

The majority of compounds in Cluster D (Figure 3D) are CHON compounds, present in the region of 1.1 < H/C < 2 and 0.2 < O/C < 0.9. Previous studies suggest that in this region oxidation products of biogenic emissions appear.^{26,39,77} We confirm this cluster as partly biogenic as we detect the compounds MBTCA (C₈H₁₂O₆) and pinic acid (C₉H₁₄O₄), which are widely used as oxidation tracers of α-pinene (Figure

S9D,E).^{78–81} However, we cannot exclude the contribution of anthropogenic compounds in this cluster. For instance, the CHO compounds with 11 and 12 carbons and $\overline{\text{OS}}_{\text{C}}$ between –1 and 0 appear with a high signal in this cluster (Figure S10C). These compounds are likely oxidation products of anthropogenic emissions since the oxidation of terpenes rarely results in C₁₁- and C₁₂-compounds.⁸²

3.3. Concentration Time Series of the Compounds in the Different Clusters and Their Relative Contribution to the Total OA. In atmospheric sciences, the use of surrogates to quantify similar compounds is a common approach when authentic standards are not available.¹¹ However, for NTA, it is impossible to allocate authentic or surrogate standards for every compound. Hence, it is a challenge to quantify nontarget screening data. Here, we used the average response of different surrogate standards to quantify the sum of the signal intensities of the four main compound clusters A–D.

We calibrated the system with eight different standards (Figure S11) and found that 4-nitrophenol and 4-nitrocatechol had the highest responses of the eight surrogates. This indicated that nitroaromatics have a higher ionization efficiency in (–)ESI than other compounds, hence, we used the average response of these two standards to quantify the nitroaromatic compounds present in clusters A and B. However, the ionization efficiency for different CHOa compounds varied greatly and, in order to minimize deviation, we tested three CHOa compounds (5,7-dihydroxy-4-phenylcoumarin, phthalic acid, and benzoic acid) and took the average of their responses to quantify the CHOa compounds in clusters A and B (Figure S11). Furthermore, camphor-10-sulfonic acid has been widely suggested to be used as the surrogate standard to quantify OSs,^{83–85} therefore, this was employed to quantify OSs in cluster C in our study. The calibration curves of MBTCA and pinic acid are very similar (Figure S11). Therefore, we used the mean response of MBTCA and pinic acid to quantify compounds in cluster D. Certainly, this approach of quantification for this large data set can easily introduce an error of a factor of 2. However, in this analysis, we observe that the Pearson correlation coefficients between the four clusters A–D and OA mass (determined by ToF-ACSM; A-OA: 0.44, B-OA: 0.70, C-OA: 0.51, and D-OA: 0.41 (Figure 4)) are all lower than the correlation coefficient between the sum of the four clusters and the OA mass (R = 0.78). This indicates that the used quantification method does not introduce any bias by giving more weight to one of the clusters, but instead explains the rather flat OA observation by the different seasonal contribution of the identified clusters (Figure 4). Furthermore, the concentration of OSs in cluster C are in the same range with other recent studies that determined the content of organic sulfates in Beijing.^{29,86}

The time series in Figure 4 reveal a strong seasonal variation of the concentration of the four different clusters. The aromatic compounds in clusters A and B show a clear increasing trend during the domestic-heating period, which provides further evidence for the OA from solid fuel combustion and traffic emissions. The lower appearance of aliphatic organosulfur-compounds (as traffic markers) in summer can be explained by a faster chemical degradation due to OH radicals, and more efficient mixing in a higher boundary layer. Cluster B shows a higher fluctuation during winter than cluster A, which might be explained as a combined meteorological and photochemical effect. In contrast, the compounds in clusters C and D are

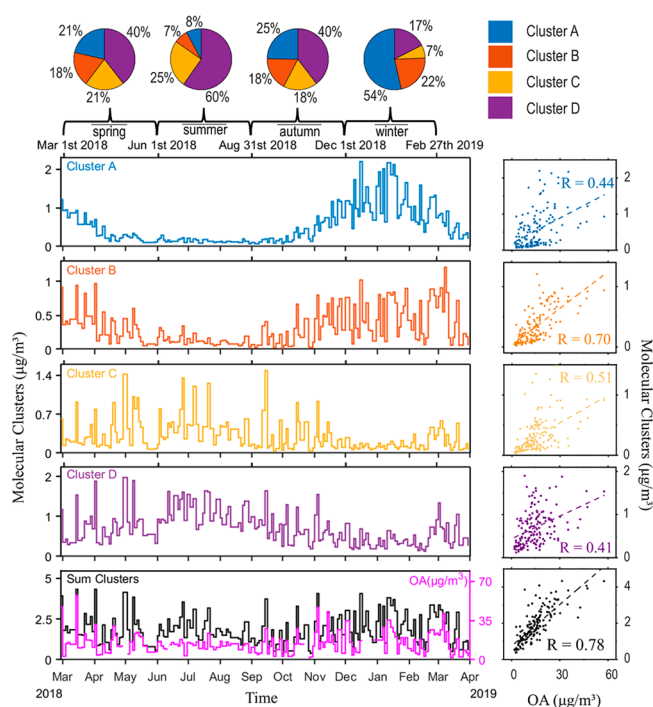


Figure 4. Concentration time series of compounds in clusters A, B, C, D, sum of the four clusters, and OA (data from ACSM). The scatter plots show the correlation between the four individual cluster and OA, as well as the correlation between the sum of the four clusters and the OA content. The pie charts display the concentration fractions of individual cluster in sum of the four clusters in spring, summer, autumn, and winter.

more abundant in summer, which indicates that these compounds partly originate from biogenic emissions. The strong positive correlation ($R = 0.75$, Figure S12) between these two clusters suggest that some of these compounds have the same source. Compounds from cluster C are elevated with increasing sulfate mass concentrations (Figure S12), which indicates the importance of sulfate in the secondary formation of OSs.³¹ The concentration of these compounds in the two clusters greatly fluctuates from day to day, and thus reveal that these clusters are largely dependent on meteorological conditions (air mass origin, relative humidity, temperature, radiation, wind speed, and so forth). It is worth mentioning that the compounds in cluster D also have a relatively high content in winter (ranging from 120 to 920 ng/m^3 , with a mean of 380 ng/m^3); this provides further evidence that a part of the compounds from this cluster are also influenced by anthropogenic activities. Interestingly, although the concentration time series of the compounds in every individual cluster shows a clear seasonal cycle, the time series for the sum concentration of the four clusters does not exhibit a seasonal variation; this is in agreement with the time series of OA from the ACSM measurement (Figure 4). Thus, there is a strong correlation between the sum of the quantified clusters and OA, indicating that the cluster analysis represents the major variability of OA seasonal cycles.

In order to investigate further the concentration fraction of the four clusters in relation to the total OA, we averaged the concentration of the sum clusters in spring, summer, autumn, and winter, respectively, the same was applied to the total OA content. As the pie charts in Figure S13 indicate, with this approach we can explain only a small fraction of OA (~11–

14%). However, in the nontarget data set we found sufficient evidence for seasonal variation; for example, clusters A and B represent emissions of solid fuel combustion and traffic, contributing with 76% to the total of the four main clusters in winter, but only 15% in summer. The CHON cluster (cluster D) showed a relative contribution of 60% in summer and only 17% in winter (see Figure 4). To gain a more complete insight on ambient OA and its sources, other ionization approaches need to be applied to enable the detection of the remaining unattributed OA.

3.4. Limitations and Implications. As limitations we emphasize that the UHPLC/HRMS technique only identifies a small fraction of the total OA, and also potential sampling artifacts cannot be ignored (e.g., α -pinene oxidation products can react with SO_2 during filter sampling⁸⁷). The six compound categories do not represent the entire organic composition since electrospray ionization is not sensitive to nonpolar compounds (e.g., nonfunctionalized polycyclic aromatic hydrocarbons, hopanes, and alkanes).¹³ Furthermore, (–)ESI is also not sensitive to compounds with no acidic protons (e.g., phthalates). To a lesser extent, there might be large-molecular weight humic-like substances (HULIS), that we do not detect in the scanning mass range of the mass spectrometer, or which do not result in sharp chromatographic peaks.⁸⁸

Nevertheless, the nontarget screening in combination with HCA can help to gain a more comprehensive understanding of urban air pollution at the molecular level. With this approach, we were able to distinguish high PM and low PM samples from different seasons and to determine the variation of the organic aerosol composition. Moreover, we can infer the different sources of the organic compounds from the chemical composition patterns and observe enhanced organosulfate formation during summer haze episodes. Further studies are needed to confirm attribution of OA winter clusters to anthropogenic emissions from coal combustion, biomass burning and traffic as well as quantitatively identify the major primary OA (POA) and SOA sources.

The calibration method in our study bridges the gap to quantify compounds from ESI-NTA. The strong correlation between the sum of the quantified clusters and OA indicates that the cluster analysis represents the major variability of OA seasonal cycles. We suggest that future nontarget studies of OA could follow the direction of combining different ionization techniques to provide a more comprehensive data set for NTA of ambient filters. Joint effort is needed to establish a mass spectrometry database that contains molecular fingerprints of chamber-generated organic aerosol, in order to identify sources and their contribution to OA in ambient samples.

■ ASSOCIATED CONTENT

Supporting Information

The Supporting Information is available free of charge at <https://pubs.acs.org/doi/10.1021/acs.est.1c06905>.

Detailed information on the ACSM measurement; CD-workflow settings and identified molecules; additional information on the $\text{PM}_{2.5}$ correlation between monitoring sites and ACSM; QA/QC of UHPLC/HRMS measurements; data preparation for HCA; molecular fingerprints (average intensity); histogram of $\text{PM}_{2.5}$ mass of clusters SH, SL, WL, and WH; backward trajectory and wind rose of the sampling period; Van Krevelen-

diagram of clusters E and F; MS/MS fragmentation spectra of quantified compounds; Kroll-diagram of clusters B, C, and D; calibration curves; relationship between clusters C and D and sulfate; and fraction of the four clusters to the total OA (PDF)

AUTHOR INFORMATION

Corresponding Authors

Kaspar R. Daellenbach – Aerosol and Haze Laboratory, Beijing Advanced Innovation Center for Soft Matter Science and Engineering, Beijing University of Chemical Technology, 100029 Beijing, P. R. China; Institute for Atmospheric and Earth System Research/Physics, Faculty of Science, University of Helsinki, 00014 Helsinki, Finland; Laboratory of Atmospheric Chemistry, Paul Scherrer Institute, 5232 Villigen, Switzerland; Email: kaspar.daellenbach@psi.ch

Alexander L. Vogel – Institute for Atmospheric and Environmental Sciences, Goethe-University Frankfurt, 60438 Frankfurt am Main, Germany; orcid.org/0000-0002-1293-6370; Email: vogel@iau.uni-frankfurt.de

Authors

Jialiing Ma – Institute for Atmospheric and Environmental Sciences, Goethe-University Frankfurt, 60438 Frankfurt am Main, Germany; orcid.org/0000-0003-0815-4066

Florian Ungeheuer – Institute for Atmospheric and Environmental Sciences, Goethe-University Frankfurt, 60438 Frankfurt am Main, Germany; orcid.org/0000-0002-4557-3844

Feixue Zheng – Aerosol and Haze Laboratory, Beijing Advanced Innovation Center for Soft Matter Science and Engineering, Beijing University of Chemical Technology, 100029 Beijing, P. R. China

Wei Du – Aerosol and Haze Laboratory, Beijing Advanced Innovation Center for Soft Matter Science and Engineering, Beijing University of Chemical Technology, 100029 Beijing, P. R. China; Institute for Atmospheric and Earth System Research/Physics, Faculty of Science, University of Helsinki, 00014 Helsinki, Finland

Yonghong Wang – Aerosol and Haze Laboratory, Beijing Advanced Innovation Center for Soft Matter Science and Engineering, Beijing University of Chemical Technology, 100029 Beijing, P. R. China; Institute for Atmospheric and Earth System Research/Physics, Faculty of Science, University of Helsinki, 00014 Helsinki, Finland; Research Center for Eco-Environmental Sciences, Chinese Academy of Sciences, 100085 Beijing, P. R. China; orcid.org/0000-0003-2498-9143

Jing Cai – Aerosol and Haze Laboratory, Beijing Advanced Innovation Center for Soft Matter Science and Engineering, Beijing University of Chemical Technology, 100029 Beijing, P. R. China; Institute for Atmospheric and Earth System Research/Physics, Faculty of Science, University of Helsinki, 00014 Helsinki, Finland

Ying Zhou – Aerosol and Haze Laboratory, Beijing Advanced Innovation Center for Soft Matter Science and Engineering, Beijing University of Chemical Technology, 100029 Beijing, P. R. China

Chao Yan – Aerosol and Haze Laboratory, Beijing Advanced Innovation Center for Soft Matter Science and Engineering, Beijing University of Chemical Technology, 100029 Beijing, P. R. China; Institute for Atmospheric and Earth System

Research/Physics, Faculty of Science, University of Helsinki, 00014 Helsinki, Finland

Yongchun Liu – Aerosol and Haze Laboratory, Beijing Advanced Innovation Center for Soft Matter Science and Engineering, Beijing University of Chemical Technology, 100029 Beijing, P. R. China; orcid.org/0000-0002-9055-970X

Markku Kulmala – Aerosol and Haze Laboratory, Beijing Advanced Innovation Center for Soft Matter Science and Engineering, Beijing University of Chemical Technology, 100029 Beijing, P. R. China; Institute for Atmospheric and Earth System Research/Physics, Faculty of Science, University of Helsinki, 00014 Helsinki, Finland

Complete contact information is available at: <https://pubs.acs.org/10.1021/acs.est.1c06905>

Author Contributions

J.M. did the majority of data curation and analysis, and wrote the original manuscript. J.M. and F.U. performed the UHPLC/HRMS measurements and nontarget analysis. F.U. synthesized standards. F.Z., W.D., Y.W., J.C., Y.Z., C.Y., and Y.L. collected the ambient filters and performed the ACSM measurement. K.R.D., M.K., and A.L.V. managed the project, advised on data analysis, edited and revised the manuscript. All authors have contributed to the scientific discussion and have given approval to the final version of the manuscript.

Notes

The authors declare no competing financial interest.

Data availability. The data underlying this study are openly available in zenodo.org at DOI: 10.5281/zenodo.6354745.

ACKNOWLEDGMENTS

J.M. thanks the China Scholarship Council (CSC) for the life expense covering (NO.202008080054). K.R.D. acknowledges support by the SNF mobility grant P2EZP2_181599. M.K. acknowledges the following projects: ACCC Flagship funded by the Academy of Finland grant number 337549, Academy professorship funded by the Academy of Finland (grant no. 302958), Academy of Finland projects no. 1325656, 316114, and 325647, “Quantifying carbon sink, CarbonSink+, and their interaction with air quality” INAR project funded by Jane and Aatos Erkkö Foundation, European Research Council (ERC) project ATM-GTP Contract No. 742206. This research has been supported by the Deutsche Forschungsgemeinschaft (DFG; German Research Foundation) (grant no. 410009325).

ABBREVIATIONS

AI, aromaticity index; BUCT, Beijing University of Chemical Technology; CCN, cloud condensation nuclei; CD, Compound Discoverer; CNEMC, China National Environmental Monitoring Center; DBE, double bond equivalent; ESI, electrospray ionization; HCA, hierarchical cluster analysis; (U)HPLC, (ultra)high performance liquid chromatography; HR/AM, high-resolution and accurate mass; HRMS, High-resolution mass spectrometry; MBTCA, 3-methyl-1,2,3-butanetricarboxylic acid; NTA, nontarget analysis; OA, organic aerosols; OSs, organosulfates; PM, particulate matter; PMF, positive matrix factorization; POA, primary organic aerosol; PTFE, polytetrafluoroethylene; SOA, secondary organic aerosol; ToF-ACSM, Time-of-Flight aerosol chemical speciation monitor; Xc, aromaticity equivalent

REFERENCES

- (1) Daellenbach, K. R.; Uzu, G.; Jiang, J.; Cassagnes, L.-E.; Leni, Z.; Vlachou, A.; Stefanelli, G.; Canonaco, F.; Weber, S.; Segers, A.; Kuenen, J. J. P.; Schaap, M.; Favez, O.; Albinet, A.; Aksoyoglu, S.; Dommen, J.; Baltensperger, U.; Geiser, M.; El Haddad, I.; Jaffrezo, J.-L.; Prévôt, A. S. H. Sources of Particulate-Matter Air Pollution and Its Oxidative Potential in Europe. *Nature* **2020**, *587* (7834), 414–419.
- (2) Lelieveld, J.; Pozzer, A.; Pöschl, U.; Fnais, M.; Haines, A.; Münzel, T. Loss of Life Expectancy from Air Pollution Compared to Other Risk Factors: A Worldwide Perspective. *Cardiovasc. Res.* **2020**, *116* (11), 1910–1917.
- (3) Stocker, T. F.; Qin, D.; Plattner, G.; Tignor, M. M. B.; Allen, S. K.; Boschung, J.; Nauels, A.; Xia, Y.; Bex, V.; Midgley, P. M. *Climate Change 2013 The Physical Science Basis*; Cambridge University Press: Geneva, 2013 https://www.ipcc.ch/site/assets/uploads/2021/08/IPCC_WGI-AR6-Press-Release_en.pdf.
- (4) Jimenez, J. L.; Canagaratna, M. R.; Donahue, N. M.; Prevot, A. S. H.; Zhang, Q.; Kröll, J. H.; DeCarlo, P. F.; Allan, J. D.; Coe, H.; Ng, N. L.; Aiken, A. C.; Docherty, K. S.; Ulbrich, I. M.; Grieshop, A. P.; Robinson, A. L.; Duplissy, J.; Smith, J. D.; Wilson, K. R.; Lanz, V. A.; Hueglin, C.; Sun, Y. L.; Tian, J.; Laaksonen, A.; Raatikainen, T.; Rautiainen, J.; Vaattovaara, P.; Ehn, M.; Kulmala, M.; Tomlinson, J. M.; Collins, D. R.; Cubison, M. J.; Dunlea, J. E.; Huffman, J. A.; Onasch, T. B.; Alfarra, M. R.; Williams, P. I.; Bower, K.; Kondo, Y.; Schneider, J.; Drewnick, F.; Borrmann, S.; Weimer, S.; Demerjian, K.; Salcedo, D.; Cottrell, L.; Griffin, R.; Takami, A.; Miyoshi, T.; Hatakeyama, S.; Shimojo, A.; Sun, J. Y.; Zhang, Y. M.; Dzepina, K.; Kimmel, J. R.; Sueper, D.; Jayne, J. T.; Herndon, S. C.; Trimborn, A. M.; Williams, L. R.; Wood, E. C.; Middlebrook, A. M.; Kolb, C. E.; Baltensperger, U.; Worsnop, D. R. Evolution of Organic Aerosols in the Atmosphere. *Science* **2009**, *326* (5959), 1525–1529.
- (5) Zhang, Q.; Jimenez, J. L.; Canagaratna, M. R.; Allan, J. D.; Coe, H.; Ulbrich, I.; Alfarra, M. R.; Takami, A.; Middlebrook, A. M.; Sun, Y. L.; Dzepina, K.; Dunlea, E.; Docherty, K.; DeCarlo, P. F.; Salcedo, D.; Onasch, T.; Jayne, J. T.; Miyoshi, T.; Shimojo, A.; Hatakeyama, S.; Takegawa, N.; Kondo, Y.; Schneider, J.; Drewnick, F.; Borrmann, S.; Weimer, S.; Demerjian, K.; Williams, P.; Bower, K.; Bahreini, R.; Cottrell, L.; Griffin, R. J.; Rautiainen, J.; Sun, J. Y.; Zhang, Y. M.; Worsnop, D. R. Ubiquity and Dominance of Oxygenated Species in Organic Aerosols in Anthropogenically-Influenced Northern Hemisphere Midlatitudes. *Geophys. Res. Lett.* **2007**, *34* (13).
- (6) Tang, R.; Lu, Q.; Guo, S.; Wang, H.; Song, K.; Yu, Y.; Tan, R.; Liu, K.; Shen, R.; Chen, S.; Zeng, L.; Jorga, S. D.; Zhang, Z.; Zhang, W.; Shuai, S.; Robinson, A. L. Measurement Report: Distinct Emissions and Volatility Distribution of Intermediate-Volatility Organic Compounds from on-Road Chinese Gasoline Vehicles: Implication of High Secondary Organic Aerosol Formation Potential. *Atmos. Chem. Phys.* **2021**, *21* (4), 2569–2583.
- (7) Murphy, D. M.; Cziczó, D. J.; Froyd, K. D.; Hudson, P. K.; Matthew, B. M.; Middlebrook, A. M.; Peltier, R. E.; Sullivan, A.; Thomson, D. S.; Weber, R. J. Single-Particle Mass Spectrometry of Tropospheric Aerosol Particles. *J. Geophys. Res. Atmos.* **2006**, *111* (D23), 23–32.
- (8) Kanakidou, M.; Seinfeld, J. H.; Pandis, S. N.; Barnes, I.; Dentener, F. J.; Facchini, M. C.; Van Dingenen, R.; Ervens, B.; Nenes, A.; Nielsen, C. J.; Swietlicki, E.; Putaud, J. P.; Balkanski, Y.; Fuzzi, S.; Horth, J.; Moortgat, G. K.; Winterhalter, R.; Myhre, C. E. L.; Tsigaridis, K.; Vignati, E.; Stephanou, E. G.; Wilson, J. Organic Aerosol and Global Climate Modelling: A Review. *Atmos. Chem. Phys.* **2005**, *5* (4), 1053–1123.
- (9) Zhang, Y.; Cai, J.; Wang, S.; He, K.; Zheng, M. Review of Receptor-Based Source Apportionment Research of Fine Particulate Matter and Its Challenges in China. *Sci. Total Environ.* **2017**, *586*, 917–929.
- (10) Huang, R.-J.; Zhang, Y.; Bozzetti, C.; Ho, K.-F.; Cao, J.-J.; Han, Y.; Daellenbach, K. R.; Slowik, J. G.; Platt, S. M.; Canonaco, F.; Zotter, P.; Wolf, R.; Pieber, S. M.; Bruns, E. A.; Crippa, M.; Ciarelli, G.; Piazzalunga, A.; Schwikowski, M.; Abbaszade, G.; Schnelle-Kreis, J.; Zimmermann, R.; An, Z.; Szidat, S.; Baltensperger, U.; Haddad, I. E.; Prevot, A. S. H. High Secondary Aerosol Contribution to Particulate Pollution during Haze Events in China. *Nature* **2014**, *514* (7521), 218–222.
- (11) Nozière, B.; Kalberer, M.; Claeys, M.; Allan, J.; D'Anna, B.; Decesari, S.; Finessi, E.; Glasius, M.; Grgić, I.; Hamilton, J. F.; Hoffmann, T.; Iinuma, Y.; Jaoui, M.; Kahnt, A.; Kampf, C. J.; Kourtchev, I.; Maenhaut, W.; Marsden, N.; Saarikoski, S.; Schnelle-Kreis, J.; Surratt, J. D.; Szidat, S.; Szmigielski, R.; Wisthaler, A. The Molecular Identification of Organic Compounds in the Atmosphere: State of the Art and Challenges. *Chem. Rev.* **2015**, *115* (10), 3919–3983.
- (12) Tao, S.; Lu, X.; Levac, N.; Bateman, A. P.; Nguyen, T. B.; Bones, D. L.; Nizkorodov, S. A.; Laskin, J.; Laskin, A.; Yang, X. Molecular Characterization of Organosulfates in Organic Aerosols from Shanghai and Los Angeles Urban Areas by Nanospray-Desorption Electrospray Ionization High-Resolution Mass Spectrometry. *Environ. Sci. Technol.* **2014**, *48* (18), 10993–11001.
- (13) Lin, P.; Rincon, A. G.; Kalberer, M.; Yu, J. Z. Elemental Composition of HULIS in the Pearl River Delta Region, China: Results Inferred from Positive and Negative Electrospray High Resolution Mass Spectrometric Data. *Environ. Sci. Technol.* **2012**, *46* (14), 7454–7462.
- (14) Blair, S. L.; MacMillan, A. C.; Drozd, G. T.; Goldstein, A. H.; Chu, R. K.; Paša-Tolić, L.; Shaw, J. B.; Tolić, N.; Lin, P.; Laskin, J.; Laskin, A.; Nizkorodov, S. A. Molecular Characterization of Organosulfur Compounds in Biodiesel and Diesel Fuel Secondary Organic Aerosol. *Environ. Sci. Technol.* **2017**, *51* (1), 119–127.
- (15) Vogel, A. L.; Schneider, J.; Müller-Tautges, C.; Phillips, G. J.; Pöhlker, M. L.; Rose, D.; Zuth, C.; Makkonen, U.; Hakola, H.; Crowley, J. N.; Andreae, M. O.; Pöschl, U.; Hoffmann, T. Aerosol Chemistry Resolved by Mass Spectrometry: Linking Field Measurements of Cloud Condensation Nuclei Activity to Organic Aerosol Composition. *Environ. Sci. Technol.* **2016**, *50* (20), 10823–10832.
- (16) Vogel, A. L.; Schneider, J.; Müller-Tautges, C.; Klimach, T.; Hoffmann, T. Aerosol Chemistry Resolved by Mass Spectrometry: Insights into Particle Growth after Ambient New Particle Formation. *Environ. Sci. Technol.* **2016**, *50* (20), 10814–10822.
- (17) Hoffmann, T.; Huang, R. J.; Kalberer, M. Atmospheric Analytical Chemistry. *Anal. Chem.* **2011**, *83* (12), 4649–4664.
- (18) Wang, X.; Hayeck, N.; Brüggemann, M.; Yao, L.; Chen, H.; Zhang, C.; Emmelin, C.; Chen, J.; George, C.; Wang, L. Chemical Characteristics of Organic Aerosols in Shanghai: A Study by Ultrahigh-Performance Liquid Chromatography Coupled With Orbitrap Mass Spectrometry. *J. Geophys. Res. Atmos.* **2017**, *122* (21), 11703–11722.
- (19) Wang, K.; Zhang, Y.; Huang, R. J.; Cao, J.; Hoffmann, T. UHPLC-Orbitrap Mass Spectrometric Characterization of Organic Aerosol from a Central European City (Mainz, Germany) and a Chinese Megacity (Beijing). *Atmos. Environ.* **2018**, *189*, 22–29.
- (20) Kourtchev, I.; Godoi, R. H. M.; Connors, S.; Levine, J. G.; Archibald, A. T.; Godoi, A. F. L.; Paralovo, S. L.; Barbosa, C. G. G.; Souza, R. A. F.; Manzi, A. O.; Seco, R.; Sjøstedt, S.; Park, J.-H.; Guenther, A.; Kim, S.; Smith, J.; Martin, S. T.; Kalberer, M. Molecular Composition of Organic Aerosols in Central Amazonia: An Ultra-High-Resolution Mass Spectrometry Study. *Atmos. Chem. Phys.* **2016**, *16* (18), 11899–11913.
- (21) Lin, P.; Yu, J. Z.; Engling, G.; Kalberer, M. Organosulfates in Humic-like Substance Fraction Isolated from Aerosols at Seven Locations in East Asia: A Study by Ultra-High-Resolution Mass Spectrometry. *Environ. Sci. Technol.* **2012**, *46* (24), 13118–13127.
- (22) Rincón, A. G.; Calvo, A. I.; Dietzel, M.; Kalberer, M. Seasonal Differences of Urban Organic Aerosol Composition – an Ultra-High Resolution Mass Spectrometry Study. *Environ. Chem.* **2012**, *9* (3), 298.
- (23) Huo, Y.; Guo, Z.; Li, Q.; Wu, D.; Ding, X.; Liu, A.; Huang, D.; Qiu, G.; Wu, M.; Zhao, Z.; Sun, H.; Song, W.; Li, X.; Chen, Y.; Wu, T.; Chen, J. Chemical Fingerprinting of HULIS in Particulate Matters Emitted from Residential Coal and Biomass Combustion. *Environ. Sci. Technol.* **2021**, *55* (6), 3593–3603.

- (24) Wang, K.; Huang, R. J.; Brüggemann, M.; Zhang, Y.; Yang, L.; Ni, H.; Guo, J.; Wang, M.; Han, J.; Bilde, M.; Glasius, M.; Hoffmann, T. Urban Organic Aerosol Composition in Eastern China Differs from North to South: Molecular Insight from a Liquid Chromatography–Mass Spectrometry (Orbitrap) Study. *Atmos. Chem. Phys.* **2021**, *21* (11), 9089–9104.
- (25) Hohrenk, L. L.; Itzel, F.; Baetz, N.; Tuerk, J.; Vosough, M.; Schmidt, T. C. Comparison of Software Tools for Liquid Chromatography–High-Resolution Mass Spectrometry Data Processing in Nontarget Screening of Environmental Samples. *Anal. Chem.* **2020**, *92* (2), 1898–1907.
- (26) Vogel, A. L.; Lauer, A.; Fang, L.; Arturi, K.; Bachmeier, F.; Daellenbach, K. R.; Kaser, T.; Vlachou, A.; Pospisilova, V.; Baltensperger, U.; Haddad, I. E.; Schwikowski, M.; Bjelic, S. A Comprehensive Nontarget Analysis for the Molecular Reconstruction of Organic Aerosol Composition from Glacier Ice Cores. *Environ. Sci. Technol.* **2019**, *53* (21), 12565–12575.
- (27) Zhao, J.; Qiu, Y.; Zhou, W.; Xu, W.; Wang, J.; Zhang, Y.; Li, L.; Xie, C.; Wang, Q.; Du, W.; Worsnop, D. R.; Canagaratna, M. R.; Zhou, L.; Ge, X.; Fu, P.; Li, J.; Wang, Z.; Donahue, N. M.; Sun, Y. Organic Aerosol Processing During Winter Severe Haze Episodes in Beijing. *J. Geophys. Res. Atmos.* **2019**, *124* (17–18), 10248–10263.
- (28) Li, X.; Yang, Y.; Liu, S.; Zhao, Q.; Wang, G.; Wang, Y. Light Absorption Properties of Brown Carbon (BrC) in Autumn and Winter in Beijing: Composition, Formation and Contribution of Nitrated Aromatic Compounds. *Atmos. Environ.* **2020**, *223*, 117289.
- (29) Bryant, D. J.; Dixon, W. J.; Hopkins, J. R.; Dunmore, R. E.; Pereira, K. L.; Shaw, M.; Squires, F. A.; Bannan, T. J.; Mehra, A.; Worrall, S. D.; Bacak, A.; Coe, H.; Percival, C. J.; Whalley, L. K.; Heard, D. E.; Slater, E.; Ouyang, B.; Cui, T.; Surratt, J. D.; Liu, D.; Shi, Z.; Harrison, R.; Sun, Y.; Xu, W.; Lewis, A. C.; Lee, J. D.; Rickard, A. R.; Hamilton, J. F. Strong Anthropogenic Control of Secondary Organic Aerosol Formation from Isoprene in Beijing. *Atmos. Chem. Phys.* **2020**, *20* (12), 7531–7552.
- (30) Xie, Q.; Su, S.; Chen, S.; Zhang, Q.; Yue, S.; Zhao, W.; Du, H.; Ren, H.; Wei, L.; Cao, D.; Xu, Y.; Sun, Y.; Wang, Z.; Fu, P. Molecular Characterization of Size-Segregated Organic Aerosols in the Urban Boundary Layer in Wintertime Beijing by FT-ICR MS. *Faraday Discuss.* **2021**, *226* (0), 457–478.
- (31) Wang, Y.; Hu, M.; Guo, S.; Wang, Y.; Zheng, J.; Yang, Y.; Zhu, W.; Tang, R.; Li, X.; Liu, Y.; Le Breton, M.; Du, Z.; Shang, D.; Wu, Y.; Wu, Z.; Song, Y.; Lou, S.; Hallquist, M.; Yu, J. The Secondary Formation of Organosulfates under Interactions between Biogenic Emissions and Anthropogenic Pollutants in Summer in Beijing. *Atmos. Chem. Phys.* **2018**, *18* (14), 10693–10713.
- (32) Du, W.; Dada, L.; Zhao, J.; Chen, X.; Daellenbach, K. R.; Xie, C.; Wang, W.; He, Y.; Cai, J.; Yao, L.; Zhang, Y.; Wang, Q.; Xu, W.; Wang, Y.; Tang, G.; Cheng, X.; Kokkonen, T. V.; Zhou, W.; Yan, C.; Chu, B.; Zha, Q.; Hakala, S.; Kurppa, M.; Järvi, L.; Liu, Y.; Li, Z.; Ge, M.; Fu, P.; Nie, W.; Bianchi, F.; Petäjä, T.; Paasonen, P.; Wang, Z.; Worsnop, D. R.; Kerminen, V.-M.; Kulmala, M.; Sun, Y. A 3D Study on the Amplification of Regional Haze and Particle Growth by Local Emissions. *npj Clim. Atmos. Sci.* **2021**, *4* (1), 1–8.
- (33) Steimer, S. S.; Patton, D. J.; Vu, T. V.; Panagi, M.; Monks, P. S.; Harrison, R. M.; Fleming, Z. L.; Shi, Z.; Kalberer, M. Differences in the Composition of Organic Aerosols between Winter and Summer in Beijing: A Study by Direct-Infusion Ultrahigh-Resolution Mass Spectrometry. *Atmos. Chem. Phys.* **2020**, *20* (21), 13303–13318.
- (34) Liu, Y.; Yan, C.; Feng, Z.; Zheng, F.; Fan, X.; Zhang, Y.; Li, C.; Zhou, Y.; Lin, Z.; Guo, Y.; Zhang, Y.; Ma, L.; Zhou, W.; Liu, Z.; Dada, L.; Dällenbach, K.; Kontkanen, J.; Cai, R.; Chan, T.; Chu, B.; Du, W.; Yao, L.; Wang, Y.; Cai, J.; Kangasluoma, J.; Kokkonen, T.; Kujansuu, J.; Rusanen, A.; Deng, C.; Fu, Y.; Yin, R.; Li, X.; Lu, Y.; Lian, C.; Yang, D.; Wang, W.; Ge, M.; Wang, Y.; Worsnop, D. R.; Junninen, H.; He, H.; Kerminen, V.-M.; Zheng, J.; Wang, L.; Jiang, J.; Petäjä, T.; Bianchi, F.; Kulmala, M. Continuous and Comprehensive Atmospheric Observations in Beijing: A Station to Understand the Complex Urban Atmospheric Environment. *Big Earth Data* **2020**, *4* (3), 295–321.
- (35) Cai, J.; Chu, B.; Yao, L.; Yan, C.; Heikkinen, L. M.; Zheng, F.; Li, C.; Fan, X.; Zhang, S.; Yang, D.; Wang, Y.; Kokkonen, T. V.; Chan, T.; Zhou, Y.; Dada, L.; Liu, Y.; He, H.; Paasonen, P.; Kujansuu, J. T.; Petäjä, T.; Mohr, C.; Kangasluoma, J.; Bianchi, F.; Sun, Y.; Croteau, P. L.; Worsnop, D. R.; Kerminen, V. M.; Du, W.; Kulmala, M.; Daellenbach, K. R. Size-Segregated Particle Number and Mass Concentrations from Different Emission Sources in Urban Beijing. *Atmos. Chem. Phys.* **2020**, *20* (21), 12721–12740.
- (36) Zhao, Y.; Hallar, A. G.; Mazzoleni, L. R. Atmospheric Organic Matter in Clouds: Exact Masses and Molecular Formula Identification Using Ultrahigh-Resolution FT-ICR Mass Spectrometry. *Atmos. Chem. Phys.* **2013**, *13* (24), 12343–12362.
- (37) Yassine, M. M.; Harir, M.; Dabek-Zlotorzynska, E.; Schmitt-Kopplin, P. Structural Characterization of Organic Aerosol Using Fourier Transform Ion Cyclotron Resonance Mass Spectrometry: Aromaticity Equivalent Approach. *Rapid Commun. Mass Spectrom.* **2014**, *28* (22), 2445–2454.
- (38) Koch, B. P.; Dittmar, T. From Mass to Structure: An Aromaticity Index for High-Resolution Mass Data of Natural Organic Matter. *Rapid Commun. Mass Spectrom.* **2006**, *20* (5), 926–932.
- (39) Daellenbach, K. R.; Kourtchev, I.; Vogel, A. L.; Bruns, E. A.; Jiang, J.; Petäjä, T.; Jaffrezo, J.-L.; Aksoyoglu, S.; Kalberer, M.; Baltensperger, U.; El Haddad, I.; Prévôt, A. S. H. Impact of Anthropogenic and Biogenic Sources on the Seasonal Variation in the Molecular Composition of Urban Organic Aerosols: A Field and Laboratory Study Using Ultra-High-Resolution Mass Spectrometry. *Atmos. Chem. Phys.* **2019**, *19* (9), 5973–5991.
- (40) Priestley, M.; Bannan, T. J.; Le Breton, M.; Worrall, S. D.; Kang, S.; Pullinen, I.; Schmitt, S.; Tillmann, R.; Kleist, E.; Zhao, D.; Wildt, J.; Garmash, O.; Mehra, A.; Bacak, A.; Shallcross, D. E.; Kiendler-Scharr, A.; Hallquist, Å. M.; Ehn, M.; Coe, H.; Percival, C. J.; Hallquist, M.; Mentel, T. F.; McFiggans, G. Chemical Characterisation of Benzene Oxidation Products under High- And Low-NOx Conditions Using Chemical Ionisation Mass Spectrometry. *Atmos. Chem. Phys.* **2021**, *21* (5), 3473–3490.
- (41) Koss, A. R.; Canagaratna, M. R.; Zaytsev, A.; Krechmer, J. E.; Breitenlechner, M.; Nihill, K. J.; Lim, C. Y.; Rowe, J. C.; Roscioli, J. R.; Keutsch, F. N.; Kroll, J. H. Dimensionality-Reduction Techniques for Complex Mass Spectrometric Datasets: Application to Laboratory Atmospheric Organic Oxidation Experiments. *Atmos. Chem. Phys.* **2020**, *20* (2), 1021–1041.
- (42) Slater, J.; Tonttila, J.; McFiggans, G.; Coe, H.; Romakkaniemi, S.; Sun, Y.; Xu, W.; Fu, P.; Wang, Z. Using a Coupled LES Aerosol–Radiation Model to Investigate the Importance of Aerosol–Boundary Layer Feedback in a Beijing Haze Episode. *Faraday Discuss.* **2021**, *226* (0), 173–190.
- (43) Fleming, L. T.; Ali, N. N.; Blair, S. L.; Roveretto, M.; George, C.; Nizkorodov, S. A. Formation of Light-Absorbing Organosulfates during Evaporation of Secondary Organic Material Extracts in the Presence of Sulfuric Acid. *ACS Earth Sp. Chem.* **2019**, *3* (6), 947–957.
- (44) Estillore, A. D.; Hettiyadura, A. P. S.; Qin, Z.; Leckrone, E.; Wombacher, B.; Humphry, T.; Stone, E. A.; Grassian, V. H. Water Uptake and Hygroscopic Growth of Organosulfate Aerosol. *Environ. Sci. Technol.* **2016**, *50* (8), 4259–4268.
- (45) Peng, C.; Razafindrambinina, P. N.; Malek, K. A.; Chen, L.; Wang, W.; Huang, R. J.; Zhang, Y.; Ding, X.; Ge, M.; Wang, X.; Asa-Awuku, A. A.; Tang, M. Interactions of Organosulfates with Water Vapor under Sub- And Supersaturated Conditions. *Atmos. Chem. Phys.* **2021**, *21* (9), 7135–7148.
- (46) Brüggemann, M.; Xu, R.; Tilgner, A.; Kwong, K. C.; Mutzel, A.; Poon, H. Y.; Otto, T.; Schaefer, T.; Poulain, L.; Chan, M. N.; Herrmann, H. Organosulfates in Ambient Aerosol: State of Knowledge and Future Research Directions on Formation, Abundance, Fate, and Importance. *Environ. Sci. Technol.* **2020**, *54* (7), 3767–3782.
- (47) Lu, C.; Wang, X.; Li, R.; Gu, R.; Zhang, Y.; Li, W.; Gao, R.; Chen, B.; Xue, L.; Wang, W. Emissions of Fine Particulate Nitrated Phenols from Residential Coal Combustion in China. *Atmos. Environ.* **2019**, *203*, 10–17.

- (48) Olson, M. R.; Victoria Garcia, M.; Robinson, M. A.; Van Rooy, P.; Diitenberger, M. A.; Bergin, M.; Schauer, J. J. Investigation of Black and Brown Carbon Multiple-Wavelength-Dependent Light Absorption from Biomass and Fossil Fuel Combustion Source Emissions. *J. Geophys. Res. Atmos.* **2015**, *120* (13), 6682–6697.
- (49) Lin, P.; Fleming, L. T.; Nizkorodov, S. A.; Laskin, J.; Laskin, A. Comprehensive Molecular Characterization of Atmospheric Brown Carbon by High Resolution Mass Spectrometry with Electrospray and Atmospheric Pressure Photoionization. *Anal. Chem.* **2018**, *90* (21), 12493–12502.
- (50) Wang, X.; Gu, R.; Wang, L.; Xu, W.; Zhang, Y.; Chen, B.; Li, W.; Xue, L.; Chen, J.; Wang, W. Emissions of Fine Particulate Nitrated Phenols from the Burning of Five Common Types of Biomass. *Environ. Pollut.* **2017**, *230*, 405–412.
- (51) Teich, M.; Van Pinxteren, D.; Wang, M.; Kecorius, S.; Wang, Z.; Müller, T.; Močnik, G.; Herrmann, H. Contributions of Nitrated Aromatic Compounds to the Light Absorption of Water-Soluble and Particulate Brown Carbon in Different Atmospheric Environments in Germany and China. *Atmos. Chem. Phys.* **2017**, *17* (3), 1653–1672.
- (52) Taneda, S.; Mori, Y.; Kamata, K.; Hayashi, H.; Furuta, C.; Li, C.; Seki, K. I.; Sakushima, A.; Yoshino, S.; Yamaki, K.; Watanabe, G.; Taya, K.; Suzuki, A. K. Estrogenic and Anti-Androgenic Activity of Nitrophenols in Diesel Exhaust Particles (DEP). *Biol. Pharm. Bull.* **2004**, *27* (6), 835–837.
- (53) Inomata, S.; Tanimoto, H.; Fujitani, Y.; Sekimoto, K.; Sato, K.; Fushimi, A.; Yamada, H.; Hori, S.; Kumazawa, Y.; Shimono, A.; Hikida, T. On-Line Measurements of Gaseous Nitro-Organic Compounds in Diesel Vehicle Exhaust by Proton-Transfer-Reaction Mass Spectrometry. *Atmos. Environ.* **2013**, *73*, 195–203.
- (54) Perrone, M. G.; Carbone, C.; Faedo, D.; Ferrero, L.; Maggioni, A.; Sangiorgi, G.; Bolzacchini, E. Exhaust Emissions of Polycyclic Aromatic Hydrocarbons, n-Alkanes and Phenols from Vehicles Coming within Different European Classes. *Atmos. Environ.* **2014**, *82*, 391–400.
- (55) Lu, C.; Wang, X.; Dong, S.; Zhang, J.; Li, J.; Zhao, Y.; Liang, Y.; Xue, L.; Xie, H.; Zhang, Q.; Wang, W. Emissions of Fine Particulate Nitrated Phenols from Various On-Road Vehicles in China. *Environ. Res.* **2019**, *179*.
- (56) Yuan, W.; Huang, R. J.; Yang, L.; Wang, T.; Duan, J.; Guo, J.; Ni, H.; Chen, Y.; Chen, Q.; Li, Y.; Dusek, U.; O'Dowd, C.; Hoffmann, T. Measurement Report: PM_{2.5}-Bound Nitrated Aromatic Compounds in Xi'an, Northwest China - Seasonal Variations and Contributions to Optical Properties of Brown Carbon. *Atmos. Chem. Phys.* **2021**, *21* (5), 3685–3697.
- (57) Kitanovski, Z.; Grgić, I.; Vermeylen, R.; Claeys, M.; Maenhaut, W. Liquid Chromatography Tandem Mass Spectrometry Method for Characterization of Monoaromatic Nitro-Compounds in Atmospheric Particulate Matter. *J. Chromatogr. A* **2012**, *1268*, 35–43.
- (58) Mohr, C.; Lopez-Hilfiker, F. D.; Zotter, P.; Prevot, A. S. H.; Xu, L.; Ng, N. L.; Herndon, S. C.; Williams, L. R.; Franklin, J. P.; Zahniser, M. S.; Worsnop, D. R.; Knighton, W. B.; Aiken, A. C.; Gorkowski, K. J.; Dubey, M. K.; Allan, J. D.; Thornton, J. A. Contribution of Nitrated Phenols to Wood Burning Brown Carbon Light Absorption in Detling, United Kingdom during Winter Time. *Environ. Sci. Technol.* **2013**, *47* (12), 6316–6324.
- (59) Kautzman, K. E.; Surratt, J. D.; Chan, M. N.; Chan, A. W. H.; Hersey, S. P.; Chhabra, P. S.; Dalleska, N. F.; Wennberg, P. O.; Flagan, R. C.; Seinfeld, J. H. Chemical Composition of Gas- and Aerosol-Phase Products from the Photooxidation of Naphthalene. *J. Phys. Chem. A* **2010**, *114* (2), 913–934.
- (60) Wang, K.; Huang, R.-J. J.; Brüggemann, M.; Zhang, Y.; Yang, L.; Ni, H.; Guo, J.; Wang, M.; Han, J.; Bilde, M.; Glasius, M.; Hoffmann, T. Urban Organic Aerosol Composition in Eastern China Differs from North to South: Molecular Insight from a Liquid Chromatography-Orbitrap Mass Spectrometry Study. *Atmos. Chem. Phys.* **2021**, *21* (11), 9089–9104.
- (61) Tuhkanen Tuula, A.; Beltrán Fernando, J. Intermediates of the Oxidation of Naphthalene in Water with the Combination of Hydrogen Peroxide and UV Radiation. *Chemosphere* **1995**, *30* (8), 1463–1475.
- (62) He, X.; Huang, X. H. H.; Chow, K. S.; Wang, Q.; Zhang, T.; Wu, D.; Yu, J. Z. Abundance and Sources of Phthalic Acids, Benzene-Tricarboxylic Acids, and Phenolic Acids in PM_{2.5} at Urban and Suburban Sites in Southern China. *ACS Earth Sp. Chem.* **2018**, *2* (2), 147–158.
- (63) Fraser, M. P.; Cass, G. R.; Simoneit, B. R. T. Gas-Phase and Particle-Phase Organic Compounds Emitted from Motor Vehicle Traffic in a Los Angeles Roadway Tunnel. *Environ. Sci. Technol.* **1998**, *32* (14), 2051–2060.
- (64) Li, M.; McDow, S. R.; Tollerud, D. J.; Mazurek, M. A. Seasonal Abundance of Organic Molecular Markers in Urban Particulate Matter from Philadelphia, PA. *Atmos. Environ.* **2006**, *40* (13), 2260–2273.
- (65) Duan, X.; Li, Y. Sources and Fates of BTEX in the General Environment and Its Distribution in Coastal Cities of China. *J. Environ. Sci. Public Heal.* **2017**, *1* (2), 86–106.
- (66) Jüttner, F. Emission of Aromatic Hydrocarbons and Aldehydes into the Water by a Four-Stroke Outboard Motor: Quantitative Measurements. *Chemosphere* **1994**, *29* (2), 191–200.
- (67) Wu, T. G.; Chang, J. C.; Huang, S. H.; Lin, W. Y.; Chan, C. C.; Wu, C. F. Exposures and Health Impact for Bicycle and Electric Scooter Commuters in Taipei. *Transp. Res. Part D Transp. Environ.* **2021**, *91*, 102696.
- (68) Hsieh, P. Y.; Shearston, J. A.; Hilpert, M. Benzene Emissions from Gas Station Clusters: A New Framework for Estimating Lifetime Cancer Risk. *J. Environ. Heal. Sci. Eng.* **2021**, *19* (1), 273–283.
- (69) Varjani, S. J.; Gnansounou, E.; Pandey, A. Comprehensive Review on Toxicity of Persistent Organic Pollutants from Petroleum Refinery Waste and Their Degradation by Microorganisms. *Chemosphere* **2017**, *188*, 280–291.
- (70) Wang, X. K.; Rossignol, S.; Ma, Y.; Yao, L.; Wang, M. Y.; Chen, J. M.; George, C.; Wang, L. Molecular Characterization of Atmospheric Particulate Organosulfates in Three Megacities at the Middle and Lower Reaches of the Yangtze River. *Atmos. Chem. Phys.* **2016**, *16* (4), 2285–2298.
- (71) Surratt, J. D.; Gómez-González, Y.; Chan, A. W. H.; Vermeylen, R.; Shahgholi, M.; Kleindienst, T. E.; Edney, E. O.; Offenberg, J. H.; Lewandowski, M.; Jaoui, M.; Maenhaut, W.; Claeys, M.; Flagan, R. C.; Seinfeld, J. H. Organosulfate Formation in Biogenic Secondary Organic Aerosol. *J. Phys. Chem. A* **2008**, *112* (36), 8345–8378.
- (72) Hettiyadura, A. P. S.; Stone, E. A.; Kundu, S.; Baker, Z.; Geddes, E.; Richards, K.; Humphry, T. Determination of Atmospheric Organosulfates Using HILIC Chromatography with MS Detection. *Atmos. Meas. Technol.* **2015**, *8* (6), 2347–2358.
- (73) Barbosa, T. S.; Riva, M.; Chen, Y.; da Silva, C. M.; Almeida, J. C. S.; Zhang, Z.; Gold, A.; Arbilla, G.; Bauerfeldt, G. F.; Surratt, J. D. Chemical Characterization of Organosulfates from the Hydroxyl Radical-Initiated Oxidation and Ozonolysis of Cis-3-Hexen-1-ol. *Atmos. Environ.* **2017**, *162*, 141–151.
- (74) Wang, K.; Zhang, Y.; Huang, R. J.; Wang, M.; Ni, H.; Kampf, C. J.; Cheng, Y.; Bilde, M.; Glasius, M.; Hoffmann, T. Molecular Characterization and Source Identification of Atmospheric Particulate Organosulfates Using Ultrahigh Resolution Mass Spectrometry. *Environ. Sci. Technol.* **2019**, *53* (11), 6192–6202.
- (75) Gómez-González, Y.; Surratt, J. D.; Cuyckens, F.; Szmigielski, R.; Vermeylen, R.; Jaoui, M.; Lewandowski, M.; Offenberg, J. H.; Kleindienst, T. E.; Edney, E. O.; Blockhuys, F.; Van Alsenoy, C.; Maenhaut, W.; Claeys, M. Characterization of Organosulfates from the Photooxidation of Isoprene and Unsaturated Fatty Acids in Ambient Aerosol Using Liquid Chromatography/(–) Electrospray Ionization Mass Spectrometry. *J. Mass Spectrom.* **2008**, *43* (3), 371–382.
- (76) Glasius, M.; Hansen, A. M. K.; Claeys, M.; Henzing, J. S.; Jedynska, A. D.; Kasper-Giebl, A.; Kistler, M.; Kristensen, K.; Martinsson, J.; Maenhaut, W.; Nøjgaard, J. K.; Spindler, G.; Stenström, K. E.; Swietlicki, E.; Szidat, S.; Simpson, D.; Yttri, K. E.

Composition and Sources of Carbonaceous Aerosols in Northern Europe during Winter. *Atmos. Environ.* **2018**, *173*, 127–141.

(77) Zhang, Y.; Wang, K.; Tong, H.; Huang, R.; Hoffmann, T. The Maximum Carbonyl Ratio (MCR) as a New Index for the Structural Classification of Secondary Organic Aerosol Components. *Rapid Commun. Mass Spectrom.* **2021**, *35*, e9113.

(78) Müller, L.; Reinnig, M.-C.; Naumann, K. H.; Saathoff, H.; Mentel, T. F.; Donahue, N. M.; Hoffmann, T. Formation of 3-Methyl-1,2,3-Butanetricarboxylic Acid via Gas Phase Oxidation of Pinonic Acid – a Mass Spectrometric Study of SOA Aging. *Atmos. Chem. Phys.* **2012**, *12* (3), 1483–1496.

(79) Christoffersen, T. S.; Hjorth, J.; Horie, O.; Jensen, N. R.; Kotzias, D.; Molander, L. L.; Neeb, P.; Ruppert, L.; Winterhalter, R.; Virkkula, A.; Wirtz, K.; Larsen, B. R. Cis-Pinic Acid, a Possible Precursor for Organic Aerosol Formation from Ozonolysis of α -Pinene. *Atmos. Environ.* **1998**, *32* (10), 1657–1661.

(80) Jenkin, M. E.; Shallcross, D. E.; Harvey, J. N. Development and Application of a Possible Mechanism for the Generation of Cis-Pinic Acid from the Ozonolysis of α - and β -Pinene. *Atmos. Environ.* **2000**, *34* (18), 2837–2850.

(81) Koch, S.; Winterhalter, R.; Uherek, E.; Koloff, A.; Neeb, P.; Moortgat, G. K. Formation of New Particles in the Gas-Phase Ozonolysis of Monoterpenes. *Atmos. Environ.* **2000**, *34* (23), 4031–4042.

(82) Kroll, J. H.; Donahue, N. M.; Jimenez, J. L.; Kessler, S. H.; Canagaratna, M. R.; Wilson, K. R.; Altieri, K. E.; Mazzoleni, L. R.; Wozniak, A. S.; Bluhm, H.; Mysak, E. R.; Smith, J. D.; Kolb, C. E.; Worsnop, D. R. Carbon Oxidation State as a Metric for Describing the Chemistry of Atmospheric Organic Aerosol. *Nat. Chem.* **2011**, *3* (2), 133–139.

(83) Brüggemann, M.; van Pinxteren, D.; Wang, Y.; Yu, J. Z.; Herrmann, H. Quantification of Known and Unknown Terpenoid Organosulfates in PM10 Using Untargeted LC–HRMS/MS: Contrasting Summertime Rural Germany and the North China Plain. *Environ. Chem.* **2019**, *16* (5), 333.

(84) Wang, Y.; Ren, J.; Huang, X. H. H.; Tong, R.; Yu, J. Z. Synthesis of Four Monoterpene-Derived Organosulfates and Their Quantification in Atmospheric Aerosol Samples. *Environ. Sci. Technol.* **2017**, *51* (12), 6791–6801.

(85) Kristensen, K.; Glasius, M. Organosulfates and Oxidation Products from Biogenic Hydrocarbons in Fine Aerosols from a Forest in North West Europe during Spring. *Atmos. Environ.* **2011**, *45* (27), 4546–4556.

(86) Bryant, D. J.; Elzein, A.; Newland, M.; White, E.; Swift, S.; Watkins, A.; Deng, W.; Song, W.; Wang, S.; Zhang, Y.; Wang, X.; Rickard, A. R.; Hamilton, J. F. Importance of Oxidants and Temperature in the Formation of Biogenic Organosulfates and Nitrooxy Organosulfates. *ACS Earth Sp. Chem.* **2021**, *5* (9), 2291–2306.

(87) Brüggemann, M.; Riva, M.; Perrier, S.; Poulain, L.; George, C.; Herrmann, H. Overestimation of Monoterpene Organosulfate Abundance in Aerosol Particles by Sampling in the Presence of SO₂. *Environ. Sci. Technol. Lett.* **2021**, *8* (3), 206–211.

(88) Kourtchev, I.; Doussin, J. F.; Giorio, C.; Mahon, B.; Wilson, E. M.; Maurin, N.; Pangui, E.; Venables, D. S.; Wenger, J. C.; Kalberer, M. Molecular Composition of Fresh and Aged Secondary Organic Aerosol from a Mixture of Biogenic Volatile Compounds: A High-Resolution Mass Spectrometry Study. *Atmos. Chem. Phys.* **2015**, *15* (10), 5683–5695.

Recommended by ACS

Aerosol Mass Spectral Profiles from NAMaSTE Field-Sampled South Asian Combustion Sources

J. Douglas Goetz, Peter F. DeCarlo, *et al.*

NOVEMBER 03, 2022
ACS EARTH AND SPACE CHEMISTRY

READ 

Molecular Tracer Characterization during COVID-19 Pandemic in Shanghai: Changes in the Aerosol Aqueous Environment and Implications for Secondary Organic Ae...

Fan Fan, Qingyan Fu, *et al.*

DECEMBER 06, 2022
ACS EARTH AND SPACE CHEMISTRY

READ 

Source Diversity of Intermediate Volatility *n*-Alkanes Revealed by Compound-Specific $\delta^{13}\text{C}$ – δD Isotopes

Tiangang Tang, Gan Zhang, *et al.*

OCTOBER 07, 2022
ENVIRONMENTAL SCIENCE & TECHNOLOGY

READ 

Can Online Aerosol Mass Spectrometry Analysis Classify Secondary Organic Aerosol (SOA) and Oxidized Primary Organic Aerosol (OPOA)? A Case Study of Laboratory a...

Sri Hapsari Budisulistiorini, Mikinori Kuwata, *et al.*

NOVEMBER 29, 2021
ACS EARTH AND SPACE CHEMISTRY

READ 

Get More Suggestions >

Supporting Material to:

Nontarget Screening Exhibits a Seasonal Cycle of PM_{2.5}

Organic Aerosol Composition in Beijing

Jialiang Ma [†], Florian Ungeheuer [†], Feixue Zheng [‡], Wei Du ^{‡, §}, Yonghong Wang ^{‡, §, ||}, Jing Cai ^{‡, §},
5 Ying Zhou [‡], Chao Yan ^{‡, §}, Yongchun Liu [‡], Markku Kulmala ^{‡, §}, Kaspar R. Daellenbach ^{‡, §, ⊥ *} , and
Alexander L. Vogel ^{†, *}

[†] Institute for Atmospheric and Environmental Sciences, Goethe-University Frankfurt, 60438
Frankfurt am Main, Germany

[‡]Aerosol and Haze Laboratory, Beijing Advanced Innovation Center for Soft Matter Science
10 and Engineering, Beijing University of Chemical Technology, 100029 Beijing, China

[§] Institute for Atmospheric and Earth System Research/Physics, Faculty of Science,
University of Helsinki, 00014 Helsinki, Finland.

[⊥] Laboratory of Atmospheric Chemistry, Paul Scherrer Institute, 5232 Villigen, Switzerland

^{||} Research Center for Eco-Environmental Sciences, Chinese Academy of Sciences, 100085
15 Beijing, China

*(K.R.D.) E-mail: kaspar.daellenbach@psi.ch

*(A.L.V.) E-mail: vogel@iau.uni-frankfurt.de

Document Contains:

25 Pages

20 13 Figures

2 Tables

Contents

25	I, Aerosol Chemical Speciation Monitor Measurement.....	S3
	II, Figure S1, PM2.5 mass correlation.....	S4
	III, Figure S2, Reproducibility of signal intensity.....	S5
	IV, Figure S3, Mass accuracy during measurement period.....	S6
	V, Table S1, Detailed settings of the CD-workflow	S7
30	VI, Figure S4, Data preparation for hierarchical cluster analysis	S14
	VII, Figure S5, Molecular fingerprints (average intensity).....	S15
	VIII, Figure S6, The PM2.5 mass distribution of clusters SH, SL, WL, and WH	S16
	IX, Figure S7, Meteorological conditions during the sampling period.....	S17
	X, Figure S8, Van Krevelen-diagram of clusters E and F.....	S18
35	XI, Figure S9, MS/MS fragmentation patterns	S19
	XII, Figure S10, Kroll-diagram of clusters B, C, and D	S20
	XIII, Figure S11, Calibration curves	S21
	XIV, Figure S12, Relationship between clusters C and D and sulfate.....	S22
	XV, Figure S13, Fraction of the four clusters to the total OA	S23
40	XVI, Table S2, Detailed information for identified molecules	S24
	Reference:.....	S25

I, Aerosol Chemical Speciation Monitor Measurement

45

The Aerodyne Time-of-Flight Aerosol Chemical Speciation Monitor (ACSM) was deployed at Beijing University of Chemical Technology (BUCT, 39°58'N, 116°25'E), China. BUCT is an urban site which is located north-east of Beijing. A PM_{2.5} cyclone was installed in front of the sampling line on the rooftop with a flow rate of 3 L/min and the aerosol was dried using a

50 Nafion dryer (Perma Pure, MD-700-24F-3).

II, Figure S1, PM_{2.5} mass correlation

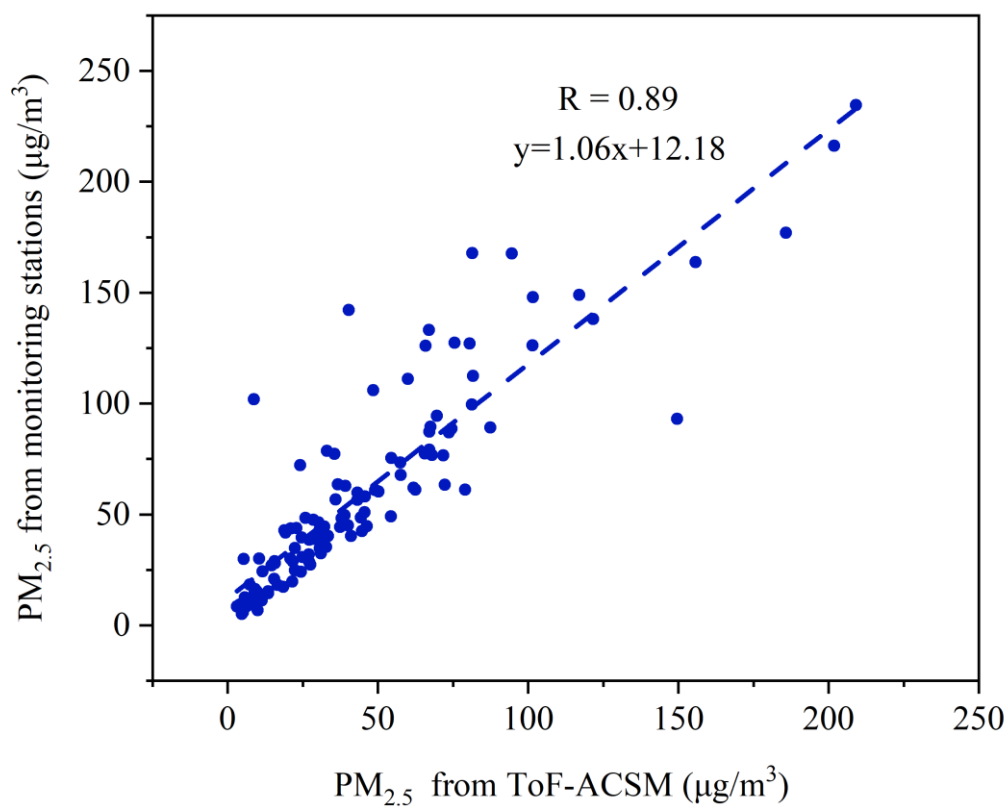
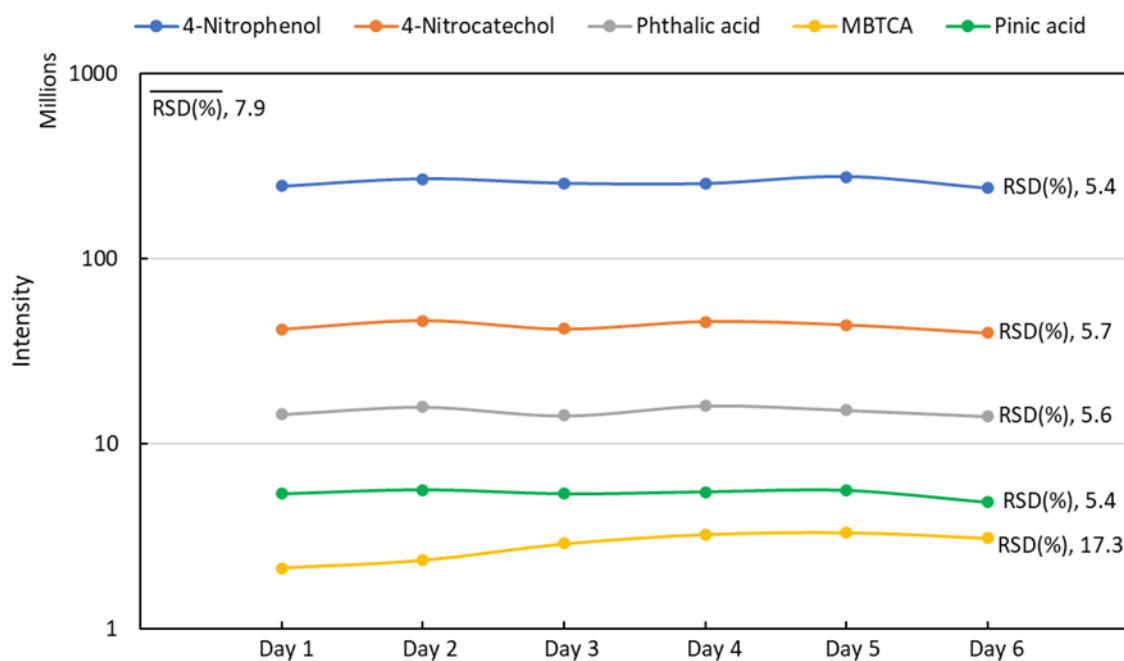


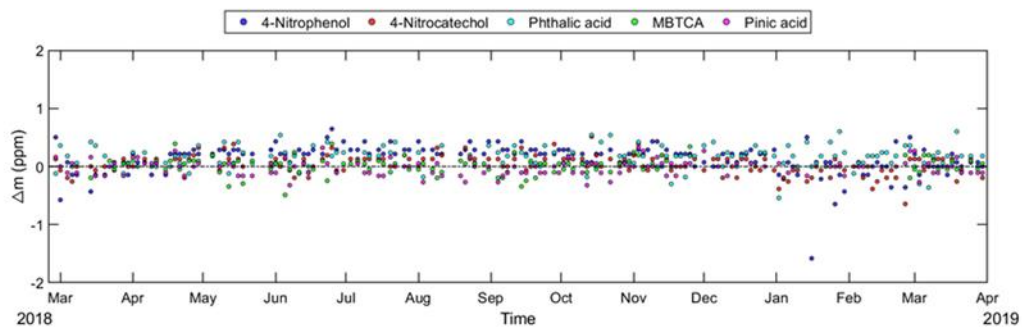
Figure S1. Concentration correlation of PM_{2.5} mass concentrations measured by ToF-ACSM
55 and the mean PM_{2.5} mass concentrations measured at Wanliu, Gucheng, Wanshouxigong, and
Guanyuan monitoring stations.

III, Figure S2, Reproducibility of signal intensity



60 **Figure S2.** Intensity variation of the five quantified compounds (4-Nitrophenol, 4-Nitrocatechol, Phthalic acid, 3-methyl-1,2,3-butanetricarboxylic acid (MBTCA), Pinic acid) of the sample which was measured repeatedly on a daily basis to monitor the performance of the instrument (sample of 30.03.2019).

65 **IV, Figure S3, Mass accuracy during measurement period**



70 **Figure S3.** The mass accuracy (deviation between theoretical and measured mass) of 4-Nitrophenol, 4-Nitrocatechol, Phthalic acid, MBTCA, and Pinic acid in all measured samples.

V, Table S1, Detailed settings of the CD-workflow

75 Processing node 1: Select Spectra

1. General Settings:

- Precursor Selection: Use MS1 Precursor
- Use Isotope Pattern in Precursor Reevaluation: True
- 80 - Provide Profile Spectra: Automatic
- Store Chromatograms: False

2. Spectrum Properties Filter:

- Lower RT Limit: 0
- 85 - Upper RT Limit: 0
- First Scan: 0
- Last Scan: 0
- Ignore Specified Scans: (not specified)
- Lowest Charge State: 0
- 90 - Highest Charge State: 0
- Min. Precursor Mass: 0 Da
- Max. Precursor Mass: 5000 Da
- Total Intensity Threshold: 1000000
- Minimum Peak Count: 1

95

3. Scan Event Filters:

- Mass Analyzer: Is FTMS
- MS Order: Is MS2; MS1
- Activation Type: Is HCD
- 100 - Min. Collision Energy: 0
- Max. Collision Energy: 1000
- Scan Type: Any
- Polarity Mode: (not specified)

4. Peak Filters:

105 - S/N Threshold (FT-only): 1.5

5. Replacements for Unrecognized Properties:

- Unrecognized Charge Replacements: 1

- Unrecognized Mass Analyzer Replacements: ITMS

110 - Unrecognized MS Order Replacements: MS2

- Unrecognized Activation Type Replacements: CID

- Unrecognized Polarity Replacements: -

- Unrecognized MS Resolution@200 Replacements: 60000

- Unrecognized MSn Resolution@200 Replacements: 30000

115 -----

Processing node 2: Align Retention Times

1. General Settings:

- Alignment Model: Adaptive curve

120 - Alignment Fallback: Use Linear Model

- Maximum Shift [min]: 0.5

- Shift Reference File: True

- Mass Tolerance: 4 ppm

- Remove Outlier: True

125 -----

Processing node 3: Detect Compounds

1. General Settings:

- Mass Tolerance [ppm]: 4 ppm

130 - Intensity Tolerance [%]: 10

- S/N Threshold: 3

- Min. Peak Intensity: 500000

- Ions:

[2M+FA-H]-1

135 [2M-H]-1

[M+FA-H]-1

[M-H]-1

[M-H-H₂O]-1

- Base Ions: [M-H]-1

140 - Min. Element Counts: C H

- Max. Element Counts: C90 H190 Br3 Cl4 N4 O20 P S3

2. Peak Detection:

- Filter Peaks: True

145 - Max. Peak Width [min]: 0.3

- Remove Singlets: True

- Min. # Scans per Peak: 5

- Min. # Isotopes: 2

150 Processing node 5: Group Compounds

1. Compound Consolidation:

- Mass Tolerance: 2 ppm

- RT Tolerance [min]: 0.1

155

2. Fragment Data Selection:

- Preferred Ions: [M-H]-1

Processing node 6: Fill Gaps

160

1. General Settings:

- Mass Tolerance: 2 ppm

- S/N Threshold: 1.5

- Use Real Peak Detection: True

165

Processing node 7: Mark Background Compounds

1. General Settings:

- Max. Sample/Blank: 3
- 170 - Max. Blank/Sample: 0
- Hide Background: False

Processing node 9: Assign Compound Annotations

175 1. General Settings:

- Mass Tolerance: 2 ppm

2. Data Sources:

- Data Source #1: mzCloud Search
- 180 - Data Source #2: Predicted Compositions
- Data Source #3: (not specified)
- Data Source #4: ChemSpider Search
- Data Source #5: (not specified)
- Data Source #6: (not specified)
- 185 - Data Source #7: (not specified)

3. Scoring Rules:

- Use mzLogic: True
- Use Spectral Distance: True
- 190 - SFit Threshold: 20
- SFit Range: 20

Processing node 10: Search mzCloud

195 1. General Settings:

- Compound Classes: All
- Precursor Mass Tolerance: 5 ppm
- FT Fragment Mass Tolerance: 5 ppm
- IT Fragment Mass Tolerance: 0.4 Da

- 200 - Library: Autoprocessed; Reference
- Post Processing: Recalibrated
- Max. # Results: 10
- Annotate Matching Fragments: False
- 205 2. DDA Search:
- Identity Search: HighChem HighRes
- Match Activation Type: True
- Match Activation Energy: Match with Tolerance
- Activation Energy Tolerance: 20
- 210 - Apply Intensity Threshold: True
- Similarity Search: Similarity Forward
- Match Factor Threshold: 60

3. DIA Search:

- 215 - Use DIA Scans for Search: False
- Max. Isolation Width [Da]: 500
- Match Activation Type: False
- Match Activation Energy: Any
- Activation Energy Tolerance: 100
- 220 - Apply Intensity Threshold: False
- Match Factor Threshold: 20

Processing node 8: Predict Compositions

- 225 1. Prediction Settings:
- Mass Tolerance: 2 ppm
- Min. Element Counts: C H
- Max. Element Counts: C90 H190 Br3 Cl4 N4 O20 P S3
- Min. RDBE: 0
- 230 - Max. RDBE: 40
- Min. H/C: 0.1

- Max. H/C: 3.5
- Max. # Candidates: 10
- Max. # Internal Candidates: 200

235

2. Pattern Matching:

- Intensity Tolerance [%]: 10
- Intensity Threshold [%]: 0.1
- S/N Threshold: 3

240

- Min. Spectral Fit [%]: 30
- Min. Pattern Cov. [%]: 90
- Use Dynamic Recalibration: True

3. Fragments Matching:

245

- Use Fragments Matching: True
- Mass Tolerance: 5 ppm
- S/N Threshold: 3

Processing node 11: Search ChemSpider

250

1. Search Settings:

- Database(s):

EAWAG Biocatalysis/Biodegradation Database

Nature Chemistry

255

Sigma-Aldrich

- Search Mode: By Formula Only

- Mass Tolerance: 2 ppm

- Max. # of results per compound: 100

- Max. # of Predicted Compositions to be searched per Compound: 3

260

- Result Order (for Max. # of results per compound): Order By Reference Count (DESC)

2. Predicted Composition Annotation:

- Check All Predicted Compositions: True

265 Processing node 12: Apply mzLogic

1. Search Settings:

- FT Fragment Mass Tolerance: 10 ppm

- IT Fragment Mass Tolerance: 0.4 Da

270 - Max. # Compounds: 0

- Max. # mzCloud Similarity Results to consider per Compound: 10

- Match Factor Threshold: 30

Processing node 13: Apply Spectral Distance

275 -----

1. Pattern Matching:

- Mass Tolerance: 5 ppm

- Intensity Tolerance [%]: 30

- Intensity Threshold [%]: 0.1

280 - S/N Threshold: 3

- Use Dynamic Recalibration: True

Processing node 4: Merge Features

285 1. Peak Consolidation:

- Mass Tolerance: 2 ppm

- RT Tolerance [min]: 0.2

VI, Figure S4, Data preparation for hierarchical cluster analysis

290

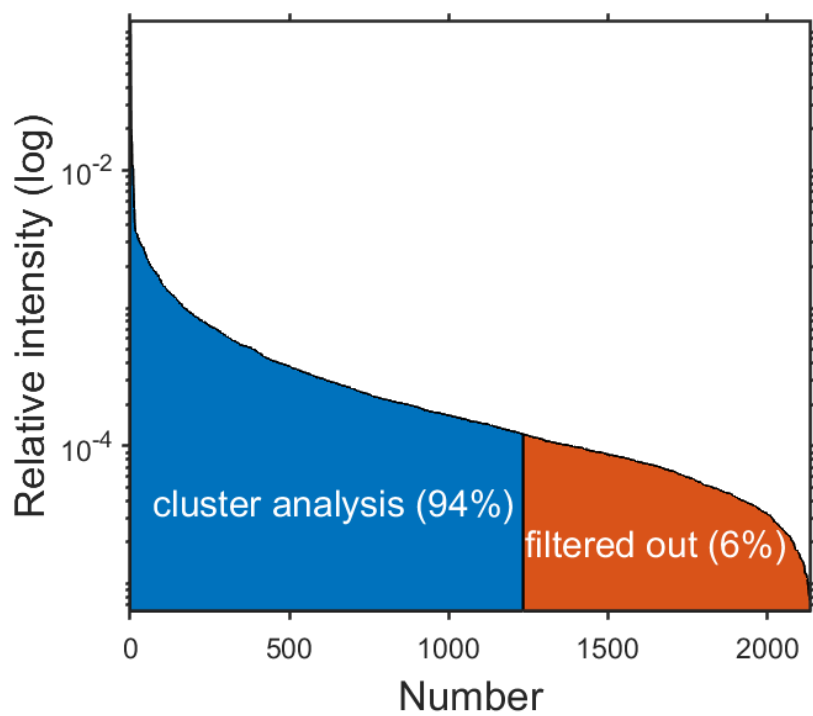


Figure S4. Data preparation for hierarchical cluster analysis.

VII, Figure S5, Molecular fingerprints (average intensity)

295

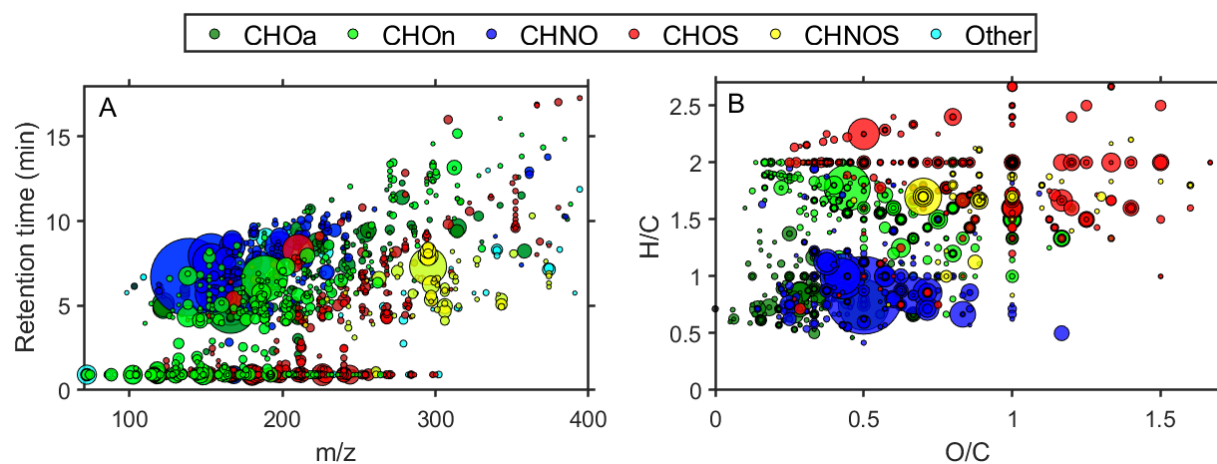
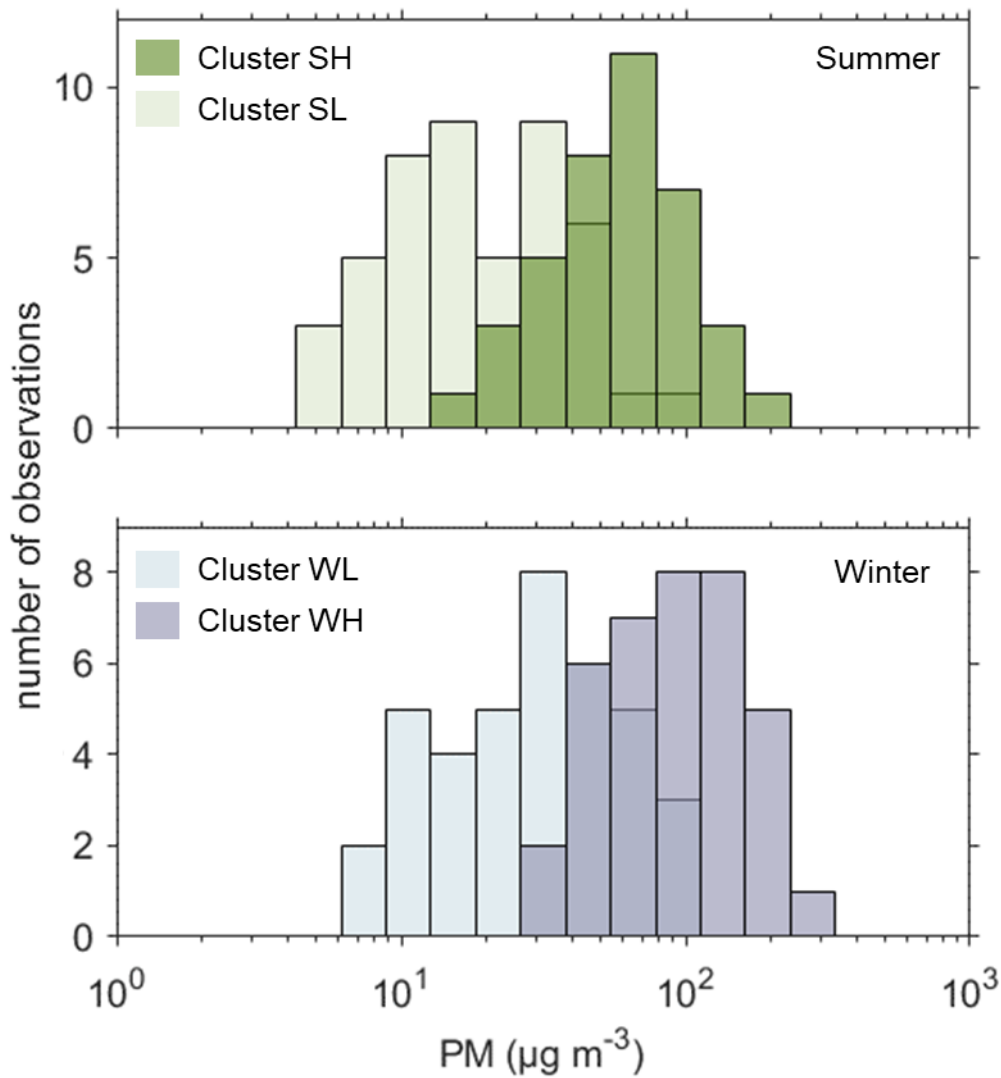


Figure S5. Molecular fingerprints of average intensity for 13 months' samples (after data filtering). (A), m/z vs RT plot. (B), Van Krevelen-diagram.

300 **VIII, Figure S6, The PM_{2.5} mass distribution of clusters SH, SL, WL, and WH**



305 **Figure S6.** The PM_{2.5} mass distribution of clusters SH, SL, WL, and WH. The standard deviations of the four clusters are 37, 16, 26, and 52 $\mu\text{g m}^{-3}$, respectively.

IX, Figure S7, Meteorological conditions during the sampling period

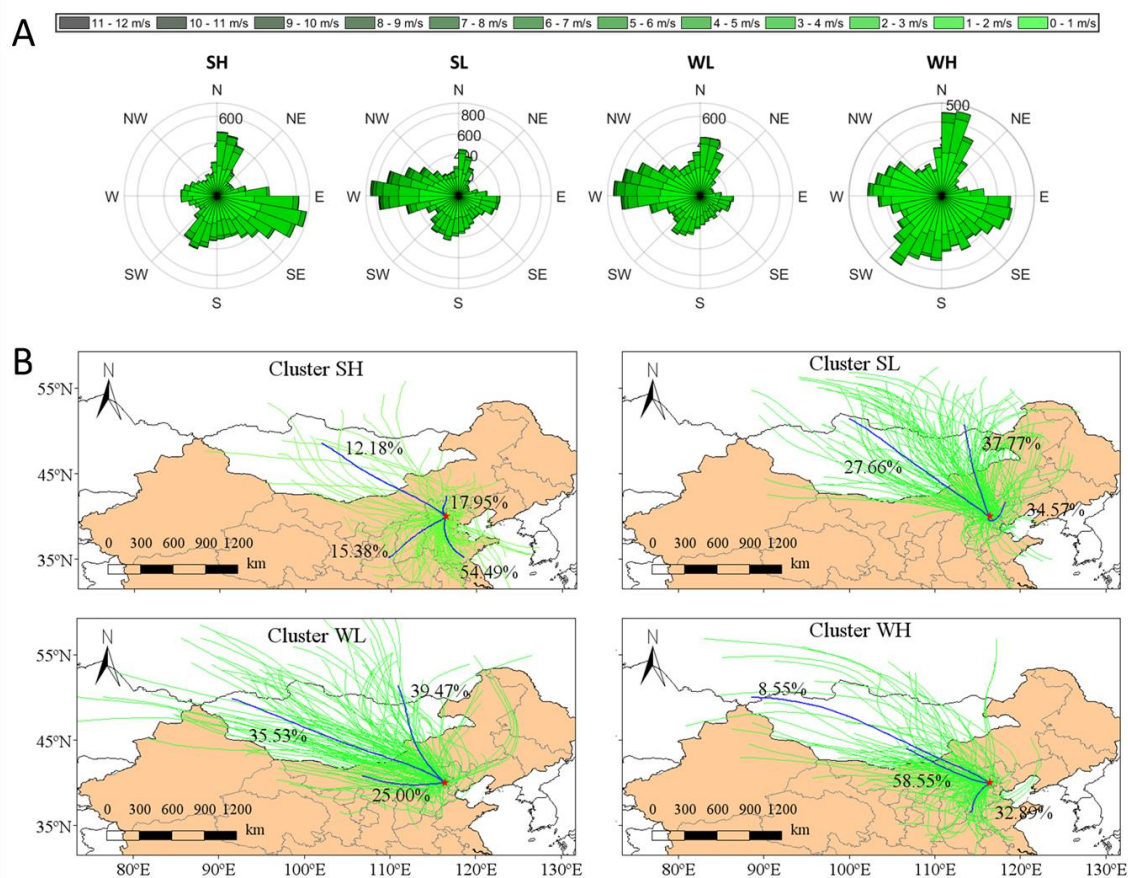
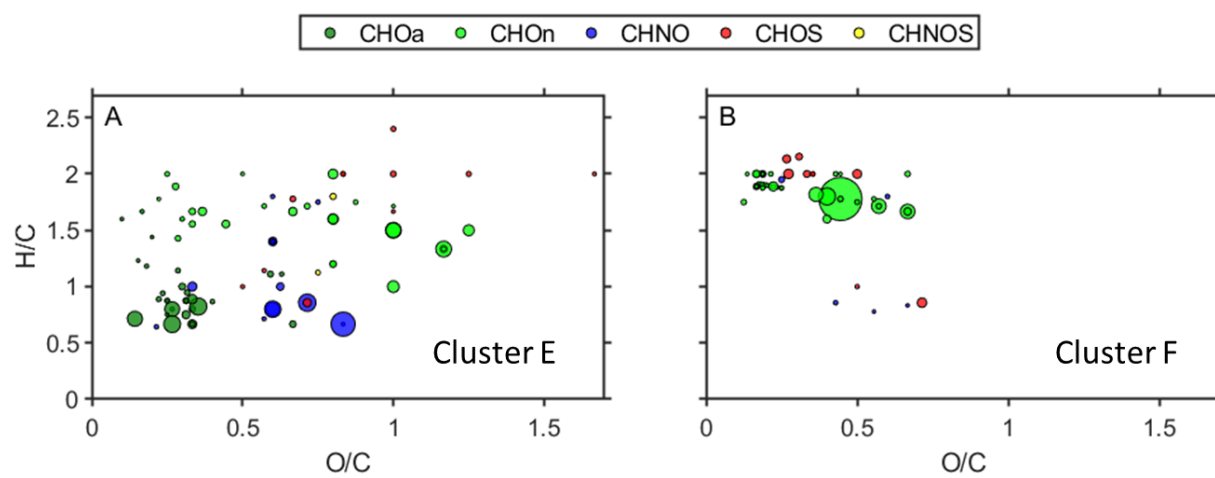


Figure S7. Meteorological conditions during the sampling period. (A) Wind direction and wind speed at Beijing University of Chemical Technology (BUCT); (B) Comparison of air mass trajectories for the different clusters based on 48 h backward HYSPLIT-trajectories.¹

310

X, Figure S8, Van Krevelen-diagram of clusters E and F



315

Figure S8. Van Krevelen-diagram (average intensity for 13 months' samples) of (A) cluster E and (B) cluster F from HCA.

XI, Figure S9, MS/MS fragmentation patterns

320

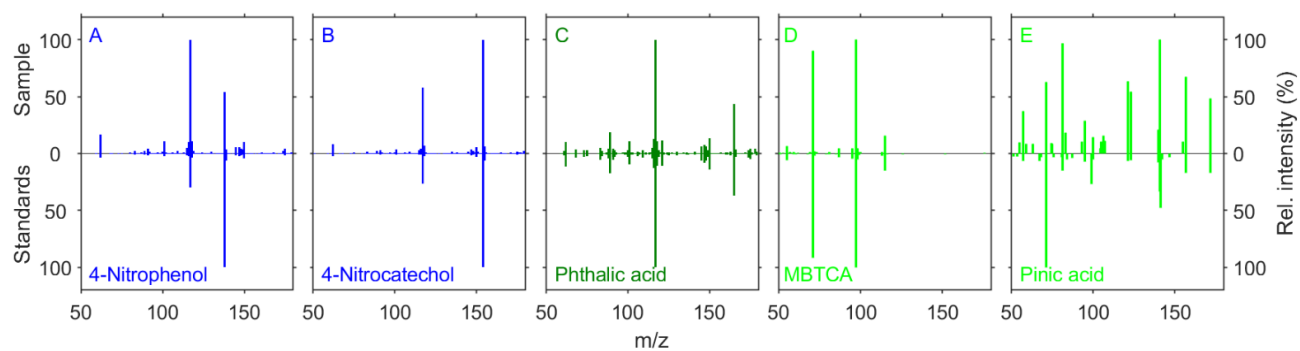
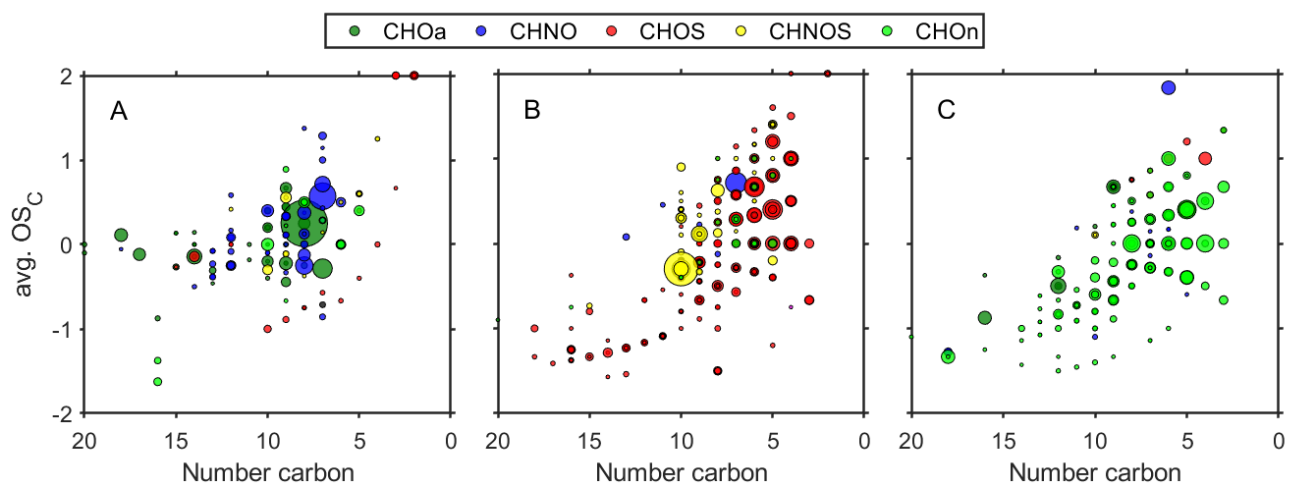


Figure S9. Comparison of the MS/MS fragmentation patterns of (A) 4-nitrophenol, (B) 4-nitrocatechol, (C) phthalic acid, (D) MBTCA, and (E) pinic acid measured in ambient samples (upward spectra) and their standards (downward spectra).

325

XII, Figure S10, Kroll-diagram of clusters B, C, and D



330 **Figure S10.** Kroll-diagram of (A) cluster B, (B) cluster C, and (E) cluster D from HCA.

XIII, Figure S11, Calibration curves

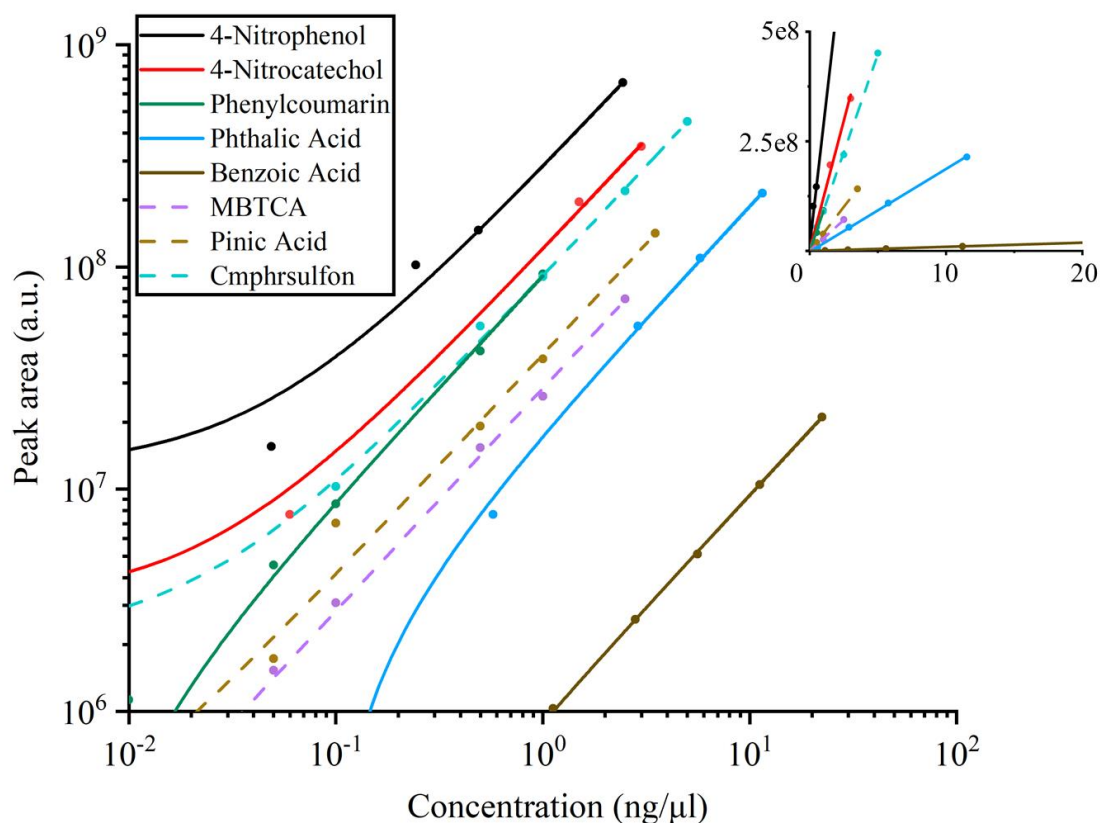


Figure S11. Calibration curves of selected compounds detected by (–)ESI, solid lines represent aromatic compounds while dashed lines non-aromatic compounds. The inset shows the calibration curves on a linear scale. Abbreviations: Phenylcoumarin (5, 7-Dihydroxy-4-phenylcoumarin), MBTCA (3-methyl-1, 2, 3-butanetricarboxylic acid), and Cmphrsulfon (camphor-10-sulfonic acid).

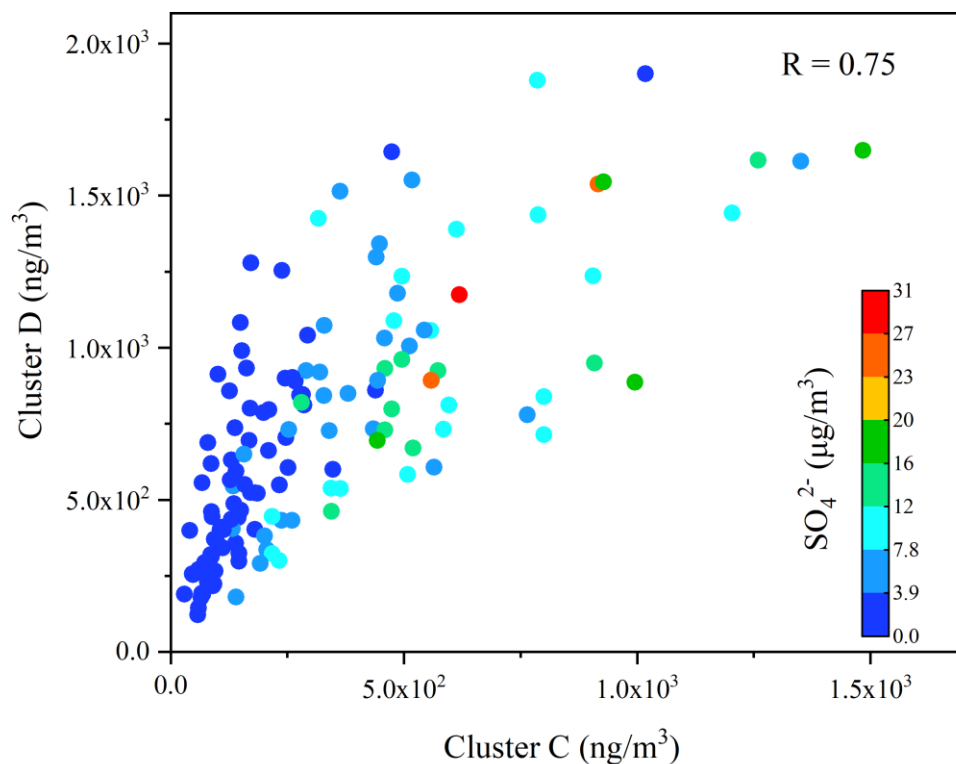


Figure S12. Correlation coefficient of total compound concentrations in cluster C and cluster D. The circles are colored according to the SO_4^{2-} mass concentration (data from ACSM).

XV, Figure S13, Fraction of the four clusters to the total OA

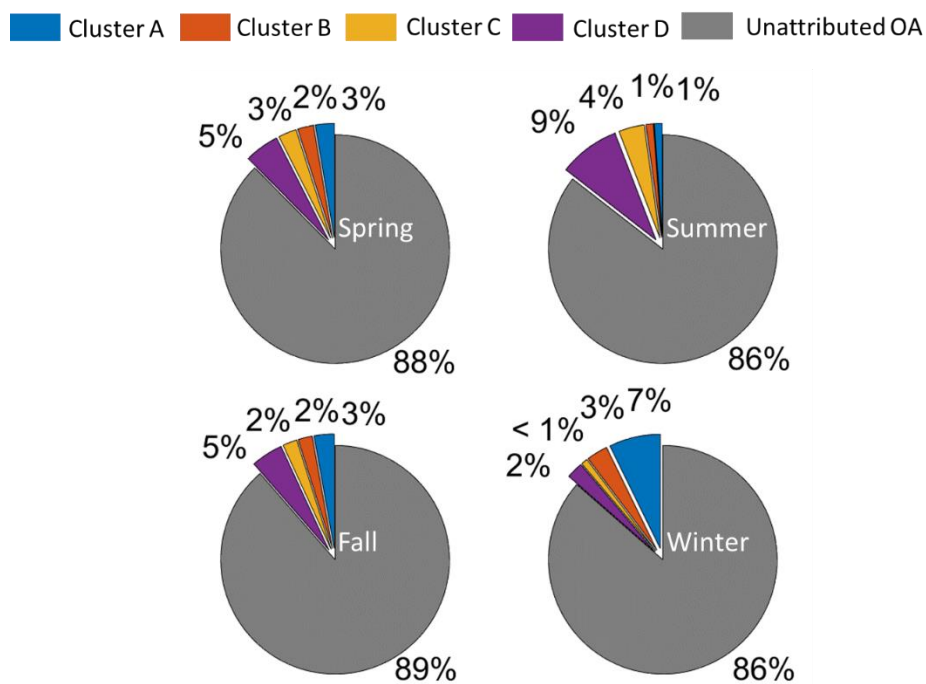
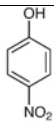
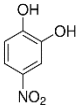
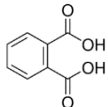
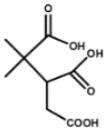
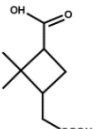


Figure S13. The concentration fraction of the four clusters to the total OA (data from ACSM)

350 in spring, summer, autumn, and winter.

XVI, Table S2, Detailed information for identified molecules

Common name	Formula	Structure	Theoretical [M-H] ⁻	ΔMass (ppm)
4-Nitrophenol	C ₆ H ₅ NO ₃		138.0197	-0.72
4-Nitrocatechol	C ₆ H ₅ NO ₄		154.0146	-0.39
Phthalic acid	C ₈ H ₆ O ₄		165.0193	-0.76
MBTCA	C ₈ H ₁₂ O ₆		203.0561	-0.14
Pinic acid	C ₉ H ₁₄ O ₄		185.0819	-0.52

355 ΔMass (ppm): Difference between measured and theoretical mass in ppm.

Reference:

- (1) Stein, A. F.; Draxler, R. R.; Rolph, G. D.; Stunder, B. J. B.; Cohen, M. D.; Ngan, F.
360 NOAA's HYSPLIT Atmospheric Transport and Dispersion Modeling System. *Bull. Am. Meteorol. Soc.* **2015**, *96* (12), 2059–2077. <https://doi.org/10.1175/BAMS-D-14-00110.1>.

6. Summary and Outlook

The organic chemical composition and formation of aviation-related ultrafine particles (UFPs) was analysed. By using a 13-stage impactor system (Nano-MOUDI), aluminium-filter samples were collected at an air quality monitoring station four kilometres north of the Frankfurt International Airport. UFPs in the size ranges 10-18 nm, 18-32 nm and 32-56 nm were chemically characterized by ultra-high-performance liquid chromatography (UHPLC), followed by heated electrospray ionisation (HESI) and mass analysis using an Orbitrap high-resolution mass spectrometer (HRMS). The characterization of particles with aerodynamic diameters < 56 nm required the detection of low picogram levels of organic molecules. Using non-target screening, the majority of detected compounds belonged to homologous series of two different kinds of organic esters. Jet engine oil base stocks and additives were identified in the UFPs by matching retention time, exact mass and MS/MS fragmentation pattern of single organic molecules in reference to five different jet oils of various manufacturers. The created molecular fingerprints showed a characteristic pattern of the jet oil constituents. The largest signals were identified as homologous series of pentaerythritol esters (PEEs) and trimethylolpropane esters (TMPEs), which are utilized in aircraft lubrication oils as base stock. The source attribution approach based on the analysed ambient synthetic esters pattern revealed that jet engine oil emissions are the source of the pentaerythritol esters detected in the aviation-related UFP samples. Trimethylolpropane esters have been detected as well in the UFP samples, compared to the pentaerythritol esters these esters contribute much less to the UFPs chemical composition. Different jet oil additives (e.g. tricresyl phosphate, TCP) were detected as well. The absence of the harmful tri-*ortho* isomer was confirmed by targeted screening, whereas a thermal transformation product of TMPE-based lubrication oil (trimethylolpropane phosphate, TMP-P) was identified.

Furthermore, the new-particle formation potential of a commonly used synthetic jet engine lubrication oil was investigated based on laboratory experiments. This was supported by a quantitative analysis of the whole spectrum of jet engine oil constituents in ambient UFPs with diameters < 56 nm, based on the collected ambient filter samples. Thermodenuder measurements enabled the monitoring of the gas-to-particle partitioning behaviour of jet engine oils at different temperatures. At 300 °C a reduction of the jet oil mass fraction by ~99% was observable compared to the experiment at 20 °C, indicating the volatile character of jet engine oils. Particles with a mean diameter of ~10 nm were formed at significantly higher numbers in

the 300 °C experiment compared to the 20 °C experiment, resulting in a more than fivefold increase in total particle numbers.

The particle diameters of the newly formed oil particles in the laboratory experiment were in the same size range as those of the UFPs coming from Frankfurt Airport, while particles coming from the direction of Frankfurt city centre had larger diameters. To further support these results quantification of the jet engine oil constituents was carried out, as the relevance of the chemical composition of UFPs regarding human health is depending on the mass contribution of each compound. This was achieved by standard addition of purchased original standards to the native UFP filter extracts. Two amines serving as stabilizers, one organophosphate used as an anti-wear agent/metal deactivator and two ester base stocks were quantified. Quantification of the two homologous ester series was carried out using one ester compound and cross-calibration. Sampling losses within the Nano-MOUDI were determined for each size stage, whereby the obtained loss factors were used for correction accordingly.

The contribution of jet engine oil to the UFP mass was determined based on particle-number size distribution measurements, conducted parallel to the filter sampling.

The results showed that aircraft emissions strongly affect the total mass of the 10-18 nm particles. The proportion of jet oil decreases for larger particles (e.g. 18-56 nm), suggesting that these oils form new particles in the cooling exhaust from aircraft engines. Accordingly, the volatility of the single ester compounds was analysed, which allows the esters to be divided into different volatility classes. The gas-to-particle partitioning behaviour of compounds is strongly determined by their volatility. The hypothesis that jet oil synthetic esters can initiate rapid nucleation in the exhaust plume of aircraft engines was supported by the three largest pentaerythritol esters showing ultra-low volatilities. Esters with higher volatilities can then condensate on these newly formed particles supporting particle growth. Furthermore, the temperature at which gas-phase supersaturation is reached was calculated with the largest pentaerythritol esters reaching supersaturation at first around 60 °C.

The hereby introduced method allows the qualitative and quantitative assignment of aircraft emissions towards the chemical composition and total mass of airport-related UFPs. Although there is strong evidence that nucleation of gaseous jet oil emissions forms new particles, open questions remain to be answered. In real emission plumes, non-volatile particulate matter (nvPM) could scavenge nucleation by providing surfaces for condensation of oil vapours.

Furthermore, *in vitro* bioassays and non-target screening were applied on aviation-related PM_{2.5} filter samples to give a first indication of toxicity drivers, depending on different wind

directions and airport operations. Three different sampling conditions are represented by the collected filter samples with air masses emerging from the Frankfurt city centre and airport direction (Frankfurt International Airport, Germany) during normal airport operations and a strike event. This allowed to differentiate between airport emissions and urban background emissions from downtown Frankfurt. PM_{2.5} samples were used in this study, as the mass of the collected ultrafine particle samples was not sufficient for the applied Microtox- and AChE inhibition biotests. The basic toxicity of PM_{2.5} was investigated by applying the Microtox assay (*Aliivibrio fischeri*), while the more specific AChE-inhibition assay accounted for neurotoxic effects. Results revealed the influence of the sampled air mass towards the organic chemical PM_{2.5} composition and consequently towards the baseline toxicity and neurotoxicity.

In the city condition samples, the overall highest signal intensities and variety of compounds were detectable. In the airport samples only organophosphorus compounds were more dominant. The highest luminescence- (Microtox assay) and AChE inhibition was detected in PM_{2.5} samples collected under the city wind direction while samples of the airport strike event showed the lowest inhibitions. Only small differences in the AChE inhibition assay were observable for the two different airport sampling conditions. The AChE assay showed a higher sensitivity towards the PM_{2.5} filter extracts compared to the Microtox assay. The sum of the signals from the detected organic compounds correlated strongly with the results of both conducted biotests and their specific mode of toxicity. However, the bioassays of some samples with a high summed signal intensity showed less toxicity compared to samples with lower intensity. This indicates that the samples toxicity is strongly influenced by the chemical composition and the individual compound concentrations.

Generally, the organic fraction of PM_{2.5} emissions from the Frankfurt city centre showed a higher toxicity compared to emissions from the airport. Findings from bioassays are certainly not directly transferrable to human health, but this approach may allow to reveal adverse human health effects related to PM exposure.

The last study of this work about the seasonality of the PM_{2.5} organic aerosol composition in Beijing showed the benefit of combining the non-target screening approach with hierarchical cluster analysis to get more insight into urban air pollution. Different sources of the detected organic compounds could be derived from the chemical composition patterns (e.g. traffic and solid fuel combustion emissions shown by the cluster analysis). Furthermore, samples with high and low particulate matter loadings from different seasons could be distinguished and the variation of the organic aerosol composition determined. An increased formation of

organosulphates during summer haze periods was observable. By the applied quantification approach the contribution of each cluster to the total organic aerosol could be determined. This study revealed clear seasonal variations of the organic aerosol composition although, only ~11-14% of the mass could be explained.

The studies described provide insight into the organic-chemical composition of airborne particulate matter of different sizes, which originate from different sources. Furthermore, statements on the toxicity of aerosols from different sources could be made. However, these studies have limitations that restrict their conclusions. Potential sampling artefacts should be taken into account and the applied UHPLC-HESI-HRMS technique is able to capture only a small part of the organic PM fraction. Using electrospray ionisation non-polar compounds without functionalisation like alkanes and polycyclic aromatic hydrocarbons are not measurable (Lin et al., 2012). Future studies should combine different ionisation techniques to gain a more complete overview about the organic chemical composition of aerosols. Furthermore, the total organic composition is certainly not fully represented by a classification by six compound classes in the non-target screening.

Due to limitations regarding the used extraction techniques and ionisation method a large part of the sampled PM_{2.5} fraction is not represented by the conducted analyses and also the correlation analysis can only provide indications for potential toxicologically relevant compounds. A direct link between the observed bioassay inhibition effects and compound classes or single compounds cannot be assessed as whole filter extracts were analysed by the *in vitro* bioassays. Therefore, fractionation of the filter extracts should be conducted prior to biotesting to improve the identification of toxicologically relevant compounds. In addition, refinements should be made with respect to *in vitro* assays to account for toxicity due to metabolic activation (for example by adding liver extract).

Earlier studies describe aviation-related UFPs as volatile under high vacuum (Mazaheri et al., 2013), therefore, it appears likely that a large number of particles smaller than 20 nm that are observed downwind of airports (Stacey, 2019; Pirhadi et al., 2020) are formed via nucleation of jet oil vapours. Nevertheless, more studies are needed to further investigate the formation of aviation-related ultrafine particles. Experiments should be carried out in which the volatile and non-volatile parts of the particles are chemically characterized individually to assess their respective fractions and sources. More analytical techniques should be applied to gain a more comprehensive overview of the chemical composition. The role of sulphuric acid in the UFP

nucleation process is still rather unclear, implying chemical-ionisation mass spectrometry measurements in the future to assess the respective contribution. Accordingly, the UFP mass fraction of metals, organic- and elemental carbon should be determined. Measurements already carried out using the collected ambient ultrafine particle filter samples did not lead to any result due to insufficient mass.

Finally, the chemical composition of the analysed particulate matter should be used to further assess potential health hazards related to exposure to aviation-related ultrafine particles, as scientific knowledge in this area is still scarce. In this context, air propagation measurements should be carried out to identify in which regions around airports people are particularly exposed. Airport and aircraft operations should be analysed in terms of their contribution to emissions in order to develop efficient reduction strategies.

7. Zusammenfassung

Die organisch-chemische Zusammensetzung und Bildung luftfahrtbedingter ultrafeiner Partikel (UFPs) wurde analysiert. Aluminiumfilter-Proben wurden an einer Luftqualitätsüberwachungsstation 4 km nördlich des internationalen Flughafens Frankfurt am Main mit einem 13-stufigen Impaktorsystem (Nano-MOUDI) gesammelt.

Die chemische Charakterisierung von UFPs im Größenbereich von 10-18 nm, 18-32 nm und 32-56 nm erfolgte durch Ultra-Hochleistungs-Flüssigkeitschromatographie (UHPLC), gefolgt von Elektrospray-Ionisation (HESI) und Detektion durch ein hochauflösendes Orbitrap-Massenspektrometer (HRMS). Die Charakterisierung von Partikeln mit aerodynamischen Durchmessern < 56 nm erfordert den Nachweis von organischen Molekülen im niedrigen Pikogramm-Bereich. Im Rahmen des Non-Target-Screenings konnte die Mehrzahl der nachgewiesenen Verbindungen homologen Reihen zweier verschiedener Arten von organischen Estern zugeordnet werden. Diese dienen als Basiskomponenten in Flugzeugschmierölen. Basierend auf fünf verschiedenen Triebwerksschmierölen verschiedener Hersteller wurden die entsprechenden Basisverbindungen und Additive in den UFPs anhand der übereinstimmenden Retentionszeit, der genauen Masse und des MS/MS-Fragmentierungsmusters einzelner organischer Moleküle identifiziert.

Die erstellten molekularen Fingerabdrücke zeigten ein charakteristisches Muster der Triebwerksöl-Bestandteile. Die größten Signale wurden als homologe Reihen von Pentaerythritolestern (PEEs) und Trimethylolpropanestern (TMPEs) identifiziert, die in Flugzeugschmierölen als Basis verwendet werden. Die Quellenzuordnung auf Grundlage des analysierten Musters der synthetischen Ester ergab, dass Triebwerksölemissionen die Quelle der in den luftfahrtbezogenen UFP-Proben nachgewiesenen Pentaerythritolester sind. Auch Trimethylolpropanester wurden in den UFP-Proben nachgewiesen, im Vergleich zu den Pentaerythritolestern tragen diese jedoch wesentlich weniger zur chemischen Zusammensetzung der UFPs bei.

Auch verschiedene Additive (z. B. Trikresylphosphat) wurden nachgewiesen. Die Abwesenheit des schädlichen Tri-*ortho*-Isomers wurde durch gezieltes Screening bestätigt, während ein thermisches Umwandlungsprodukt von Ölen auf TMPE-Basis (Trimethylolpropanphosphat, TMP-P) identifiziert wurde.

Darüber hinaus wurde das Potenzial zur Partikelneubildung eines häufig verwendeten synthetischen Triebwerköls anhand von Laborexperimenten untersucht. Unterstützt wurde dies

durch eine quantitative Analyse der Triebwerksölbestandteile in UFPs mit Durchmessern < 56 nm. Thermodenuder-Messungen ermöglichten die Untersuchung von Triebwerksölen hinsichtlich ihrer Verteilung zwischen der Gas- und Partikelphase bei unterschiedlichen Temperaturen. Bei 300 °C war eine Verringerung des Massenanteils des Triebwerksöls um $\sim 99\%$ im Vergleich zum Versuch bei 20 °C festzustellen, was auf den flüchtigen Charakter der Öle hinweist. Bei 300 °C werden deutlich mehr Partikel mit einem mittleren Durchmesser von ~ 10 nm gebildet, was zu einem mehr als fünffachen Anstieg der Gesamtpartikelzahl im Vergleich zur 20 °C Messung führt. Die Durchmesser der neu gebildeten Ölpartikel im Laborexperiment lagen im gleichen Größenbereich wie die der UFPs aus Richtung des Frankfurter Flughafens. Partikel, die aus Richtung des Frankfurter Stadtzentrums kamen, wiesen größere Durchmesser auf.

Um die Ergebnisse des Laborexperiments weiter zu untermauern und da die Relevanz der chemischen Zusammensetzung von UFPs für die menschliche Gesundheit vom Massenanteil der einzelnen Verbindungen abhängt, wurden die Öl-Bestandteile in den gesammelten UFPs quantifiziert. Dies geschah durch Standardaddition von gekauften Standards zu den nativen UFP-Filterextrakten. Zwei Amine, die als Stabilisatoren dienen, ein Organophosphat das als Antiverschleißmittel/Metalldeaktivator verwendet wird und zwei Estergrundstoffe wurden quantifiziert. Die Quantifizierung der beiden homologen Ester-Reihen wurde mit einer Esterverbindung mittels Kreuzkalibrierung durchgeführt.

Durch die Charakterisierung des Nano-MOUDI konnten die Sammelverluste für jede Größenstufe bestimmt und die Ergebnisse entsprechend korrigiert werden. Messungen der Partikelgrößenverteilung, die parallel zur Filterbeprobung durchgeführt wurden, ermöglichten die Bestimmung des Anteils der Triebwerksöle an der UFP-Masse.

Die Ergebnisse zeigen, dass Flugzeugemissionen die Gesamtmasse der $10-18$ nm großen Partikel stark beeinflussen. Der Anteil des Triebwerksöls nimmt bei größeren Partikeln (z. B. $18-56$ nm) ab, was darauf hindeutet, dass diese Öle in den sich abkühlenden Abgasen von Flugzeugtriebwerken neue Partikel bilden. Dementsprechend wurde die Flüchtigkeit der einzelnen Esterverbindungen analysiert, wodurch die Ester in verschiedene Flüchtigkeitsklassen eingeteilt werden konnten.

Das Gas-zu-Partikel-Verteilungsverhalten von Verbindungen wird stark durch ihre Flüchtigkeit bestimmt. Die Hypothese, dass synthetische Ester eine schnelle Keimbildung in der Abgasfahne von Flugzeugtriebwerken auslösen können, wurde dadurch gestützt, dass die drei größten Pentaerythritolester eine sehr geringe Flüchtigkeit aufwiesen. Ester mit höherer Flüchtigkeit können dann auf diesen neu gebildeten Partikeln kondensieren und das Partikelwachstum

fördern. Darüber hinaus wurde die Temperatur berechnet, bei der eine Übersättigung der Gasphase erreicht wird, wobei die größten Pentaerythritolester als erste Verbindungen diese bei etwa 60 °C erreichen.

Die hier vorgestellte Methode ermöglicht die qualitative und quantitative Zuordnung von Flugzeugemissionen zur chemischen Zusammensetzung und Gesamtmasse flughafenbezogener UFPs.

Darüber hinaus wurden In-vitro-Bioassays und ein Non-Target-Screening an PM_{2,5}-Filterproben durchgeführt, um toxikologisch relevante Verbindungen in Abhängigkeit von verschiedenen Windrichtungen und dem Flughafenbetrieb zu bestimmen. Drei verschiedene Probenahmebedingungen werden durch die gesammelten Filterproben repräsentiert, wobei die beprobten Luftmassen aus dem Frankfurter Stadtzentrum und aus Richtung des Flughafens während des normalen Flughafenbetriebs und eines Streikereignisses stammten. Dies ermöglichte die Unterscheidung zwischen Flughafenemissionen und Hintergrundemissionen aus der Frankfurter Innenstadt.

In dieser Studie wurden PM_{2,5}-Proben verwendet, da die Masse der gesammelten UFP-Proben für die durchgeführten Microtox- und AChE-biotests nicht ausreichte. Die Basistoxizität von PM_{2,5} wurde mit dem Microtox-Test (*Aliivibrio fischeri*) untersucht, während der spezifischere AChE-Test neurotoxische Effekte berücksichtigte.

Die Ergebnisse zeigen den Einfluss der beprobten Luftmasse auf die organisch-chemische PM_{2,5}-Zusammensetzung und folglich auf die Basistoxizität und Neurotoxizität. In den Stadtproben waren insgesamt die meisten Verbindungen und die höchsten Signalintensitäten nachweisbar, lediglich phosphororganische Verbindungen waren in den Flughafenproben dominanter. Die stärkste Lumineszenz- (Microtox-Assay) und AChE-Hemmung wurde in PM_{2,5}-Proben festgestellt die bei Windrichtung aus der Stadt gesammelt wurden, während die Proben des Flughafenstreiks die geringsten Hemmungen aufwiesen. Es konnten zudem nur geringe Unterschiede in der AChE-Hemmung zwischen den Proben des regulären Flughafenbetriebs und des Streiks beobachtet werden. Der AChE-Assay zeigte eine höhere Empfindlichkeit gegenüber den PM_{2,5}-Filterextrakten als der Microtox-Assay. Die Summe der Signale der nachgewiesenen organischen Verbindungen korrelierte stark mit den Ergebnissen der beiden durchgeführten Biotests und ihrer spezifischen Art der Toxizität. Allerdings zeigten die Biotests einiger Proben mit einer hohen summierten Signalintensität eine geringere Toxizität als Proben mit geringerer Intensität.

Darüber hinaus zeigte der organische PM_{2,5}-Anteil der Partikelemissionen aus der Frankfurter Innenstadt eine höhere Toxizität verglichen mit den Emissionen des Frankfurter Flughafens. Generell hat diese Studie gezeigt, dass sowohl die Konzentration als auch die individuelle Zusammensetzung der organischen PM_{2,5}-Fraktion die Toxizität bestimmen. Die Ergebnisse von Bioassays sind sicherlich nicht direkt auf die menschliche Gesundheit übertragbar, aber dieser Ansatz kann es ermöglichen, negative Auswirkungen einer Aerosol-Exposition auf die menschliche Gesundheit aufzuzeigen.

Die letzte Studie dieser Arbeit über die saisonale Zusammensetzung der organischen PM_{2,5}-Fraktion von Aerosolen aus Peking hat gezeigt, dass es von Vorteil ist, den Non-Target-Screening-Ansatz mit der hierarchischen Clusteranalyse zu kombinieren. Dies ermöglicht es einen besseren Einblick in die städtische Luftverschmutzung zu erhalten. Aus den Mustern der chemischen Zusammensetzung konnten verschiedene Quellen der organischen Verbindungen abgeleitet werden, z. B. Emissionen aus dem Verkehr und der Verbrennung fester Brennstoffe, Proben mit hoher und niedriger Feinstaubbelastung aus verschiedenen Jahreszeiten unterschieden und die Variation der organischen Aerosolzusammensetzung bestimmt werden. Eine verstärkte Bildung von Organosulfaten während sommerlicher Dunstperioden war ebenfalls zu beobachten. Anhand der durchgeführten Quantifizierung konnte der Beitrag jedes Clusters zum gesamten organischen Aerosol bestimmt werden. Deutliche saisonale Schwankungen der Zusammensetzung des organischen Aerosols konnten durch diese Studie aufgezeigt werden, obwohl aufgrund der genutzten Analyseverfahren nur ~11-14% der Masse erklärt werden konnten.

Die beschriebenen Untersuchungen geben einen Einblick in die organisch-chemische Zusammensetzung von luftgetragenen Feinstaubfraktionen unterschiedlicher Größe aus den verschiedensten Quellen. Zudem konnten Aussagen über die Toxizität der Aerosole getroffen werden. Diese Studien unterliegen jedoch Einschränkungen, die ihre Schlussfolgerungen limitieren. Für zukünftige Arbeiten sollte berücksichtigt werden, dass Artefakte bei der Probenahme auftreten können und dass die angewandte UHPLC-HESI-HRMS-Messmethode nur einen kleinen Teil der organischen Aerosol-Fraktion erfassen kann. Mit der Elektrospray-Ionisierung sind unpolare Verbindungen ohne Funktionalisierung wie Alkane und polyzyklische aromatische Kohlenwasserstoffe (PAKs) nicht messbar (Lin et al., 2012).

In künftigen Studien sollten verschiedene Ionisierungstechniken kombiniert werden, um einen vollständigeren Überblick über die organisch-chemische Zusammensetzung von Aerosolen zu

erhalten. Darüber hinaus kann die gesamte organische Zusammensetzung mit hoher Wahrscheinlichkeit nicht durch eine Unterscheidung in nur sechs Verbindungsklassen vollständig dargestellt werden.

Dementsprechend ist auch ein großer Teil der beprobten PM_{2,5}-Fraktionen durch die durchgeführten Analysen nicht repräsentiert, was auf die Limitierungen der verwendeten Extraktionstechniken und Ionisierungsverfahren zurückzuführen ist. Darüber hinaus kann die durchgeführte Korrelationsanalyse nur Hinweise auf potentiell toxikologisch relevante Verbindungen liefern. Ein direkter Zusammenhang zwischen den beobachteten Bioassay-Ergebnissen und Verbindungsklassen oder einzelnen Verbindungen kann nicht hergestellt werden, da vollständige Filterextrakte in den *in vitro* Bioassays analysiert wurden. Daher sollte vor der Durchführung von Biotests eine Fraktionierung der Filterextrakte durchgeführt werden, um die Identifizierung toxikologisch relevanter Verbindungen zu verbessern. Darüber hinaus sollten die In-vitro-Tests verfeinert werden, um eine Toxizität aufgrund von Metabolisierung zu berücksichtigen.

Obwohl es deutliche Hinweise darauf gibt, dass die Nukleation gasförmiger Ölemissionen zur Bildung neuer Partikel führt, sind noch offene Fragen zu klären. In Emissionsfahnen könnten nichtflüchtige Partikel (nvPM) die Keimbildung verhindern, indem sie Oberflächen für die Kondensation von Öldämpfen bieten. Frühere Studien beschreiben jedoch luftfahrtbedingte UFPs als flüchtig unter Hochvakuum (Mazaheri et al., 2013), weshalb es wahrscheinlich ist, dass eine große Anzahl von Partikeln kleiner 20 nm, die in der Abluft von Flughäfen beobachtet werden (Stacey, 2019; Pirhadi et al., 2020), durch Nukleation von Öldämpfen gebildet werden. Dennoch sind weitere Studien erforderlich, um die Bildung von luftfahrtbedingten ultrafeinen Partikeln zu untersuchen. Es sollten Experimente durchgeführt werden, bei denen die flüchtigen und nicht flüchtigen Bestandteile der Partikel einzeln chemisch charakterisiert werden, um ihre jeweiligen Anteile und Quellen zu ermitteln. Zusätzlich sollten weitere Analysetechniken angewendet werden, um einen umfassenderen Überblick über die chemische Zusammensetzung zu erhalten. Der Einfluss von Schwefelsäure auf die Bildung von luftfahrtbedingten UFPs ist noch nicht vollständig geklärt, so dass in Zukunft Messungen mittels chemischer Ionisation und Massenspektrometrie durchgeführt werden sollten, um den entsprechenden Beitrag zu ermitteln. Ebenso sollte der UFP-Massenanteil von Metallen sowie organischem- und elementarem Kohlenstoff bestimmt werden. Bereits durchgeführte Analysen der gesammelten UFP-Filterproben führten aufgrund unzureichender Masse zu keinem aussagekräftigen Ergebnis.

Schließlich muss die ermittelte chemische Zusammensetzung der Aerosole genutzt werden, um potenzielle Gesundheitsgefahren im Zusammenhang mit der Exposition gegenüber luftfahrtbedingten ultrafeinen Partikeln weiter zu bewerten, da die wissenschaftlichen Erkenntnisse in diesem Bereich noch gering sind. In diesem Zusammenhang sollten Ausbreitungsmessungen durchgeführt werden, um festzustellen, in welchen Regionen in der Nähe von Flughäfen Menschen besonders exponiert sind. Flughafen- und Flugbetrieb sollten hinsichtlich ihres Beitrags zu den Emissionen analysiert werden, um effiziente Minderungsstrategien zu entwickeln.

8. Personal Contribution to the Publications

1.) Ungeheuer, F., van Pinxteren, D., and Vogel, A. L.: Identification and source attribution of organic compounds in ultrafine particles near Frankfurt International Airport, *Atmos. Chem. Phys.*, 21, 3763–3775, <https://doi.org/10.5194/acp-21-3763-2021>, 2021.

This publication describes the chemical characterization of airborne ultrafine particles (UFPs) with aerodynamic diameters smaller than 56 nm collected near Frankfurt Airport by combining UHPLC-HRMS measurements with a non-target screening approach. From August to October 2019 I collected UFP filter samples at an air quality monitoring site using a cascade impactor sampler (Nano-MOUDI). I developed the sample preparation procedure, the UHPLC-HRMS method and carried out the UHPLC-HRMS measurements. I analysed the data by performing a software based non-target screening. Thereby, I identified a strong contribution of jet engine lubrication oils to the organic chemical composition of aviation-related UFPs based on single compound identification. I depicted the data and wrote the manuscript.

2.) Ungeheuer, F., Caudillo, L., Ditas, F. et al. Nucleation of jet engine oil vapours is a large source of aviation-related ultrafine particles. *Commun Earth Environ* 3, 319 (2022). <https://doi.org/10.1038/s43247-022-00653-w>.

This publication describes the volatility and new-particle-formation ability of jet engine oil vapours based on laboratory thermodenuder experiments. This is further supported by quantification of jet engine oil constituents in three ambient ultrafine particle (UFP) size fractions (< 56 nm) downwind Frankfurt International Airport. Lucia and I together performed the thermodenuder measurements and Nano-MOUDI characterization in the laboratory. I conducted the respective UHPLC-HRMS measurements, analysed the data and depicted the results. From August to October 2019 I collected UFP filter samples at an air quality monitoring site using a cascade impactor sampler (Nano-MOUDI). By performing targeted UHPLC-HRMS measurements and standard addition quantification I determined the mass contribution of the individual jet oil constituents to the three ambient UFP size fractions. Therefore, I developed the sample preparation procedure, the UHPLC-HRMS method and carried out the UHPLC-HRMS measurements. Thereby, I identified the strongest contribution of jet engine lubrication oils to the organic chemical composition of the smallest UFP size fraction (10-18

nm). Based on the ambient concentrations I analysed the volatility of the individual jet oil constituents. I depicted the data and wrote the manuscript.

3.) Wallraff, J. P.¹, Ungeheuer, F.¹, Dombrowski, A., Oehlmann, J., and Vogel, A. L.: Occurrence and in vitro toxicity of organic compounds in urban background PM_{2.5}, *The Science of the total environment*, 817, 152779, <https://doi.org/10.1016/j.scitotenv.2021.152779>, 2022.

¹ These authors contributed equally.

This publication describes the in vitro toxicity of the organic fraction of atmospheric particulate matter with aerodynamic diameters smaller than 2.5 μm (PM_{2.5}). It combines the toxicological assessment with a comprehensive chemical characterization by UHPLC-HRMS and non-target screening. Jonas P. Wallraff and I collected PM_{2.5} filter samples at an air quality monitoring station 4km north of Frankfurt Airport. We jointly developed the sample preparation procedure. I developed to a large extent the UHPLC-HRMS and non-target screening method and was significantly involved in the UHPLC-HRMS measurements and chemical data analysis. Jonas P. Wallraff carried out the in vitro tests and evaluation of the corresponding results. I conducted various measurements to verify identified compounds using purchased standards. Final results point out a high correlation of the aerosol toxicity with the origin of the sampled air masses. Air masses originating from the Frankfurt city direction showed a higher in vitro toxicity and varying chemical composition than air masses advected over Frankfurt Airport. I contributed to creating the figures and writing the manuscript.

4.) Ma, J., Ungeheuer, F., Zheng, F., Du, W., Wang, Y., Cai, J., Zhou, Y., Yan, C., Liu, Y., Kulmala, M., Daellenbach, K. R., and Vogel, A. L.: Nontarget Screening Exhibits a Seasonal Cycle of PM_{2.5} Organic Aerosol Composition in Beijing, *Environ. Sci. Technol.*, <https://doi.org/10.1021/acs.est.1c06905>, 2022.

This publication describes the seasonal variation of the organic molecular composition of atmospheric particulate matter based on PM_{2.5} filter samples collected over a one year period in Beijing, China. The study combines UHPLC-HRMS non-target screening, hierarchical cluster analysis (HCA) and ToF-ACSM measurements. I developed to a large extent the

UHPLC-HRMS- and sample preparation method and was significantly involved in the UHPLC-HRMS measurements and data verification. Furthermore, I synthesised organic standards to quantify the contribution of several compound clusters to the total organic aerosol mass and contributed to the scientific discussion.

9. References

- Aammi, S., Karaca, F., and Petek, M.: A toxicological and genotoxicological indexing study of ambient aerosols (PM_{2.5-10}) using in vitro bioassays, *Chemosphere*, 174, 490–498, <https://doi.org/10.1016/j.chemosphere.2017.01.141>, 2017.
- Acir, I.-H. and Guenther, K.: Endocrine-disrupting metabolites of alkylphenol ethoxylates - A critical review of analytical methods, environmental occurrences, toxicity, and regulation, *The Science of the total environment*, 635, 1530–1546, <https://doi.org/10.1016/j.scitotenv.2018.04.079>, 2018.
- Albrecht, B. A.: Aerosols, cloud microphysics, and fractional cloudiness, *Science (New York, N.Y.)*, 245, 1227–1230, <https://doi.org/10.1126/science.245.4923.1227>, 1989.
- Allan, J. D., Williams, P. I., Morgan, W. T., Martin, C. L., Flynn, M. J., Lee, J., Nemitz, E., Phillips, G. J., Gallagher, M. W., and Coe, H.: Contributions from transport, solid fuel burning and cooking to primary organic aerosols in two UK cities, *Atmos. Chem. Phys.*, 10, 647–668, <https://doi.org/10.5194/acp-10-647-2010>, 2010.
- Andrade-Oliva, M.-A., Escamilla-Sánchez, J., Debray-García, Y., Morales-Rubio, R. A., González-Pantoja, R., Uribe-Ramírez, M., Amador-Muñoz, O., Díaz-Godoy, R. V., Vizcaya-Ruiz, A. de, and Arias-Montaña, J.-A.: In vitro exposure to ambient fine and ultrafine particles alters dopamine uptake and release, and D2 receptor affinity and signaling, *Environmental Toxicology and Pharmacology*, 80, 103484, <https://doi.org/10.1016/j.etap.2020.103484>, available at: <https://www.sciencedirect.com/science/article/pii/S1382668920301605>, 2020.
- Anenberg, S. C., Mohegh, A., Goldberg, D. L., Kerr, G. H., Brauer, M., Burkart, K., Hystad, P., Larkin, A., Wozniak, S., and Lamsal, L.: Long-term trends in urban NO₂ concentrations and associated paediatric asthma incidence: estimates from global datasets, *The Lancet Planetary Health*, 6, e49-e58, [https://doi.org/10.1016/S2542-5196\(21\)00255-2](https://doi.org/10.1016/S2542-5196(21)00255-2), 2022.
- Arias-Pérez, R. D., Tabora, N. A., Gómez, D. M., Narvaez, J. F., Porras, J., and Hernandez, J. C.: Inflammatory effects of particulate matter air pollution, *Environmental science and pollution research international*, 27, 42390–42404, <https://doi.org/10.1007/s11356-020-10574-w>, 2020.
- Baldauf, R. W., Devlin, R. B., Gehr, P., Giannelli, R., Hassett-Sipple, B., Jung, H., Martini, G., McDonald, J., Sacks, J. D., and Walker, K.: Ultrafine Particle Metrics and Research Considerations: Review of the 2015 UFP Workshop, *Int. J. Environ. Res. Public Health*, 13, <https://doi.org/10.3390/ijerph13111054>, 2016.
- Bates, J. T., Weber, R. J., Abrams, J., Verma, V., Fang, T., Klein, M., Strickland, M. J., Sarnat, S. E., Chang, H. H., Mulholland, J. A., Tolbert, P. E., and Russell, A. G.: Reactive Oxygen Species Generation Linked to Sources of Atmospheric Particulate Matter and Cardiorespiratory Effects, *Environ. Sci. Technol.*, 49, 13605–13612, <https://doi.org/10.1021/acs.est.5b02967>, 2015.
- Bauer, S. E., Tsigaridis, K., and Miller, R.: Significant atmospheric aerosol pollution caused by world food cultivation, *Geophys. Res. Lett.*, 43, 5394–5400, <https://doi.org/10.1002/2016GL068354>, 2016.
- Bergé, A., Cladière, M., Gasperi, J., Coursimault, A., Tassin, B., and Moilleron, R.: Meta-analysis of environmental contamination by alkylphenols, *Environmental science and*

- pollution research international, 19, 3798–3819, <https://doi.org/10.1007/s11356-012-1094-7>, 2012.
- Beyersdorf, A. J., Timko, M. T., Ziemba, L. D., Bulzan, D., Corporan, E., Herndon, S. C., Howard, R., Miake-Lye, R., Thornhill, K. L., Winstead, E., Wey, C., Yu, Z., and Anderson, B. E.: Reductions in aircraft particulate emissions due to the use of Fischer–Tropsch fuels, *Atmos. Chem. Phys.*, 14, 11–23, <https://doi.org/10.5194/acp-14-11-2014>, 2014.
- Bird, R. B., Stewart, W. E., and Lightfoot, E. N.: *Transport phenomena*, Rev. 2. ed., Wiley, New York, 905 pp., 2007.
- Blair, S. L., MacMillan, A. C., Drozd, G. T., Goldstein, A. H., Chu, R. K., Paša-Tolić, L., Shaw, J. B., Tolić, N., Lin, P., Laskin, J., Laskin, A., and Nizkorodov, S. A.: Molecular Characterization of Organosulfur Compounds in Biodiesel and Diesel Fuel Secondary Organic Aerosol, *Environ. Sci. Technol.*, 51, 119–127, <https://doi.org/10.1021/acs.est.6b03304>, 2017.
- Boer, J. de, Antelo, A., van der Veen, I., Brandsma, S., and Lammertse, N.: Tricresyl phosphate and the aerotoxic syndrome of flight crew members--current gaps in knowledge, *Chemosphere*, 119 Suppl, S58-61, <https://doi.org/10.1016/j.chemosphere.2014.05.015>, 2015.
- Bowery, N. G., Collins, J. F., Hill, R. G., and Pearson, S.: t-Butyl bicyclo phosphate: a convulsant and GABA antagonist more potent than bicuculline, *Br. J. Pharmacol.*, 60, 275–276, 1977.
- Bowery, N. G., Collins, J. F., Hill, R. G., and Pearson, S.: GABA antagonism as a possible basis for the convulsant action of a series of bicyclic phosphorus esters, *Br. J. Pharmacol.*, 57, P435-P436, 1976.
- Brack, W.: Effect-directed analysis: a promising tool for the identification of organic toxicants in complex mixtures?, *Analytical and bioanalytical chemistry*, 377, 397–407, <https://doi.org/10.1007/s00216-003-2139-z>, 2003.
- Bristow, A. W. T.: Accurate mass measurement for the determination of elemental formula--a tutorial, *Mass spectrometry reviews*, 25, 99–111, <https://doi.org/10.1002/mas.20058>, 2006.
- Brüggemann, M., Xu, R., Tilgner, A., Kwong, K. C., Mutzel, A., Poon, H. Y., Otto, T., Schaefer, T., Poulain, L., Chan, M. N., and Herrmann, H.: Organosulfates in Ambient Aerosol: State of Knowledge and Future Research Directions on Formation, Abundance, Fate, and Importance, *Environ. Sci. Technol.*, 54, 3767–3782, <https://doi.org/10.1021/acs.est.9b06751>, 2020.
- Brüggemann, M., van Pinxteren, D., Wang, Y., Yu, J. Z., and Herrmann, H.: Quantification of known and unknown terpenoid organosulfates in PM10 using untargeted LC–HRMS/MS: contrasting summertime rural Germany and the North China Plain, *Environ. Chem.*, 16, 333, <https://doi.org/10.1071/EN19089>, 2019.
- Bryant, D. J., Dixon, W. J., Hopkins, J. R., Dunmore, R. E., Pereira, K. L., Shaw, M., Squires, F. A., Bannan, T. J., Mehra, A., Worrall, S. D., Bacak, A., Coe, H., Percival, C. J., Whalley, L. K., Heard, D. E., Slater, E. J., Ouyang, B., Cui, T., Surratt, J. D., Di Liu, Shi, Z., Harrison, R., Sun, Y., Xu, W., Lewis, A. C., Lee, J. D., Rickard, A. R., and Hamilton, J. F.: Strong anthropogenic control of secondary organic aerosol formation from isoprene in Beijing, *Atmos. Chem. Phys.*, 20, 7531–7552, <https://doi.org/10.5194/acp-20-7531-2020>, 2020.

- Cai, J., Chu, B., Yao, L., Yan, C., Heikkinen, L. M., Zheng, F., Li, C., Fan, X., Zhang, S., Yang, D., Wang, Y., Kokkonen, T. V., Chan, T., Zhou, Y., Dada, L., Liu, Y., He, H., Paasonen, P., Kujansuu, J. T., Petäjä, T., Mohr, C., Kangasluoma, J., Bianchi, F., Sun, Y., Croteau, P. L., Worsnop, D. R., Kerminen, V.-M., Du, W., Kulmala, M., and Daellenbach, K. R.: Size-segregated particle number and mass concentrations from different emission sources in urban Beijing, *Atmos. Chem. Phys.*, 20, 12721–12740, <https://doi.org/10.5194/acp-20-12721-2020>, 2020.
- Callahan, A. B., Tappan, D. V., Mooney, L. W., and Heyder, E.: Analysis of Hydraulic Fluids and Lubricating Oils for the Formation of Trimethylolpropane Phosphate (TMP-P), Naval Submarine Medical Research Lab Groton CT, 98 pp., 1989.
- Campen, M. J., Nolan, J. P., Schladweiler, M. C., Kodavanti, U. P., Evansky, P. A., Costa, D. L., and Watkinson, W. P.: Cardiovascular and thermoregulatory effects of inhaled PM-associated transition metals: a potential interaction between nickel and vanadium sulfate, *Toxicol. Sci.*, 64, 243–252, <https://doi.org/10.1093/toxsci/64.2.243>, 2001.
- Carletti, E., Colletier, J.-P., Schopfer, L. M., Santoni, G., Masson, P., Lockridge, O., Nachon, F., and Weik, M.: Inhibition pathways of the potent organophosphate CBDP with cholinesterases revealed by X-ray crystallographic snapshots and mass spectrometry, *Chemical research in toxicology*, 26, 280–289, <https://doi.org/10.1021/tx3004505>, 2013.
- Cena, L. G., Chisholm, W. P., Keane, M. J., Cumpston, A., and Chen, B. T.: Size Distribution and Estimated Respiratory Deposition of Total Chromium, Hexavalent Chromium, Manganese, and Nickel in Gas Metal Arc Welding Fume Aerosols, *Aerosol Sci. Technol.*, 48, 1254–1263, <https://doi.org/10.1080/02786826.2014.980883>, 2014.
- Centers, P. W.: Potential neurotoxin formation in thermally degraded synthetic ester turbine lubricants, *Arch. Toxicol.*, 66, 679–680, <https://doi.org/10.1007/BF01981509>, 1992.
- Chalupa, D. C., Morrow, P. E., Oberdörster, G., Utell, M. J., and Frampton, M. W.: Ultrafine particle deposition in subjects with asthma, *Environ. Health Persp.*, 112, 879–882, <https://doi.org/10.1289/ehp.6851>, 2004.
- Chang, Y., Cui, H., Jiang, X., and Li, M.: Comparative assessment of neurotoxicity impacts induced by alkyl tri-n-butyl phosphate and aromatic tricresyl phosphate in PC12 cells, *Environ. Toxicol.*, <https://doi.org/10.1002/tox.22997>, 2020.
- Chatkin, J., Correa, L., and Santos, U.: External Environmental Pollution as a Risk Factor for Asthma, *Clinical reviews in allergy & immunology*, <https://doi.org/10.1007/s12016-020-08830-5>, 2021.
- Chen, C., Yao, M., Luo, X., Zhu, Y., Liu, Z., Zhuo, H., and Zhao, B.: Outdoor-to-indoor transport of ultrafine particles: Measurement and model development of infiltration factor, *Environ. Pollut.*, 267, 115402, <https://doi.org/10.1016/j.envpol.2020.115402>, 2020.
- Chen, G., Zhang, S., Jin, Y., Wu, Y., Liu, L., Qian, H., and Fu, Z.: TPP and TCEP induce oxidative stress and alter steroidogenesis in TM3 Leydig cells, *Reproductive toxicology (Elmsford, N.Y.)*, 57, 100–110, <https://doi.org/10.1016/j.reprotox.2015.05.011>, 2015.
- Costa, D. L. and Dreher, K. L.: Bioavailable Transition Metals in Particulate Matter Mediate Cardiopulmonary Injury in Healthy and Compromised Animal Models, *Environ. Health Persp.*, 105, 1053, <https://doi.org/10.2307/3433509>, 1997.
- Cronin, M. T. and Schultz, T. W.: Structure-toxicity relationships for three mechanisms of action of toxicity to *Vibrio fischeri*, *Ecotoxicology and Environmental Safety*, 39, 65–69, <https://doi.org/10.1006/eesa.1997.1618>, 1998.
- Daellenbach, K. R., Uzu, G., Jiang, J., Cassagnes, L.-E., Leni, Z., Vlachou, A., Stefenelli, G., Canonaco, F., Weber, S., Segers, A., Kuenen, J. J. P., Schaap, M., Favez, O., Albinet, A.,

- Aksoyoglu, S., Dommen, J., Baltensperger, U., Geiser, M., El Haddad, I., Jaffrezou, J.-L., and Prévôt, A. S. H.: Sources of particulate-matter air pollution and its oxidative potential in Europe, *Nature*, 587, 414–419, <https://doi.org/10.1038/s41586-020-2902-8>, 2020.
- Daellenbach, K. R., Kourtchev, I., Vogel, A. L., Bruns, E. A., Jiang, J., Petäjä, T., Jaffrezou, J.-L., Aksoyoglu, S., Kalberer, M., Baltensperger, U., El Haddad, I., and Prévôt, A. S. H.: Impact of anthropogenic and biogenic sources on the seasonal variation in the molecular composition of urban organic aerosols: a field and laboratory study using ultra-high-resolution mass spectrometry, *Atmos. Chem. Phys.*, 19, 5973–5991, <https://doi.org/10.5194/acp-19-5973-2019>, 2019.
- Daigle, C. C., Chalupa, D. C., Gibb, F. R., Morrow, P. E., Oberdörster, G., Utell, M. J., and Frampton, M. W.: Ultrafine particle deposition in humans during rest and exercise, *Inhalation toxicology*, 15, 539–552, <https://doi.org/10.1080/08958370304468>, 2003.
- Delfino, R. J., Sioutas, C., and Malik, S.: Potential role of ultrafine particles in associations between airborne particle mass and cardiovascular health, *Environ. Health Persp.*, 113, 934–946, <https://doi.org/10.1289/ehp.7938>, 2005.
- Díaz-Robles, L. A., Fu, J. S., Vergara-Fernández, A., Etcharren, P., Schiappacasse, L. N., Reed, G. D., and Silva, M. P.: Health risks caused by short term exposure to ultrafine particles generated by residential wood combustion: a case study of Temuco, Chile, *Environ. Int.*, 66, 174–181, <https://doi.org/10.1016/j.envint.2014.01.017>, 2014.
- Ditas, F., Rose, D., and Jacobi, S.: 4. Bericht zur Untersuchung der regionalen Luftqualität auf ultrafeine Partikel im Bereich des Flughafens Frankfurt des Flughafens Frankfurt: Überblick über die bisherigen Messungen zu ultrafeinen Partikeln in der Region, Hessisches Landesamt für Naturschutz, Umwelt und Geologie, Wiesbaden, 40 pp., 2022.
- Donahue, N. M., Kroll, J. H., Pandis, S. N., and Robinson, A. L.: A two-dimensional volatility basis set – Part 2: Diagnostics of organic-aerosol evolution, *Atmos. Chem. Phys.*, 12, 615–634, <https://doi.org/10.5194/acp-12-615-2012>, 2012.
- Donahue, N. M., Epstein, S. A., Pandis, S. N., and Robinson, A. L.: A two-dimensional volatility basis set: 1. organic-aerosol mixing thermodynamics, *Atmos. Chem. Phys.*, 11, 3303–3318, <https://doi.org/10.5194/acp-11-3303-2011>, 2011.
- Donahue, N. M., Robinson, A. L., Stanier, C. O., and Pandis, S. N.: Coupled partitioning, dilution, and chemical aging of semivolatile organics, *Environ. Sci. Technol.*, 40, 2635–2643, <https://doi.org/10.1021/es052297c>, 2006.
- Donahue, N. M., Ortega, I. K., Chuang, W., Riipinen, I., Riccobono, F., Schobesberger, S., Dommen, J., Baltensperger, U., Kulmala, M., Worsnop, D. R., and Vehkamäki, H.: How do organic vapors contribute to new-particle formation?, *Faraday discussions*, 165, 91–104, <https://doi.org/10.1039/c3fd00046j>, 2013.
- Donaldson, K., Stone, V., Gilmour, P. S., Brown, D. M., and MacNee, W.: Ultrafine particles: mechanisms of lung injury, *Philosophical Transactions of the Royal Society of London. Series A: Mathematical, Physical and Engineering Sciences*, 358, 2741–2749, <https://doi.org/10.1098/rsta.2000.0681>, 2000.
- Donaldson, K., Brown, D., Clouter, A., Duffin, R., MacNee, W., Renwick, L., Tran, L., and Stone, V.: The pulmonary toxicology of ultrafine particles, *Journal of aerosol medicine the official journal of the International Society for Aerosols in Medicine*, 15, 213–220, <https://doi.org/10.1089/089426802320282338>, 2002.
- Du Han, H. and Masuko, M.: Elucidation of the Antiwear Performance of Several Organic Phosphates Used with Different Polyol Ester Base Oils from the Aspect of Interaction

- between Additive and Base Oil, *Tribol. T.*, 41, 600–604, <https://doi.org/10.1080/10402009808983788>, 1998.
- Duangkaewmanee, S. and Petsom, A.: Synergistic and antagonistic effects on oxidation stability of antioxidants in a synthetic ester based oil, *Tribol. Int.*, 44, 266–271, <https://doi.org/10.1016/j.triboint.2010.10.028>, 2011.
- Durdina, L., Brem, B. T., Abegglen, M., Lobo, P., Rindlisbacher, T., Thomson, K. A., Smallwood, G. J., Hagen, D. E., Sierau, B., and Wang, J.: Determination of PM mass emissions from an aircraft turbine engine using particle effective density, *Atmos. Environ.*, 99, 500–507, <https://doi.org/10.1016/j.atmosenv.2014.10.018>, 2014.
- E. Jenkin, M., Shallcross, D. E., and Harvey, J. N.: Development and application of a possible mechanism for the generation of cis-pinic acid from the ozonolysis of α - and β -pinene, *Atmos. Environ.*, 34, 2837–2850, [https://doi.org/10.1016/S1352-2310\(00\)00087-X](https://doi.org/10.1016/S1352-2310(00)00087-X), 2000.
- Eastwick, C. N., Simmons, K., Wang, Y., and Hibberd, S.: Study of aero-engine oil-air separators, *Proceedings of the Institution of Mechanical Engineers, Part A: Journal of Power and Energy*, 220, 707–717, <https://doi.org/10.1243/09576509JPE116>, 2006.
- EEA: Health impacts of air pollution in Europe, 2021, European Environment Agency, <https://www.eea.europa.eu/publications/health-risks-of-air-pollution/health-impacts-of-air-pollution>, last access: 15 November 2021, 2021.
- Ehrich, M., Jortner, B. S., and Padilla, S.: Relationship of neuropathy target esterase inhibition to neuropathology and ataxia in hens given organophosphorus esters, *Chem-Biol. Interact.*, 87, 431–437, [https://doi.org/10.1016/0009-2797\(93\)90071-6](https://doi.org/10.1016/0009-2797(93)90071-6), 1993.
- Eliuk, S. and Makarov, A.: Evolution of Orbitrap Mass Spectrometry Instrumentation, *Annual review of analytical chemistry (Palo Alto, Calif.)*, 8, 61–80, <https://doi.org/10.1146/annurev-anchem-071114-040325>, 2015.
- Ellison, S. L. R. and Thompson, M.: Standard additions: myth and reality, *The Analyst*, 133, 992–997, <https://doi.org/10.1039/b717660k>, 2008.
- Ellman, G. L., Courtney, K., Andres, V., and Featherstone, R. M.: A new and rapid colorimetric determination of acetylcholinesterase activity, *Biochemical Pharmacology*, 7, 88–95, [https://doi.org/10.1016/0006-2952\(61\)90145-9](https://doi.org/10.1016/0006-2952(61)90145-9), 1961.
- El-Sayed, A. F.: Aircraft propulsion and gas turbine engines, Second edition, CRC Press Taylor & Francis Group, Boca Raton, FL, 1447 pp., 2017.
- Epstein, S. A., Riipinen, I., and Donahue, N. M.: A semiempirical correlation between enthalpy of vaporization and saturation concentration for organic aerosol, *Environ. Sci. Technol.*, 44, 743–748, <https://doi.org/10.1021/es902497z>, 2010.
- Escher, B. I., Allinson, M., Altenburger, R., Bain, P. A., Balaguer, P., Busch, W., Crago, J., Denslow, N. D., Dopp, E., Hilscherova, K., Humpage, A. R., Kumar, A., Grimaldi, M., Jayasinghe, B. S., Jarosova, B., Jia, A., Makarov, S., Maruya, K. A., Medvedev, A., Mehinto, A. C., Mendez, J. E., Poulsen, A., Prochazka, E., Richard, J., Schifferli, A., Schlenk, D., Scholz, S., Shiraishi, F., Snyder, S., Su, G., Tang, J. Y. M., van der Burg, B., van der Linden, S. C., Werner, I., Westerheide, S. D., Wong, C. K. C., Yang, M., Yeung, B. H. Y., Zhang, X., and Leusch, F. D. L.: Benchmarking organic micropollutants in wastewater, recycled water and drinking water with in vitro bioassays, *Environ. Sci. Technol.*, 48, 1940–1956, <https://doi.org/10.1021/es403899t>, 2014.
- Escher, B. I., Bramaz, N., Quayle, P., Rutishauser, S., and Vermeirssen, E. L. M.: Monitoring of the ecotoxicological hazard potential by polar organic micropollutants in sewage treatment plants and surface waters using a mode-of-action based test battery, *J. Environ. Monit.*, 10, 622–631, <https://doi.org/10.1039/b800951a>, 2008.

- Eto, M., Casida, J. E., and Eto, T.: Hydroxylation and cyclization reactions involved in the metabolism of tri-O-cresyl phosphate, *Biochemical Pharmacology*, 11, 337–352, [https://doi.org/10.1016/0006-2952\(62\)90056-4](https://doi.org/10.1016/0006-2952(62)90056-4), 1962.
- Ettre, L. S. and Sakodinskii, K. I.: M. S. Tswett and the discovery of chromatography I: Early work (1899–1903), *Chromatographia*, 35, 223–231, <https://doi.org/10.1007/BF02269707>, 1993.
- Eurocontrol: Charting the European Aviation recovery: 2021 COVID-19 impacts and 2022 outlook: Think Paper #15 – 1 January 2022, Brussels, 22 pp., 2022.
- Eurocontrol: Forecast Update 2021-2027 European Flight Movements and Service Units: Three Scenarios for Recovery from COVID-19, Brussels, 16 pp., 2021a.
- Eurocontrol: What COVID-19 did to European Aviation in 2020, and Outlook 2021: Think Paper #8 – 1 January 2021, Brussels, 12 pp., 2021b.
- Eurocontrol: European Aviation in 2040: Challenges of Growth, Annex1 Flight Forecast to 2040, European Organisation for the Safety of Air Navigation, 92 pp., 2018.
- Eyer, P.: Neuropsychopathological changes by organophosphorus compounds--a review, *Hum. Exp. Toxicol.*, 14, 857–864, <https://doi.org/10.1177/096032719501401101>, 1995.
- Felitsyn, N., Peschke, M., and Kebarle, P.: Origin and number of charges observed on multiply-protonated native proteins produced by ESI, *International Journal of Mass Spectrometry*, 219, 39–62, [https://doi.org/10.1016/S1387-3806\(02\)00588-2](https://doi.org/10.1016/S1387-3806(02)00588-2), 2002.
- Focsa, C., Duca, D., Noble, J. A., Vojkovic, M., Carpentier, Y., Pirim, C., Betrancourt, C., Desgroux, P., Tritscher, T., Spielvogel, J., Rahman, M., Boies, A., Lee, K. F., Bhave, A. N., Legendre, S., Lancry, O., Kreutziger, P., and Rieker, M.: Multi-technique physico-chemical characterization of particles generated by a gasoline engine: Towards measuring tailpipe emissions below 23 nm, *Atmos. Environ.*, 235, 117642, <https://doi.org/10.1016/j.atmosenv.2020.117642>, 2020.
- Fort, K. L., van de Waterbeemd, M., Boll, D., Reinhardt-Szyba, M., Belov, M. E., Sasaki, E., Zschoche, R., Hilvert, D., Makarov, A. A., and Heck, A. J. R.: Expanding the structural analysis capabilities on an Orbitrap-based mass spectrometer for large macromolecular complexes, *The Analyst*, 143, 100–105, <https://doi.org/10.1039/c7an01629h>, 2017.
- Fraport AG: Fraport-Verkehrszahlen 2019: Über 70,5 Millionen Passagiere am Flughafen Frankfurt, last access: 14 January 2021, 2020.
- Freudenthal, R. I., Rausch, L., Gerhart, J. M., Barth, M. L., Mackerer, C. R., and Bisinger, E. C.: Subchronic Neurotoxicity of Oil Formulations Containing Either Tricresyl Phosphate or Tri-Orthocresyl Phosphate, *J. Am. Coll. Toxicol.*, 12, 409–416, <https://doi.org/10.1177/109158189301200410>, 1993.
- Fröhlich-Nowoisky, J., Kampf, C. J., Weber, B., Huffman, J. A., Pöhlker, C., Andreae, M. O., Lang-Yona, N., Burrows, S. M., Gunthe, S. S., Elbert, W., Su, H., Hoor, P., Thines, E., Hoffmann, T., Després, V. R., and Pöschl, U.: Bioaerosols in the Earth system: Climate, health, and ecosystem interactions, *Atmospheric Research*, 182, 346–376, <https://doi.org/10.1016/j.atmosres.2016.07.018>, 2016.
- Fujitani, Y., Takahashi, K., Saitoh, K., Fushimi, A., Hasegawa, S., Kondo, Y., Tanabe, K., Takami, A., and Kobayashi, S.: Contribution of industrial and traffic emissions to ultrafine, fine, coarse particles in the vicinity of industrial areas in Japan, *Environmental Advances*, 5, 100101, <https://doi.org/10.1016/j.envadv.2021.100101>, 2021.
- Fushimi, A., Saitoh, K., Fujitani, Y., and Takegawa, N.: Identification of jet lubrication oil as a major component of aircraft exhaust nanoparticles, *Atmos. Chem. Phys.*, 19, 6389–6399, <https://doi.org/10.5194/acp-19-6389-2019>, 2019.

- Givehchi, R. and Tan, Z.: An Overview of Airborne Nanoparticle Filtration and Thermal Rebound Theory, *Aerosol Air Qual. Res.*, 14, 46–63, <https://doi.org/10.4209/aaqr.2013.07.0239>, 2014.
- Glish, G. L.: Multiple stage mass spectrometry: the next generation tandem mass spectrometry experiment, *The Analyst*, 119, 533, <https://doi.org/10.1039/an9941900533>, 1994.
- Glish, G. L. and Vachet, R. W.: The basics of mass spectrometry in the twenty-first century, *Nature reviews. Drug discovery*, 2, 140–150, <https://doi.org/10.1038/nrd1011>, 2003.
- Gross, J. H. and Roepstorff, P.: *Mass Spectrometry: A Textbook*, 2. 2nd ed. 2011, Springer Berlin Heidelberg, Berlin, Heidelberg, 753 pp., 2011.
- Habre, R., Zhou, H., Eckel, S. P., Enebish, T., Fruin, S., Bastain, T., Rappaport, E., and Gilliland, F.: Short-term effects of airport-associated ultrafine particle exposure on lung function and inflammation in adults with asthma, *Environ. Int.*, 118, 48–59, <https://doi.org/10.1016/j.envint.2018.05.031>, 2018.
- Hageman, G., Mackenzie Ross, S. J., Nihom, J., and van der Laan, G.: Aerotoxic syndrome: A new occupational disease caused by contaminated cabin air?, in: *Occupational Neurotoxicology*, edited by: Aschner, M., Elsevier Science & Technology, San Diego, 77–132, <https://doi.org/10.1016/bs.ant.2022.04.001>, 2022.
- Hallquist, M., Wenger, J. C., Baltensperger, U., Rudich, Y., Simpson, D., Claeys, M., Dommen, J., Donahue, N. M., George, C., Goldstein, A. H., Hamilton, J. F., Herrmann, H., Hoffmann, T., Iinuma, Y., Jang, M., Jenkin, M. E., Jimenez, J. L., Kiendler-Scharr, A., Maenhaut, W., McFiggans, G., Mentel, T. F., Monod, A., Prévôt, A. S. H., Seinfeld, J. H., Surratt, J. D., Szmigielski, R., and Wildt, J.: The formation, properties and impact of secondary organic aerosol: current and emerging issues, *Atmos. Chem. Phys.*, 9, 5155–5236, <https://doi.org/10.5194/acp-9-5155-2009>, 2009.
- Hanhela, P. J., Kibby, J., DeNola, G., and Mazurek, W.: Organophosphate and Amine Contamination of Cockpit Air in the Hawk, F-111 and Hercules C-130 Aircraft, Maritime Platforms Division Platforms Sciences Laboratory, 506 Lorimer St Fishermans Bend, Victoria 3207 Australia, 31 pp., 2005.
- Hardman, M. and Makarov, A. A.: Interfacing the orbitrap mass analyzer to an electrospray ion source, *Anal. Chem.*, 75, 1699–1705, <https://doi.org/10.1021/ac0258047>, 2003.
- Haywood, J. and Boucher, O.: Estimates of the direct and indirect radiative forcing due to tropospheric aerosols: A review, *Rev. Geophys.*, 38, 513–543, <https://doi.org/10.1029/1999RG000078>, 2000.
- He, R.-W., Gerlofs-Nijland, M. E., Boere, J., Fokkens, P., Leseman, D., Janssen, N. A. H., and Cassee, F. R.: Comparative toxicity of ultrafine particles around a major airport in human bronchial epithelial (Calu-3) cell model at the air-liquid interface, *Toxicology in vitro an international journal published in association with BIBRA*, 68, 104950, <https://doi.org/10.1016/j.tiv.2020.104950>, 2020.
- Heald, C. L. and Spracklen, D. V.: Land use change impacts on air quality and climate, *Chemical reviews*, 115, 4476–4496, <https://doi.org/10.1021/cr500446g>, 2015.
- Hecht, E. S., Eliuk, S., Scigelova, M., and Makarov, A.: Fundamentals and Advances of Orbitrap Mass Spectrometry, *Encyclopedia of Analytical Chemistry* 2019, 1–40, <https://doi.org/10.1002/9780470027318.a9309.pub2>, 2019.
- Hermann, M., Wehner, B., Bischof, O., Han, H.-S., Krinke, T., Liu, W., Zerrath, A., and Wiedensohler, A.: Particle counting efficiencies of new TSI condensation particle

- counters, *J. Aerosol Sci.*, 38, 674–682, <https://doi.org/10.1016/j.jaerosci.2007.05.001>, 2007.
- Hermens, J., Busser, F., Leeuwangh, P., and Musch, A.: Quantitative structure-activity relationships and mixture toxicity of organic chemicals in *Photobacterium phosphoreum*: The microtox test, *Ecotoxicology and Environmental Safety*, 9, 17–25, [https://doi.org/10.1016/0147-6513\(85\)90030-2](https://doi.org/10.1016/0147-6513(85)90030-2), 1985.
- Herndon, S. C., Jayne, J. T., Lobo, P., Onasch, T. B., Fleming, G., Hagen, D. E., Whitefield, P. D., and Miake-Lye, R. C.: Commercial aircraft engine emissions characterization of in-use aircraft at Hartsfield-Jackson Atlanta International Airport, *Environ. Sci. Technol.*, 42, 1877–1883, <https://doi.org/10.1021/es072029>, 2008.
- HLNUG: Measurement Data Portal [WWW Document], <https://www.hlnug.de/messwerte/datenportal/messstelle/2/1/0619>, last access: 25 August 2022, 2019.
- Hoffmann, T., Huang, R.-J., and Kalberer, M.: Atmospheric analytical chemistry, *Anal. Chem.*, 83, 4649–4664, <https://doi.org/10.1021/ac2010718>, 2011.
- Hsu, H.-H., Adamkiewicz, G., Houseman, E. A., Zarubiak, D., Spengler, J. D., and Levy, J. I.: Contributions of aircraft arrivals and departures to ultrafine particle counts near Los Angeles International Airport, *Sci. Total Environ.*, 444, 347–355, <https://doi.org/10.1016/j.scitotenv.2012.12.010>, 2013.
- Hsu, H.-H., Adamkiewicz, G., Andres Houseman, E., Vallarino, J., Melly, S. J., Wayson, R. L., Spengler, J. D., and Levy, J. I.: The relationship between aviation activities and ultrafine particulate matter concentrations near a mid-sized airport, *Atmos. Environ.*, 50, 328–337, <https://doi.org/10.1016/j.atmosenv.2011.12.002>, 2012.
- Hu, S., Fruin, S., Kozawa, K., Mara, S., Winer, A. M., and Paulson, S. E.: Aircraft emission impacts in a neighborhood adjacent to a general aviation airport in southern California, *Environ. Sci. Technol.*, 43, 8039–8045, <https://doi.org/10.1021/es900975f>, 2009.
- Hudda, N. and Fruin, S. A.: International Airport Impacts to Air Quality: Size and Related Properties of Large Increases in Ultrafine Particle Number Concentrations, *Environ. Sci. Technol.*, 50, 3362–3370, <https://doi.org/10.1021/acs.est.5b05313>, 2016.
- Hudda, N., Simon, M. C., Zamore, W., and Durant, J. L.: Aviation-Related Impacts on Ultrafine Particle Number Concentrations Outside and Inside Residences near an Airport, *Environ. Sci. Technol.*, 52, 1765–1772, <https://doi.org/10.1021/acs.est.7b05593>, 2018.
- Hudda, N., Durant, L. W., Fruin, S. A., and Durant, J. L.: Impacts of Aviation Emissions on Near-Airport Residential Air Quality, *Environ. Sci. Technol.*, 54, 8580–8588, <https://doi.org/10.1021/acs.est.0c01859>, 2020.
- Hudda, N., Gould, T., Hartin, K., Larson, T. V., and Fruin, S. A.: Emissions from an international airport increase particle number concentrations 4-fold at 10 km downwind, *Environ. Sci. Technol.*, 48, 6628–6635, <https://doi.org/10.1021/es5001566>, 2014.
- Ikonomou, M. G., Blades, A. T., and Kebarle, P.: Electrospray-ion spray: a comparison of mechanisms and performance, *Anal. Chem.*, 63, 1989–1998, <https://doi.org/10.1021/ac00018a017>, 1991.
- International Civil Aviation Organization: Environmental Report Aviation And Environment: Destination Green The Next Chapter, International Civil Aviation Organization, Montreal, QC, Canada, 2019.
- IPCC: Technical Summary. In *Climate Change 2021: The Physical Science Basis: Contribution of Working Group I to the Sixth Assessment Report of the Intergovernmental Panel on Climate Change*, Masson-Delmotte, V., P. Zhai, A. Pirani, S.L. Connors, C.

- Péan, S. Berger, N. Caud, Y. Chen, L. Goldfarb, M.I. Gomis, M. Huang, K. Leitzell, E. Lonnoy, J.B.R. Matthews, T.K. Maycock, T. Waterfield, O. Yelekçi, R. Yu, and B. Zhou (eds.), Cambridge University Press, Cambridge, United Kingdom and New York, NY, USA, 33–144, 2021.
- Iribarne, J. V.: On the evaporation of small ions from charged droplets, *J. Chem. Phys.*, 64, 2287, <https://doi.org/10.1063/1.432536>, 1976.
- ISO 11348-3:2007: Water Quality - Determination of the Inhibitory Effect of Water, International Organization for Standardization (ISO), Geneva, Switzerland, 2007.
- Jacobson, M. C., Hansson, H.-C., Noone, K. J., and Charlson, R. J.: Organic atmospheric aerosols: Review and state of the science, *Rev. Geophys.*, 38, 267–294, <https://doi.org/10.1029/1998RG000045>, 2000.
- Jaques, P. A. and Kim, C. S.: Measurement of total lung deposition of inhaled ultrafine particles in healthy men and women, *Inhalation toxicology*, 12, 715–731, <https://doi.org/10.1080/08958370050085156>, 2000.
- Ji, X., Li, N., Ma, M., Rao, K., Yang, R., and Wang, Z.: Tricresyl phosphate isomers exert estrogenic effects via G protein-coupled estrogen receptor-mediated pathways, *Environ. Pollut.*, 264, 114747, <https://doi.org/10.1016/j.envpol.2020.114747>, 2020.
- Jimenez, J. L., Canagaratna, M. R., Donahue, N. M., Prevot, A. S. H., Zhang, Q., Kroll, J. H., DeCarlo, P. F., Allan, J. D., Coe, H., Ng, N. L., Aiken, A. C., Docherty, K. S., Ulbrich, I. M., Grieshop, A. P., Robinson, A. L., Duplissy, J., Smith, J. D., Wilson, K. R., Lanz, V. A., Hueglin, C., Sun, Y. L., Tian, J., Laaksonen, A., Raatikainen, T., Rautiainen, J., Vaattovaara, P., Ehn, M., Kulmala, M., Tomlinson, J. M., Collins, D. R., Cubison, M. J., Dunlea, E. J., Huffman, J. A., Onasch, T. B., Alfarra, M. R., Williams, P. I., Bower, K., Kondo, Y., Schneider, J., Drewnick, F., Borrmann, S., Weimer, S., Demerjian, K., Salcedo, D., Cottrell, L., Griffin, R., Takami, A., Miyoshi, T., Hatakeyama, S., Shimojo, A., Sun, J. Y., Zhang, Y. M., Dzepina, K., Kimmel, J. R., Sueper, D., Jayne, J. T., Herndon, S. C., Trimborn, A. M., Williams, L. R., Wood, E. C., Middlebrook, A. M., Kolb, C. E., Baltensperger, U., and Worsnop, D. R.: Evolution of organic aerosols in the atmosphere, *Science (New York, N.Y.)*, 326, 1525–1529, <https://doi.org/10.1126/science.1180353>, 2009.
- Jonsdottir, H. R., Delaval, M., Leni, Z., Keller, A., Brem, B. T., Siegerist, F., Schönenberger, D., Durdina, L., Elser, M., Burtscher, H., Liati, A., and Geiser, M.: Non-volatile particle emissions from aircraft turbine engines at ground-idle induce oxidative stress in bronchial cells, *Commun. Biol.*, 2, 90, <https://doi.org/10.1038/s42003-019-0332-7>, 2019.
- Junkermann, W. and Hacker, J. M.: Ultrafine Particles in the Lower Troposphere: Major Sources, Invisible Plumes, and Meteorological Transport Processes, *Bull. Amer. Meteor. Soc.*, 99, 2587–2602, <https://doi.org/10.1175/BAMS-D-18-0075.1>, 2018.
- Kahnt, A., Iinuma, Y., Mutzel, A., Böge, O., Claeys, M., and Herrmann, H.: Campholenic aldehyde ozonolysis: a mechanism leading to specific biogenic secondary organic aerosol constituents, *Atmos. Chem. Phys.*, 14, 719–736, <https://doi.org/10.5194/acp-14-719-2014>, 2014.
- Kanninen, K. M., Lampinen, R., Rantanen, L. M., Odendaal, L., Jalava, P., Chew, S., and White, A. R.: Olfactory cell cultures to investigate health effects of air pollution exposure: Implications for neurodegeneration, *Neurochemistry international*, 136, 104729, <https://doi.org/10.1016/j.neuint.2020.104729>, 2020.
- Kärcher, B.: Formation and radiative forcing of contrail cirrus, *Nature communications*, 9, 1824, <https://doi.org/10.1038/s41467-018-04068-0>, 2018.

- Kautzman, K. E., Surratt, J. D., Chan, M. N., Chan, A. W. H., Hersey, S. P., Chhabra, P. S., Dalleska, N. F., Wennberg, P. O., Flagan, R. C., and Seinfeld, J. H.: Chemical composition of gas- and aerosol-phase products from the photooxidation of naphthalene, *The journal of physical chemistry. A*, 114, 913–934, <https://doi.org/10.1021/jp908530s>, 2010.
- Kebarle, P.: A brief overview of the present status of the mechanisms involved in electrospray mass spectrometry, *J. Mass Spectrom.*, 35, 804–817, [https://doi.org/10.1002/1096-9888\(200007\)35:7<804:AID-JMS22>3.0.CO;2-Q](https://doi.org/10.1002/1096-9888(200007)35:7<804:AID-JMS22>3.0.CO;2-Q), 2000.
- Kendrick, E.: A Mass Scale Based on CH₂ = 14.0000 for High Resolution Mass Spectrometry of Organic Compounds, *Anal. Chem.*, 35, 2146–2154, <https://doi.org/10.1021/ac60206a048>, 1963.
- Keuken, M. P., Moerman, M., Zandveld, P., Henzing, J. S., and Hoek, G.: Total and size-resolved particle number and black carbon concentrations in urban areas near Schiphol airport (the Netherlands), *Atmos. Environ.*, 104, 132–142, <https://doi.org/10.1016/j.atmosenv.2015.01.015>, 2015.
- Kılıç, D., El Haddad, I., Brem, B. T., Bruns, E., Bozetti, C., Corbin, J., Durdina, L., Huang, R.-J., Jiang, J., Klein, F., Lavi, A., Pieber, S. M., Rindlisbacher, T., Rudich, Y., Slowik, J. G., Wang, J., Baltensperger, U., and Prévôt, A. S. H.: Identification of secondary aerosol precursors emitted by an aircraft turbofan, *Atmos. Chem. Phys.*, 18, 7379–7391, <https://doi.org/10.5194/acp-18-7379-2018>, 2018.
- Kim, B.-G., Park, M.-K., Lee, P.-H., Lee, S.-H., Hong, J., Aung, M. M. M., Moe, K. T., Han, N. Y., and Jang, A.-S.: Effects of nanoparticles on neuroinflammation in a mouse model of asthma, *Respiratory physiology & neurobiology*, 271, 103292, <https://doi.org/10.1016/j.resp.2019.103292>, 2020.
- Kim, C. S. and Jaques, P. A.: Respiratory dose of inhaled ultrafine particles in healthy adults, *Philosophical Transactions of the Royal Society of London. Series A: Mathematical, Physical and Engineering Sciences*, 358, 2693–2705, <https://doi.org/10.1098/rsta.2000.0678>, 2000.
- Kim, S. C., Harrington, M. S., and Pui, D. Y. H.: Experimental study of nanoparticles penetration through commercial filter media, *J Nanopart Res*, 9, 117–125, <https://doi.org/10.1007/s11051-006-9176-4>, 2006.
- Kingdon, K. H.: A Method for the Neutralization of Electron Space Charge by Positive Ionization at Very Low Gas Pressures, *Phys. Rev.*, 21, 408–418, <https://doi.org/10.1103/PhysRev.21.408>, 1923.
- Kitanovski, Z., Grgić, I., Vermeulen, R., Claeys, M., and Maenhaut, W.: Liquid chromatography tandem mass spectrometry method for characterization of monoaromatic nitro-compounds in atmospheric particulate matter, *J. Chromatogr. A*, 1268, 35–43, <https://doi.org/10.1016/j.chroma.2012.10.021>, available at: <https://www.sciencedirect.com/science/article/pii/S0021967312015762>, 2012.
- Knight, R. D.: Storage of ions from laser-produced plasmas, *Appl. Phys. Lett.*, 38, 221–223, <https://doi.org/10.1063/1.92315>, 1981.
- Kolossa-Gehring, M., Becker, K., Conrad, A., Schröter-Kermani, C., Schulz, C., and Seiwert, M.: Chapter 2A. Health-related Environmental Monitoring in Germany: German Environmental Survey (GerES) and Environmental Specimen Bank (ESB), in: *Biomarkers and human biomonitoring: Volume 1*, edited by: Knudsen, L. and Merlo, D. F., Royal Society of Chemistry, Cambridge, 16–45, <https://doi.org/10.1039/9781849733373-00016>, 2011.

- Kroll, J. H., Donahue, N. M., Jimenez, J. L., Kessler, S. H., Canagaratna, M. R., Wilson, K. R., Altieri, K. E., Mazzoleni, L. R., Wozniak, A. S., Bluhm, H., Mysak, E. R., Smith, J. D., Kolb, C. E., and Worsnop, D. R.: Carbon oxidation state as a metric for describing the chemistry of atmospheric organic aerosol, *Nat. Chem.*, 3, 133–139, <https://doi.org/10.1038/nchem.948>, 2011.
- Kromidas, S. (Ed.): *The HPLC-MS Handbook for Practitioners*, Wiley-VCH Verlag GmbH & Co. KGaA, Weinheim, 260 pp., 2017.
- Kulkarni, P.: *Aerosol Measurement: Principles, Techniques, and Applications*, 3rd ed., John Wiley & Sons Incorporated, Hoboken, 904 pp., 2011.
- Kumar, P., Morawska, L., Birmili, W., Paasonen, P., Hu, M., Kulmala, M., Harrison, R. M., Norford, L., and Britter, R.: Ultrafine particles in cities, *Environ. Int.*, 66, 1–10, <https://doi.org/10.1016/j.envint.2014.01.013>, 2014.
- Lammers, A., Janssen, N. A. H., Boere, A. J. F., Berger, M., Longo, C., Vijverberg, S. J. H., Neerincx, A. H., Maitland-van der Zee, A. H., and Cassee, F. R.: Effects of short-term exposures to ultrafine particles near an airport in healthy subjects, *Environ. Int.*, 141, 105779, <https://doi.org/10.1016/j.envint.2020.105779>, 2020.
- Laskin, J., Laskin, A., and Nizkorodov, S. A.: Mass Spectrometry Analysis in Atmospheric Chemistry, *Anal. Chem.*, 90, 166–189, <https://doi.org/10.1021/acs.analchem.7b04249>, 2018.
- Lee, D. S., Pitari, G., Grewe, V., Gierens, K., Penner, J. E., Petzold, A., Prather, M. J., Schumann, U., Bais, A., Berntsen, T., Iachetti, D., Lim, L. L., and Sausen, R.: Transport impacts on atmosphere and climate: Aviation, *Atmos. Environ.*, 44, 4678–4734, <https://doi.org/10.1016/j.atmosenv.2009.06.005>, 2010.
- Lee, D. S., Fahey, D. W., Forster, P. M., Newton, P. J., Wit, R. C. N., Lim, L. L., Owen, B., and Sausen, R.: Aviation and global climate change in the 21st century, *Atmos. Environ.*, 43, 3520–3537, <https://doi.org/10.1016/j.atmosenv.2009.04.024>, 2009.
- Leikauf, G. D., Kim, S.-H., and Jang, A.-S.: Mechanisms of ultrafine particle-induced respiratory health effects, *Exp. Mol. Med.*, 52, 329–337, <https://doi.org/10.1038/s12276-020-0394-0>, 2020.
- Lelieveld, J., Klingmüller, K., Pozzer, A., Pöschl, U., Fnais, M., Daiber, A., and Münzel, T.: Cardiovascular disease burden from ambient air pollution in Europe reassessed using novel hazard ratio functions, *European Heart Journal*, 40, 1590–1596, <https://doi.org/10.1093/eurheartj/ehz135>, 2019.
- Lewis Sr., R. J., Larrañaga, M. D., and Lewis, R. A.: *Hawley's Condensed Chemical Dictionary*, John Wiley & Sons, Incorporated, Hoboken, UNITED STATES, 2016.
- Li, N., Sioutas, C., Cho, A., Schmitz, D., Misra, C., Sempf, J., Wang, M., Oberley, T., Froines, J., and Nel, A.: Ultrafine particulate pollutants induce oxidative stress and mitochondrial damage, *Environ. Health Persp.*, 111, 455–460, <https://doi.org/10.1289/ehp.6000>, 2003.
- Lin, P., Rincon, A. G., Kalberer, M., and Yu, J. Z.: Elemental composition of HULIS in the Pearl River Delta Region, China: results inferred from positive and negative electrospray high resolution mass spectrometric data, *Environ. Sci. Technol.*, 46, 7454–7462, <https://doi.org/10.1021/es300285d>, 2012.
- Liu, Y., Yan, C., Feng, Z., Zheng, F., Fan, X., Zhang, Y., Li, C., Zhou, Y., Lin, Z., Guo, Y., Zhang, Y., Ma, L., Zhou, W., Liu, Z., Dada, L., Dällenbach, K., Kontkanen, J., Cai, R., Chan, T., Chu, B., Du, W., Yao, L., Wang, Y., Cai, J., Kangasluoma, J., Kokkonen, T., Kujansuu, J., Rusanen, A., Deng, C., Fu, Y., Yin, R., Li, X., Lu, Y., Liu, Y., Lian, C.,

- Yang, D., Wang, W., Ge, M., Wang, Y., Worsnop, D. R., Junninen, H., He, H., Kerminen, V.-M., Zheng, J., Wang, L., Jiang, J., Petäjä, T., Bianchi, F., and Kulmala, M.: Continuous and comprehensive atmospheric observations in Beijing: a station to understand the complex urban atmospheric environment, *Big Earth Data*, 4, 295–321, <https://doi.org/10.1080/20964471.2020.1798707>, 2020.
- Lobo, P., Durdina, L., Smallwood, G. J., Rindlisbacher, T., Siegerist, F., Black, E. A., Yu, Z., Mensah, A. A., Hagen, D. E., Miake-Lye, R. C., Thomson, K. A., Brem, B. T., Corbin, J. C., Abegglen, M., Sierau, B., Whitefield, P. D., and Wang, J.: Measurement of Aircraft Engine Non-Volatile PM Emissions: Results of the Aviation-Particle Regulatory Instrumentation Demonstration Experiment (A-PRIDE) 4 Campaign, *Aerosol Sci. Technol.*, 49, 472–484, <https://doi.org/10.1080/02786826.2015.1047012>, 2015.
- Lu, D., Luo, Q., Chen, R., Zhuansun, Y., Jiang, J., Wang, W., Yang, X., Zhang, L., Liu, X., Li, F., Liu, Q., and Jiang, G.: Chemical multi-fingerprinting of exogenous ultrafine particles in human serum and pleural effusion, *Nature communications*, 11, 2567, <https://doi.org/10.1038/s41467-020-16427-x>, 2020.
- Ma, J., Ungeheuer, F., Zheng, F., Du, W., Wang, Y., Cai, J., Zhou, Y., Yan, C., Liu, Y., Kulmala, M., Daellenbach, K. R., and Vogel, A. L.: Nontarget Screening Exhibits a Seasonal Cycle of PM_{2.5} Organic Aerosol Composition in Beijing, *Environ. Sci. Technol.*, <https://doi.org/10.1021/acs.est.1c06905>, 2022.
- MacNee, W. and Donaldson, K.: Mechanism of lung injury caused by PM₁₀ and ultrafine particles with special reference to COPD, *The European respiratory journal. Supplement*, 40, 47s-51s, <https://doi.org/10.1183/09031936.03.00403203>, 2003.
- Makarov, A., Denisov, E., Kholomeev, A., Balschun, W., Lange, O., Strupat, K., and Horning, S.: Performance evaluation of a hybrid linear ion trap/orbitrap mass spectrometer, *Anal. Chem.*, 78, 2113–2120, <https://doi.org/10.1021/ac0518811>, 2006.
- Marklund, A., Andersson, B., and Haglund, P.: Traffic as a source of organophosphorus flame retardants and plasticizers in snow, *Environ. Sci. Technol.*, 39, 3555–3562, <https://doi.org/10.1021/es0482177>, 2005.
- Marple, V. A., Rubow, K. L., and Behm, S. M.: A Microorifice Uniform Deposit Impactor (MOUDI): Description, Calibration, and Use, *Aerosol Sci. Technol.*, 14, 434–446, <https://doi.org/10.1080/02786829108959504>, 1991.
- Martin, A. J. and Synge, R. L.: A new form of chromatogram employing two liquid phases: A theory of chromatography. 2. Application to the micro-determination of the higher monoamino-acids in proteins, *The Biochemical journal*, 35, 1358–1368, <https://doi.org/10.1042/bj0351358>, available at: <https://www.thermofisher.com/document-connect/document-connect.html?url=https://assets.thermofisher.com/TFS-Assets%2FCMD%2FSpecification-Sheets%2FPS-72075-LC-Vanquish-Binary-Pump-F-PS72075-EN.pdf>, 1941.
- Masiol, M. and Harrison, R. M.: Aircraft engine exhaust emissions and other airport-related contributions to ambient air pollution: A review, *Atmos. Environ.*, 95, 409–455, <https://doi.org/10.1016/j.atmosenv.2014.05.070>, 2014.
- Masiol, M., Harrison, R. M., Vu, T. V., and Beddows, D. C. S.: Sources of sub-micrometre particles near a major international airport, *Atmos. Chem. Phys.*, 17, 12379–12403, <https://doi.org/10.5194/acp-17-12379-2017>, 2017.
- Mattsson, H.: Bicyclic phosphates increase the cyclic GMP level in rat cerebellum, presumably due to reduced GABA inhibition, *Brain Res.*, 181, 175–184, [https://doi.org/10.1016/0006-8993\(80\)91267-6](https://doi.org/10.1016/0006-8993(80)91267-6), 1980.

- Mazaheri, M., Bostrom, T. E., Johnson, G. R., and Morawska, L.: Composition and morphology of particle emissions from in-use aircraft during takeoff and landing, *Environ. Sci. Technol.*, 47, 5235–5242, <https://doi.org/10.1021/es3046058>, 2013.
- McLuckey, S. A.: Principles of collisional activation in analytical mass spectrometry, *J. Am. Soc. Mass Spectrom.*, 3, 599–614, [https://doi.org/10.1016/1044-0305\(92\)85001-Z](https://doi.org/10.1016/1044-0305(92)85001-Z), 1992.
- Mei, F., Setyan, A., Zhang, Q., and Wang, J.: CCN activity of organic aerosols observed downwind of urban emissions during CARES, *Atmos. Chem. Phys.*, 13, 12155–12169, <https://doi.org/10.5194/acp-13-12155-2013>, 2013.
- Merzenich, H., Riccetti, N., Hoffmann, B., Blettner, M., Forastiere, F., and Gianicolo, E.: Air pollution and airport apron workers: A neglected occupational setting in epidemiological research, *International journal of hygiene and environmental health*, 231, 113649, <https://doi.org/10.1016/j.ijheh.2020.113649>, 2021.
- Michalski, A., Damoc, E., Hauschild, J.-P., Lange, O., Wieghaus, A., Makarov, A., Nagaraj, N., Cox, J., Mann, M., and Horning, S.: Mass spectrometry-based proteomics using Q Exactive, a high-performance benchtop quadrupole Orbitrap mass spectrometer, *Molecular & Cellular Proteomics MCP*, 10, M111.011015, <https://doi.org/10.1074/mcp.M111.011015>, 2011.
- Miller, M. R., Raftis, J. B., Langrish, J. P., McLean, S. G., Samutrtai, P., Connell, S. P., Wilson, S., Vesey, A. T., Fokkens, P. H. B., Boere, A. J. F., Krystek, P., Campbell, C. J., Hadoke, P. W. F., Donaldson, K., Cassee, F. R., Newby, D. E., Duffin, R., and Mills, N. L.: Inhaled Nanoparticles Accumulate at Sites of Vascular Disease, *ACS nano*, 11, 4542–4552, <https://doi.org/10.1021/acsnano.6b08551>, 2017.
- Mills, N. L., Donaldson, K., Hadoke, P. W., Boon, N. A., MacNee, W., Cassee, F. R., Sandström, T., Blomberg, A., and Newby, D. E.: Adverse cardiovascular effects of air pollution, *Nature clinical practice. Cardiovascular medicine*, 6, 36–44, <https://doi.org/10.1038/ncpcardio1399>, 2009.
- Moise, T., Flores, J. M., and Rudich, Y.: Optical properties of secondary organic aerosols and their changes by chemical processes, *Chemical reviews*, 115, 4400–4439, <https://doi.org/10.1021/cr5005259>, 2015.
- Møller, K. L., Brauer, C., Mikkelsen, S., Bonde, J. P., Loft, S., Helweg-Larsen, K., and Thygesen, L. C.: Cardiovascular disease and long-term occupational exposure to ultrafine particles: A cohort study of airport workers, *International journal of hygiene and environmental health*, 223, 214–219, <https://doi.org/10.1016/j.ijheh.2019.08.010>, 2020.
- Morawska, L., Ristovski, Z., Jayaratne, E. R., Keogh, D. U., and Ling, X.: Ambient nano and ultrafine particles from motor vehicle emissions: Characteristics, ambient processing and implications on human exposure, *Atmos. Environ.*, 42, 8113–8138, <https://doi.org/10.1016/j.atmosenv.2008.07.050>, 2008.
- Mordas, G., Manninen, H. E., Petäjä, T., Aalto, P. P., Hämeri, K., and Kulmala, M.: On Operation of the Ultra-Fine Water-Based CPC TSI 3786 and Comparison with Other TSI Models (TSI 3776, TSI 3772, TSI 3025, TSI 3010, TSI 3007), *Aerosol Sci. Technol.*, 42, 152–158, <https://doi.org/10.1080/02786820701846252>, 2008.
- Müller, L., Reinnig, M.-C., Naumann, K. H., Saathoff, H., Mentel, T. F., Donahue, N. M., and Hoffmann, T.: Formation of 3-methyl-1,2,3-butanetricarboxylic acid via gas phase oxidation of pinonic acid – a mass spectrometric study of SOA aging, *Atmos. Chem. Phys.*, 12, 1483–1496, <https://doi.org/10.5194/acp-12-1483-2012>, 2012.
- Nel, A., Xia, T., Mädler, L., and Li, N.: Toxic potential of materials at the nanolevel, *Science (New York, N.Y.)*, 311, 622–627, <https://doi.org/10.1126/science.1114397>, 2006.

- Newby, D. E., Mannucci, P. M., Tell, G. S., Baccarelli, A. A., Brook, R. D., Donaldson, K., Forastiere, F., Franchini, M., Franco, O. H., Graham, I., Hoek, G., Hoffmann, B., Hoylaerts, M. F., Künzli, N., Mills, N., Pekkanen, J., Peters, A., Piepoli, M. F., Rajagopalan, S., and Storey, R. F.: Expert position paper on air pollution and cardiovascular disease, *European Heart Journal*, 36, 83-93b, <https://doi.org/10.1093/eurheartj/ehu458>, 2015.
- Nguyen, H. P. and Schug, K. A.: The advantages of ESI-MS detection in conjunction with HILIC mode separations: Fundamentals and applications, *Journal of separation science*, 31, 1465–1480, <https://doi.org/10.1002/jssc.200700630>, 2008.
- Nola, G. de, Kibby, J., and Mazurek, W.: Determination of ortho-cresyl phosphate isomers of tricresyl phosphate used in aircraft turbine engine oils by gas chromatography and mass spectrometry, *J. Chromatogr. A*, 1200, 211–216, <https://doi.org/10.1016/j.chroma.2008.05.035>, 2008.
- Nolting, D., Malek, R., and Makarov, A.: Ion traps in modern mass spectrometry, *Mass spectrometry reviews*, 38, 150–168, <https://doi.org/10.1002/mas.21549>, 2019.
- Nozière, B., Kalberer, M., Claeys, M., Allan, J., D'Anna, B., Decesari, S., Finessi, E., Glasius, M., Grgić, I., Hamilton, J. F., Hoffmann, T., Iinuma, Y., Jaoui, M., Kahnt, A., Kampf, C. J., Kourtschev, I., Maenhaut, W., Marsden, N., Saarikoski, S., Schnelle-Kreis, J., Surratt, J. D., Szidat, S., Szmigielski, R., and Wisthaler, A.: The molecular identification of organic compounds in the atmosphere: state of the art and challenges, *Chemical reviews*, 115, 3919–3983, <https://doi.org/10.1021/cr5003485>, 2015.
- Oberdörster, G.: Pulmonary effects of inhaled ultrafine particles, *International archives of occupational and environmental health*, 74, 1–8, <https://doi.org/10.1007/s004200000185>, 2001.
- Oberdörster, G., Sharp, Z., Atudorei, V., Elder, A., Gelein, R., Kreyling, W., and Cox, C.: Translocation of inhaled ultrafine particles to the brain, *Inhalation toxicology*, 16, 437–445, <https://doi.org/10.1080/08958370490439597>, 2004.
- Oberdörster, G., Oberdörster, E., and Oberdörster, J.: Nanotoxicology: an emerging discipline evolving from studies of ultrafine particles, *Environ. Health. Persp.*, 113, 823–839, <https://doi.org/10.1289/ehp.7339>, 2005.
- Oberdörster, G., Sharp, Z., Atudorei, V., Elder, A., Gelein, R., Lunts, A., Kreyling, W., and Cox, C.: Extrapulmonary translocation of ultrafine carbon particles following whole-body inhalation exposure of rats, *Journal of Toxicology and Environmental Health, Part A*, 65, 1531–1543, <https://doi.org/10.1080/00984100290071658>, 2002.
- O'Callaghan, J. P.: Neurotoxic esterase: not so toxic?, *Nat. Genet.*, 33, 437–438, <https://doi.org/10.1038/ng1135>, 2003.
- Ohlwein, S., Kappeler, R., Kutlar Joss, M., Künzli, N., and Hoffmann, B.: Health effects of ultrafine particles: a systematic literature review update of epidemiological evidence, *International journal of public health*, 64, 547–559, <https://doi.org/10.1007/s00038-019-01202-7>, 2019.
- Olsen, J. V., Macek, B., Lange, O., Makarov, A., Horning, S., and Mann, M.: Higher-energy C-trap dissociation for peptide modification analysis, *Nature methods*, 4, 709–712, <https://doi.org/10.1038/nmeth1060>, 2007.
- Otto, M.: *Analytische Chemie*, 3., vollst. überarb. und erw. Aufl., Wiley-VCH, Weinheim, 733 pp., 2006.

- Paasonen, P., Kupiainen, K., Klimont, Z., Visschedijk, A., van der Denier Gon, H. A. C., and Amann, M.: Continental anthropogenic primary particle number emissions, *Atmos. Chem. Phys.*, 16, 6823–6840, <https://doi.org/10.5194/acp-16-6823-2016>, 2016.
- Pankow, J. F. and Asher, W. E.: SIMPOL.1: a simple group contribution method for predicting vapor pressures and enthalpies of vaporization of multifunctional organic compounds, *Atmos. Chem. Phys.*, 8, 2773–2796, <https://doi.org/10.5194/acp-8-2773-2008>, 2008.
- Pekkanen, J. and Kulmala, M.: Exposure assessment of ultrafine particles in epidemiologic time-series studies, *Scandinavian Journal of Work, Environment & Health*, 30 Suppl 2, 9–18, 2004.
- Penner, J. E. and Novakov, T.: Carbonaceous particles in the atmosphere: A historical perspective to the Fifth International Conference on Carbonaceous Particles in the Atmosphere, *J. Geophys. Res.*, 101, 19373–19378, <https://doi.org/10.1029/96JD01175>, 1996.
- Peters, A.: Ambient air pollution and Alzheimer's disease: the role of the composition of fine particles, *Proc Natl Acad Sci USA*, 120, e2220028120, <https://doi.org/10.1073/pnas.2220028120>, 2023.
- Petzold, A., Ogren, J. A., Fiebig, M., Laj, P., Li, S.-M., Baltensperger, U., Holzer-Popp, T., Kinne, S., Pappalardo, G., Sugimoto, N., Wehrli, C., Wiedensohler, A., and Zhang, X.-Y.: Recommendations for reporting "black carbon" measurements, *Atmos. Chem. Phys.*, 13, 8365–8379, <https://doi.org/10.5194/acp-13-8365-2013>, 2013.
- Pirhadi, M., Mousavi, A., Sowlat, M. H., Janssen, N. A. H., Cassee, F. R., and Sioutas, C.: Relative contributions of a major international airport activities and other urban sources to the particle number concentrations (PNCs) at a nearby monitoring site, *Environ. Pollut.*, 260, 114027, <https://doi.org/10.1016/j.envpol.2020.114027>, 2020.
- Plachá, D., Vaculík, M., Mikeska, M., Dutko, O., Peikertová, P., Kukutschová, J., Mamulová Kutláková, K., Růžicková, J., Tomášek, V., and Filip, P.: Release of volatile organic compounds by oxidative wear of automotive friction materials, *Wear*, 376-377, 705–716, <https://doi.org/10.1016/j.wear.2016.12.016>, 2017.
- Reemtsma, T., Quintana, J. B., Rodil, R., Garcí'a-López, M., and Rodri'guez, I.: Organophosphorus flame retardants and plasticizers in water and air I. Occurrence and fate, *TrAC Trends in Analytical Chemistry*, 27, 727–737, <https://doi.org/10.1016/j.trac.2008.07.002>, 2008.
- Rider, C. V., Janardhan, K. S., Rao, D., Morrison, J. P., McPherson, C. A., and Harry, G. J.: Evaluation of N-butylbenzenesulfonamide (NBBS) neurotoxicity in Sprague-Dawley male rats following 27-day oral exposure, *Neurotoxicology*, 33, 1528–1535, <https://doi.org/10.1016/j.neuro.2012.07.002>, available at: <https://www.sciencedirect.com/science/article/pii/S0161813X1200188X>, 2012.
- Riesz, P., Berdahl, D., and Christman, C. L.: Free radical generation by ultrasound in aqueous and nonaqueous solutions, *Environ. Health Persp.*, 64, 233–252, <https://doi.org/10.1289/ehp.8564233>, 1985.
- Riipinen, I., Yli-Juuti, T., Pierce, J. R., Petäjä, T., Worsnop, D. R., Kulmala, M., and Donahue, N. M.: The contribution of organics to atmospheric nanoparticle growth, *Nature Geosci*, 5, 453–458, <https://doi.org/10.1038/ngeo1499>, 2012.
- Riley, E. A., Gould, T., Hartin, K., Fruin, S. A., Simpson, C. D., Yost, M. G., and Larson, T.: Ultrafine particle size as a tracer for aircraft turbine emissions, *Atmos. Environ.*, 139, 20–29, <https://doi.org/10.1016/j.atmosenv.2016.05.016>, 2016.

- Rivas, I., Beddows, D. C. S., Amato, F., Green, D. C., Järvi, L., Hueglin, C., Reche, C., Timonen, H., Fuller, G. W., Niemi, J. V., Pérez, N., Aurela, M., Hopke, P. K., Alastuey, A., Kulmala, M., Harrison, R. M., Querol, X., and Kelly, F. J.: Source apportionment of particle number size distribution in urban background and traffic stations in four European cities, *Environ. Int.*, 135, 105345, <https://doi.org/10.1016/j.envint.2019.105345>, 2020.
- Roig, N., Sierra, J., Rovira, J., Schuhmacher, M., Domingo, J. L., and Nadal, M.: In vitro tests to assess toxic effects of airborne PM(10) samples. Correlation with metals and chlorinated dioxins and furans, *The Science of the total environment*, 443, 791–797, <https://doi.org/10.1016/j.scitotenv.2012.11.022>, 2013.
- Rönkkö, T., Kuuluvainen, H., Karjalainen, P., Keskinen, J., Hillamo, R., Niemi, J. V., Pirjola, L., Timonen, H. J., Saarikoski, S., Saukko, E., Järvinen, A., Silvennoinen, H., Rostedt, A., Olin, M., Yli-Ojanperä, J., Nousiainen, P., Kousa, A., and Dal Maso, M.: Traffic is a major source of atmospheric nanocluster aerosol, *Proc. Natl. Acad. Sci. U S A*, 114, 7549–7554, <https://doi.org/10.1073/pnas.1700830114>, 2017.
- Rose, D., Ditas, F., and Jacobi, S.: 3. Bericht zur Untersuchung der regionalen Luftqualität auf ultrafeine Partikel im Bereich des Flughafens Frankfurt: Auswirkungen des reduzierten Flugbetriebs während der COVID-19-Pandemie, Hessisches Landesamt für Naturschutz, Umwelt und Geologie, Wiesbaden, 30 pp., 2020.
- Samet, J. M., Dominici, F., Curriero, F. C., Coursac, I., and Zeger, S. L.: Fine particulate air pollution and mortality in 20 U.S. cities, 1987–1994, *The New England journal of medicine*, 343, 1742–1749, <https://doi.org/10.1056/NEJM200012143432401>, 2000.
- Schmidt, E. M., Pudenzi, M. A., Santos, J. M., Angolini, C. F. F., Pereira, R. C. L., Rocha, Y. S., Denisov, E., Damoc, E., Makarov, A., and Eberlin, M. N.: Petroleomics via Orbitrap mass spectrometry with resolving power above 1 000 000 at m/z 200, *RSC Adv.*, 8, 6183–6191, <https://doi.org/10.1039/C7RA12509G>, 2018.
- Schreiber, B., Fischer, J., Schiwy, S., Hollert, H., and Schulz, R.: Towards more ecological relevance in sediment toxicity testing with fish: Evaluation of multiple bioassays with embryos of the benthic weatherfish (*Misgurnus fossilis*), *The Science of the total environment*, 619–620, 391–400, <https://doi.org/10.1016/j.scitotenv.2017.11.122>, 2018.
- Schultz, T. W. and Cronin, M. T. D.: Quantitative structure-activity relationships for weak acid respiratory uncouplers to *Vibrio fisheri*, *Environ Toxicol Chem*, 16, 357–360, <https://doi.org/10.1002/etc.5620160235>, 1997.
- Schymanski, E. L., Singer, H. P., Slobodnik, J., Ipolyi, I. M., Oswald, P., Krauss, M., Schulze, T., Haglund, P., Letzel, T., Grosse, S., Thomaidis, N. S., Bletsou, A., Zwiener, C., Ibáñez, M., Portolés, T., Boer, R. de, Reid, M. J., Onghena, M., Kunkel, U., Schulz, W., Guillon, A., Noyon, N., Leroy, G., Bados, P., Bogialli, S., Stipaničev, D., Rostkowski, P., and Hollender, J.: Non-target screening with high-resolution mass spectrometry: critical review using a collaborative trial on water analysis, *Analytical and bioanalytical chemistry*, 407, 6237–6255, <https://doi.org/10.1007/s00216-015-8681-7>, 2015.
- Schymanski, E. L., Jeon, J., Gulde, R., Fenner, K., Ruff, M., Singer, H. P., and Hollender, J.: Identifying small molecules via high resolution mass spectrometry: communicating confidence, *Environ. Sci. Technol.*, 48, 2097–2098, <https://doi.org/10.1021/es5002105>, 2014.
- Scigelova, M. and Makarov, A.: Orbitrap mass analyzer--overview and applications in proteomics, *Proteomics*, 6 Suppl 2, 16–21, <https://doi.org/10.1002/pmic.200600528>, 2006.
- Seinfeld, J. H. and Pandis, S. N.: *Atmospheric Chemistry and Physics: From Air Pollution to Climate Change*, 3rd ed., Wiley, s.l., 2185 pp., 2016.

- Shi, Q., Wang, M., Shi, F., Yang, L., Guo, Y., Feng, C., Liu, J., and Zhou, B.: Developmental neurotoxicity of triphenyl phosphate in zebrafish larvae, *Aquatic toxicology* (Amsterdam, Netherlands), 203, 80–87, <https://doi.org/10.1016/j.aquatox.2018.08.001>, 2018.
- Shirmohammadi, F., Sowlat, M. H., Hasheminassab, S., Saffari, A., Ban-Weiss, G., and Sioutas, C.: Emission rates of particle number, mass and black carbon by the Los Angeles International Airport (LAX) and its impact on air quality in Los Angeles, *Atmos. Environ.*, 151, 82–93, <https://doi.org/10.1016/j.atmosenv.2016.12.005>, 2017.
- Shrivastava, M., Cappa, C. D., Fan, J., Goldstein, A. H., Guenther, A. B., Jimenez, J. L., Kuang, C., Laskin, A., Martin, S. T., Ng, N. L., Petaja, T., Pierce, J. R., Rasch, P. J., Roldin, P., Seinfeld, J. H., Shilling, J., Smith, J. N., Thornton, J. A., Volkamer, R., Wang, J., Worsnop, D. R., Zaveri, R. A., Zelenyuk, A., and Zhang, Q.: Recent advances in understanding secondary organic aerosol: Implications for global climate forcing, *Rev. Geophys.*, 55, 509–559, <https://doi.org/10.1002/2016RG000540>, 2017.
- Sigma-Aldrich: Acetylcholinesterase Inhibitor Screening Kit MAK324 - Technical Bulletin: [WWW Document], <https://www.sigmaaldrich.com/deepweb/assets/sigmaaldrich/>, last access: 25 August 2022, 2018.
- Simmonds, M. A.: Classification of Some GABA Antagonists With Regard to Site of Action and Potency in Slices of Rat Cuneate Nucleus, *Eur. J. Pharmacol.*, 80, 347–358, 1982.
- Solbu, K., Daae, H. L., Olsen, R., Thorud, S., Ellingsen, D. G., Lindgren, T., Bakke, B., Lundanes, E., and Molander, P.: Organophosphates in aircraft cabin and cockpit air--method development and measurements of contaminants, *J. Environ. Monit.*, 13, 1393–1403, <https://doi.org/10.1039/c0em00763c>, 2011.
- Solbu, K., Daae, H. L., Thorud, S., Ellingsen, D. G., Lundanes, E., and Molander, P.: Exposure to airborne organophosphates originating from hydraulic and turbine oils among aviation technicians and loaders, *J. Environ. Monit.*, 12, 2259–2268, <https://doi.org/10.1039/c0em00273a>, 2010.
- Southerland, V. A., Brauer, M., Mohegh, A., Hammer, M. S., van Donkelaar, A., Martin, R. V., Apte, J. S., and Anenberg, S. C.: Global urban temporal trends in fine particulate matter (PM_{2.5}) and attributable health burdens: estimates from global datasets, *The Lancet Planetary Health*, [https://doi.org/10.1016/S2542-5196\(21\)00350-8](https://doi.org/10.1016/S2542-5196(21)00350-8), 2022.
- Sparkman, O. D.: *Gas Chromatography and Mass Spectrometry: A Practical Guide*, 2nd ed., Elsevier Science & Technology, San Diego, 633 pp., 2011.
- Spolnik, G., Wach, P., Rudzinski, K. J., Skotak, K., Danikiewicz, W., and Szmigielski, R.: Improved UHPLC-MS/MS Methods for Analysis of Isoprene-Derived Organosulfates, *Anal. Chem.*, 90, 3416–3423, <https://doi.org/10.1021/acs.analchem.7b05060>, 2018.
- Squires, G.: Francis Aston and the mass spectrograph, *J. Chem. Soc., Dalton Trans.*, 3893–3900, <https://doi.org/10.1039/a804629h>, 1998.
- Stacey, B.: Measurement of ultrafine particles at airports: A review, *Atmos. Environ.*, 198, 463–477, <https://doi.org/10.1016/j.atmosenv.2018.10.041>, 2019.
- Stafoggia, M., Cattani, G., Forastiere, F., Di Menno Bucchianico, A., Gaeta, A., and Ancona, C.: Particle number concentrations near the Rome-Ciampino city airport, *Atmos. Environ.*, 147, 264–273, <https://doi.org/10.1016/j.atmosenv.2016.09.062>, 2016.
- Steimer, S. S., Patton, D. J., Vu, T. V., Panagi, M., Monks, P. S., Harrison, R. M., Fleming, Z. L., Shi, Z., and Kalberer, M.: Differences in the composition of organic aerosols between winter and summer in Beijing: a study by direct-infusion ultrahigh-resolution mass spectrometry, *Atmos. Chem. Phys.*, 20, 13303–13318, <https://doi.org/10.5194/acp-20-13303-2020>, 2020.

- Stolzenburg, D., Fischer, L., Vogel, A. L., Heinritzi, M., Schervish, M., Simon, M., Wagner, A. C., Dada, L., Ahonen, L. R., Amorim, A., Baccarini, A., Bauer, P. S., Baumgartner, B., Bergen, A., Bianchi, F., Breitenlechner, M., Brilke, S., Buenrostro Mazon, S., Chen, D., Dias, A., Draper, D. C., Duplissy, J., El Haddad, I., Finkenzeller, H., Frege, C., Fuchs, C., Garmash, O., Gordon, H., He, X., Helm, J., Hofbauer, V., Hoyle, C. R., Kim, C., Kirkby, J., Kontkanen, J., Kürten, A., Lampilahti, J., Lawler, M., Lehtipalo, K., Leiminger, M., Mai, H., Mathot, S., Mentler, B., Molteni, U., Nie, W., Nieminen, T., Nowak, J. B., Ojdanic, A., Onnela, A., Passananti, M., Petäjä, T., Quéléver, L. L. J., Rissanen, M. P., Sarnela, N., Schallhart, S., Tauber, C., Tomé, A., Wagner, R., Wang, M., Weitz, L., Wimmer, D., Xiao, M., Yan, C., Ye, P., Zha, Q., Baltensperger, U., Curtius, J., Dommen, J., Flagan, R. C., Kulmala, M., Smith, J. N., Worsnop, D. R., Hansel, A., Donahue, N. M., and Winkler, P. M.: Rapid growth of organic aerosol nanoparticles over a wide tropospheric temperature range, *Proc Natl Acad Sci USA*, 115, 9122–9127, <https://doi.org/10.1073/pnas.1807604115>, 2018.
- Surratt, J. D., Gómez-González, Y., Chan, A. W. H., Vermeulen, R., Shahgholi, M., Kleindienst, T. E., Edney, E. O., Offenberg, J. H., Lewandowski, M., Jaoui, M., Maenhaut, W., Claeys, M., Flagan, R. C., and Seinfeld, J. H.: Organosulfate formation in biogenic secondary organic aerosol, *The journal of physical chemistry. A*, 112, 8345–8378, <https://doi.org/10.1021/jp802310p>, 2008.
- Takegawa, N., Murashima, Y., Fushimi, A., Misawa, K., Fujitani, Y., Saitoh, K., and Sakurai, H.: Characteristics of sub-10 nm particle emissions from in-use commercial aircraft observed at Narita International Airport, *Atmos. Chem. Phys.*, 21, 1085–1104, <https://doi.org/10.5194/acp-21-1085-2021>, 2021.
- Tao, S., Lu, X., Levac, N., Bateman, A. P., Nguyen, T. B., Bones, D. L., Nizkorodov, S. A., Laskin, J., Laskin, A., and Yang, X.: Molecular characterization of organosulfates in organic aerosols from Shanghai and Los Angeles urban areas by nanospray-desorption electrospray ionization high-resolution mass spectrometry, *Environ. Sci. Technol.*, 48, 10993–11001, <https://doi.org/10.1021/es5024674>, 2014.
- Taylor, G. I.: Disintegration of water drops in an electric field, *Proc. R. Soc. Lond. A*, 280, 383–397, <https://doi.org/10.1098/rspa.1964.0151>, 1964.
- Terzano, C., Di Stefano, F., Conti, V., Graziani, E., and Petroianni, A.: Air pollution ultrafine particles: toxicity beyond the lung, *European Review for Medical and Pharmacological Sciences*, 14, 809–821, available at: https://www.researchgate.net/publication/49743881_Air_pollution_ultrafine_particles_Toxicity_beyond_the_lung, 2010.
- Thermo Fisher Scientific: Vanquish™ Flex UHPLC Systems, <https://www.thermofisher.com/order/catalog/product/IQLAAAGABHFAPUMBHV>, last access: 18 November 2021, 2021.
- Thomson, B. A. and Iribarne, J. V.: Field induced ion evaporation from liquid surfaces at atmospheric pressure, *J. Chem. Phys.*, 71, 4451–4463, <https://doi.org/10.1063/1.438198>, 1979.
- Ticku, M. K. and Ramanjaneyulu, R.: Differential interactions of GABA agonists, depressant and convulsant drugs with [35S]-t-butylbicyclophosphorothionate binding sites in cortex and cerebellum, *Pharmacol. Biochem. Be.*, 21, 151–158, [https://doi.org/10.1016/0091-3057\(84\)90145-X](https://doi.org/10.1016/0091-3057(84)90145-X), 1984.
- Timko, M. T., Fortner, E., Franklin, J., Yu, Z., Wong, H.-W., Onasch, T. B., Miake-Lye, R. C., and Herndon, S. C.: Atmospheric measurements of the physical evolution of aircraft

- exhaust plumes, *Environ. Sci. Technol.*, 47, 3513–3520, <https://doi.org/10.1021/es304349c>, 2013.
- Timko, M. T., Yu, Z., Onasch, T. B., Wong, H.-W., Miake-Lye, R. C., Beyersdorf, A. J., Anderson, B. E., Thornhill, K. L., Winstead, E. L., Corporan, E., DeWitt, M. J., Klingshirm, C. D., Wey, C., Tacina, K., Liscinsky, D. S., Howard, R., and Bhargava, A.: Particulate Emissions of Gas Turbine Engine Combustion of a Fischer–Tropsch Synthetic Fuel, *Energ. Fuel.*, 24, 5883–5896, <https://doi.org/10.1021/ef100727t>, 2010.
- Timko, M. T., Albo, S. E., Onasch, T. B., Fortner, E. C., Yu, Z., Miake-Lye, R. C., Canagaratna, M. R., Ng, N. L., and Worsnop, D. R.: Composition and Sources of the Organic Particle Emissions from Aircraft Engines, *Aerosol Sci. Technol.*, 48, 61–73, <https://doi.org/10.1080/02786826.2013.857758>, 2014.
- Turóczy, B., Hoffer, A., Tóth, Á., Kováts, N., Ács, A., Ferincz, Á., Kovács, A., and Gelencsér, A.: Comparative assessment of ecotoxicity of urban aerosol, *Atmos. Chem. Phys.*, 12, 7365–7370, <https://doi.org/10.5194/acp-12-7365-2012>, 2012.
- Turpin, B. J., Saxena, P., and Andrews, E.: Measuring and simulating particulate organics in the atmosphere: problems and prospects, *Atmos. Environ.*, 34, 2983–3013, [https://doi.org/10.1016/S1352-2310\(99\)00501-4](https://doi.org/10.1016/S1352-2310(99)00501-4), 2000.
- Twomey, S.: The Influence of Pollution on the Shortwave Albedo of Clouds, *J. Atmos. Sci.*, 34, 1149–1152, [https://doi.org/10.1175/1520-0469\(1977\)034<1149:TIOPOT>2.0.CO;2](https://doi.org/10.1175/1520-0469(1977)034<1149:TIOPOT>2.0.CO;2), 1977.
- Ungeheuer, F., Caudillo, L., Ditas, F., Simon, M., van Pinxteren, D., Kılıç, D., Rose, D., Jacobi, S., Kürten, A., Curtius, J., and Vogel, A. L.: Nucleation of jet engine oil vapours is a large source of aviation-related ultrafine particles, *Commun Earth Environ*, 3, <https://doi.org/10.1038/s43247-022-00653-w>, 2022.
- Ungeheuer, F., van Pinxteren, D., and Vogel, A. L.: Identification and source attribution of organic compounds in ultrafine particles near Frankfurt International Airport, *Atmos. Chem. Phys.*, 21, 3763–3775, <https://doi.org/10.5194/acp-21-3763-2021>, 2021.
- United States Environmental Protection Agency: US EPA. [2021]. Estimation Programs Interface Suite™ v 4.11, Washington, DC, USA, 2012.
- van Netten, C. and Leung, V.: Comparison of the constituents of two jet engine lubricating oils and their volatile pyrolytic degradation products, *Appl. Occup. Environ. Hyg.*, 15, 277–283, <https://doi.org/10.1080/104732200301593>, 2000.
- Vanhanen, J., Mikkilä, J., Lehtipalo, K., Sipilä, M., Manninen, H. E., Siivola, E., Petäjä, T., and Kulmala, M.: Particle Size Magnifier for Nano-CN Detection, *Aerosol Sci. Technol.*, 45, 533–542, <https://doi.org/10.1080/02786826.2010.547889>, 2011.
- Vazquez-Duhalt, R.: Environmental impact of used motor oil, *Sci. Total Environ.*, 79, 1–23, [https://doi.org/10.1016/0048-9697\(89\)90049-1](https://doi.org/10.1016/0048-9697(89)90049-1), available at: <http://www.sciencedirect.com/science/article/pii/0048969789900491>, 1989.
- Vert, C., Meliefste, K., and Hoek, G.: Outdoor ultrafine particle concentrations in front of fast food restaurants, *J Expo Sci Environ Epidemiol*, 26, 35–41, <https://doi.org/10.1038/jes.2015.64>, 2016.
- Vogel, A. L., Lauer, A., Fang, L., Arturi, K., Bachmeier, F., Daellenbach, K. R., Käser, T., Vlachou, A., Pospisilova, V., Baltensperger, U., Haddad, I. E., Schwikowski, M., and Bjelić, S.: A Comprehensive Nontarget Analysis for the Molecular Reconstruction of Organic Aerosol Composition from Glacier Ice Cores, *Environ. Sci. Technol.*, 53, 12565–12575, <https://doi.org/10.1021/acs.est.9b03091>, 2019.

- Völker, J., Vogt, T., Castronovo, S., Wick, A., Ternes, T. A., Joss, A., Oehlmann, J., and Wagner, M.: Extended anaerobic conditions in the biological wastewater treatment: Higher reduction of toxicity compared to target organic micropollutants, *Water research*, 116, 220–230, <https://doi.org/10.1016/j.watres.2017.03.030>, 2017.
- Wallraff, J. P., Ungeheuer, F., Dombrowski, A., Oehlmann, J., and Vogel, A. L.: Occurrence and in vitro toxicity of organic compounds in urban background PM_{2.5}, *The Science of the total environment*, 817, 152779, <https://doi.org/10.1016/j.scitotenv.2021.152779>, 2022.
- Wang, K., Huang, R.-J., Brüggemann, M., Zhang, Y., Yang, L., Ni, H., Guo, J., Wang, M., Han, J., Bilde, M., Glasius, M., and Hoffmann, T.: Urban organic aerosol composition in eastern China differs from north to south: molecular insight from a liquid chromatography–mass spectrometry (Orbitrap) study, *Atmos. Chem. Phys.*, 21, 9089–9104, <https://doi.org/10.5194/acp-21-9089-2021>, 2021.
- Wang, M., Kong, W., Marten, R., He, X.-C., Chen, D., Pfeifer, J., Heitto, A., Kontkanen, J., Dada, L., Kürten, A., Yli-Juuti, T., Manninen, H. E., Amanatidis, S., Amorim, A., Baalbaki, R., Baccarini, A., Bell, D. M., Bertozzi, B., Bräkling, S., Brilke, S., Murillo, L. C., Chiu, R., Chu, B., Menezes, L.-P. de, Duplissy, J., Finkenzeller, H., Carracedo, L. G., Granzin, M., Guida, R., Hansel, A., Hofbauer, V., Krechmer, J., Lehtipalo, K., Lamkaddam, H., Lampimäki, M., Lee, C. P., Makhmutov, V., Marie, G., Mathot, S., Mauldin, R. L., Mentler, B., Müller, T., Onnela, A., Partoll, E., Petäjä, T., Philippov, M., Pospisilova, V., Ranjithkumar, A., Rissanen, M., Rörup, B., Scholz, W., Shen, J., Simon, M., Sipilä, M., Steiner, G., Stolzenburg, D., Tham, Y. J., Tomé, A., Wagner, A. C., Wang, D. S., Wang, Y., Weber, S. K., Winkler, P. M., Wlasits, P. J., Wu, Y., Xiao, M., Ye, Q., Zauner-Wieczorek, M., Zhou, X., Volkamer, R., Riipinen, I., Dommen, J., Curtius, J., Baltensperger, U., Kulmala, M., Worsnop, D. R., Kirkby, J., Seinfeld, J. H., El-Haddad, I., Flagan, R. C., and Donahue, N. M.: Rapid growth of new atmospheric particles by nitric acid and ammonia condensation, *Nature*, 581, 184–189, <https://doi.org/10.1038/s41586-020-2270-4>, 2020.
- Wang, S. C. and Flagan, R. C.: Scanning Electrical Mobility Spectrometer, *Aerosol Sci. Technol.*, 13, 230–240, <https://doi.org/10.1080/02786829008959441>, 1990.
- Wang, X., Hayeck, N., Brüggemann, M., Yao, L., Chen, H., Zhang, C., Emmelin, C., Chen, J., George, C., and Wang, L.: Chemical Characteristics of Organic Aerosols in Shanghai: A Study by Ultrahigh-Performance Liquid Chromatography Coupled With Orbitrap Mass Spectrometry, *J. Geophys. Res. Atmos.*, 122, 11,703–11,722, <https://doi.org/10.1002/2017JD026930>, 2017.
- Wang, Y., Hu, M., Guo, S., Wang, Y., Zheng, J., Yang, Y., Zhu, W., Tang, R., Li, X., Liu, Y., Le Breton, M., Du, Z., Shang, D., Wu, Y., Wu, Z., Song, Y., Lou, S., Hallquist, M., and Yu, J.: The secondary formation of organosulfates under interactions between biogenic emissions and anthropogenic pollutants in summer in Beijing, *Atmos. Chem. Phys.*, 18, 10693–10713, <https://doi.org/10.5194/acp-18-10693-2018>, 2018.
- Wei, G.-L., Li, D.-Q., Zhuo, M.-N., Liao, Y.-S., Xie, Z.-Y., Guo, T.-L., Li, J.-J., Zhang, S.-Y., and Liang, Z.-Q.: Organophosphorus flame retardants and plasticizers: sources, occurrence, toxicity and human exposure, *Environ. Pollut.*, 196, 29–46, <https://doi.org/10.1016/j.envpol.2014.09.012>, 2015.
- Weichenthal, S., Olaniyan, T., Christidis, T., Lavigne, E., Hatzopoulou, M., van Ryswyk, K., Tjepkema, M., and Burnett, R.: Within-city Spatial Variations in Ambient Ultrafine

- Particle Concentrations and Incident Brain Tumors in Adults, *Epidemiology* (Cambridge, Mass.), 31, 177–183, <https://doi.org/10.1097/EDE.0000000000001137>, 2020.
- Weiden, S.-L. von der, Drewnick, F., and Borrmann, S.: Particle Loss Calculator – a new software tool for the assessment of the performance of aerosol inlet systems, *Atmos. Meas. Tech.*, 2, 479–494, <https://doi.org/10.5194/amt-2-479-2009>, 2009.
- Wey, C. C., Anderson, B. E., Wey, C., Miake-Lye, R. C., Whitefield, P., and Howard, R.: Overview on the Aircraft Particle Emissions Experiment (APEX), *J. Propul. Power*, 23, 898–905, <https://doi.org/10.2514/1.26406>, 2007.
- WHO: WHO global air quality guidelines: Particulate matter (PM_{2.5} and PM₁₀), ozone, nitrogen dioxide, sulfur dioxide and carbon monoxide, World Health Organization, European Centre for Environment and Health, Bonn, Germany, 285 pp., 2021.
- WHO: Review of evidence on health aspects of air pollution – REVIHAAP, World Health Organization, Scherfigsvej 8, DK-2100 Copenhagen Ø, Denmark, 33 pp., 2013.
- WHO: Air Quality Guidelines: Global Update 2005. Particulate Matter, Ozone, Nitrogen Dioxide and Sulfur Dioxide: Particulate Matter, Ozone, Nitrogen Dioxide and Sulfur Dioxide, World Health Organization, Europe, 496 pp., 2006.
- Willenborg, K., Klingsporn, M., Tebby, S., Ratcliffe, T., Gorse, P., Dullenkopf, K., and Wittig, S.: Experimental Analysis of Air/Oil Separator Performance, *Journal of Engineering for Gas Turbines and Power*, 130, <https://doi.org/10.1115/1.2795785>, 2008.
- Winder, C. and Balouet, J.-C.: The toxicity of commercial jet oils, *Environ. Res.*, 89, 146–164, <https://doi.org/10.1006/enrs.2002.4346>, 2002.
- Winder, C. and Balouet, J.-C.: Aircrew Exposure to Chemicals in Aircraft: Symptoms of Irritation and Toxicity, *J. Occup. Health Safety*, 471–483, 2001.
- Wright, R. L.: Formation of the Neurotoxin TMPP from TMPE-Phosphate Formulations, *Tribol. T.*, 39, 827–834, <https://doi.org/10.1080/10402009608983601>, 1996.
- Wu, A. H., Fruin, S., Larson, T. V., Tseng, C.-C., Wu, J., Yang, J., Jain, J., Shariff-Marco, S., Inamdar, P. P., Setiawan, V. W., Porcel, J., Stram, D. O., Le Marchand, L., Ritz, B., and Cheng, I.: Association between Airport-Related Ultrafine Particles and Risk of Malignant Brain Cancer: A Multiethnic Cohort Study, *Cancer research*, 81, 4360–4369, <https://doi.org/10.1158/0008-5472.CAN-21-1138>, 2021.
- Wu, Y., Li, W., Zhang, M., and Wang, X.: Improvement of oxidative stability of trimethylolpropane trioleate lubricant, *Thermochim. Acta*, 569, 112–118, <https://doi.org/10.1016/j.tca.2013.05.033>, 2013.
- Wyman, J. F., Porvaznik, M., Serve, P., Hobson, D., and Uddin, D. E.: High Temperature Decomposition of Military Specification L-23699 Synthetic Aircraft Lubricants, *J. Fire Sci.*, 5, 162–177, <https://doi.org/10.1177/073490418700500303>, 1987.
- Yamashita, M. and Fenn, J. B.: Electrospray ion source. Another variation on the free-jet theme, *J. Phys. Chem.*, 88, 4451–4459, <https://doi.org/10.1021/j150664a002>, 1984.
- Yang, L., Li, C., and Tang, X.: The Impact of PM_{2.5} on the Host Defense of Respiratory System, *Frontiers in cell and developmental biology*, 8, 91, <https://doi.org/10.3389/fcell.2020.00091>, 2020.
- Yassine, M. M., Harir, M., Dabek-Zlotorzynska, E., and Schmitt-Kopplin, P.: Structural characterization of organic aerosol using Fourier transform ion cyclotron resonance mass spectrometry: aromaticity equivalent approach, *Rapid communications in mass spectrometry RCM*, 28, 2445–2454, <https://doi.org/10.1002/rcm.7038>, 2014.

- Ying, G.-G., Williams, B., and Kookana, R.: Environmental fate of alkylphenols and alkylphenol ethoxylates—a review, *Environment International*, 28, 215–226, [https://doi.org/10.1016/S0160-4120\(02\)00017-X](https://doi.org/10.1016/S0160-4120(02)00017-X), 2002.
- Yu, Z., Timko, M. T., Herndon, S. C., Miake-Lye, R. C., Beyersdorf, A. J., Ziemba, L. D., Winstead, E. L., and Anderson, B. E.: Mode-specific, semi-volatile chemical composition of particulate matter emissions from a commercial gas turbine aircraft engine, *Atmos. Environ.*, 218, 116974, <https://doi.org/10.1016/j.atmosenv.2019.116974>, 2019.
- Yu, Z., Liscinsky, D. S., Fortner, E. C., Yacovitch, T. I., Croteau, P., Herndon, S. C., and Miake-Lye, R. C.: Evaluation of PM emissions from two in-service gas turbine general aviation aircraft engines, *Atmos. Environ.*, 160, 9–18, <https://doi.org/10.1016/j.atmosenv.2017.04.007>, 2017.
- Yu, Z., Herndon, S. C., Ziemba, L. D., Timko, M. T., Liscinsky, D. S., Anderson, B. E., and Miake-Lye, R. C.: Identification of lubrication oil in the particulate matter emissions from engine exhaust of in-service commercial aircraft, *Environ. Sci. Technol.*, 46, 9630–9637, <https://doi.org/10.1021/es301692t>, 2012.
- Yu, Z., Liscinsky, D. S., Winstead, E. L., True, B. S., Timko, M. T., Bhargava, A., Herndon, S. C., Miake-Lye, R. C., and Anderson, B. E.: Characterization of lubrication oil emissions from aircraft engines, *Environ. Sci. Technol.*, 44, 9530–9534, <https://doi.org/10.1021/es102145z>, 2010.
- Yuan, W., Huang, R.-J., Yang, L., Wang, T., Duan, J., Guo, J., Ni, H., Chen, Y., Chen, Q., Li, Y., Dusek, U., O'Dowd, C., and Hoffmann, T.: Measurement report: PM_{2.5}-bound nitrated aromatic compounds in Xi'an, Northwest China – seasonal variations and contributions to optical properties of brown carbon, *Atmos. Chem. Phys.*, 21, 3685–3697, <https://doi.org/10.5194/acp-21-3685-2021>, 2021.
- Zhang, X., Karl, M., Zhang, L., and Wang, J.: Influence of Aviation Emission on the Particle Number Concentration near Zurich Airport, *Environ. Sci. Technol.*, 54, 14161–14171, <https://doi.org/10.1021/acs.est.0c02249>, 2020.
- Zhu, Y., Fanning, E., Yu, R. C., Zhang, Q., and Froines, J. R.: Aircraft emissions and local air quality impacts from takeoff activities at a large International Airport, *Atmos. Environ.*, 45, 6526–6533, <https://doi.org/10.1016/j.atmosenv.2011.08.062>, 2011.
- Zhu, Y., Hinds, W. C., Kim, S., Shen, S., and Sioutas, C.: Study of ultrafine particles near a major highway with heavy-duty diesel traffic, *Atmos. Environ.*, 36, 4323–4335, [https://doi.org/10.1016/S1352-2310\(02\)00354-0](https://doi.org/10.1016/S1352-2310(02)00354-0), 2002a.
- Zhu, Y., Hinds, W. C., Kim, S., and Sioutas, C.: Concentration and size distribution of ultrafine particles near a major highway, *J. Air Waste Manag. Assoc.*, 52, 1032–1042, <https://doi.org/10.1080/10473289.2002.10470842>, 2002b.
- Zubarev, R. A. and Makarov, A.: Orbitrap mass spectrometry, *Anal. Chem.*, 85, 5288–5296, <https://doi.org/10.1021/ac4001223>, 2013.
- Zuth, C., Vogel, A. L., Ockenfeld, S., Huesmann, R., and Hoffmann, T.: Ultrahigh-Resolution Mass Spectrometry in Real Time: Atmospheric Pressure Chemical Ionization Orbitrap Mass Spectrometry of Atmospheric Organic Aerosol, *Anal. Chem.*, 90, 8816–8823, <https://doi.org/10.1021/acs.analchem.8b00671>, 2018.

10. Curriculum Vitae



